FTC-SD-70-20

AD876862L

FTC-SD-70-20

STALL/NEAR STALL INVESTIGATION OF THE F-4E AIRCRAFT

AFFTC

COLLET E. McELROY
First Lieutenant, USAF
Stability and Control
Engineer

PATRICK S. SHARP
Sergeant, USAF
Assistant Stability
and Control Engineer

SUBSTANTIATING DOCUMENT No. 70-20

OCTOBER 1970

This document may be further distributed by any holder only with specific prior approval of ASD (ASZMT), Wright-Patterson AFB, Ohio 45433.

AIR FORCE FLIGHT TEST CENTER
EDWARDS AIR FORCE BASE, CALIFORNIA
AIR FORCE SYSTEMS COMMAND
UNITED STATES AIR FORCE

FTC-SD-70-20

STALL/NEAR STALL INVESTIGATION OF THE F-4E AIRCRAFT

COLLET E. McELROY
First lieutenant, USAF
Stability and Control Engineer

PATRICK S. SHARP
Sergeant, USAF
Assistant Stability and Control Engineer

This document may be further distributed by any holder only with specific prior approval of ASD (ASZMT), Wright-Patterson AFB, Ohio 45433.

FOREWORD

This report presents substantiating data for a previously published technical report (reference 1) on an Air Force evaluation of the F-4E stall characteristics. The flight tests were conducted from 2 December 1969 to 22 June 1970 at the Air Force Flight Test Center, Edwards Air Force Base, California. A total of 57 flights were flown for a total of 63.8 hours.

The tests were conducted under the authority of Headquarters, Air Force Systems Command, as directed by AFFTC Project Directive 70-30, 23 September 1969, amended by Project Directive 70-30A, 18 November 1969. The project engineer was Mr. Elbert L. Rutan and the project officer and pilot was Major Jerauld R. Gentry, USAF.

The authors of this report wish to thank Mr. B.J. Brockhagen, Mr. D.A. Warren, and Mr. R.H. Hendrell, McDonnell-Douglas Corporation, for their engineering assistance.

Prepared by:

Collet E. McElroy

COLLET E. McELROY
First Lieutenant, USAF
Stability and Control Engineer

Patrick S. Sharp

PATRICK S. SHARP
Sergeant, USAF
Assistant Stability and Control Engineer

Reviewed and approved by:
25 September 1970

Crowell D. Skene (?) Col
for THOMAS J. CECIL
Colonel, USAF
Commander, 6512th Test Group

Robert M. White

ROBERT M. WHITE
Brigadier General, USAF
Commander

ABSTRACT

This report includes test techniques, data reduction methods, analytical studies and substantiating data for the Stall/Near Stall Investigation of the F-4E aircraft. Discussion of results, conclusions, and recommendations were included in FTC-TR-70-20, Stall/Near Stall Investigation of the F-4E Aircraft, August 1970.

Table of Contents

List of Illustrations

Figure	Title	Page
Symmetric-High Drag Loadings		
53	Rolling Departure with Opposite Recovery Rolls	258-259
54	Recovery Rolls from a Rolling Departure	260-261
55	2 Turn, Steep-Oscillatory Spin	262-267
56	Drag Chute Deployment at Departure	268-272
57	2 Turn Steep-Oscillatory Spin	274-278
58	Rolling Departure	280-283
59	Recovery Rolls from a Rolling Departure	284-290
Comparison Plots		
60	Comparison of Flat Spin Entries	292-293
61	Comparison of Flat and Steep-Mildly Oscillatory Spin Entries	294-307
Flat Spins		
62	Flat Spin with Asymmetric Loading	308-315
63	Flat Spin with Clean Loading	316-323
Wind Tunnel Data		
64-65	Pitching Moment Coefficient vs. Angle of Attack	324-325
66	Yawing Moment Coefficient vs. Angle of Attack	326
67	Rolling Moment Coefficient vs. Angle of Attack	327
68	Stabilator Effectiveness vs. Angle of Attack	328
69	Rudder Effectiveness vs. Angle of Attack	329
70	Yawing Moment due to Aileron Deflection	330
71	Rolling Moment due to Rudder Deflection	331
72	Aileron Roll Effectiveness vs. Angle of Attack	332

List of Abbreviations and Symbols

Item	Definition	Units
AGL	above ground level	- - -
AND	aircraft nose down	- - -
ANL	aircraft nose left	- - -
ANR	aircraft nose right	- - -
ANU	aircraft nose up	- - -
AOA	angle of attack	deg for true AOA; units for pilot's AOA
ARI	aileron-rudder interconnect	- - -
b	wing span	ft
$\bar{c}$	length of MAC	feet
B/M	bellmouth	- - -
cal, calib	calibration	- - -
C_m	pitching moment coefficient	dimensionless
C_n	yawing moment coefficient	dimensionless
C_ℓ	rolling moment coefficient	dimensionless
C_{m_α}	$\partial C_m/\partial \alpha$	per deg
$C_{m_{\delta_s}}$	$\partial C_m/\partial \delta_s$	per deg
C_{m_β}	$\partial C_m/\partial \beta$	per deg
C_{m_Ω}	$\partial C_m/\partial \left(\frac{\Omega b}{2V_t}\right)$	per rad

Item	Definition	Units
C_{m_q}	$\partial C_m / \partial \left(\frac{q\bar{c}}{2V_t}\right)$	per rad
C_{n_β}	$\partial C_n / \partial \beta$	per deg
$C_{n_{\delta_a}}$	$\partial C_n / \partial \delta_a$	per deg
$C_{n_{\delta_r}}$	$\partial C_n / \partial \delta_r$	per deg
C_{n_r}	$\partial C_n / \partial \left(\frac{rb}{2V_t}\right)$	per rad
C_{n_p}	$\partial C_n / \partial \left(\frac{pb}{2V_t}\right)$	per rad
C_{n_Ω}	$\partial C_n / \partial \left(\frac{\Omega b}{2V_t}\right)$	per rad
C_{ℓ_β}	$\partial C_\ell / \partial \beta$	per deg
$C_{\ell_{\delta_a}}$	$\partial C_\ell / \partial \delta_a$	per deg
$C_{\ell_{\delta_r}}$	$\partial C_\ell / \partial \delta_r$	per deg
C_{ℓ_p}	$\partial C_\ell / \partial \left(\frac{pb}{2V_t}\right)$	per rad
C_{ℓ_r}	$\partial C_\ell / \partial \left(\frac{rb}{2V_t}\right)$	per rad
F_c	parachute riser tension	lb
FAT	free air temperature	deg C
FS	fuselage station	- - -
I_{ENG}	engine moment of inertia	slug-ft^2
IGV	inlet guide vane	- - -
INOP	inoperative	- - -
I_X	moment of inertia about x axis	slug-ft^2
I_{XZ}, I_{XY}, I_{XZ}	cross products of inertia	slug-ft^2

Item	Definition	Units
I_Y	moment of inertia about y axis	slug-ft^2
I_Z	moment of inertia about z axis	slug-ft^2
KCAS	knots calibrated airspeed	knots
KEAS	knots equivalent airspeed	knots
lat	lateral	- - -
LH	left hand	- - -
Long	longitudinal	- - -
LWD	left wing down	- - -
m	mass	slugs
MAC	mean aerodynamic chord	- - -
M_X, M_Y, M_Z	aerodynamic moments about the x, y, and z axes respectively	ft-lb
n, n_z	normal load factor along body z axis	dimensionless
n_Y	load factor along the body y axis	dimensionless
n_X	load factor along the body x axis	dimensionless
P	Pitch axis of SAS	- - -
p	body axis roll rate	deg/sec
PED	pedal	- - -
POS'N	position	- - -
q	body axis pitch rate	deg/sec
$\bar{q}$	free stream dynamic pressure	lb/ft^2
R	roll axis of SAS	- - -
r	body axis yaw rate	deg/sec
RH	right hand	- - -
R.O.	rear observer	- - -
RUD	rudder	- - -
RWD	right wing down	- - -
S	wing area	ft^2

Item	Definition	Units
SAS	stability augmentation system	- - -
SMO	steep-mildly oscillatory (spin mode)	- - -
sta	station	- - -
STK	stick	- - -
TDP	turbine discharge pressure	psia
TED	trailing edge down	- - -
TEL	trailing edge left	- - -
TER	trailing edge right	- - -
TEU	trailing edge up	- - -
TOT	turbine outlet temperature	deg C
V_{ic}	indicated instrument corrected airspeed	knots
V_t, V	true airspeed	knots or ft/sec
WT, W	weight	lb
Y	yaw axis of SAS	- - -
Y_c	relative dimension measured from film to locate chute displacement in Y direction	inches at FS 567
Z_c	relative dimension measured from film to locate chute displacement in Z direction	inches at FS 567
X_c	distance from aircraft cg to parachute attachment point	inches
α_{B_C}	true angle of attack (noseboom AOA corrected for pitch rate effects)	deg
β_C	true sideslip angle (noseboom β corrected for AOA and yaw rate effects)	deg
κ	chute riser angle measured to the plane of symmetry	deg
λ	chute riser angle measured to the xy plane	deg
δ_a	aileron deflection	deg
δ_r	rudder deflection	deg

Item	Definition	Units
δ_s	stabilator deflection	deg
Ω	total angular velocity	deg/sec or rad/sec
Ω_{eng}	engine rotation speed	rpm or rad/sec

Sign Conventions

Parameter	Sign Convention
Y Side Force	+ RT
L Rolling Moment	+ RWD
M Pitching Moment	+ ANU
N Yawing Moment	+ ANR
p Roll Rate	+ RWD
r Yaw Rate	+ ANR
q Pitch Rate	+ ANU
α Angle of Attack	+ ANU
β Sideslip Angle	+ ANL
ϕ Bank Angle	+ RWD
δ_s Stabilator Deflection	+ TEU
δ_a Aileron Deflection	+ RWD
δ_r Rudder Deflection	+ TER
F_e Longitudinal Stick Force	+ Pull
Lateral Stick Position	+ RT

INTRODUCTION

This report includes test techniques, data reduction methods, analytical studies, and substantiating data for the Stall/Near Stall Investigation of the F-4E aircraft. Discussion of results, conclusions and recommendations were included in FTC-70-20, Stall/Near Stall Investigation of the F-4E Aircraft, August 1970. The data represent out-of-control characteristics of the aircraft with a variety of representative loadings. Data pertaining to departure, spin susceptibility, and spin prevention and recovery techniques are included. The results of analytical studies as presented herein should provide a more thorough understanding of the F-4E flight dynamics at high angle of attack.

Table I lists the external store loadings flown during this program. Table II is a summary of the aircraft configurations referred to in this report.

TABLE I
LOADING SUMMARY
F-4E USAF S/N 66-265

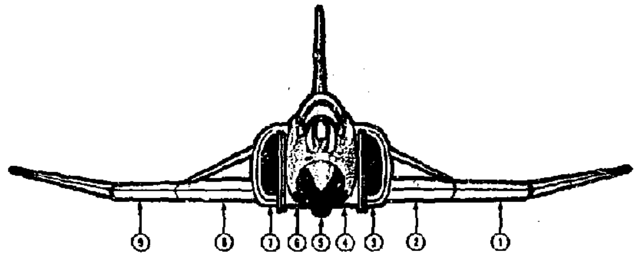

LOADING NO.	ENGINE START GROSS WEIGHT (lb)	ENGINE START CG (% MAC)	FLIGHT MANUAL STABILITY INDEX	FLIGHT MANUAL DRAG INDEX	LOADING ASYMMETRY (ft-lb)	LOADING ASYMMETRY (% OF MAX ALLOWABLE)	ARMAMENT STATIONS 9	8	7	6	5	4	3	2	1
1	41,400	33.3	11.4	10.4	0	0	CLEAN	MAU-12B/A PYLON	AIM-7 (SPARROW)	AIM-7 (SPARROW)	CLEAN	AIM-7 (SPARROW)	AIM-7 (SPARROW)	MAU-12B/A PYLON	CLEAN
1A	44,700	32.6	11.4	7.1	0	0	CLEAN	MAU-12B/A PYLON	CLEAN	AIM-7 (SPARROW)	CLEAN	AIM-7 (SPARROW)	CLEAN	MAU-12B/A PYLON	CLEAN
1B	44,500	34.6	11.6	7.0	0	0	CLEAN	MAU-12B/A PYLON	AIM-7 (SPARROW)	CLEAN	CLEAN	CLEAN	AIM-7 (SPARROW)	MAU-12B/A PYLON	CLEAN
1C	44,400	34.9	0	2.4	0	0	CLEAN	CLEAN	AIM-7 (SPARROW)	CLEAN	CLEAN	CLEAN	AIM-7 (SPARROW)	CLEAN	CLEAN
1D	40,900	33.1	0	2.1	0	0	CLEAN	CLEAN	CLEAN	AIM-7 (SPARROW)	CLEAN	AIM-7 (SPARROW)	CLEAN	CLEAN	CLEAN
1E	45,060	34.9	0	0	0	0	CLEAN	CLEAN	CLEAN	CLEAN	CLEAN	CLEAN	CLEAN	CLEAN	CLEAN
2A	50,700	31.6	22.4	10.0	0	0	MAU-12B/A PYLON	MAU-12B/A PYLON	CLEAN	CLEAN	FULL 600 GAL TANK	CLEAN	CLEAN	MAU-12B/A PYLON	MAU-12B/A PYLON
2B	–	–	22.4	19.6	0	0	MAU-12B/A PYLON	MAU-12B/A PYLON	CLEAN	CLEAN	EMPTY 600 GAL TANK	CLEAN	CLEAN	MAU-12B/A PYLON	MAU-12B/A PYLON
2C	51,000	33.0	87.2	30.3	-10,170	63	MAU-12B/A PYLON	MAU-12B/A PYLON TER THREE M117 LDGP BOMBS	CLEAN	CLEAN	CLEAN	CLEAN	CLEAN	MAU-12B/A PYLON TER TWO LAU-3/A's	MAU-12B/A PYLON ONE M117 LDGP BOMB
2D	51,000	33.0	86.1	30.3	10,170	63	MAU-12B/A PYLON ONE M117 LDGP BOMB	MAU-12B/A PYLON TER TWO LAU-3/A's	CLEAN	CLEAN	CLEAN	CLEAN	CLEAN	MAU-12B/A PYLON TER THREE M117 LDGP BOMBS	MAU-12B/A PYLON
4A	54,900	32.9	100.4	33.0	0	0	FULL 370 GAL SGT. FLETCHER TANK	MAU-12B/A PYLON TER THREE M117 LDGP BOMBS	CLEAN	CLEAN	CLEAN	CLEAN	CLEAN	MAU-12B/A PYLON TER THREE M117 LDGP BOMBS	FULL 370 GAL SGT. FLETCHER TANK
4B	–	–	114.4	33.6	0	0	EMPTY 370 GAL SGT. FLETCHER TANK	MAU-12B/A PYLON TER THREE M117 LDGP BOMBS	CLEAN	CLEAN	CLEAN	CLEAN	CLEAN	MAU-12B/A PYLON TER THREE M117 LDGP BOMBS	EMPTY 370 GAL SGT. FLETCHER TANK
5A	53,900	33.3	114.9	49.0	11,399	44	FULL 370 GAL SGT. FLETCHER TANK	MAU-12B/A PYLON TER TWO M117 RETARDED	CLEAN	CLEAN	MER & ADAPTER	CLEAN	CLEAN	MAU-12B/A PYLON TER	FULL 370 GAL SGT. FLETCHER TANK
5B	–	–	114.9	47.0	11,399	44	EMPTY 370 GAL SGT. FLETCHER TANK	MAU-12B/A PYLON TER TWO M117 RETARDED	CLEAN	CLEAN	MER & ADAPTER	CLEAN	CLEAN	MAU-12B/A PYLON TER	EMPTY 370 GAL SGT. FLETCHER TANK
6A	49,200	34.3	51.8	18.0	26,552	100	FULL 370 GAL SGT. FLETCHER TANK	MAU-12B/A PYLON	CLEAN	CLEAN	CLEAN	CLEAN	CLEAN	MAU-12B/A PYLON	EMPTY 370 GAL SGT. FLETCHER TANK
6B	–	–	51.8	18.9	0	0	EMPTY 370 GAL SGT. FLETCHER TANK	MAU-12B/A PYLON	CLEAN	CLEAN	CLEAN	CLEAN	CLEAN	MAU-12B/A PYLON	EMPTY 370 GAL SGT. FLETCHER TANK
7A	54,900	32.9	175.2	130.4	0	0	MAU-12B/A PYLON MER SIX M117 LDGP BOMBS	MAU-12B/A PYLON TER THREE LAU-3/A's	CLEAN	AIM-7 (SPARROW)	CLEAN	AIM-7 (SPARROW)	CLEAN	MAU-12B/A PYLON TER THREE LAU-3/A's	MAU-12B/A PYLON MER SIX M117 LDGP BOMBS
8A	56,000	33.1	151.0	111.0	0	0	MAU-12B/A PYLON MER THREE M117 LDGP BOMBS	MAU-12B/A PYLON TER THREE LAU-3A's	CLEAN	CLEAN	FULL 600 GAL TANK	CLEAN	CLEAN	MAU-12B/A PYLON TER THREE LAU-3A's	MAU-12B/A PYLON MER THREE M117 LDGP BOMBS
8B	–	–	151.9	111.0	0	0	MAU-12B/A PYLON MER THREE M117 LDGP BOMBS	MAU-12B/A PYLON TER THREE LAU-3A's	CLEAN	CLEAN	EMPTY 600 GAL TANK	CLEAN	CLEAN	MAU-12B/A PYLON TER THREE LAU-3A's	MAU-12B/A PYLON MER THREE M117 LDGP BOMBS
9A	52,000	31.8	73.1	42.7	4,943	35	FULL 370 GAL SGT. FLETCHER TANK	MAU-12B/A PYLON TER ONE M117 RETARDED	CLEAN	CLEAN	MER & ADAPTER	CLEAN	CLEAN	MAU-12B/A PYLON TER	FULL 370 GAL SGT. FLETCHER TANK
9B	–	–	94.3	42.7	4,943	35	EMPTY 370 GAL SGT. FLETCHER TANK	MAU-12B/A PYLON TER ONE M117 RETARDED	CLEAN	CLEAN	MER & ADAPTER	CLEAN	CLEAN	MAU-12B/A PYLON TER	EMPTY 370 GAL SGT. FLETCHER TANK

NOTE. All LAU-3A's are full of rockets and without nose or tail cones

TABLE II

AIRCRAFT CONFIGURATIONS				
Configuration	Thrust	Gear	Flaps	Speed Brake
Cruise (CR)	As required for level flight	UP	UP	UP
Combat (CO)	Augmented	UP	UP	UP
Dive (D)	IDLE	UP	UP	EXTENDED
Glide (G)	IDLE	UP	UP	UP
Power Approach (PA)	As required for level flight	DOWN	FULL or HALF*	UP
Landing (L)	IDLE	DOWN	FULL	UP

*Flaps for PA configuration tests were full unless noted as half.

AIRCRAFT DESCRIPTION

SPECIAL MODIFICATIONS

The test aircraft was a production F-4E, USAF S/N 66-285, instrumented for flying qualities testing and modified to provide a recovery capability from any out-of-control condition. Figure 1 shows the external geometry changes necessary to accommodate a 33.5-foot diameter spin-recovery chute and a production drag chute.

External stiffeners were added to the aft fuselage to absorb loads from the spin-recovery parachute. Two cameras were mounted on top of the fuselage. One camera was oriented forward to document the motions of the aircraft and the other was pointed aft to cover parachute deployments (figure 2). An additional forward-looking camera was mounted above and behind the pilot's shoulder.

Other modifications consisted of the removal of production equipment not required in the flight test program and installation of instrumentation equipment in its place. The nose gun was replaced with an emergency electrical power package and the nose radar was replaced with a MCAIR-designed and -installed instrumentation package containing the magnetic airborne data recording system and other major components.

A test noseboom was also installed with a pitot-static head for measurement of airspeed and altitude, and vanes for measurements of angle of attack and angle of sideslip (figures 2 and 3).

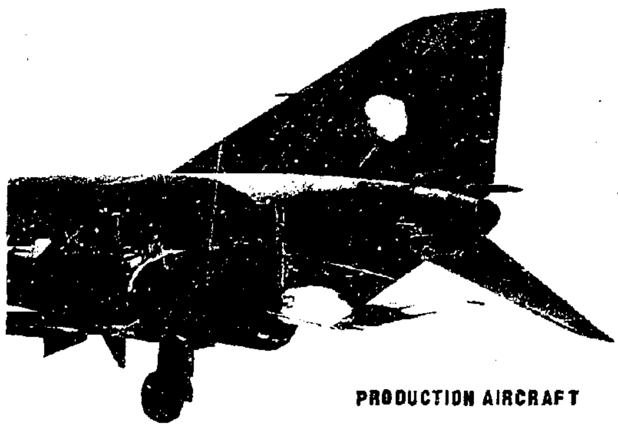

PRODUCTION AIRCRAFT

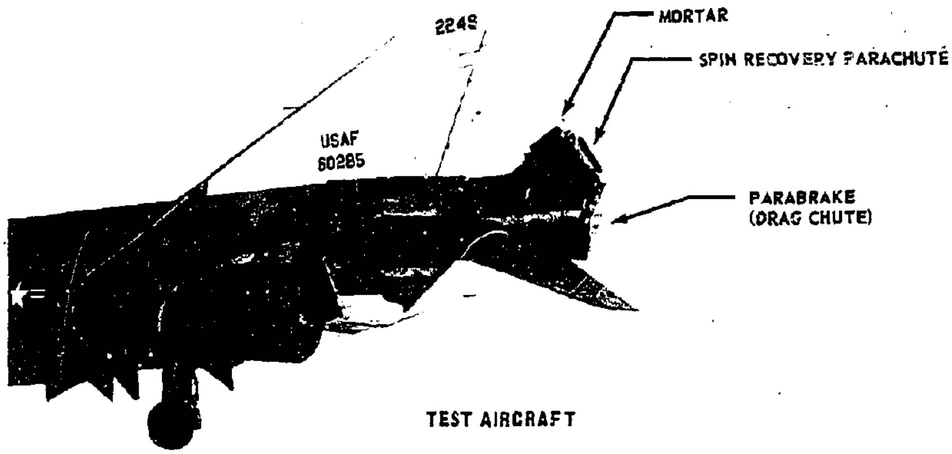

TEST AIRCRAFT

Figure 1 - AFT FUSELAGE COMPARISON

Figure 2 TEST AIRCRAFT

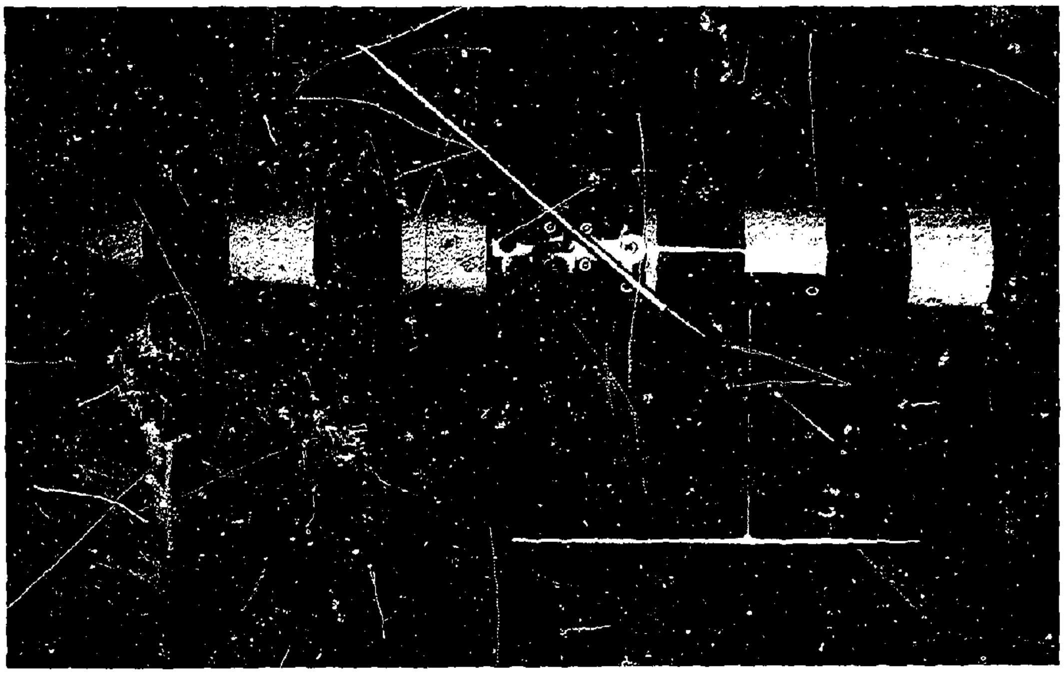

Figure 3 NOSEBOOM WITH ANGLE OF ATTACK AND SIDESLIP VANES

The forward and aft cockpits were equipped with special test systems controls (figures 4, 5, and 6). A two-position fuel transfer switch, allowing manual control of the fuel transfer from fuel cell numbers five and six, was installed on the main instrument panel to facilitate flight testing at an aft cg. An individual fuel quantity indicator, providing the capability of monitoring the fuel quantity in each fuselage tank, was also installed.

A continuous ignition system was provided to sustain engine ignition during a spin condition. Two ON/OFF switches labeled AIRCRAFT and FLIGHT TEST were installed on the pilot's main instrument panel. The switch labeled AIRCRAFT provided ignition power to both engines from the production battery system when the switch was in the ON position. In the ON position, the switch labeled FLIGHT TEST provided ignition power to both engines from the flight test battery system.

Emergency electrical power was provided by two of the four batteries in the emergency power package located in the nose gun compartment. This power was available to all instrumentation systems, the pyrotechnic busses, engine ignition system, the stabilator feel trim system, the PC-1 indicator, the intercom, and UHF radio. The batteries provided dc power to selected systems and to inverters which provided three-phase, 115-volt, 400-cps power to the systems requiring ac power. Control of the emergency electrical system was provided by a three-position switch, labeled EMERG ELECT CONT with positions, AUTO/OFF/ON, providing manaul or automatic activation of the emergency batteries. In AUTO position, the emergency batteries were activated as generator power was lost.

Two electrically driven, emergency hydraulic pumps, which receive power from two batteries in the emergency power package, were installed in the left-hand side of the center fuselage and just above the wing root. Emergency hydraulic power was available to all lateral and longitudinal controls through the PC-1 system. A three-position switch labeled EMERG HYD CONT with positions AUTO/OFF/ON was located on the pilot's forward pedestal panel, providing pilot control for either automatic or manual activation of the emergency hydraulic pumps. In the AUTO position, the emergency pumps were activated when PC-1 pressure dropped to 1,000 ± 50 psi. In the OFF position, the emergency pumps were deactivated. In the ON position, the pilot could select operation of the emergency hydraulic pumps, independent of PC-1 system pressure. A cumulative-operating-time indicator for the emergency hydraulic power system was installed on the main instrument panel in the location normally occupied by the clock. A yellow light was also provided to indicate, when illuminated, that the emergency hydraulic power was operational.

Pyrotechnic systems were provided for spin recovery chute deployment and jettison, drag chute jettison, forward and aft canopy emergency release, and arresting hook extension. Deployment of the spin recovery chute was accomplished by pulling a "T" handle installed in the missile status panel area, or by placing a guarded two-position switch, labeled ALTERNATE DEPLOY, in the deploy position. Pulling the "T" handle aft one inch would pyrotechnically jettison the drag chute, deploy the spin recovery chute, and arm the pyrotechnic jettison circuit for the recovery chute. The alternate deploy switch was provided in the event of a failure of the "T" handle switch. Pyrotechnic jettison of the drag chute could also be accomplished by using a guarded two-position jettison switch installed on the pilot's left console where the AGM-12B control handle was normally located. A guarded two-position switch, labeled CANOPY XPL REL, was installed on both forward and aft cockpits in the event normal canopy jettison would not occur when using the ejection procedure. Placing this switch in the FIRE position would cause the pyrotechnic devices in the canopy hinges and rod ends to be activated. This action severed the links but would not jettison the canopies. A two-position switch, labeled ARRESTING HOOK, was installed on the pilot's forward pedestal panel.

Placing this switch in the LOWER position would cause activation of a gas-operated device which allowed the arresting hook to fall free. A pyrotechnic control panel located on the pilot's right console panel provided a central control for the arming of all pyrotechnic systems. This panel contained a lever-lock two-position master switch labeled SAFE/ARM which had to be in the ARM position for the pyrotechnic system to operate, and fourteen circuit breakers which also had to be closed for the selected pyrotechnic system to be operational. All systems contained dual circuitry.

Three, three-inch indicators, angle of attack, angle of yaw, and yaw rate, were installed in a flight test panel in a location normally occupied by the APS-120 radar scope. In addition, a flight test airspeed indicator was installed on the main instrument panel in place of the production radar altimeter.

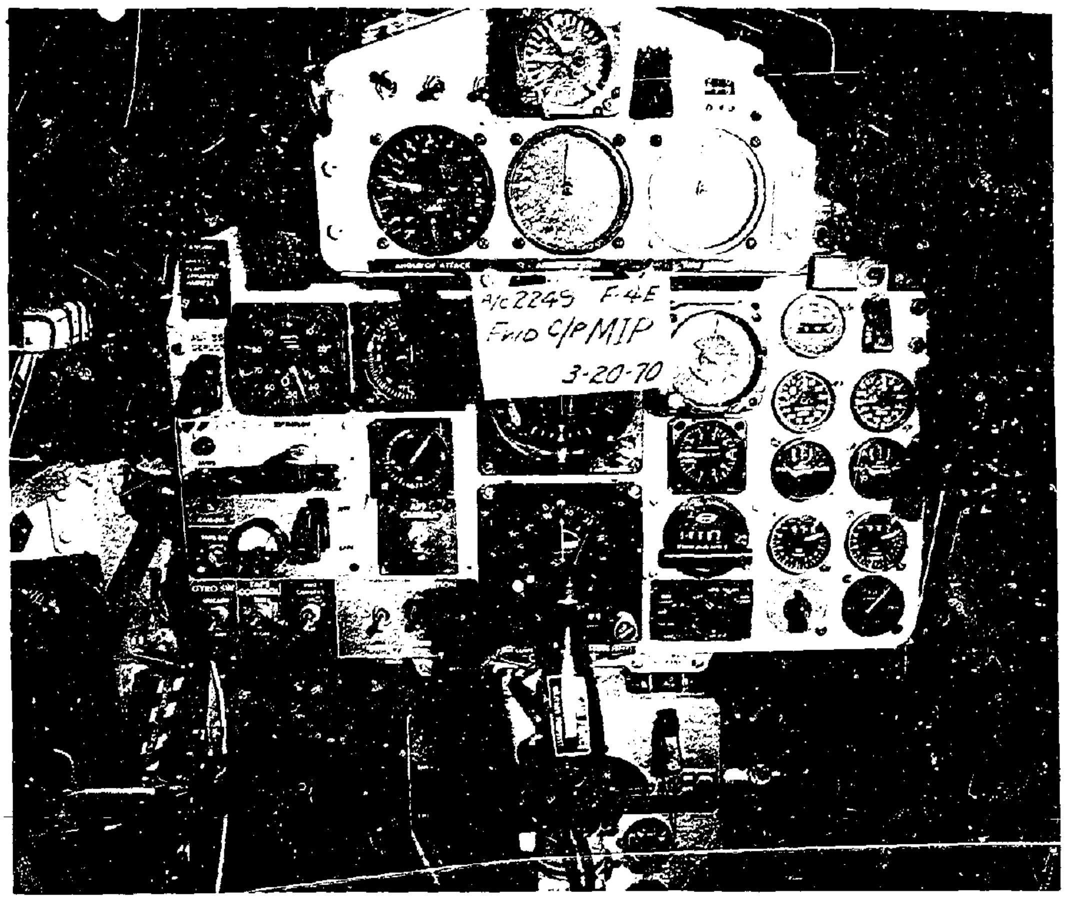

Figure 4 FORWARD COCKPIT MAIN INSTRUMENT PANEL

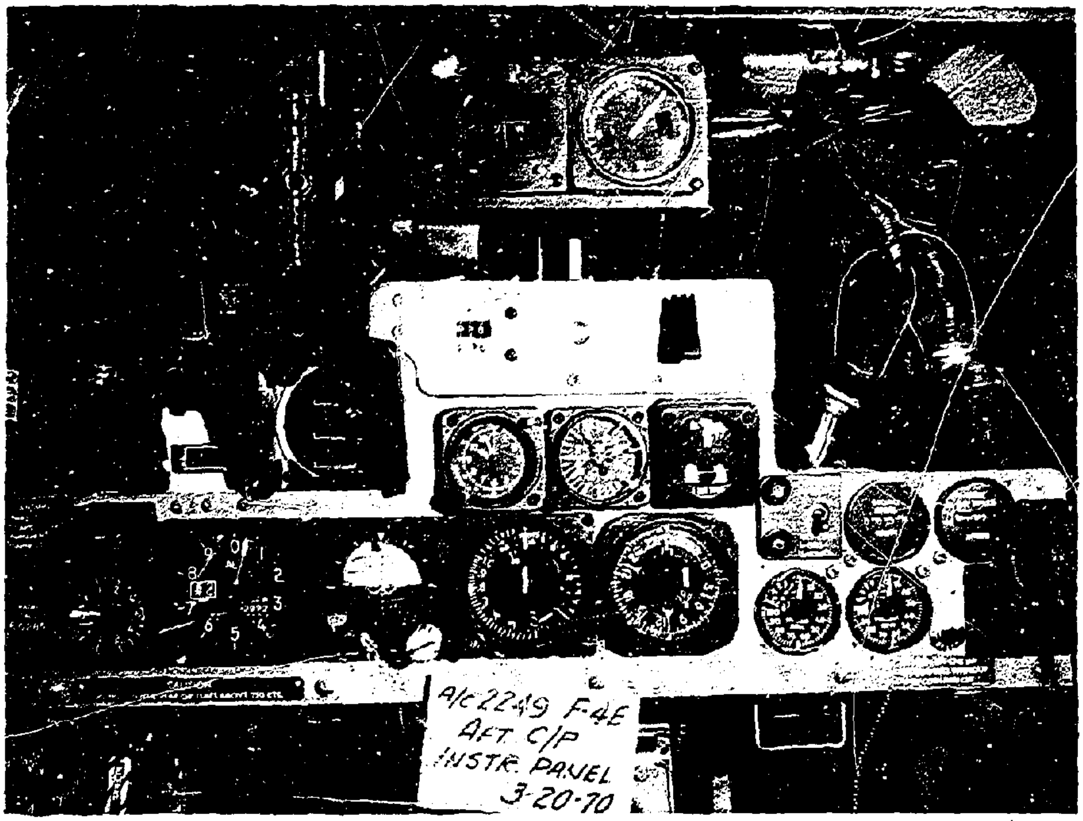

Figure 5 AFT COCKPIT MAIN INSTRUMENT PANEL

The tailcone was modified to house the 33.5-foot diameter spin-recovery chute, at a 30-degree angle above the aircraft waterline. The tailcone contained two separate compartments in which the spin-recovery chute and a conventional drag chute were installed. A pivot retaining mechanism for each chute was provided, and had to be manually locked prior to deployment. Unlocking the mechanisms would mechanically jettison the chutes after deployment. In addition, special bolts and lugs were provided to jettison the drag chute and spin-recovery chute pyrotechnically, if required.

Immediately above the spin recovery chute compartment was a mortar canister containing the spin-recovery pilot chute. The pilot chute, when fired from the mortar canister, inflates and extracts the spin-recovery chute and 70 feet of riser from its compartment.

The 33.5-foot spin-recovery chute jaw operating handle occupied the position where the arresting gear handle was normally installed. When

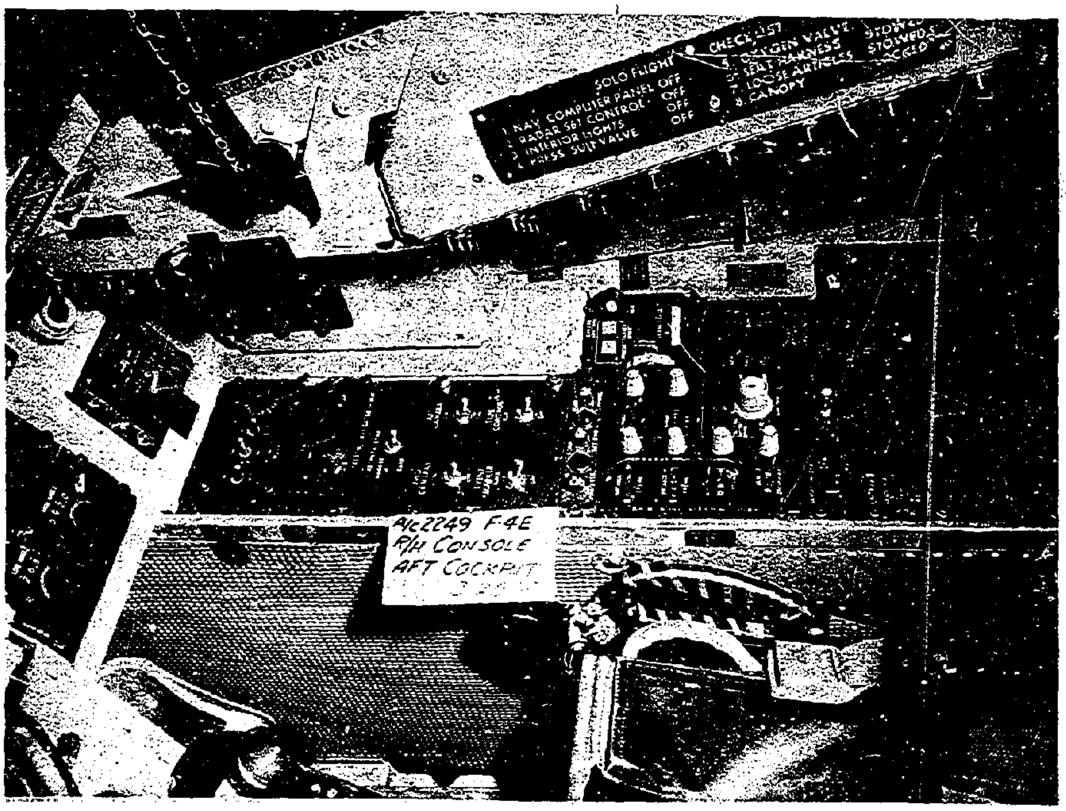

Figure 6 AFT COCKPIT R/H INSTRUMENT CONSOLE

the handle was up, the retaining jaws were open. When the handle was down, the retaining jaws were locked; a green light at the end of the handle, and the 33.5 foot chute JAWS-LOCKED green light on the spin recovery chute control panel indicated the jaws locked and pivots in place. Mechanical jettison of the spin recovery chute would occur if the handle were moved from the DOWN to the UP position after chute deployment.

The drag chute was housed in the lower compartment of the tailcone, and its operation, from a pilot's standpoint, was identical to the production F-4 installation. Drag chute deployment occurred when the production drag chute control handle was rotated aft to the locking detent. The drag chute could then be mechanically jettisoned by rotating the handle further aft to clear the detent, depressing the thumb button, and rotating the handle full forward. The drag chute was pyrotechnically jettisoned automatically upon the actuation of the spin-recovery chute deployment switch to avoid the spin-recovery pilot chute from becoming fouled in the drag chute risers or canopy.

INSTRUMENTATION

An ampex IRIG magnetic tape recording package was installed in the radome in place of the production radar package (figure 7). Two forms of data recording were used. These were frequency modulation (FM) and pulse duration modulation (PDM). The FM recording technique employs a carrier frequency modulated by the data to be recorded. A number of signal channels are recorded on a single recorder track. PDM used the instantaneous sampling of a number of signal channels on a time sequencing basis. Ninety parameters were recorded via PDM. This magnetic tape recorder was operated from either the front or aft cockpits, and the data was recorded both onboard and on the ground via telemetry. For each test mission, parameters measured, units and ranges are listed.

Parameter	Units	Range
Altitude (production)	ft	0 to 80,000
Altitude (test)	ft	0 to 80,000
Airspeed (production)	kt	0 to 1,000
Airspeed (test)	kt	0 to 1,000
FAT No. 1 L/H side	deg C	-70 to 200
Fuel quantity No. 1	lb	0 to 2,000
Fuel quantity No. 2	lb	0 to 2,000
Fuel quantity No. 3	lb	0 to 1,180
Fuel quantity No. 4	lb	0 to 1,610
Fuel quantity No. 5	lb	0 to 1,435
Fuel quantity No. 6	lb	0 to 1,685
Fuel quantity No. 7	lb	0 to 683
Fuel quantity total	lb	0 to 12,500
L/H rpm	rpm	0 to 9,000
R/H rpm	rpm	0 to 9,000
L/H TDP	psia	0 to 60.0
R/H TDP	psia	0 to 60.0
L/H TOT	deg C	0 to 1,000
R/H TOT	deg C	0 to 1,000
L/H CDP	psia	0 to 300

Parameter	Units	Range
R/H CDP	psia	0 to 300
L/H Nozzle position	in^2	280 to 665
R/H Nozzle position	in^2	280 to 665
L/H IGV position	deg	-22 to +18
R/H IGV position	deg	-22 to +18
L/H Throttle position	deg	Cutoff to max A/B
R/H Throttle position	deg	Cutoff to max A/B
L/H Inlet ramp position	in.	11 to 16
R/H Inlet ramp position	in.	11 to 16
L/H B/M position	in.	0 to 4
R/H B/M position	in.	0 to 4
Speed brake position	---	closed - open
T.E. flap position (L & R)	up - down - one-half	---
n_z at cg	g	-2 to +9
n_z at P.S.	g	-2 to +9
n_y at cg	g	-2 to +2
n_y at P.S.	g	-2 to +2
n_x at cg	g	-6 to +3
n_x at P.S.	g	-6 to +3
L/H Aileron position	deg	-30 to +1
R/H Aileron position	deg	-30 to +1
Stabilator position	deg	-10 to +30
Rudder position	deg	-30 to +30
L/H Inboard spoiler position	deg	0 to 45
L/H Outboard spoiler position	deg	0 to 45
R/H Inboard spoiler position	deg	0 to 45
R/H Outboard spoiler position	deg	0 to 45

Parameter	Units	Range
Stabilator trim position	units of trim	±5
Longitudinal stick position	deg	-12.0 to +25.0
Lateral stick position	deg	-10.0 to +10.0
Longitudinal stick force	lb	-40 to +75
Lateral stick force	lb	-30 to +30
Rudder pedal position	in.	3.09 fwd to 3.24 aft
Rudder pedal force (Differential)	lb	0 to +300
Pitch angle	deg	-120 to +120
Bank angle	deg	-180 to +180
Angle of sideslip	deg	-90 to +90
Angle of attack (production)	units	0 to 30
Angle of attack (test)	deg	-40 to +110
Rate of pitch	deg/sec	-150 to +150
Rate of roll	deg/sec	-200 to +200
Rate of yaw	deg/sec	-150 to +150
Azimuth angle	deg	0 to 360
Yaw damper position	deg of rudder	±5
Roll damper position	deg of aileron	±10
Pitch damper position	deg of elevator	±.5
Drag and spin chute deploy event	---	---
Drag and spin chute loads	---	---
Utility hydraulic pressure	psi	0 to 3,500
PC-2 hydraulic pressure	psi	0 to 3,500
PC-1 hydraulic pressure	psi	0 to 3,500
Pilots event mark	---	---
R.O. event mark	---	---

A detailed description of the test aircraft is given in reference 8.

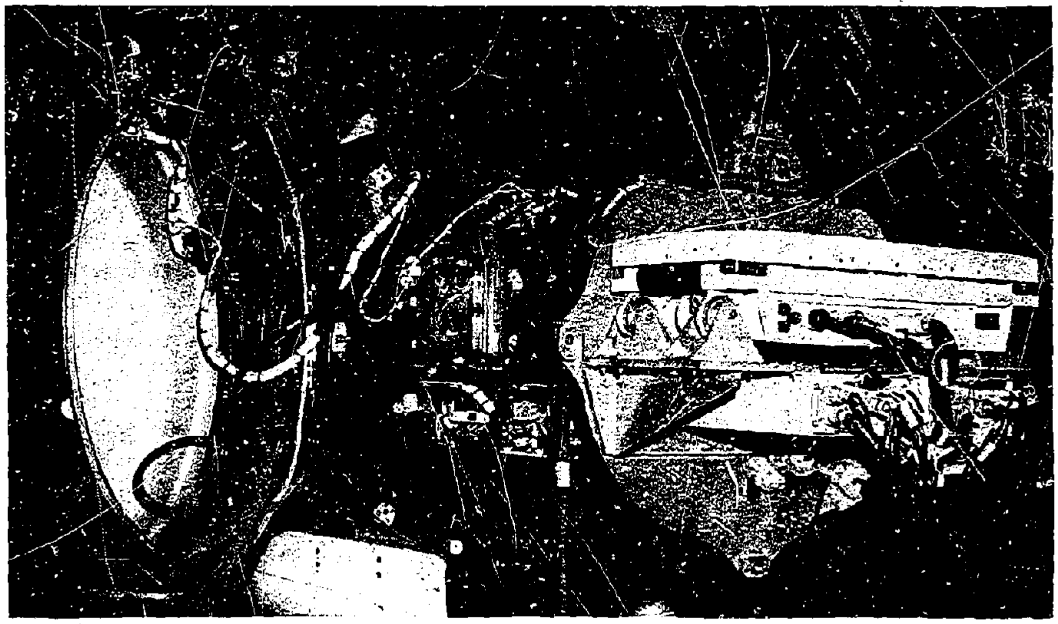

Figure 7 MCAIR INSTRUMENTATION PACKAGE

TEST TECHNIQUES AND DATA REDUCTION METHODS

BASELINE STABILITY

The test aircraft was compared with an unmodified F-4E to determine the effect of the aft fuselage modifications at AOA's below departure. This was done by comparing test data of this program to that obtained during the Air Force F-4E Category II Stability tests (references 4 and 5). The following specific tests were flown: maneuvering flight, static and dynamic stability, and rudder roll performance.

Longitudinal

The maneuvering stability test technique consisted of trimming the aircraft for 1-g flight at the aim flight condition, and then increasing normal acceleration while holding trim, throttle setting, and Mach number constant (windup turns). A descent was established to hold constant Mach number. To facilitate calculation of maneuver points, stabilator position and angle of attack were plotted against normal force coefficient, $C_N = \frac{nW}{\bar{q}S}$, (figure 1, appendix I).

Manuever points were calculated by the following technique:

a. Plots of stabilator position (δ_S) versus C_N, were grouped by Mach number for like loadings and configurations and for various cg positions.

b. Slopes of the δ_S versus C_N curves (d_{δ_S}/dC_N) were determined at various values of C_N.

c. The d_{δ_S}/dC_N values were plotted against cg positions.

d. The d_{δ_S}/dC_N values at different cg's were extrapolated to the cg for zero d_{δ_S}/dC_N for each value of C_N.

The maneuver points were plotted against C_N to summarize the maneuvering stability for a given Mach number range and are compared with an unmodified F-4E (figure 9, appendix I).

Accelerations and decelerations were performed to evaluate the stick force characteristics during speed changes throughout the flight envelope. The tests were conducted by trimming at a Mach number, changing the throttle setting, and then maintaining altitude with the longitudinal control while the aircraft accelerated or decelerated (figures 2 and 3, appendix I).

Lateral-Directional

Tests to determine static directional stability and dihedral effect were conducted by slowly applying increasing rudder pedal force and using lateral stick to maintain a constant heading. Initial trim condition for all tests was 1-g level flight.

Lateral and directional control surface positions and bank angle were plotted against sideslip angle for a stability comparison. These data are shown in figure 10, appendix I.

STALL TESTS

Stall tests were conducted in four phases. Test techniques were discussed in reference 1.

Each stall mission was photographed from a chase aircraft and by ground-to-air trackers. Each flight was also monitored and recorded on video tape, which was reviewed immediately after each flight. In addition, the following parameters were telemetered and monitored in real time by engineers at the ground station:

Azimuth angle
N_z @ cg
Yaw rate
Roll rate
Cameras on/off
16-foot chute load
Altitude (coarse)
Airspeed (coarse)

Stabilator position
Lateral stick position
Rudder position
Noseboom AOA
Production AOA
Noseboom sideslip (uncorrected)
Pitch angle
Bank angle
Intercom voice.

In order to evaluate the flight dynamics of the aircraft at stall/near stall angles of attack, measurement of most parameters recorded in normal stability and control flight testing were sufficient. The techniques employed to correct the parameters were different than for normal low AOA testing.

Position Error

Utilizing the tower fly-by method (reference 7), low AOA static position error was determined for the test aircraft (figure 4, appendix I).

Angle of attack values were frequently encountered which were greater than those at which the airplane can maintain a steady state flight condition. As a result, standard airspeed calibration methods such as pacer, tower fly-by, etc., were not adequate. Proper design of total pressure sensing systems allows for a relatively wide range of angle of attack values while maintaining negligible total pressure errors. For stall/spin testing total pressure corrections must be made since excessive angle of attack values are reached which exceed the negligible error range of the total pressure sensor.

For this program, airspeed corrections during high angle of attack maneuvers were determined in the following manner: true velocity change during a maneuver was found by integrating acceleration data:

$$\Delta V_t = \frac{dV}{dt} \; dt,$$

where: $$\frac{dV}{dt} = \left[-N_z \sin \alpha - N_x \cos \alpha\right] g - g \sin\gamma,$$

$$\gamma = \theta - \alpha \cos\phi$$

Using the integration process of obtaining ΔV_t, it was possible to go from V_t measured immediately before the maneuver (at low AOA) to V_t measured after the maneuver (at low AOA). Having V_t, free air temperature, and pressure altitude (static pressure error was found to be small - less than 100 feet), a Mach number was determined. Calibrated airspeed was determined from Mach number and pressure altitude. A corrected impact pressure $\bar{q}_c$, was then determined using V_c (for conditions during a stall/spin, V_c is within 2 knots of V_e, thus $\bar{q}_c$ was used in lieu of $\bar{q}$).

The ratio $\frac{\bar{q}_{ic}}{\bar{q}_c}$ was plotted versus angle of attack and this function

was used to determine calibrated airspeed and true airspeed in subsequent high angle of attack situations (figure 5, appendix I). Thus, rate corrections to angle of attack and sideslip, which are dependent on correct values of V_t, and stability and control derivatives, which are dependent on correct values of $\bar{q}$ and V_t, can be determined.

A typical high angle of attack maneuver showing $\bar{q}_c$ and V_t with only static pressure error corrections applied and the resultant effect of total pressure error corrections is shown in figure 6, appendix I.

Angle of Attack and Angle of Sideslip

Angles of attack and sideslip were measured by vanes attached to the flight test noseboom as shown in figure 4. Determination of angle of attack and angle of sideslip in the stall/spin regime required the application of corrections to indicated noseboom vane angles. (Note: the assumption was made that mechanical effects such as boom bending were negligible.)

Noseboom vane readings were affected by body axis pitch rate. The noseboom corrected angle of attack is given by:

$$\alpha_{B_C} = \alpha_B + \frac{R_b\, q \cos\alpha_B}{V_t}$$

where: α_B = noseboom measured angle of attack (vane position)

R_b = distance from probe to 32 percent MAC (38.4 ft)

q = pitch rate (deg/sec)

V_t = true airspeed (fps)

Corrections to indicated sideslip angle were made to account for rotation and axes orientation, i.e., the indicated angle is in a plane parallel to the X and Y axes, while the true sideslip angle is that angle between the resultant velocity vector and the projection of the resultant velocity vector on the plane of symmetry. Corrected noseboom sideslip angle is given by:

$$\beta_c = \beta_i \left|\cos \alpha_{B_C}\right| - \frac{R_s\, r}{V_t} \cos \beta_i$$

where: β_i = noseboom sideslip angle

R_s = distance from probe to 32 percent MAC (38.1 ft)

r = yaw rate (deg/sec)

V_t = true airspeed (fps)

α_{B_C} = noseboom corrected angle of attack (deg)

Corrections due to aircraft rotation were small. The magnitude was approximately 2 degrees for aircraft rotation rates as high as 100 deg/sec.

Angle of attack corrections to sideslip angle were very large. Sideslip angle values are unreliable for angles of attack above 80 degrees due to the vane position with respect to the oncoming flow.

Moment Coefficients

Spins involved a balance of inertial, engine gyroscopic and aerodynamic moments, thus it was necessary to separate these three effects for analysis. Body axes accelerations were given by:

$$\dot{p} = \frac{I_y - I_z}{I_x} qr + \frac{I_{xz}}{I_x} \dot{r} + \frac{I_{xz}}{I_x} pq + \frac{M_x}{I_x} + \frac{I_{xy}}{I_x} (\dot{q} - pr) + \frac{I_{yz}}{I_x} (q^2 - r^2)$$

$$\dot{q} = \frac{I_z - I_x}{I_y} pr + \frac{I_{xz}}{I_y} (r^2 - p^2) - \frac{I_{eng} \Omega_{eng}}{I_y} r + \frac{M_y}{I_y} + \frac{I_{xy}}{I_y} (\dot{p} + qr) + \frac{I_{yz}}{I_y} (\dot{r} + pq)$$

$$\dot{r} = \frac{I_x - I_y}{I_z} pq + \frac{I_{xz}}{I_z} (\dot{p} - qr) + \frac{I_{eng} \Omega_{eng}}{I_z} q + \frac{M_z}{I_z} + \frac{I_{xy}}{I_z} (p^2 + q^2) + \frac{I_{yz}}{I_z} (\dot{q} + pr)$$

Using fuel quantity indications and known weight data, total weight, cg position, and moments of inertia were calculated using the McDonnell-Douglas Corporation 9302 Multi-PDM Reduction Computer program. Angular accelerations were determined by calculating the slopes of the angular rate data.

With the symmetrically loaded aircraft the product of inertia terms, I_{xy} and I_{yz}, were zero. Thus, the equations reduced to:

$$\dot{p} = \frac{I_y - I_z}{I_x} qr + \frac{I_{xz}}{I_x} \dot{r} + \frac{I_{xz}}{I_x} pq + \frac{M_x}{I_x}$$

$$\dot{q} = \frac{I_z - I_x}{I_y} pr + \frac{I_{xz}}{I_y} (r^2 - p^2) - \frac{I_{eng} \Omega_{eng}}{I_y} r + \frac{M_y}{I_y}$$

$$\dot{r} = \frac{I_x - I_y}{I_z} pq + \frac{I_{xz}}{I_z} (\dot{p} - qr) + \frac{I_{eng} \Omega_{eng}}{I_z} q + \frac{M_z}{I_z}$$

The effects of the I_{xy} and the I_{yz} terms on the total angular accelerations were calculated for the asymmetric loadings and found to be negligible.

In order to determine angular accelerations produced only by aerodynamics,

$$\dot{p}_{aero} = \frac{M_x}{I_x}$$

$$\dot{q}_{aero} = \frac{M_y}{I_y}$$

$$\dot{r}_{aero} = \frac{M_z}{I_z},$$

the inertial, engine gyroscopic, and drag chute effects (where applicable) were subtracted from the calculated body axis accelerations (slope of measured body axis angular rates).

$$\dot{p}_{aero} = \dot{p} - \frac{I_y - I_z}{I_x} qr - \frac{I_{xz}}{I_x} (\dot{r} + pq)$$

$$\dot{q}_{aero} = \dot{q} - \frac{I_z - I_x}{I_y} pr - \frac{I_{xz}}{I_y} (r^2 - p^2) + \frac{I_{eng}\,\Omega_{eng}}{I_y} r - \dot{q}_{chute}$$

$$\dot{r}_{aero} = \dot{r} - \frac{I_x - I_y}{I_z} pq - \frac{I_{xz}}{I_z} (\dot{p} - qr) - \frac{I_{eng}\,\Omega_{eng}}{I_z} q - \dot{r}_{chute}$$

Time histories of inertial accelerations are presented for most spins and some rolling departures; they show the relative magnitudes of inertia coupling, gyroscopic and drag chute effects, and the solution of the aerodynamic pitch, roll and yaw moments (or accelerations), respectively. Using these accelerations, moment coefficients were determined.

The pitching moment coefficient due to all aerodynamic terms is given by:

$$\left(C_m\right)_{aero} = \frac{\dot{q}_{aero}\, I_y}{\bar{q}Sc}$$

C_m due to angle of attack was determined by subtracting from $C_{m_{aero}}$ the effects of pitch rate, stabilator position, sideslip and center of gravity position.

$$\left(C_m\right)_{\text{due to } \alpha} = \left(C_m\right)_{\text{aero}} - C_{m_q} q_{osc} \frac{\bar{c}}{2V_t} - C_{m_{\delta_s}} \delta_s - C_{m_\beta} \beta$$

$$- C_{m_\Omega} \frac{\Omega b}{2V_t} - \left(C_m\right)_{\text{due to cg}}$$

C_{m_q}, $C_{m_{\delta_s}}$, C_{m_Ω} and C_{m_β} were obtained from reference 2.

The rolling moment coefficient due to all aerodynamic terms,

$$\left(C_\ell\right)_{\text{aero}} = \frac{\dot{p} I_x}{\bar{q} S b},$$

and yawing coefficient due to all aerodynamic terms,

$$\left(C_n\right)_{\text{aero}} = \frac{\dot{r} I_z}{\bar{q} S b},$$

were calculated. However, a large degree of scatter was evidenced in these values due to instrumentation noise and the low sample rate (10 per second).

Drag Chute Measurements

Quantitative data on production drag chute effectiveness was obtained. In order to determine the yawing and pitching moments on the aircraft due to the chute, it was necessary to determine the angle at which the measured chute force was applied. The following two equations were used to obtain the chute riser angle measured relative to the XY plane and plane of symmetry, respectively. These equations neglect any aircraft interference effect on the chute.

$$\lambda = \alpha_{B_C} + \frac{q X_c}{V_t} \cos \alpha_{B_C}$$

$$\kappa = \beta_C - \frac{r X_c}{V_t} \cos \beta_C$$

An aft-looking camera mounted on the fuselage behind the canopy recorded chute activity during the maneuvers. Using the geometry shown in figure 8, the following equations were developed to obtain λ and κ from measurements taken from the film.

$$\sin \lambda = Z_c \left[.00395 \cos \lambda + .0065\right] + .202$$

$$\sin \kappa = Y_c \left[.00395 \cos \lambda + .0065\right] - .307$$

where Z_c and Y_c are vertical and lateral measurements from the film projected at fuselage station (FS)567.

Figure 7, appendix I, shows a typical time history of λ, κ, α_{B_C} and

β_c during the time that the chute was deployed. The film data showed that the parachute experienced violent oscillations, but generally followed the calculated κ and λ values.

The following three equations were used to calculate the drag coefficient of the chute, aircraft yawing moment coefficient due to the chute, and aircraft pitching moment coefficient due to the chute.

$$C_{D_C} = \frac{F_c}{\bar{q}Sc}$$

$$C_{n_c} = \frac{F_c X_c \sin \kappa}{\bar{q}Sb}$$

$$C_{m_c} = \frac{-F_c X_c \sin \lambda}{\bar{q}Sc}$$

Figure 8, appendix I, presents typical chute coefficients.

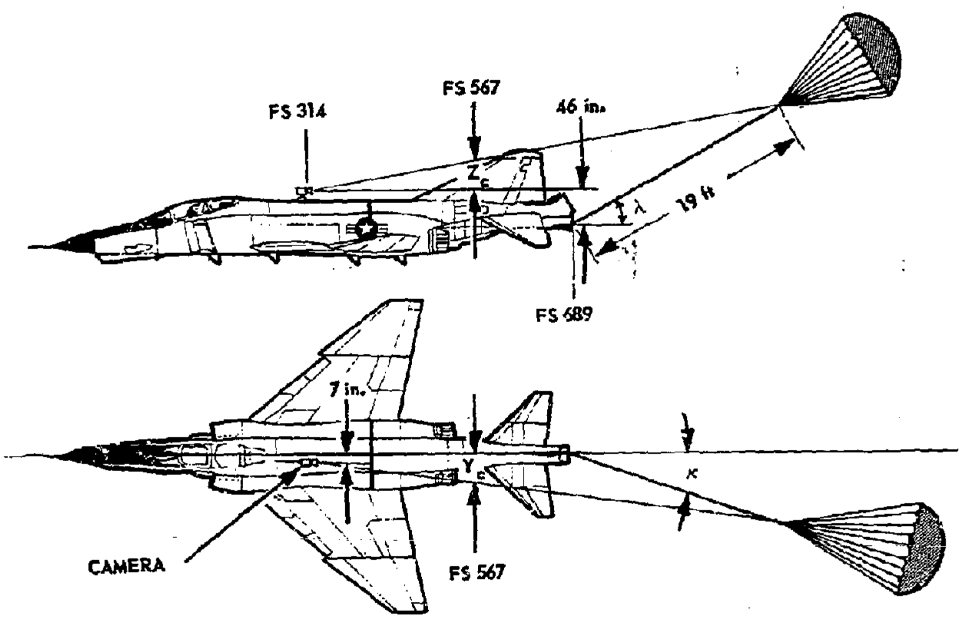

Figure 8 PARACHUTE RISER ANGLES

ANALYSIS OF OUT-OF-CONTROL DYNAMICS OF THE F-4

Analytical studies were conducted during the program to gain a more complete understanding of F-4 high angle of attack dynamics and thus support the flight test results. Out-of-control dynamics were examined in the major areas of aerodynamics and inertial coupling effects. Special computer plotting routines were developed to provide time histories which isolated inertial, engine gyroscopic, and aerodynamic characteristics from the body axis angular accelerations.

A review of the departure/spin flight test results indicated that the high AOA predicted and/or adjusted aerodynamic data (reference 2) were generally accurate and were very useful in the prediction and evaluation of the flight characteristics of the test aircraft. The data sampling rate and calibration ranges of the instrumentation system did not justify a systematic determination of stability and control derivatives at departure/spin angles of attack. However, the extracted pitch acceleration term due to aerodynamics alone appeared smooth enough to evaluate the static longitudinal stability for trends and "ball park" magnitudes. These findings are discussed in the following section.

Figures 11 through 63, appendix I, present stall approach and departure/spin flight test data for the major loading groups. These data encompass a wide range of cg positions, stall entry conditions, and types of out-of-control maneuvers. Accordingly, this set of data, along with the data in reference 2, is necessary and sufficient to describe the test aircraft behavior at high AOA. Reference will be made to specific figures in this group when discussing aerodynamics and inertial coupling characteristics in the following sections. Unless otherwise noted, all quoted values of angle of attack are referenced to the body axis ($\alpha_B = \alpha_{noseboom}$); therefore, in this discussion the interpretation of wind tunnel data includes the adjustment for AOA measured with respect to a wing reference line ($\alpha_B = \alpha_W - 1°$). Selected reproductions from reference 2 are presented in figures 64 through 76, appendix I. These data are in the body axis.

F-4 AERODYNAMICS AT HIGH AOA

Predicted Stability Derivatives

The predicted F-4 static stability aerodynamic data of references 2 and 3 indicated the following for low Mach numbers: (1) A mild pitch instability existed prior to the first local maximum in the lift-curve slope and was evident over an AOA range of approximately 3-5 degrees. Additionally, the pitching moment coefficient at a given AOA was a function of sideslip angle and this influence was highly non-linear out to 40° of sideslip. (2) Directional stability (C_{n_β}) approached zero near 21° AOA and became strongly adverse by 25° AOA. This adverse condition remained through 90° AOA and moderate sideslip angle ranges. However, for sideslip angles greater than 25°-40°, an increasingly stable yawing moment was observed. Significant yawing moment asymmetries and nonlinearties were noted for $45° < \alpha_W < 80°$. For example, zero yawing moment was evident for a sideslip angle greater than 5°. These asymmetries were also recorded for sideforce measurements but did not occur about the roll

axis. Therefore, it can be assumed that the asymmetries were primarily due to forebody and aft body effects rather than a wing-body effect. The extrapolation of any such model results to imply large asymmetries for full scale airplanes becomes a matter of utmost concern in predicting the behavior of a spinning airplane. Both asymmetric data and the adjusted data should be analyzed to determine their influence on spin entry/recovery. Model scale effects, local tunnel blockage effects, etc., should be thoroughly reviewed to establish the verity of observed asymmetries. (3) Dihedral effect (C_{ℓ_β}) through moderate sideslip angles ($-10° < \beta < 10°$) showed a marked deterioration from 14° to 19° AOA, then a neutral or slightly adverse condition through 35° AOA. The dihedral effect again became strongly favorable by 40° AOA and remained essentially constant through 90° AOA. In the AOA range from 15° to 40°, C_{ℓ_β} was very non-linear for β <20°.

Control effectiveness data from reference 2 indicated the following: (1) Stabilator pitch effectiveness ($C_{m_{\delta_s}}$) decreased rapidly after 25° AOA, and minimum values were observed for 40° <AOA< 60° for zero sideslip angle. (2) Rudder yaw power ($C_{n_{\delta_r}}$) approached zero at 40°-50° AOA and was adverse at higher AOA's under conditions of large sideslip and aft stick. (3) Aileron roll power ($C_{\ell_{\delta_a}}$) decreased rapidly between 10° and 30° AOA and approached zero by 50° AOA. (4) Aileron yaw power ($C_{n_{\delta_a}}$) for moderate sideslip angles was consistently adverse and approximately constant between 20° and 90° AOA.

The major characteristics of the predicted dynamic derivative data as they applied to stall and spin conditions were: (1) Roll rate damping (C_{ℓ_p}) was favorable (negative) over the entire positive AOA range. (2) rolling moment due to yawing velocity (C_{ℓ_r}) was coordinated (positive) over the entire positive AOA range. (3) Yawing moment due to rolling velocity (C_{n_p}) demonstrated three changes in sense over the AOA range from 0° to 90°. For the AOA range for the steeper spins, C_{n_p} was uncoordinated (negative), i.e., a yawing moment was provided away from the turn direction of the spinning aircraft whenever roll rate was in the direction of the turn. For AOA's greater than 75°, C_{n_p} was coordinated (positive), and a left wing down roll rate in a spin to the left provided an additional yawing moment in the spin direction. (4) Yawing moment due to yawing velocity (C_{n_r}) was damping if AOA is less than 75°. The magnitude of C_{n_r} was particularly small for 35° <AOA< 50°; above 75°, C_{n_r} was propelling. (5) Pitch rate damping (C_{m_q}) was favorable (negative) over the entire positive AOA range. (See figures 73 through 75, appendix I.)

Pre-Departure

Cruise Configuration, Low Mach Number (< 0.8)

The F-4 longitudinal instability condition documented in references 4, 5, and 6 is demonstrated in Figure 53, appendix I, for the test aircraft during low Mach number flight. The nose rise is shown by the unstable gradient of stabilator and angle of attack near 8 seconds on the time

history. This longitudinal instability, combined with deteriorating control effectiveness near stall AOA's, led to inadvertant excursions into the region of directional divergence when attempts were made to roll with aileron or rudder at high AOA.

For the clean loading, lateral-directional stability breakdown was usually observed to begin near 22-24 units AOA in the form of wing rock, an unstable dutch roll oscillation. Examples of wing rock are presented in figures 16 and 36, appendix I. As AOA was further increased, the oscillations, as viewed by the pilot, progressed from a primarily roll motion to excursions in yaw (nose slice). This behavior is consistent with the wind tunnel data (figures 66 and 67, appendix I) which show that there is no significant change in rolling moment for $\beta < 5°$ for AOA's between 25° and 35°. For an AOA range from 20° to 35°, directional instability increased, and the nose slice became the immediate indication of impending departure. Full lateral stick inputs near 25 units AOA produced no significant effect on aircraft motion. The adverse yaw due to aileron ($C_{n_{\delta_a}}$) was insufficient to produce a departure because lateral-directional instability was insufficient for departure, and roll effectiveness ($C_{\ell_{\delta_a}}$) was very low. Departure required a threshold value of directional instability; aileron inputs promoted a divergence of sideslip which determined departure direction, but only at AOA's above approximately 27 units. Aileron inputs alone did not produce a departure; AOA had to be in the region of directional instability.

For the symmetric-high drag loadings, the amplitude of wing rock was reduced, and nose slice was observed at a lower angle of attack than for the clean aircraft. The increased roll inertia, because of store addition, yielded lower roll acceleration. The store effect on wing lift distribution (i.e., the influence on C_{ℓ_β}) and the subsequent change in the sidewash distribution on the empennage (i.e., the influence on C_{n_β}) were also contributing factors in the change in pre-departure characteristics.

For the medium and highly asymmetric loadings, the rolling moment due to the weight asymmetry was balanced by an ever-increasing sideslip angle as AOA was increased during normal stall approaches. This is demonstrated in figure 48, appendix I. The pre-established sideslip angle negated oscillations in yaw and the first significant excursion in yaw was initial departure.

Cruise Configuration, High Mach Number (> 0.8)

High-g, transonic, decelerating turns demonstrated that, even with full aft stick, the test aircraft was limited to AOA's below those required for departure when lateral-directional controls were essentially neutral and the Mach number was greater than approximately 0.85. These characteristics were due to the static stability and stabilator effectiveness trends with Mach number, and an example is presented in figure 21, appendix I. As Mach number reduced and the center of pressure moved forward, the aircraft pitched up into an out-of-control condition. Mis-application of lateral-directional controls in the high transonic regime did lead to a departure at 1.13 M as discussed in reference 1.

The onset of wing rock always preceded stall and provided ample warning when maneuvering was conducted smoothly. The intensity of wing rock increased with increasing AOA and the frequency was much higher than for low speed flight.

Flap Effects

Wing rock in the power-approach configuration was repeatable, and the amplitude was larger than that for the aircraft in the cruise configuration. Figures 11 and 12, appendix I, indicate wing rock near 25-27 units AOA in the PA configuration. The different high-AOA flight characteristics between the CR and PA configuration are a result of the change in wing lift distribution and the sidewash flow field with leading and trailing edge flap deflection.

A normal stall approach with a half-flap/gear-up configuration is presented in figure 31, appendix I. An AOA of 52° was attained with essentially no lateral-directional divergence. This result reflects the improvement in directional stability and dihedral effect with leading edge droop noted in reference 3 and the improved high AOA flight characteristics noted during the F-4 leading edge maneuvering slat evaluation (reference 19).

Departure

Initial Departure

Departures were the result of directional instability arising from adverse sidewash at the empennage and a loss of dihedral effect due to local flow separation on the wing. The vertical tail-off data shown in reference 3 indicate that adverse sidewash causes the aft body and stabilator elements to be directionally destabilizing for $10° < AOA < 38°$. The total component build-up data indicate that as AOA is increased above 29°, the adverse sidewash field moves upward and causes the vertical tail component to be directionally destabilizing. The rapid change of directional stability and dihedral effect with angle of attack and the non-linearities of these quantities are shown in figures 66 and 67, appendix I. These non-linearities are the probable reason the test aircraft departed at an AOA higher than that predicted by the departure correlation function,

$$C_{n_{\beta_{DYN}}} = C_{n_\beta} - \frac{I_Z}{I_X} C_{\ell_\beta} \sin\alpha,$$

documented in reference 15. If C_{n_β} and C_{ℓ_β} are evaluated at $\beta = 0°$, then $C_{n_{\beta_{DYN}}}$ predicts departure at 21°, however, the clean loaded test aircraft usually departed above 30° AOA in low speed flight in the CR configuration. The interchange of angle of attack and sideslip angle during rolling motions prior to nose slice also contributed to the delay in actual departure until a sufficiently adverse directional stability condition was present.

Inadvertant AOA excursions into the region of lateral-directional instability and subsequent departure from controlled flight were possible because of the stick force lightening tendency and the potential for

statically trimming the aircraft to an AOA well past that for maximum usable lift. Figure 65, appendix I, presents static stability data for full aft stick at 33% MAC. These data indicate that for either the original wind tunnel data or the data adjusted in reference 2, there exists a trimmed AOA region for which the aircraft is directionally unstable.

Rolling Departure

As stated in reference 3, the base aircraft exhibited two types of out-of-control events: the rolling departure or the spin. The rolling departure was the most predominant maneuver for the clean aircraft during low speed flight at forward cg's[1] and for the symmetrically loaded aircraft under must conditions of stall entry.

A rolling departure developed when the departure roll and yaw rates were not severe and the cg was forward. These characteristics were observed most often for low speed departures, nose high departures, or departures that went over the top (reverse bank angle) from an accelerated stall in turning flight. Such conditions were conducive to a rapid airspeed bleed-off through the stall and departure, and as a result, the nose-up pitching moment due to inertial coupling at initial departure was insufficient to sustain an AOA for a spinning condition. A greater aerodynamic restoring moment (i.e., forward cg's) and forward stick at initial departure normally reduced AOA after one peak excursion in the 40° - 50° AOA range.

Even the highly asymmetric loadings could be limited to a rolling departure if recovery was attempted at the first indication of nose slice, before the divergent yaw rate became large. Normal lateral-directional control technique always resulted in departures away from the heavy wing because of the pre-established sideslip required to aerodynamically balance the weight moment. Figure 52, appendix I, shows that for the 25%-allowable-asymmetry loading, abrupt aft stick and cross controls were required to obtain a rolling departure into the heavy wing.

Spin Entry

No control input other than aft stick was required for entry into a spin. However, the strongly adverse aileron yaw would determine spin direction as shown in the abrupt pull-up/roll-in attempt shown in figure 19, appendix I. Spins were entered directly from initial departure and did not pass through any intermediate stage of post-stall gyrations. Those conditions that produced a spin rather than a rolling departure were aft cg's and those entry conditions that resulted in significant departure roll and yaw rates. For the clean aircraft, nose-low attitudes and high energy stalls contributed to departure severity; a good example is provided by the second flat spin presented in figure 63, appendix I.

The asymmetric loadings demonstrated an extreme susceptibility to spin. The large sideslip angle, established before departure to help aerodynamically balance the weight moment, meant that a large yawing moment existed as the AOA was increased above the value for directional instability. Additionally, the asymmetric loadings departed at a much

---

[1] For this study, 30% MAC was used as the division between forward and aft cg's.

lower average true AOA than for the symmetrically loaded aircraft. As such, the drag build-up and speed bleed-off was not as great for the asymmetrically loaded aircraft with similar gross weight and stall entry conditions, and the dynamic pressure at departure was higher.

Spin

Because of the five spin modes and many unique spin features observed during the test program, simplified but inclusive definitions were given to "spin" and "incipient spin". A spin is a sustained turning motion at a stalled AOA. There is no requirement that each turn mirror the previous turn or that the flight path be vertical. The incipient phase of a spin is that initial phase in which the balance between aerodynamic and inertial moments is insufficient to identify a spin mode in terms of average angle of attack and angular rates.

Four recoverable spin modes and one non-recoverable mode were identified during the 101 erect spins experienced during the flight test program. The key to aerodynamic recovery from the first four spin modes was a sufficiently large sideslip angle away from the turn direction. The static stability derivatives, C_{n_β} and C_{ℓ_β} were more influential than the dynamic derivatives in determining spin characteristics of the recoverable spin modes. The flat mode was dominated by the dynamic derivative, C_{n_r} (or C_{n_Ω}), which was propelling at flat spin AOA's, and no combination of control surface positions could be expected to recover the F-4 from a flat spin. Inverted spins were not attempted using pro-spin controls. However, recoveries from extremely oscillatory erect spins did result in very high roll and yaw rates at negative AOA's and only one inverted turn was recorded. Spin mode characteristics are presented in Table III.

TABLE III

SPIN MODE CHARACTERISTICS

SPIN MODE	MOST PREVALENT LOADINGS	MOST PREVALENT ENTRY SPEED	AVERAGE AOA FOR SPIN (deg)	AOA OSCILLATIONS ABOUT AVERAGE VALUE (deg)	AVERAGE YAW RATE (deg/sec)	DOES DRAG CHUTE AID RECOVERY?	IS SPIN RECOVERABLE?
Steep-Smooth	Clean or ℄ Tank Only	Low Speed	40 to 45	±5	40 to 50	Yes	Yes
Steep-Mildly Oscillatory	Clean or ℄ Tank Only	Low & High Speed (Common With Transonic Entry)	45 to 55	±10	45 to 60	Yes	Yes
Steep-Oscillatory	Clean	Low Speed	50 to 60	±20	40 to 60	Marginal	Yes
	Wing Heavy (Symmetric and Low Asymmetric)	Low & High Speed					
High Angle of Attack-Highly Oscillatory	Medium to High Asymmetry	Any Entry	60 to 80	±30	60 to 90	No	Yes
Flat	Seldom Occurs, But Possible With All Loadings	Seldom Occurs, But Possible With Any Entry	77 to 80	±5	80 to 90	No	No

Note: 1. The modes and values shown are for full forward stick and neutral ailerons and rudder.
2. The flat mode values are essentially independent of control positions.

Steep-Smooth Mode

The steep-smooth mode was occasionally observed for the clean or centerline tank-only loadings. This spin was transitory in nature; its existence was established by the relatively low sideslip values during entry conditions, and its continuation was guaranteed only when the sideslip oscillations remained fairly small. Figures 22 and 37, appendix I, demonstrate that roll rate remains coordinated with the turn direction and does not approach zero until recovery. Dihedral effect dominated the aerodynamic influence on the aircraft roll characteristics during the steep-smooth spin, so any initial disturbance of sideslip angle usually initiated a divergence of β and subsequent recovery or mode change as evidenced by roll hesitations.

Steep-Mildly Oscillatory Mode

This spin mode was the most common for the clean aircraft. Larger sideslip oscillations existed for this mode than for the previous one. There was a characteristic roll away from the turn direction at every half turn of the spin; that is, right roll rates were observed in a spin to the left.

As sideslip angle away from the spin direction promoted a roll away from the spin through favorable C_{ℓ_β}, the sideslip simultaneously provided a yawing moment away from the turn because of an unstable C_{n_β} Note that yaw rate reduced to only 16 degrees per second at one of the hesitations as shown in figure 21, appendix I.

Statistical data indicated that with aft cg's and without inboard pylons, the aircraft tended to continue in the steep-mildly oscillatory mode if only forward stick was held in for recovery. An eight turn example is presented in figure 25, appendix I, in which the drag chute was finally deployed to effect recovery.

The mode can be described as being essentially "neutrally stable" under the conditions of aft cg and inboard pylons off. The spin tended to remain spinning with forward stick only but with an imminent possibility of recovery (or less likely, a reversal) if the sideslip oscillations were slightly disturbed in the appropriate direction. The one reversal experienced during the program is presented in figure 35, appendix I. Actually, the predicted data show no autorotative rate-damping terms applicable to this spin other than the small value of positive C_{ℓ_r}; however, C_{n_r} does exhibit minimum values for the spin AOA range. Minimum yaw rate damping and an average pro-spin inertial yaw acceleration term were probably responsible for the continual nature of the spin and the requirement to use drag chute or aileron for satisfactory recovery.

Many of the spins with forward cg's and/or inboard pylons were terminated within several turns using forward stick only for recovery. An example is presented in figure 21, appendix I.

Table III shows that the steep spins (lower average AOA) turn at a slower rate, and that the average values of AOA and yaw rate for a given mode are approximately equal.

Figure 27, appendix I, shows that severity of the departure induced a large nose-up pitching moment due to inertial coupling and the aircraft spun initially at a higher AOA. Eventually the AOA and yaw rate trend was toward those values characteristic of the mode.

Several steep spins were evaluated for trends in static longitudinal stability using the equations for $(C_m)_{aero}$ and $(C_m)_{due\ to\ \alpha}$, page 19. All values other than $(C_m)_{due\ to\ \alpha}$ were assumed to be correct as given in reference 2 and $(C_m)_{due\ to\ \alpha}$ at 33% MAC were calculated from $C_{m_{aero}}$. The results are presented in figure 64, appendix I, and show that the curve adjusted in the simulator study to fit Navy flight test data was approximated by the F-4E flight test results through 50-55 degrees AOA, but above 60° AOA, there was a more stabilizing trend with increasing AOA.

Steep-Oscillatory Mode

This mode was characteristic of the symmetrically loaded aircraft. The inertia distribution effects as well as the divergent sideslip angle led to recoveries within two turns with forward stick. Again, the combination of favorable dihedral effect (negative C_{ℓ_β}) and unstable C_{n_β} provided roll and yaw away from the turn direction for β away from the spin. Examples of this mode are presented in figures 55 and 57, appendix I.

High Angle of Attack-Highly Oscillatory Mode

This mode was exclusive to the medium and highly asymmetric loadings and was highly unstable in that these spins vigorously diverged to recovery with application of forward stick only. A unique feature for the first several spin turns was an essentially horizontal flight path. Figure 51, appendix I, demonstrates that the initial turns were similar to the flat spin in terms of AOA and turn rate. The significant differences were that the aircraft initially spun flat to the horizontal flight path and not vertically, and the oscillations subsequently diverged.

Flat Mode

The flat spin was dominated by a propelling yawing moment due to yaw rate (or spin rate coefficient Ω) and to a lesser extent by a propelling value of C_{n_β}. This spin was non-recoverable. Longitudinal stick position was found to influence yaw rate only slightly after the mode had been established. In the flat spin, figure 63, appendix I, a cg change of 2% MAC after ejection produced only a slight change in yaw rate. Based on the variety of spins encountered in the test program, and the nature of spin mechanics, it is doubtful that any oscillatory spin will transition to the flat spin as long as the stick is held full forward. Flat spins will be established by very high departure rates or become probable if the stick is brought aft in the high angle of attack - highly oscillatory spins. Comparison plots of flat spin and steep-mildly oscillatory spin entries are presented in figure 60 and 61, appendix I.

Recovery

Rolling Departures

Rolling departures did not exhibit a sustained yaw rate. Therefore, pitch-up due to inertial coupling was transient, and an aero-

dynamic recovery was always attained by driving the aircraft with forward stick to a low angle of attack where lateral-directional stability was regained. The drag chute proved an effective aid to forward stick in reducing AOA during rolling departures.

Erect Spins

The use of full forward stick for spin recovery was simply an extension of the out-of-control recovery procedure. Therefore, full forward stick was normally attained during the incipient spin phase. The aircraft diverged rapidly toward recovery from the more oscillatory spins. The use of aileron or drag chute was required to aid full forward stick for a satisfactory recovery from the steeper spins.

The primary values of forward stick were:

1. Natural reaction and simple application.
2. Maintained angular oscillation required for recovery from spin.
3. Almost totally eliminated spin reversals.
4. Recovery from spinning condition signalled when aircraft unloaded to zero or negative g.
5. Helps damp recovery oscillations by keeping AOA low.

Previous to this program the use of forward stick was not considered a satisfactory spin recovery technique for the F-4 (fuselage-heavy) aircraft for fear of "wrapping up" the spin; i.e., that an increased nosedown aerodynamic pitching moment leads to an increased yaw rate, thus increasing inertial pitch-up. The contractor tried to verify this condition during initial flight test work (reference 10), but four of the five spins allotted to this demonstration recovered with forward stick before the required five turns, and one spin was actually terminated with forward stick and pro-spin aileron. Only when forward stick was delayed through the first two turns and pro-spin aileron reduced did the spin progress past five turns total. Reference 10 also stated that the cause for the increased oscillatory activity appeared to result from the increase in inter-axis coupling as a result of the greater rotational rate. This observation was validated by the F-4E flight test data which showed that full forward stick, applied at the incipient phase of recoverable spins, promoted oscillations in <u>all</u> axes, and that the most vigorous oscillations were an indication to the pilot of imminent recovery. Since the key to an aerodynamic spin recovery was a sideslip away from the spin, the application of forward stick to intensify oscillations causes it to be an effective recovery control.

The steep-smooth mode was somewhat unique. Low sideslip angle during the entry and incipient spin phase determined the relatively non-oscillatory nature of this mode. However, this situation was tenuous, and small disturbances would force a spin mode transition to steep-mildly oscillatory or abrupt recovery with aileron inputs.

Aileron full with the spin direction proved to be a very effective aid to full forward stick for recovery from the steep spins. Figures 26, 27, 29, 34, and 35, appendix I demonstrated such recoveries; the

figures show that aileron adverse yaw slowed the turn rate and displaced the sideslip oscillations in the appropriate direction required for recovery. No timing problems were encountered for neutralizing the aileron at recovery.

Predicted data indicated the rudder would be of no significant effect as an anti-spin control because of the high AOA's involved.

Recovery Rolls

The initial phase of recovery from spins or rolling departures often demonstrated a large residual sideslip angle and yaw rate as the AOA rapidly reduced through the stall region. The aircraft would begin a rapid, uncommanded rolling motion because of the favorable dihedral effect in the lower AOA range, and the subsequent high roll and yaw rates provided a nose-up pitching moment due to inertial coupling. This inertial coupling momentarily prevented full forward stick from reducing AOA. Figures 36, 37, 52, 54, and 59, appendix I, show that the AOA range for recovery rolls was from approximately 10-20 degrees. Since these rolling motions occurred in an AOA range of positive directional stability, the sideslip angle forcing the rolls was transient, and recovery rolls always damped within two or three rolls.

High-Pitch Attitude, Low-Speed Stall Entries

The near vertical stall entries usually resulted in such drastic speed bleed-offs that, even with highly adverse conditions of AOA and sideslip, the low dynamic pressures were insufficient to force the aircraft into a divergent out-of-control condition. An example presented in figure 15, appendix I, shows that local flow velocity was so low that the AOA probe stopped rotating.

Aerodynamic Peculiarities of the Test Aircraft

F-4E vs F/RF-4C, F-4D

The significant aerodynamic differences between C, D, and the test E models are nose length, nose shape, and slotted stabilator. Many qualitative reports have indicated that C and D models exhibit a more consistent and pronounced wing rock in the low speed, CR configuration. This behavior may be anticipated from a change in forebody sideforce characteristics due to flow separation and a mutual realignment of the forebody and wing-body vortex systems. Both factors would influence directional stability, and, therefore, the wing rock characteristics. Nose shape also influences the relationship between indicated production AOA and true AOA. Any qualitative comparisons of F-4 model flying qualities at high AOA should take this factor into account.

Reference 17 indicated that the propelling nature of yaw rate damping was an aft body component arrangement problem and not a forebody effect, thus nose shape is not expected to alter flat spin characteristics. It is not expected that model aerodynamic differences would materially alter spin characteristics or recovery techniques.

Test Aircraft Aft-Body Modification

A side view projection of the additional area of the aft body modification indicated that the test aircraft had an equivalent increase in vertical tail-volume coefficient of approximately 30% over a production F-4. This is a fairly significant increase, especially since local dynamic pressure reduction and sidewash reaction on aft-body components create rapid directional stability changes in the stall region under investigation. Also, spinning conditions involve some degree of balance between aerodynamic and inertial forces and moments, and the steep spins of this program demonstrated that this balance was a delicate one in terms of mode existence or recovery capability with forward stick only.

The only steady state tests that could be accomplished to determine aft-body effects were constant heading sideslips at AOA's below the stall. These maneuvers were conducted at 19 units AOA, and the data are presented in figure 10, appendix I, along with similar data from a test F-4E aircraft with a standard aft body. The results show a destabilizing change in $\beta/\delta r$ for the stall test aircraft. This finding is consistent with the data presented in reference 3 which indicate that, for specific AOA ranges, adverse sidewash causes all empennage elements to be destabilizing. It is doubtful that meaningful extrapolation of these results can be made to the test aircraft in the departure/spin region of higher angles of attack and sideslip.

The test aircraft may not exactly reflect the average departure angles of attack that a production F-4 would experience with the same store loadings. However, there is no reason to believe that the out-of-control and spin recovery procedures determined with the test aircraft would not apply to all production F-4 models.

INERTIAL AND ENGINE GYROSCOPIC COUPLING

Inertial Coupling

The specially prepared time histories showing angular acceleration components due to inertial and gyroscopic coupling proved to be valuable aids in the analysis of spin entry, spin recovery, and recovery rolls.

Appropriate equations of motion for a symmetrically loaded aircraft are given at the top of these time histories, and the angular acceleration terms due to aerodynamics alone have been resolved from the absolute body axis angular accelerations.

Spin entry, and sometimes spin mode, was greatly influenced by the principal nose up inertial coupling term $\frac{I_z - I_x}{I_y} pr$. Figure 27, appendix I, shows that this inertial term has a peak value of +110 deg/sec^2 during the incipient phase of a steep-mildly oscillatory spin while the second flat spin (figure 63, appendix I) demonstrated a peak nose up inertial value of 150 deg/sec^2 during the incipient phase.

All of the oscillatory spins demonstrated nose down inertial coupling at the characteristic hesitations (β away from the spin), and when this condition was of sufficient duration or the nose-down inertial

term was sufficiently large, spin recovery was effected. An example is shown in figure 42, appendix I.

At times, the oscillations at the initial stage of recovery were so large that the aircraft would return to a spinning condition due to inertial coupling effects although the AOA had temporarily reduced to a value below stall. Figure 44, appendix I, shows that the pilot had experienced negative g at incipient recovery and began bringing the stick aft. The angle of attack returned to a post stall value of 40° after the stick had been place forward again. Inertial coupling was responsible for another excursion of AOA to 75° before the spinning motion was finally terminated. A spin recovery such as this validates the recommendation to maintain full forward stick until the recovery oscillations cease.

Figure 24, appendix I, shows that a large, pro-spin value of the yaw acceleration term, $\frac{I_x - I_y}{I_z} pq$, maintained a turning condition even though AOA had momentarily reduced to 15°.

The nose up inertial influence during recovery rolls is evident in figures 37 and 59, appendix I.

Engine Gyroscopic Coupling

Engine gyroscopic effects can be signficant during high energy departures or during the fast-turning spin modes. The pitching term $\frac{I_{ENG}\,\Omega_{ENG}}{I_Y} r$ was calculated by averaging LH and RH engine speeds, where maximum rpm is 7460 and the polar moment of inertia per engine is 20 slug-ft^2. Figure 63, appendix I, shows that the peak value of engine gyroscopic nose-up during the incipient phase of the flat spin is as much as 50% of the average value of the primary nose-up inertial term, $\frac{I_x - I_z}{I_y} pq$, in the developed portion of the flat spin.

It is possible that the F-4 without stores will spin flat only to the left because of the engine gyroscopic pitch-up contribution with left yaw rates. The high angle of attack-highly oscillatory spins demonstrated more than a 10° higher average AOA to the left than to the right for yaw rates on the order of 80 degrees per second.

PRODUCTION DRAG CHUTE EFFECTIVENESS

Flight Manual out-of-control recovery procedures recommend deployment of the production drag chute as an aid to full forward stick for all out-of-control events. Data analysis of a steep oscillatory spin with the drag chute deployed indicated that the recovery effectiveness of the drag chute was low above an AOA of about 50 degrees. The aerodynamic effects of the drag chute on the aircraft (see page 19) are plotted vs. angle of attack in figure 8, appendix I. An important result to note is that during any oscillatory mode, the effect of sideslip dominates that of yaw rate in aligning the chute to the plane of symmetry. (See figure 7, appendix I.)

Drag chute drag coefficient (C_{D_C}, referenced to free stream $\bar{q}$) was drastically reduced at high AOA due to aircraft wake interference (figure 8, appendix I), and the yaw moments from the chute have little total effect on the aircraft rotation (at high AOA) and are actually pro-spin at times during the spin. Quantitatively, that figure also shows that the drag chute maintains some effectiveness until AOA is above 45-50 degrees. As a result, the drag chute will aid recovery from the steep-smooth and the steep-mildly oscillatory modes due to their lower average AOA's. The drag chute is ineffective as a recovery aid from the high AOA-highly oscillatory and flat spin modes. Examples of drag chute recoveries are shown in figures 20, 25, 39, and 56, appendix I. Note that figure 56, appendix I, indicates the production drag chute helped reduce AOA from 50° to 23° while the stabilator was nearly full aft during a rolling departure.

APPENDIX I
Selected Test Data

NOTES APPLICABLE TO APPENDIX I FIGURES

1. Parameters listed at top of time histories are for maneuver entry.

2. Noseboom Angle-of-Attack is referred to the fuselage reference axis (waterline).

3. Stability Augmentation System (SAS) parameters are presented in degrees of their respective commanded surface positions.

4. Sideslip data are unreliable when AOA is greater than 80 degrees.

5. Throttle positions are shown in degrees of throttle angle:

Military Thrust	=	Approximately 70 to 80 degrees
Idle Thrust	=	8 degrees
Maximum Afterburner Thrust	=	113 degrees

6. Maximum Surface Deflections or Full-stick throws are as follows:

Stabilator Position	+21	to	-9	degrees
Lateral Stick	+12	to	-12	degrees
Production AOA	0	to	30	units
Rudder Position	+30	to	-30	degrees
Spoiler Positions	0	to	45	degrees
Aileron Positions	- 2	to	+30	degrees
Yaw SAS	+ 5	to	-5	degrees
Roll SAS	+7.5	to	-7.5	degrees
Pitch SAS	+0.5	to	-0.5	degrees

7. The production AOA data shown was measured at the production AOA probe. Cockpit indications were affected by internal indicator damping.

8. Maximum engine RPM = 7460.

9. Engine Polar Moment of Inertia = 21 slug - ft^2 per engine.

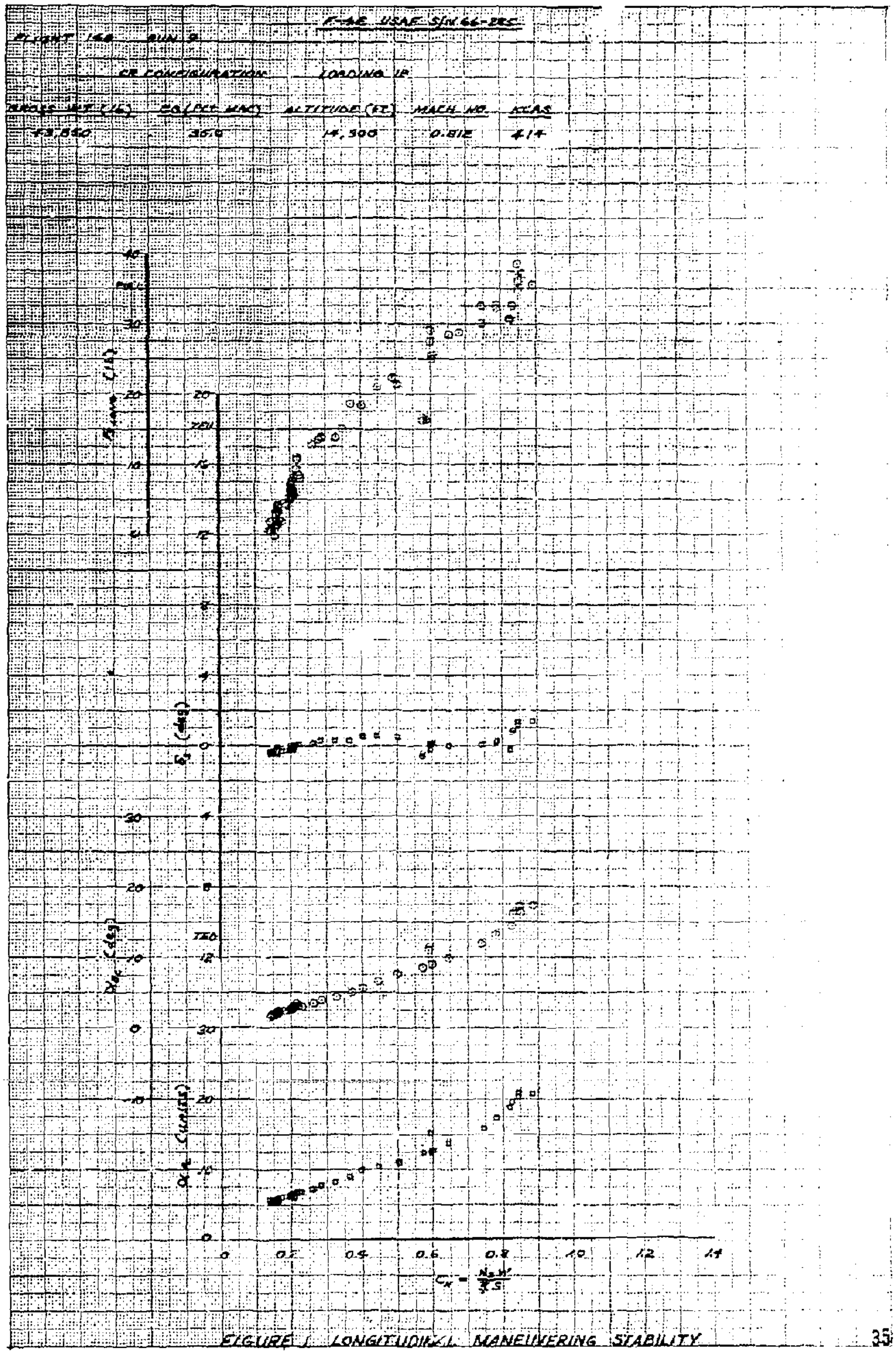

FIGURE 1 LONGITUDINAL MANEUVERING STABILITY

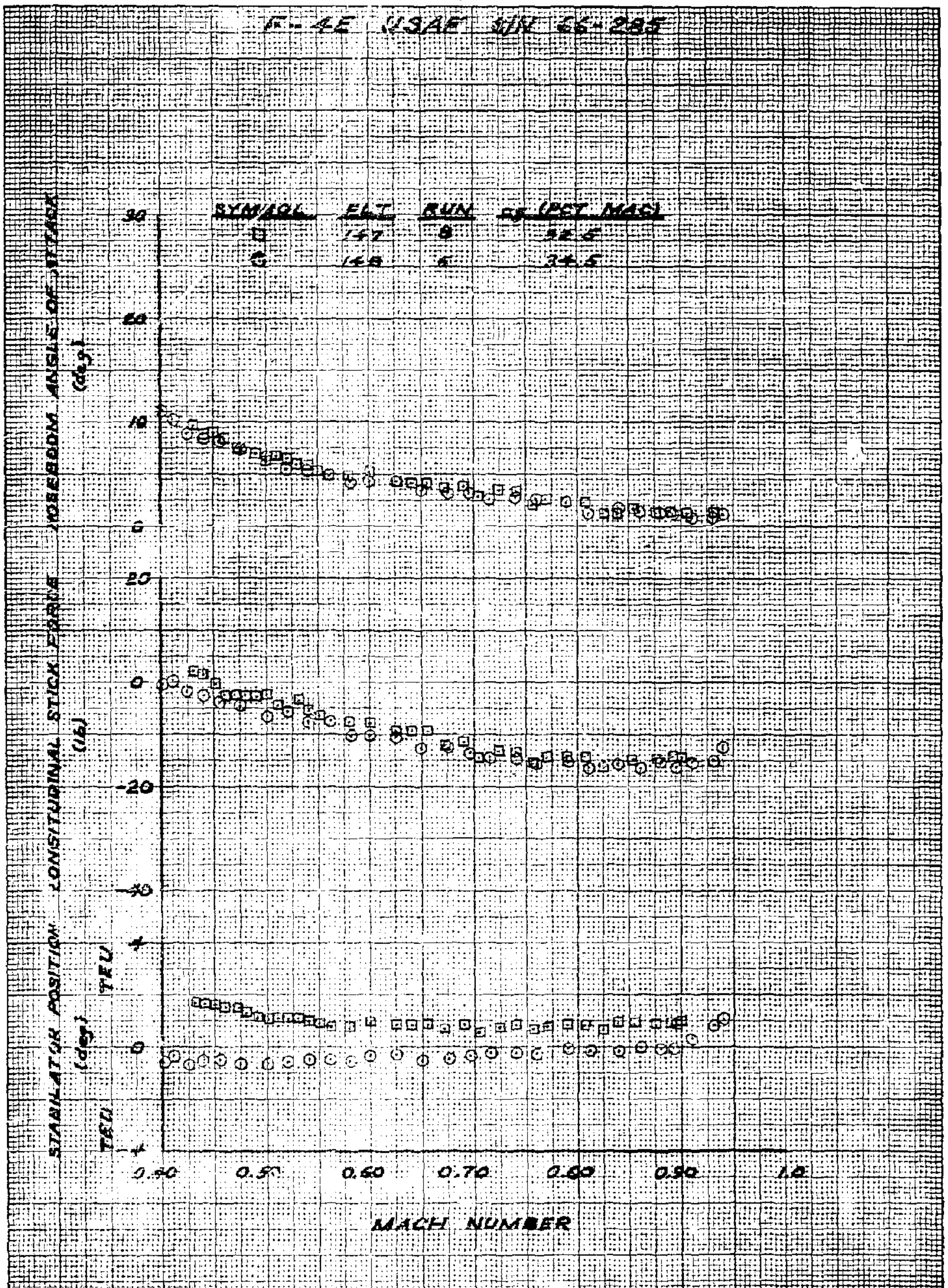

FIGURE 2 SPEED STABILITY

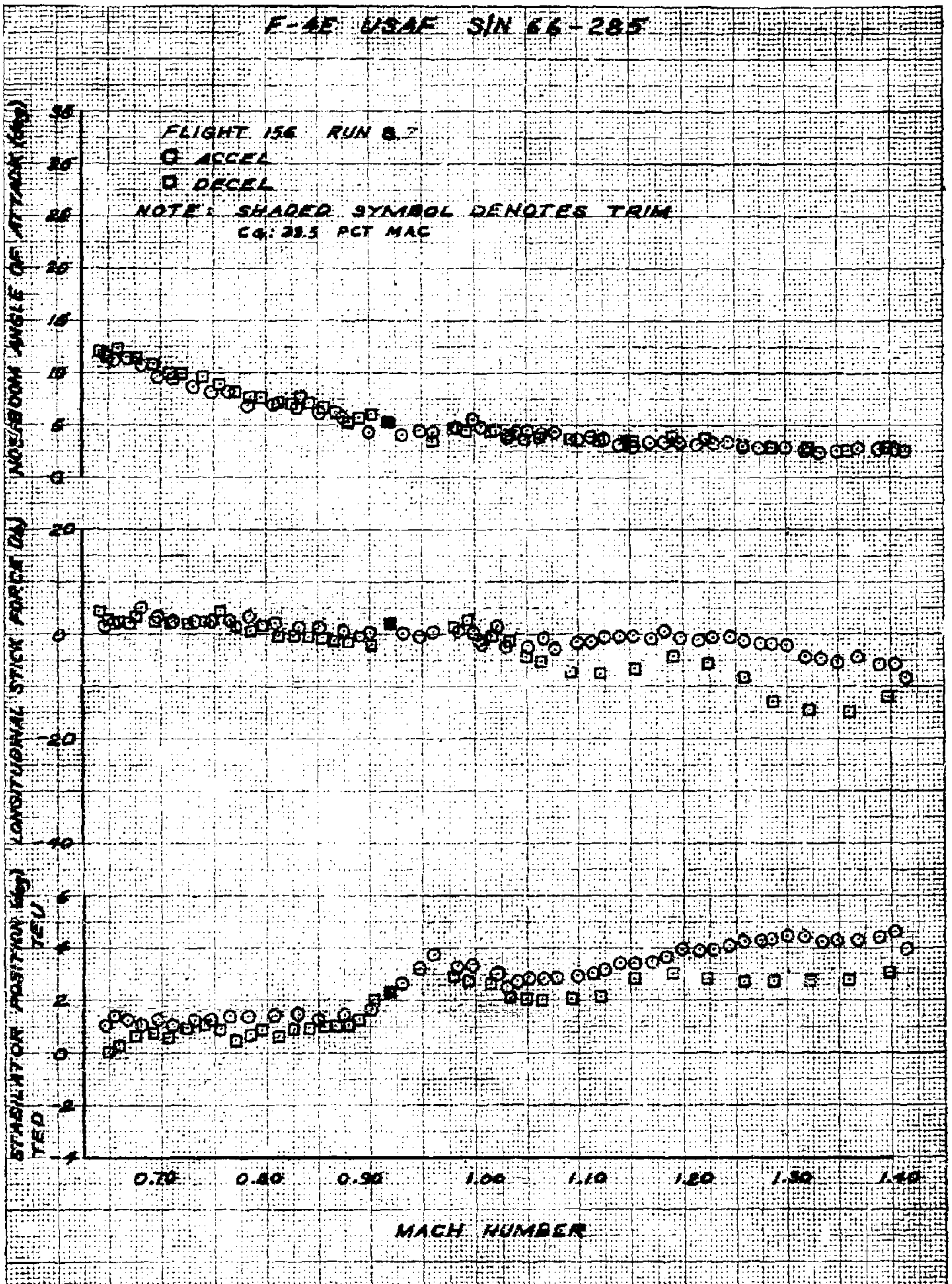

FIGURE 3 SPEED STABILITY

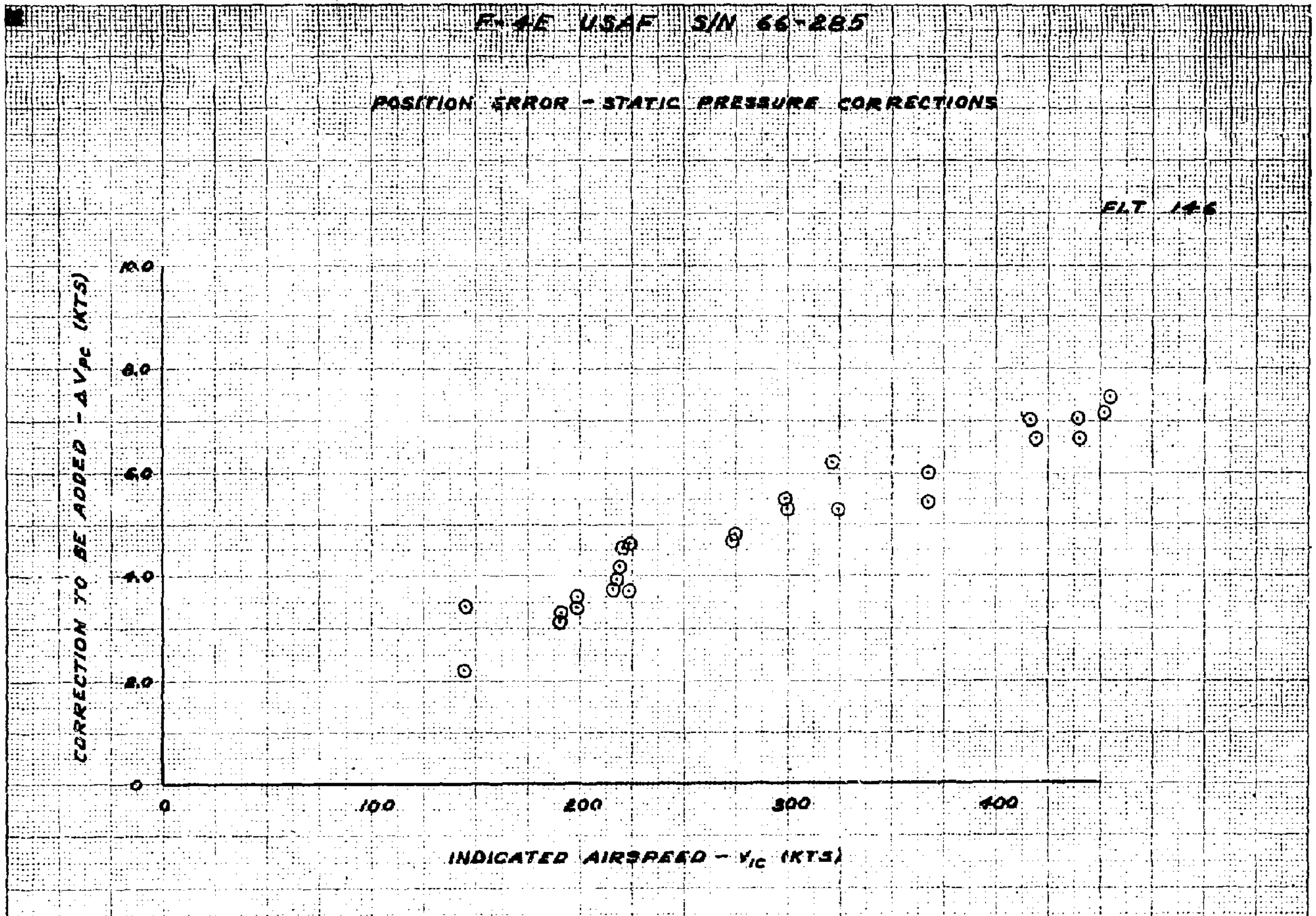

FIGURE 4 POSITION ERROR - STATIC PRESSURE CORRECTIONS

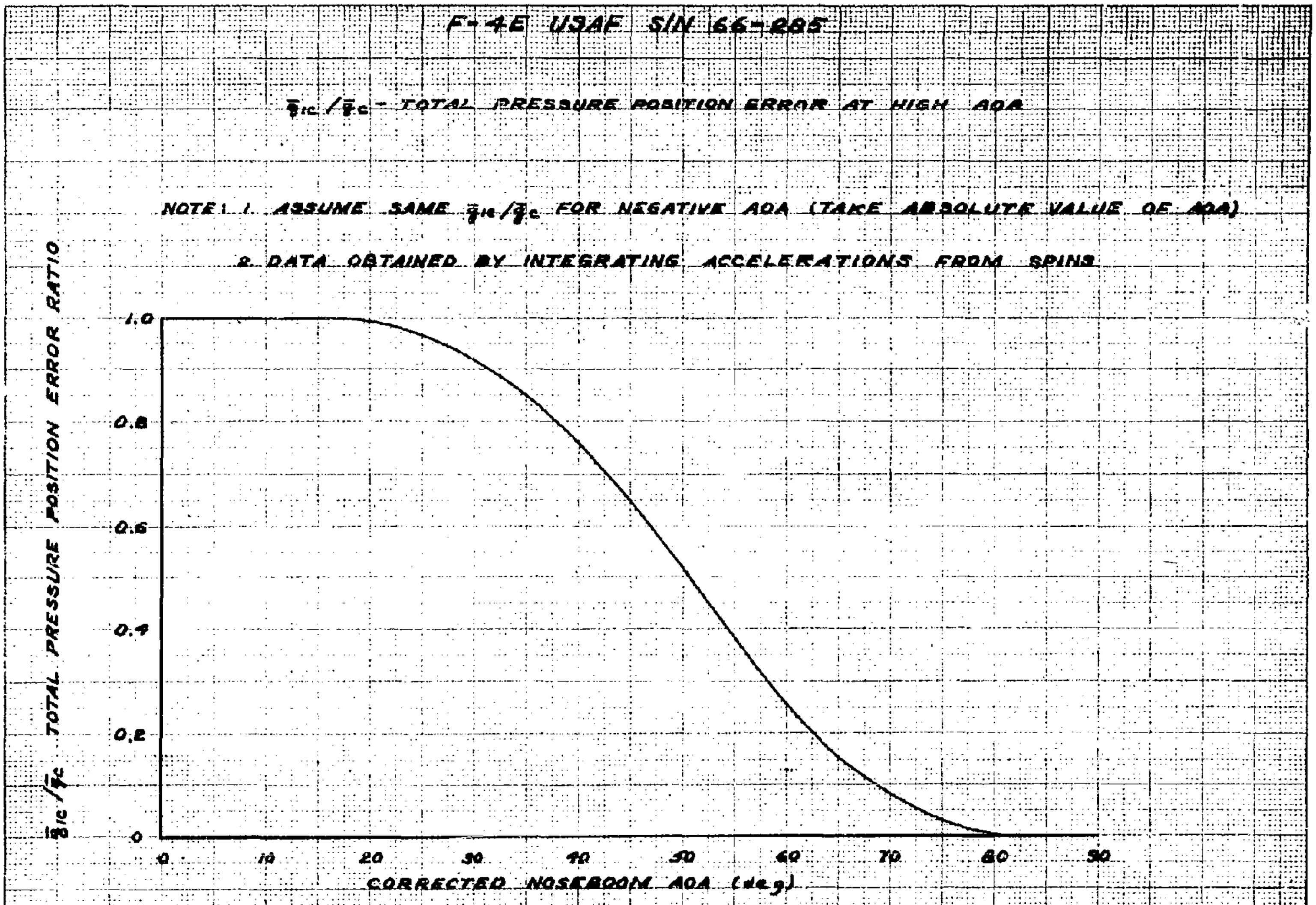

FIGURE 5 POSITION ERROR - TOTAL PRESSURE CORRECTIONS

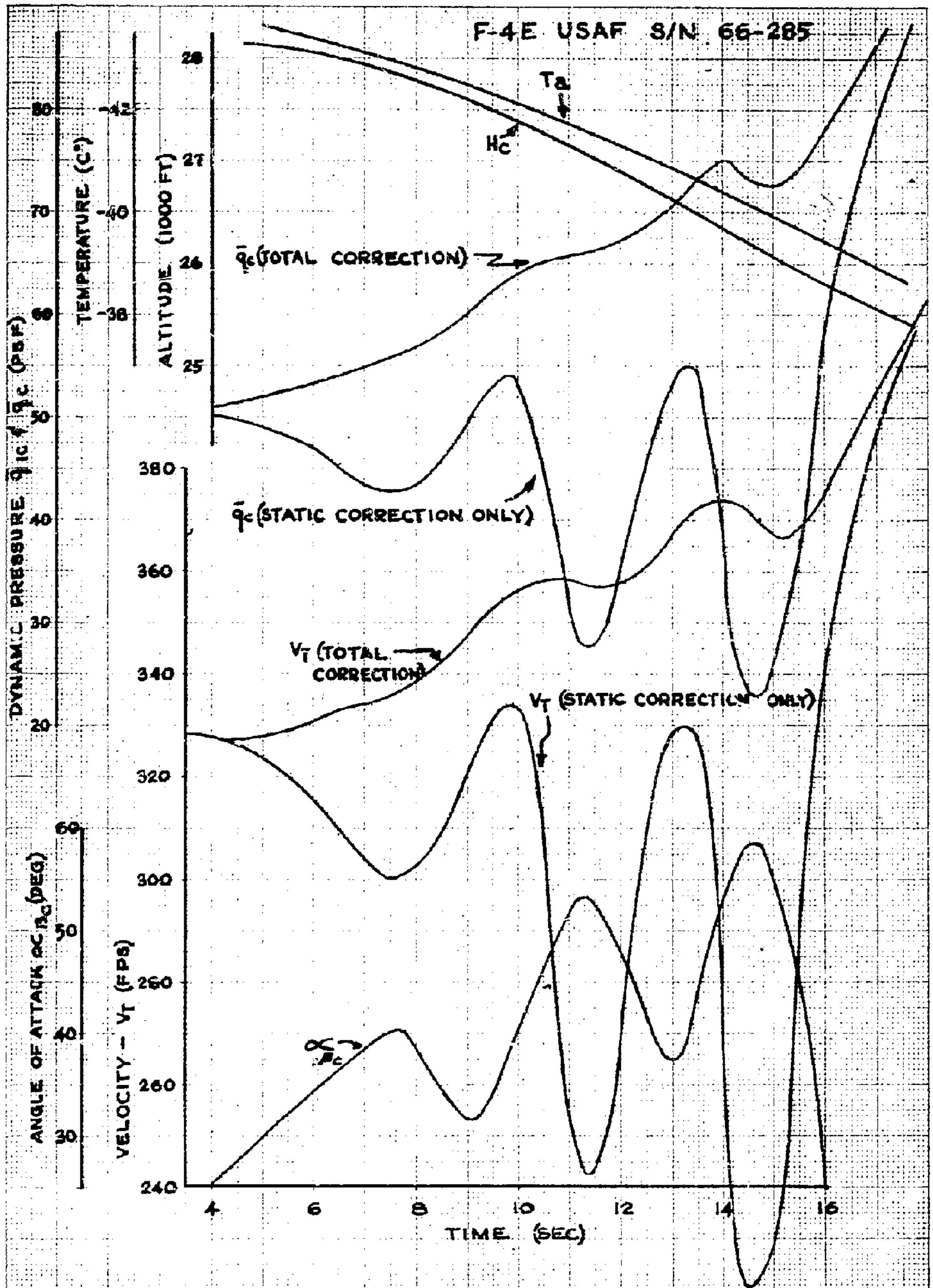

FIGURE 6 EFFECTS OF TOTAL PRESSURE CORRECTIONS ON TRUE VELOCITY AND DYNAMIC PRESSURE

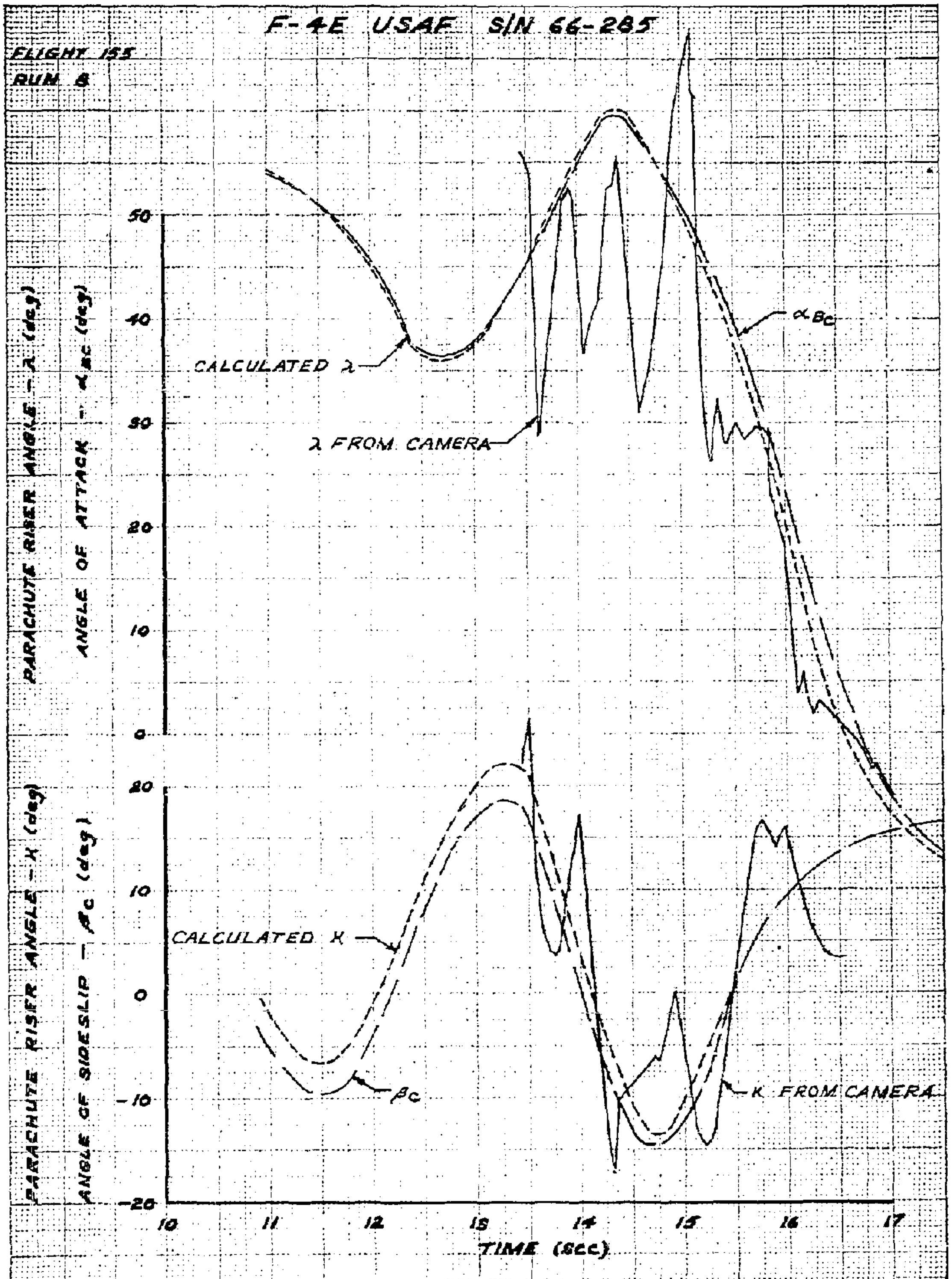

FIGURE 7 PARACHUTE RISER ANGLES

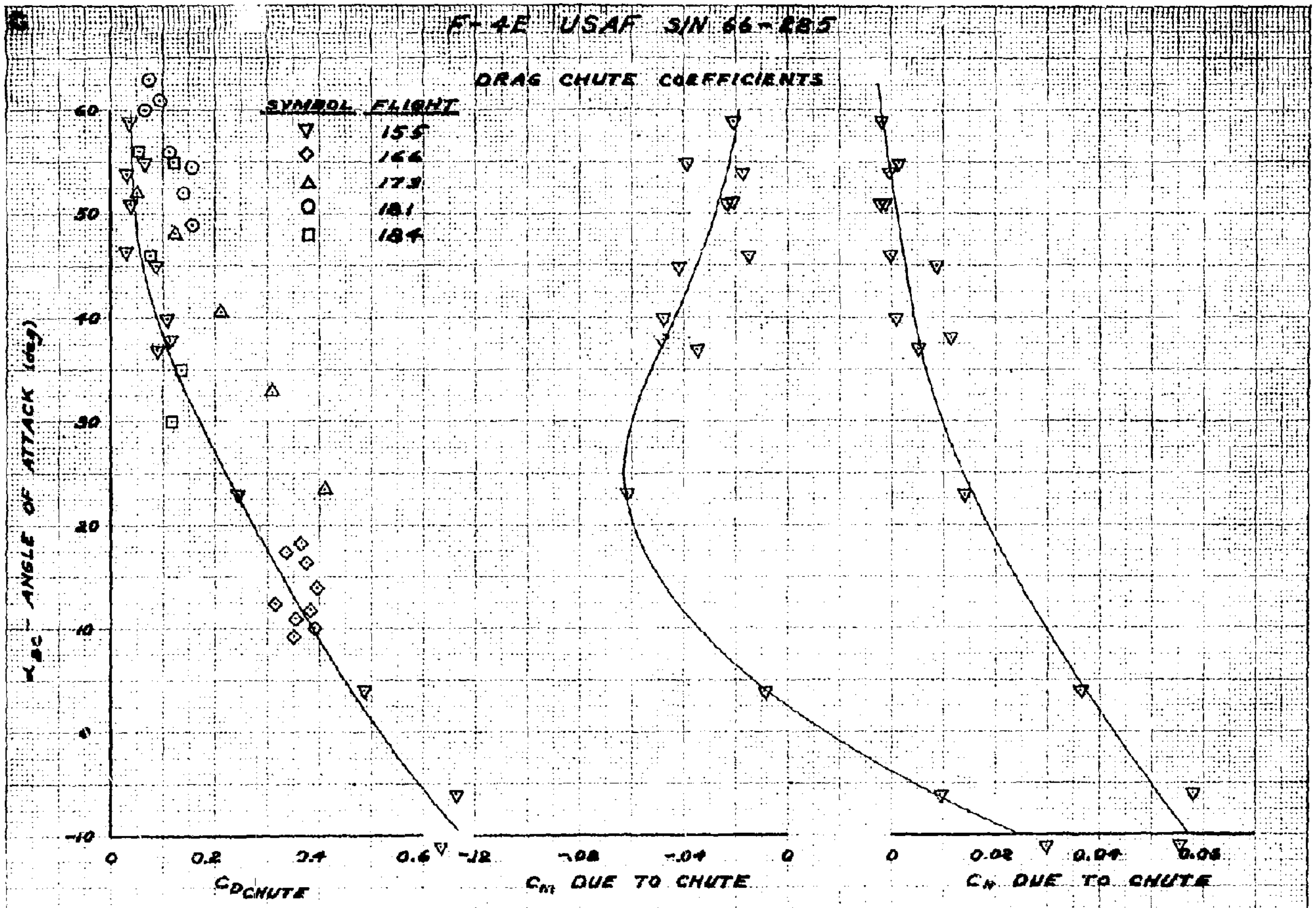

FIGURE 8 DRAG CHUTE COEFFICIENTS

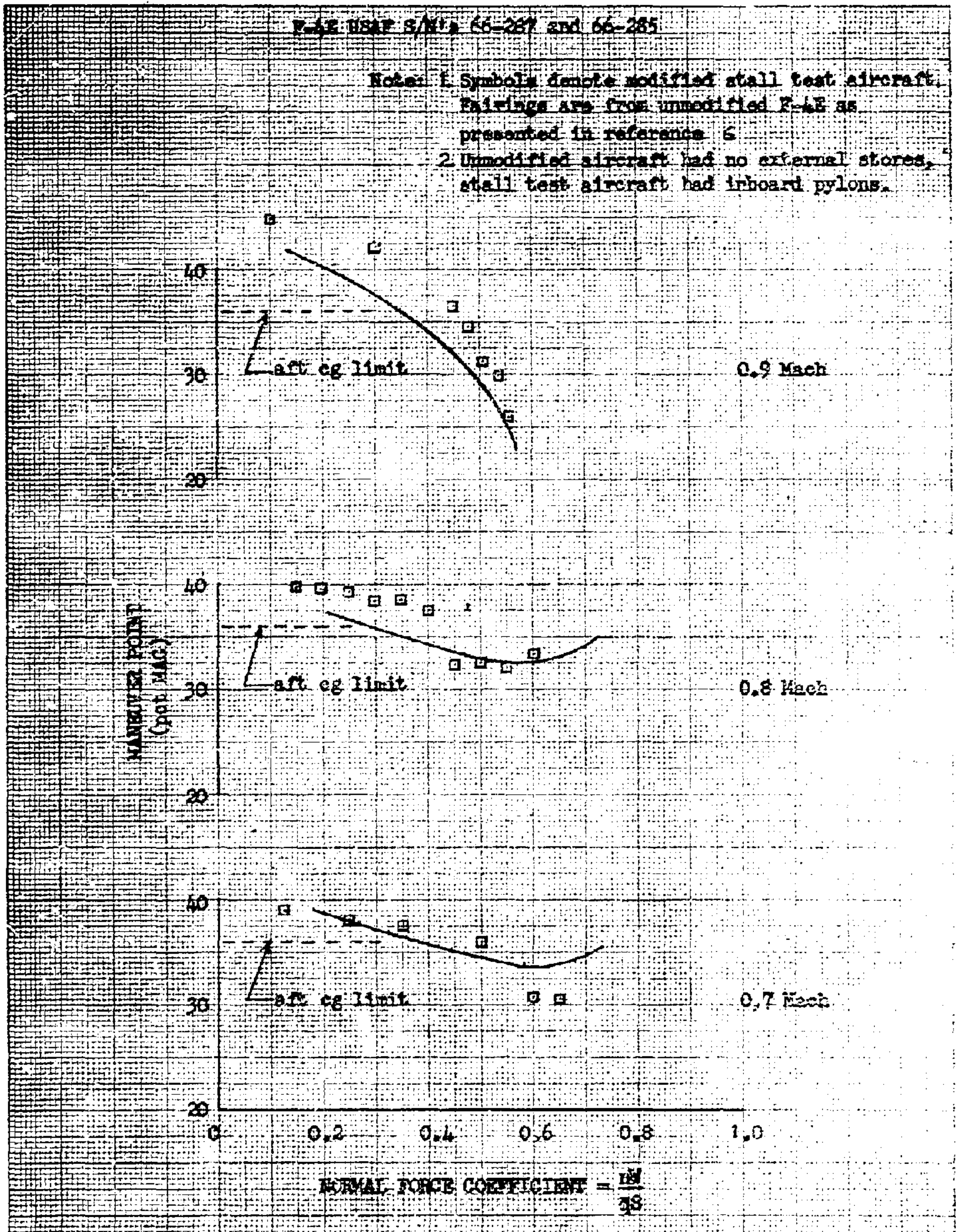

Figure 9 LONGITUDINAL MANUEVERING STABILITY COMPARISON

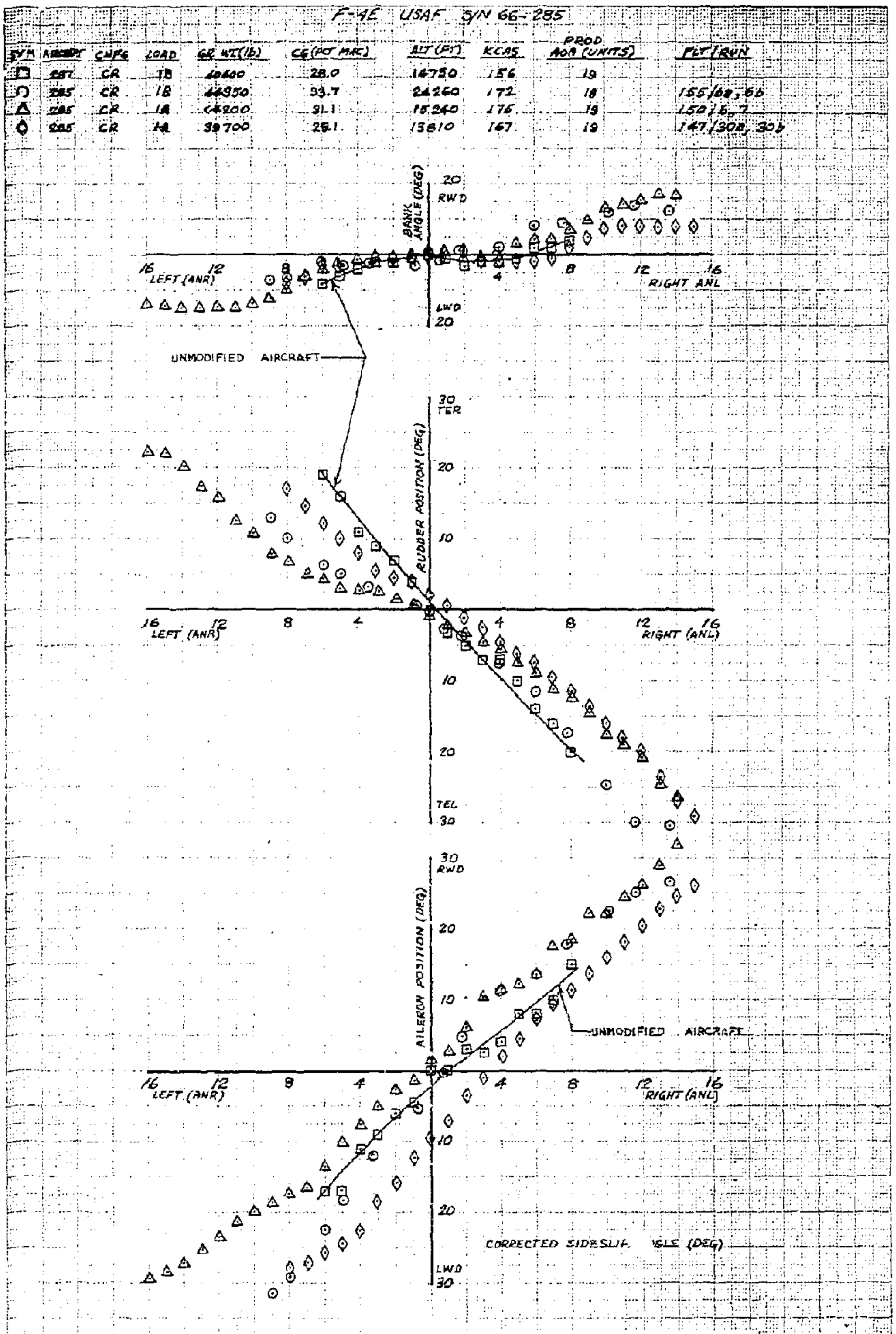

Figure 10 LATERAL-DIRECTIONAL STABILITY COMPARISON AT 19 UNITS ANGLE OF ATTACK

THIS PAGE LEFT BLANK FOR PRESENTATION PURPOSES

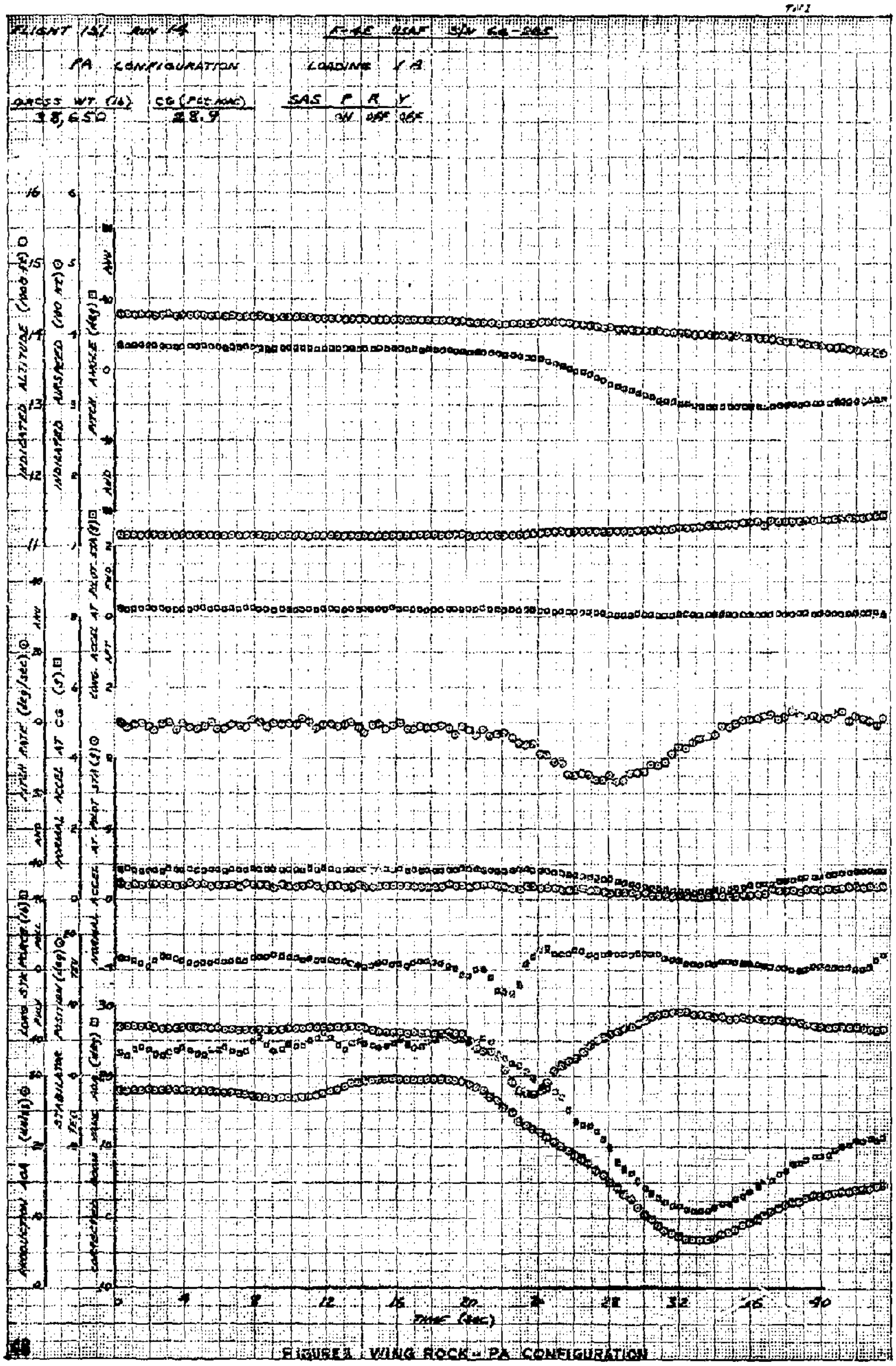

FIGURE 3. WING ROCK - PA CONFIGURATION

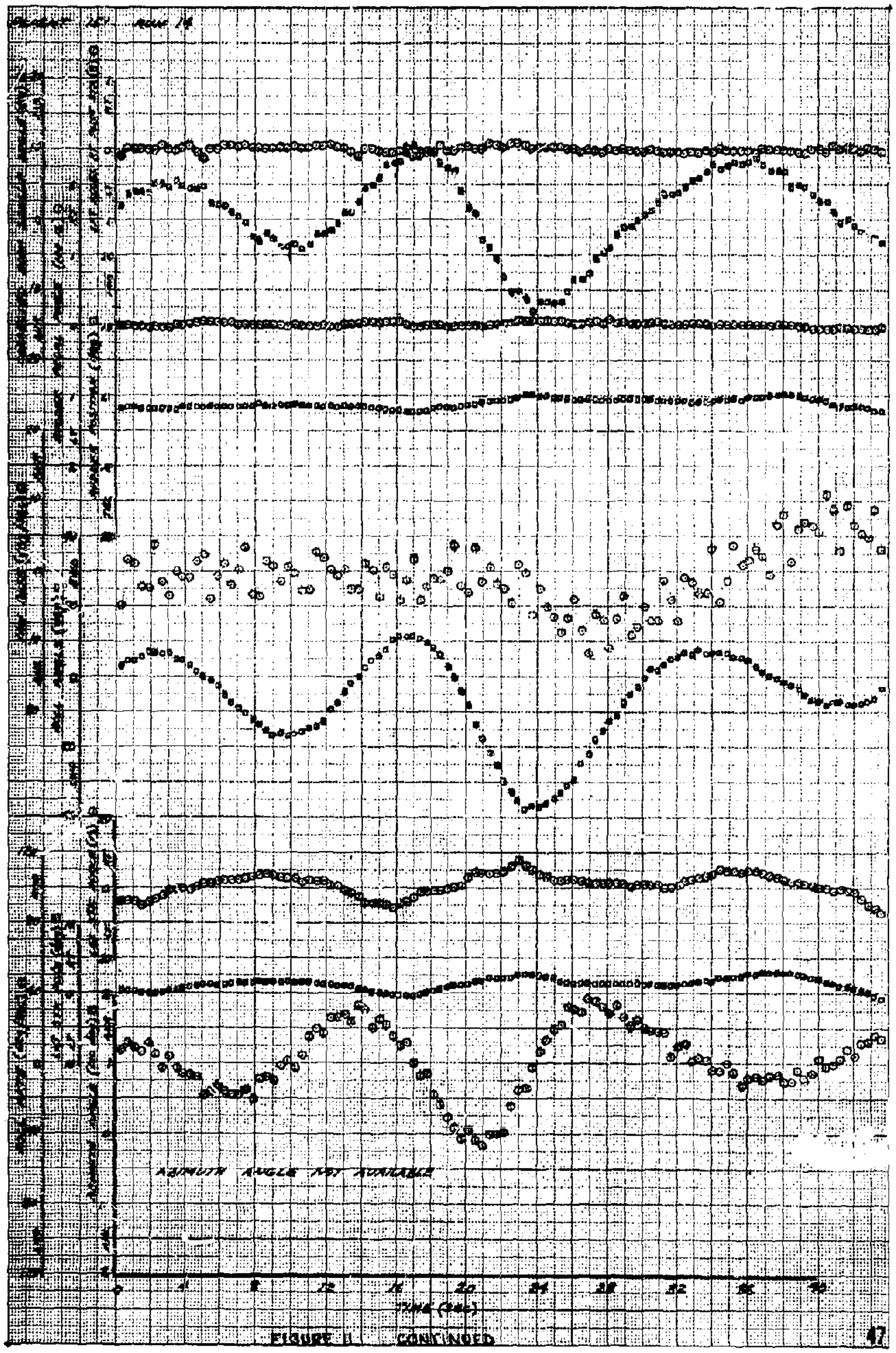

FIGURE 11 CONTINUED

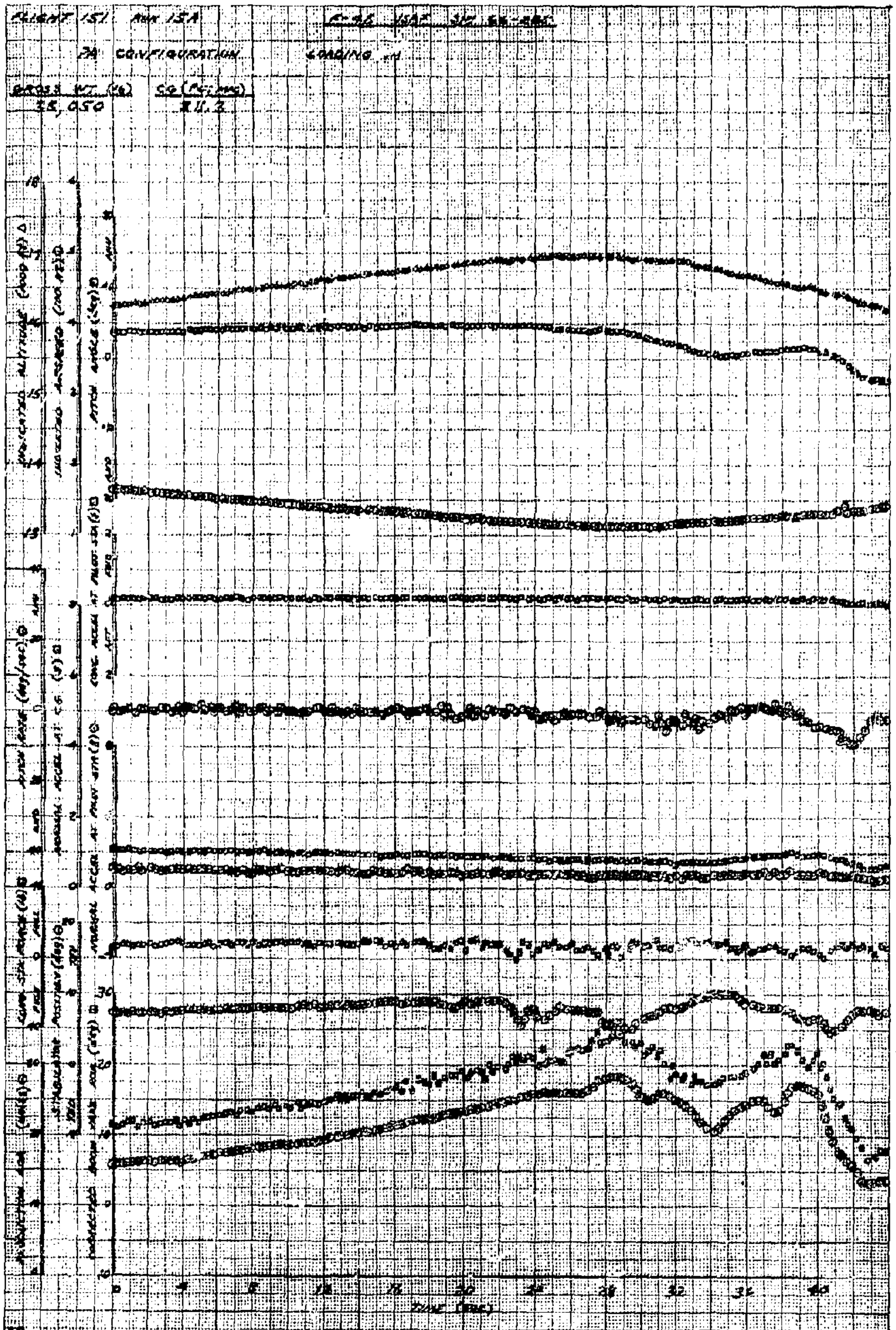

FIGURE 12 WIND ROCK - PA CONFIGURATION

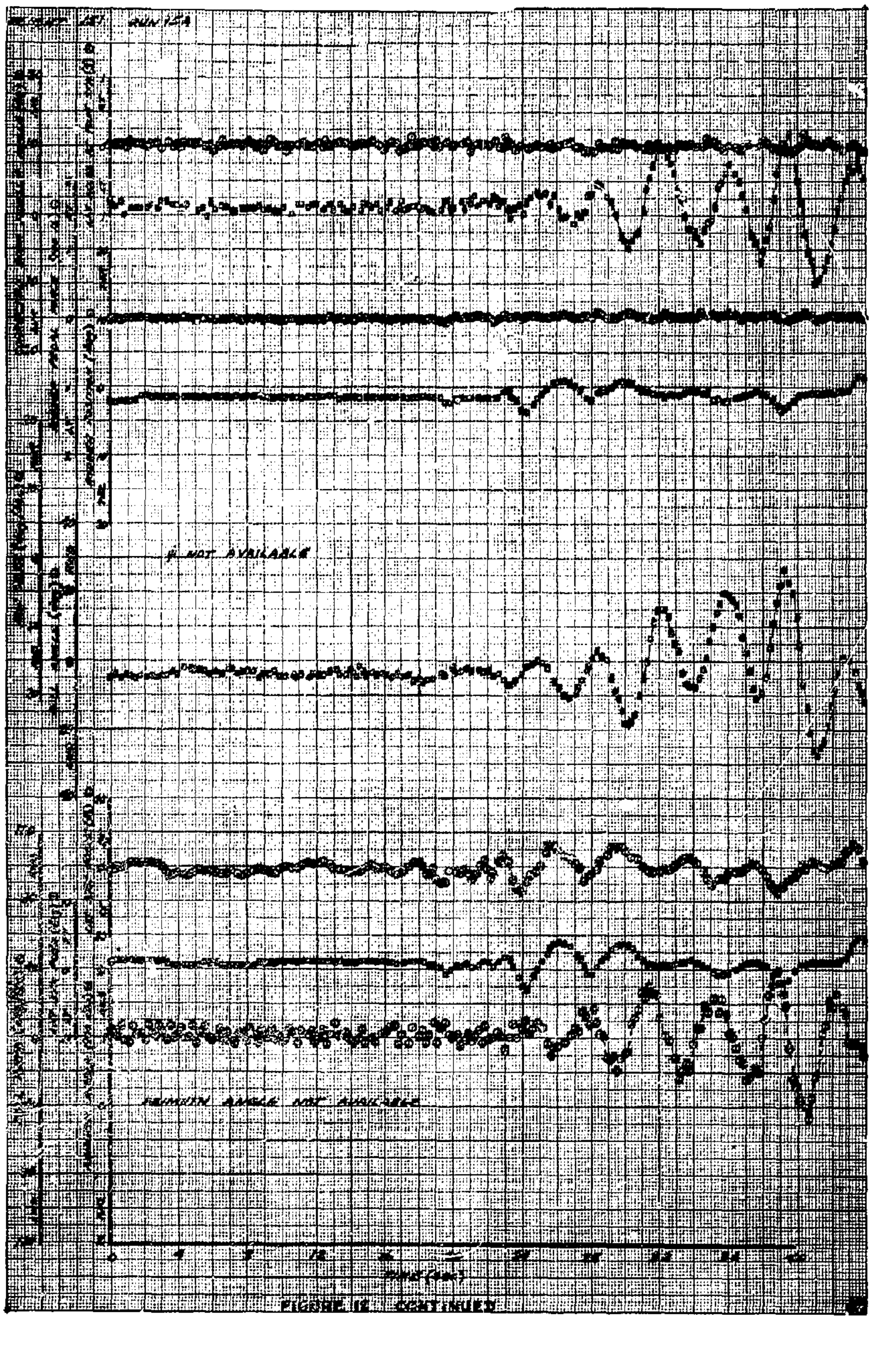

FIGURE 12 CONTINUED

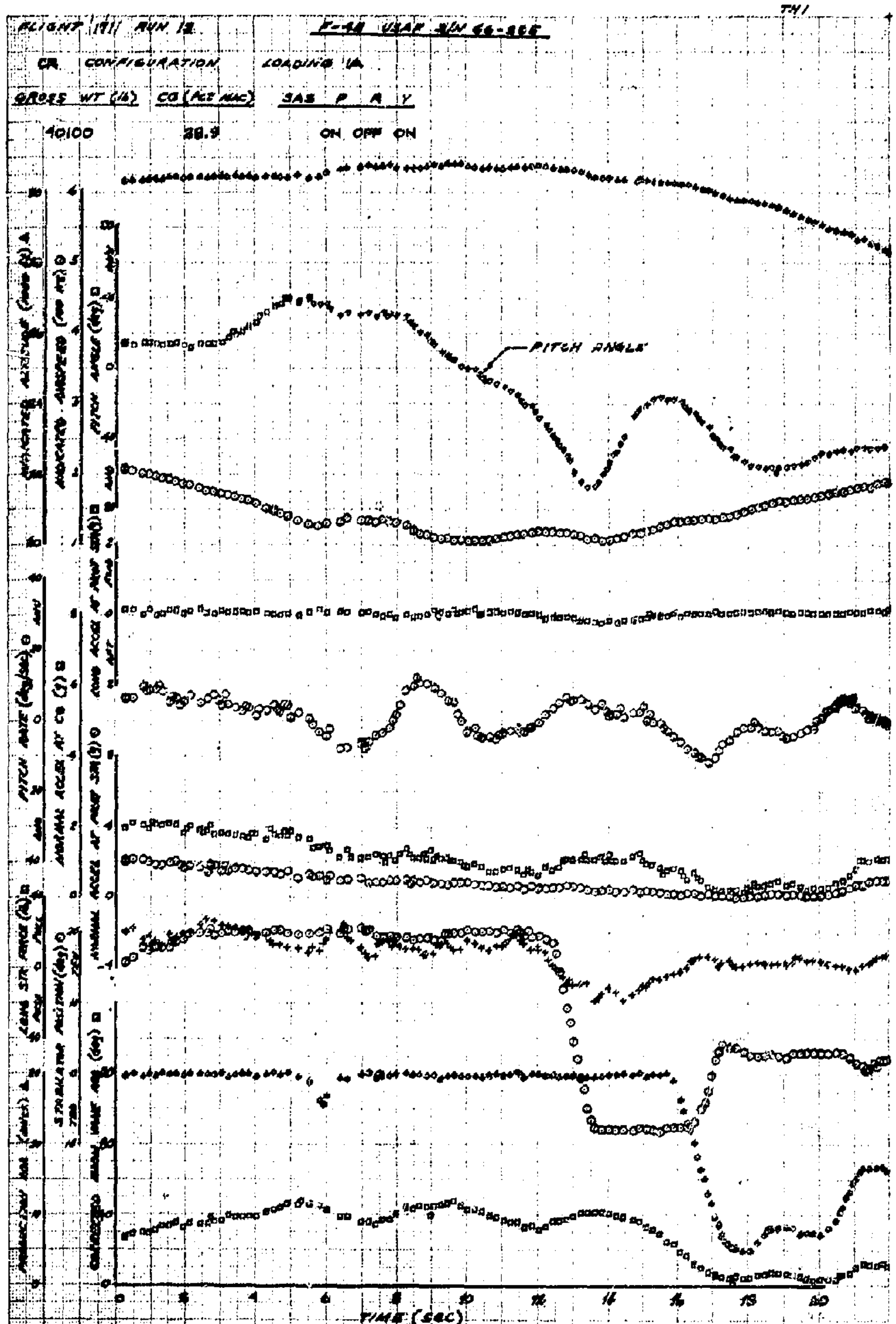

FIGURE 15 ROLLING DEPARTURE - CLEAN LOADING

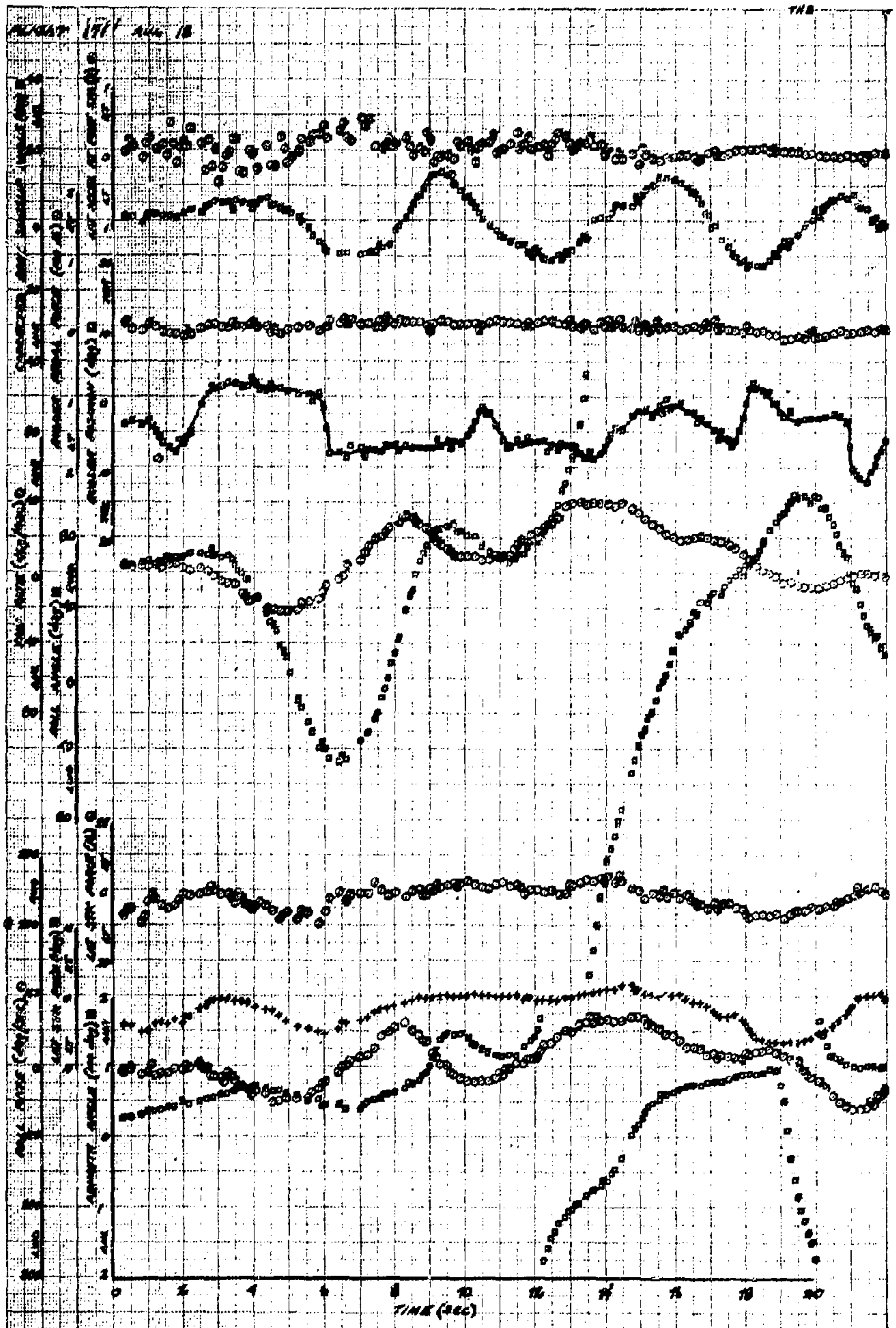

FIGURE 15 CONTINUED

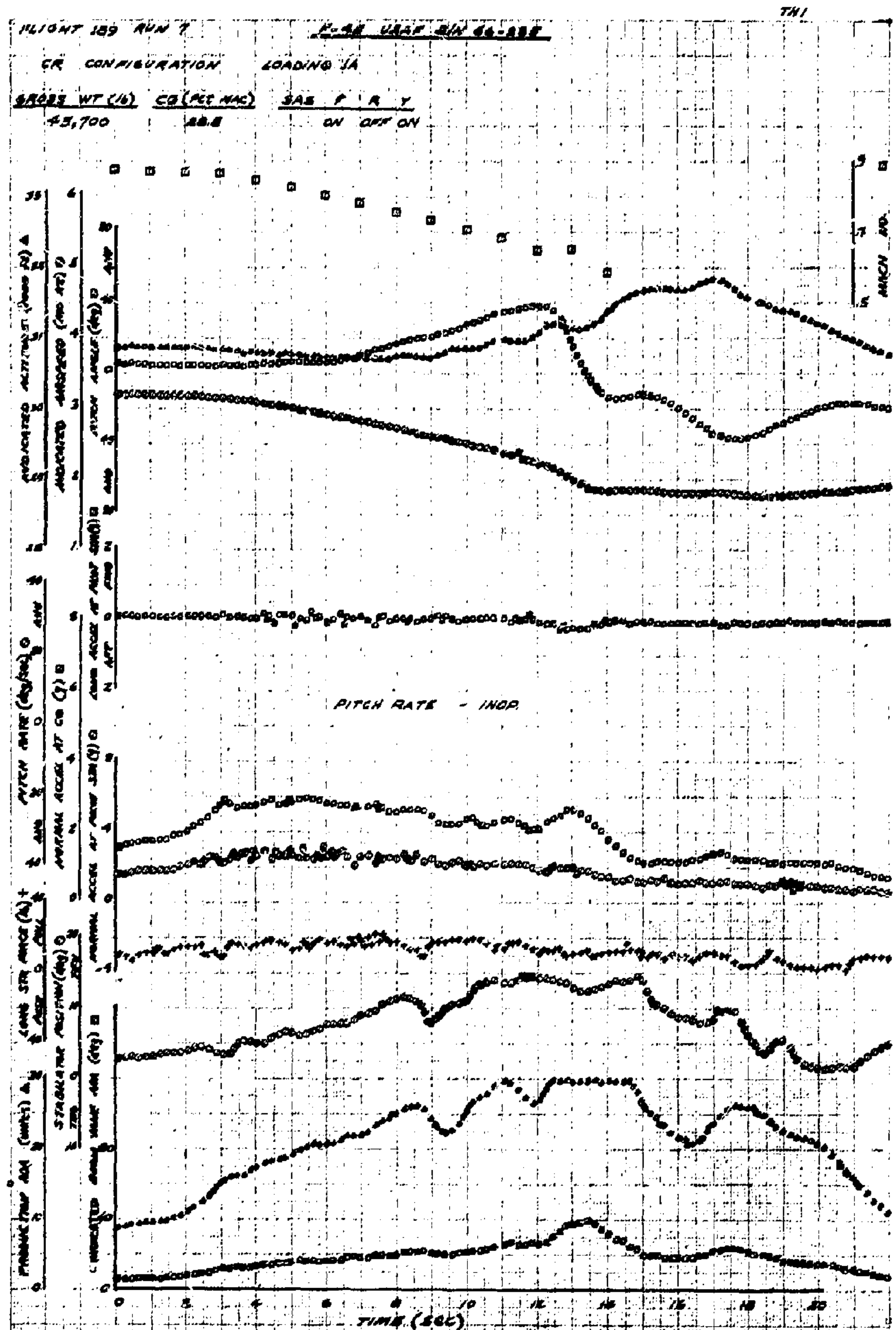

FIGURE 14 ROLLING DEPARTURE FROM A TRANSONIC DECELERATION

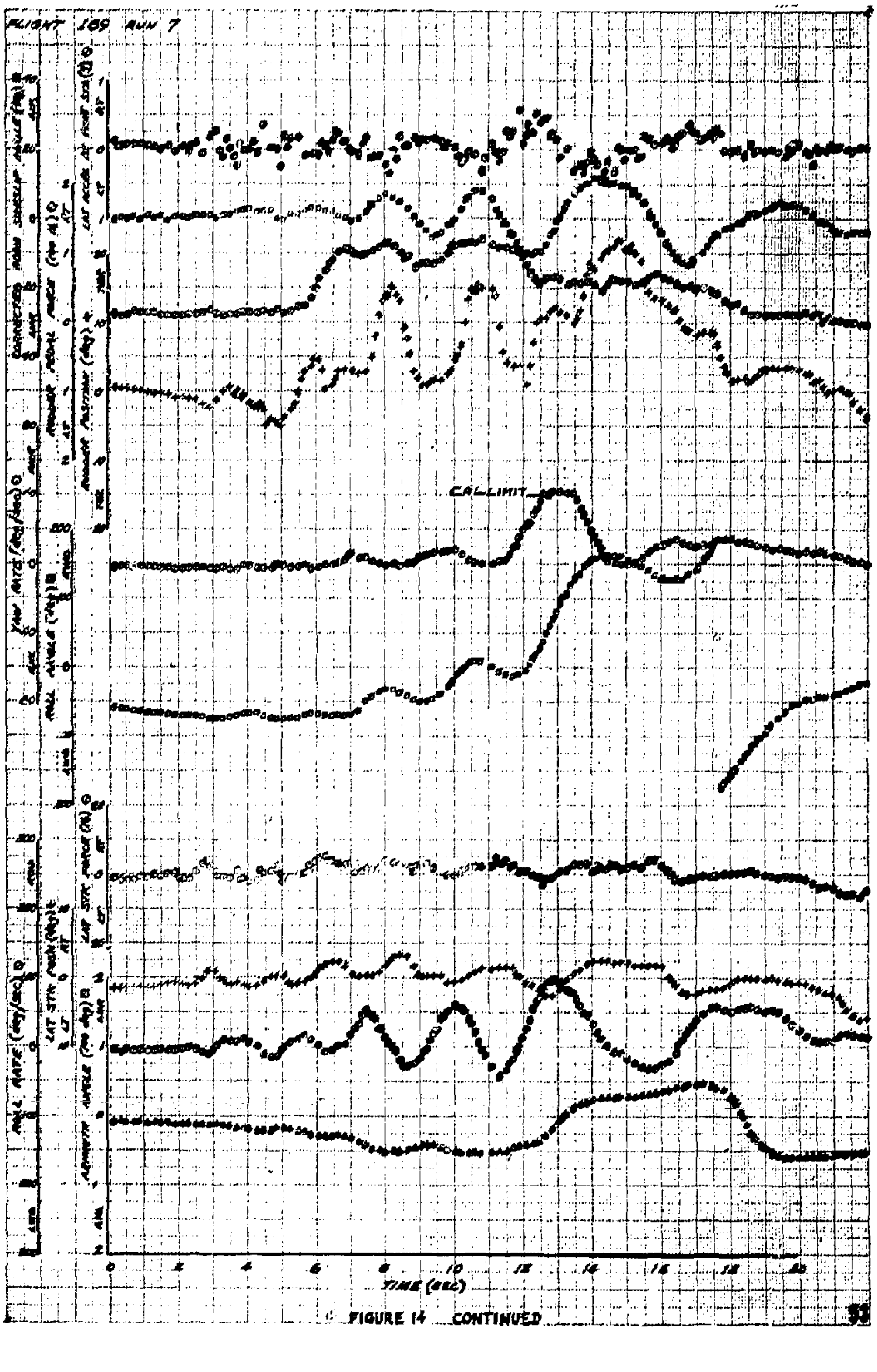

FIGURE 14 CONTINUED

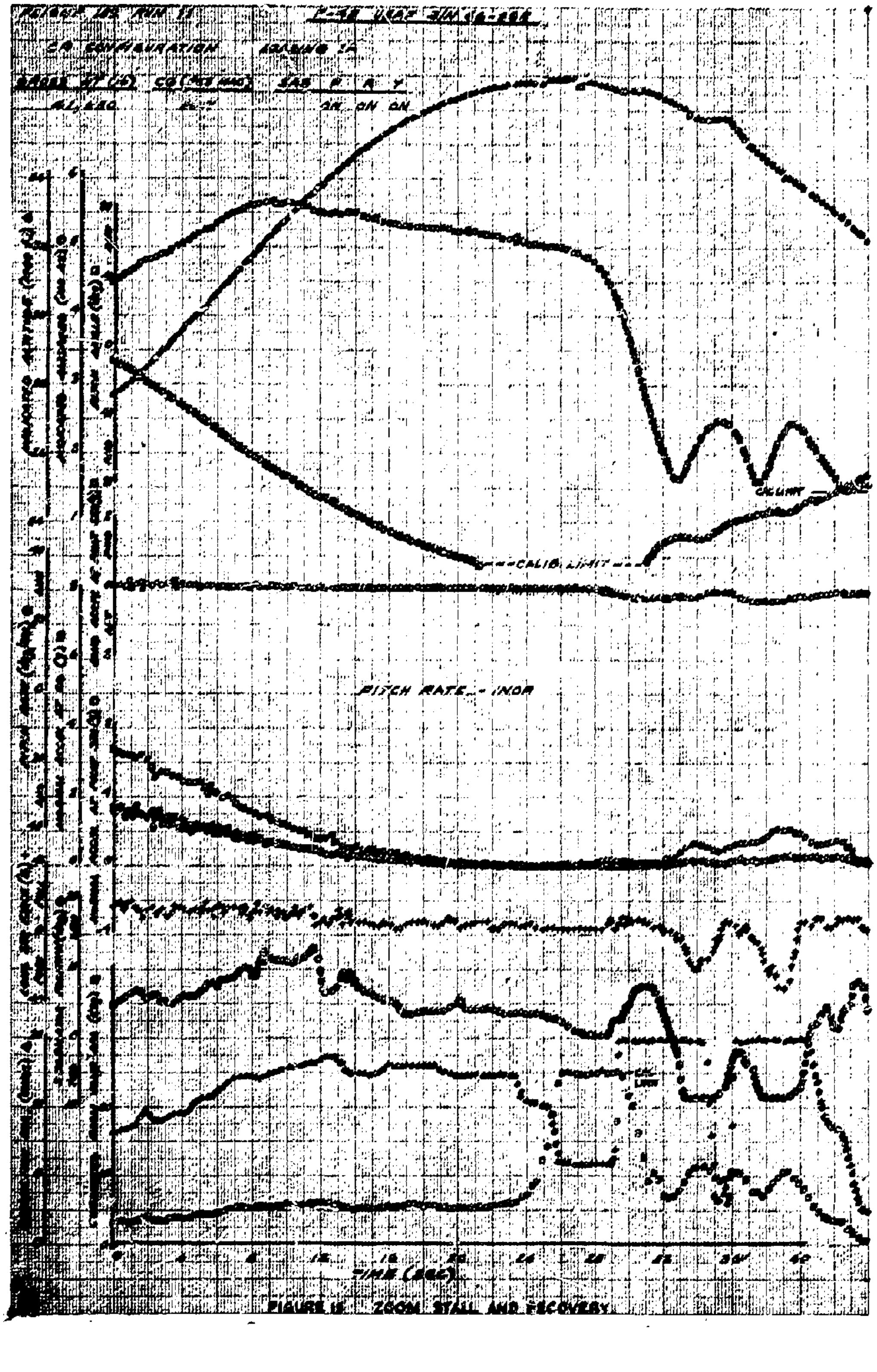

FIGURE 15. ZOOM STALL AND RECOVERY

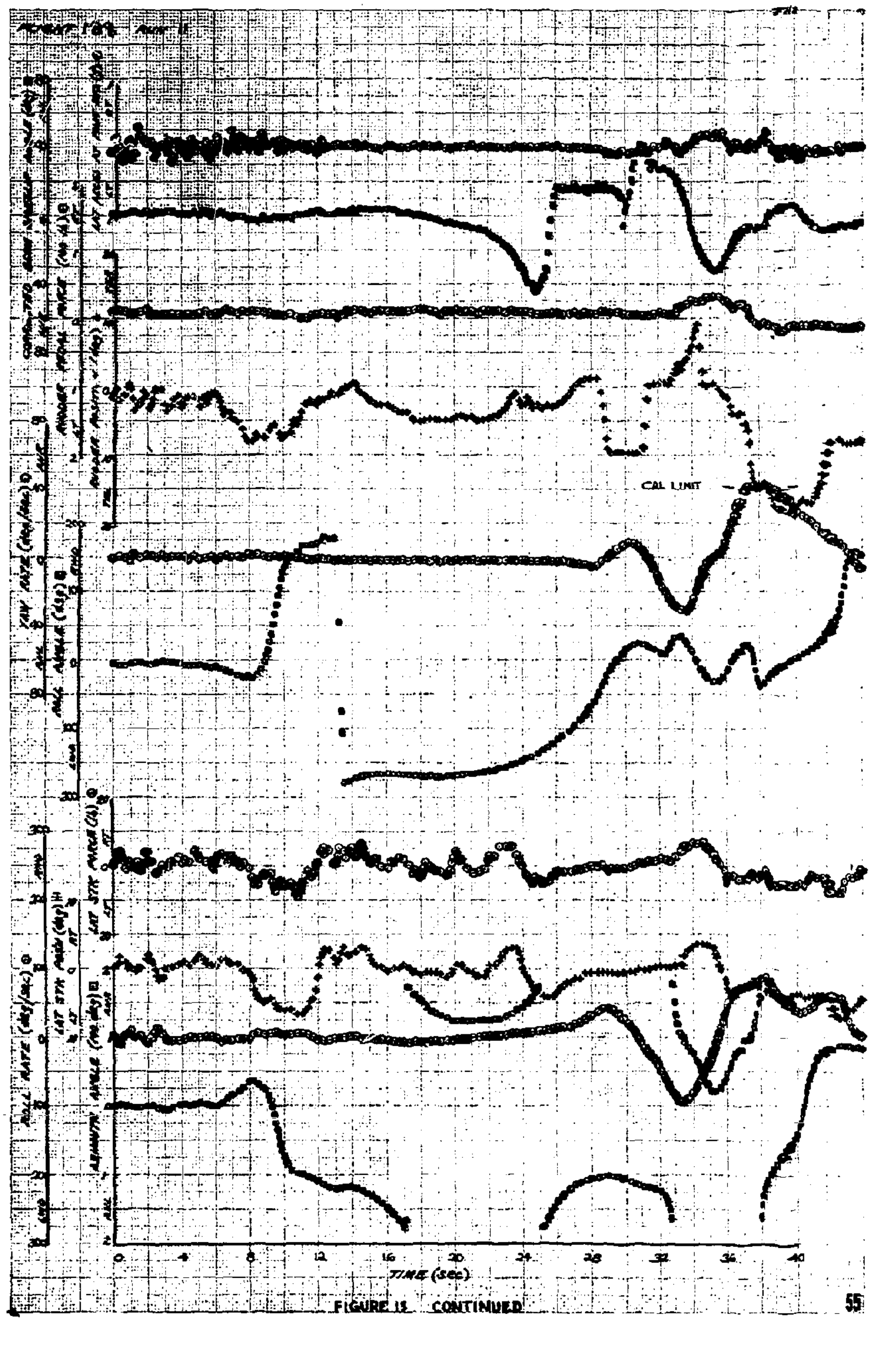

FIGURE 15 CONTINUED

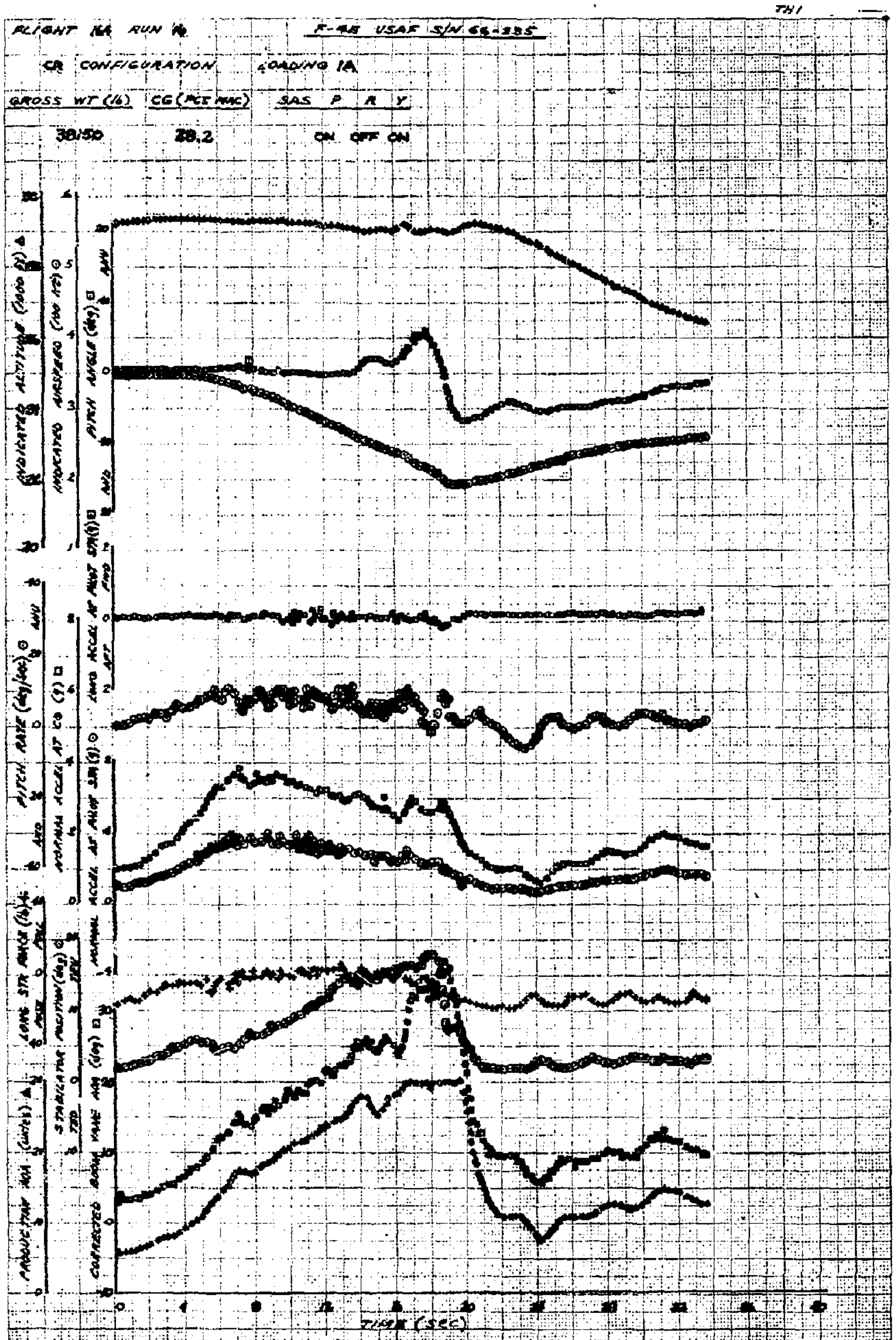

FIGURE 16 ROLLING DEPARTURE FROM A 4G RIGHT TURN

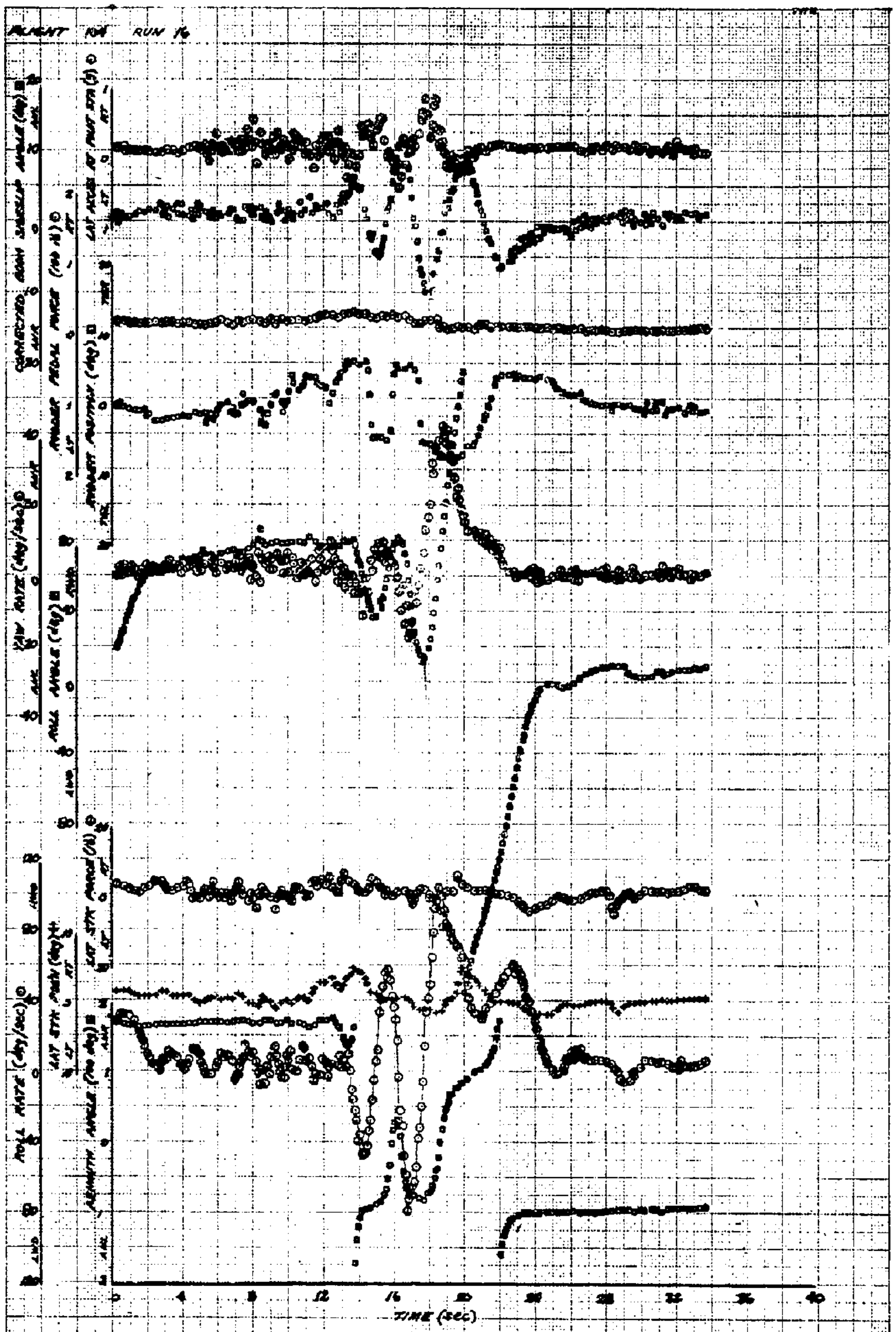

FIGURE 16 CONTINUED

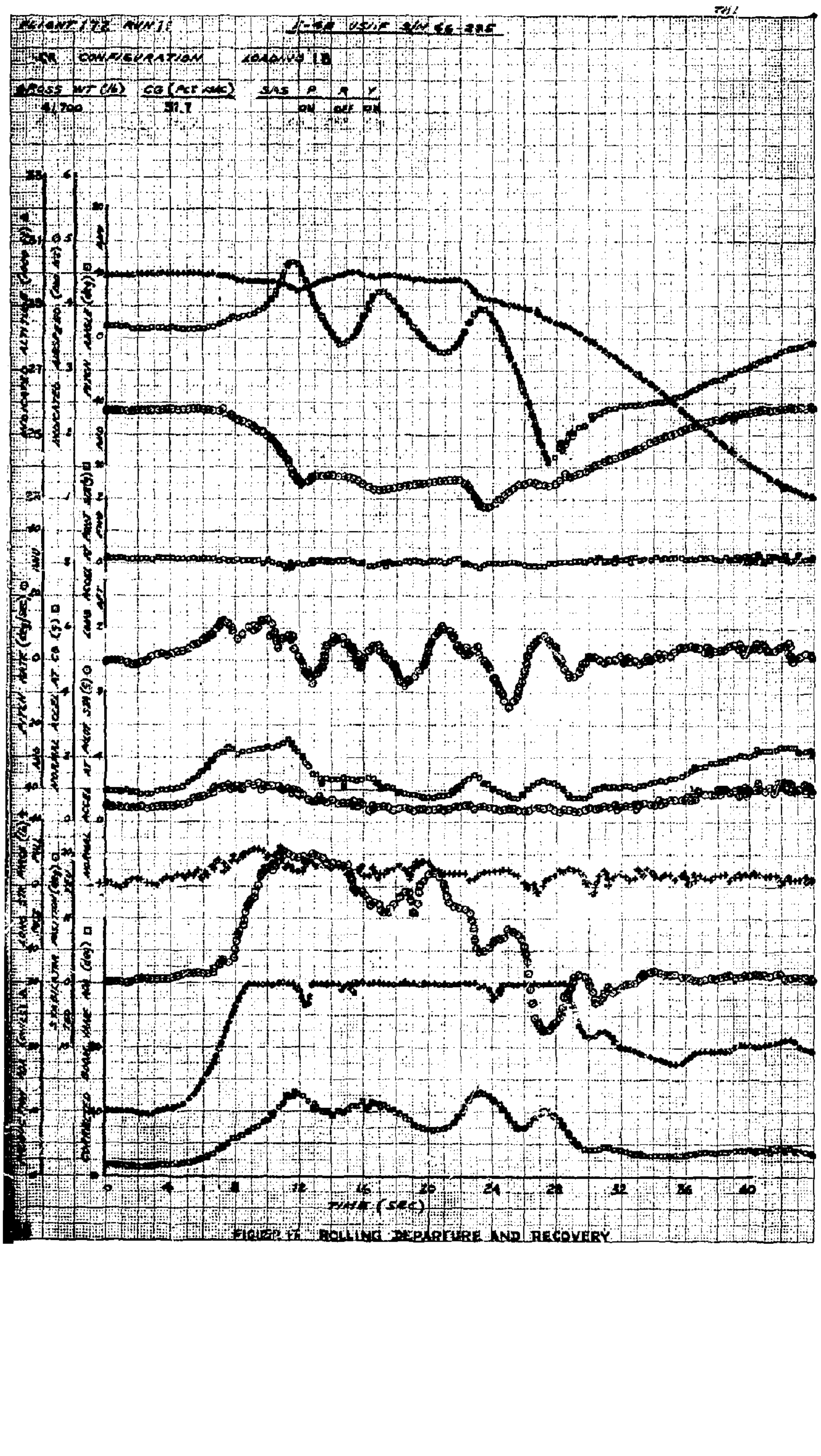

FIGURE 17 ROLLING DEPARTURE AND RECOVERY

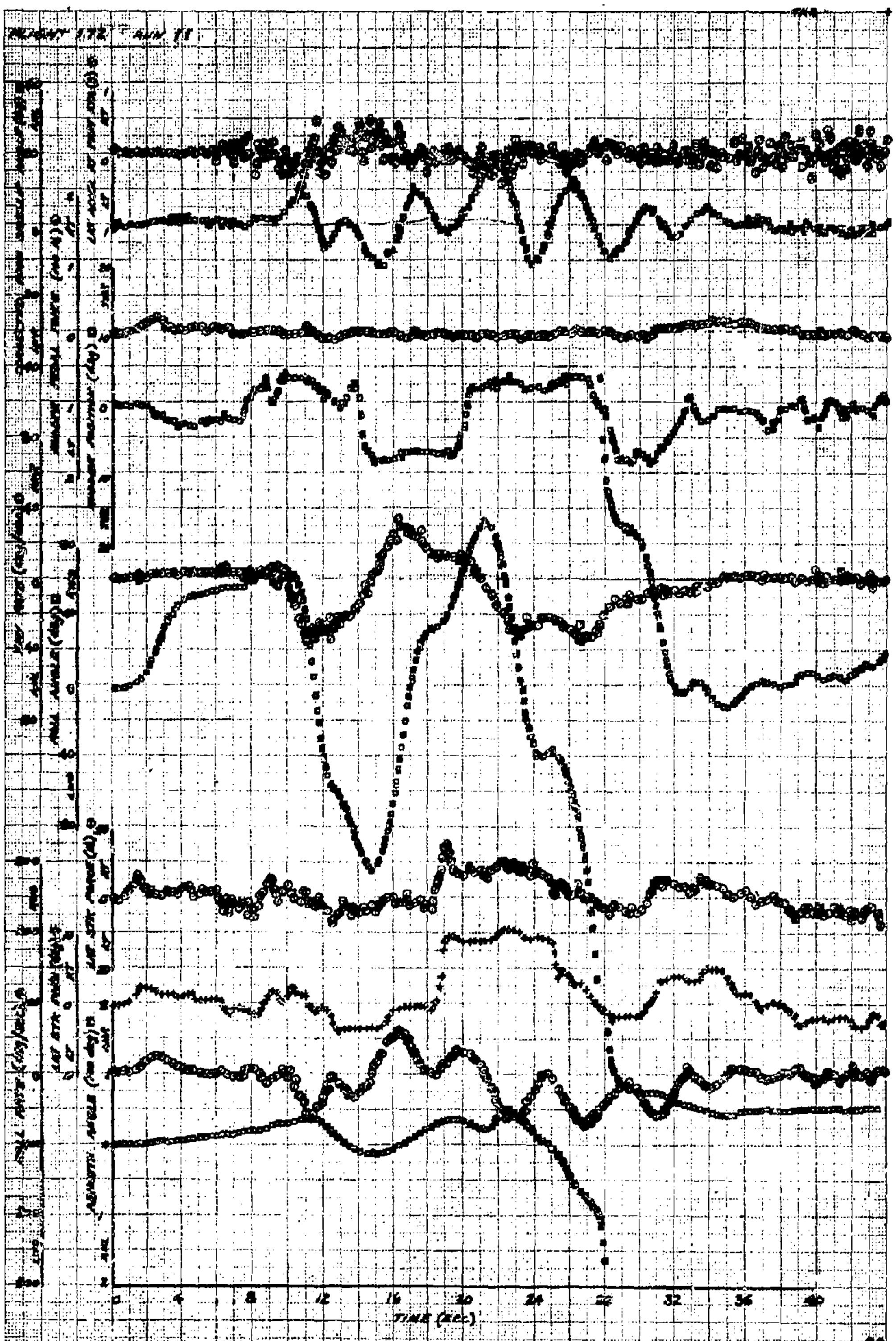

FIGURE 17 CONTINUED

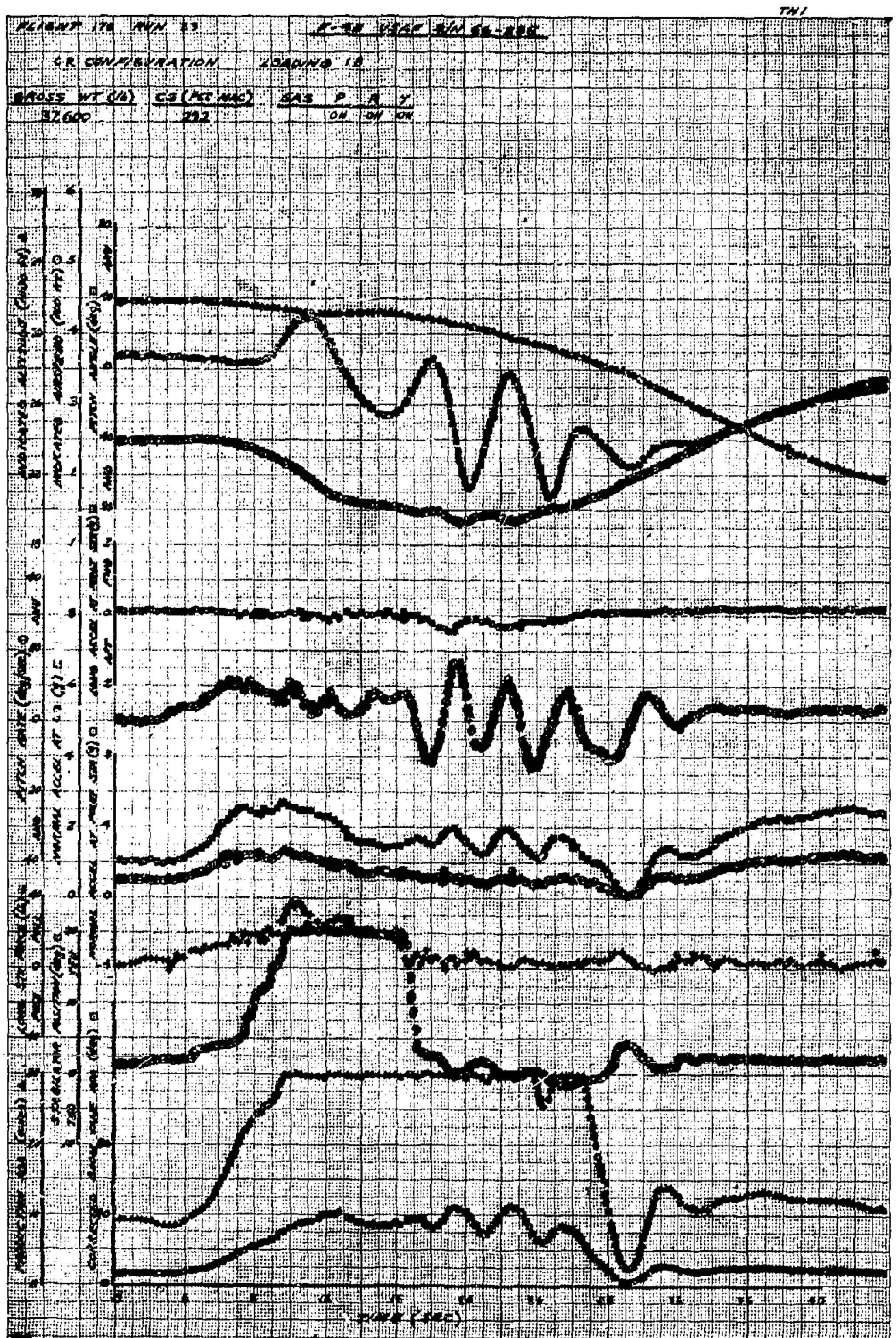

FIGURE 19 RECOVERY ROLLS FROM A ROLLING DEPARTURE

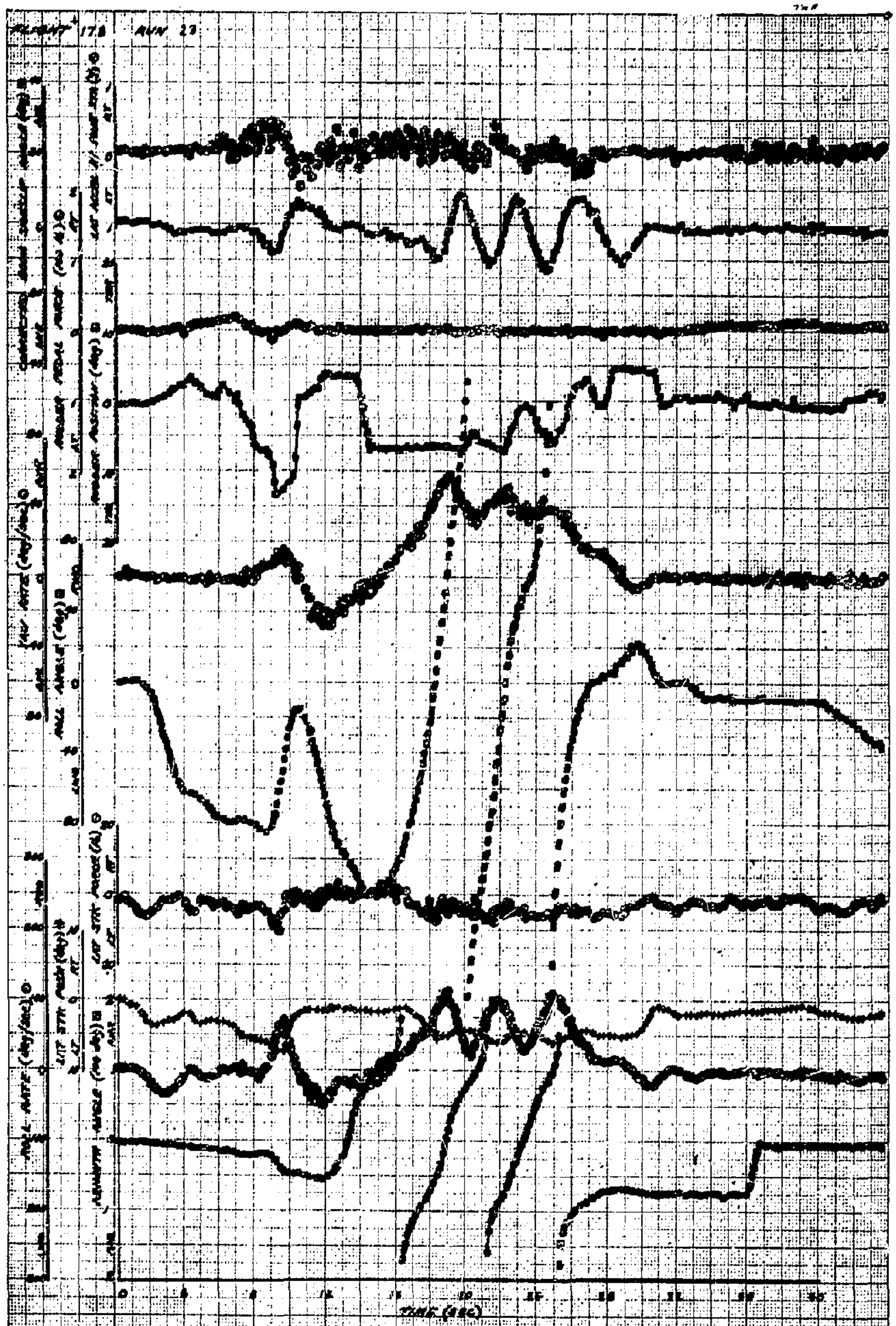

FIGURE 18 CONTINUED

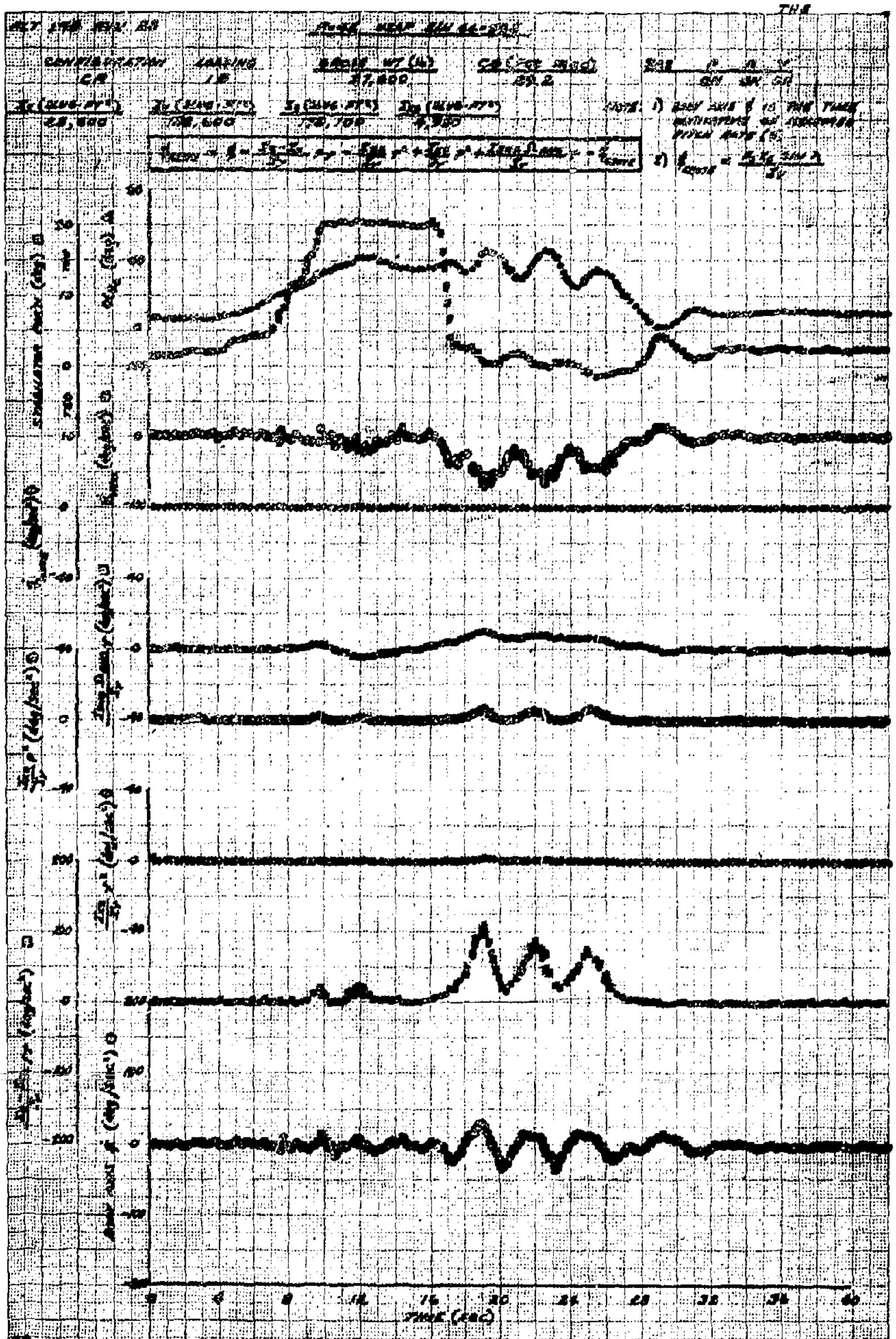

FIGURE 19 CONTINUED

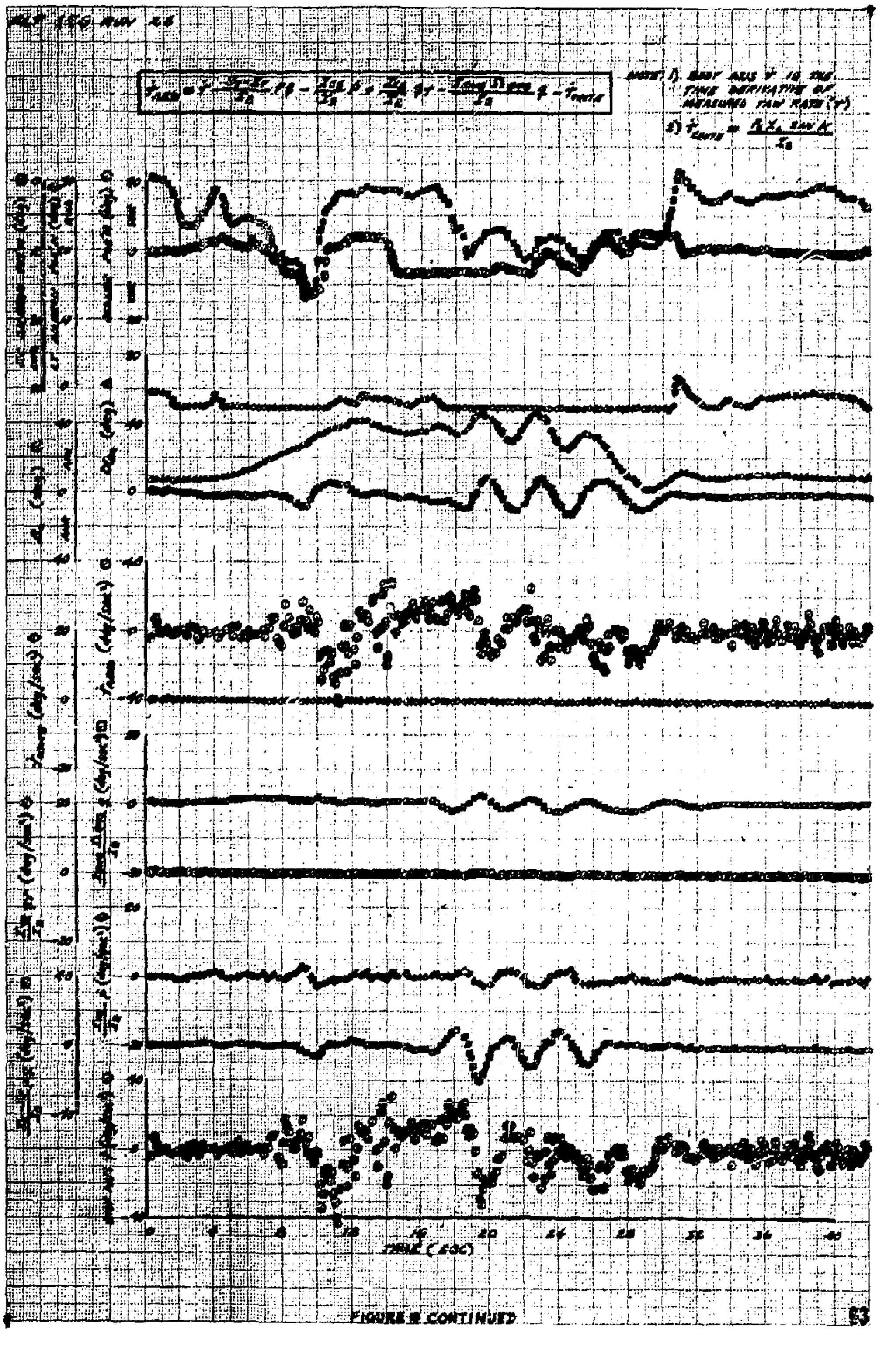

FIGURE 8 CONTINUED

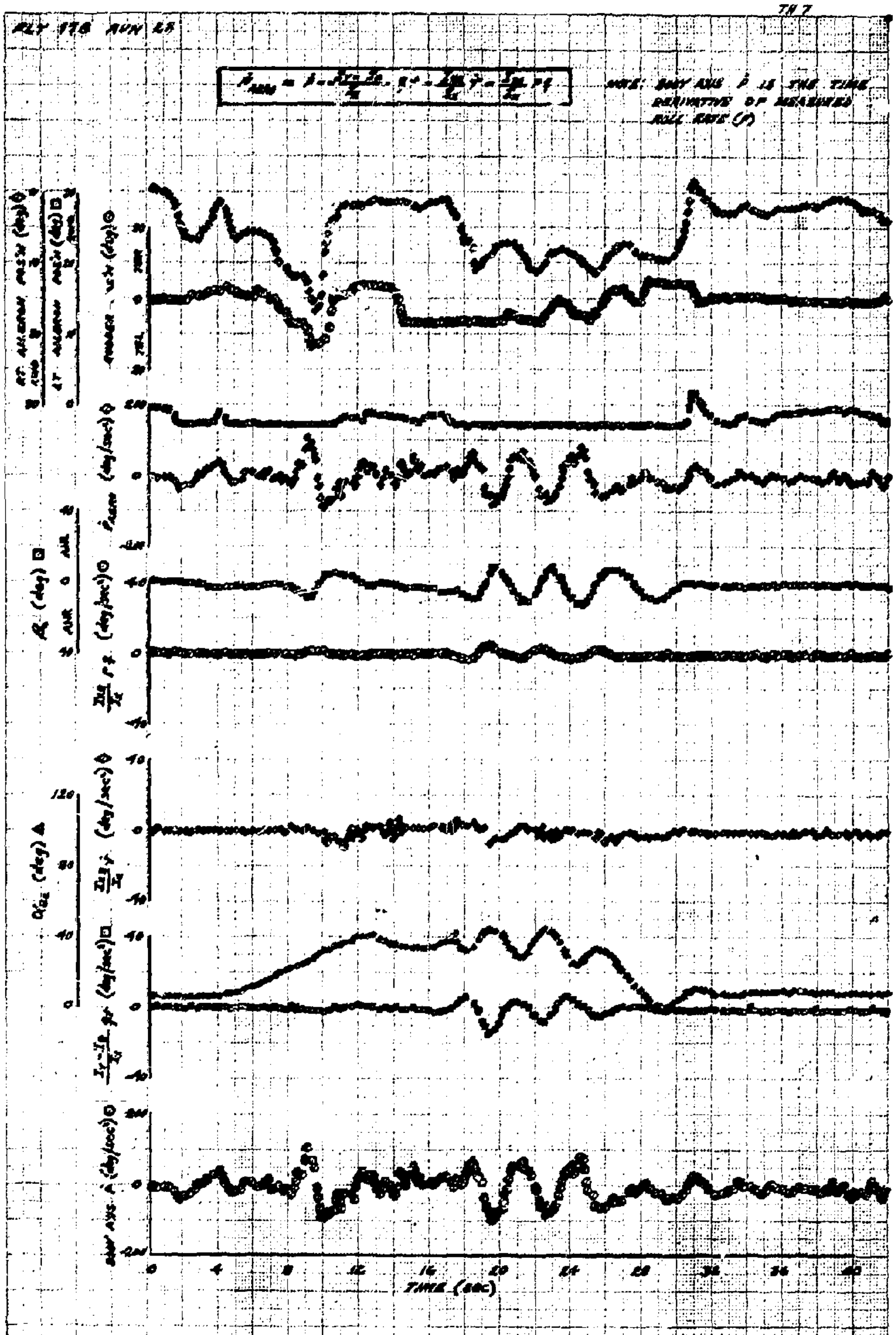

FIGURE 19 CONTINUED

THIS PAGE LEFT BLANK FOR PRESENTATION PURPOSES

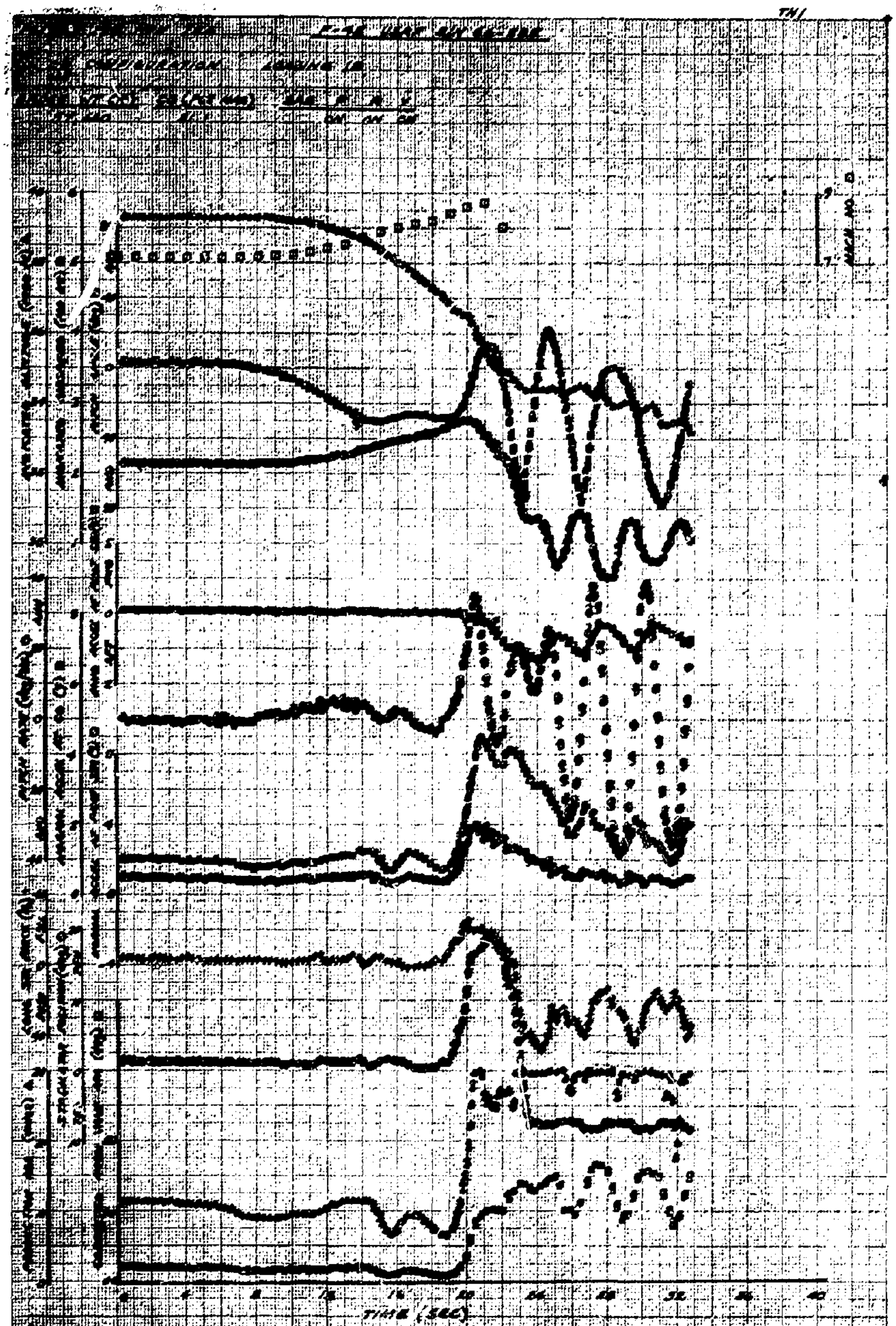

FIGURE II. 5½ TURNS, STEEP-MILDLY OSCILLATORY SPIN-DRAG CHUTE RECOVERY

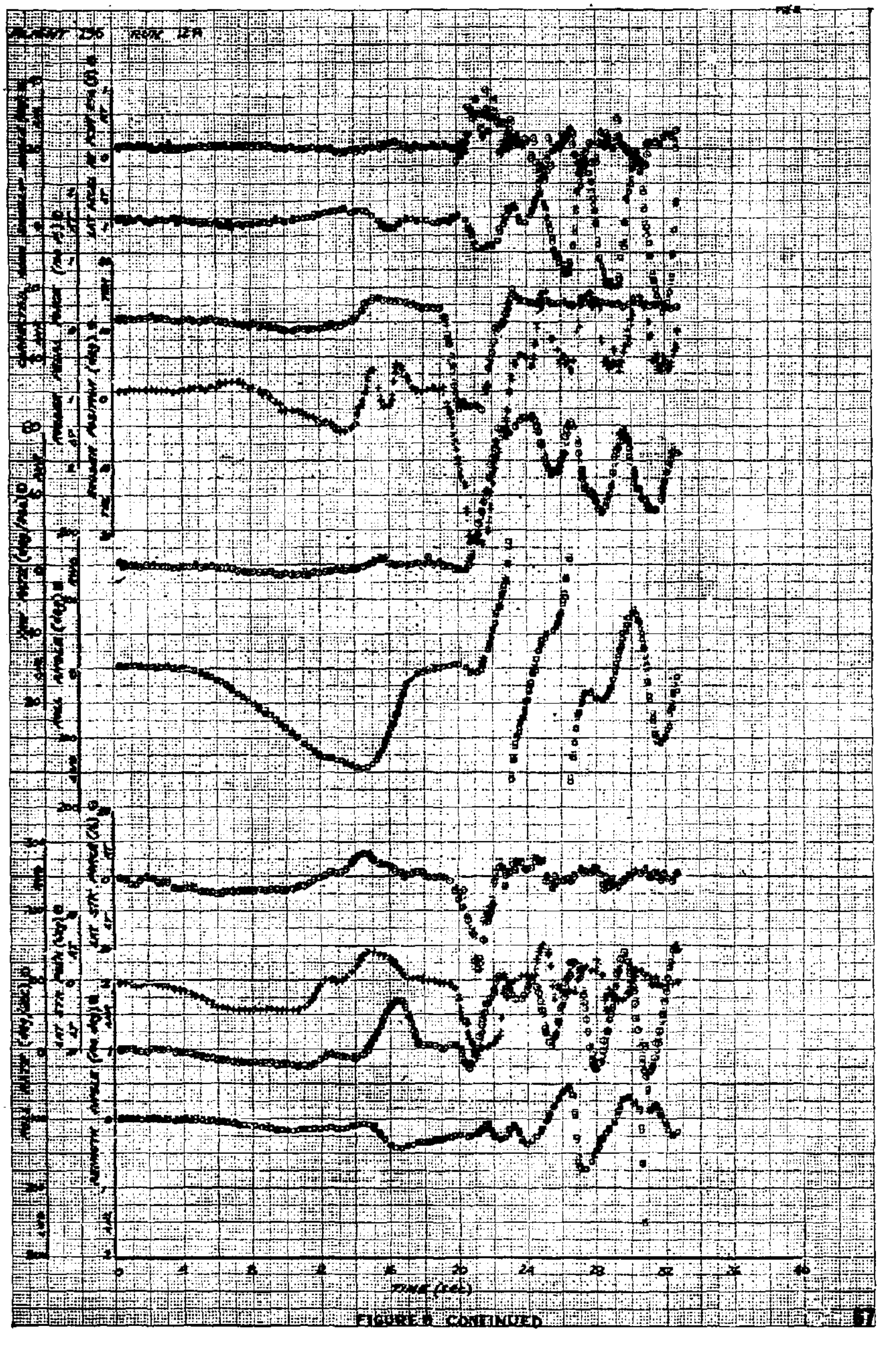

FIGURE 8 CONTINUED

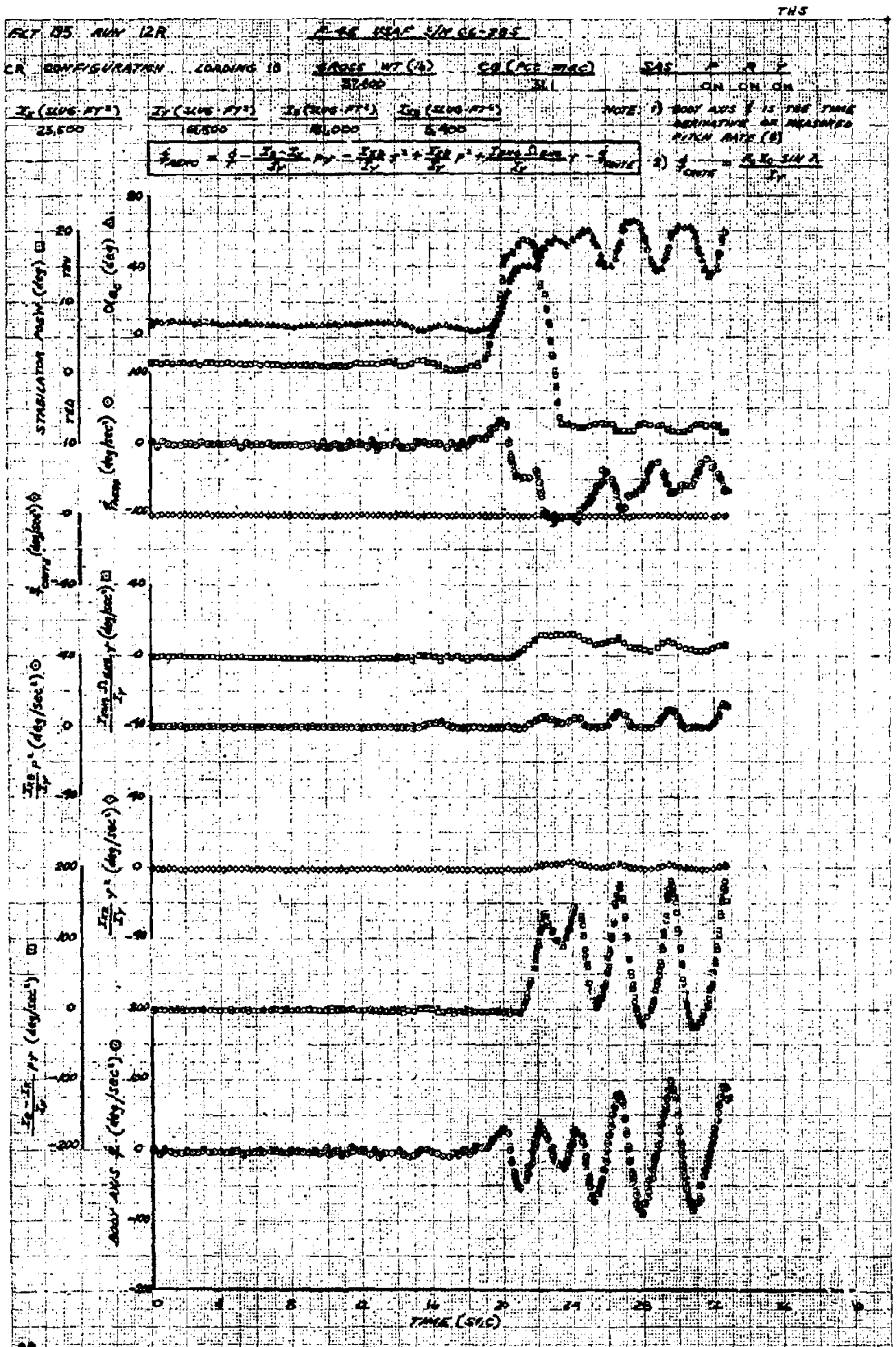

FIGURE 17 CONTINUED

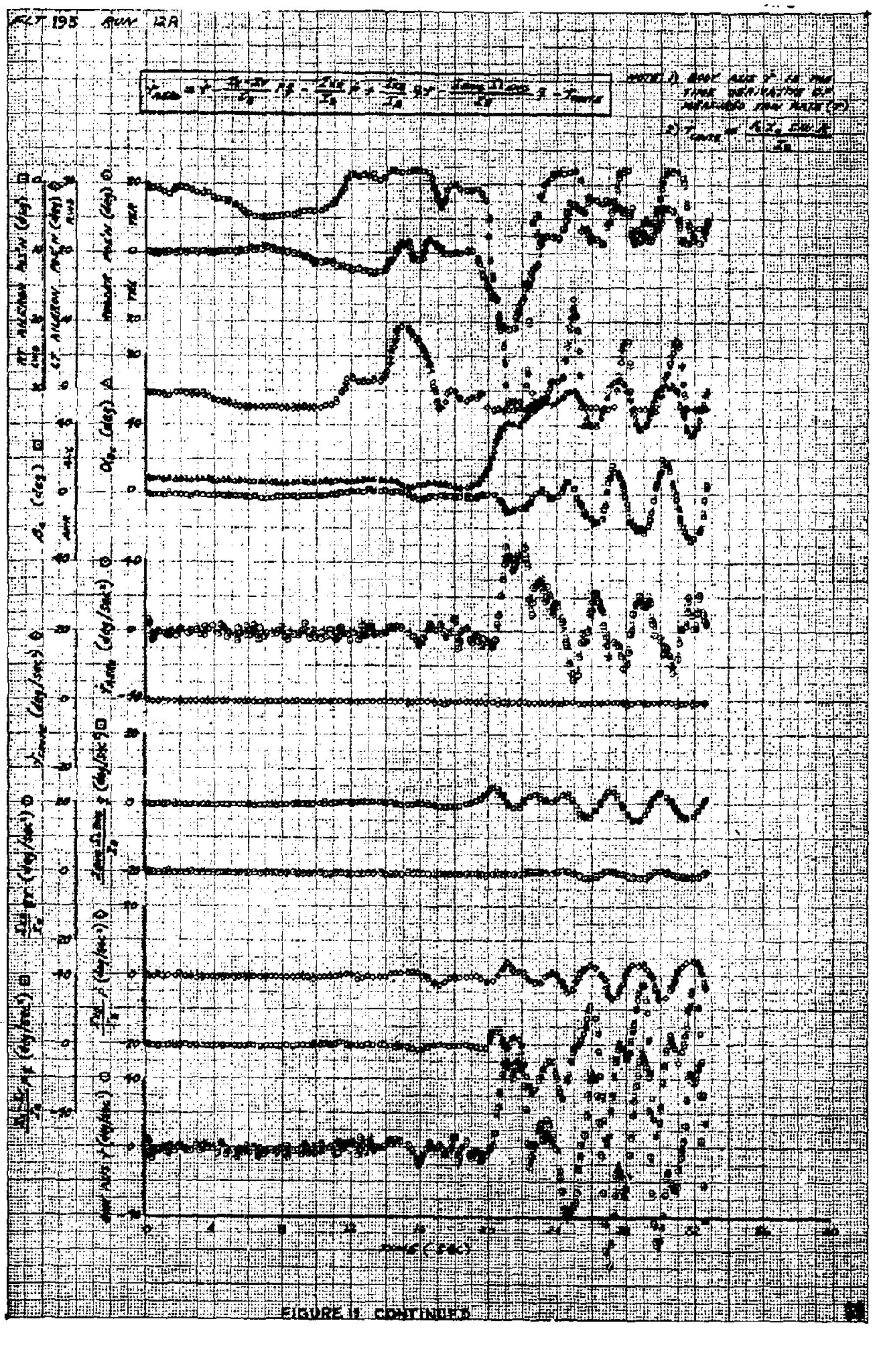

FIGURE 11 CONTINUED

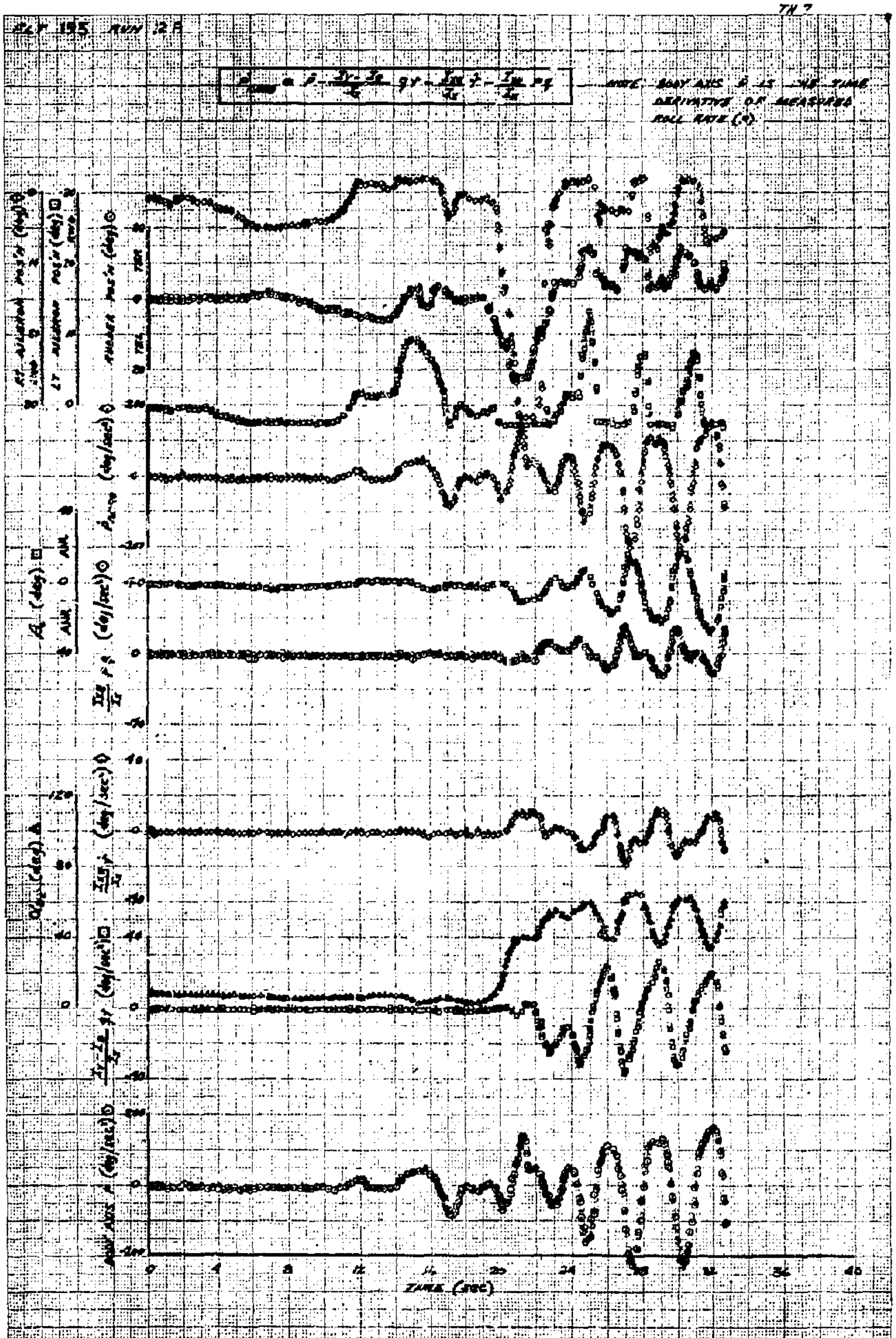

FIGURE 11 CONTINUED

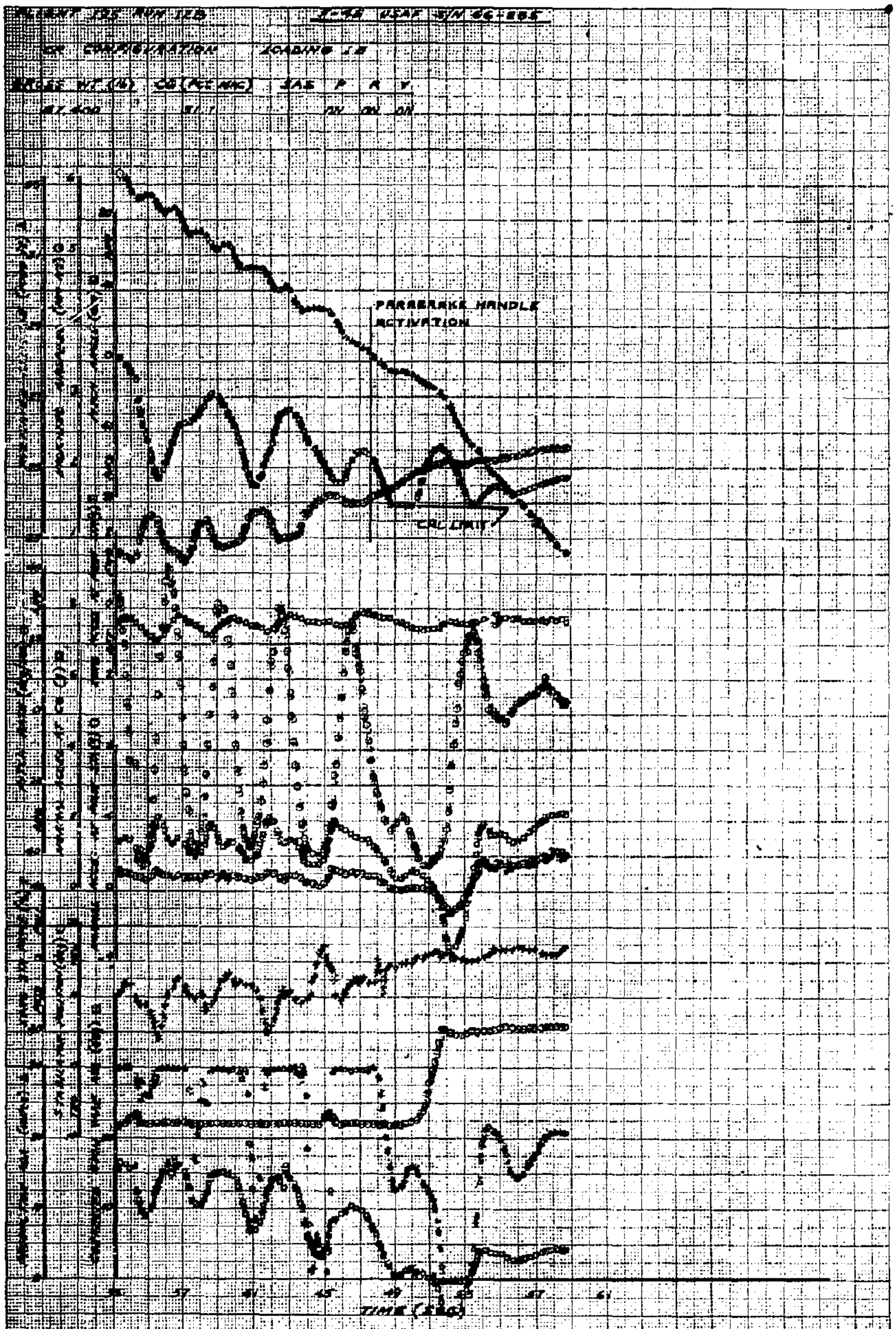

FIGURE 19 CONTINUED

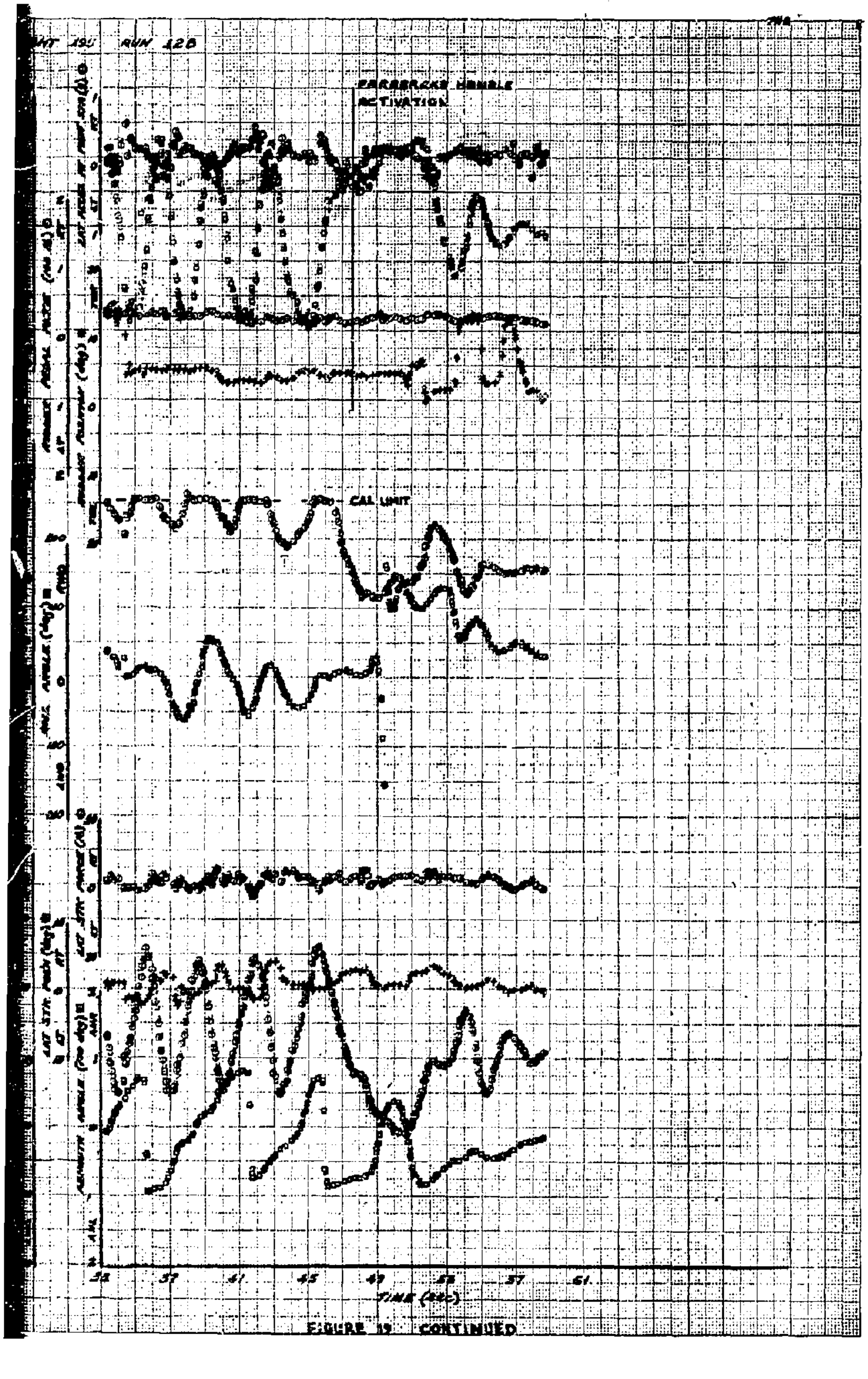

FIGURE 19 CONTINUED

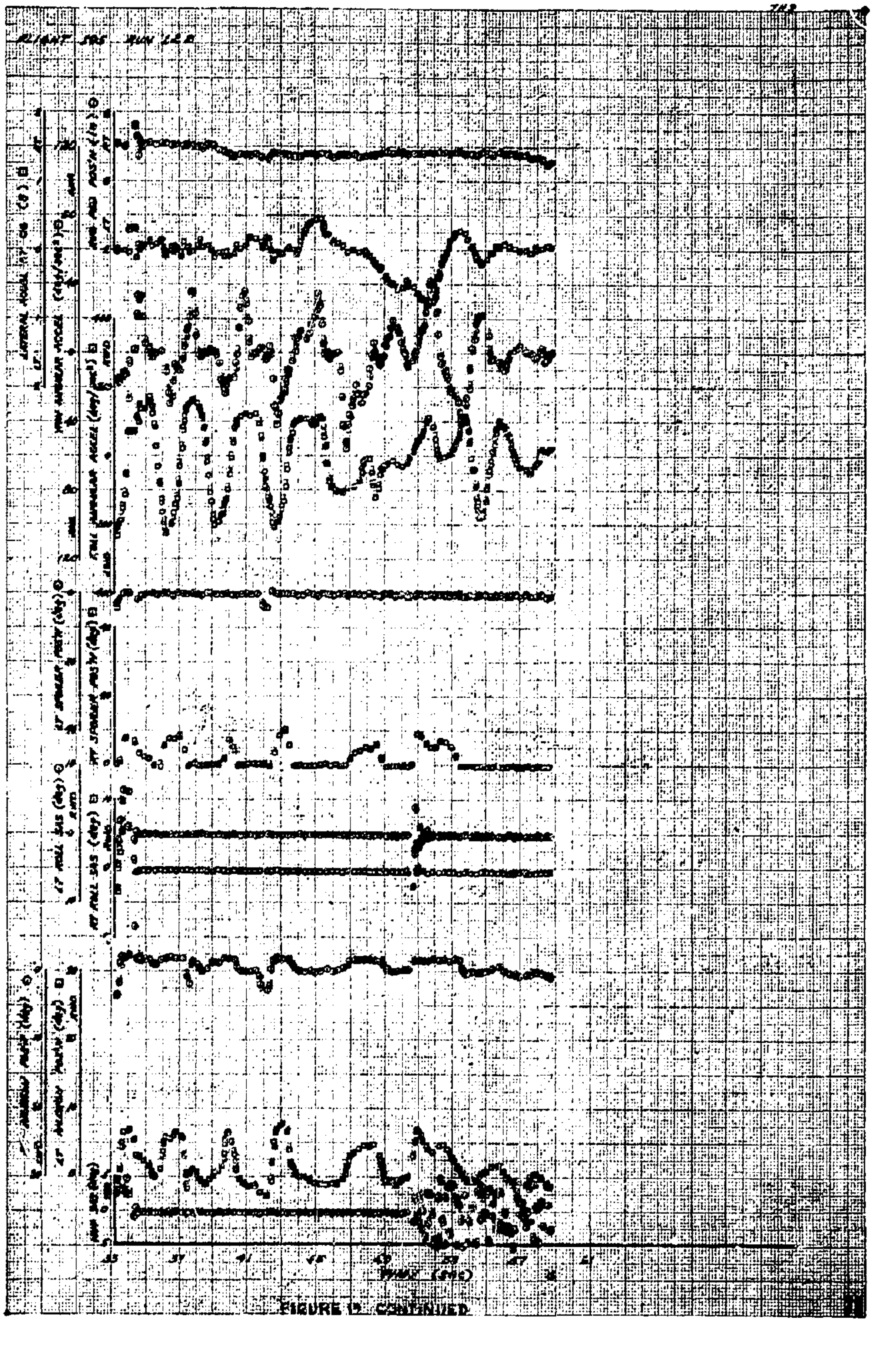

FIGURE [illegible] CONTINUED

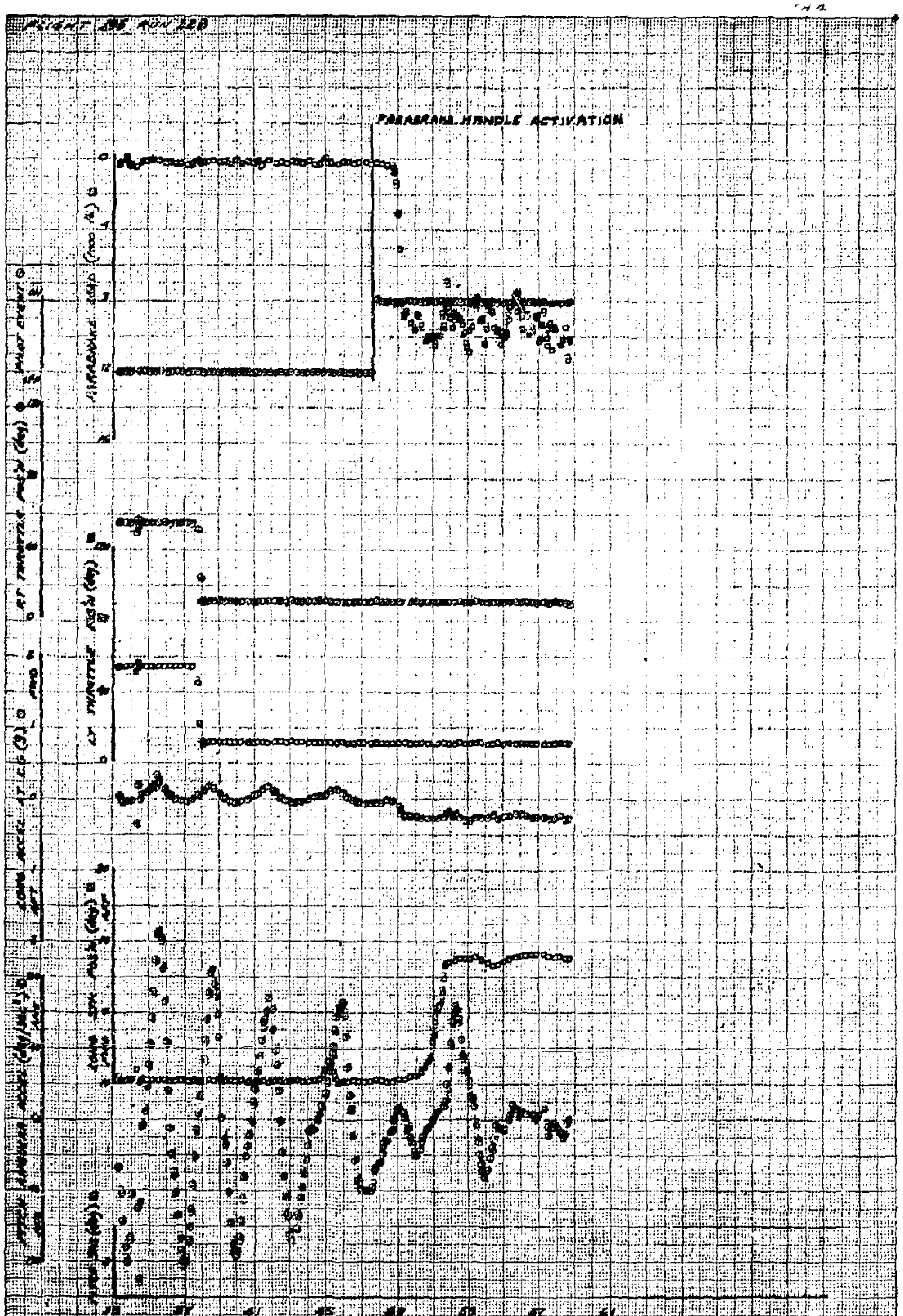

FIGURE 17 CONTINUED

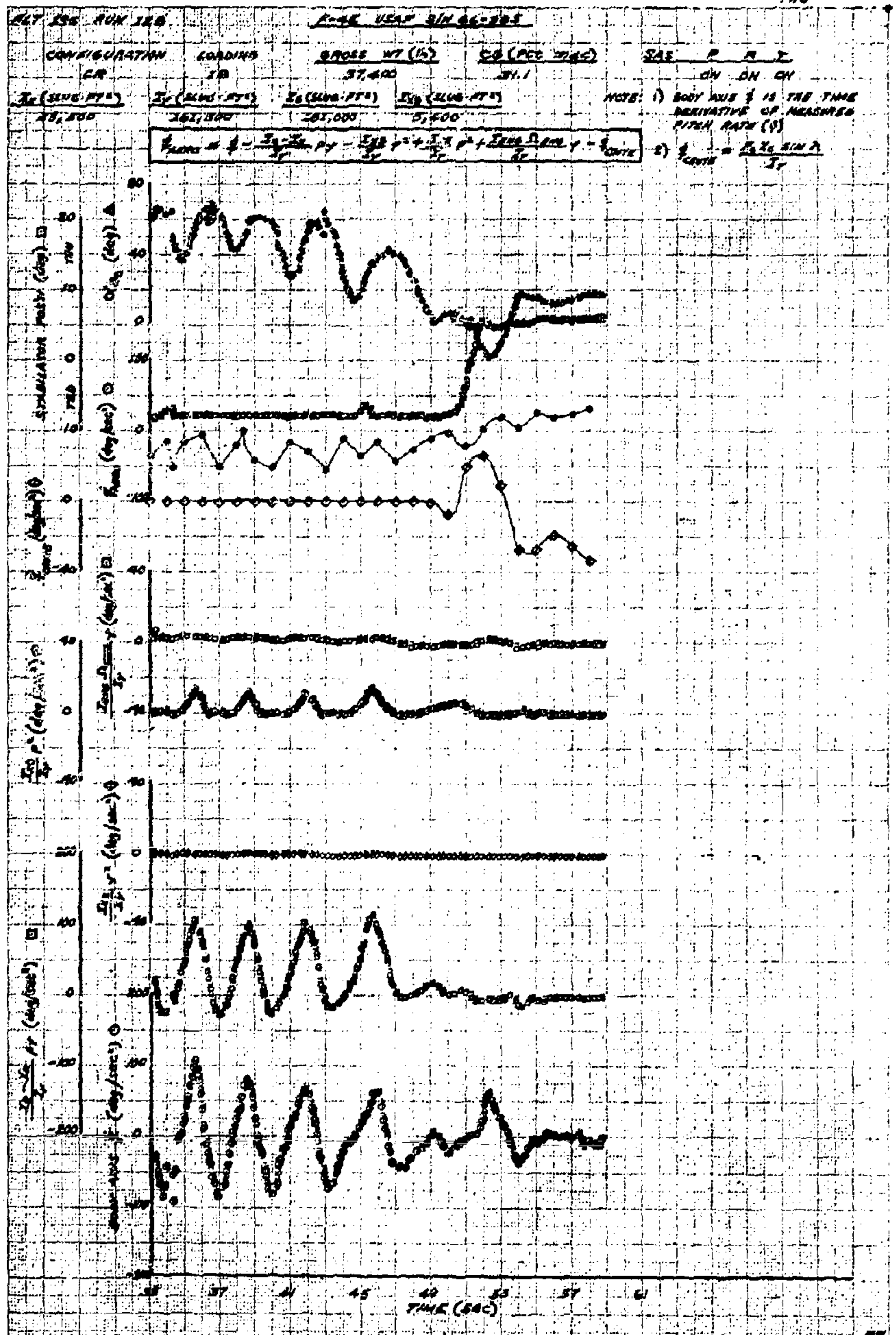

FIGURE 19 CONTINUED

7H6

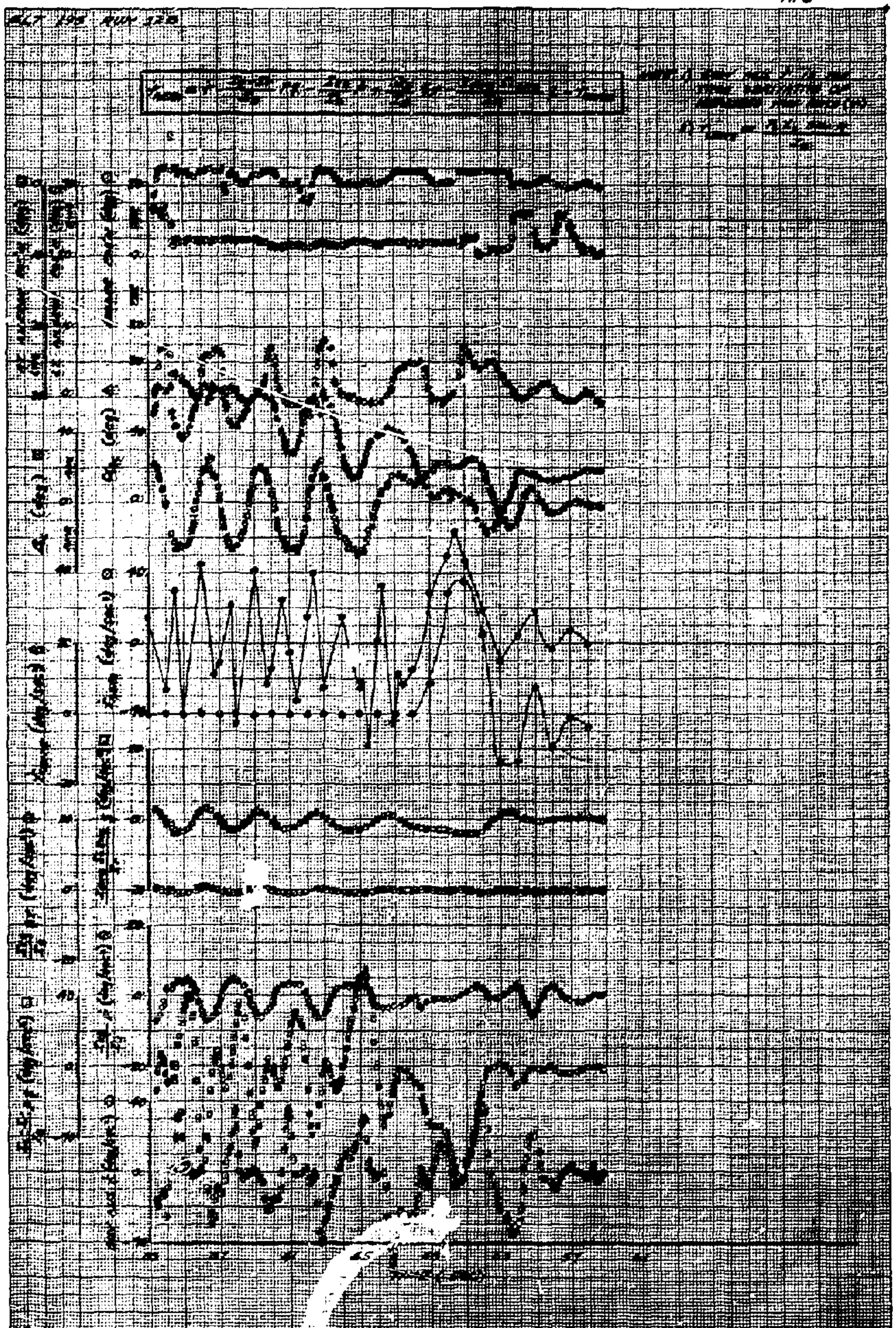

FIGURE 17. CONTINUED

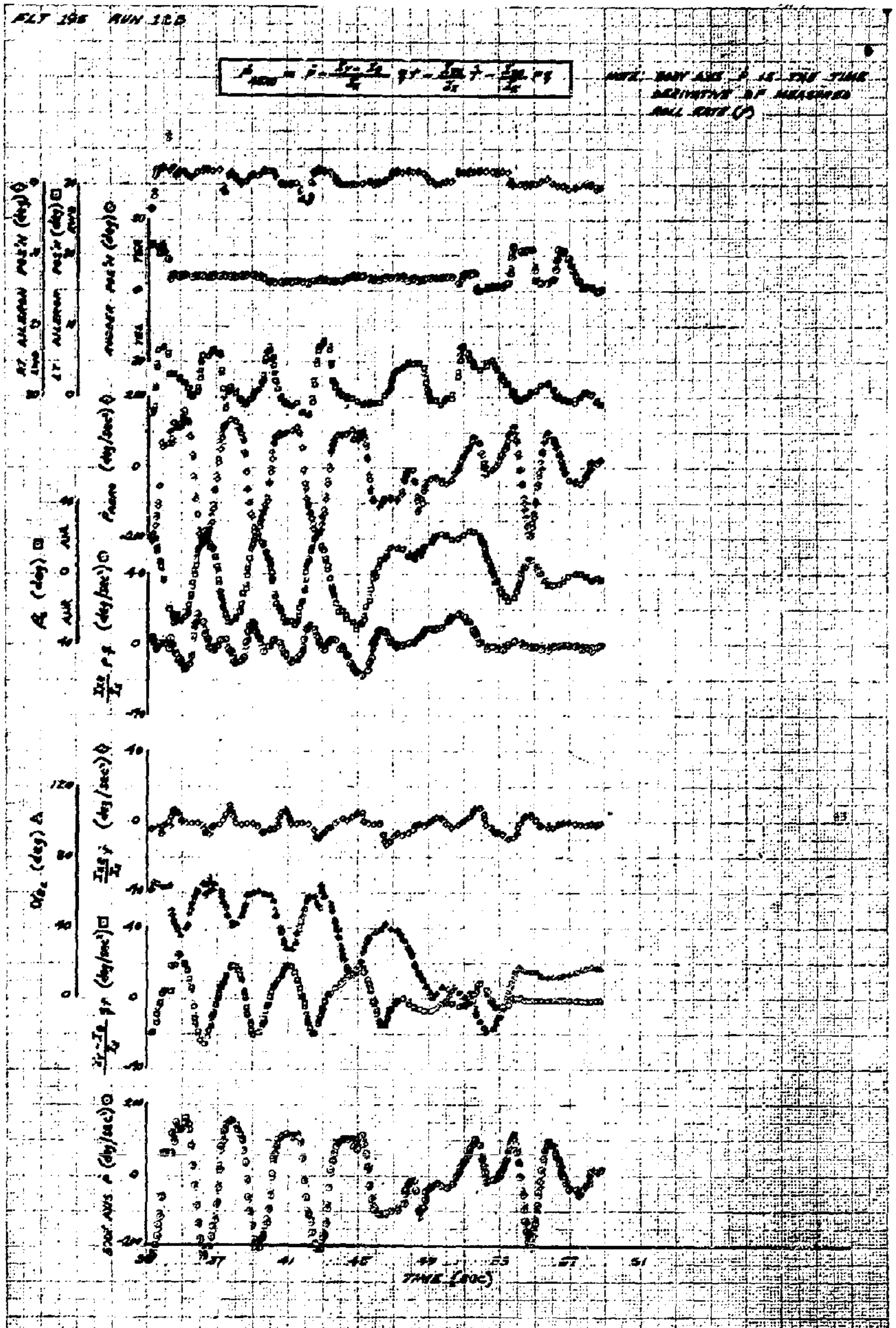

FIGURE 19 CONTINUED

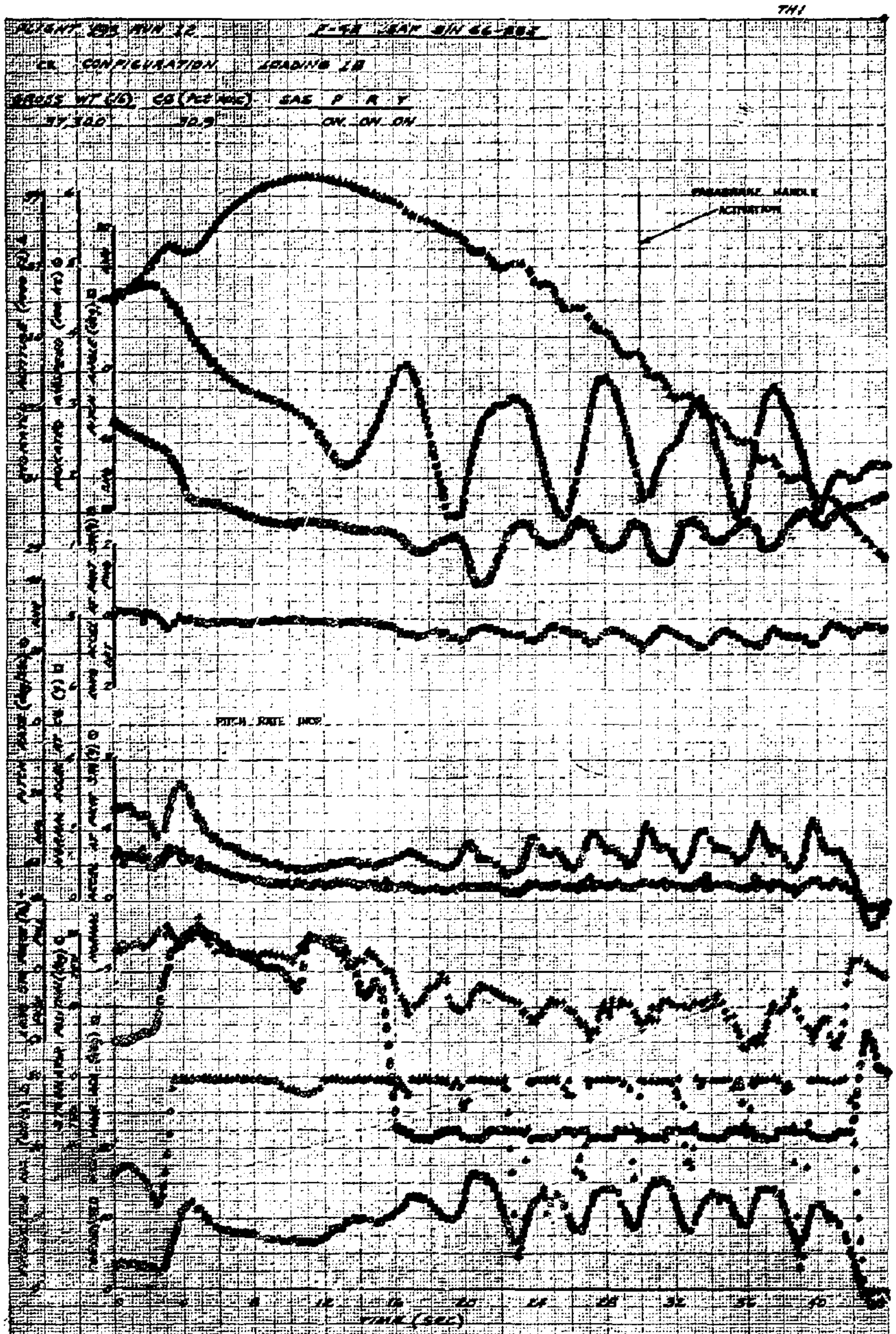

FIGURE 20 5 TURN STEEP-MILDLY OSCILLATORY SPIN FROM ACM ENTRY

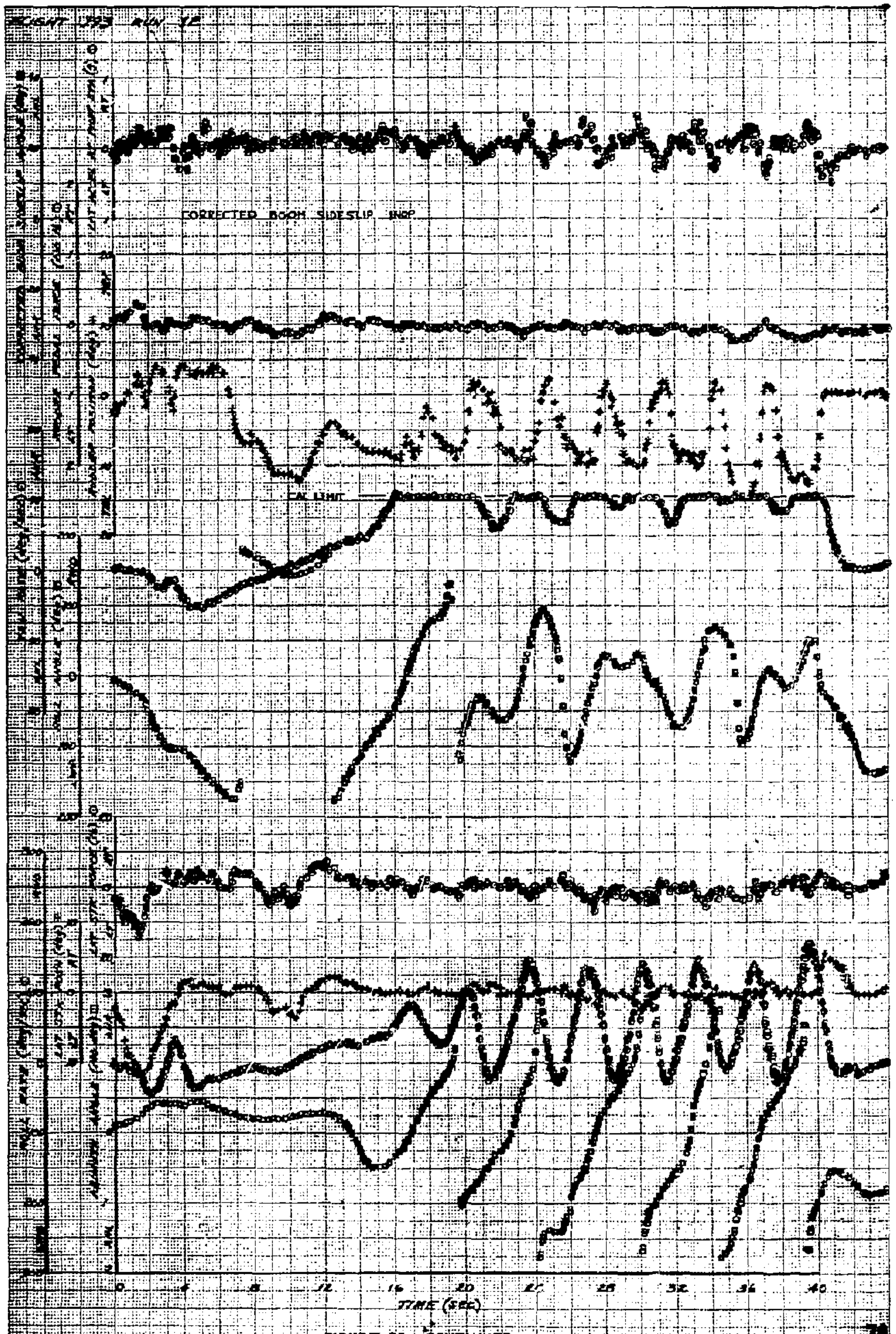

FIGURE 20 CONTINUED

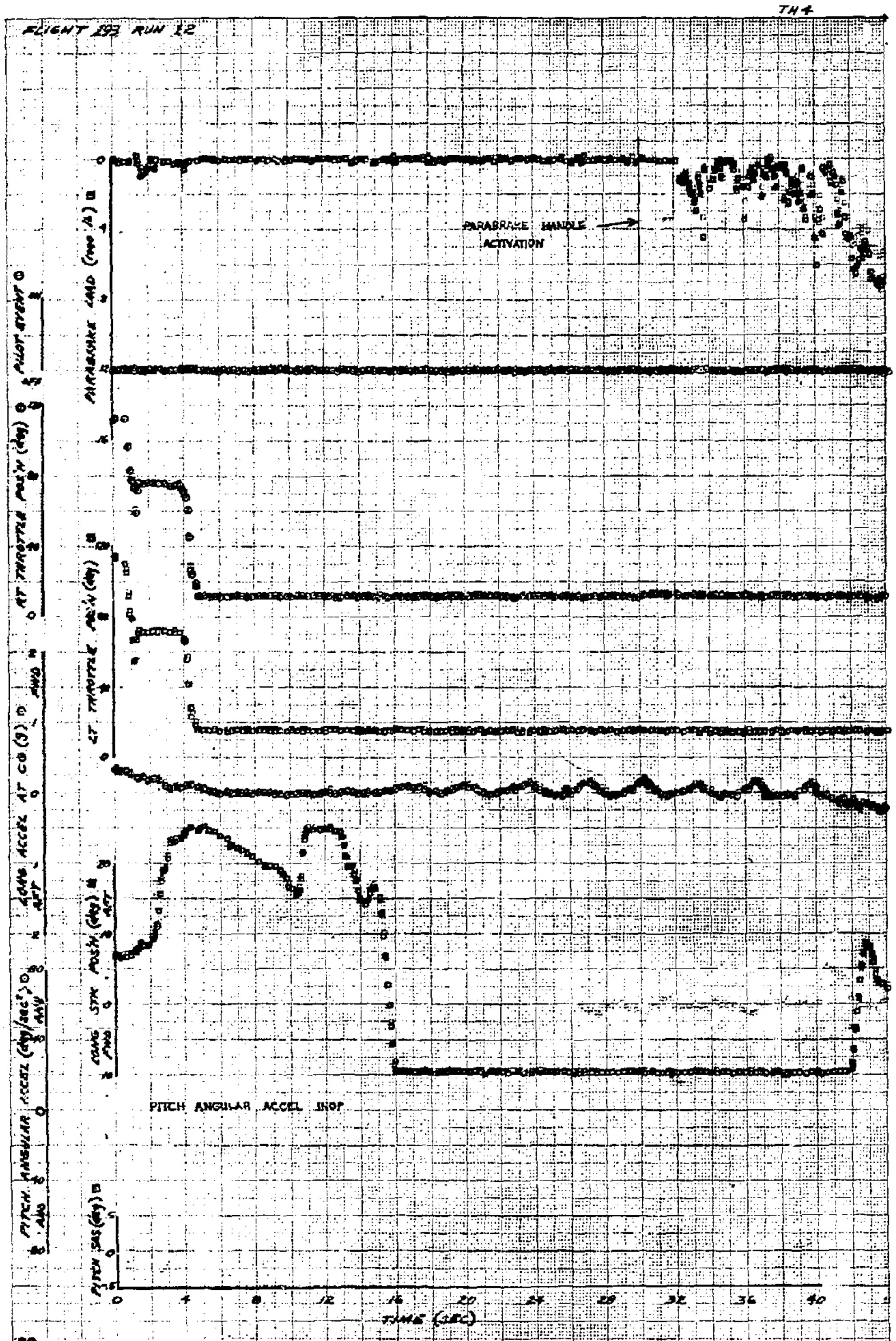

FIGURE 12 CONTINUED

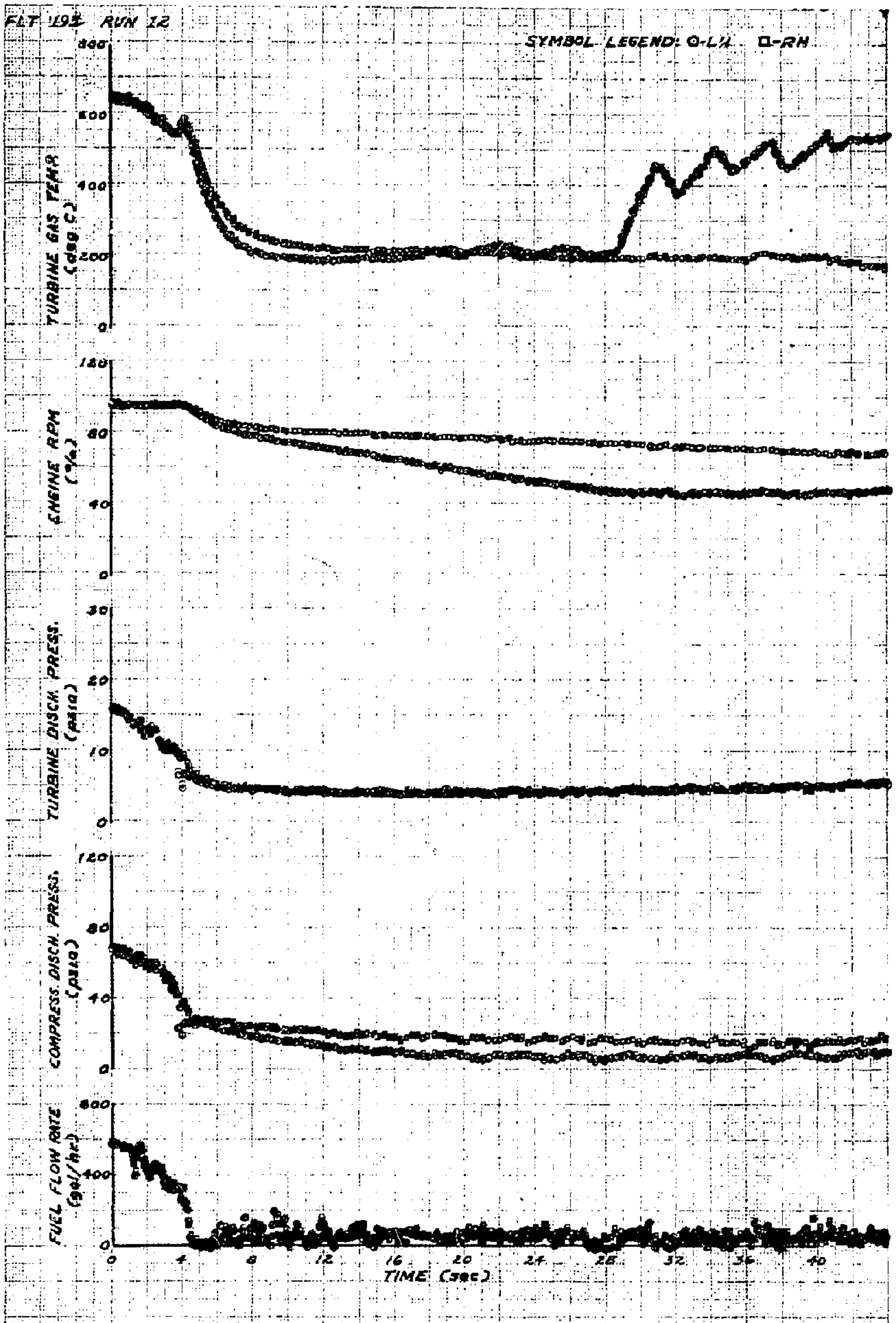

FIGURE 20 CONTINUED

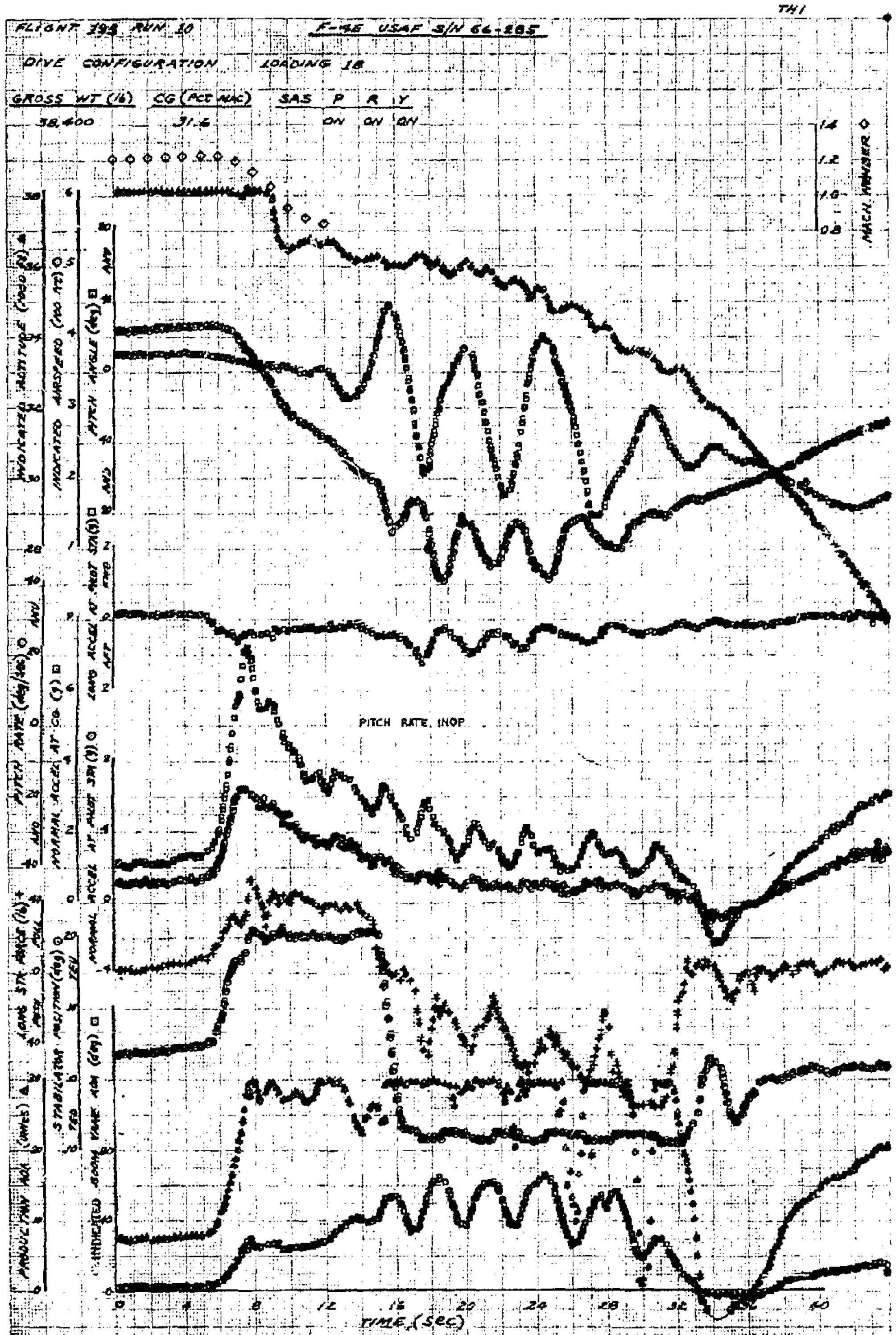

FIGURE 21 2 TURN STEEP MILDLY OSCILLATORY SPIN FROM TRANSONIC DECELERATION

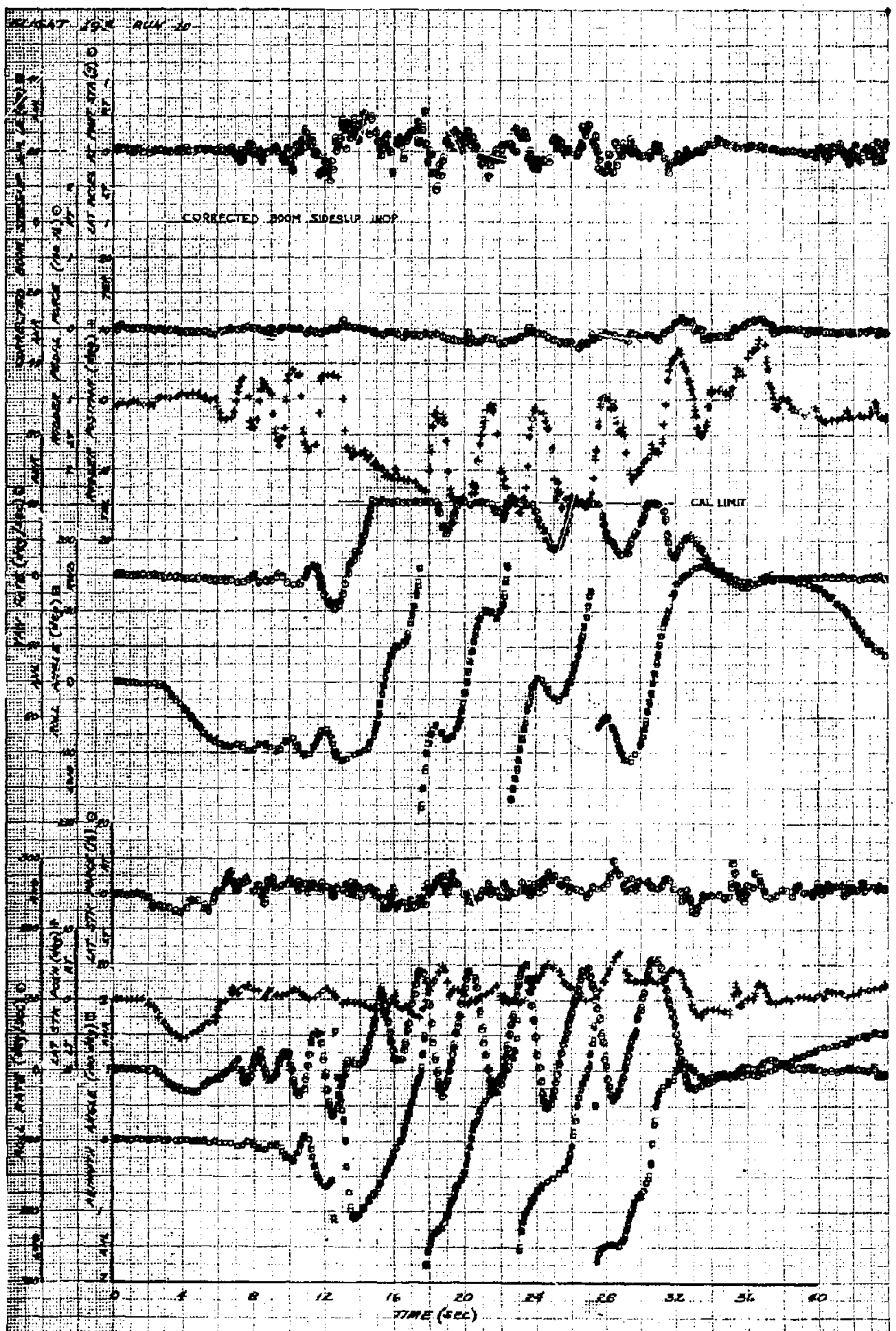

FIGURE 21 CONTINUED

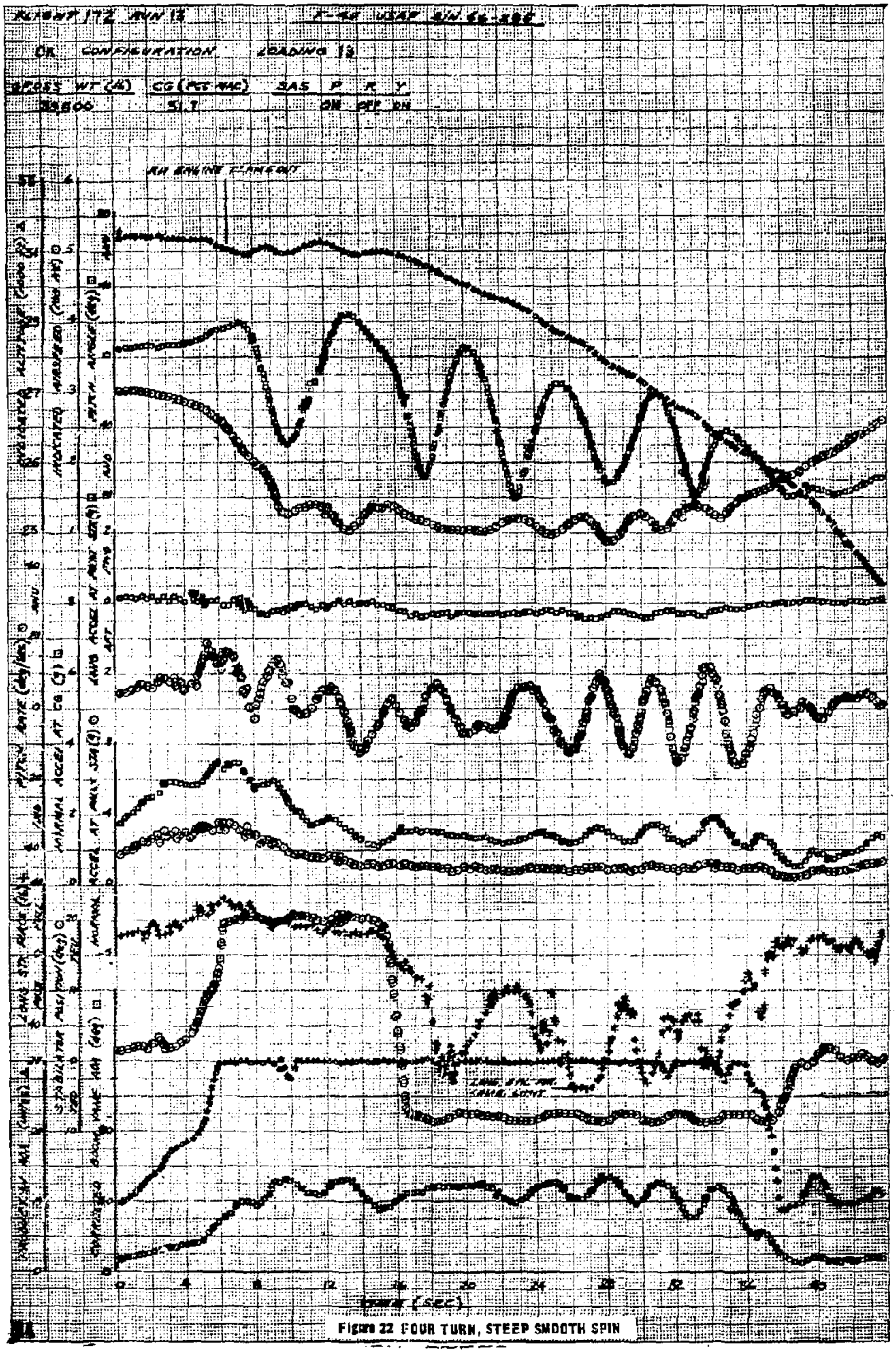

Figure 22 FOUR TURN, STEEP SMOOTH SPIN

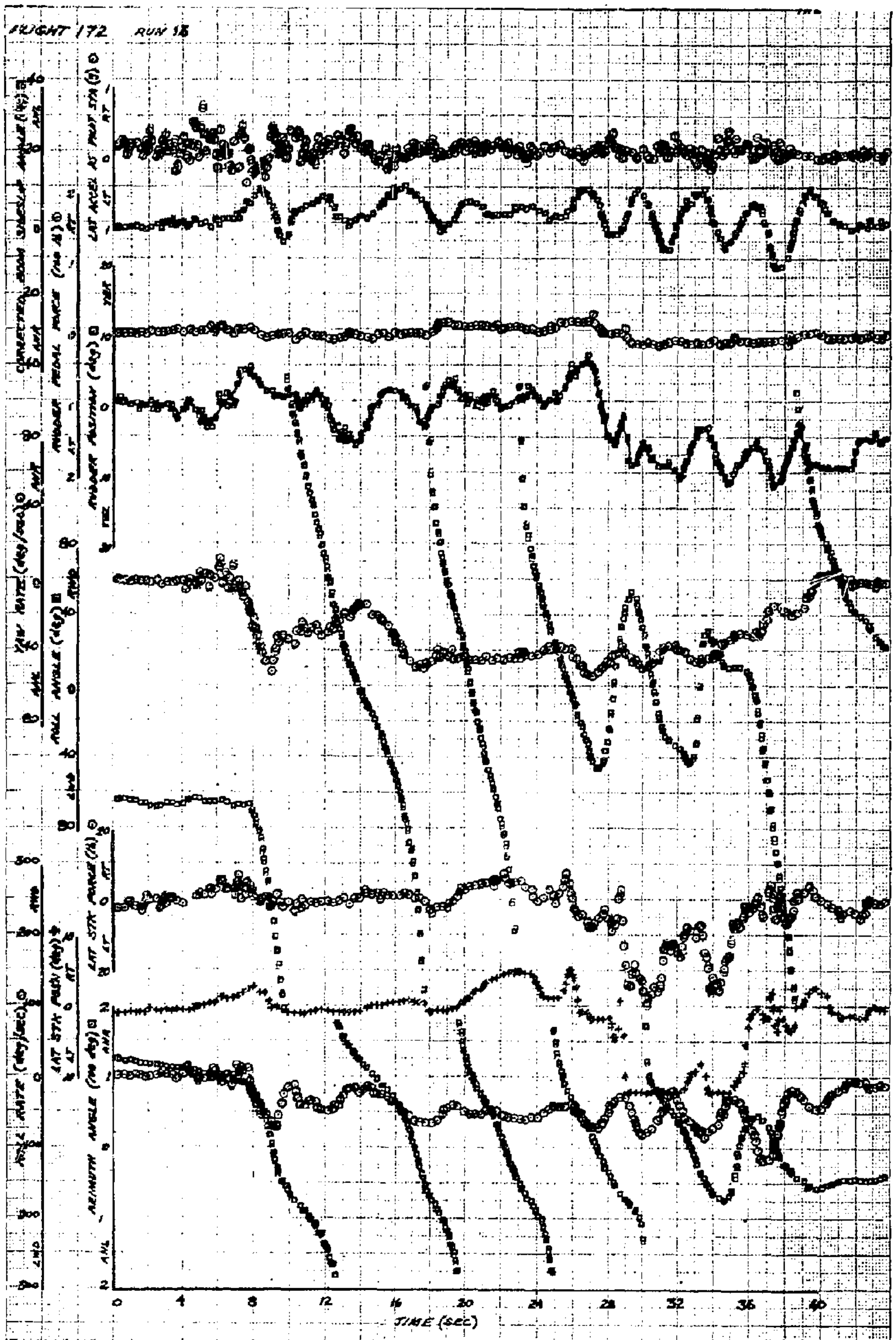

Figure 22 CONTINUED

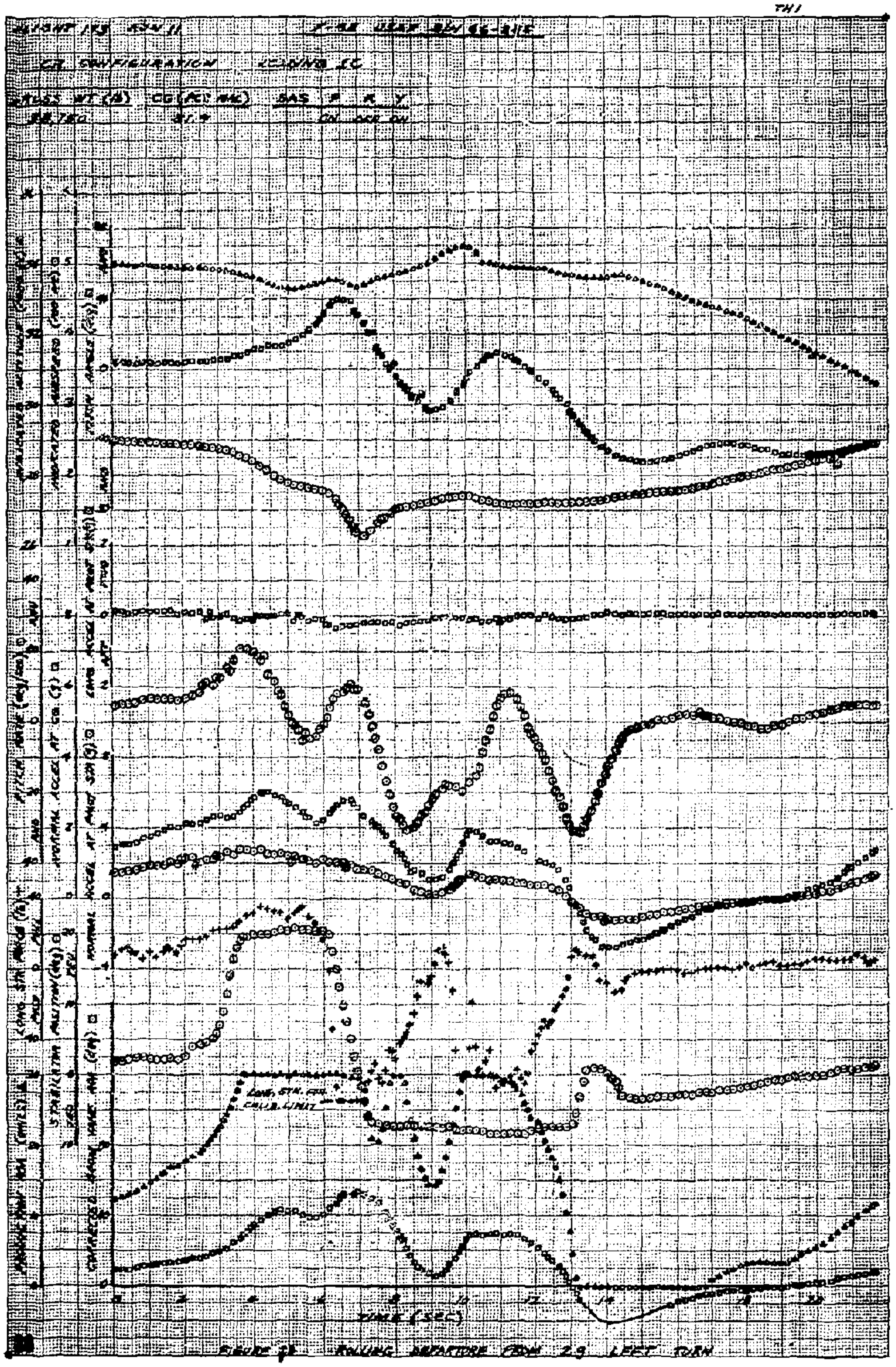

FIGURE [illegible] ROLLING DEPARTURE FROM 2.9 LEFT TURN

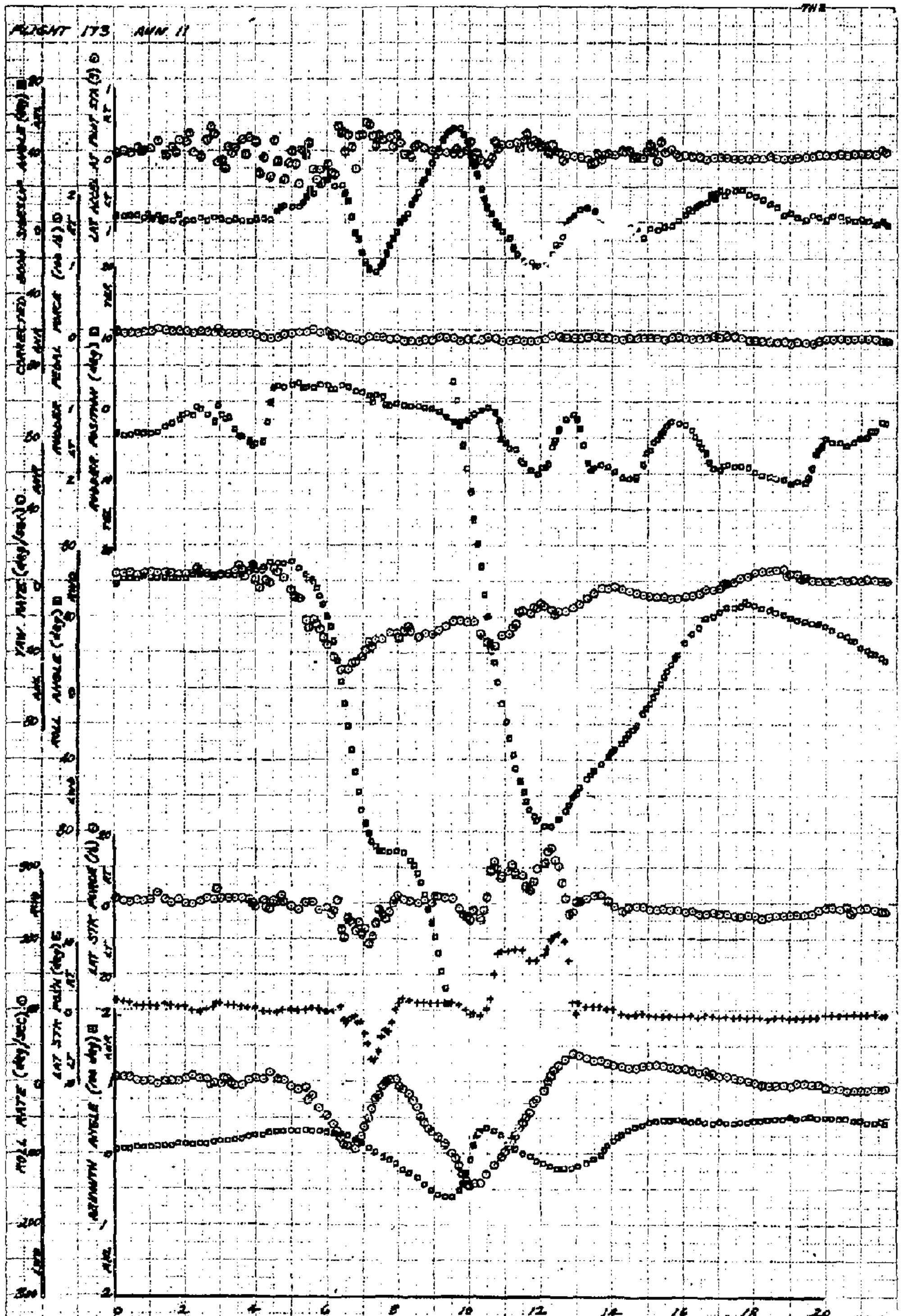

FIGURE 23 CONTINUED

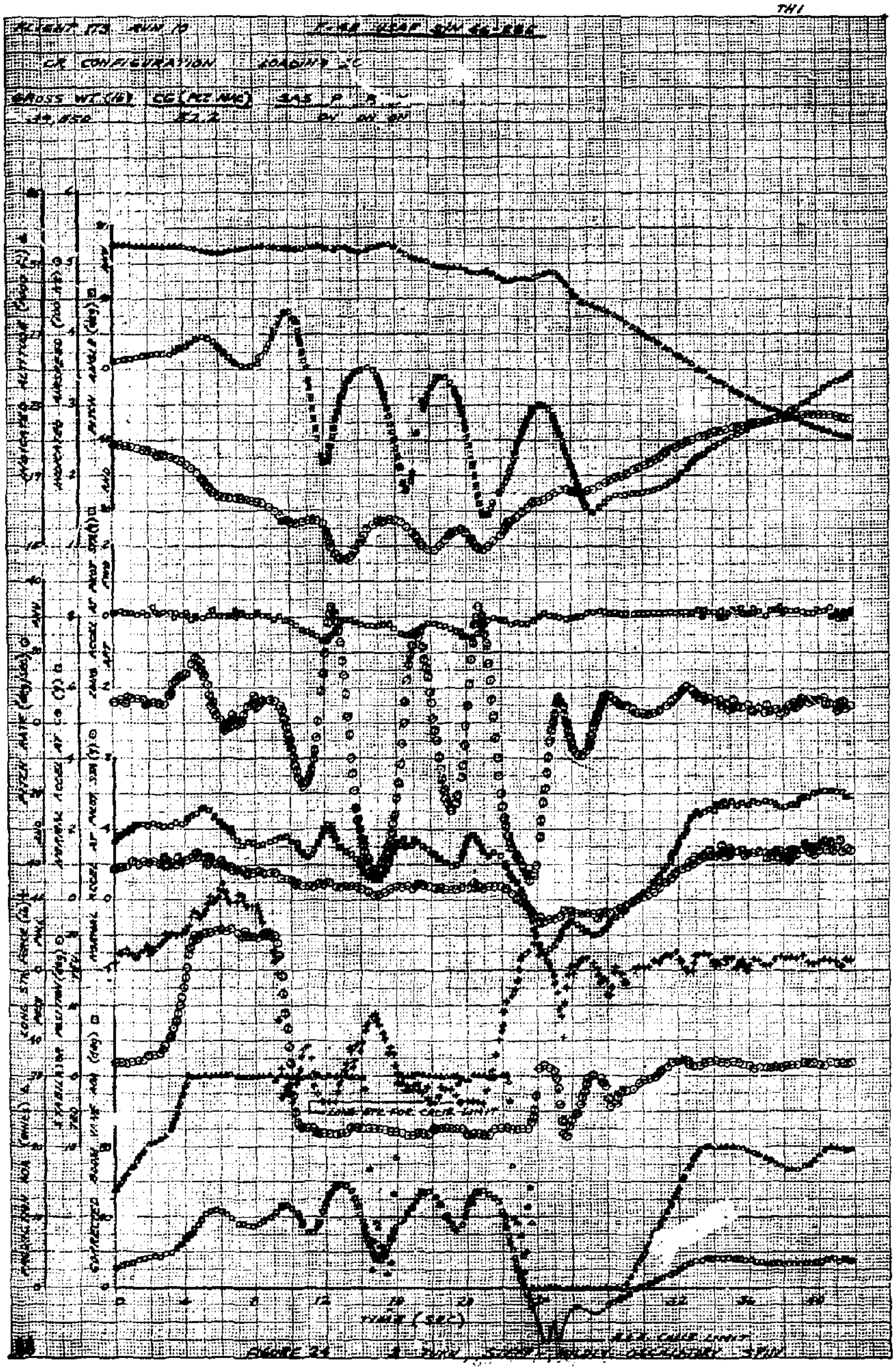
THI
CR CONFIGURATION
GROSS WT. (lb)
CG (PCT MAC)
SAS
32.2
TIME (SEC)
FIGURE 24

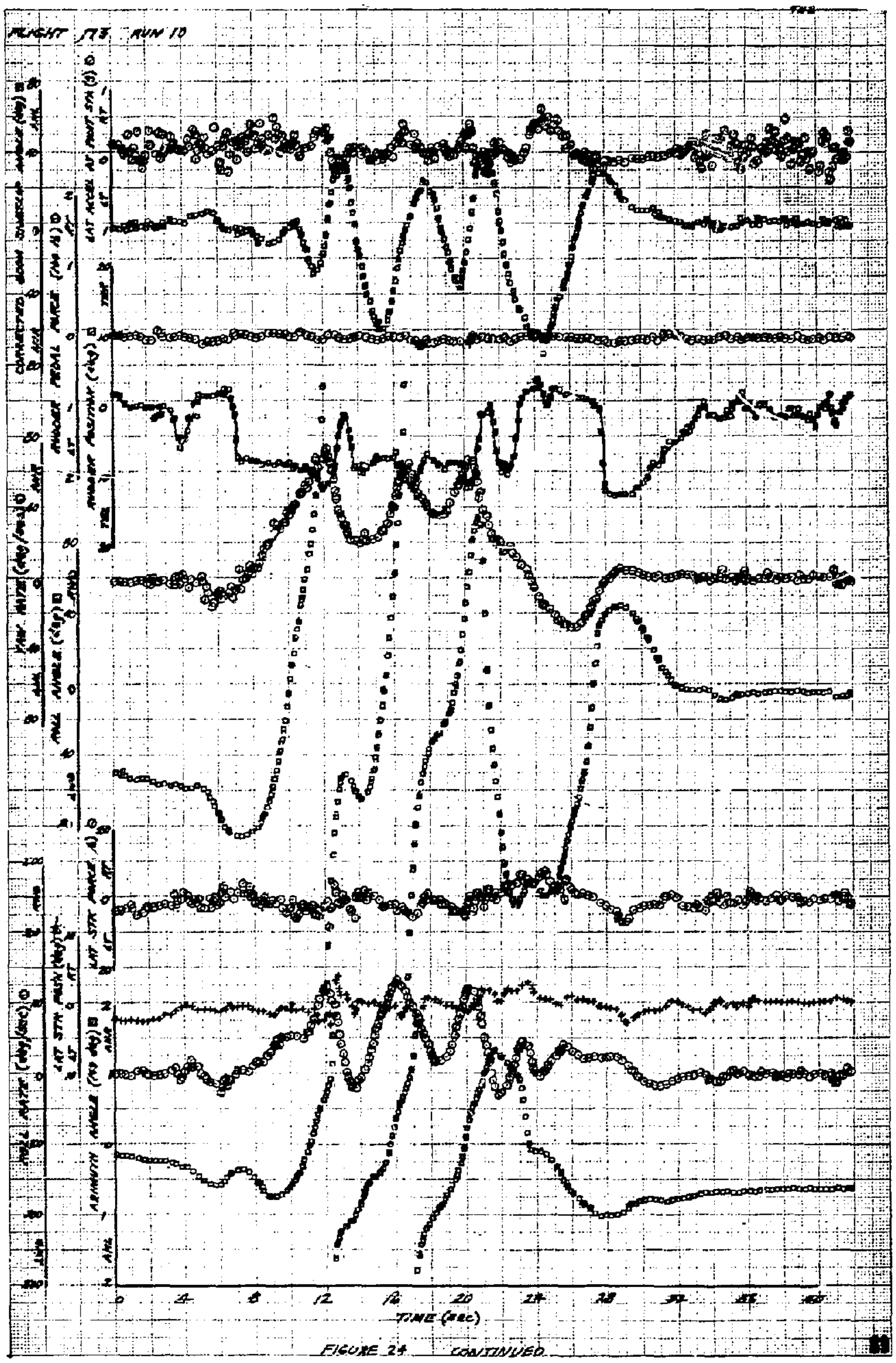

FIGURE 24 CONTINUED

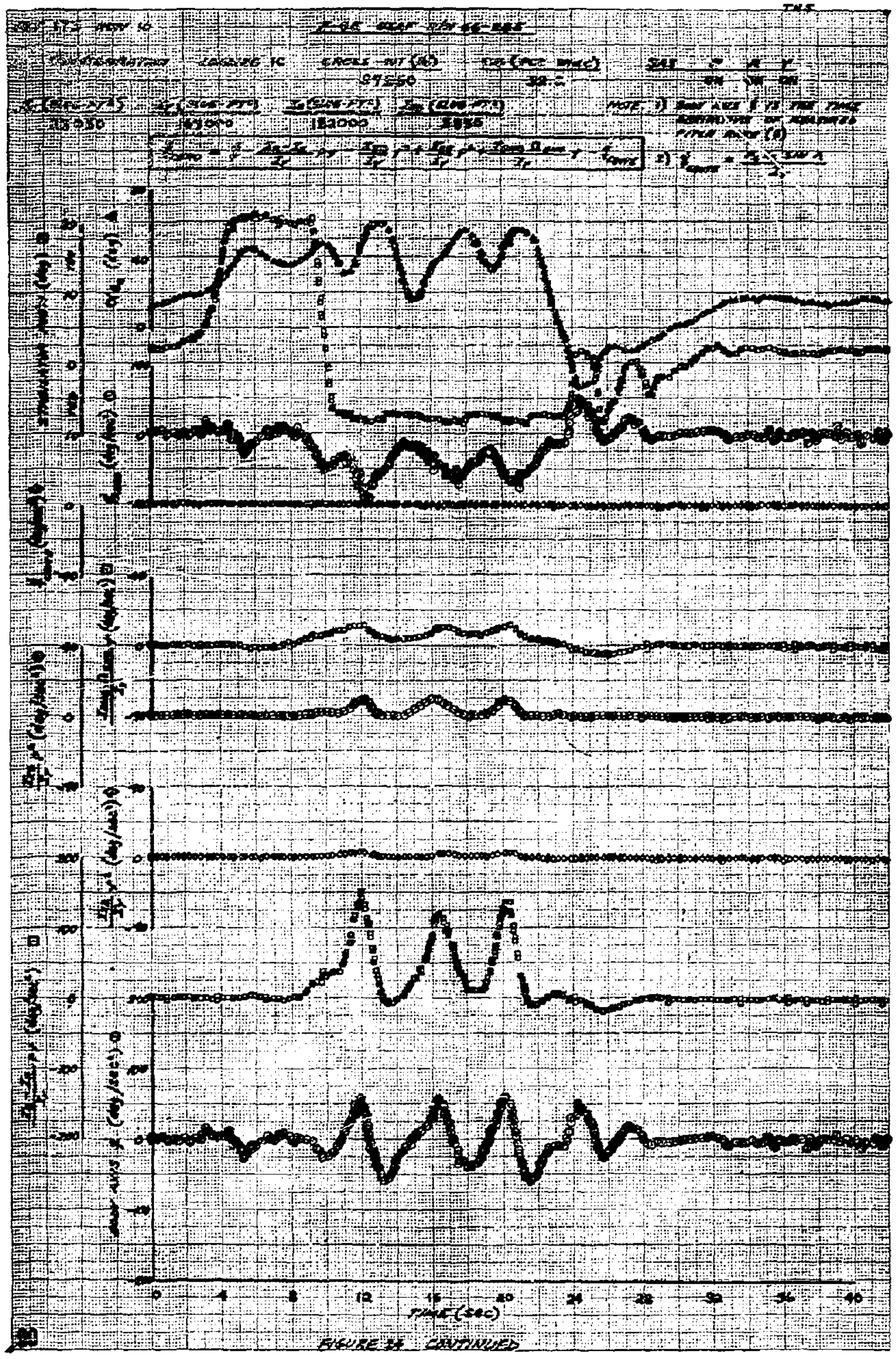

FIGURE 24 CONTINUED

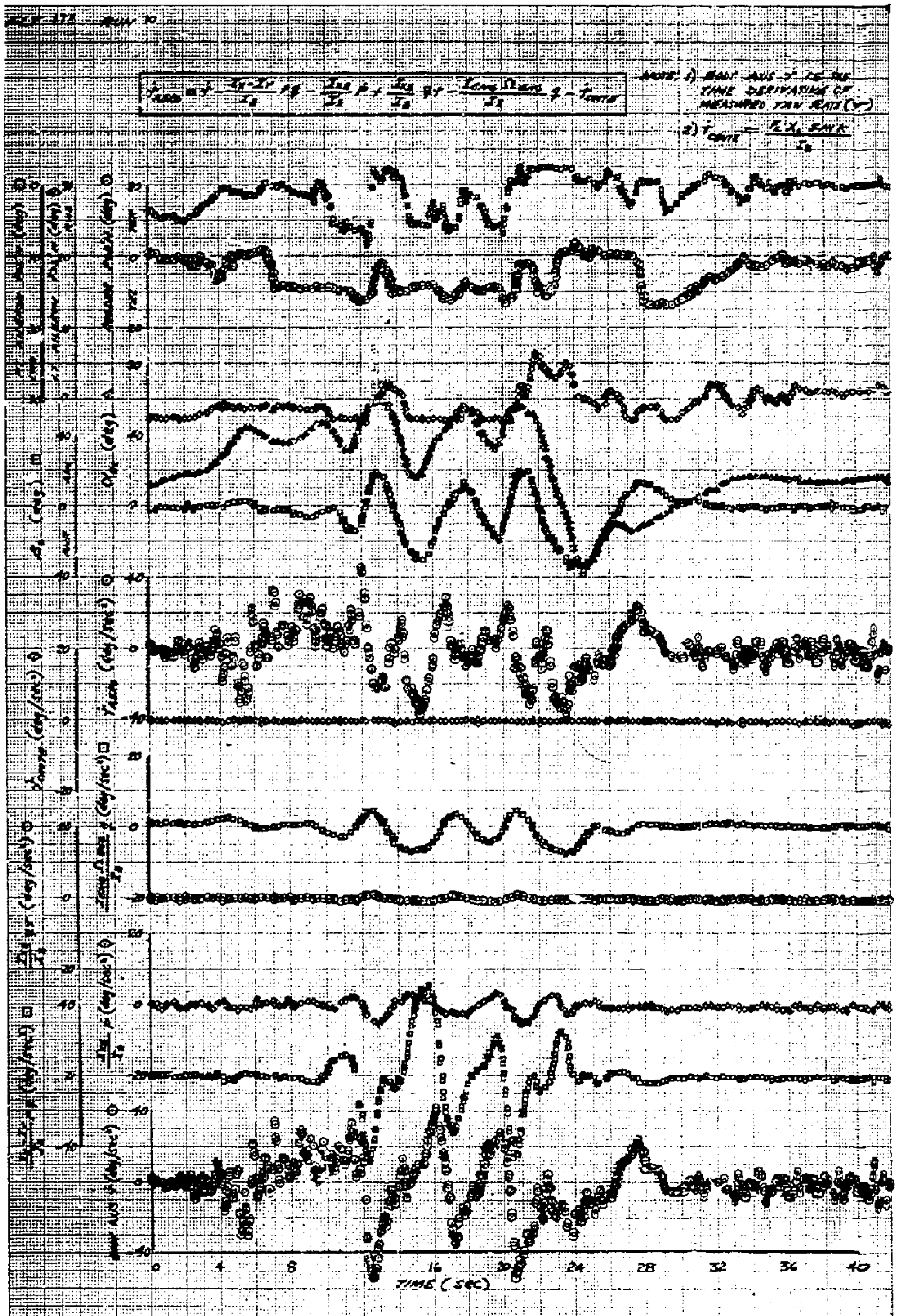

FIGURE 24 CONTINUED

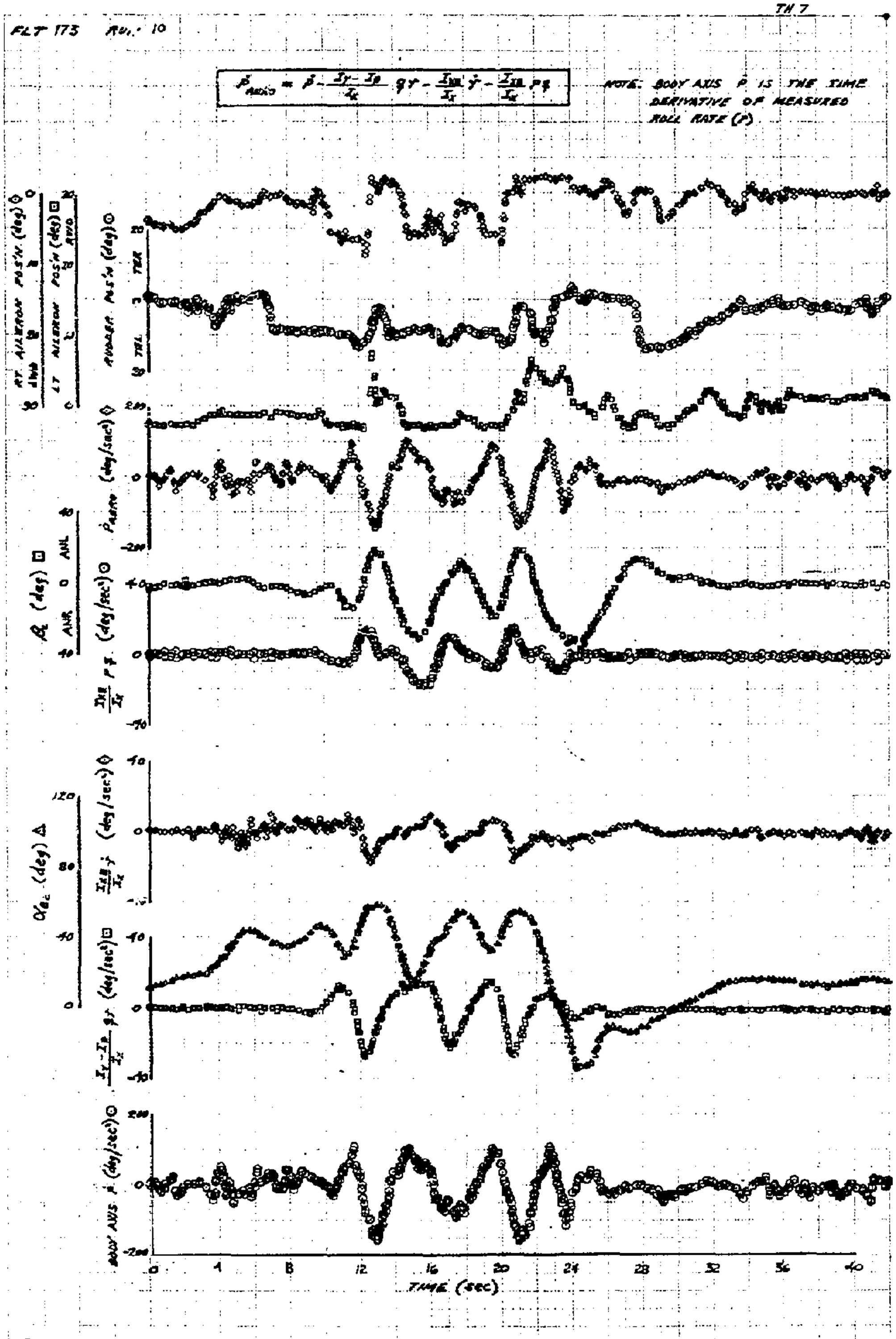

FIGURE 24 CONTINUED

THIS PAGE LEFT BLANK FOR PRESENTATION PURPOSES

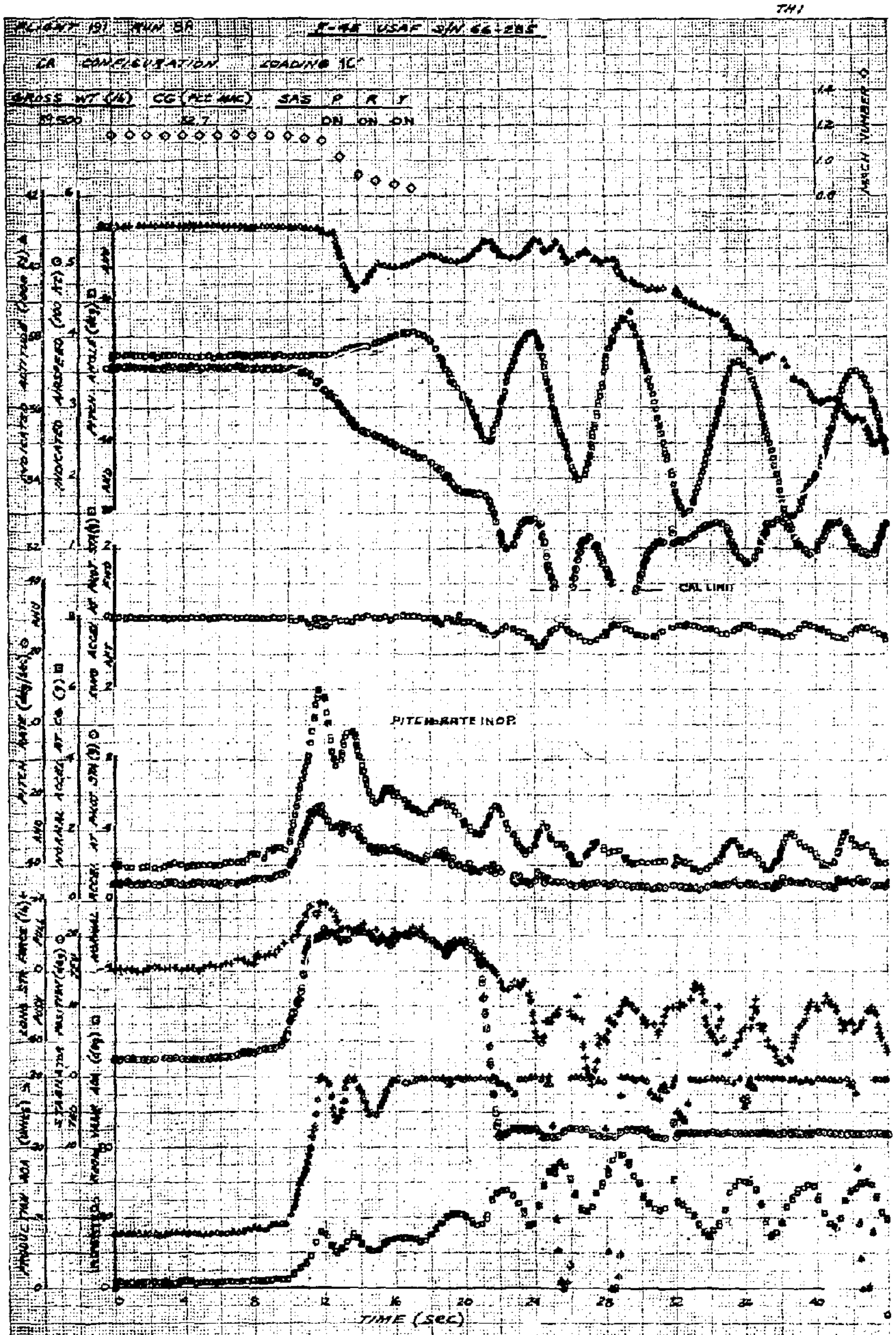

FIGURE 25 R TURN, STEEP-MILDLY OSCILLATORY SPIN, DRAG CHUTE DEPLOY

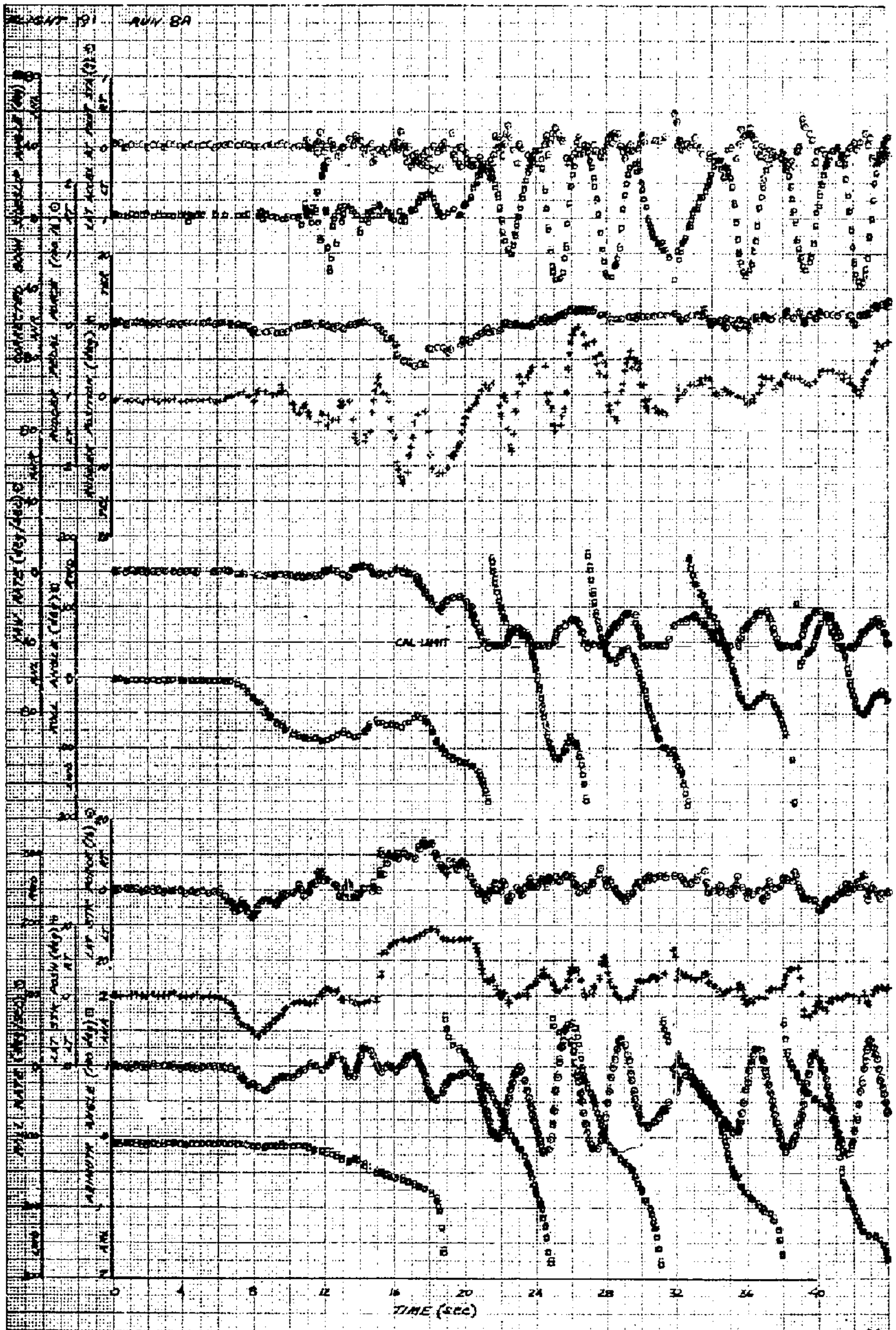

FIGURE 25 CONTINUED

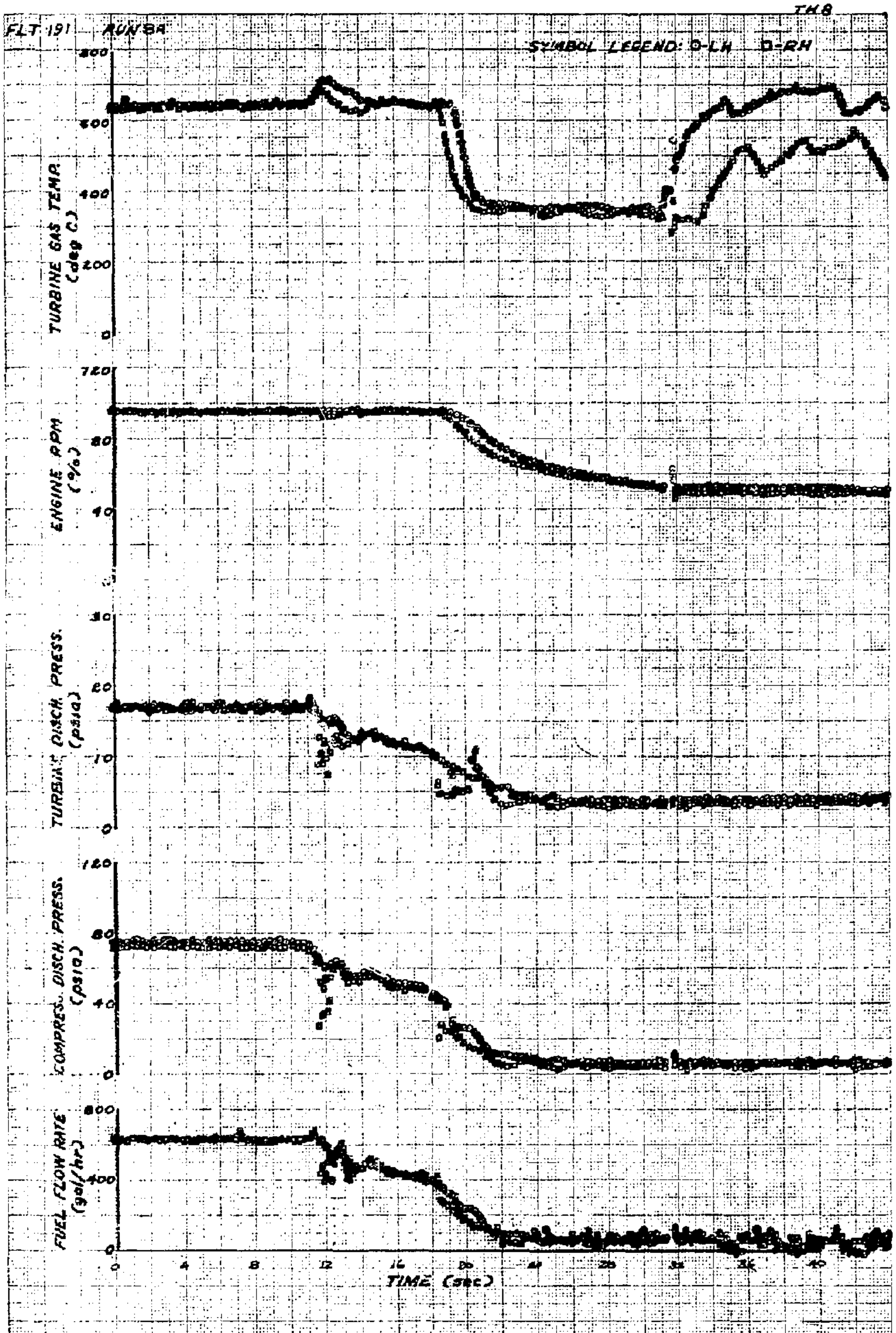

FIGURE 25 CONTINUED

FLIGHT 191 RUN 88

F-4E USAF S/N 66-285

CR CONFIGURATION LOADING 1C

GROSS WT (lb)	CG (PCT MAC)	SAS P R Y
39,500	32.7	ON ON ON

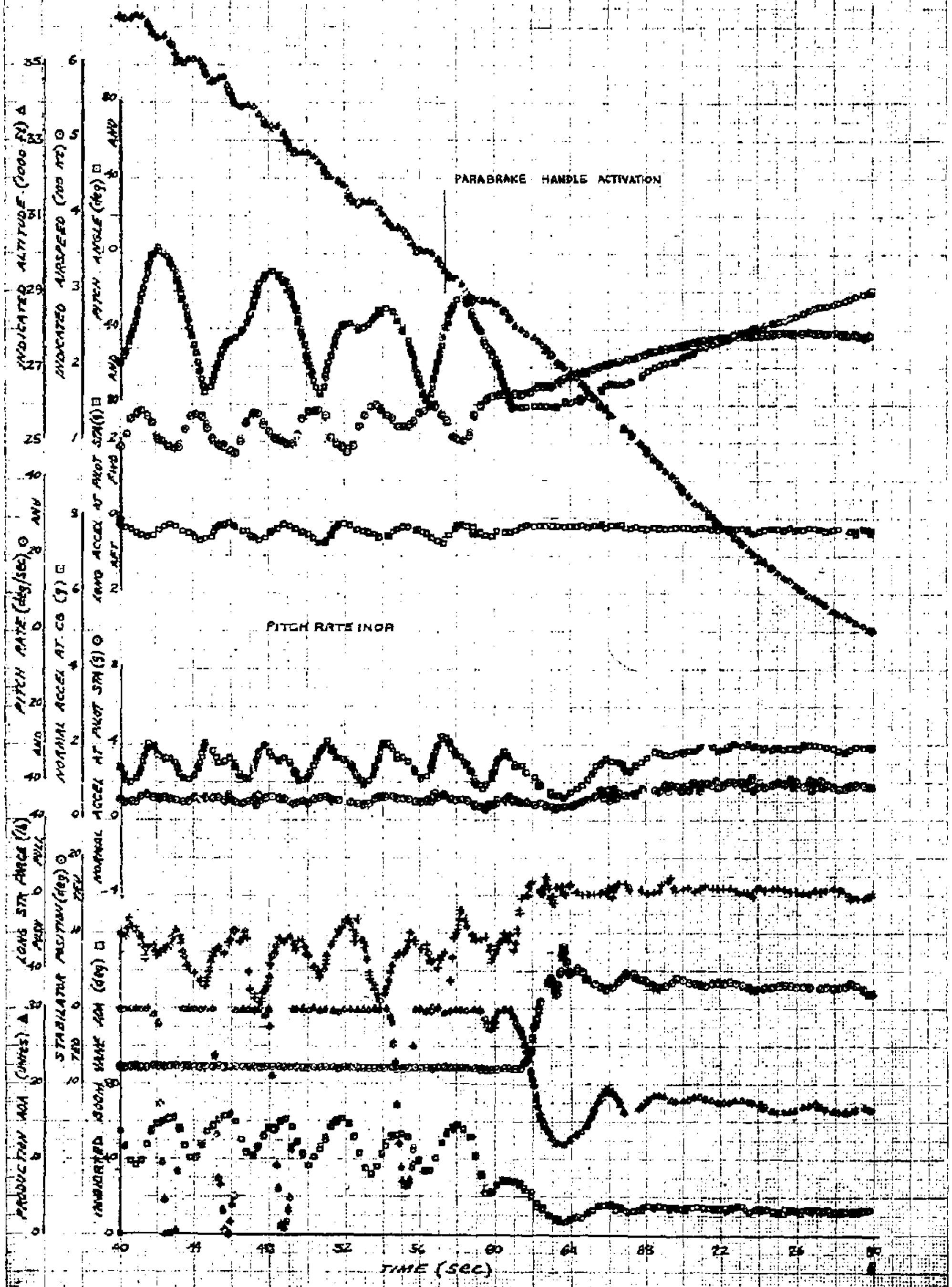

FIGURE 25 CONTINUED

TH2

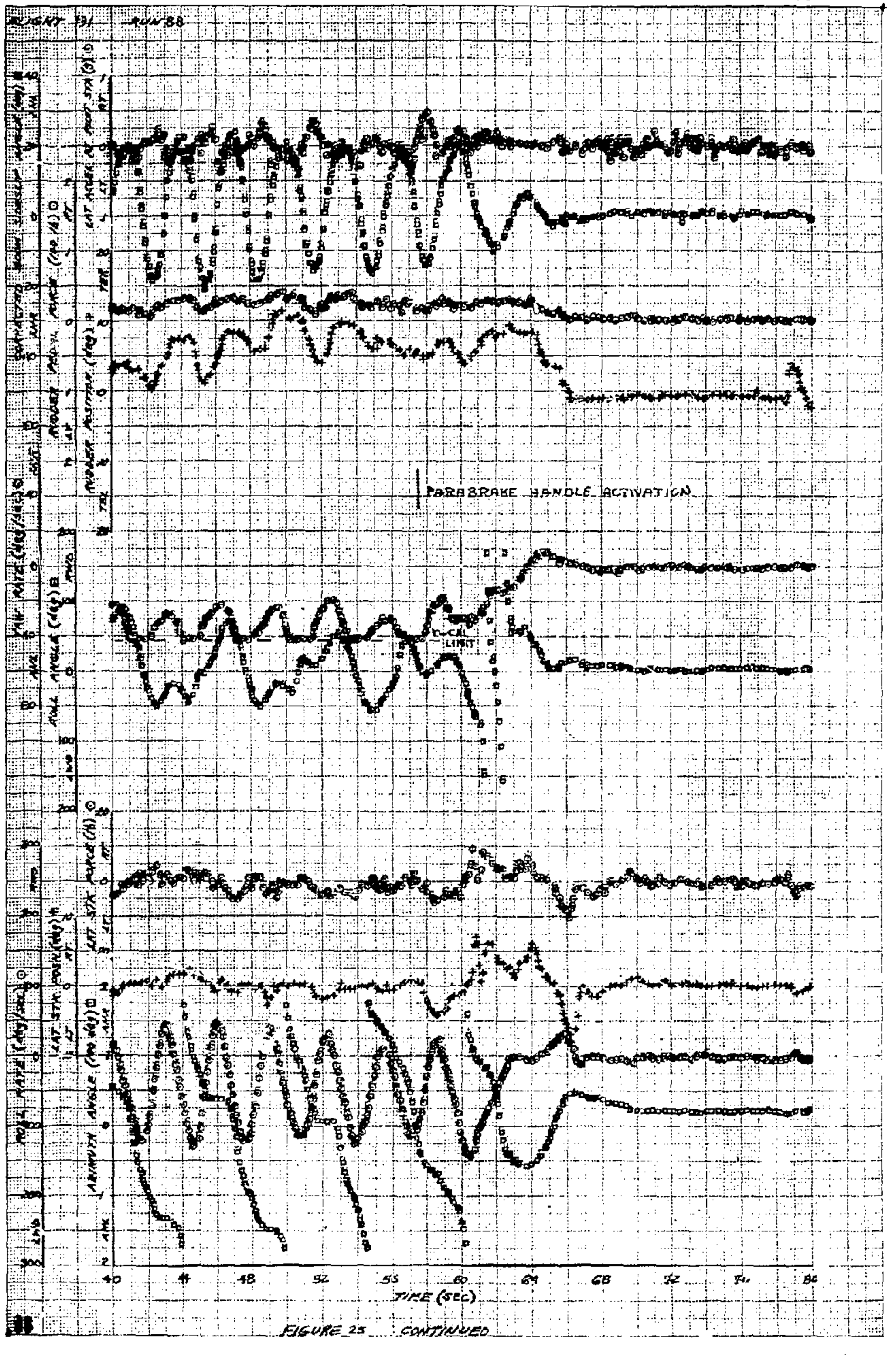

FIGURE 25 CONTINUED

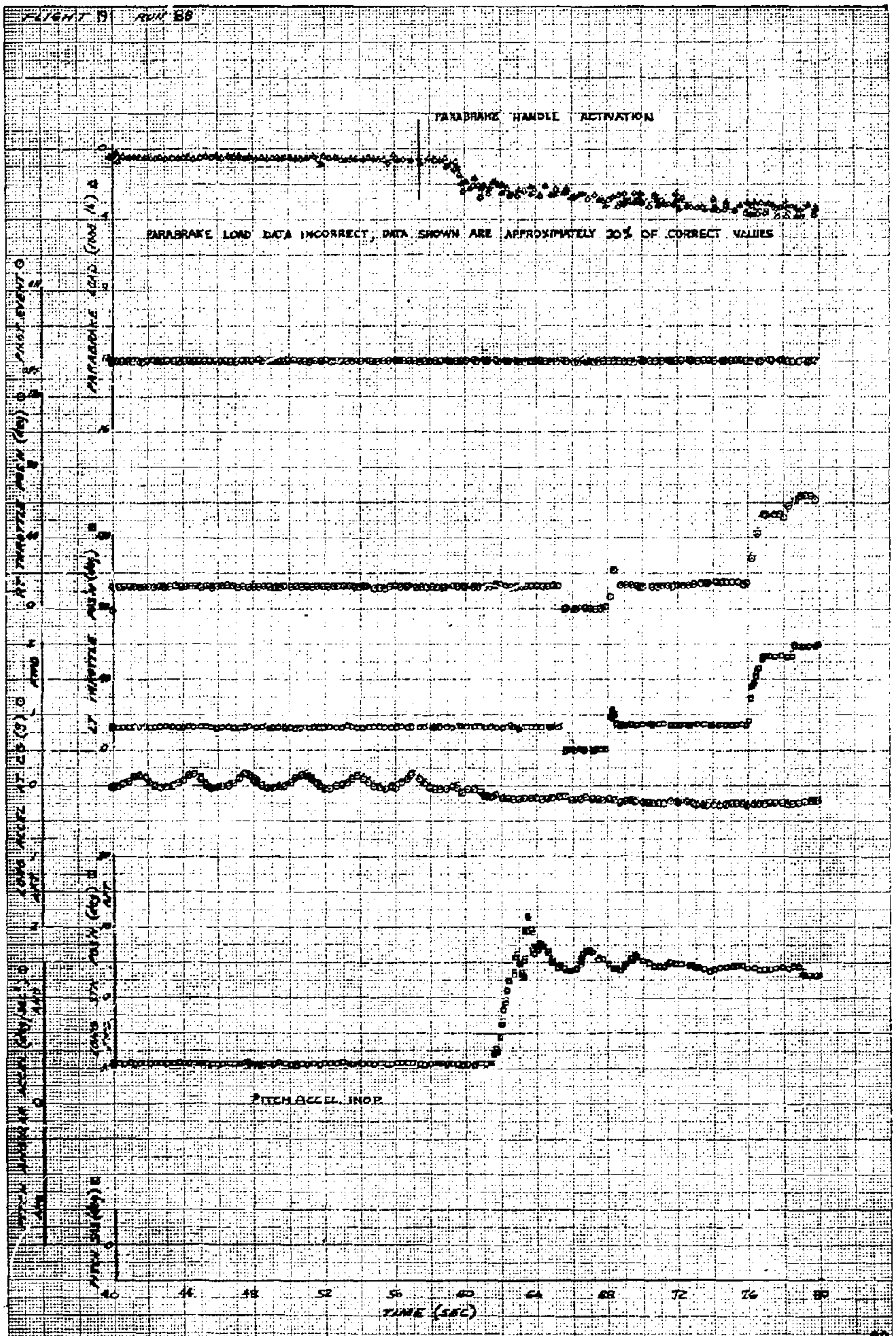

FIGURE 25 CONTINUED

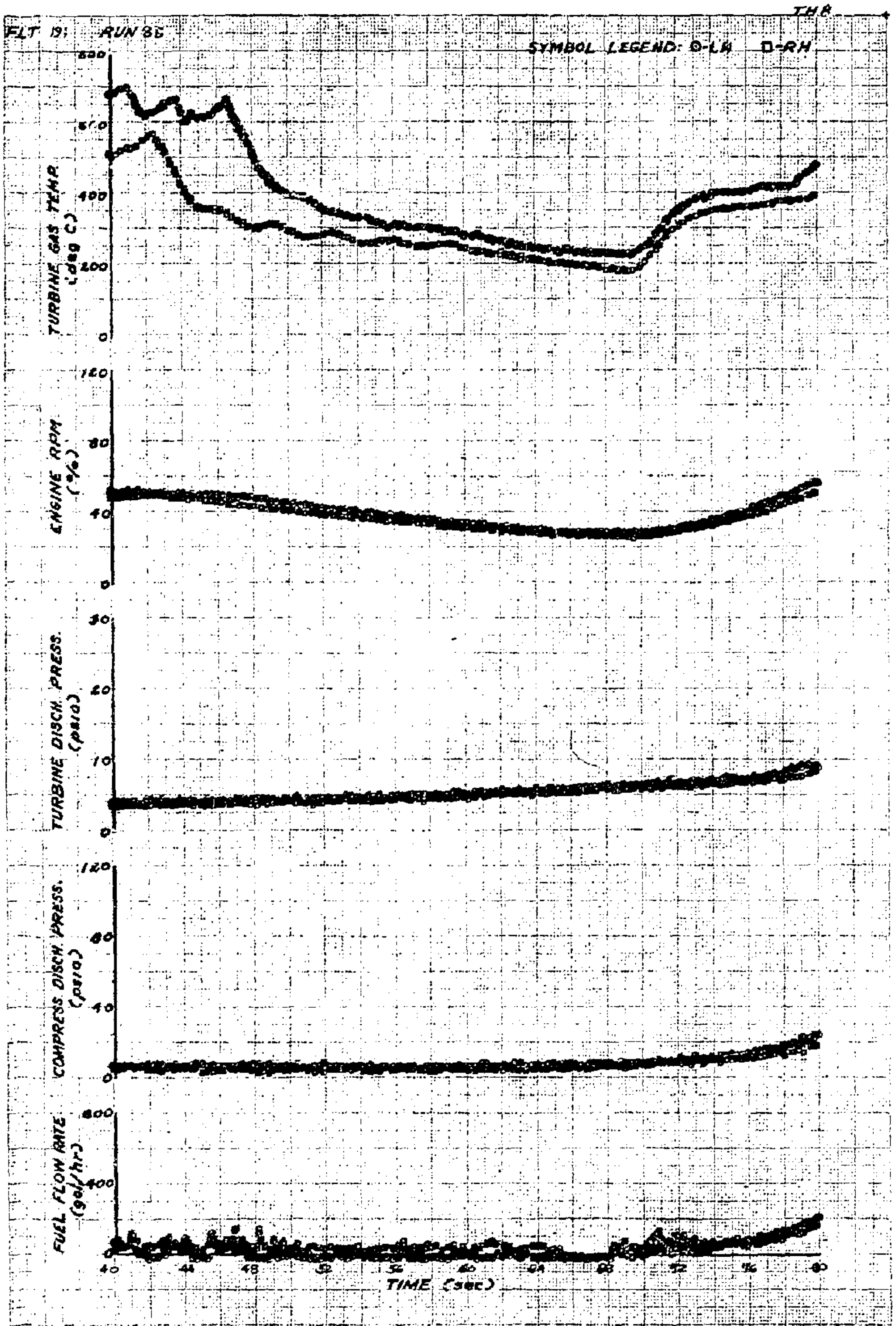

FIGURE 25 CONTINUED

THIS PAGE LEFT BLANK FOR PRESENTATION PURPOSES

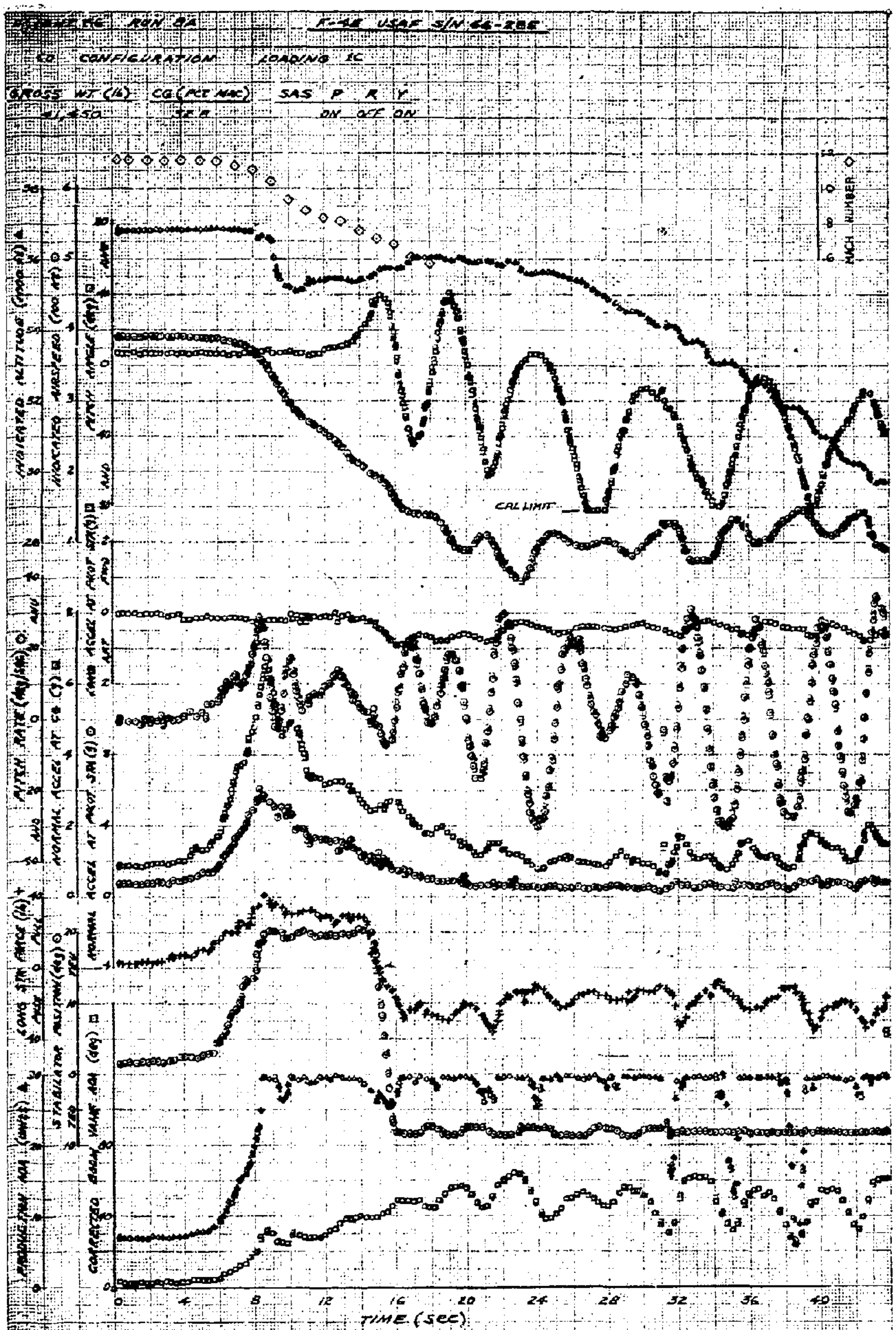

FIGURE 26. ... TURN, STEEP-MILDLY OSCILLATORY SPIN; AILERON INPUT FOR RECOVERY

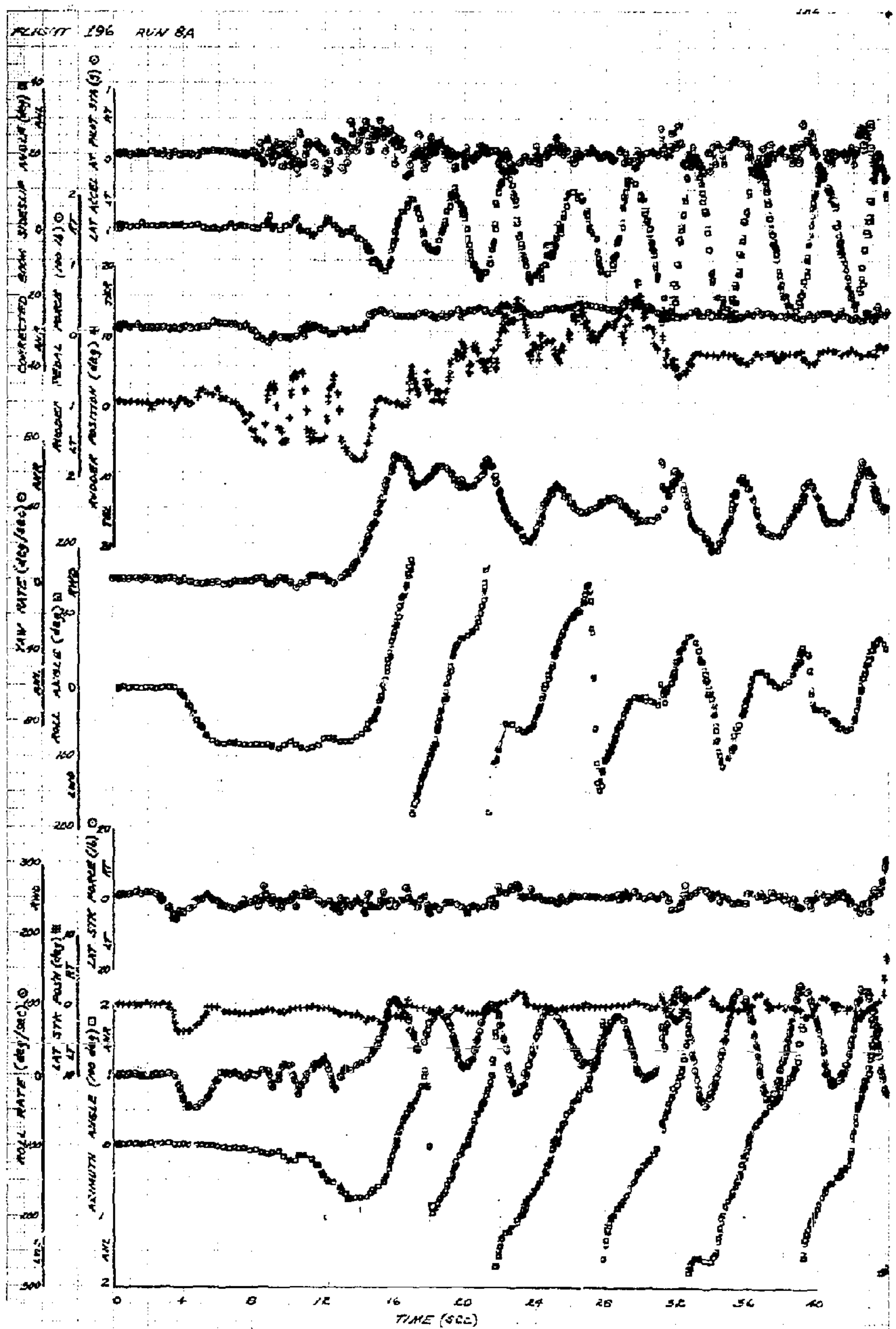

FIGURE 26 CONTINUED

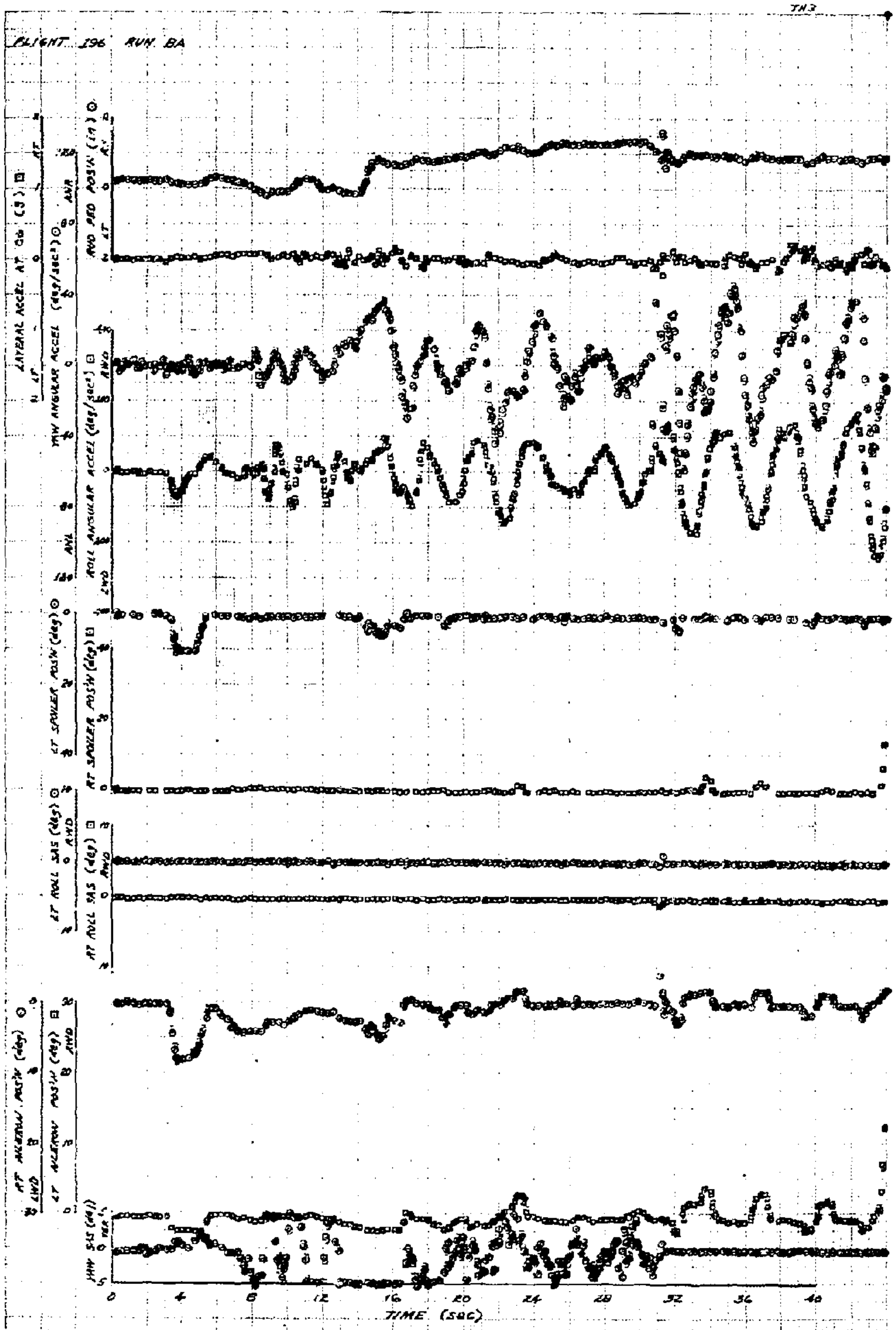

FIGURE 24 CONTINUED

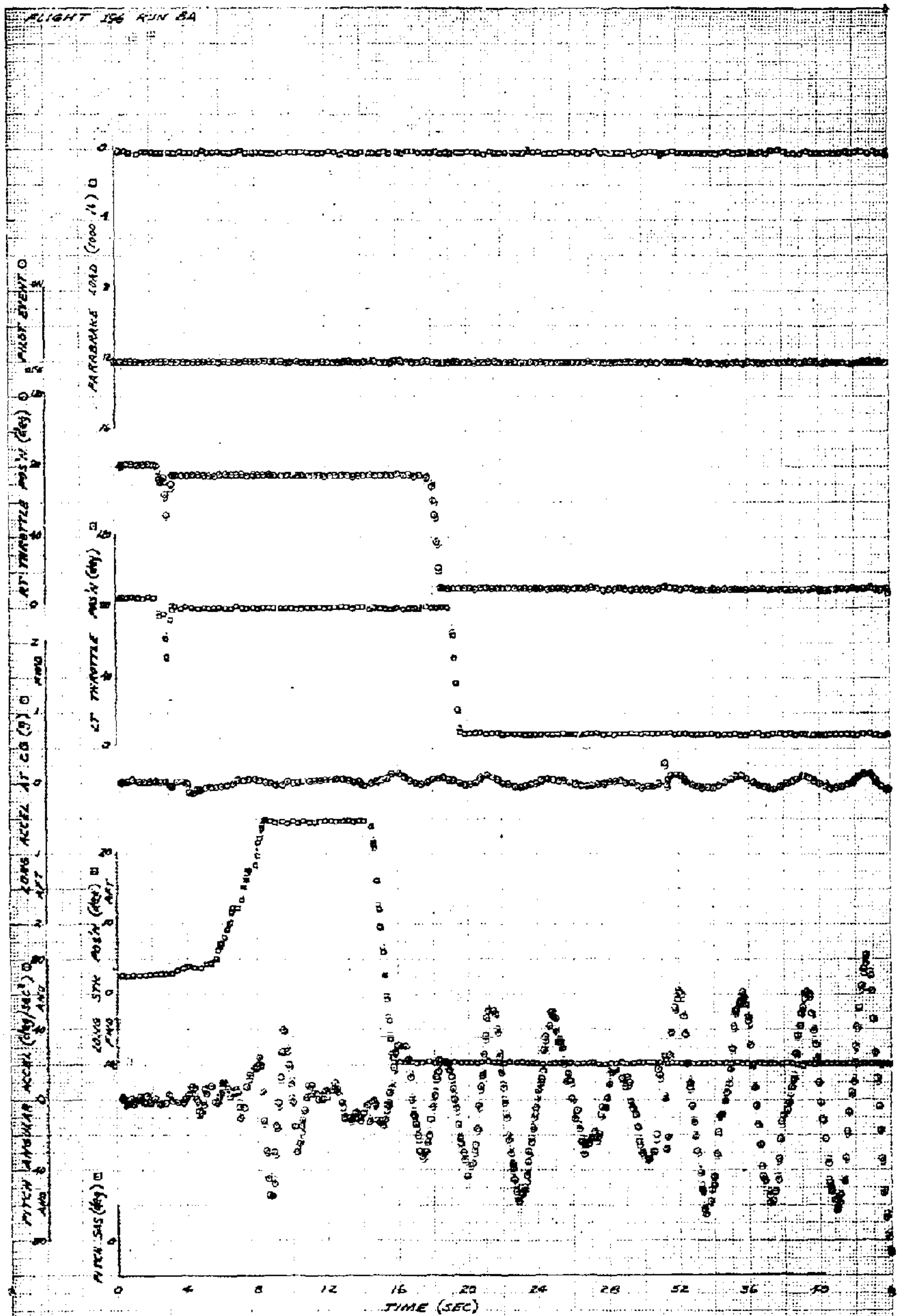

FIGURE 26 CONTINUED

THS

FLT 196 RUN 8A — F-4E USAF S/N 66-285

CONFIGURATION	LOADING	GROSS WT (lb)	CG (Pct mac)	SAS P R Y
CO	IC	41,450	32.8	ON OFF ON

I_X (SLUG-FT²)	I_Y (SLUG-FT²)	I_Z (SLUG-FT²)	I_{XZ} (SLUG-FT²)
24,200	166,000	185,000	6,200

$$\boxed{\dot{q}_{AERO} = \dot{q} - \frac{I_Z - I_X}{I_Y} pr - \frac{I_{XZ}}{I_Y} r^2 + \frac{I_{XZ}}{I_Y} p^2 + \frac{I_{ENG}\,\Omega_{ENG}}{I_Y} r - \dot{q}_{CHUTE}}$$

NOTE: 1) BODY AXIS $\dot{q}$ IS THE TIME DERIVATIVE OF MEASURED PITCH RATE (q)

2) $\dot{q}_{CHUTE} = \frac{F_c X_c \sin\lambda}{I_Y}$

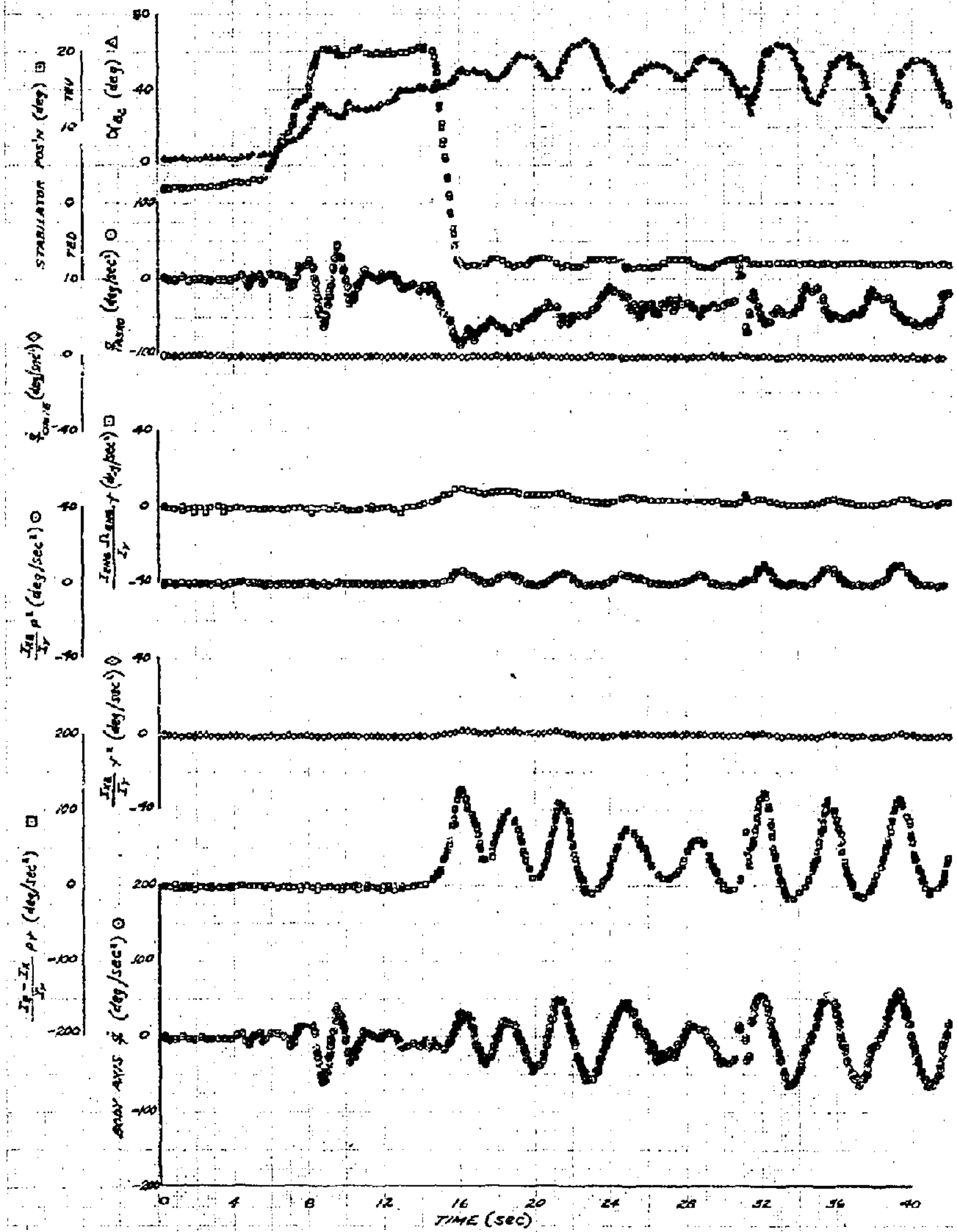

FIGURE 26 CONTINUED

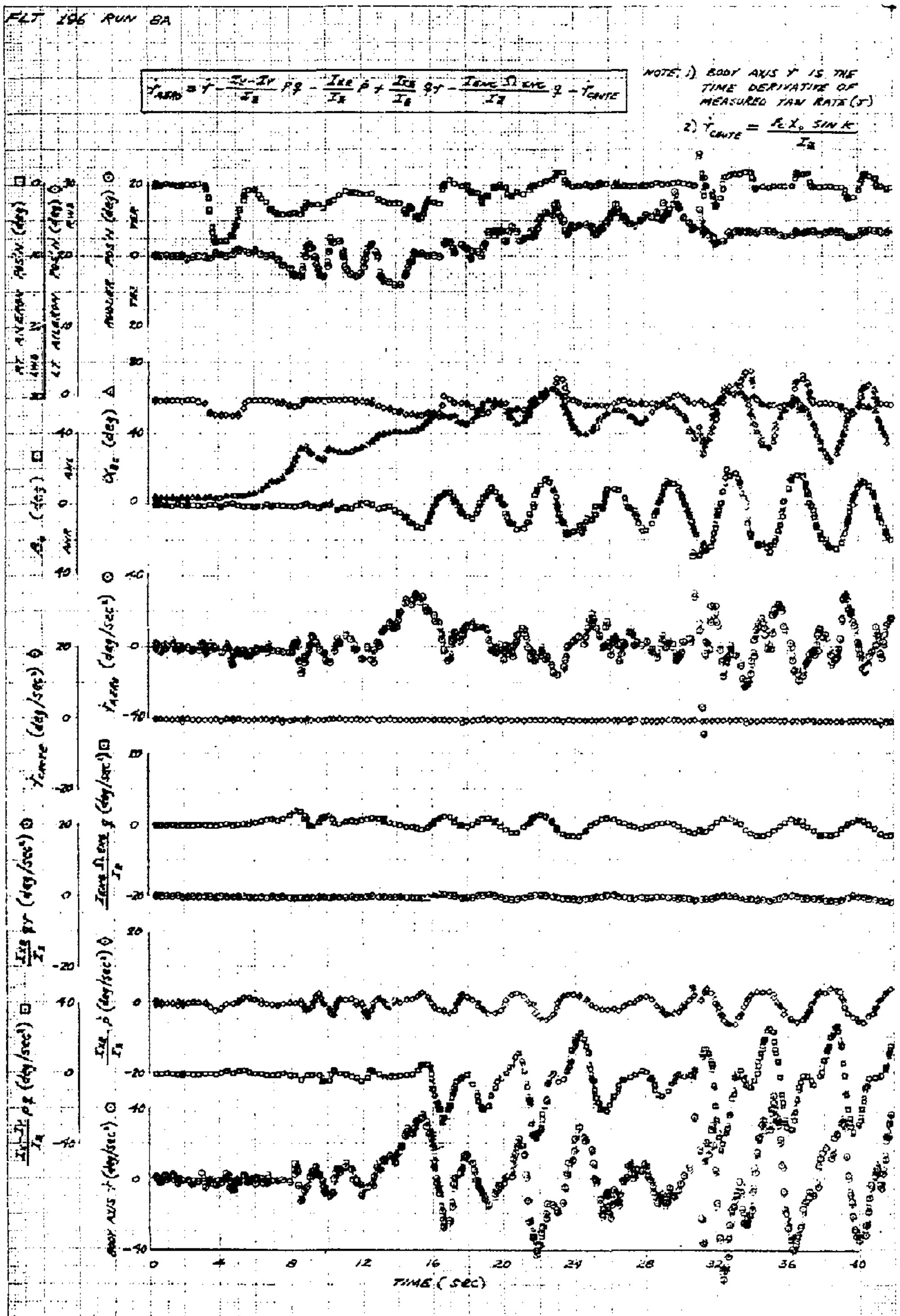

FIGURE 26 CONTINUED

FLT 296 RUN 8A

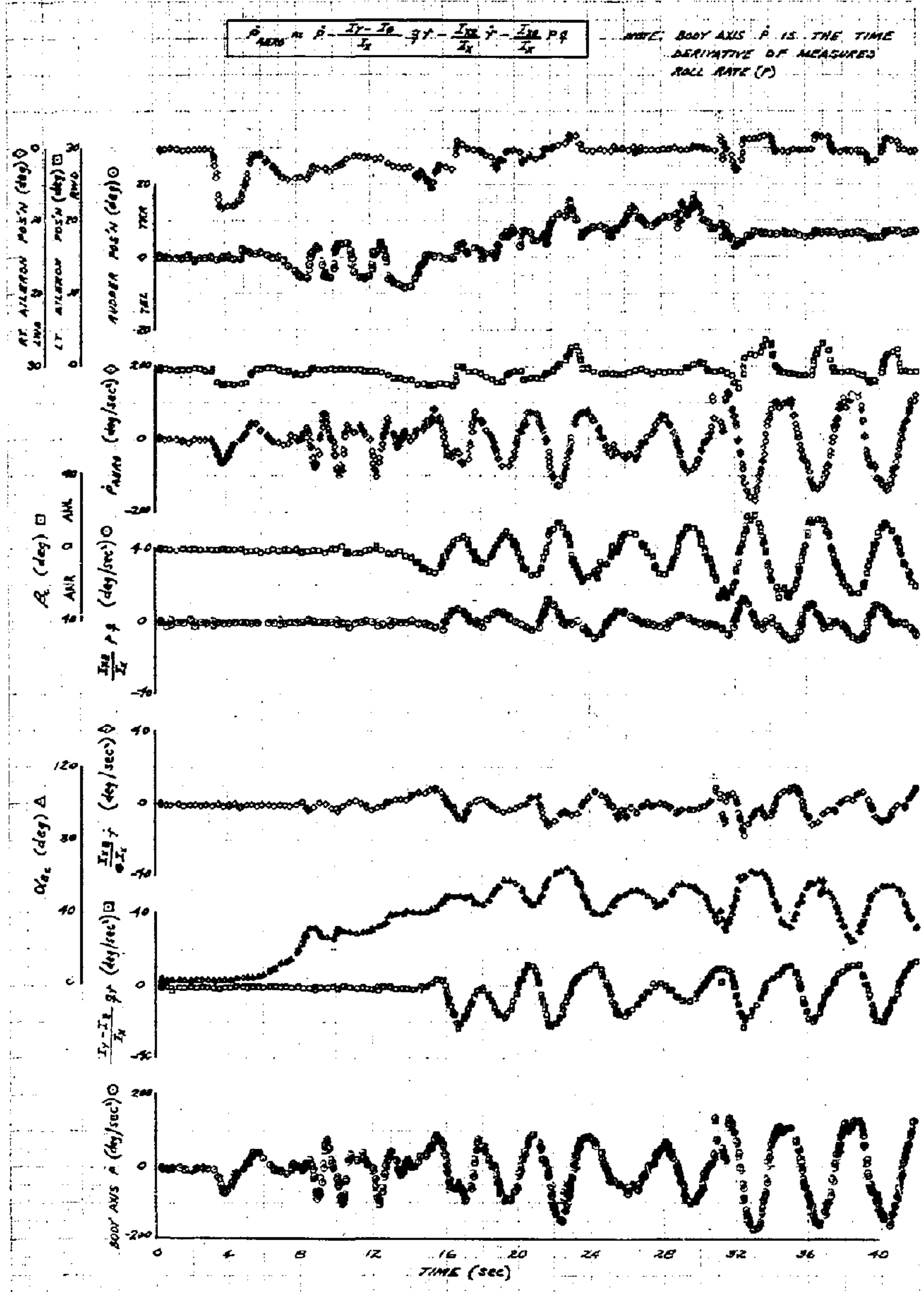

FIGURE 26 CONTINUED

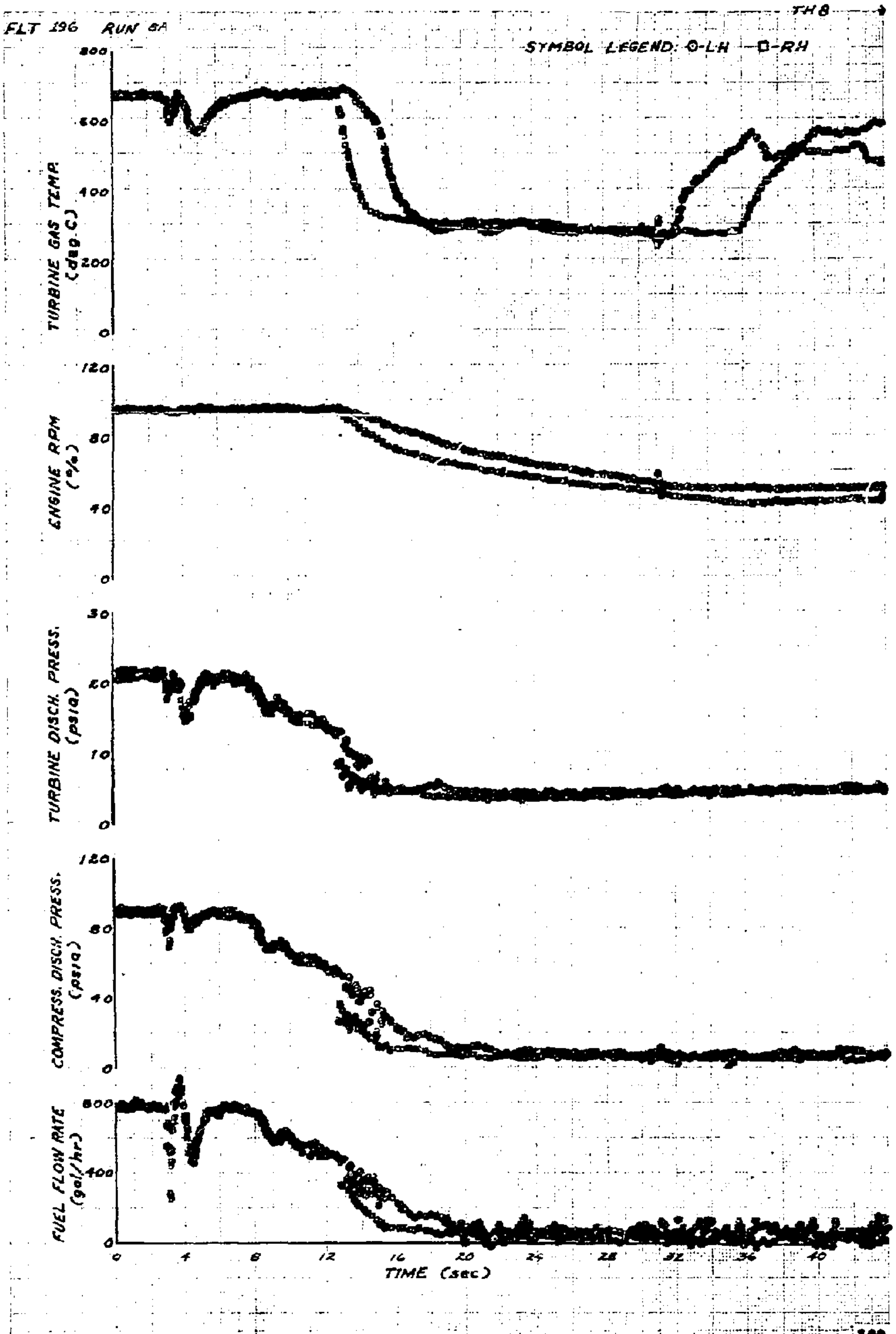

FIGURE 26 CONTINUED

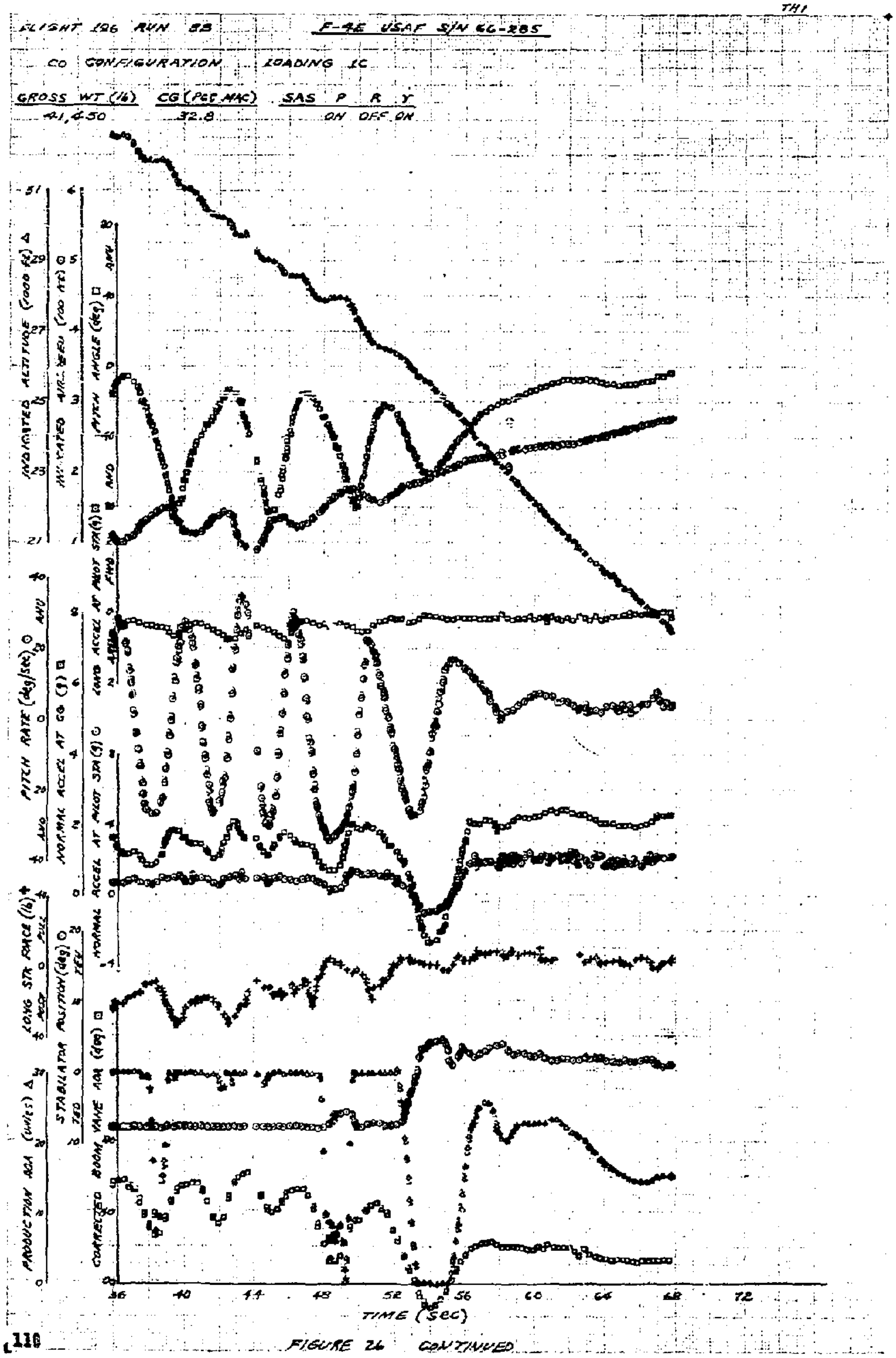

FIGURE 26 CONTINUED

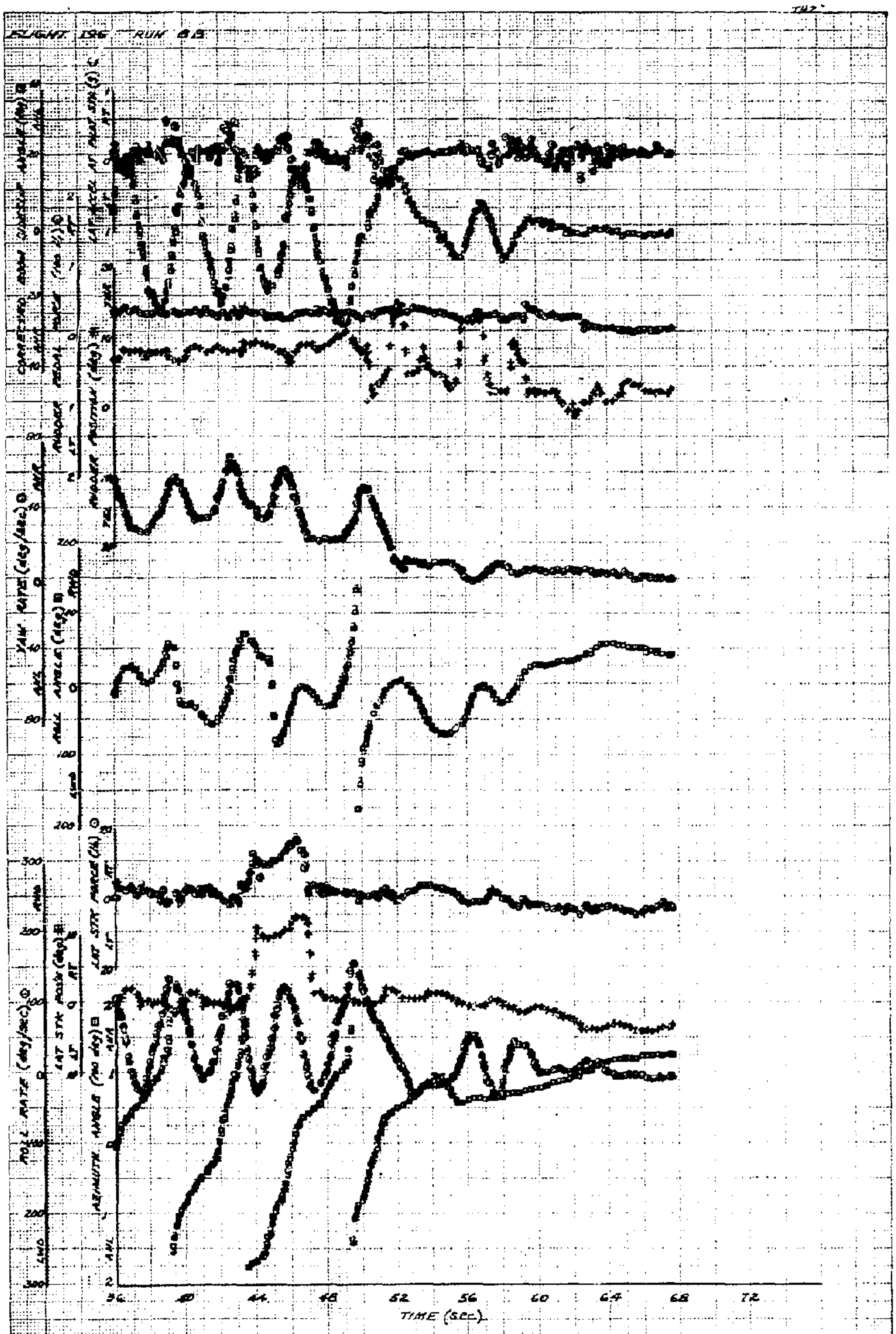

FIGURE 26 CONTINUED

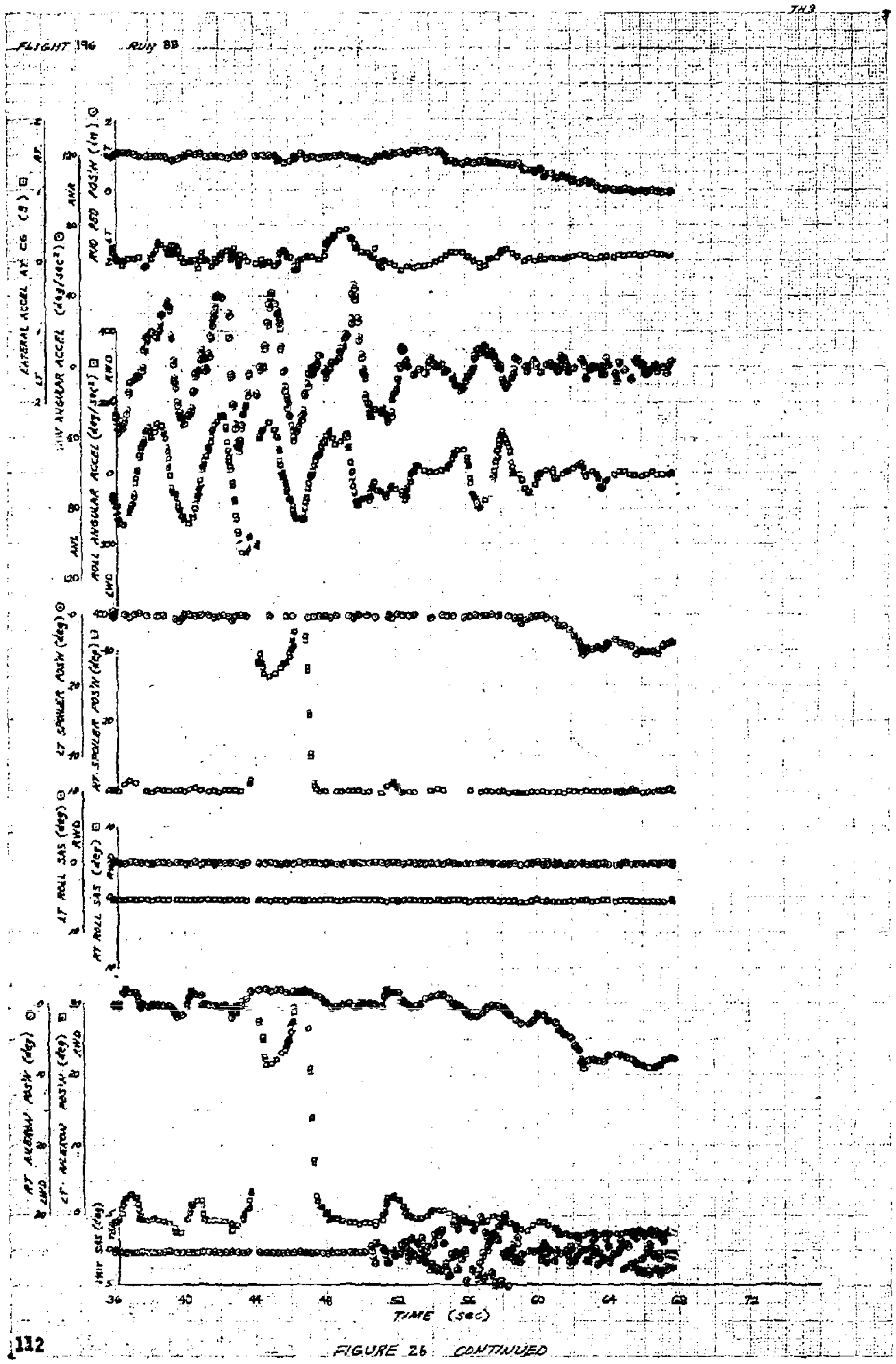

FIGURE 26 CONTINUED

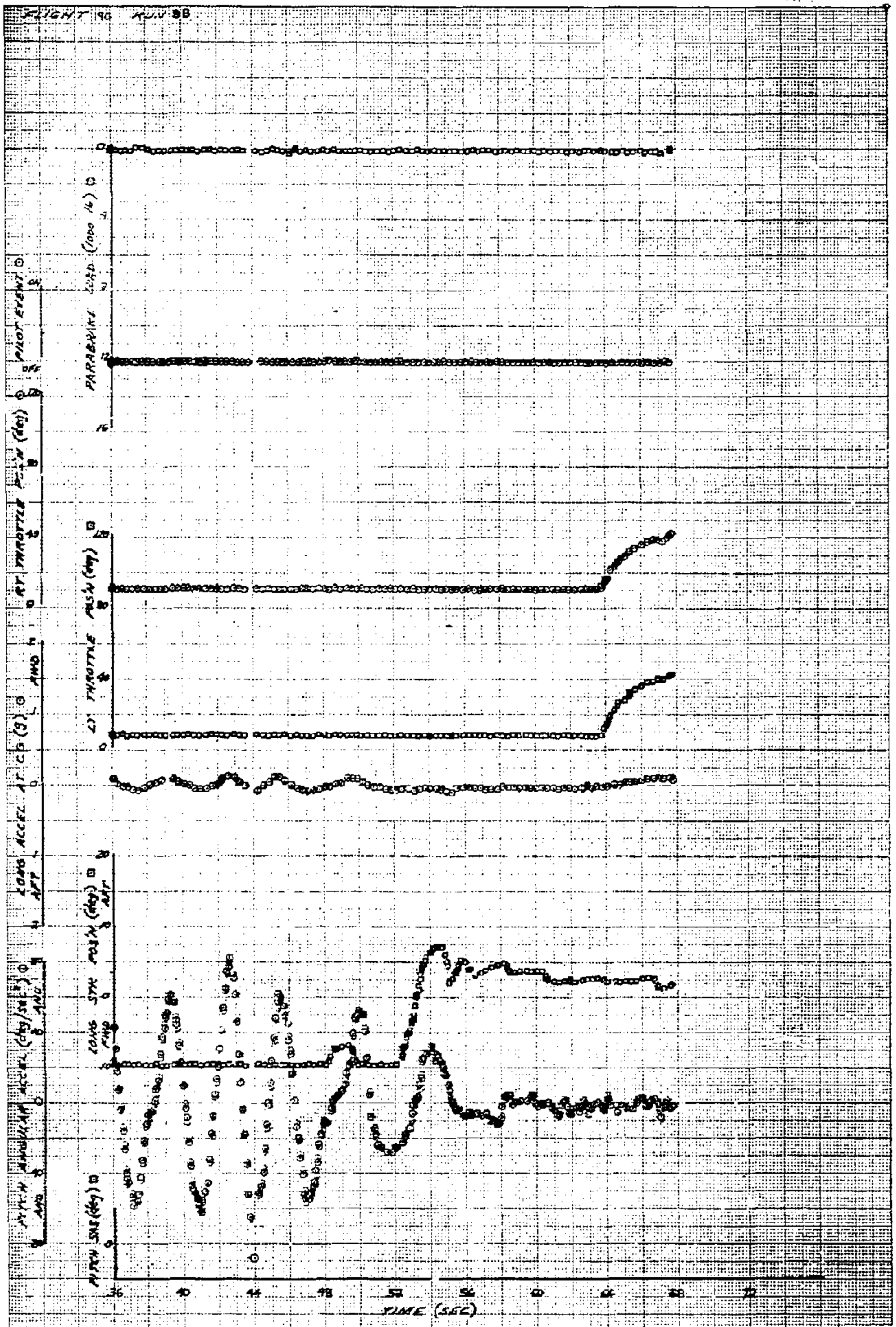

FIGURE 26 CONTINUED

THS

FLT 296 RUN 8B — F-4E USAF S/N 66-285

CONFIGURATION	LOADING	GROSS WT (lb)	CG (PCT mac)	SAS P R Y
CO	IC	41,450	32.8	ON OFF ON

I_X (SLUG-FT²)	I_Y (SLUG-FT²)	I_Z (SLUG-FT²)	I_{XZ} (SLUG-FT²)
24,200	166,000	185,000	6,200

NOTE: 1) BODY AXIS $\dot{q}$ IS THE TIME DERIVATIVE OF MEASURED PITCH RATE (q)

$$\boxed{\dot{q}_{AERO} = \dot{q} - \frac{I_Z - I_X}{I_Y}pr - \frac{I_{XZ}}{I_Y}r^2 + \frac{I_{XZ}}{I_Y}p^2 + \frac{I_{ENG}\,\Omega_{ENG}}{I_Y}r - \dot{q}_{GRVTE}}$$

2) $\dot{q}_{GRVTE} = \frac{F_C X_C \sin\lambda}{I_Y}$

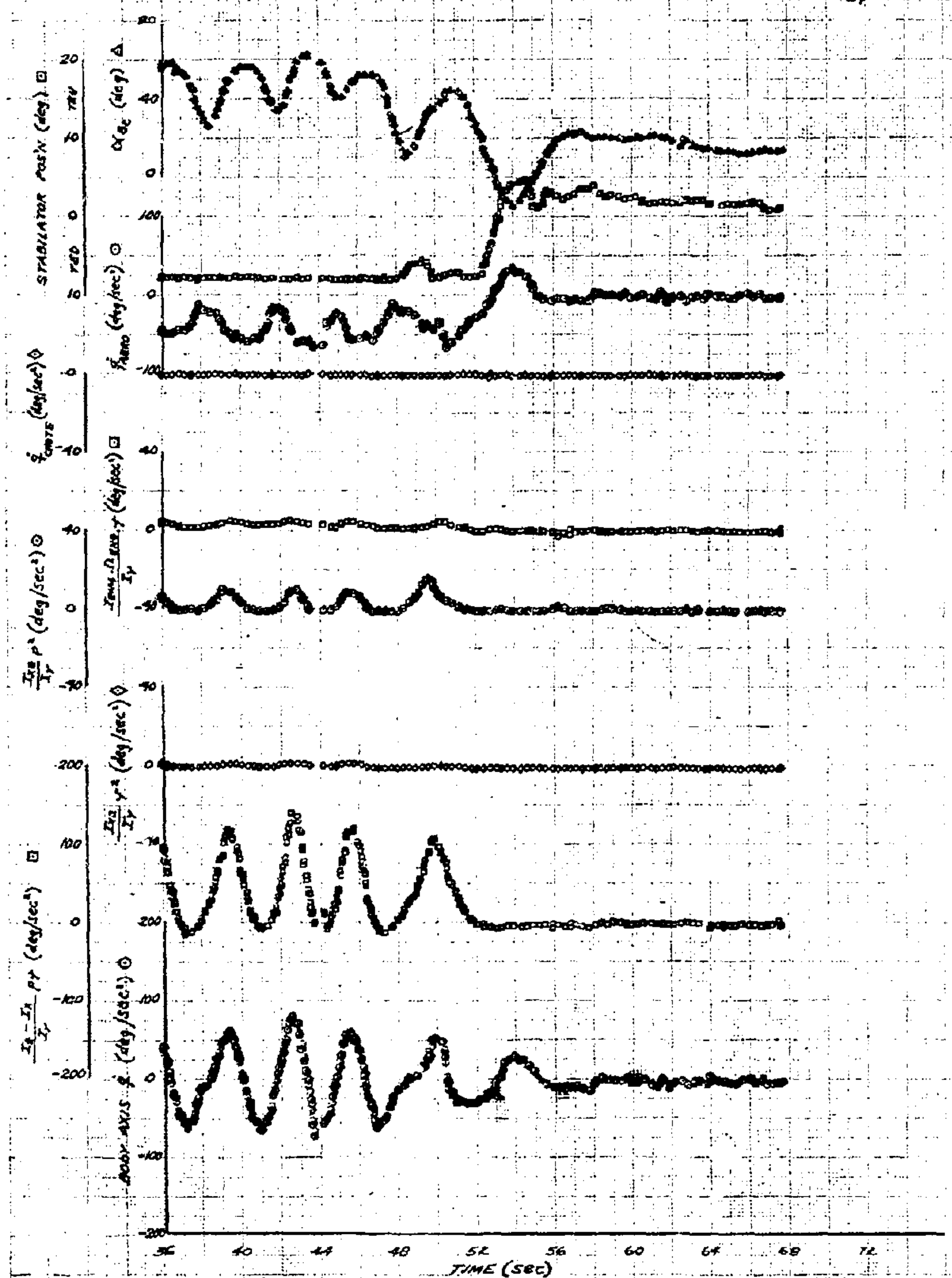

FIGURE 26 CONTINUED

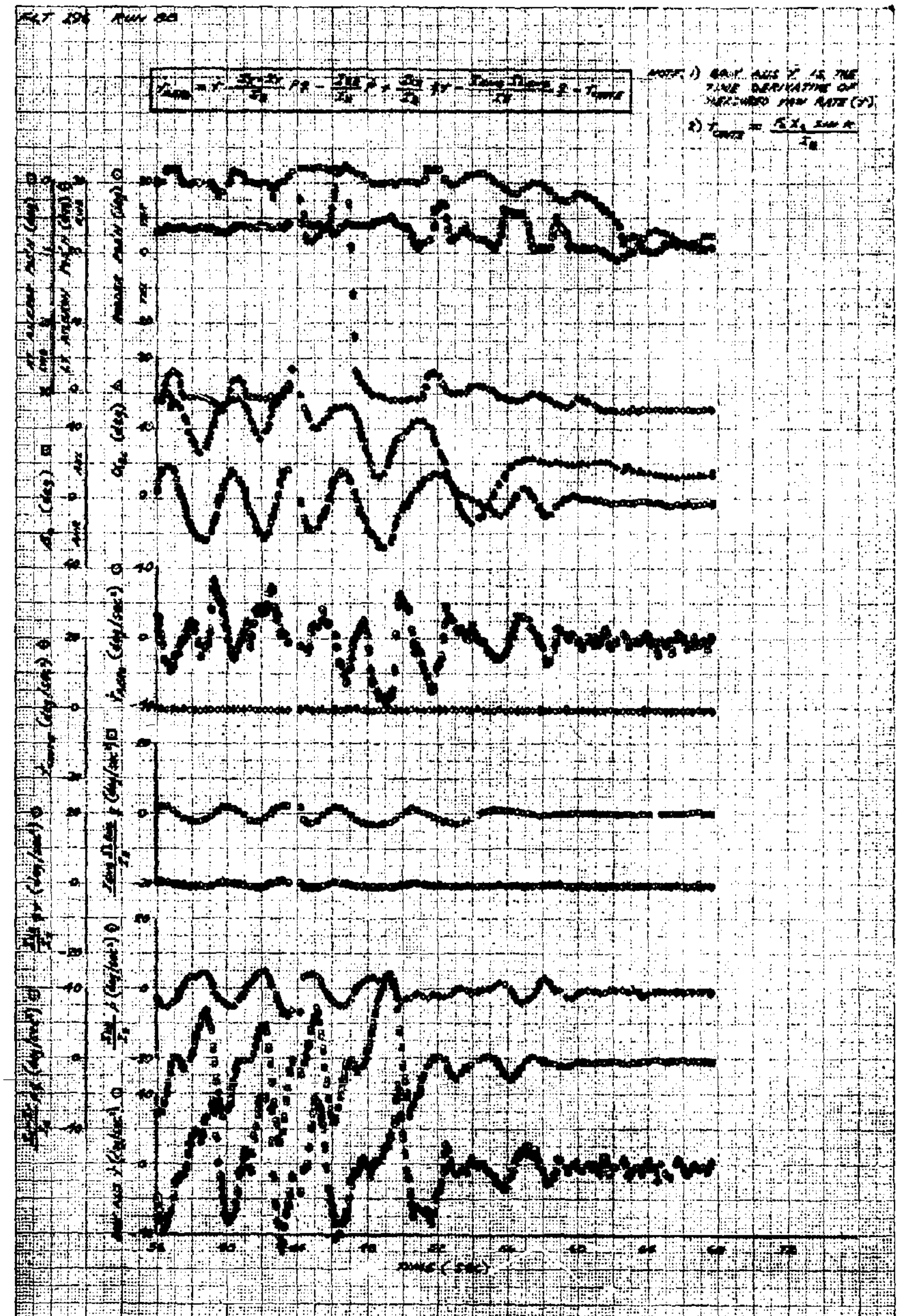

FIGURE 24 CONTINUED

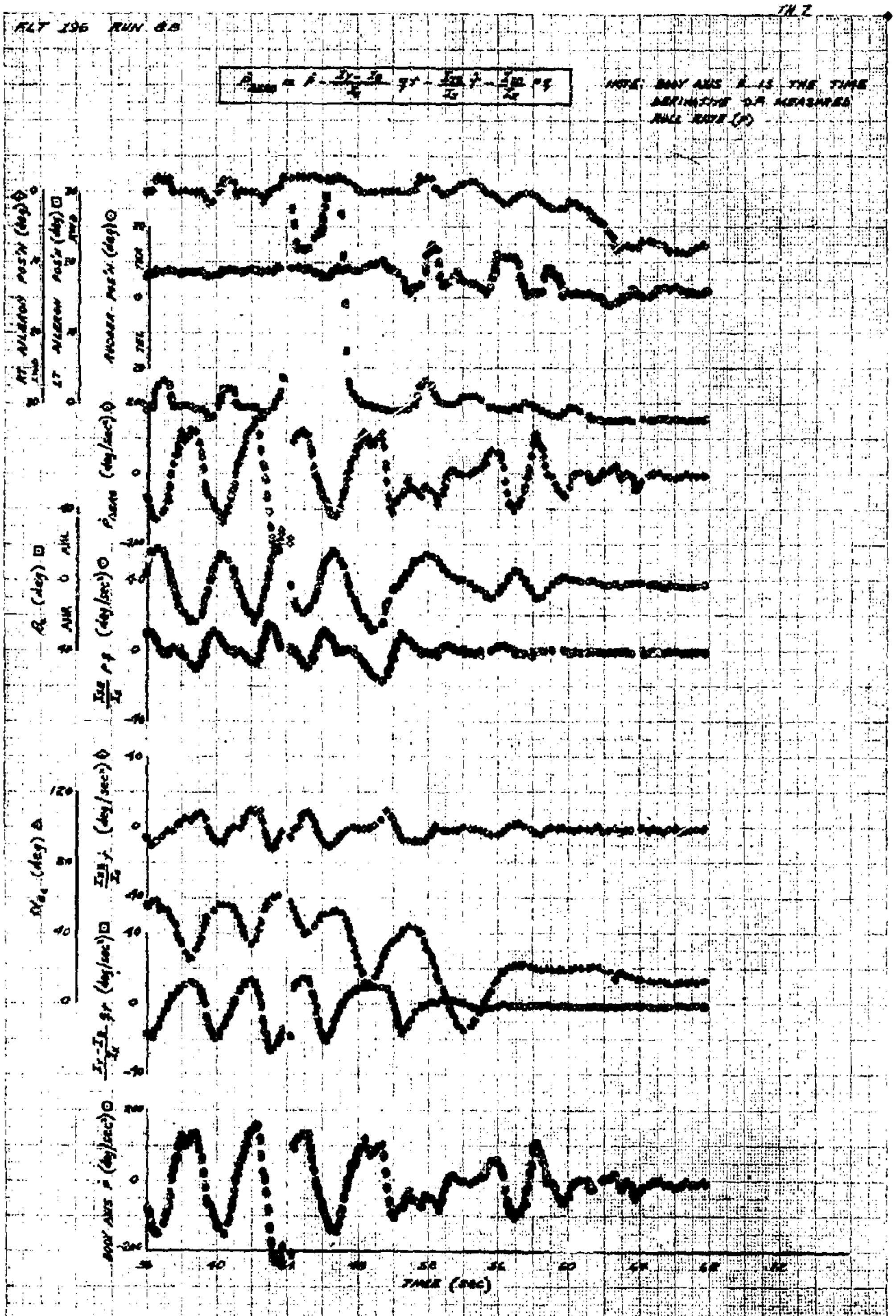

FIGURE 26 CONTINUED

THIS PAGE LEFT BLANK FOR PRESENTATION PURPOSES

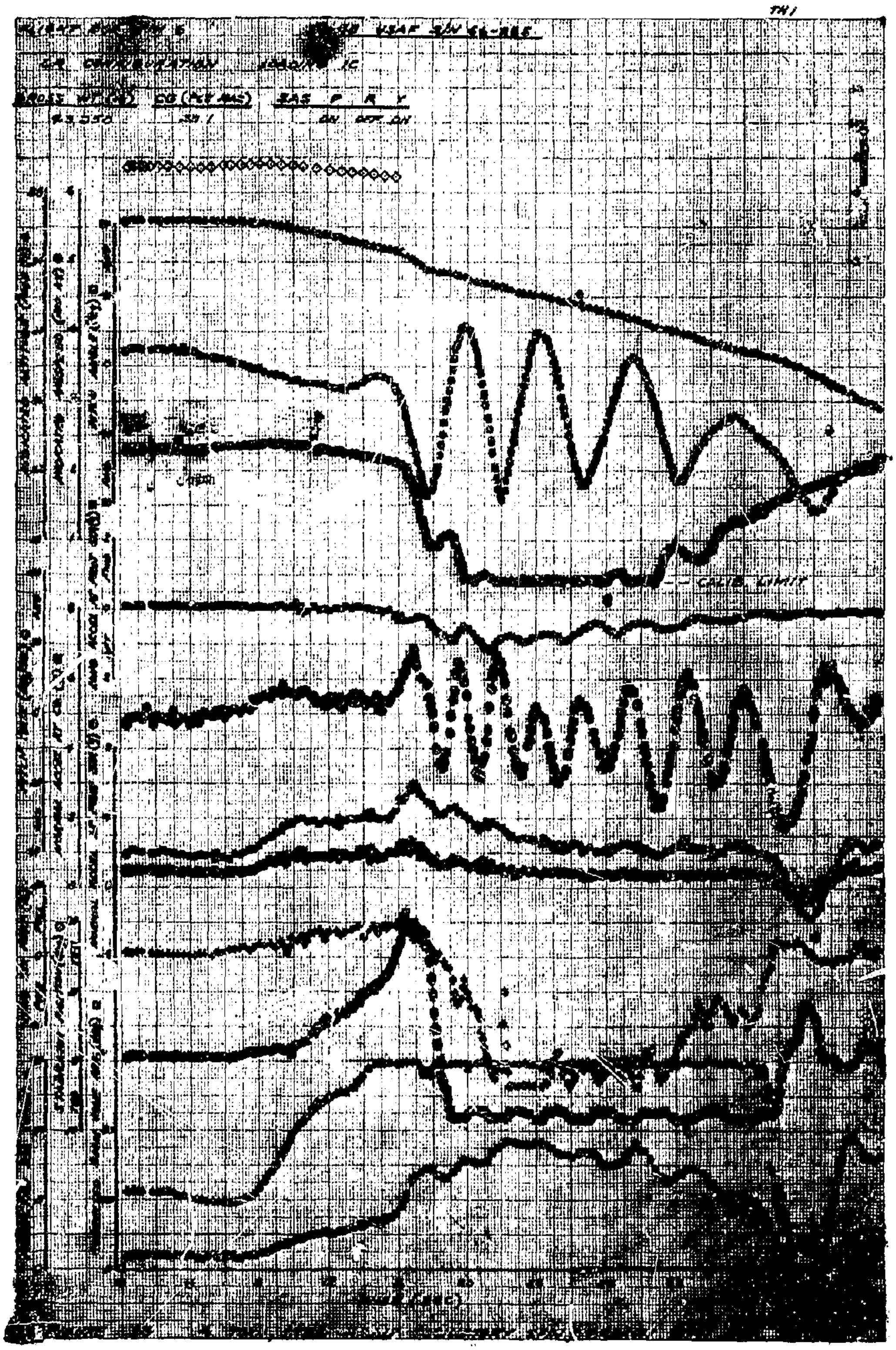

THI
USAF S/N
CALIB. LIMIT

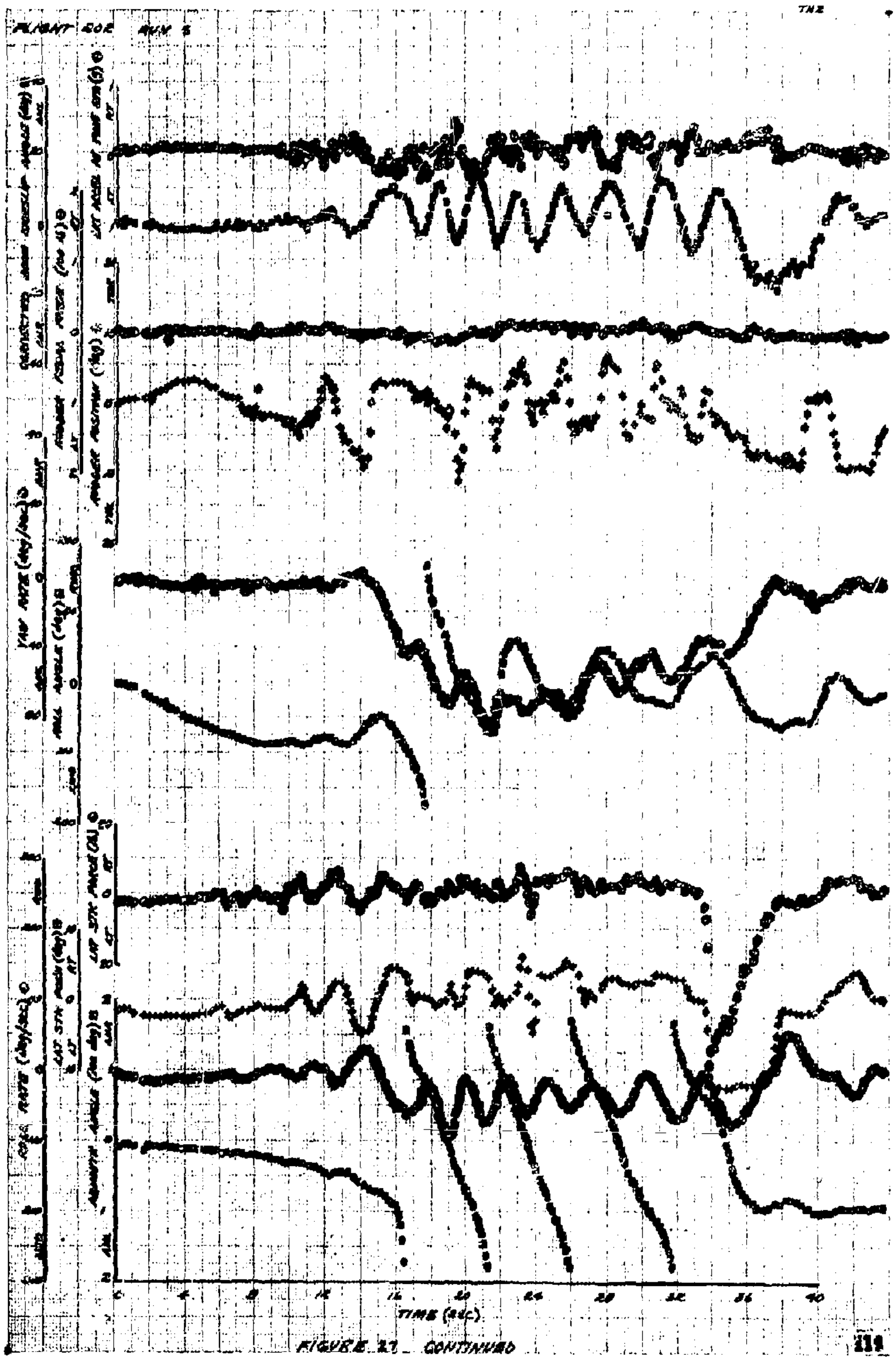

FIGURE 21 CONTINUED

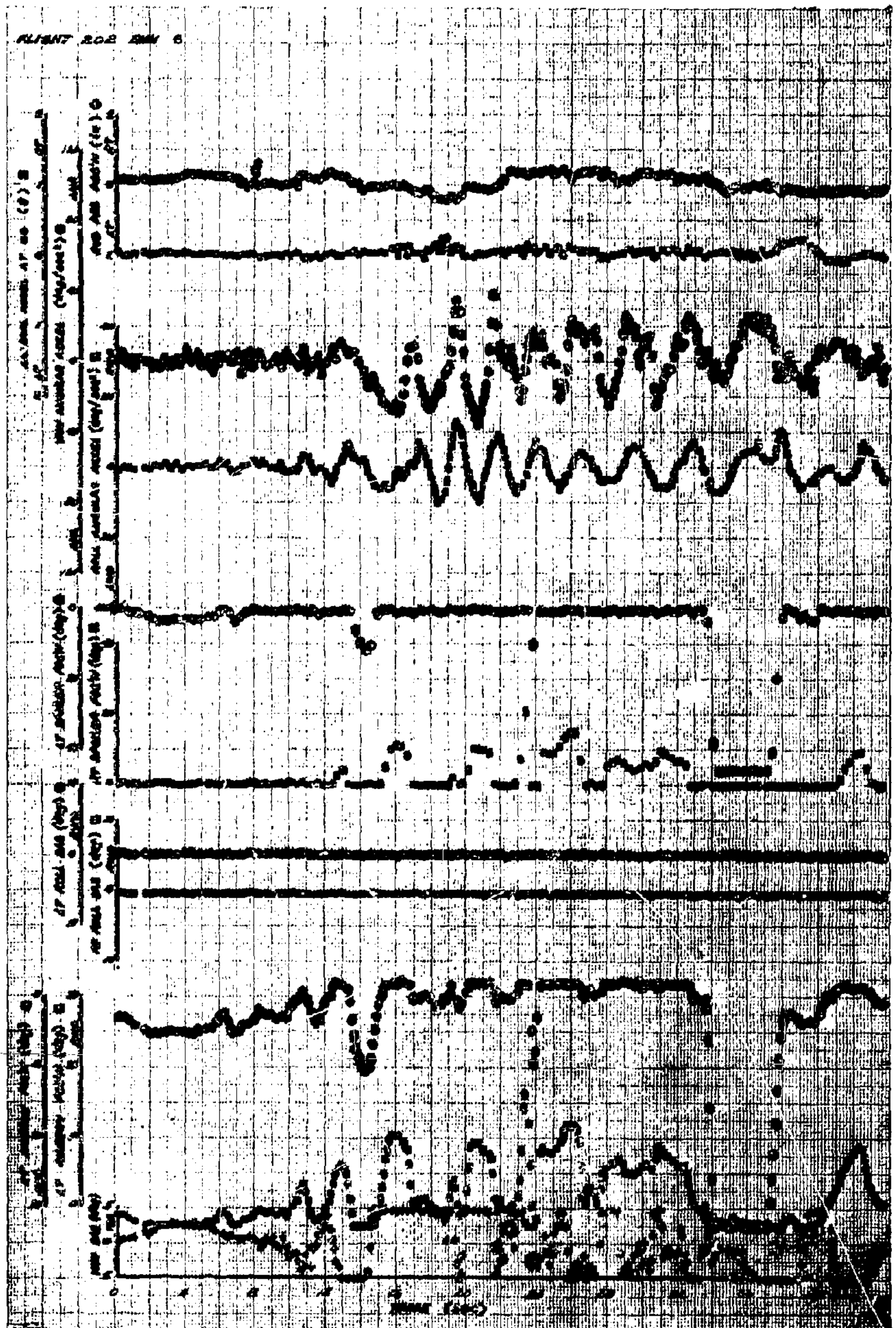

FIGURE 27 CONTINUED

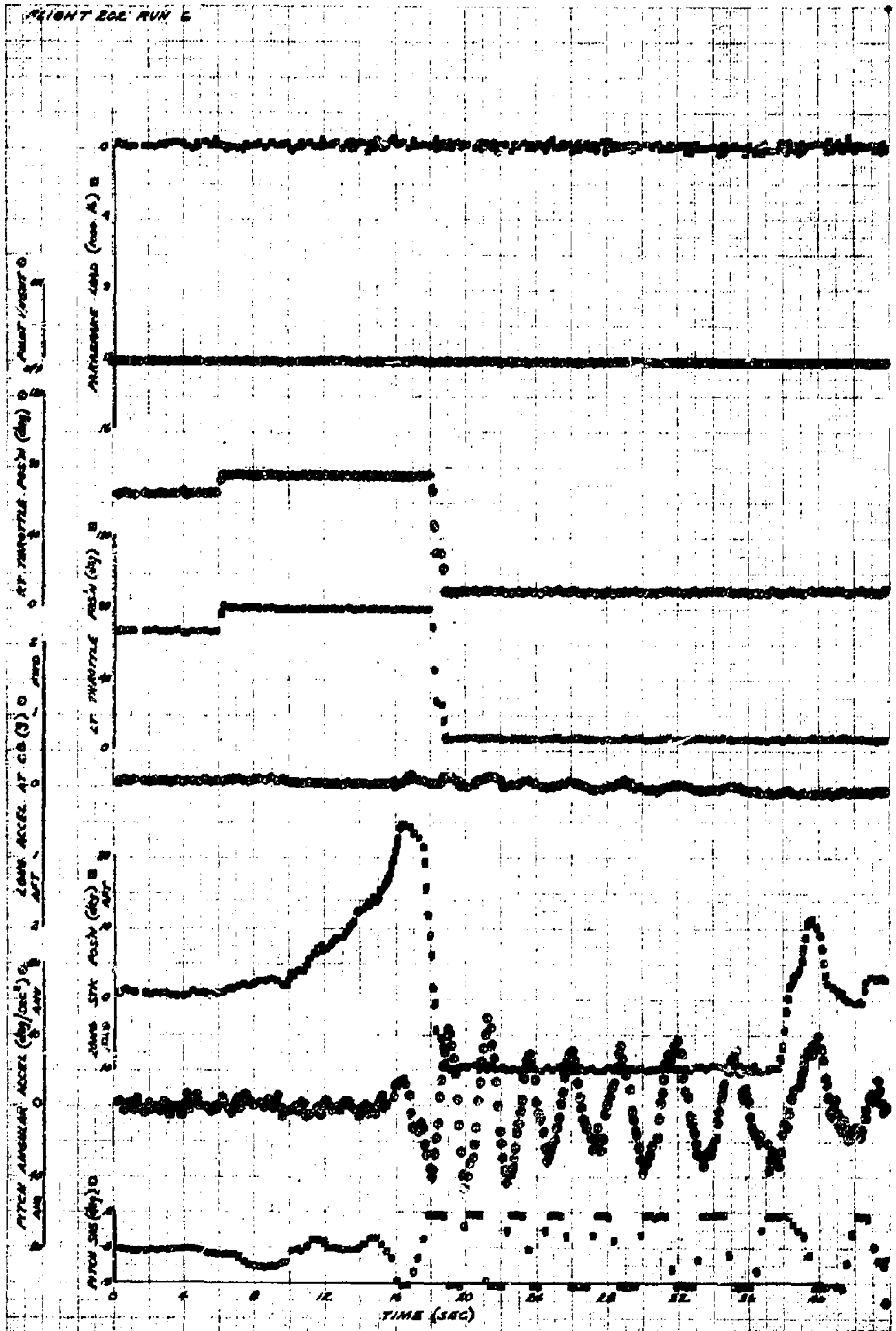

FIGURE 27 CONTINUED

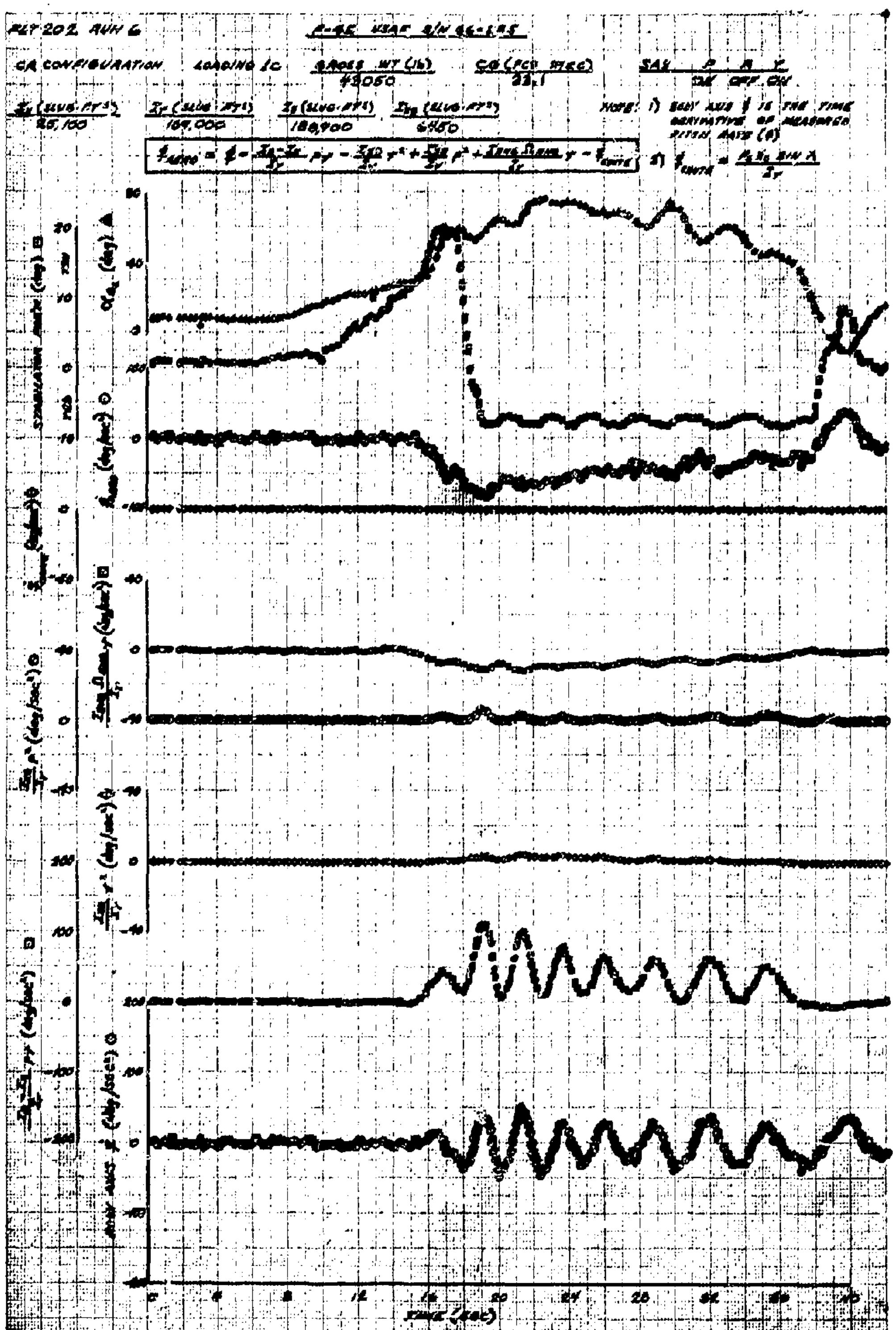

FIGURE 27 CONTINUED

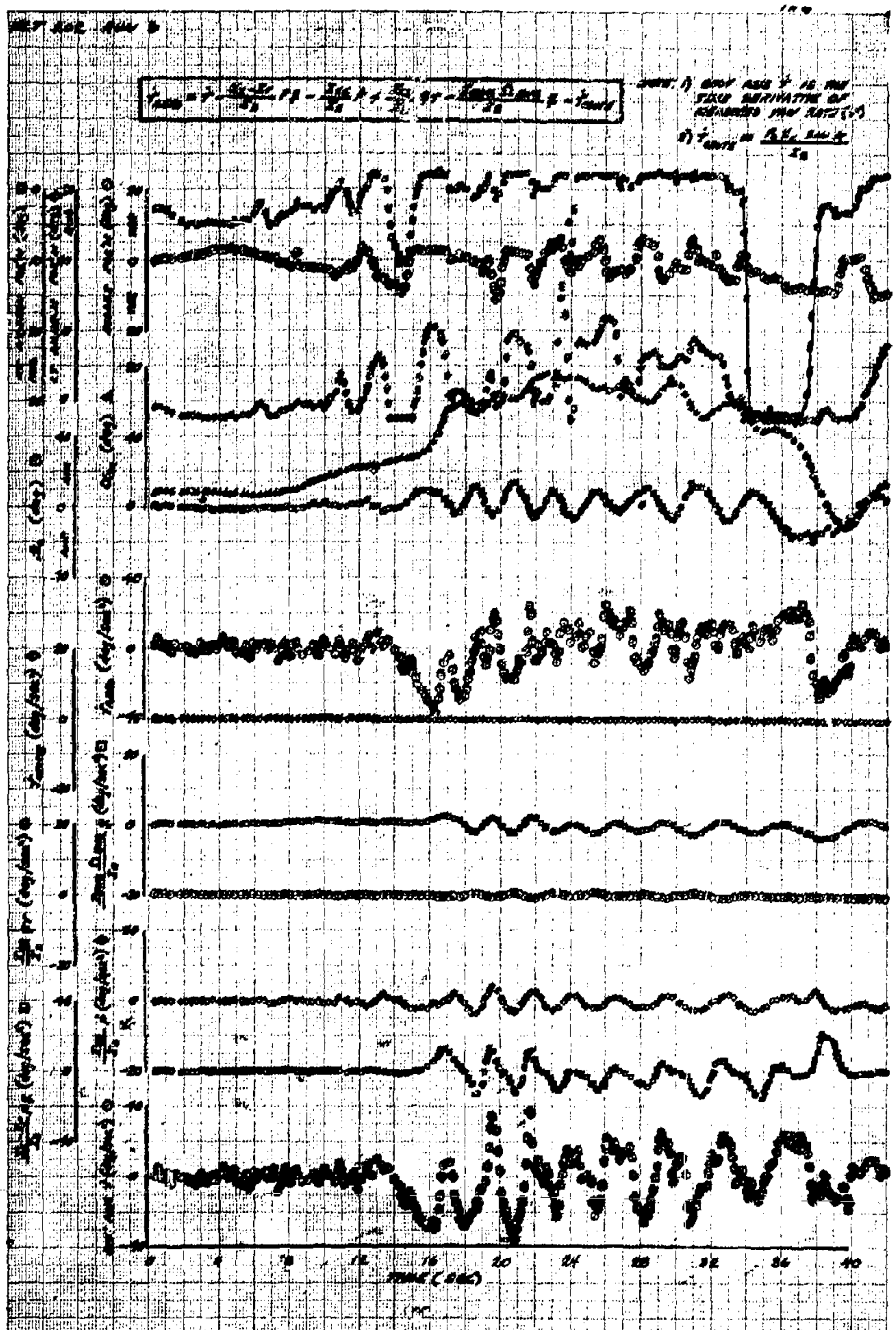

FIGURE 27 CONTINUED

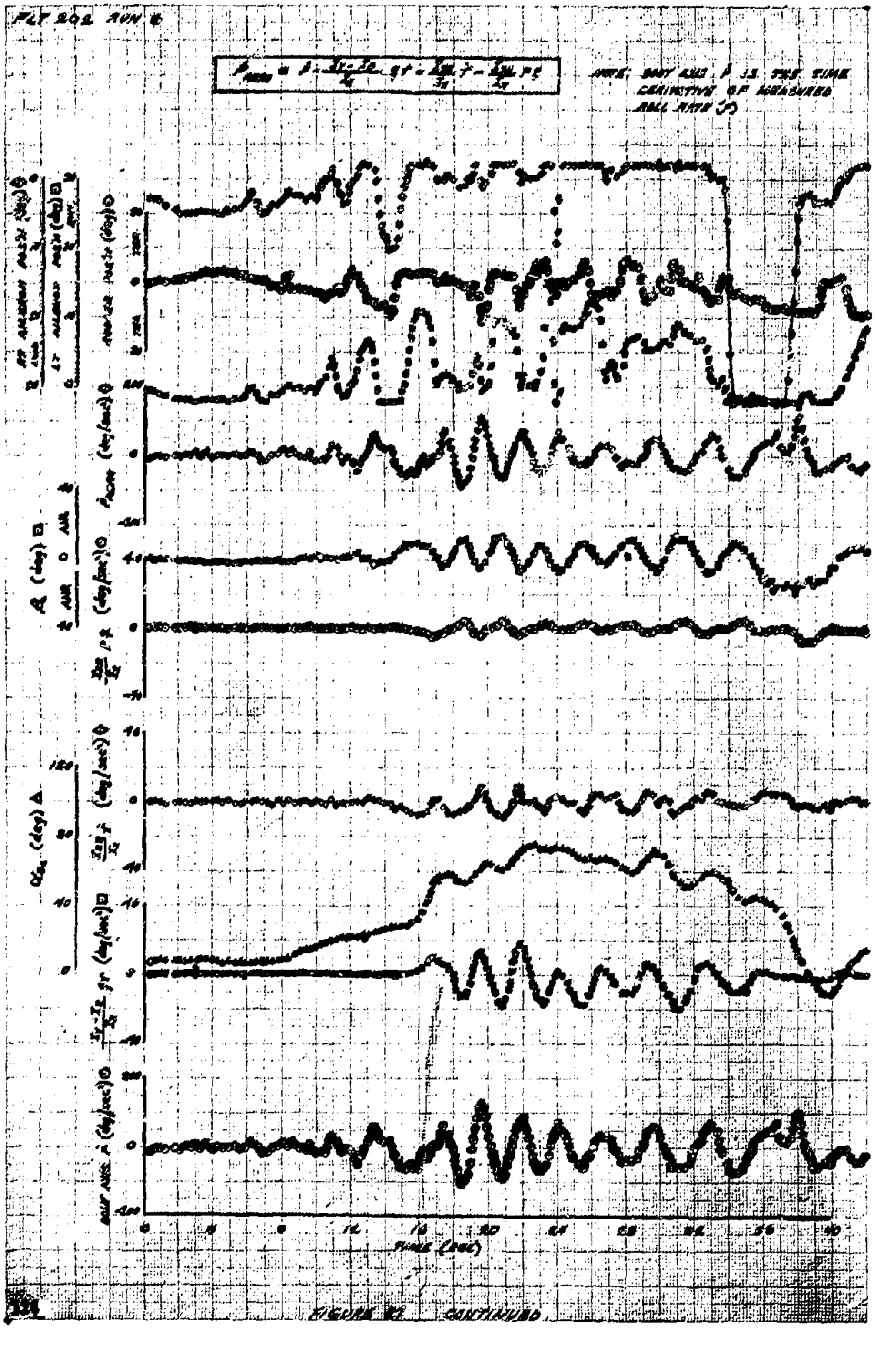

FIGURE [illegible] CONTINUED.

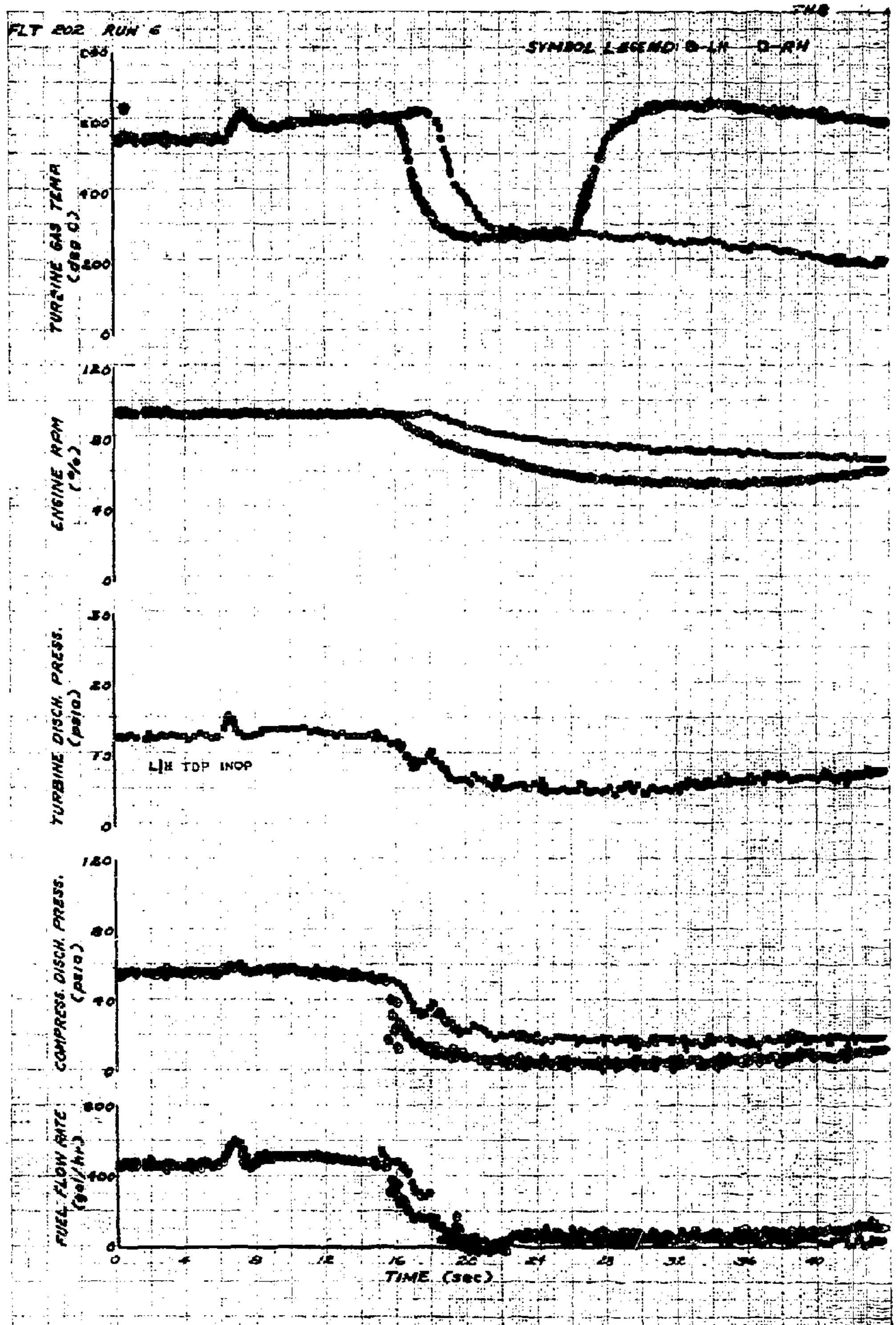

FIGURE 27 CONTINUED

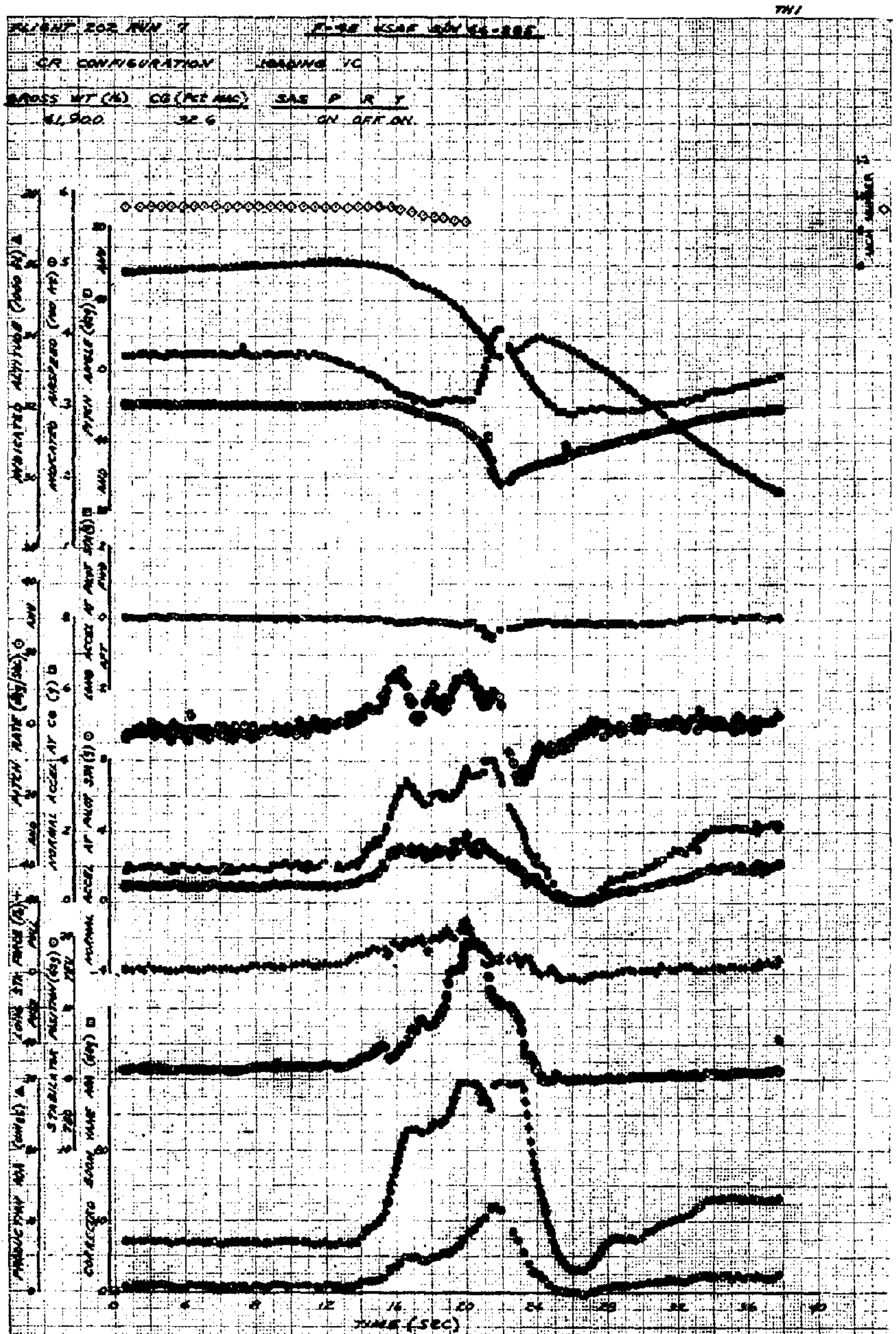

 FIGURE 28 ROLLING DEPARTURE FROM A TRANSONIC DECELERATION

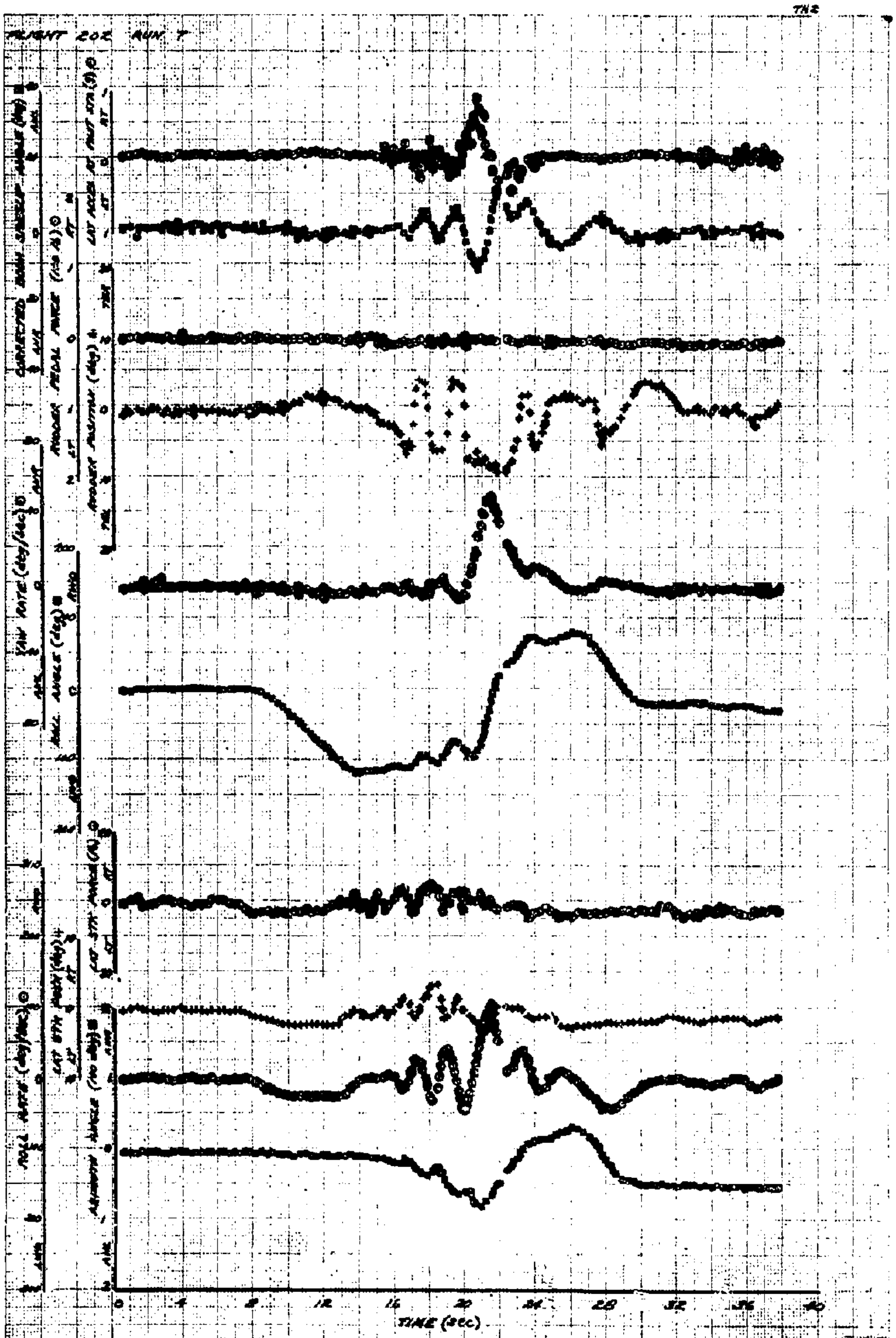

FIGURE 28 CONTINUED

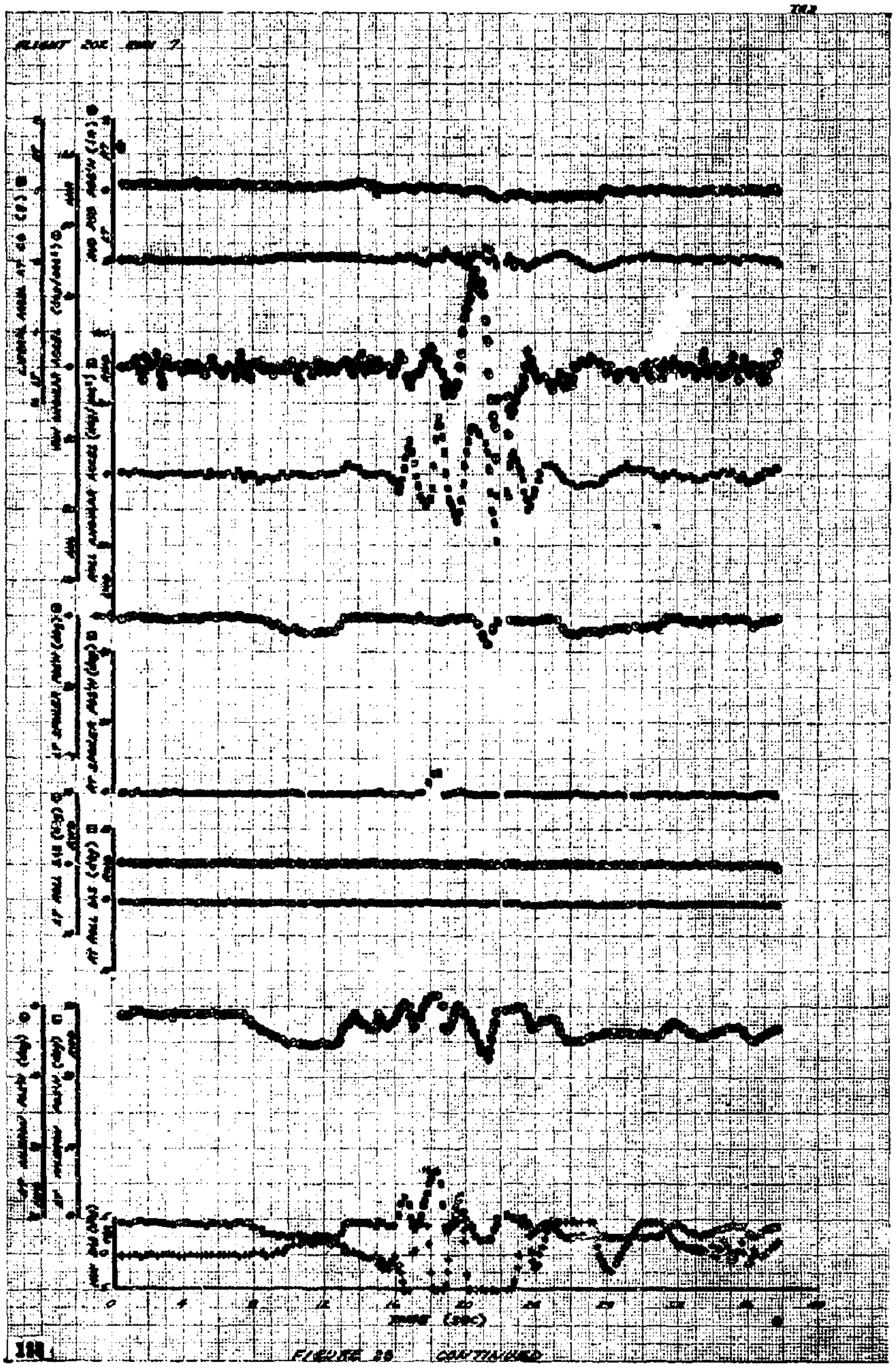

FIGURE 28 CONTINUED

FLIGHT 202 RUN 7

TH4

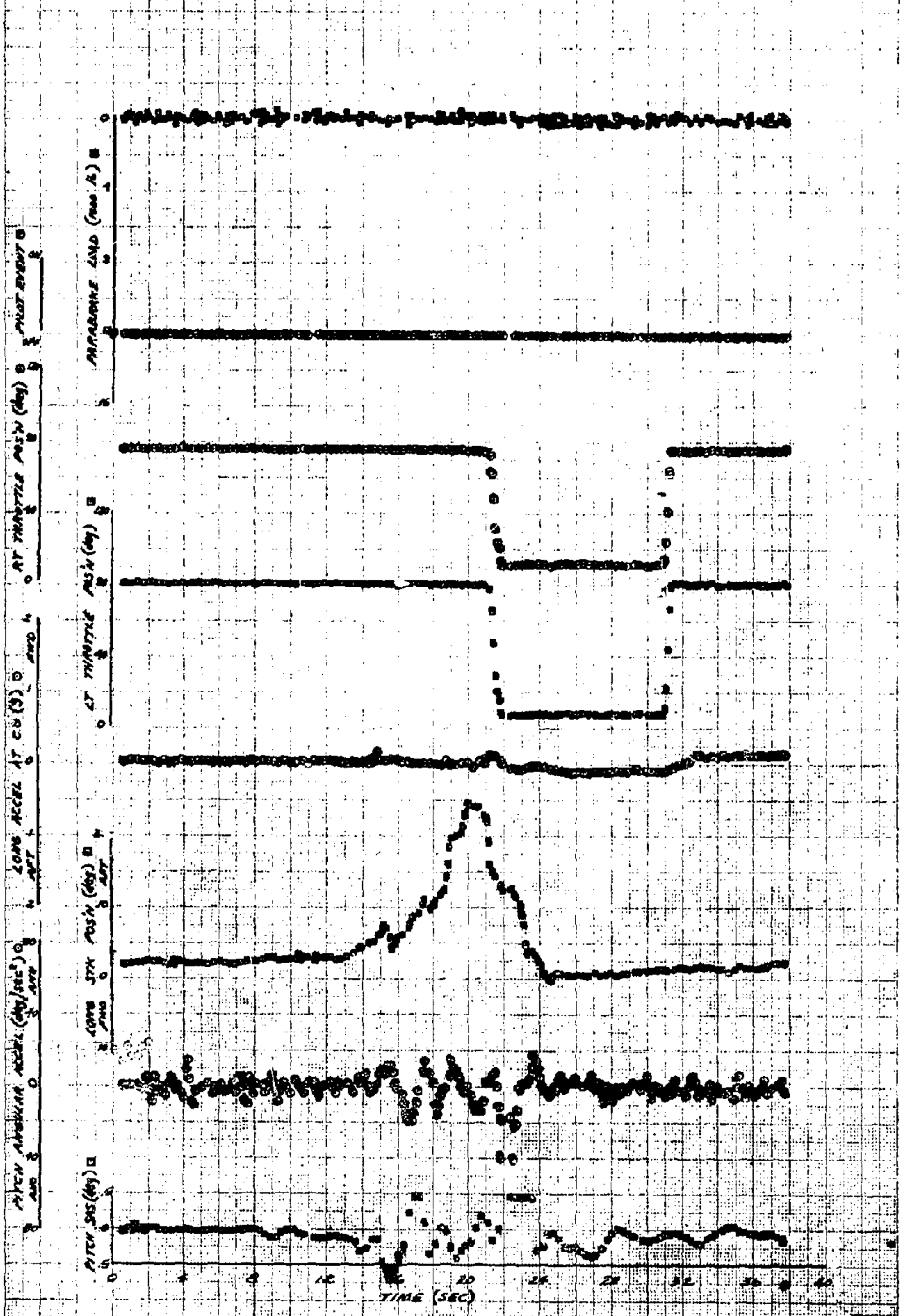

FIGURE 28 CONTINUED

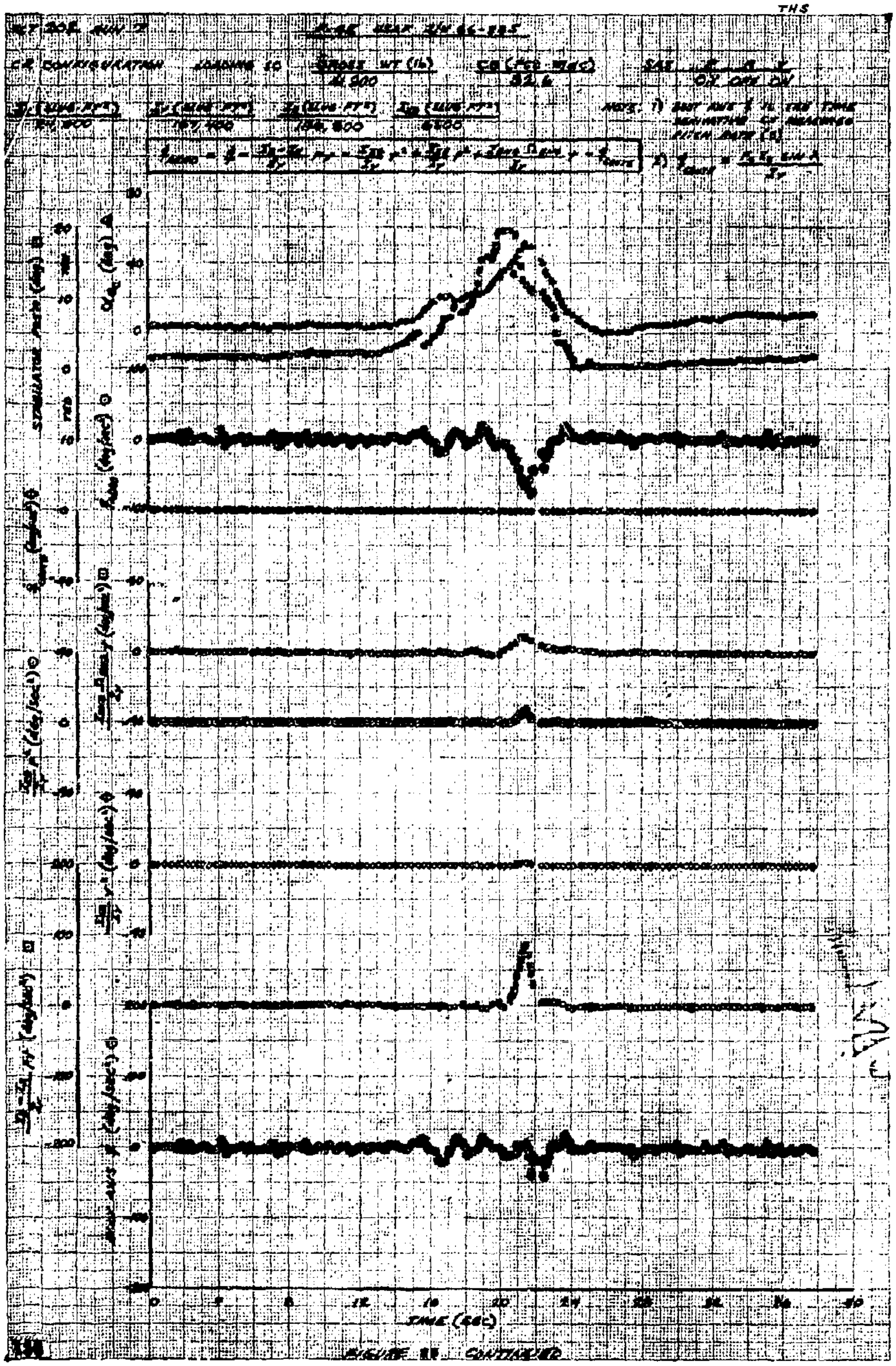

FIGURE [illegible] CONTINUED

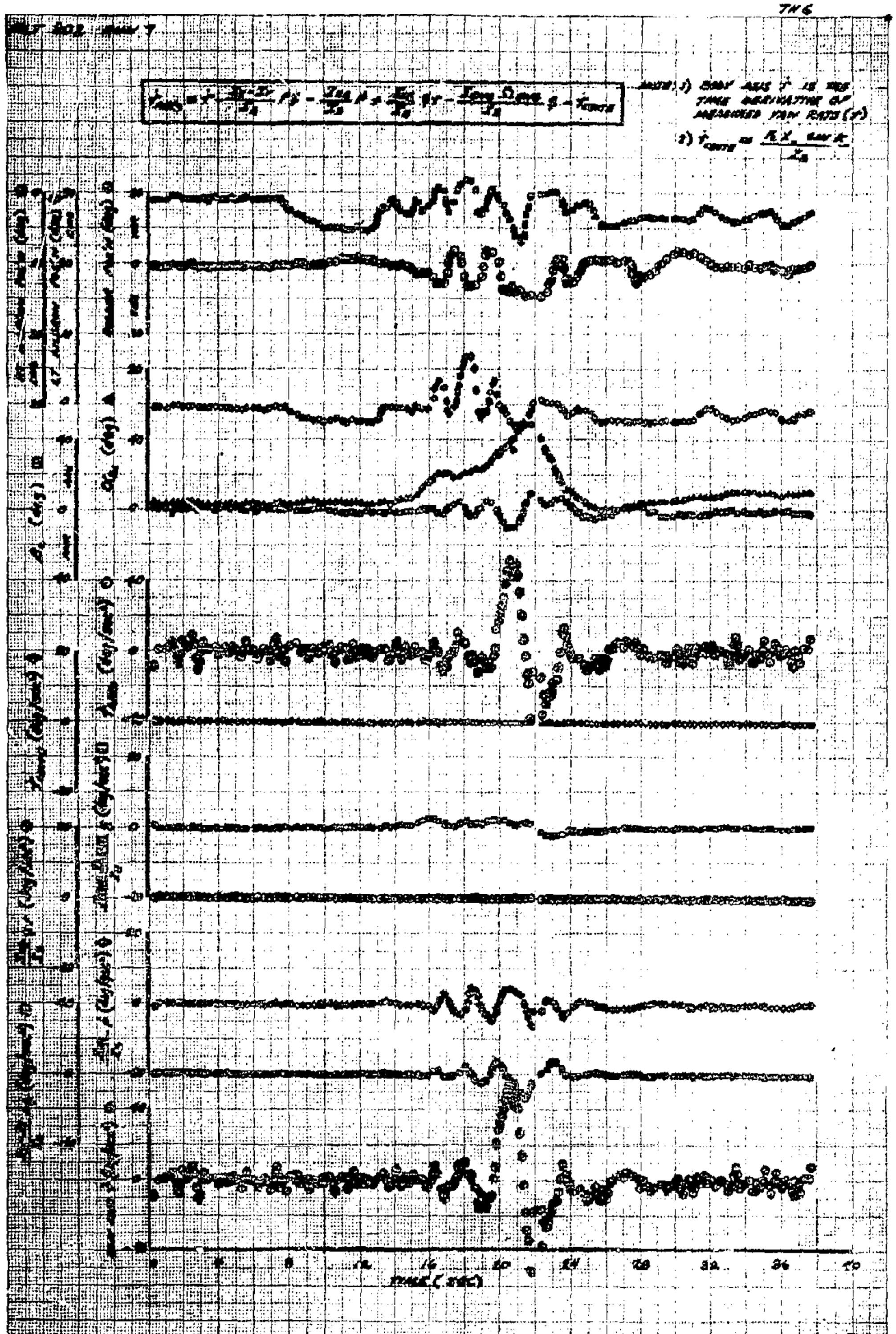

FIGURE 20 CONTINUED

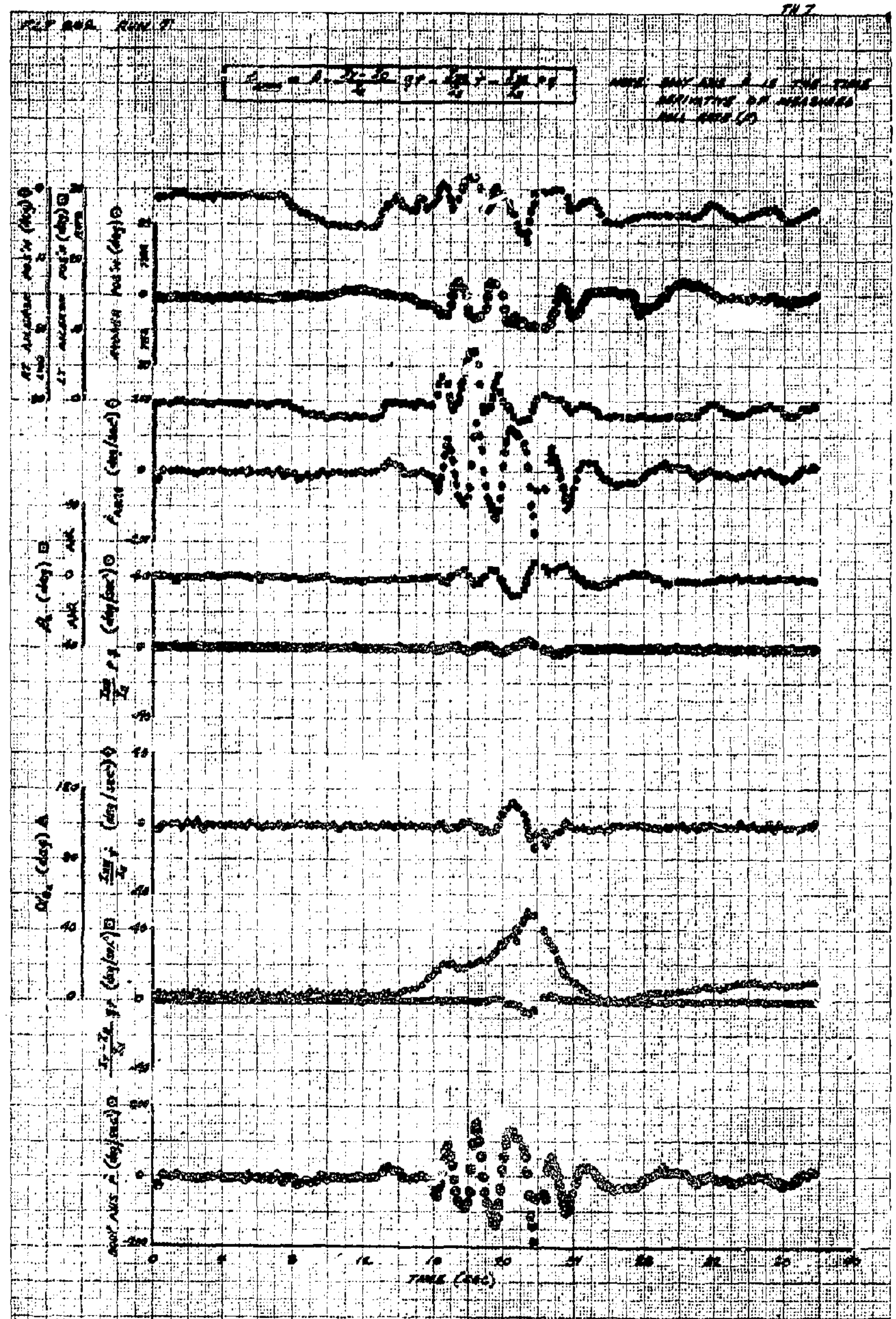

FIGURE 78 CONTINUED

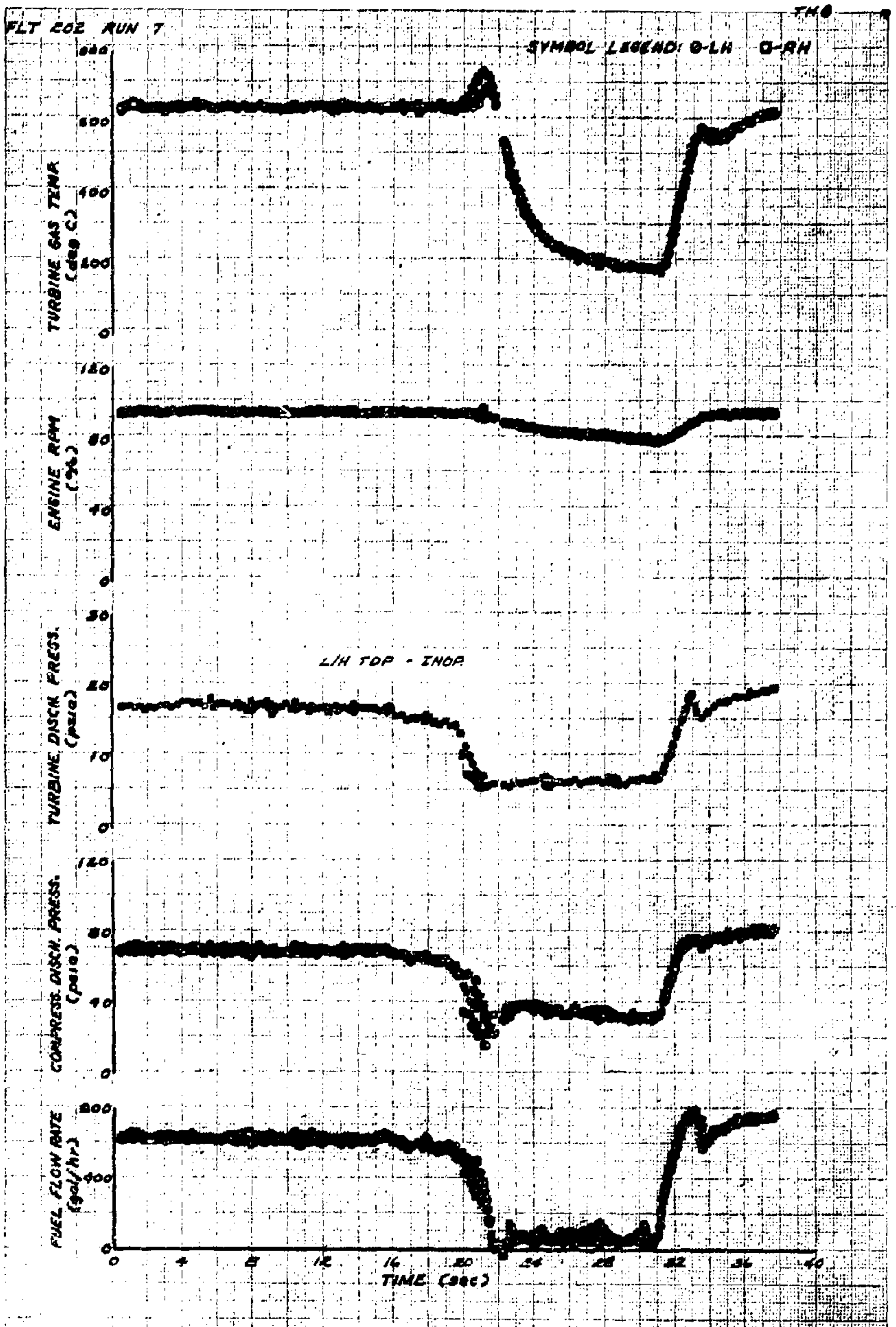

FIGURE 28 CONTINUED

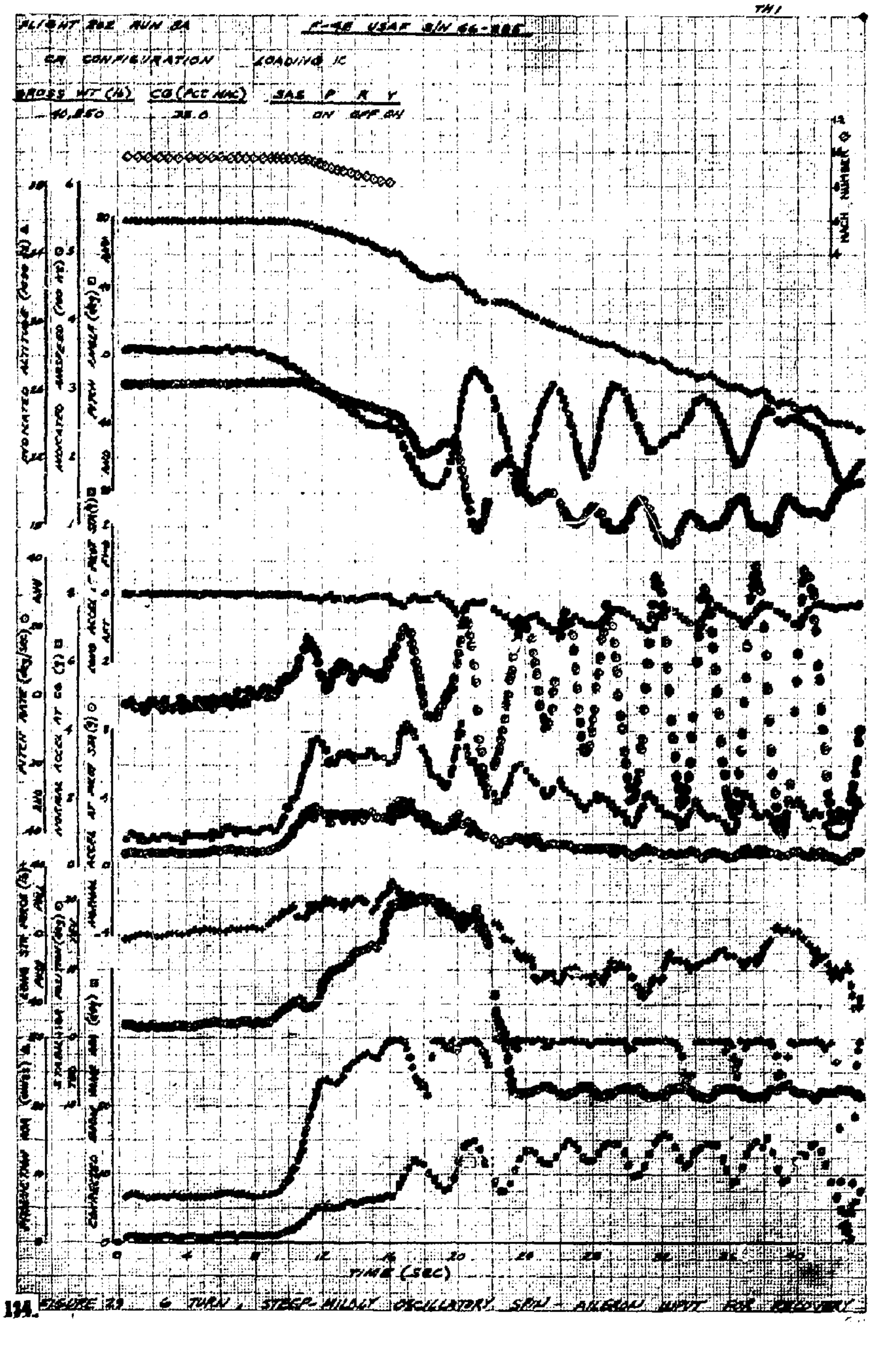

FIGURE 29 G TURN, STEEP-MILDLY OSCILLATORY SPIN - AILERON INPUT FOR RECOVERY

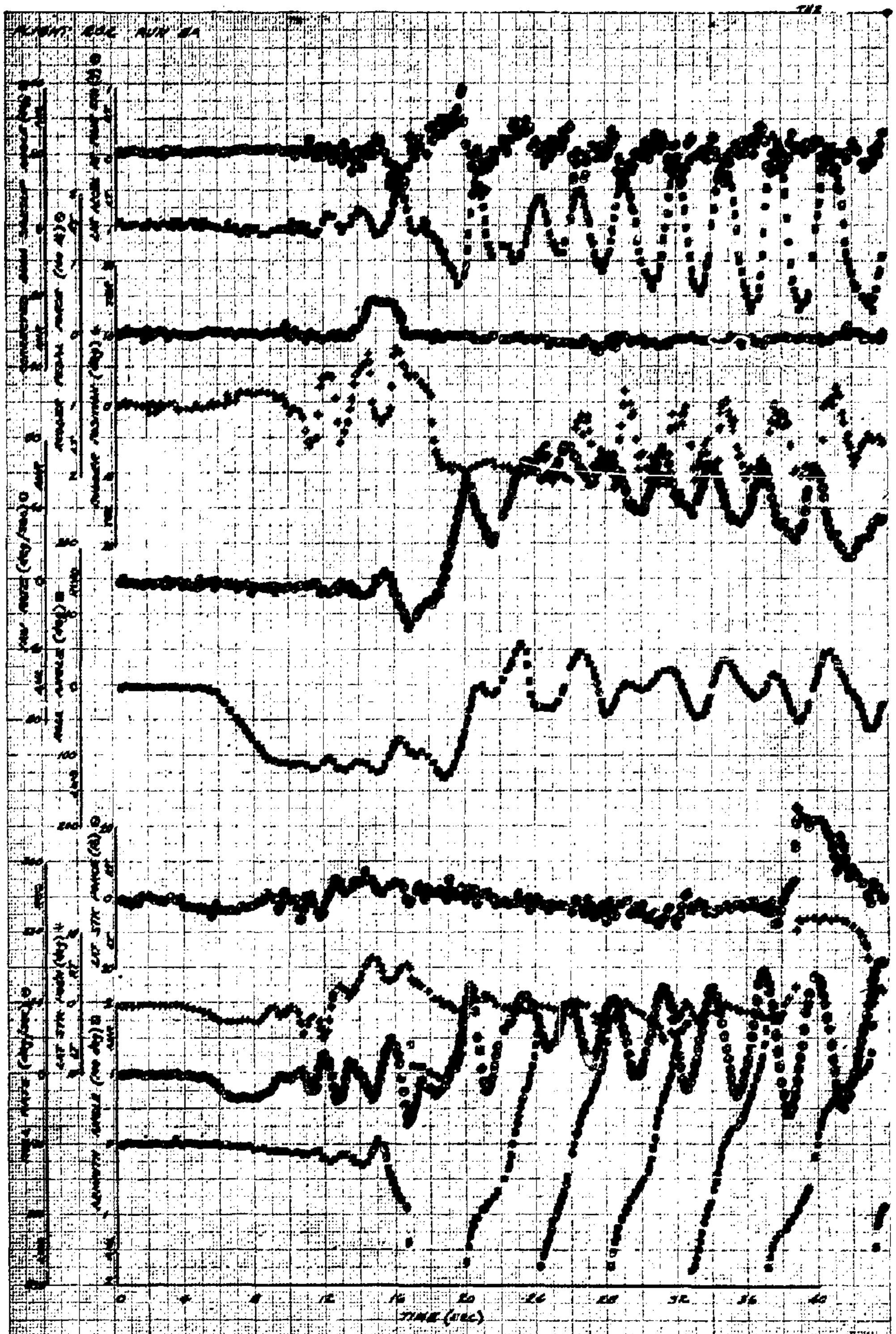

FIGURE 34 CONTINUED

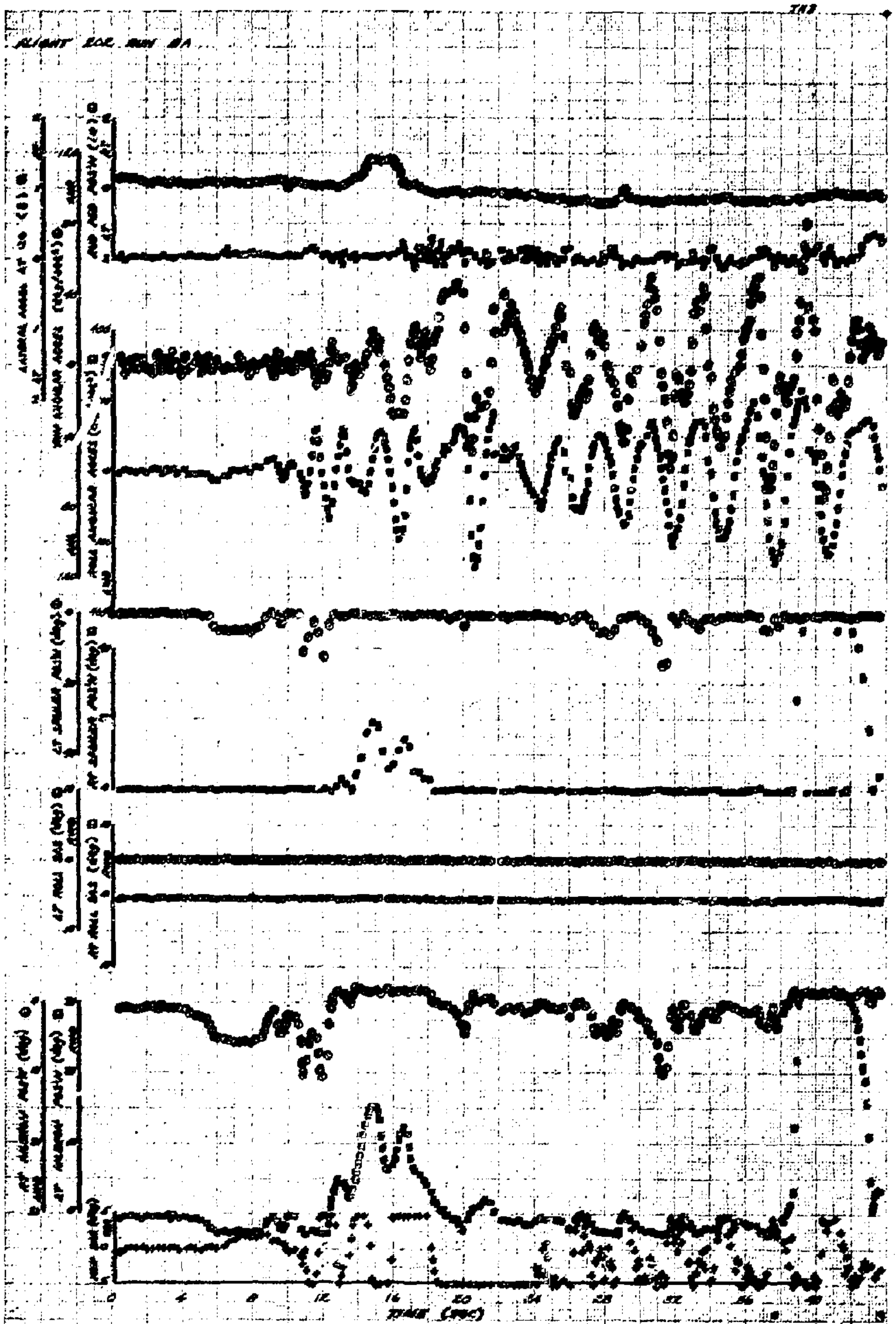

FIGURE 29 CONTINUED

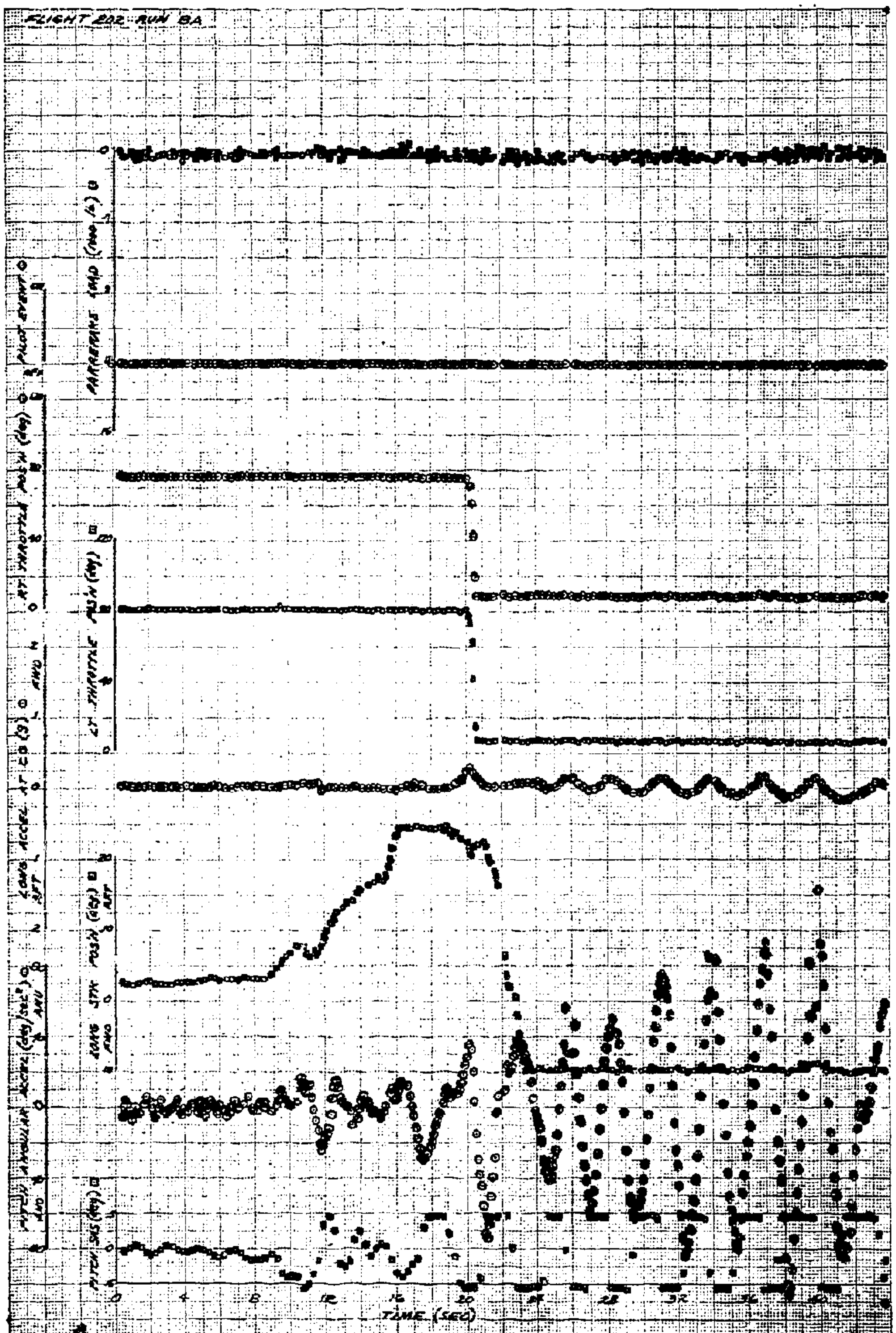

FIGURE 29 CONTINUED

TNS

FLT 202 RUN 8A

F-4E USAF S/N 66-285

CR CONFIGURATION LOADING 3C

GROSS WT (lb)	CG (PCT MAC)	SAS P R Y
40,850	33.0	ON OFF ON

I_x (SLUG·FT²)	I_y (SLUG·FT²)	I_z (SLUG·FT²)	I_{xz} (SLUG·FT²)
23,700	167,800	186,000	6150

$$\boxed{\dot{q}_{AERO} = \dot{q} - \frac{I_z - I_x}{I_y} pr - \frac{I_{xz}}{I_y} r^2 + \frac{I_{xz}}{I_y} p^2 + \frac{I_{eng}\,\Omega_{eng}}{I_y} r - \dot{q}_{CNTR}}$$

NOTE: 1) BODY AXIS $\dot{q}$ IS THE TIME DERIVATIVE OF MEASURED PITCH RATE (q)

2) $\dot{q}_{CNTR} = \frac{F_s\, \ell_c \cdot \sin\lambda}{I_y}$

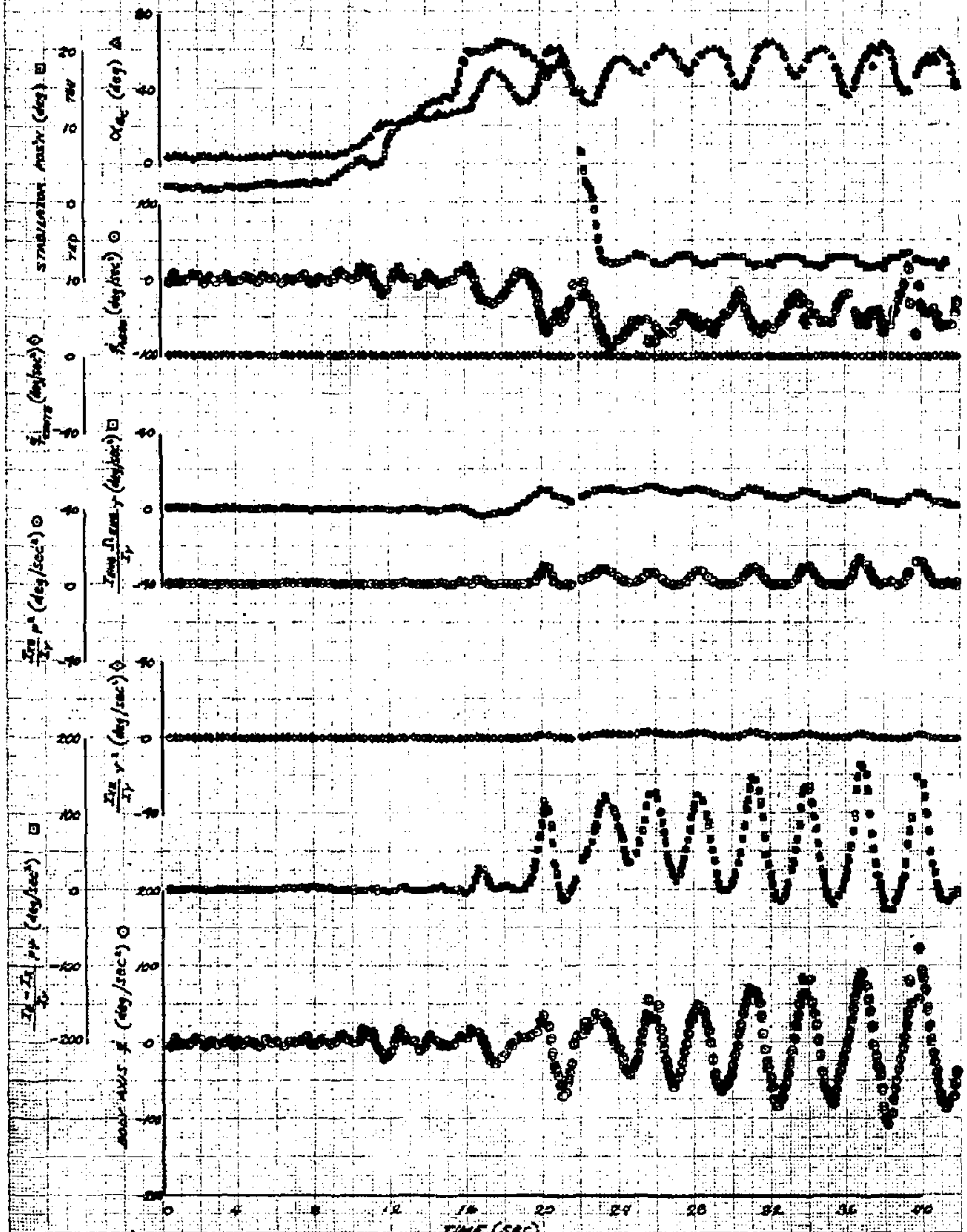

FIGURE 29 CONTINUED

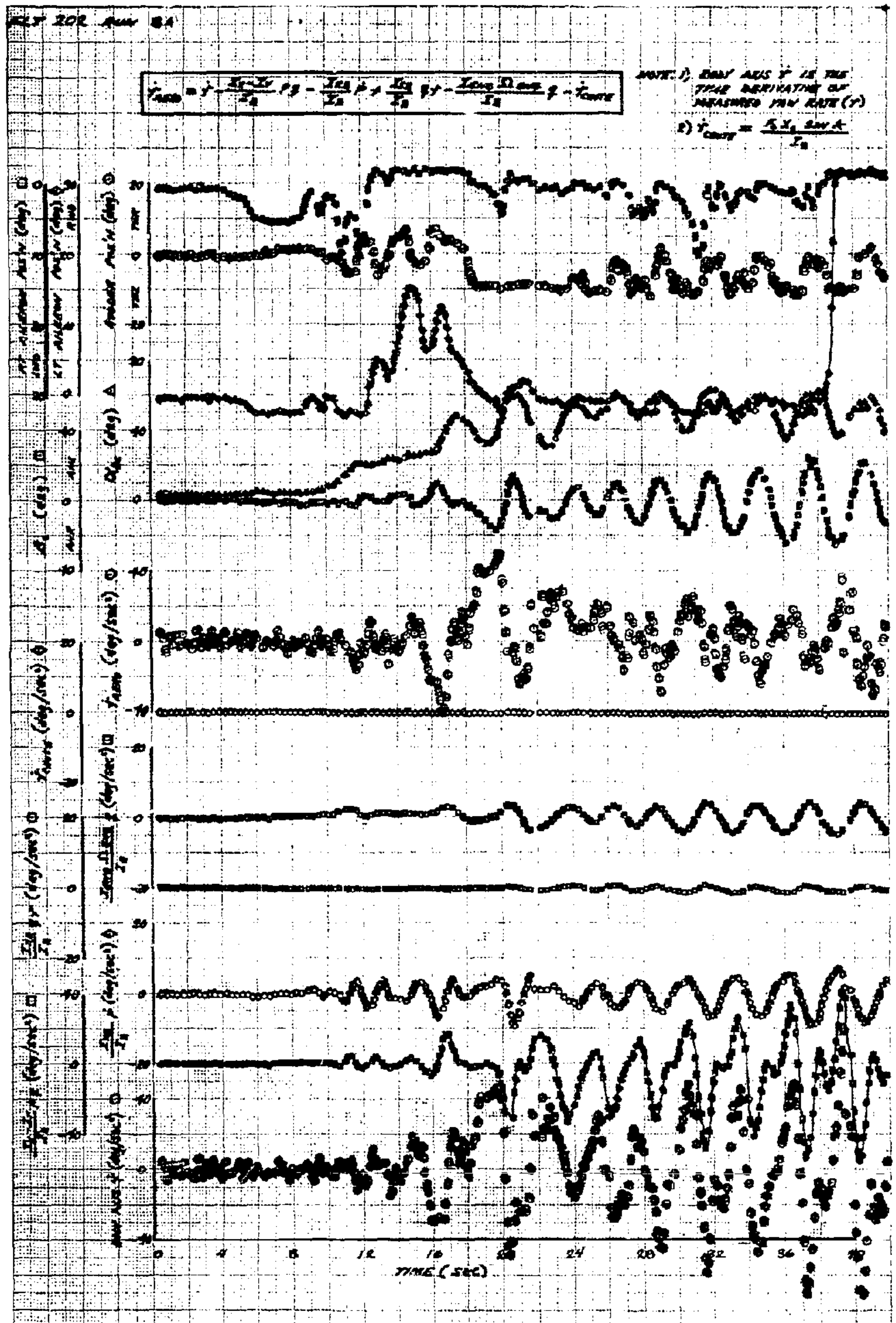

FIGURE 29 CONTINUED

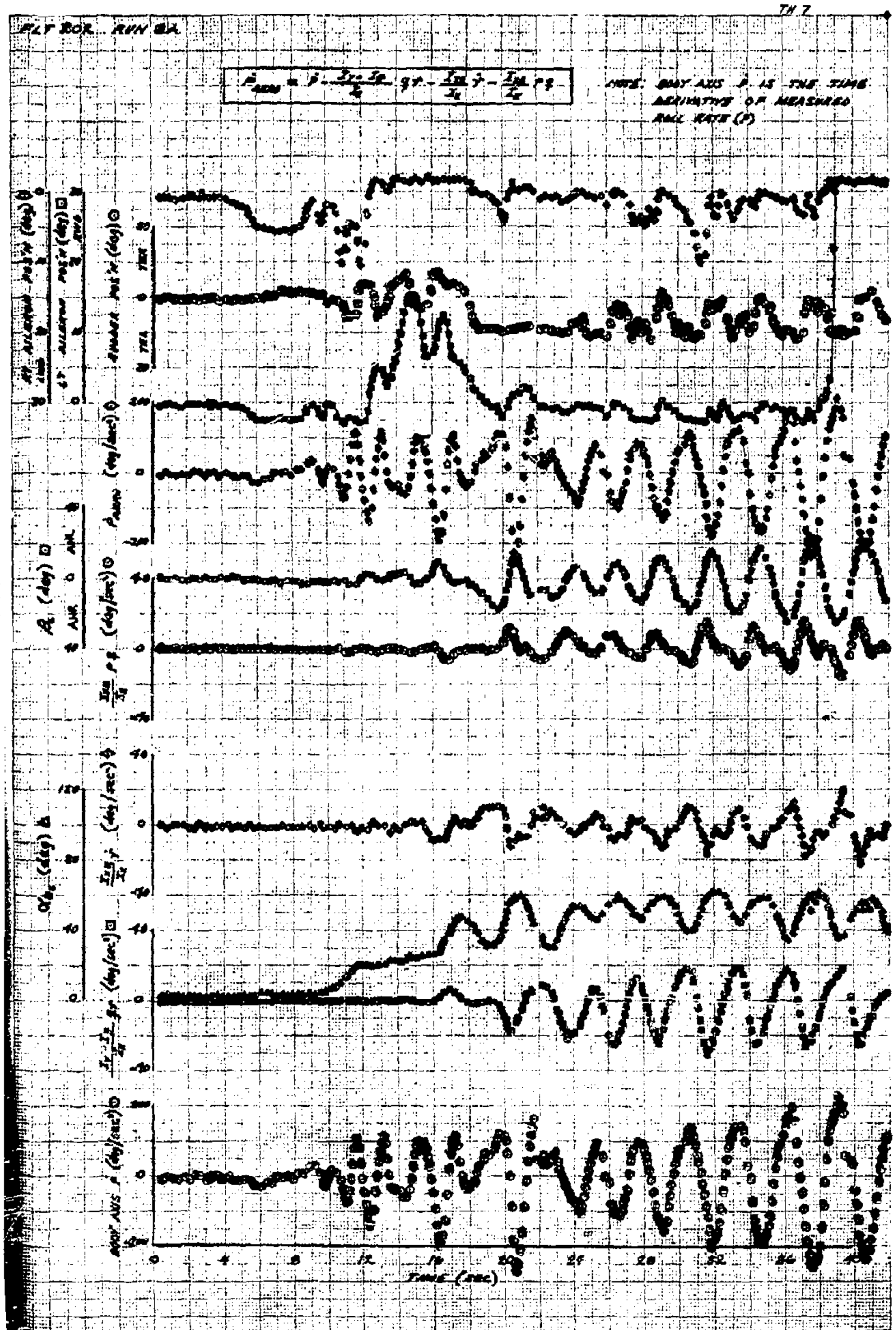

FIGURE 29 CONTINUED

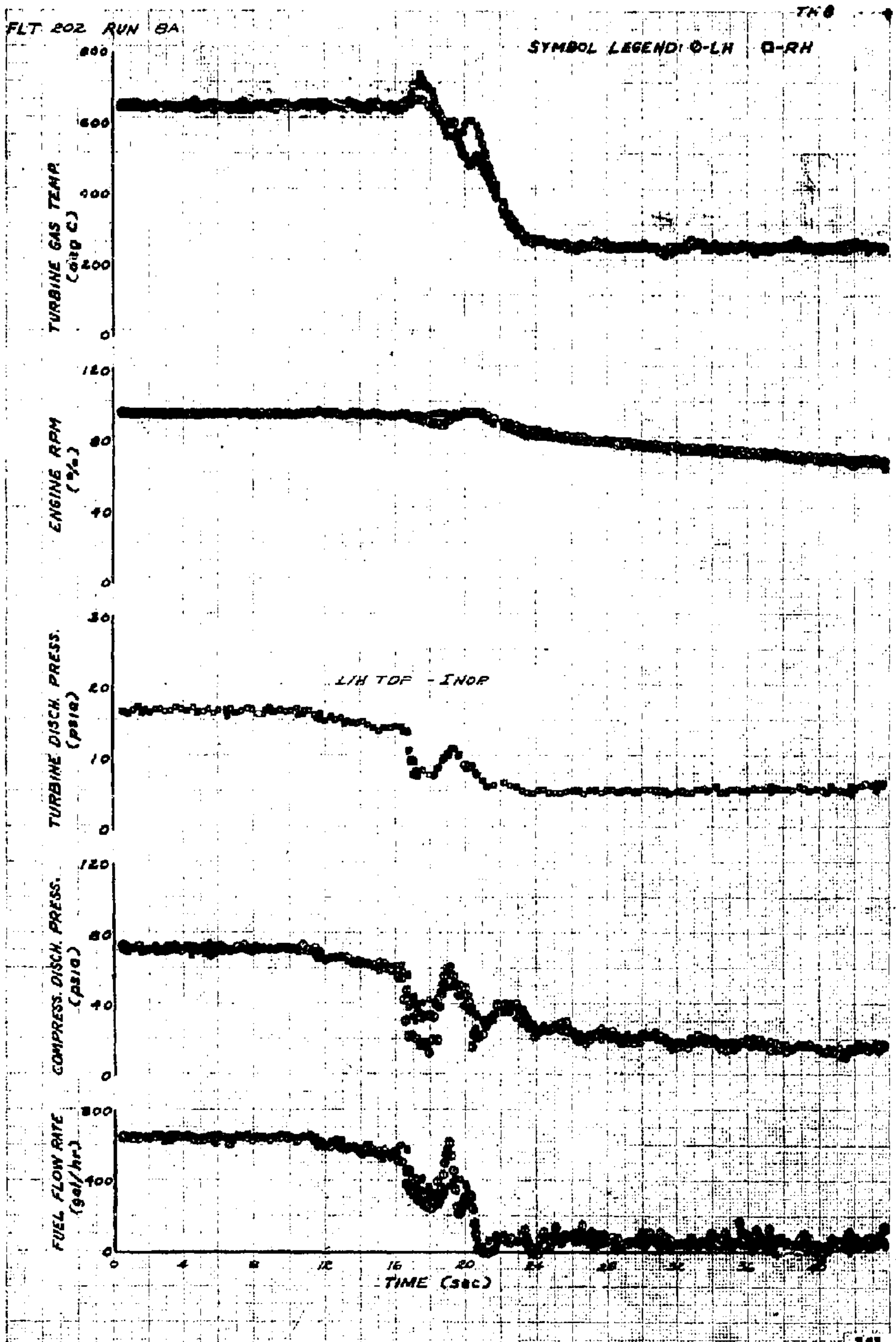

FIGURE 29 CONTINUED

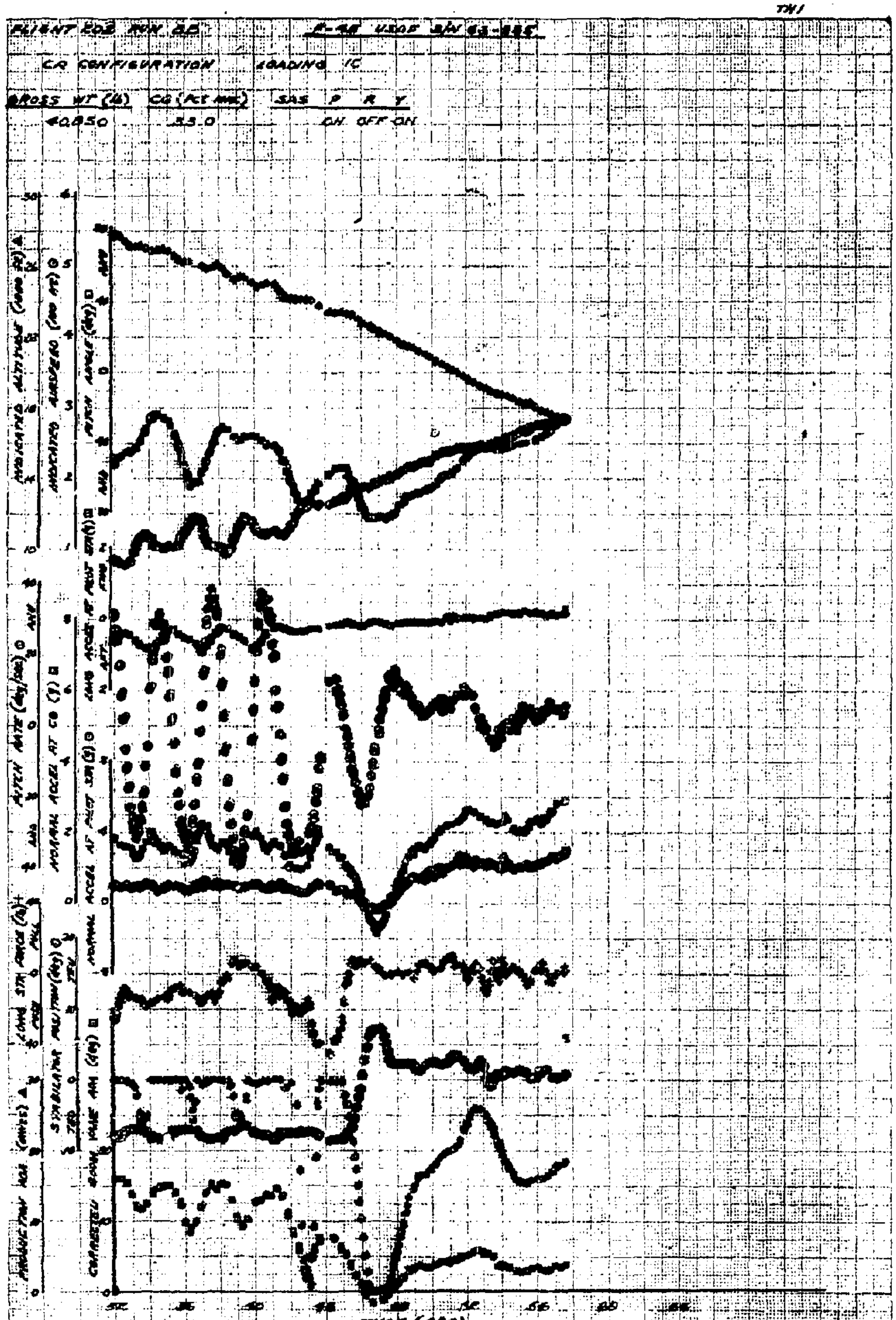

FIGURE 29 CONTINUED

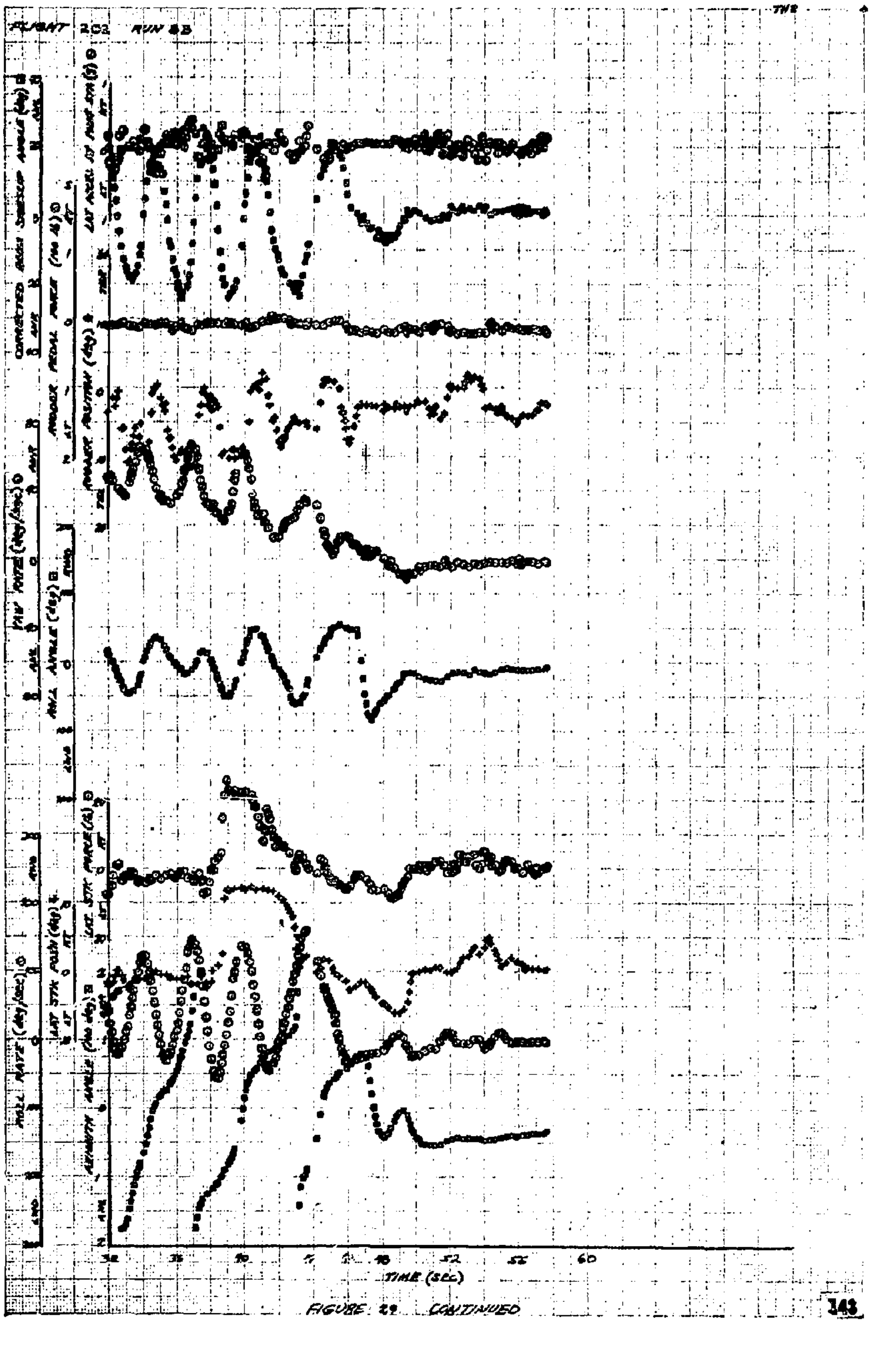

FIGURE 29 CONTINUED

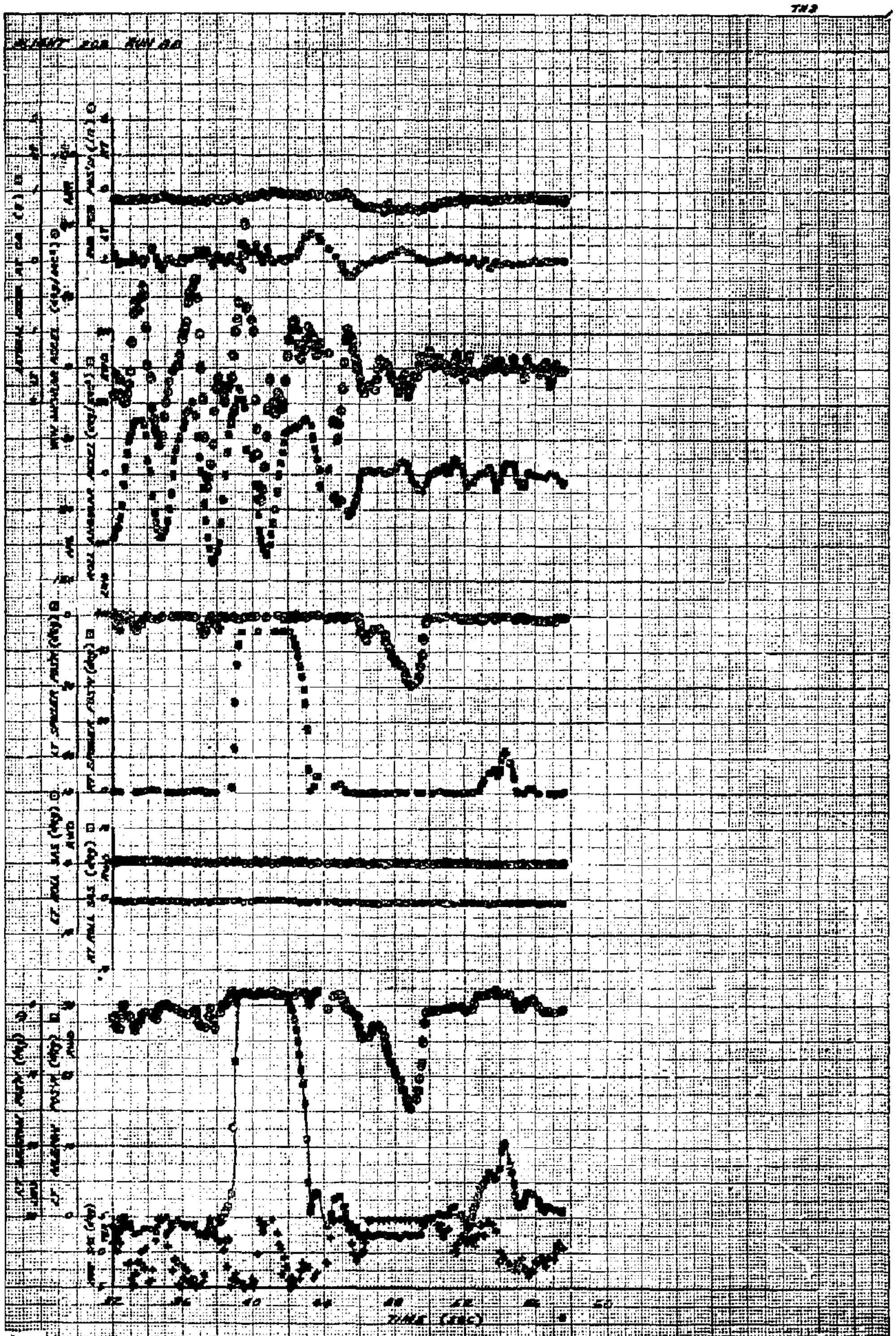

FIGURE 29 CONTINUED

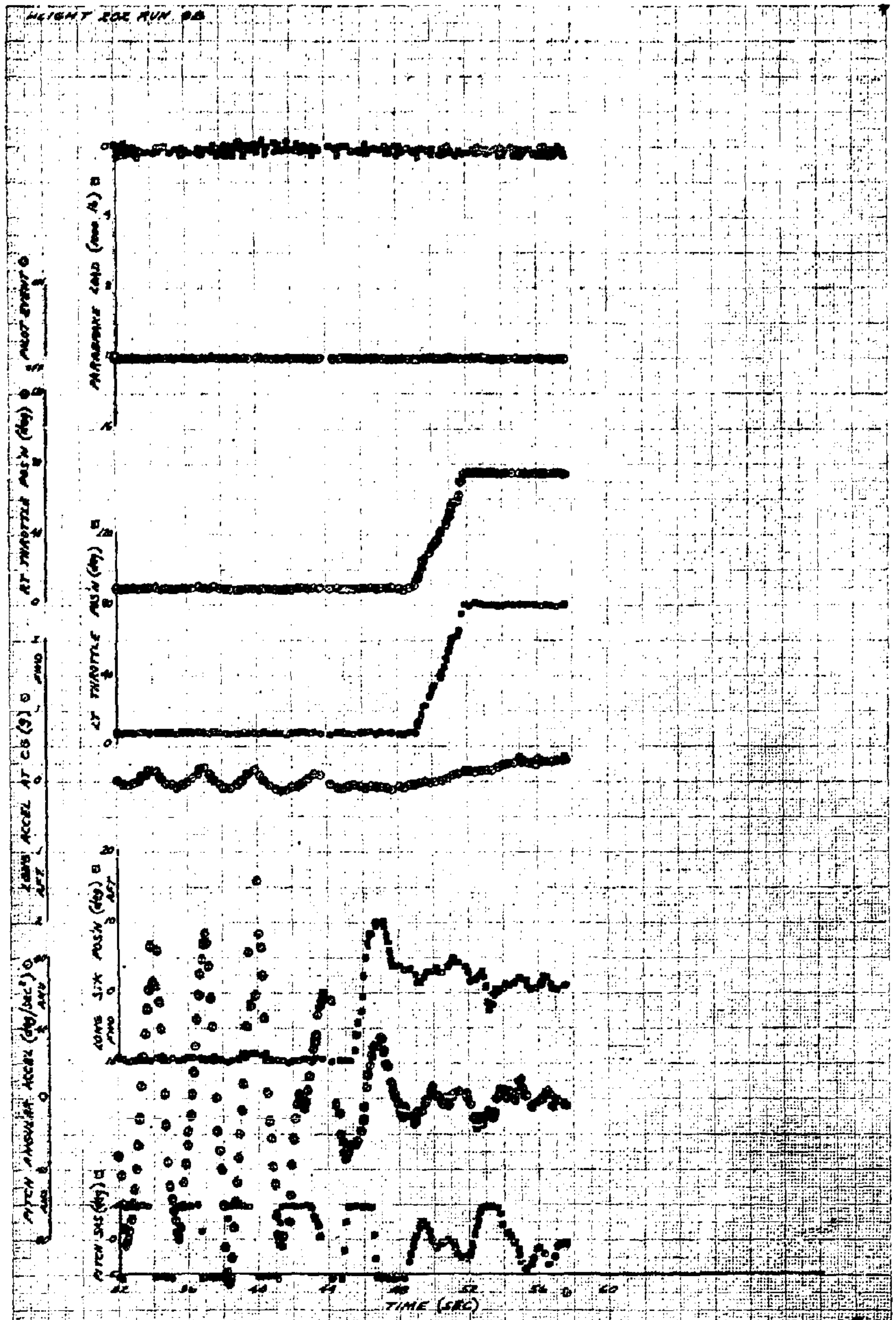

FIGURE 29 CONTINUED

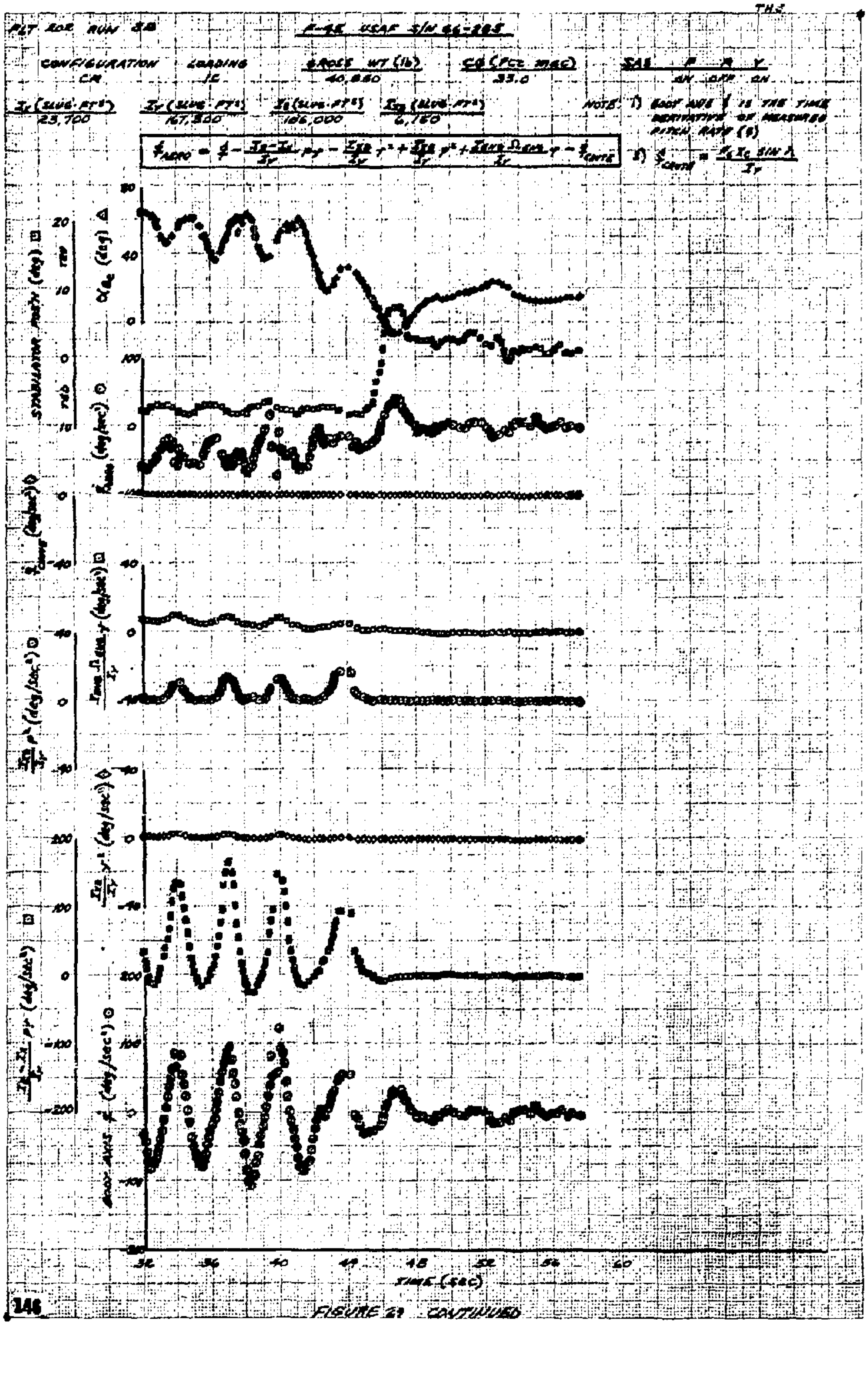

FIGURE 29 CONTINUED

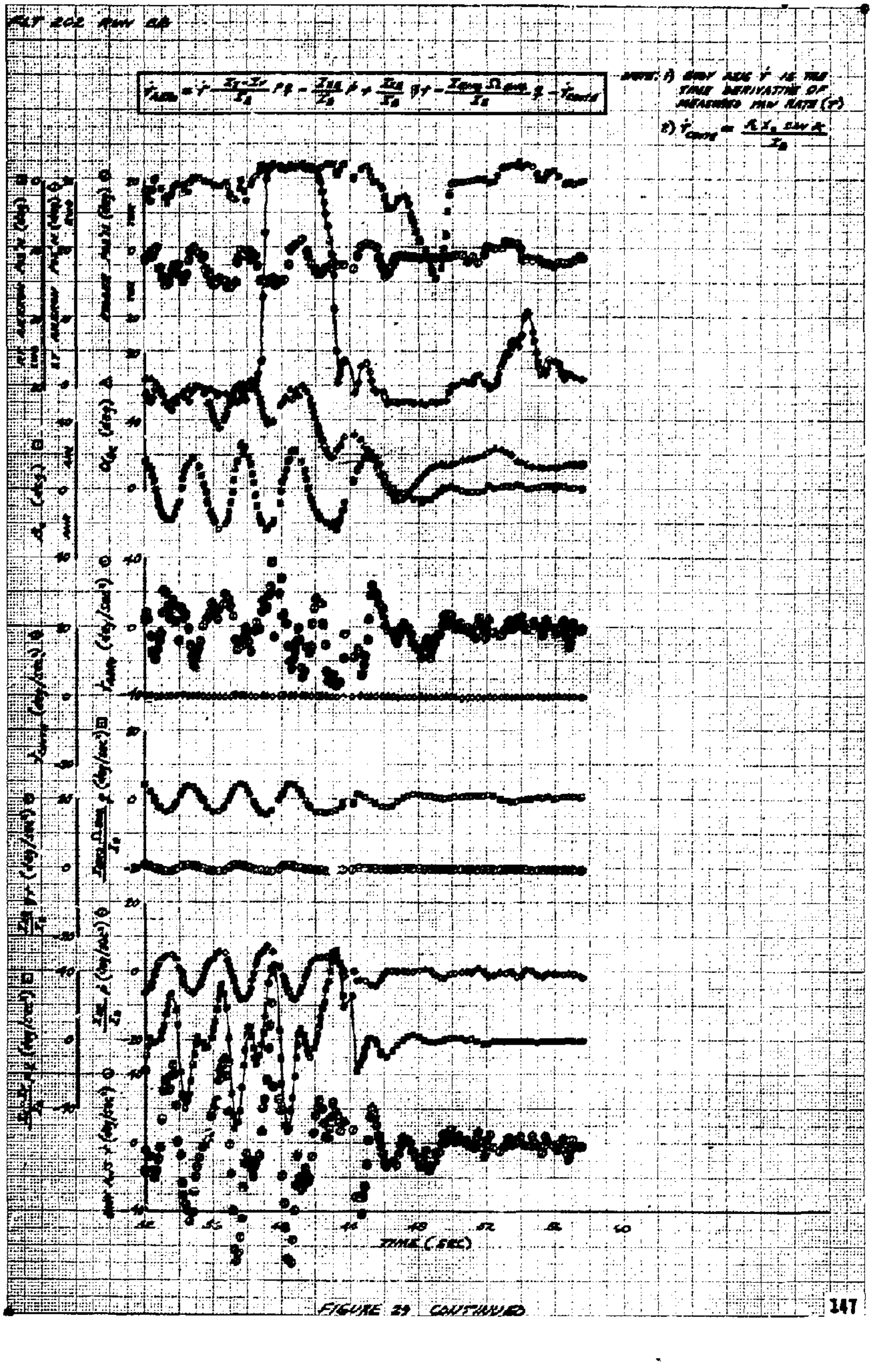

FIGURE 29 CONTINUED

FLT 202 RUN 8B

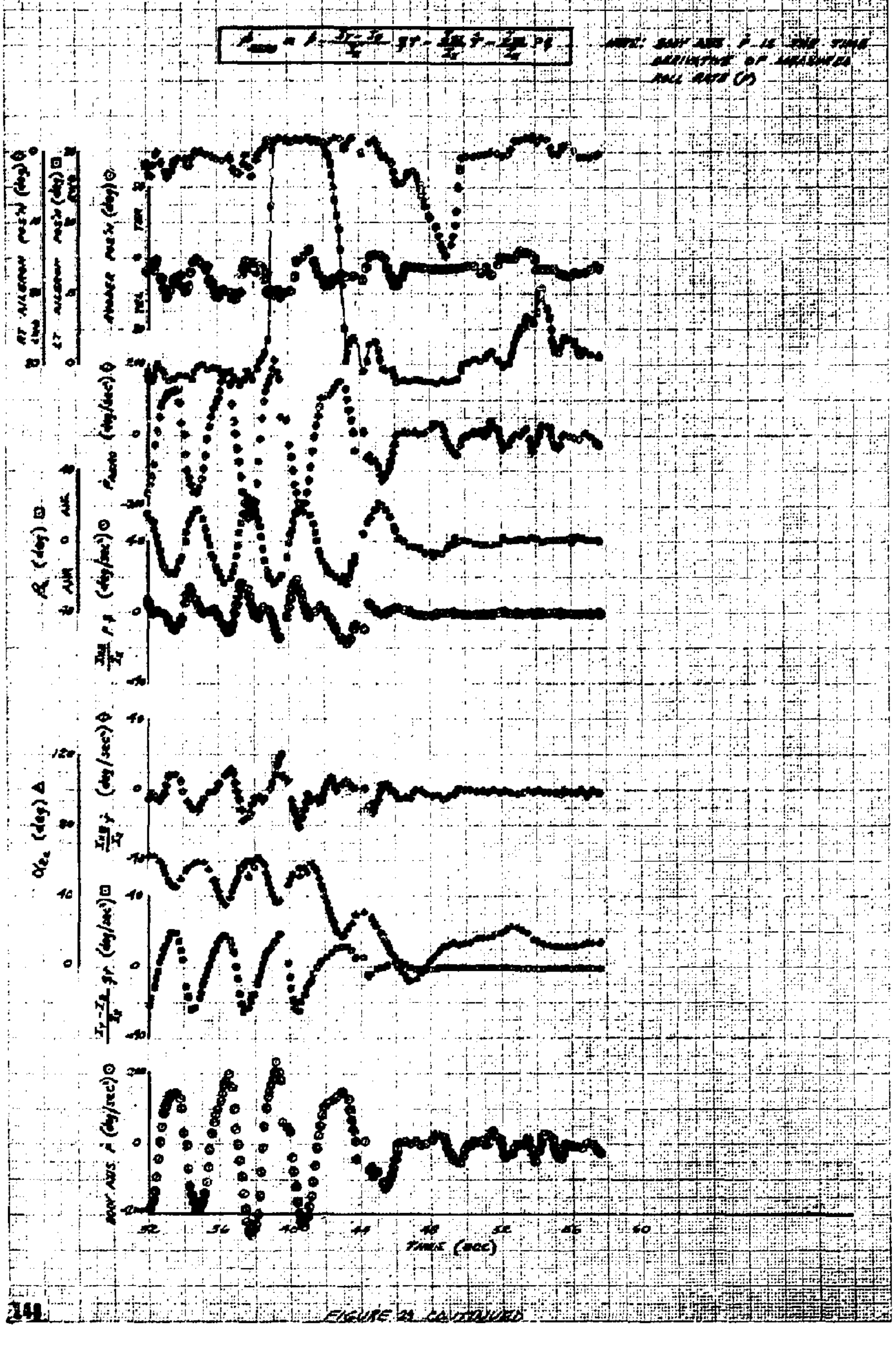

FIGURE 21 CONTINUED

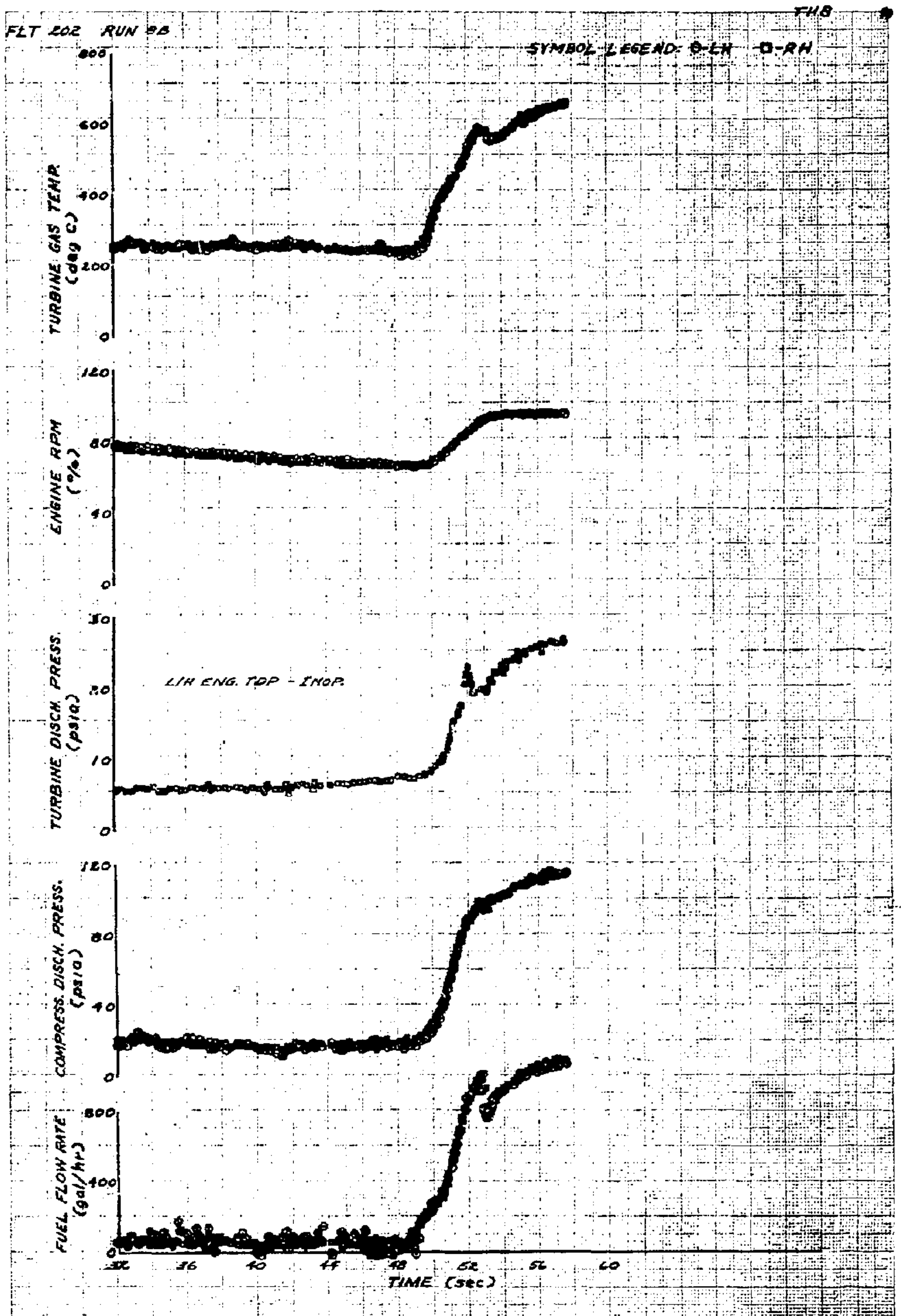

FIGURE 29 CONTINUED

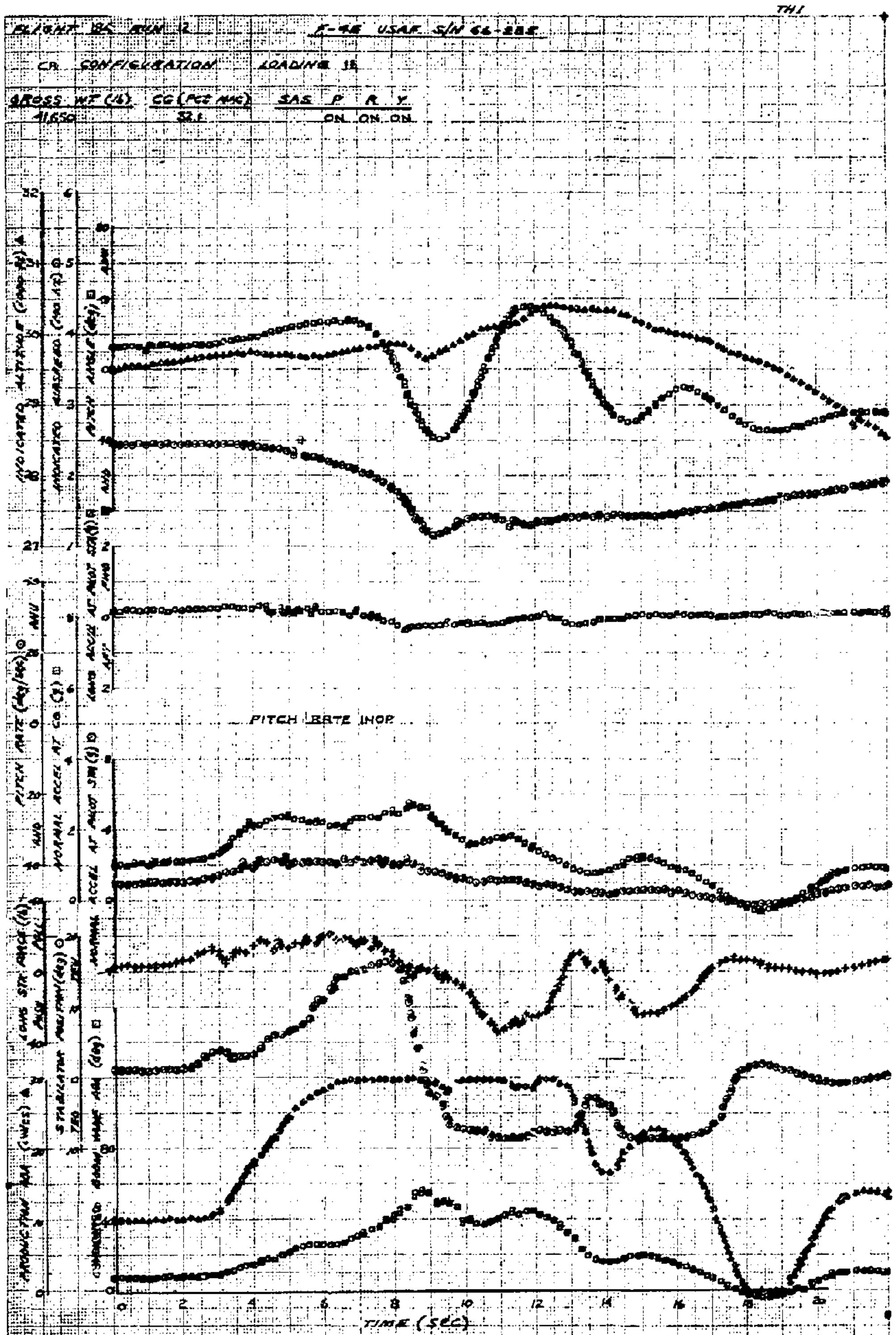

FIGURE 30 ROLLING DEPARTURE WITH OPPOSITE RECOVERY ROLL

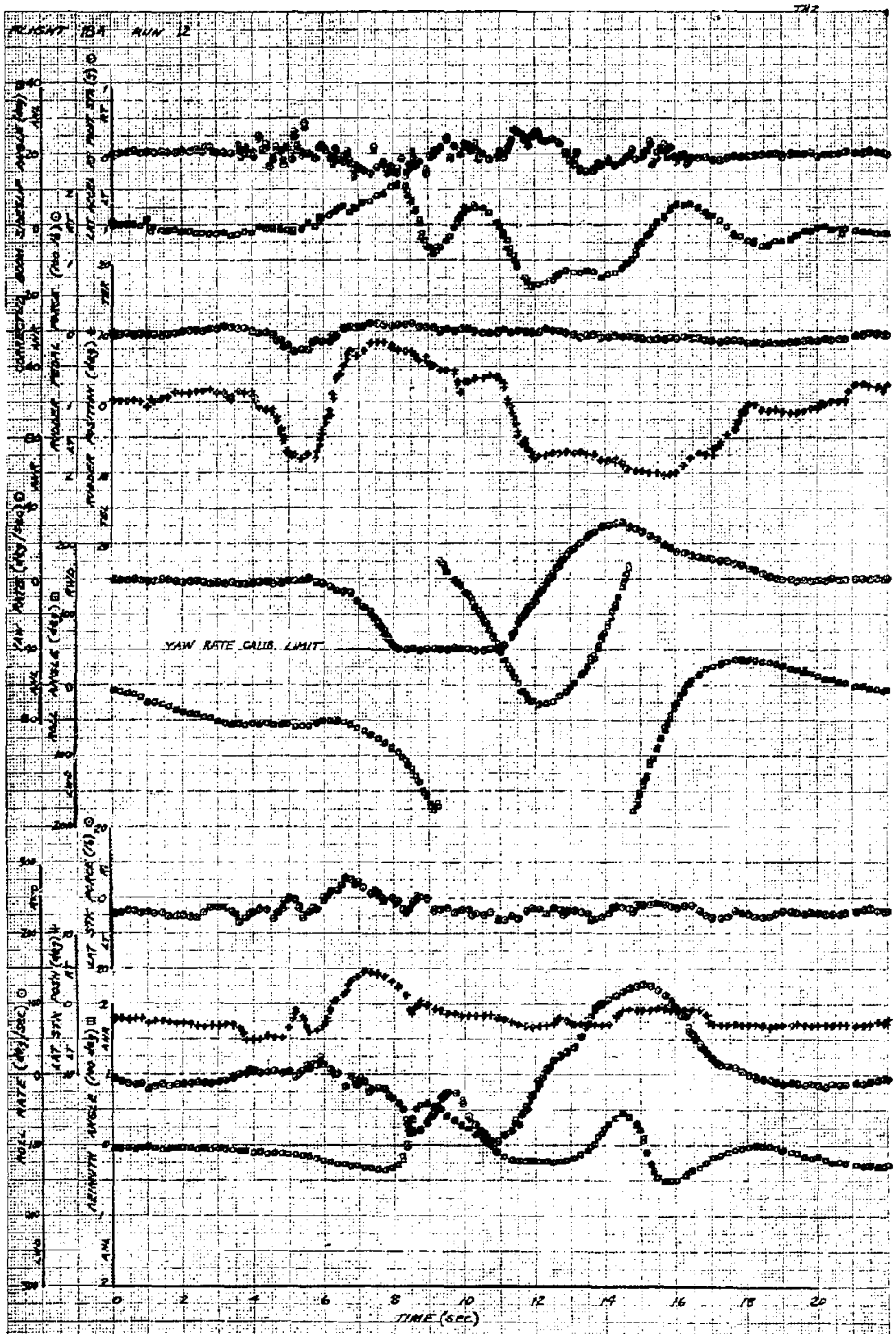

FIGURE 20 CONTINUED

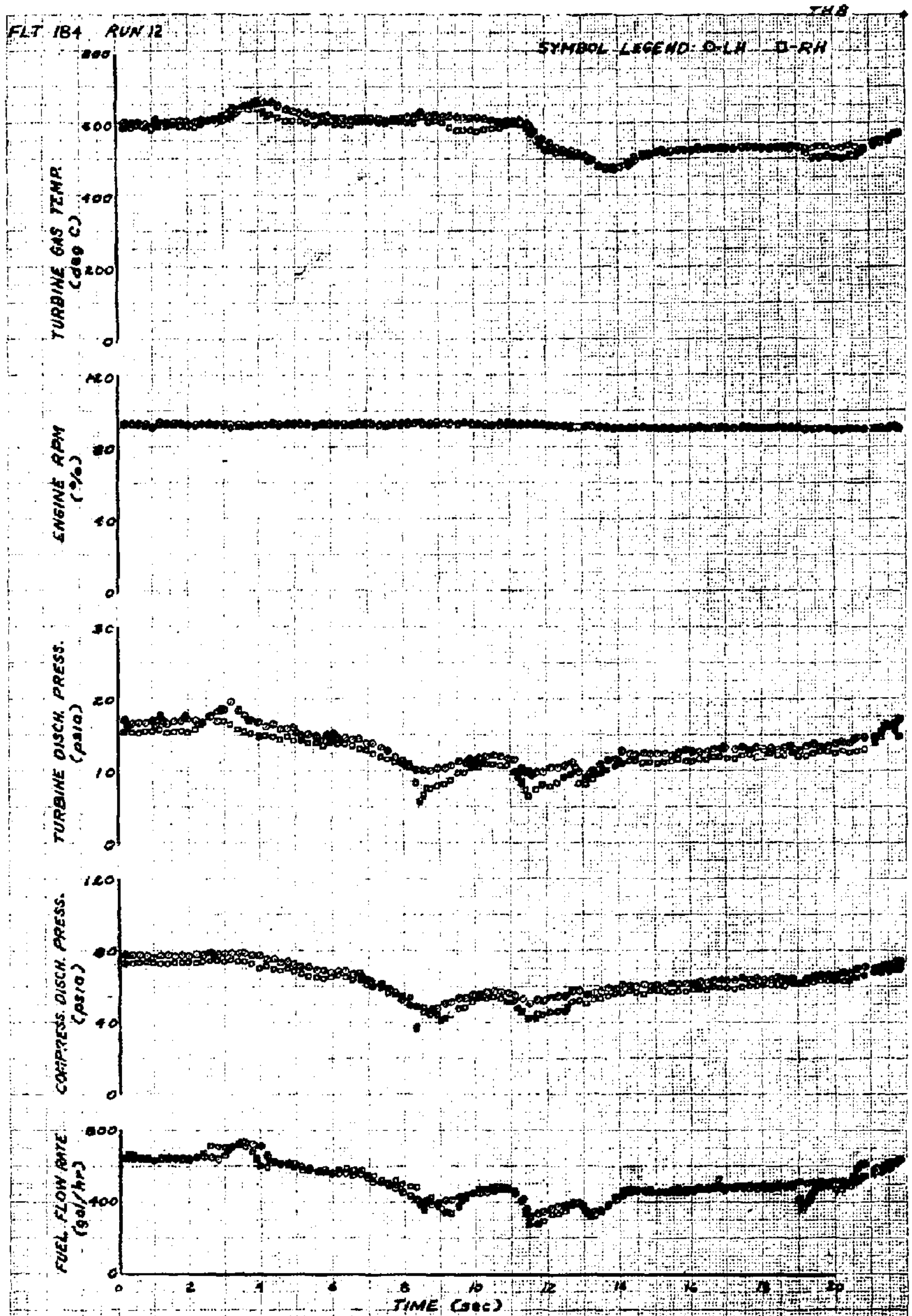

FIGURE 30 CONTINUED

THIS PAGE LEFT BLANK FOR PRESENTATION PURPOSES

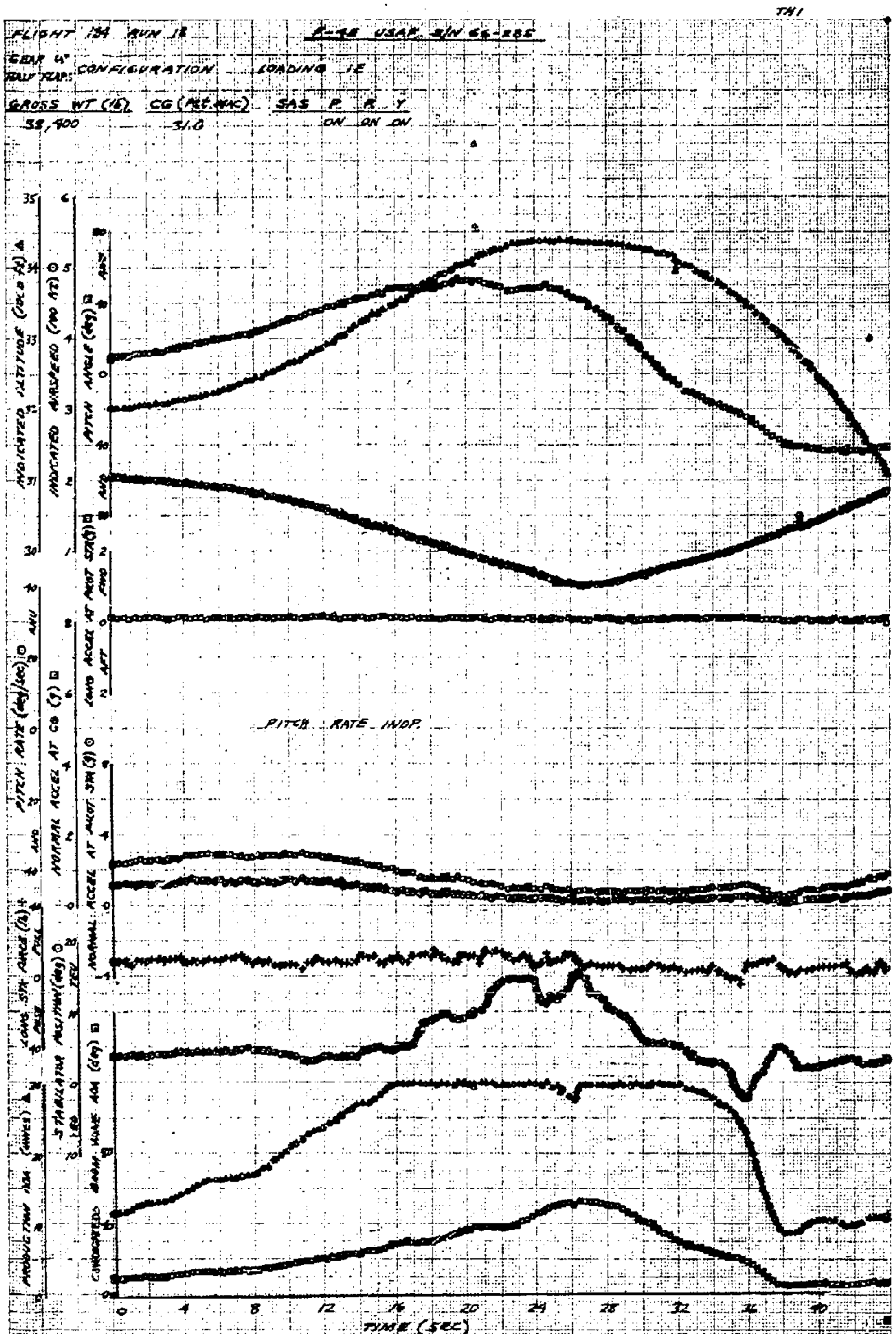

FIGURE 31 HIGH AOA STALL PENETRATION WITH HALF FLAPS

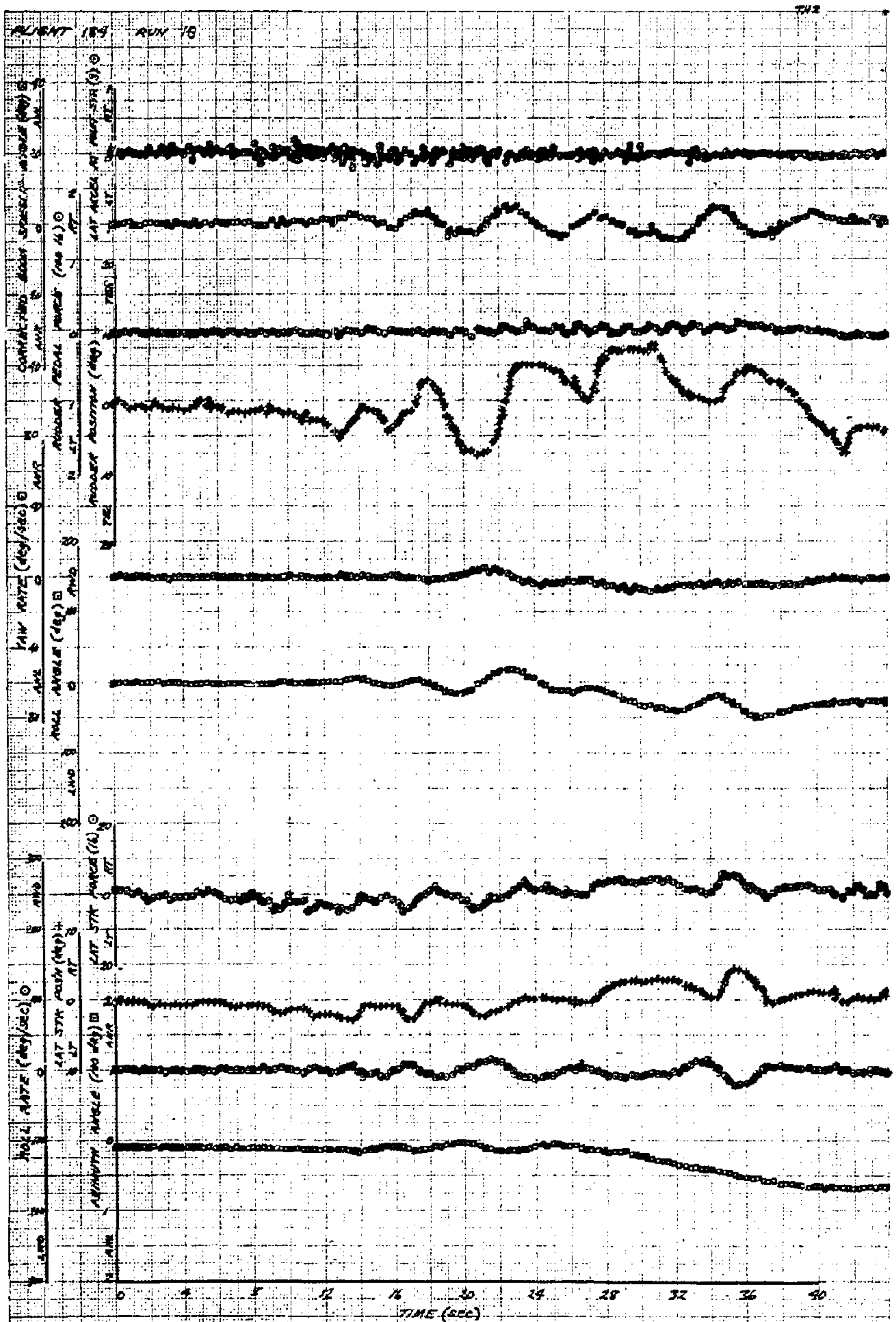

FIGURE 31 CONTINUED

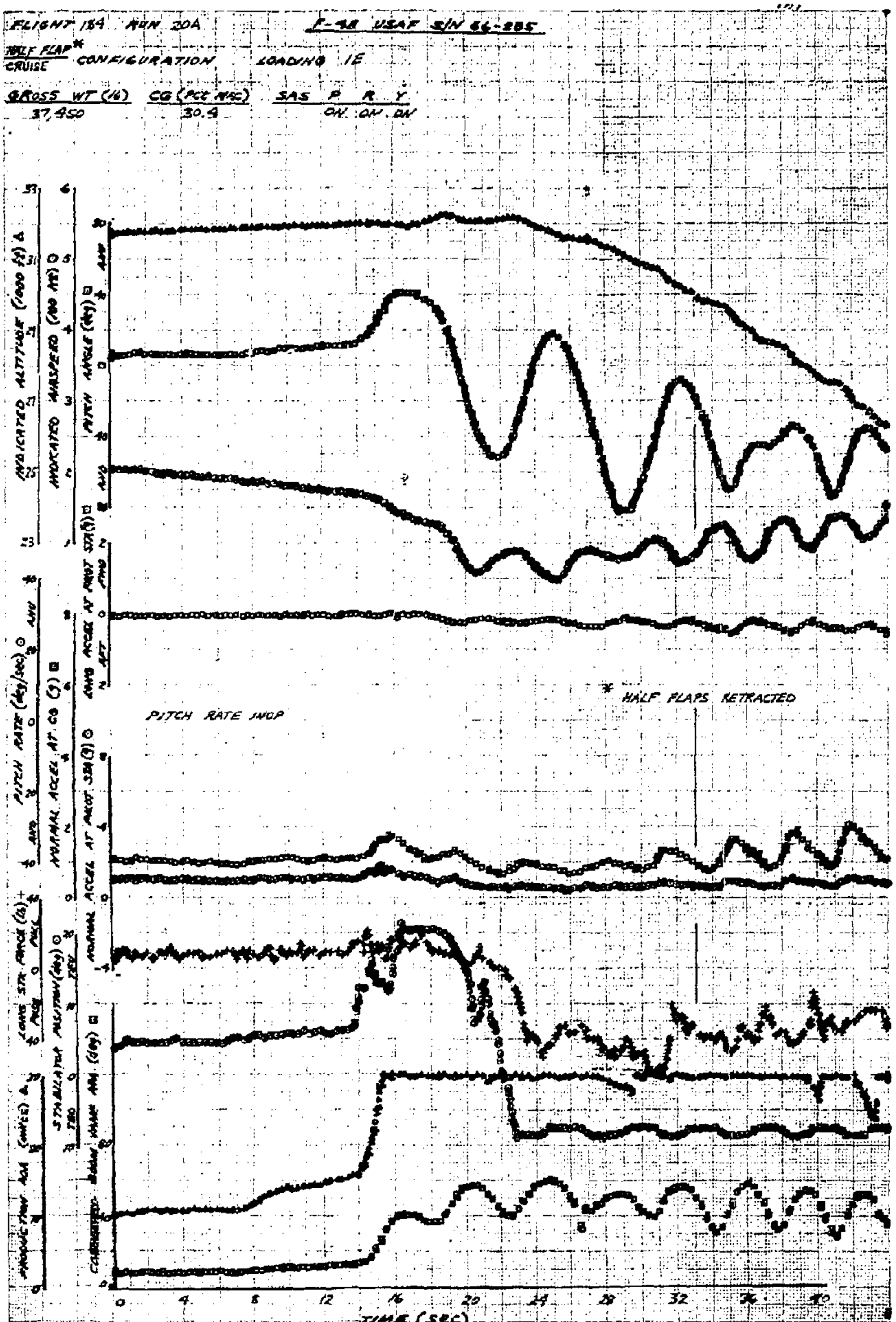

FIGURE 32 7 TURN, 2 MODE SPIN ENTERED WITH HALF FLAPS

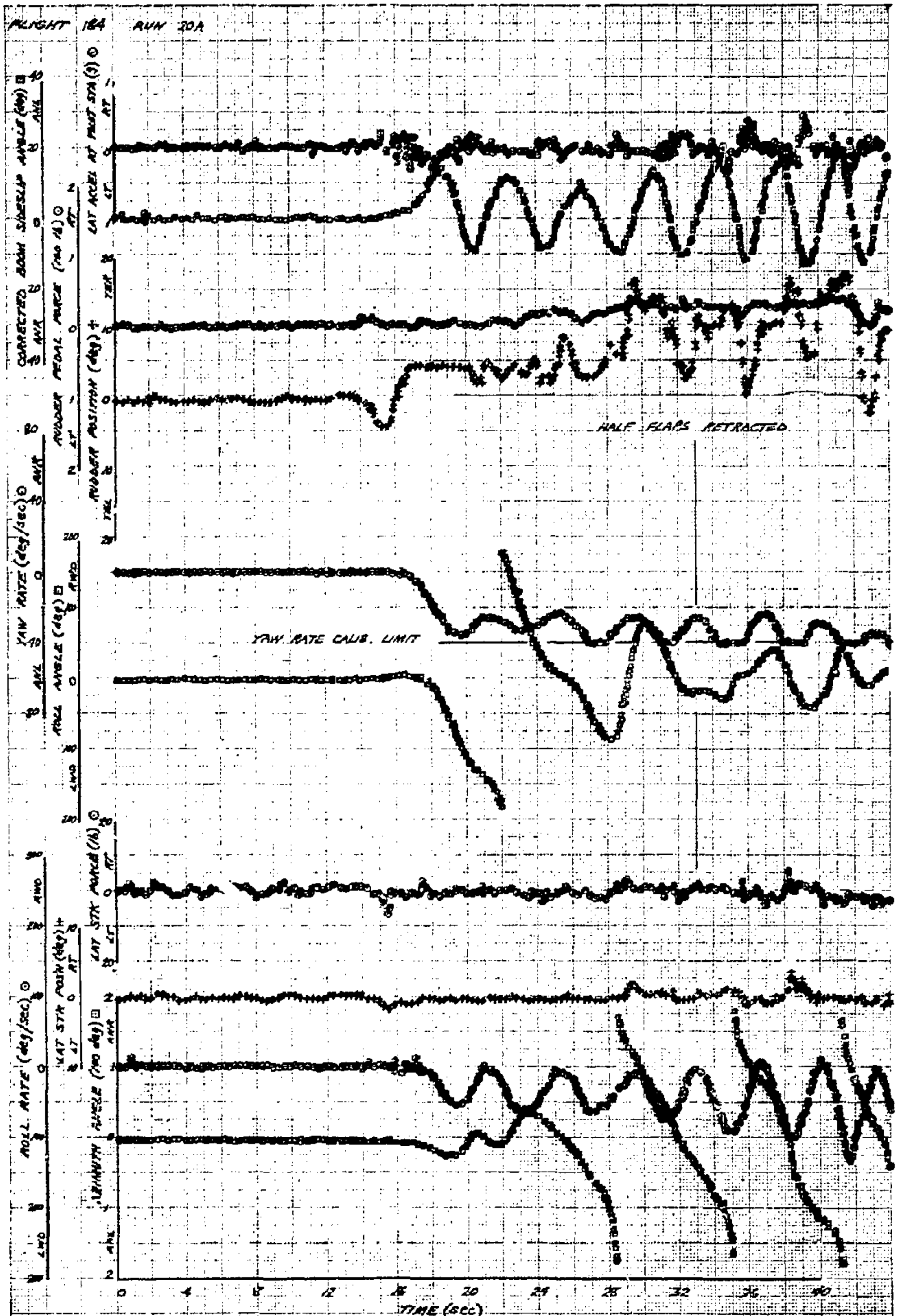

FIGURE 32 CONTINUED

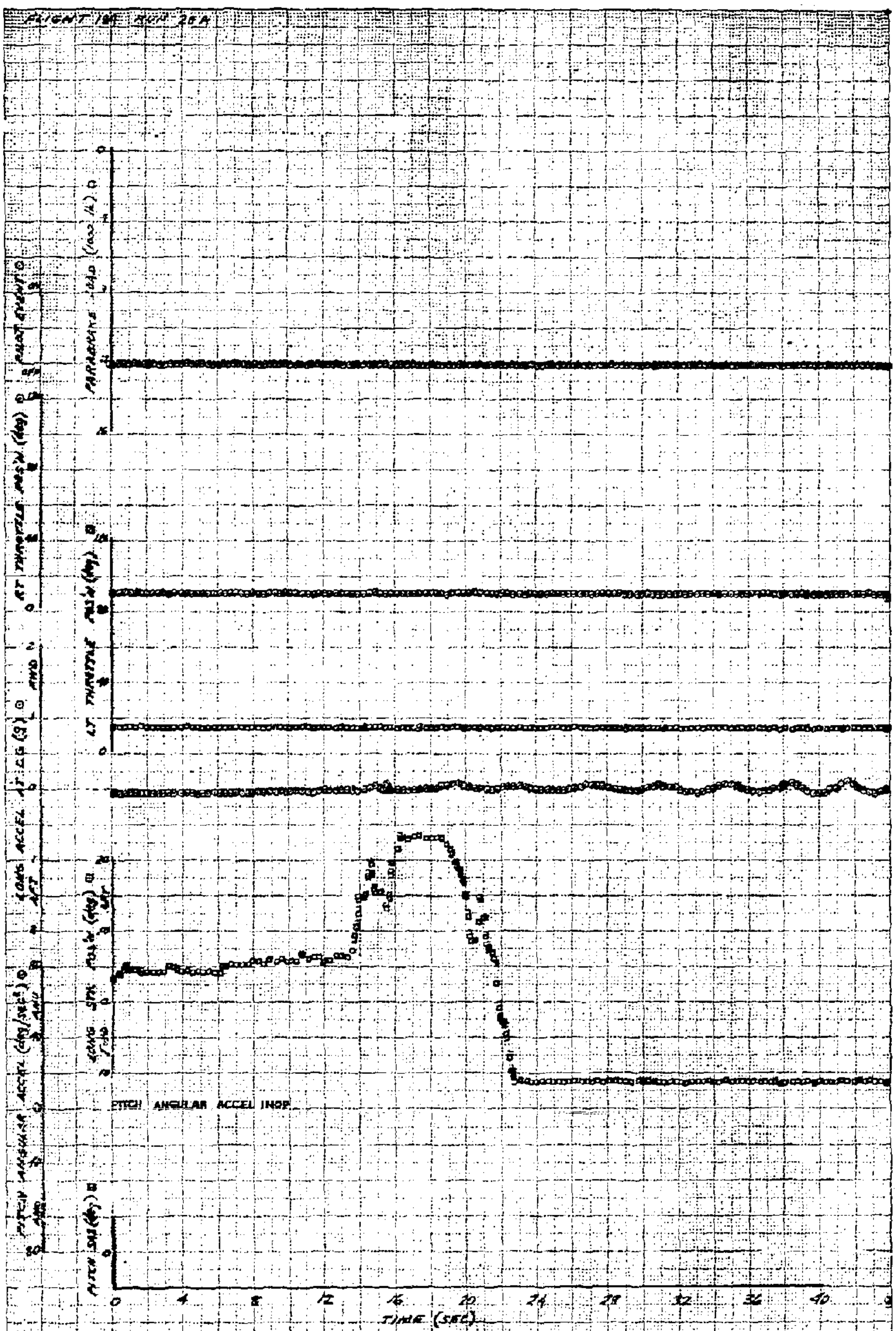

FIGURE 32 CONTINUED

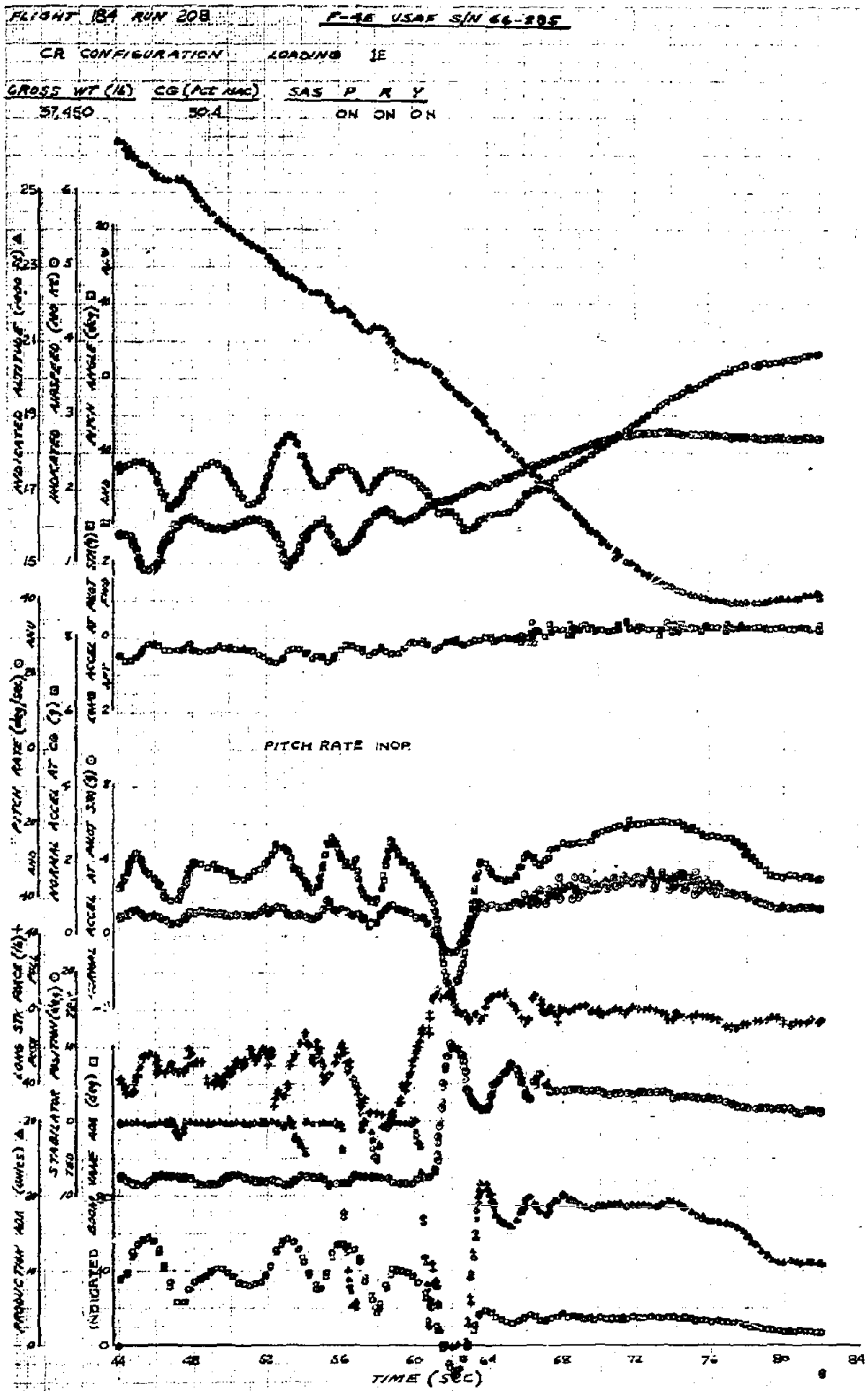

FIGURE 32 CONTINUED

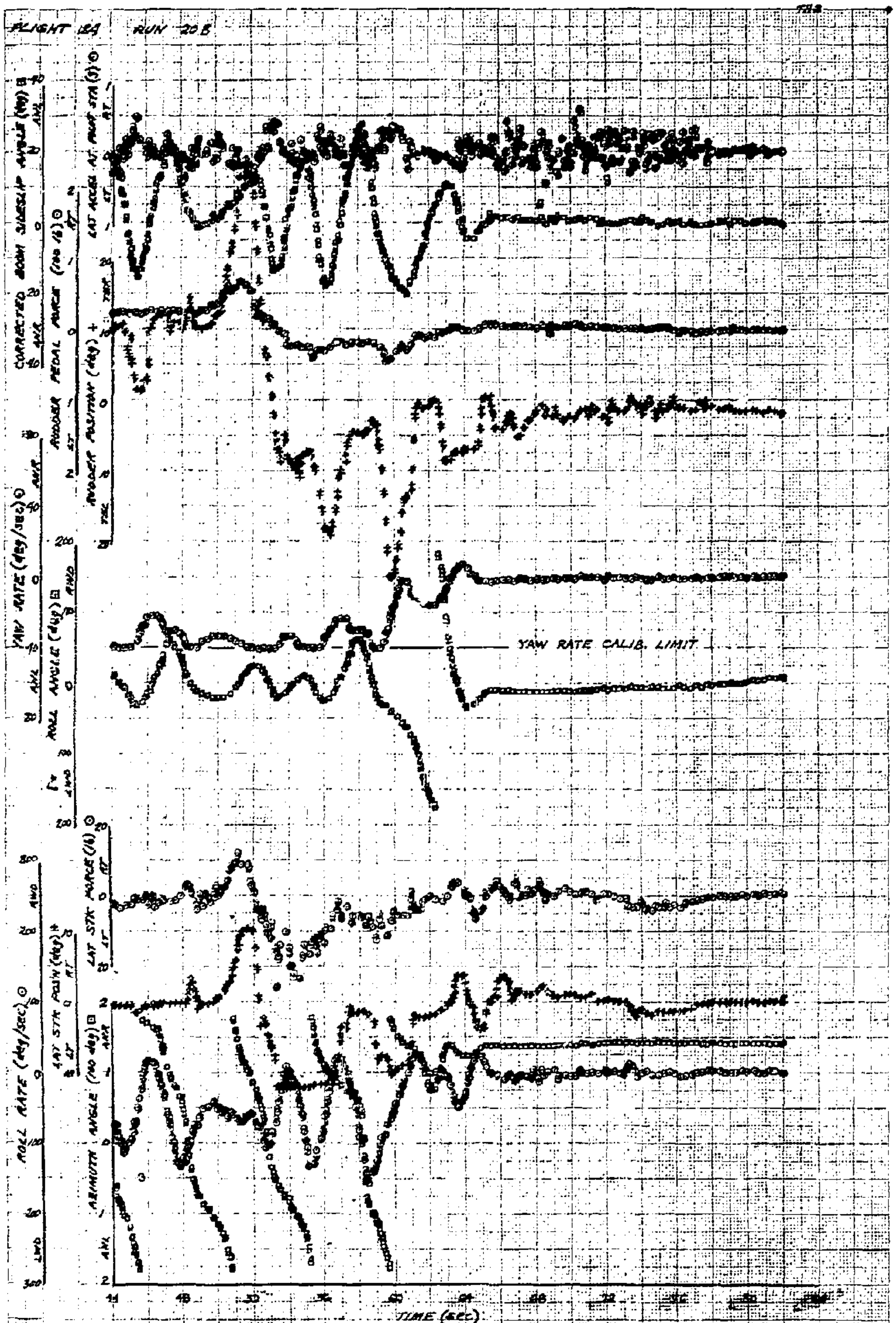

FIGURE 32 CONTINUED

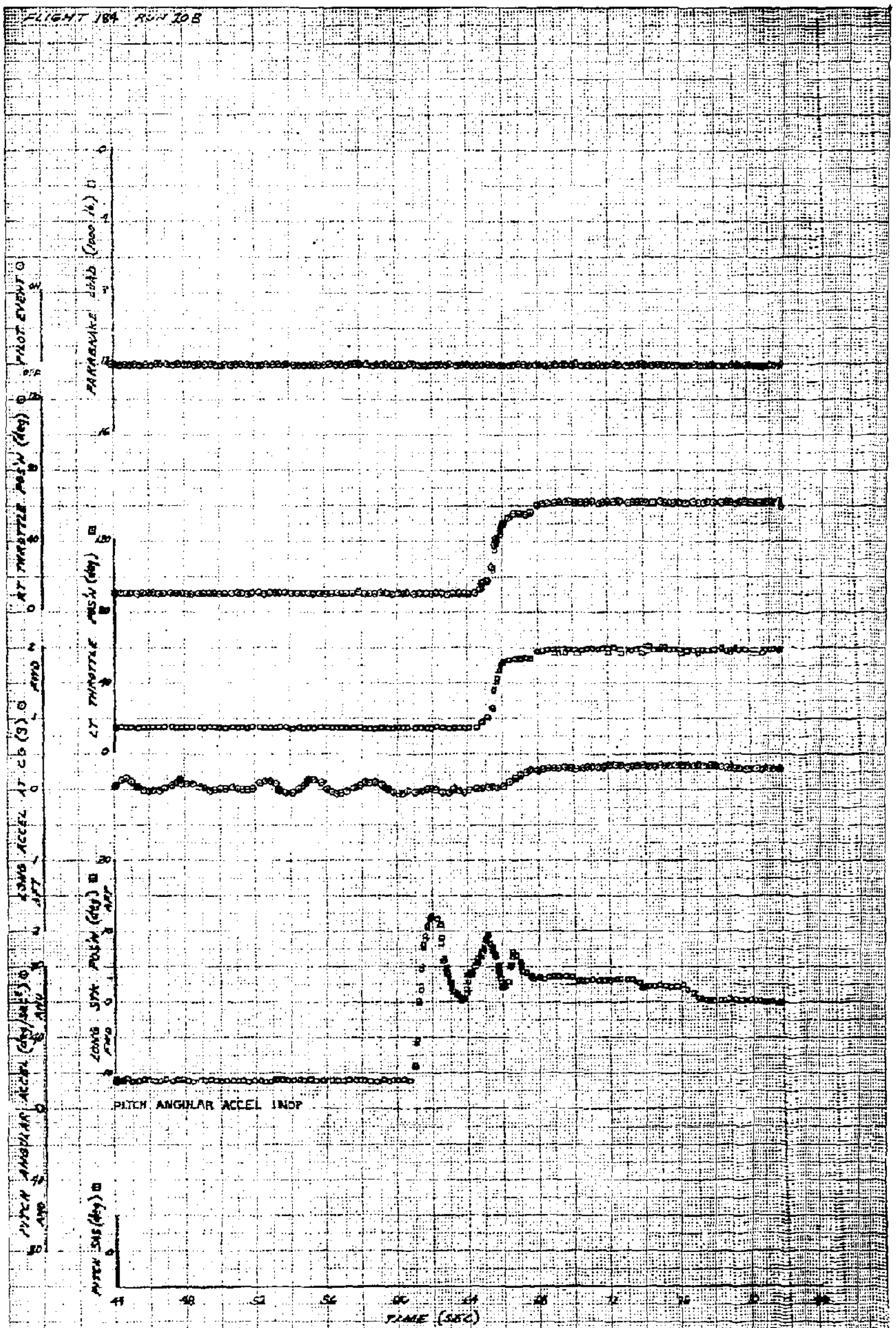

FIGURE 32 CONTINUED

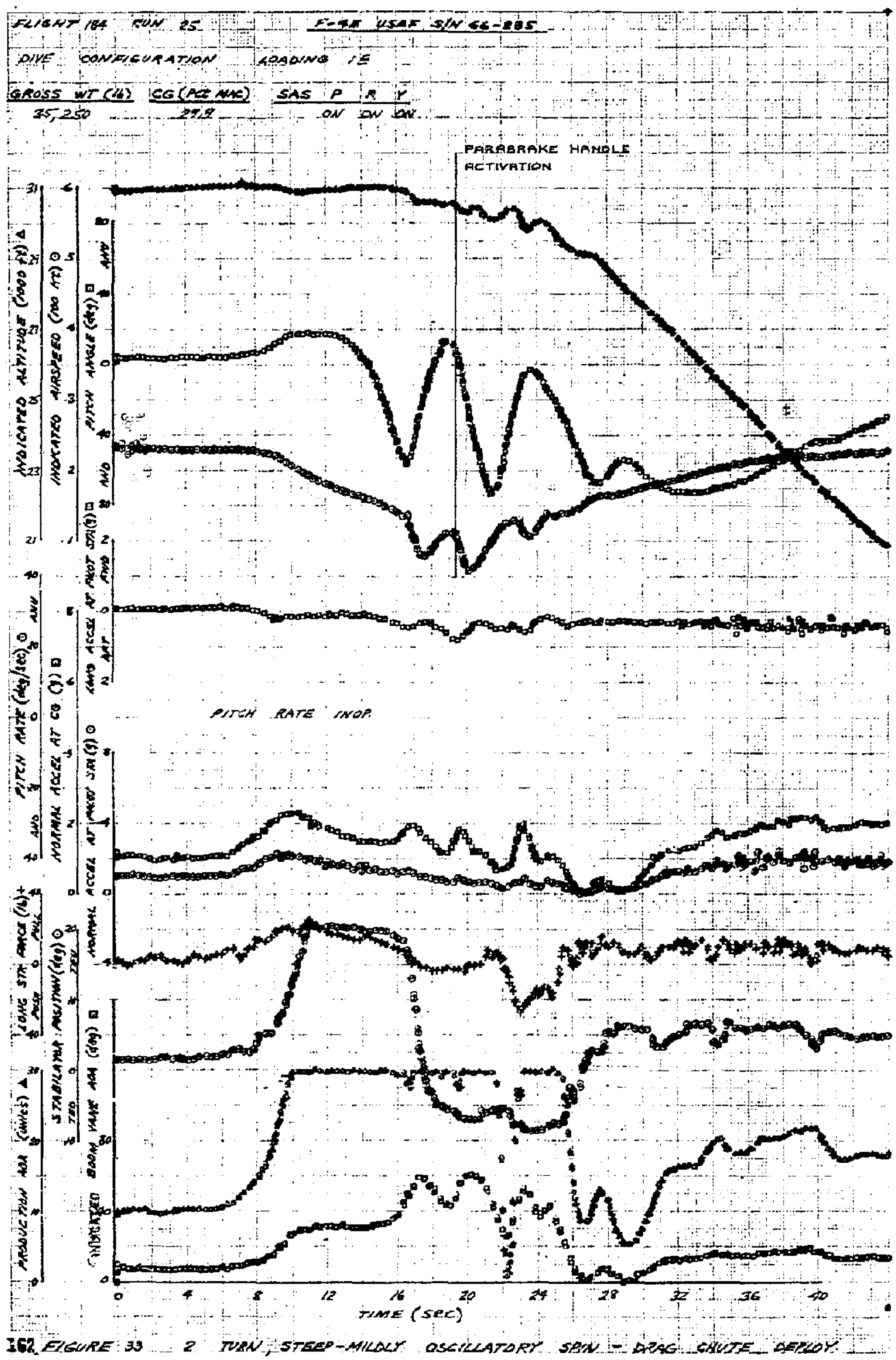

 FIGURE 33 2 TURN, STEEP-MILDLY OSCILLATORY SPIN - DRAG CHUTE DEPLOY.

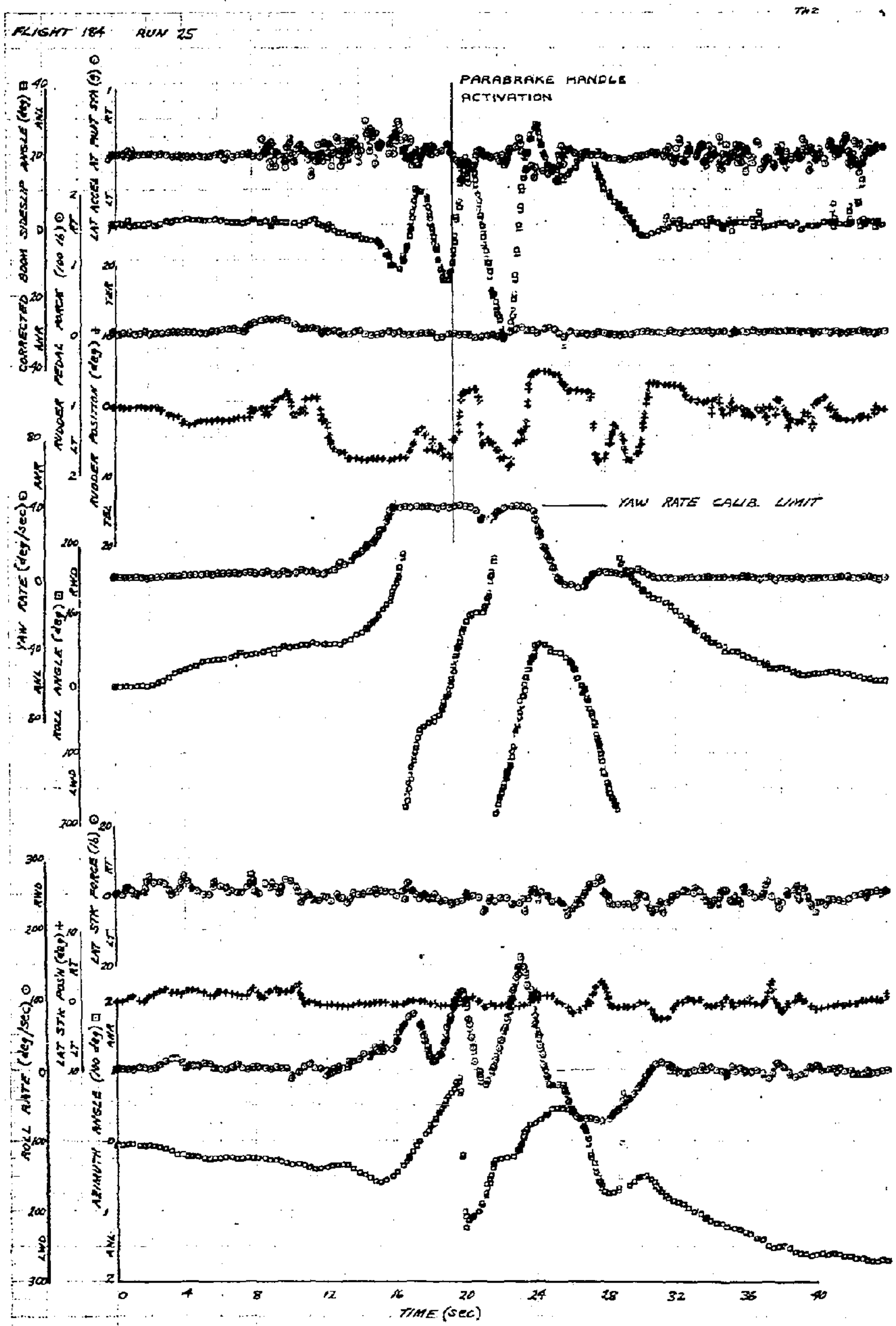

FIGURE 33 CONTINUED

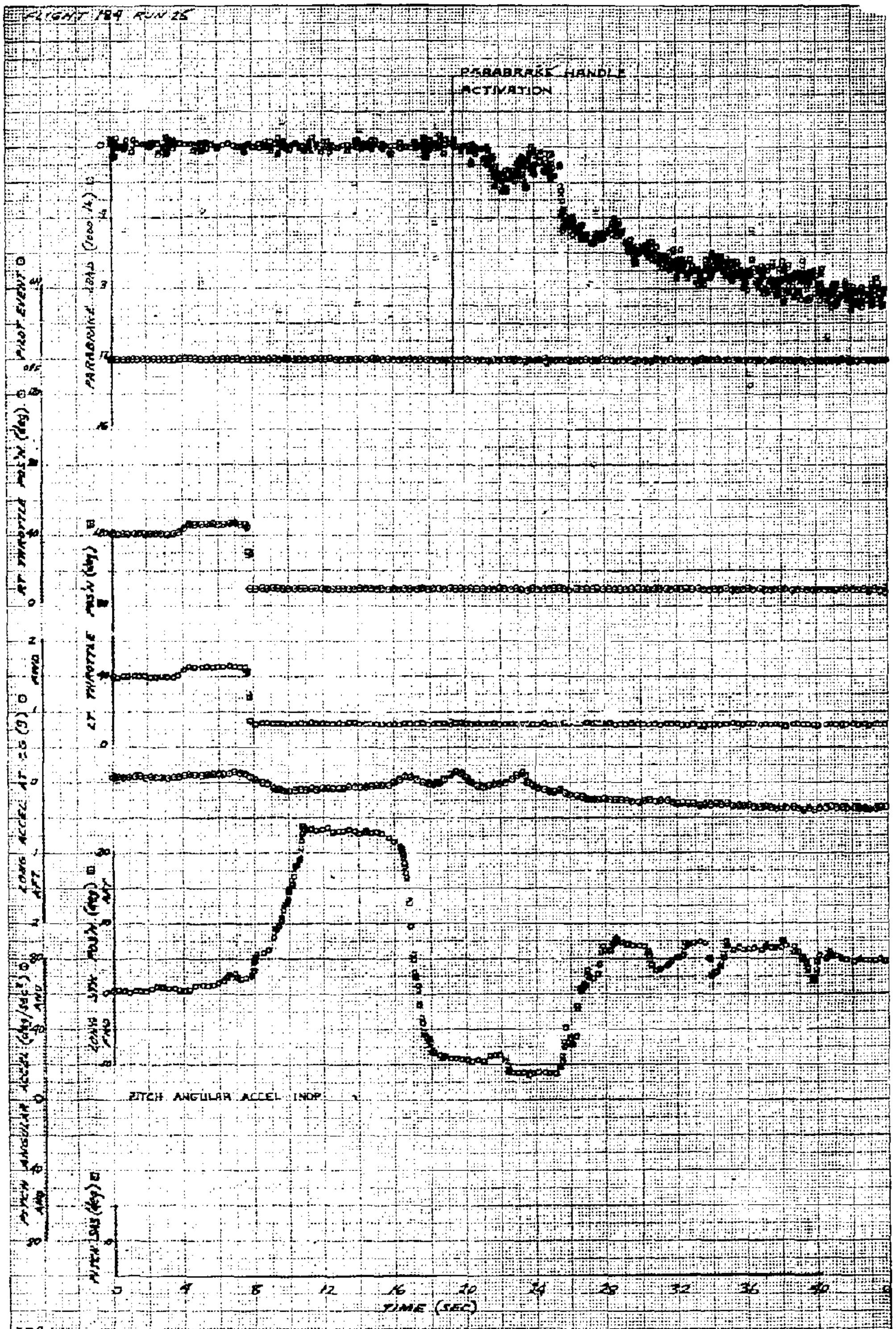

FIGURE 33 CONTINUED

THIS PAGE LEFT BLANK FOR PRESENTATION PURPOSES

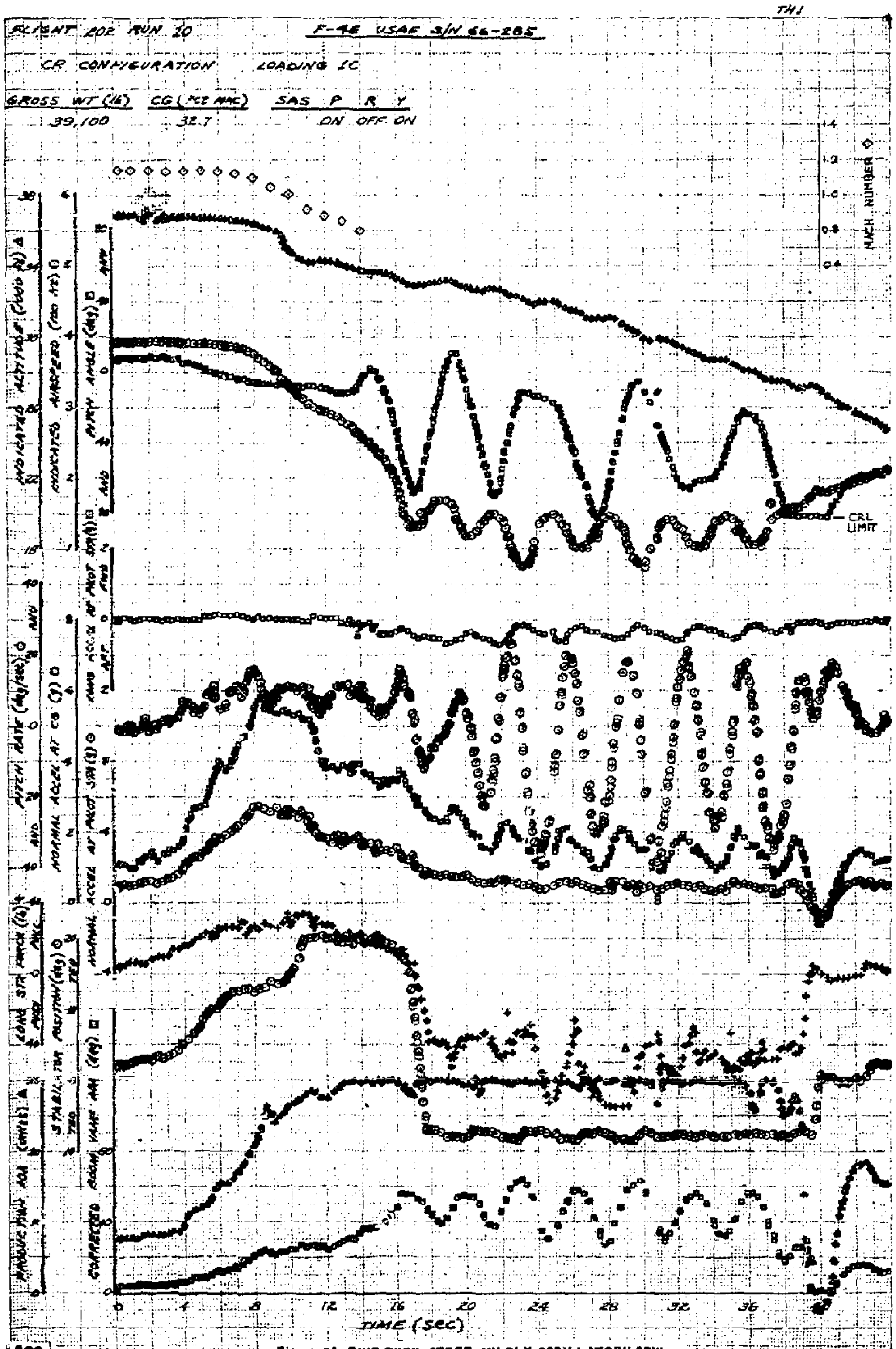

Figure 34 FIVE TURN, STEEP-MILDLY OSCILLATORY SPIN

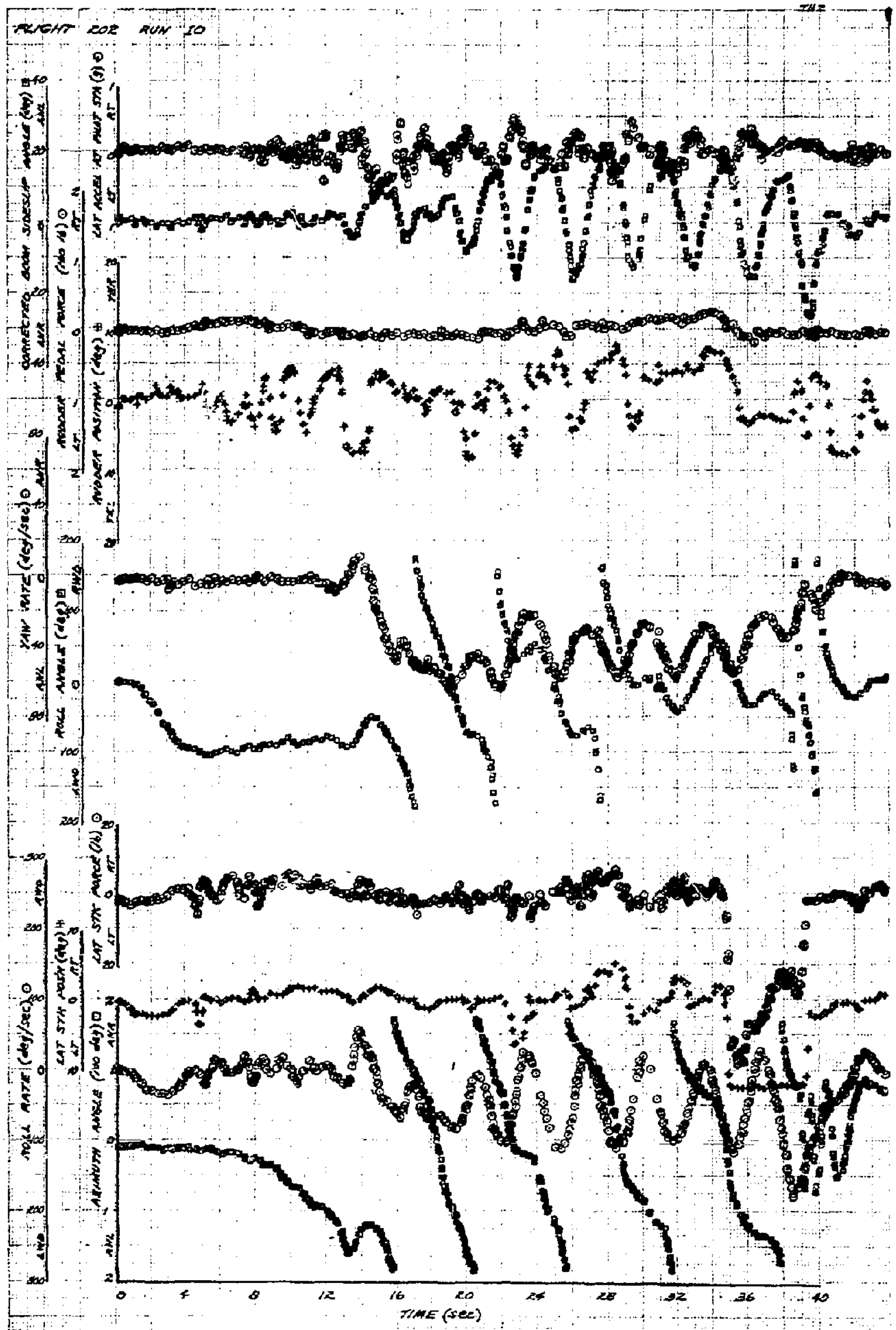

Figure 34 CONTINUED

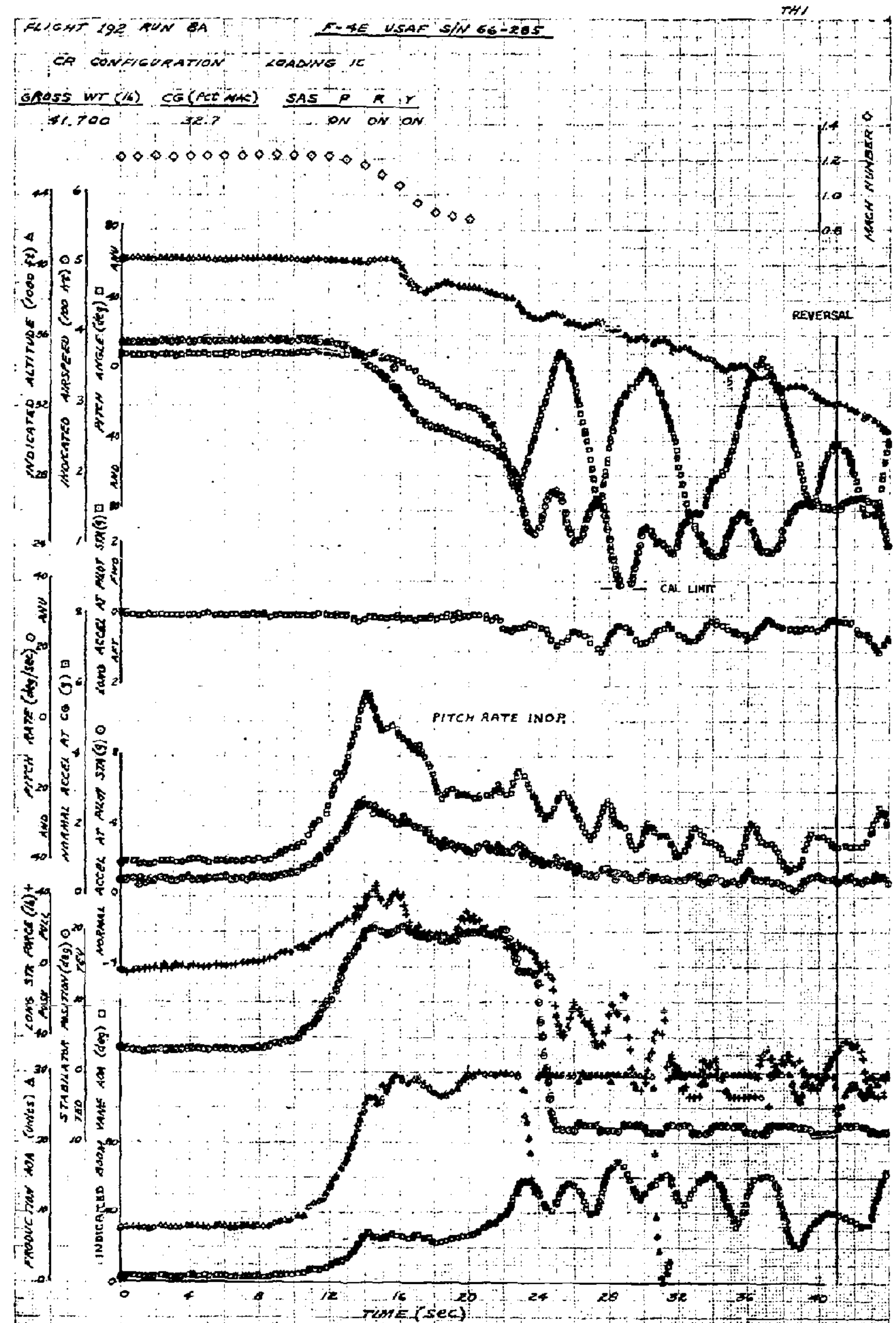

Figure 56 STEEP-MILDLY OSCILLATORY SPIN WITH REVERSAL

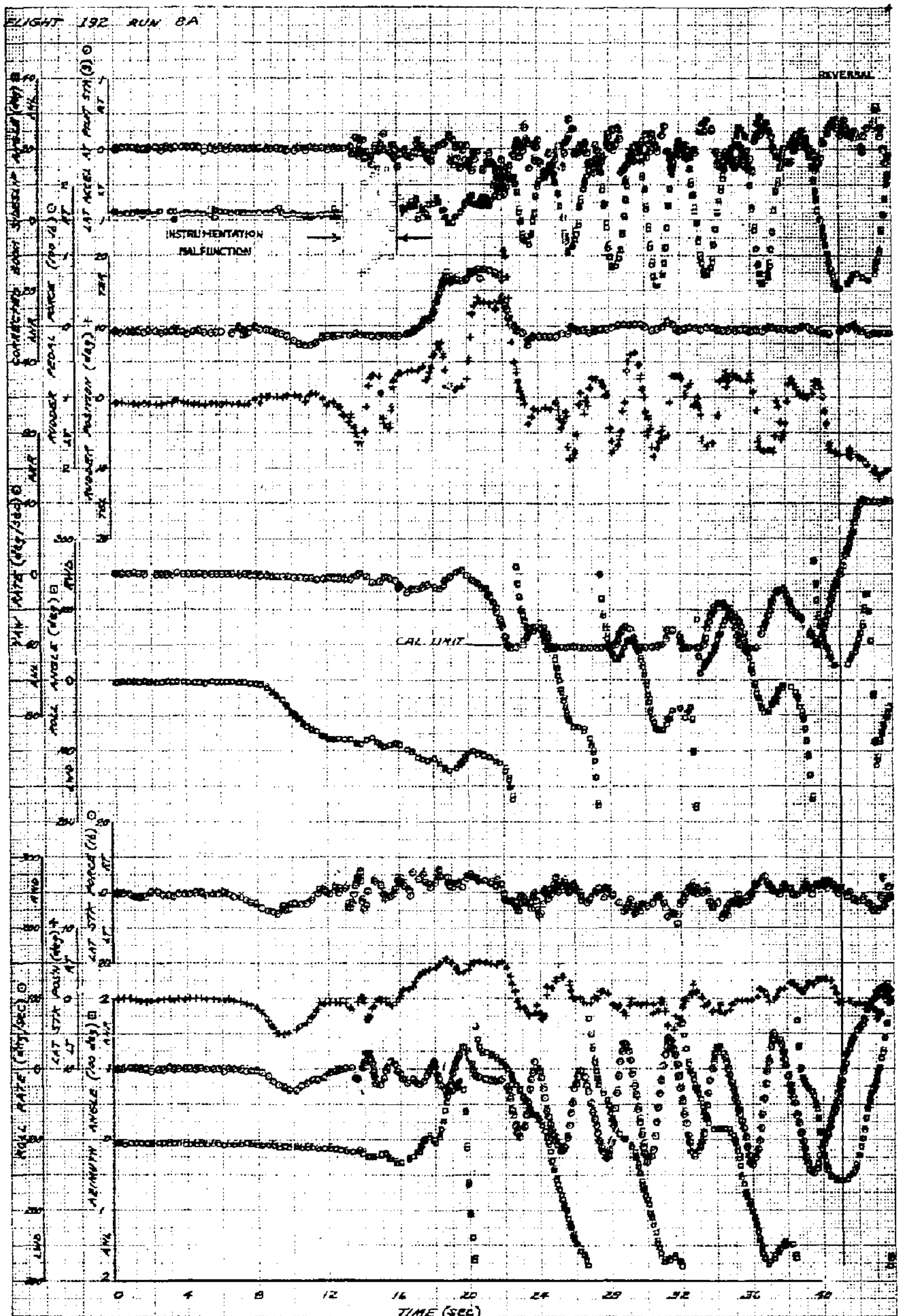

Figure 35 CONTINUED

FLIGHT 192 RUN 8B

F-4E USAF S/N 66-285

CR CONFIGURATION LOADING IC

GROSS WT (lb)	CG (PCT MAC)	SAS P	R	Y
41,700	32.7	ON	ON	ON

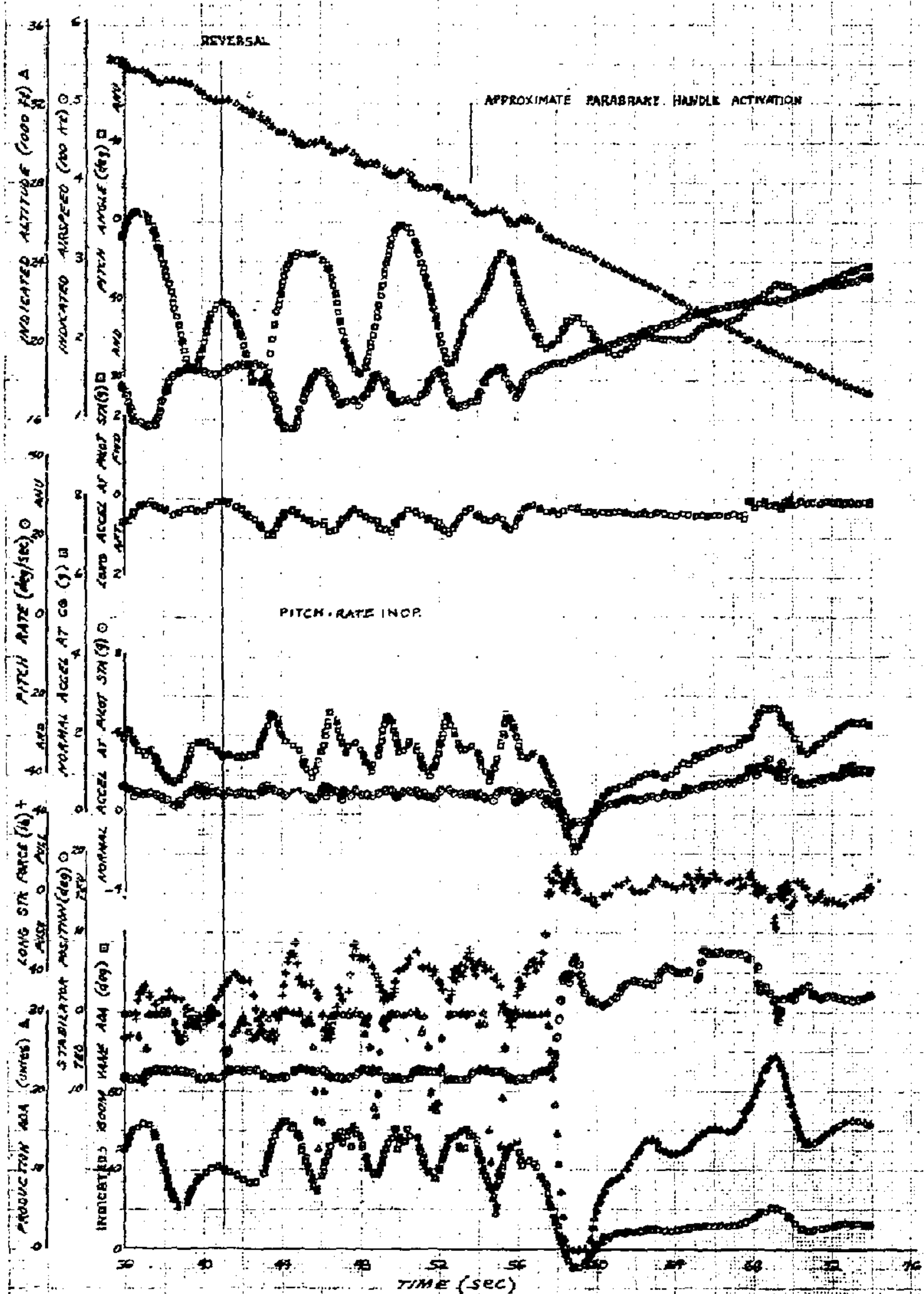

Figure 25 CONTINUED

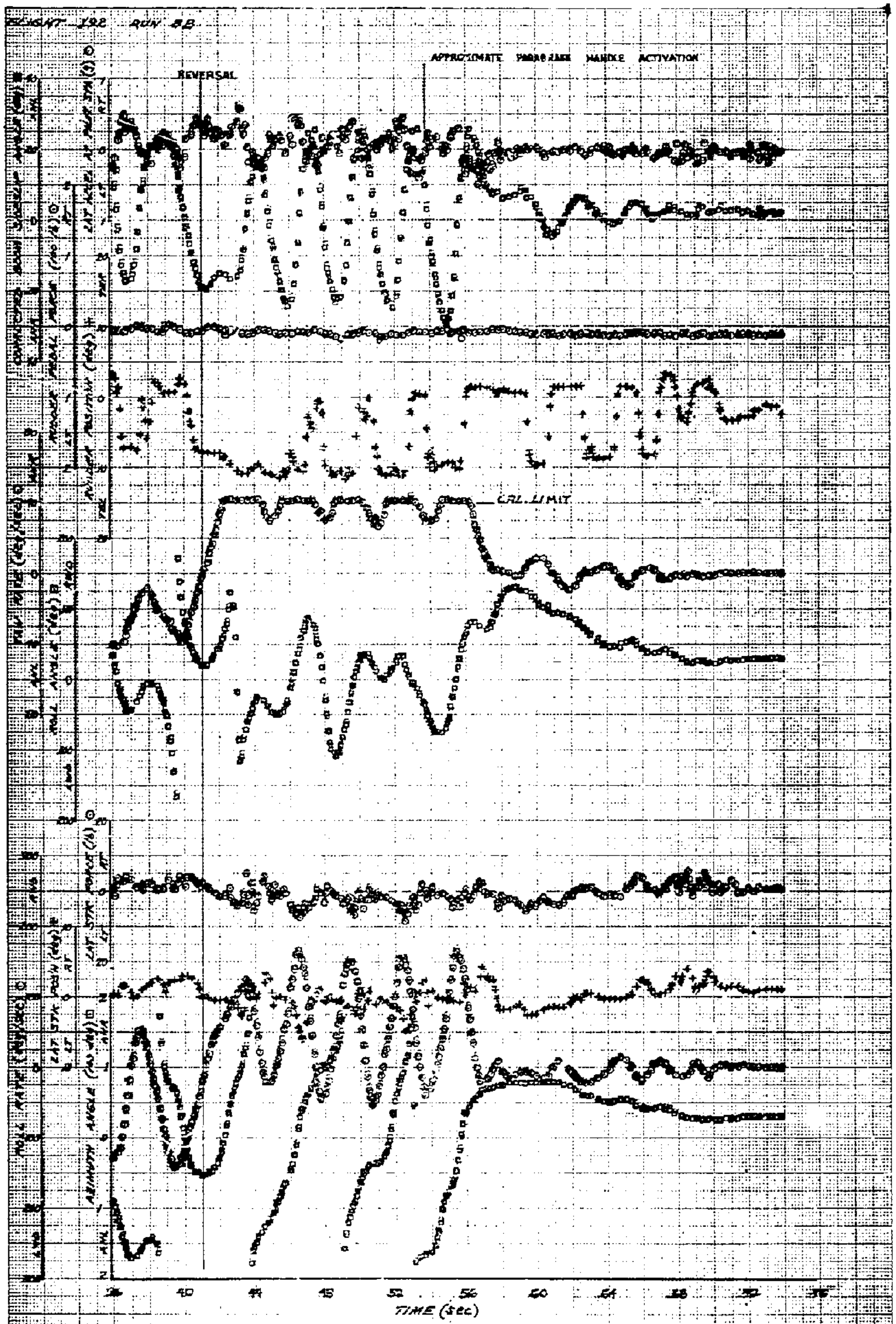

Figure 36 CONTINUED

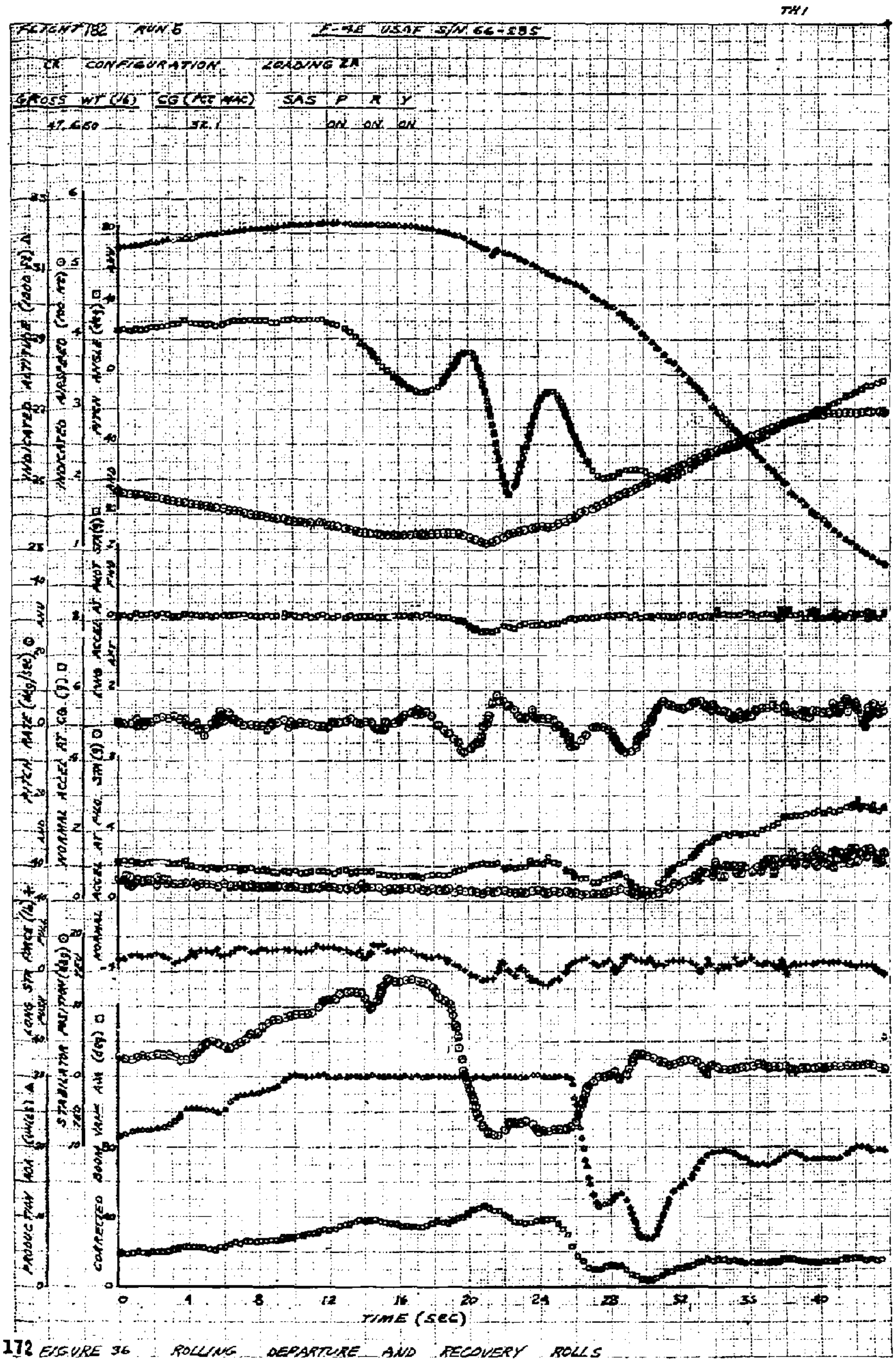

 FIGURE 36 ROLLING DEPARTURE AND RECOVERY ROLLS

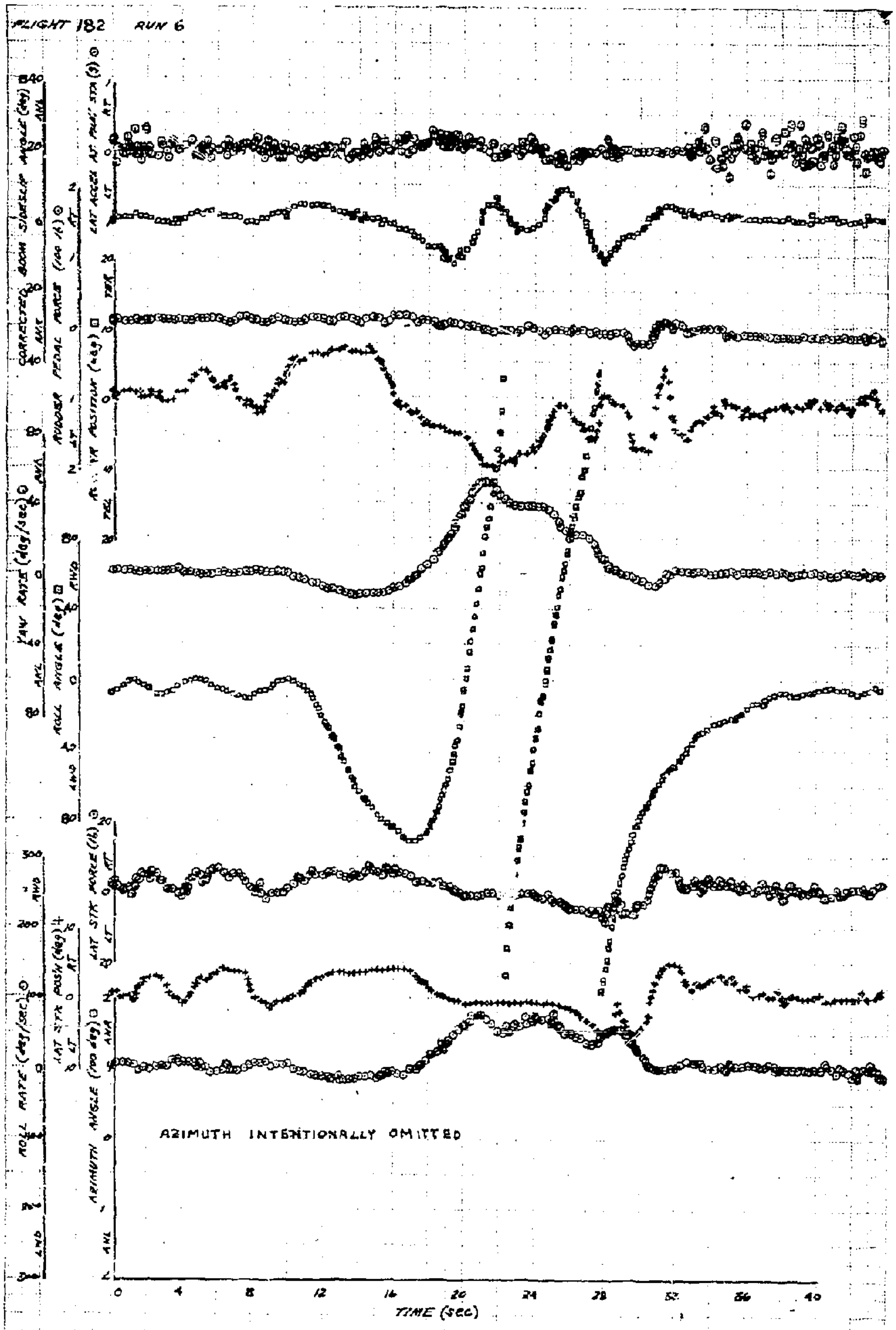

FIGURE 36 CONTINUED

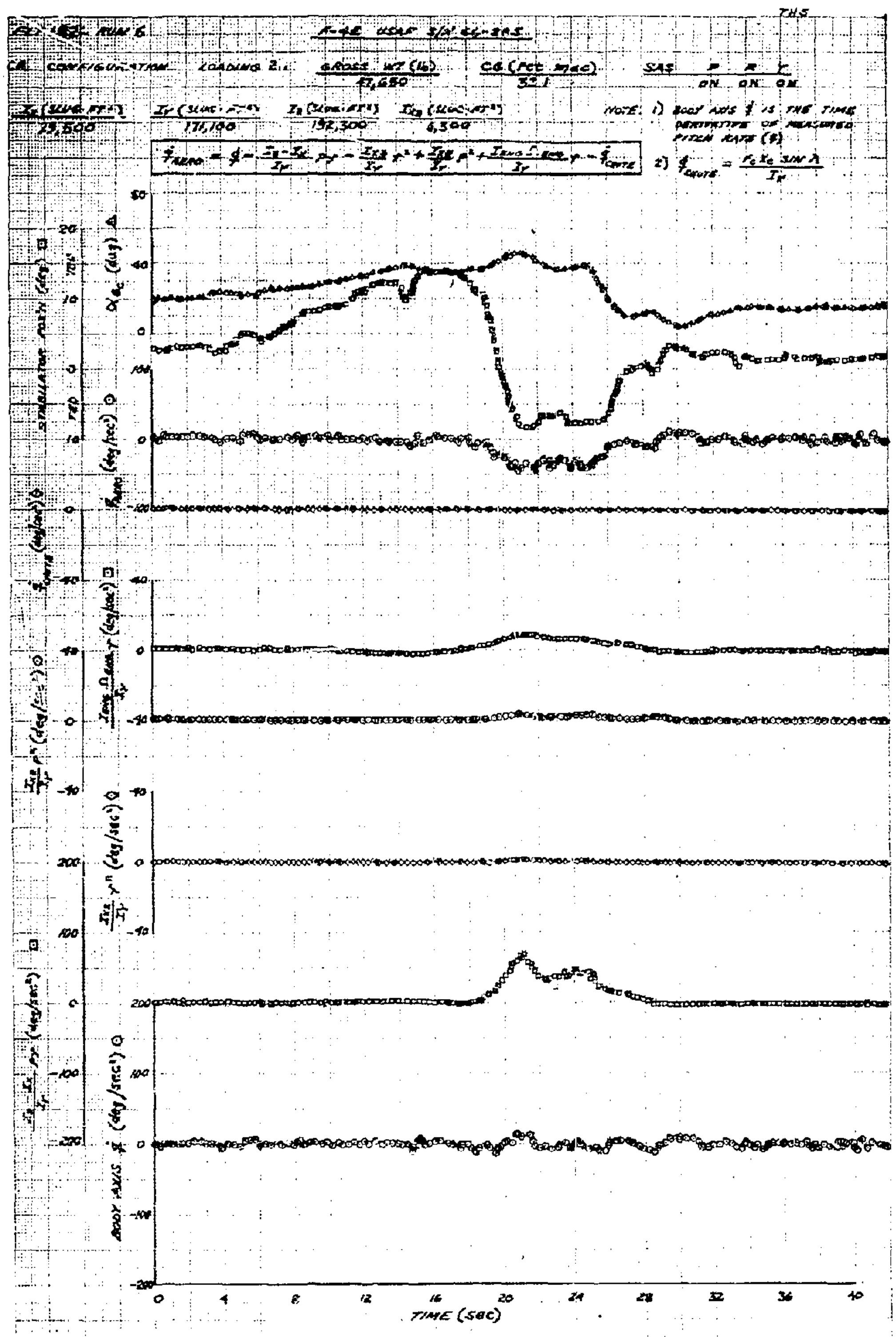

174

FIGURE 36 CONTINUED

FLT 182 RUN 6

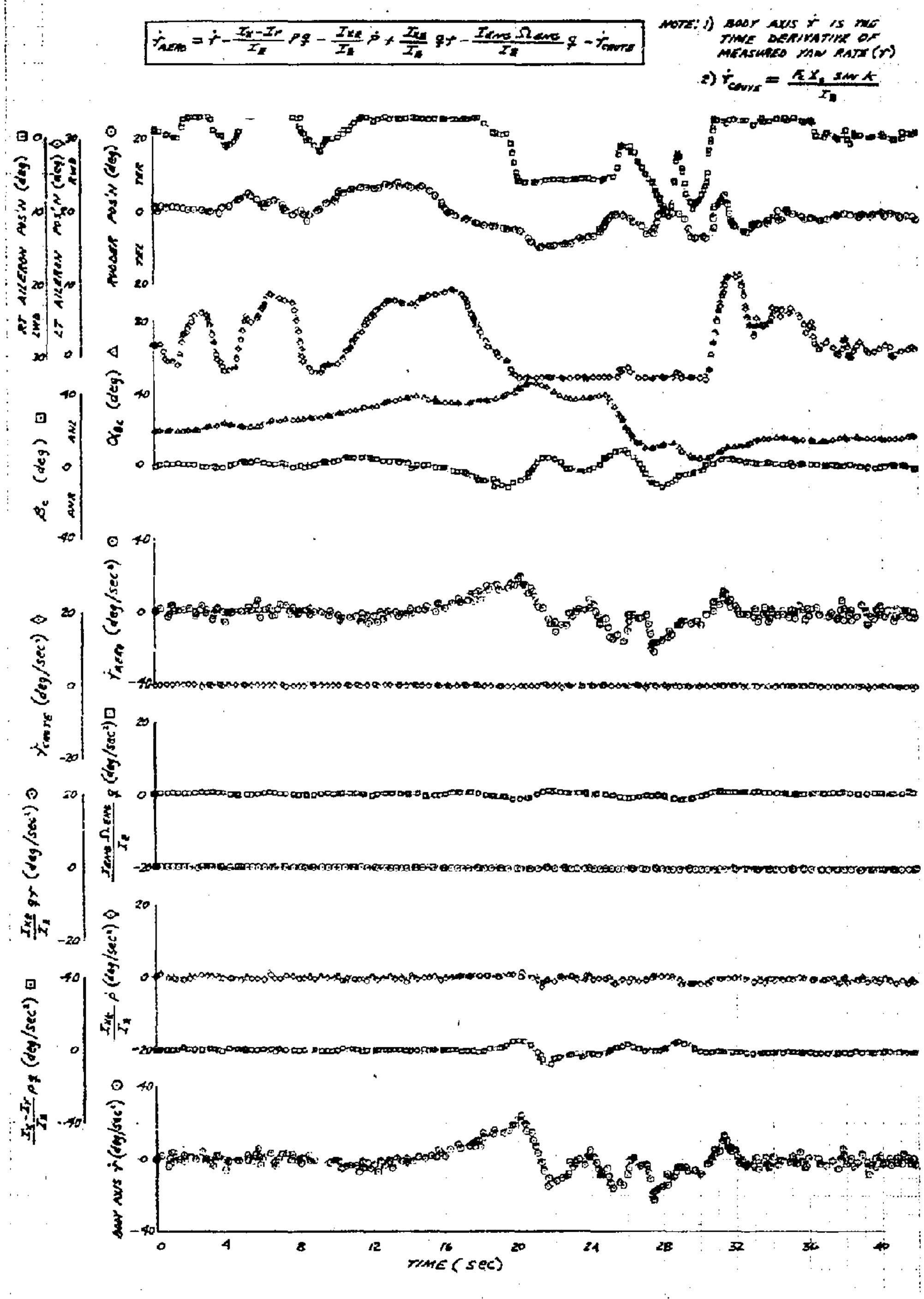

FIGURE 36 CONTINUED

FLT 182 RUN 6

$$\dot{p}_{AERO} = \dot{p} - \frac{I_Y - I_Z}{I_X} q r - \frac{I_{XZ}}{I_X}\dot{r} - \frac{I_{XZ}}{I_X} p q$$

NOTE: BODY AXIS. $\dot{p}$ IS THE TIME DERIVATIVE OF MEASURED ROLL RATE (P)

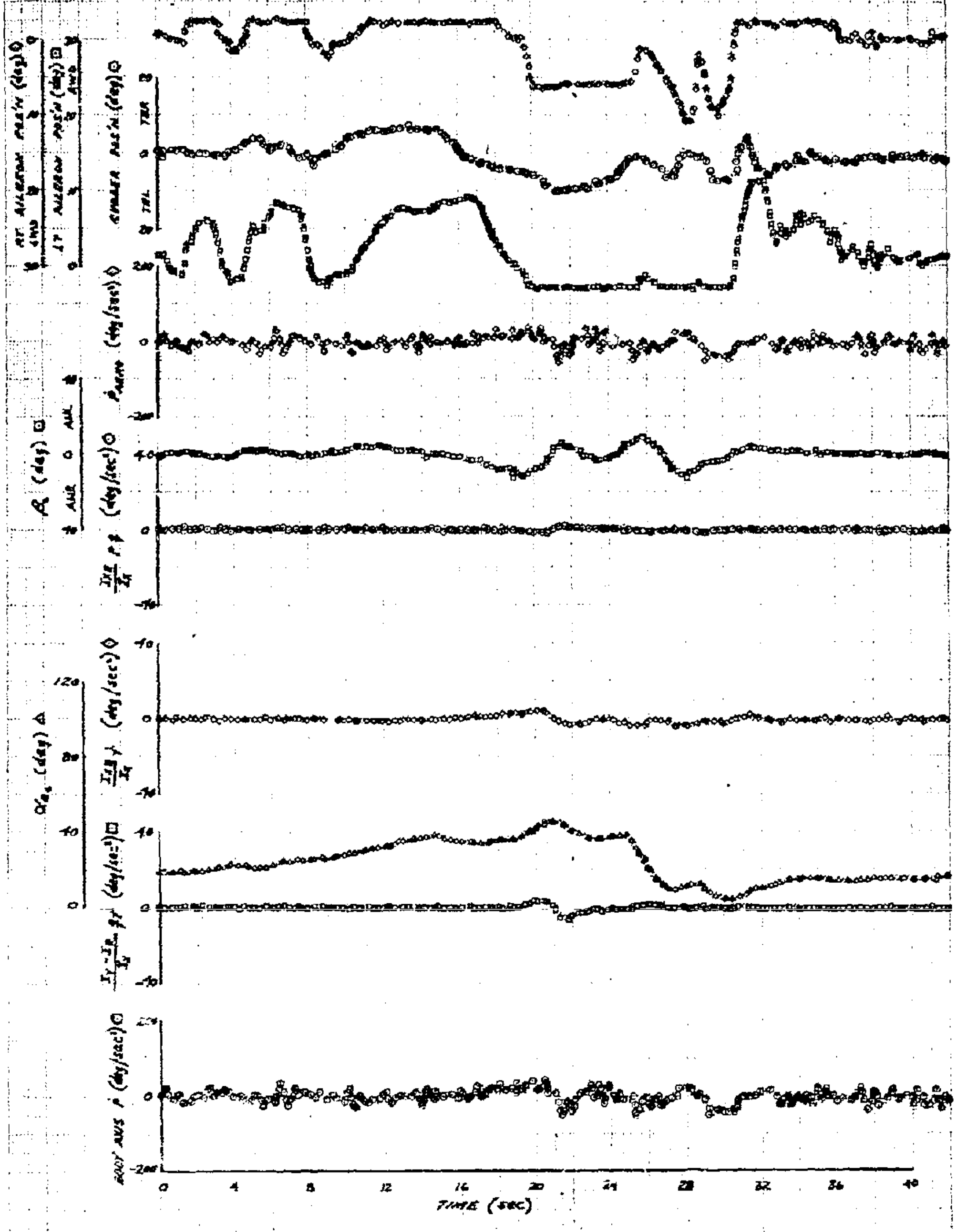

FIGURE 36 CONTINUED

THIS PAGE LEFT BLANK FOR PRESENTATION PURPOSES

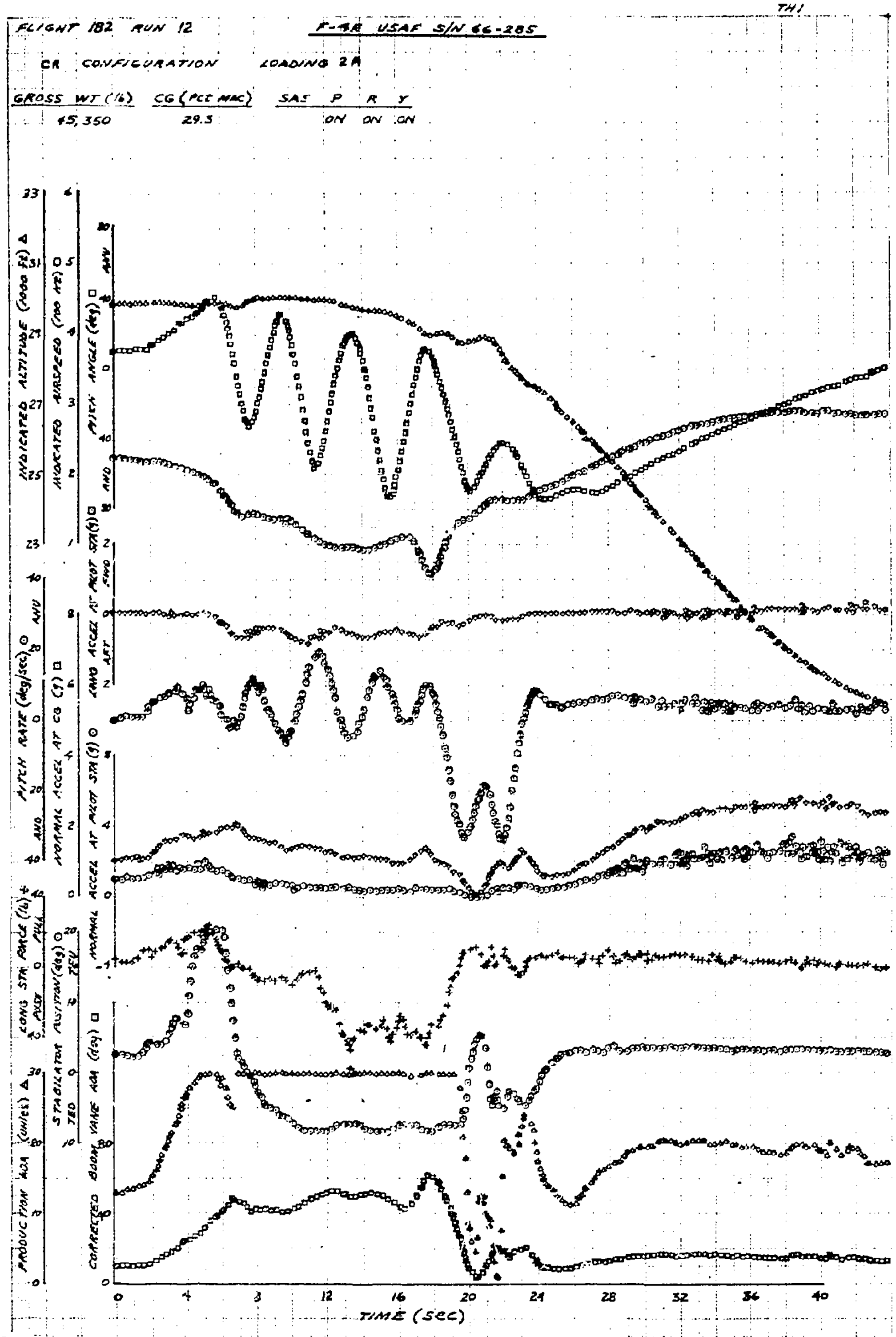

 FIGURE 37 3. TURN, STEEP--SMOOTH SPIN AND RECOVERY ROLL

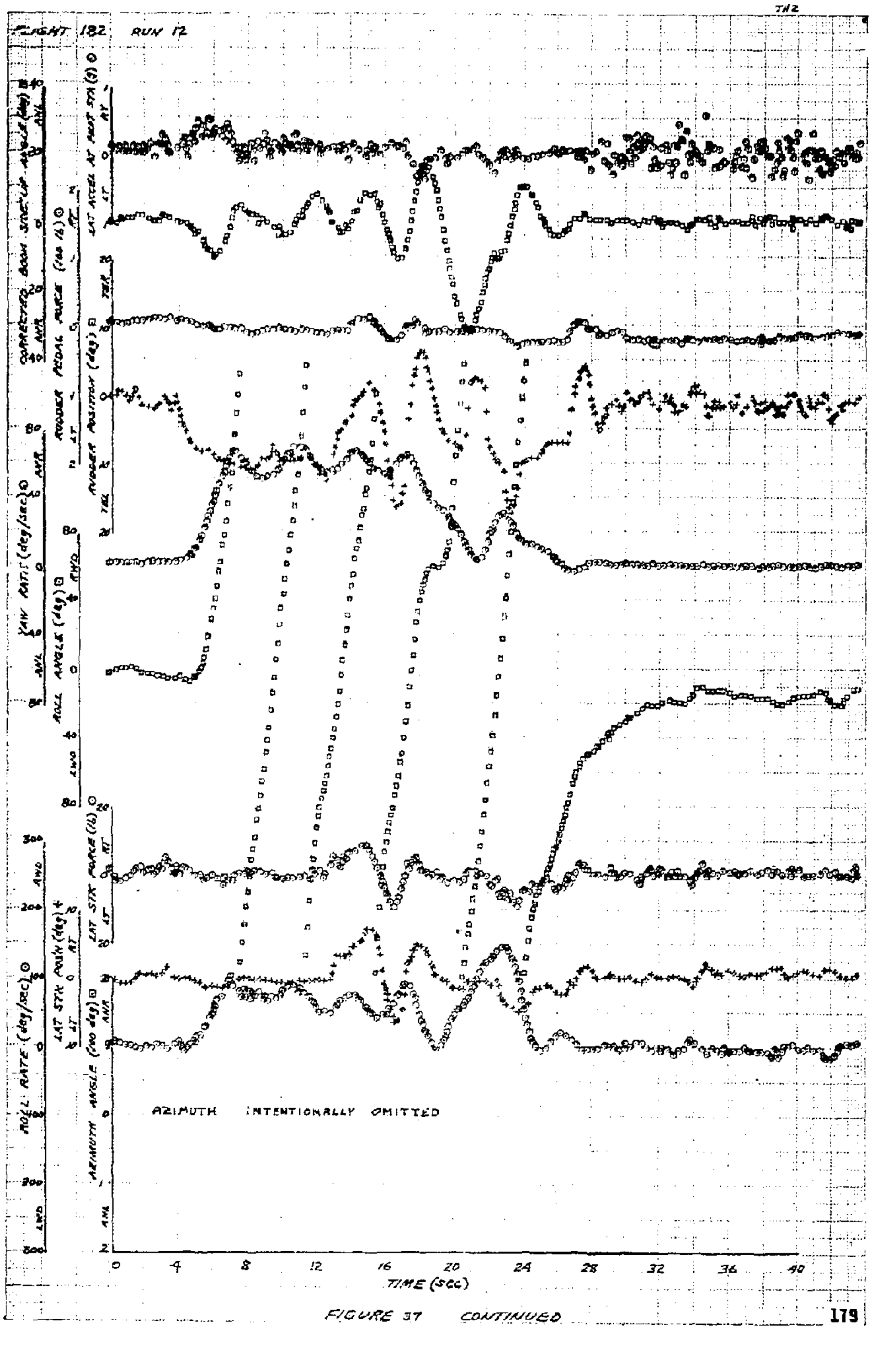

FIGURE 37 CONTINUED

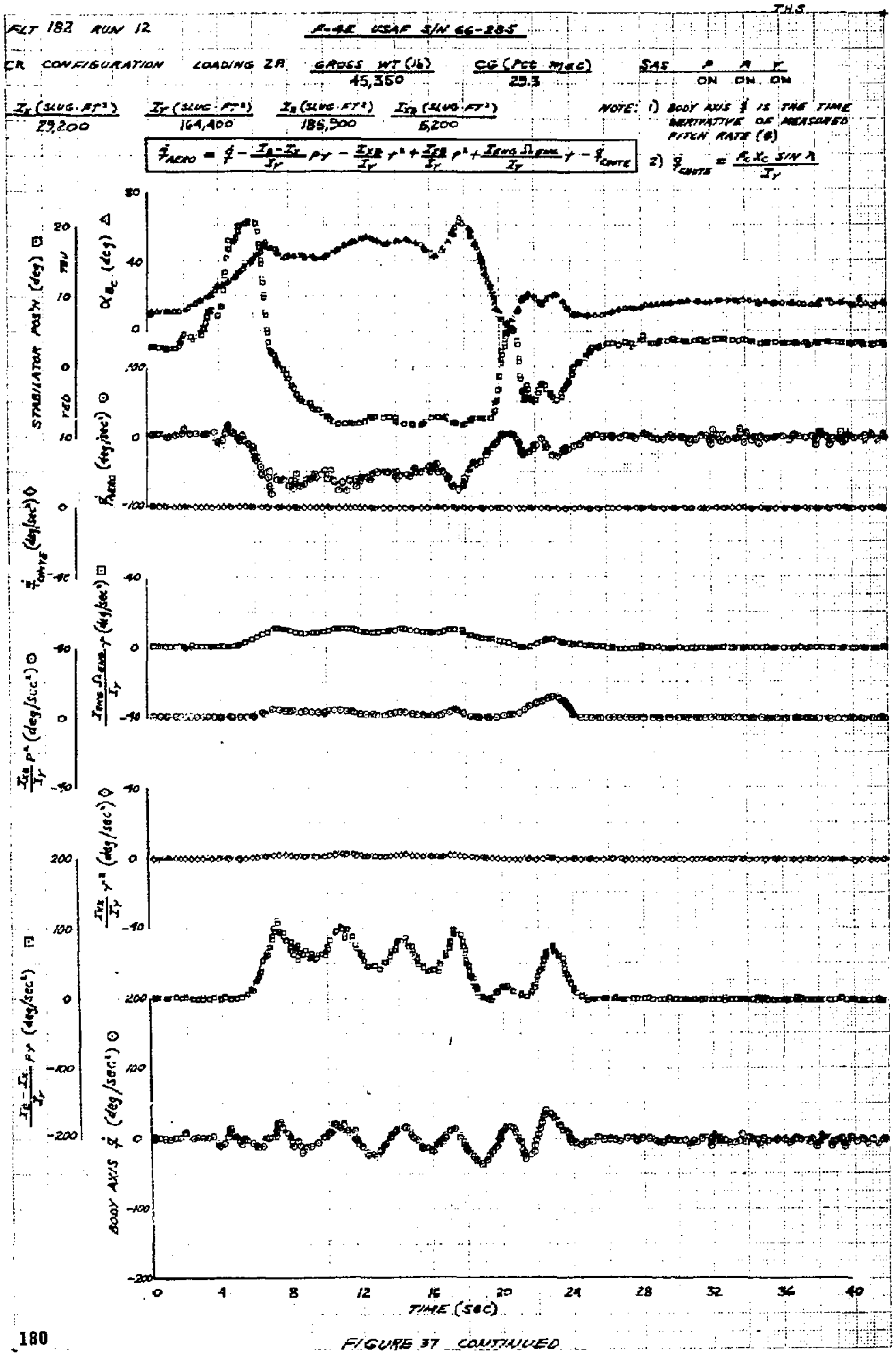

FIGURE 37 CONTINUED

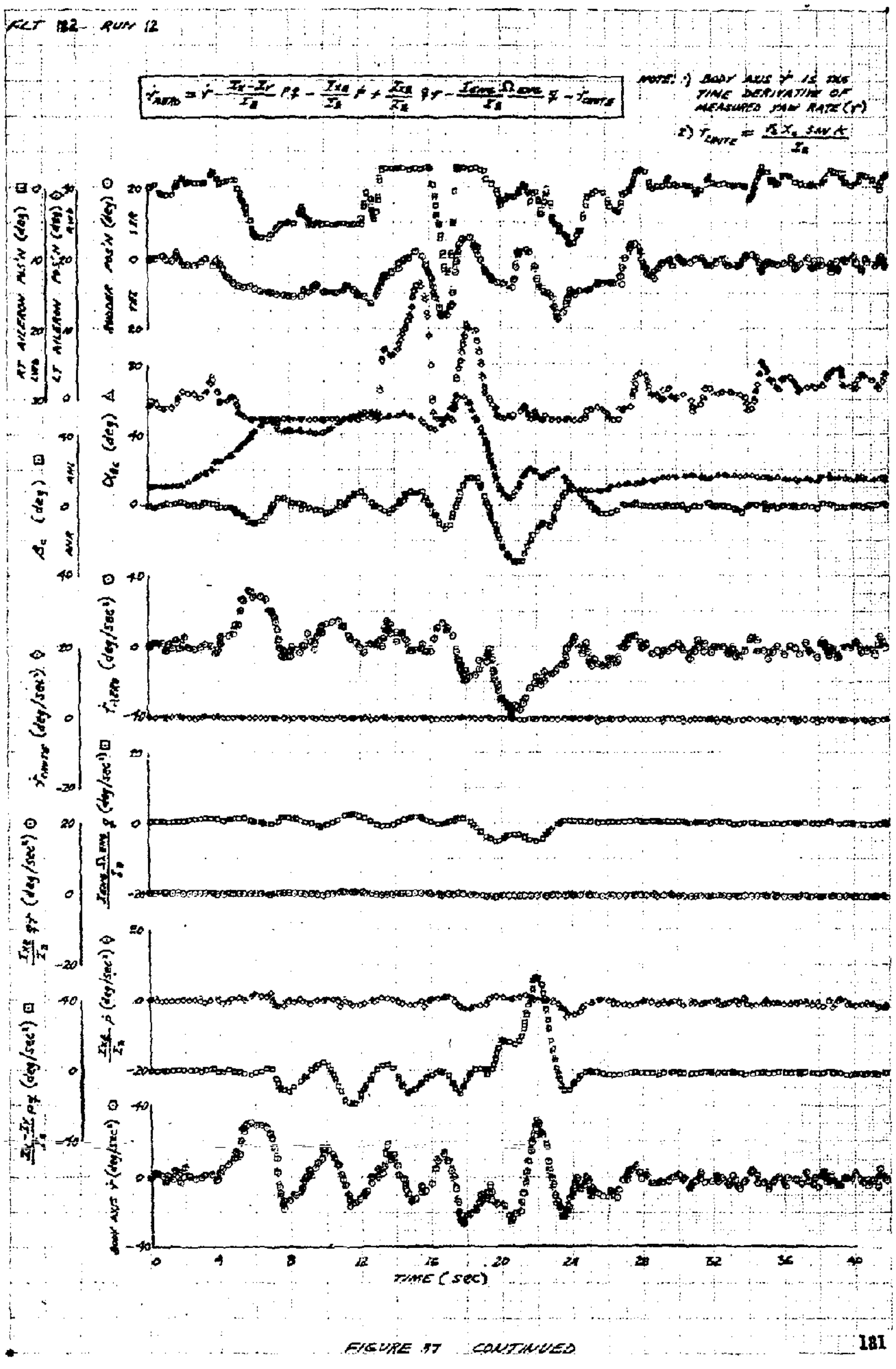

FIGURE 37 CONTINUED

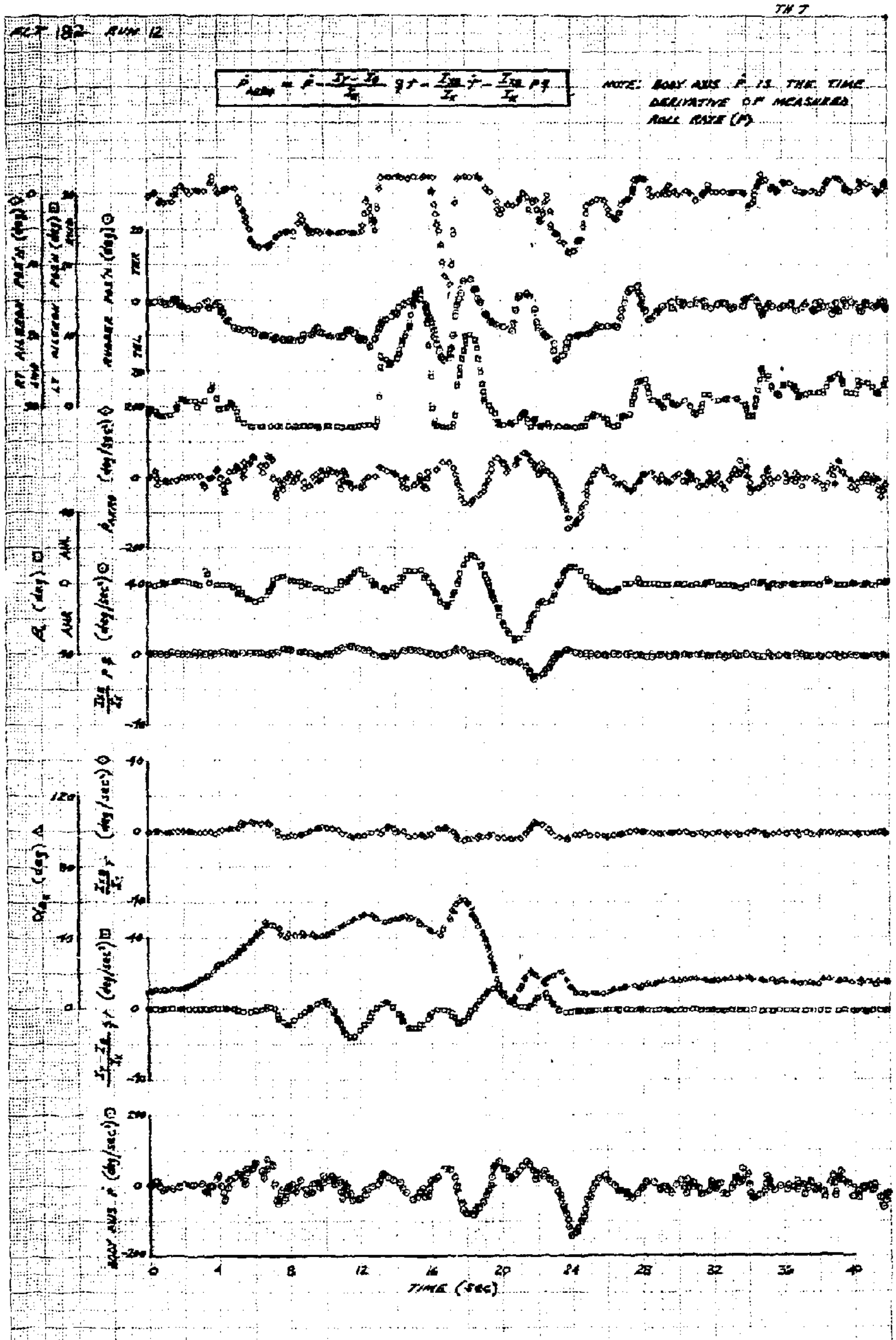

FIGURE 37 CONTINUED

THIS PAGE LEFT BLANK FOR PRESENTATION PURPOSES

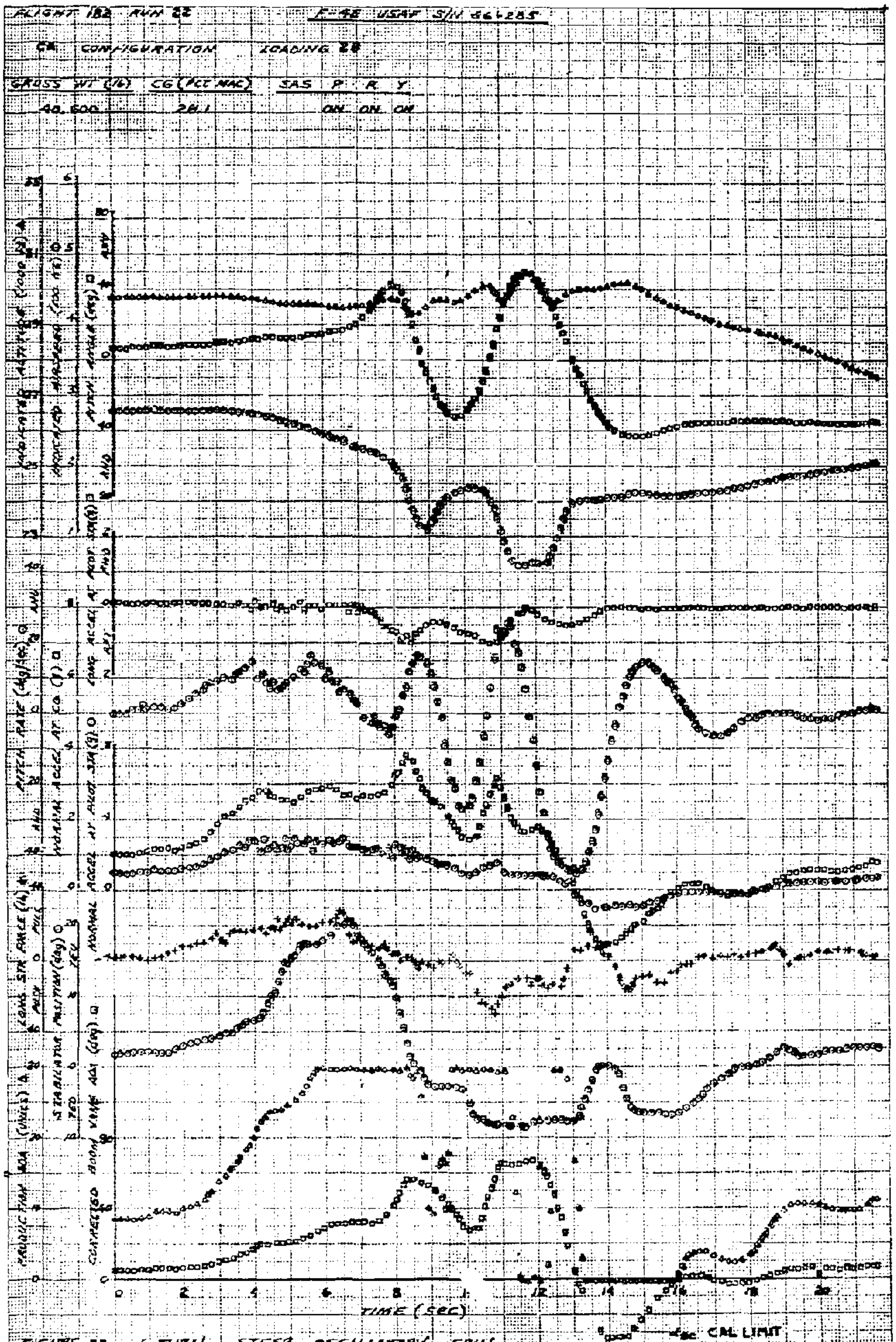

FIGURE 38 1 TURN; STEEP-OSCILLATORY SPIN

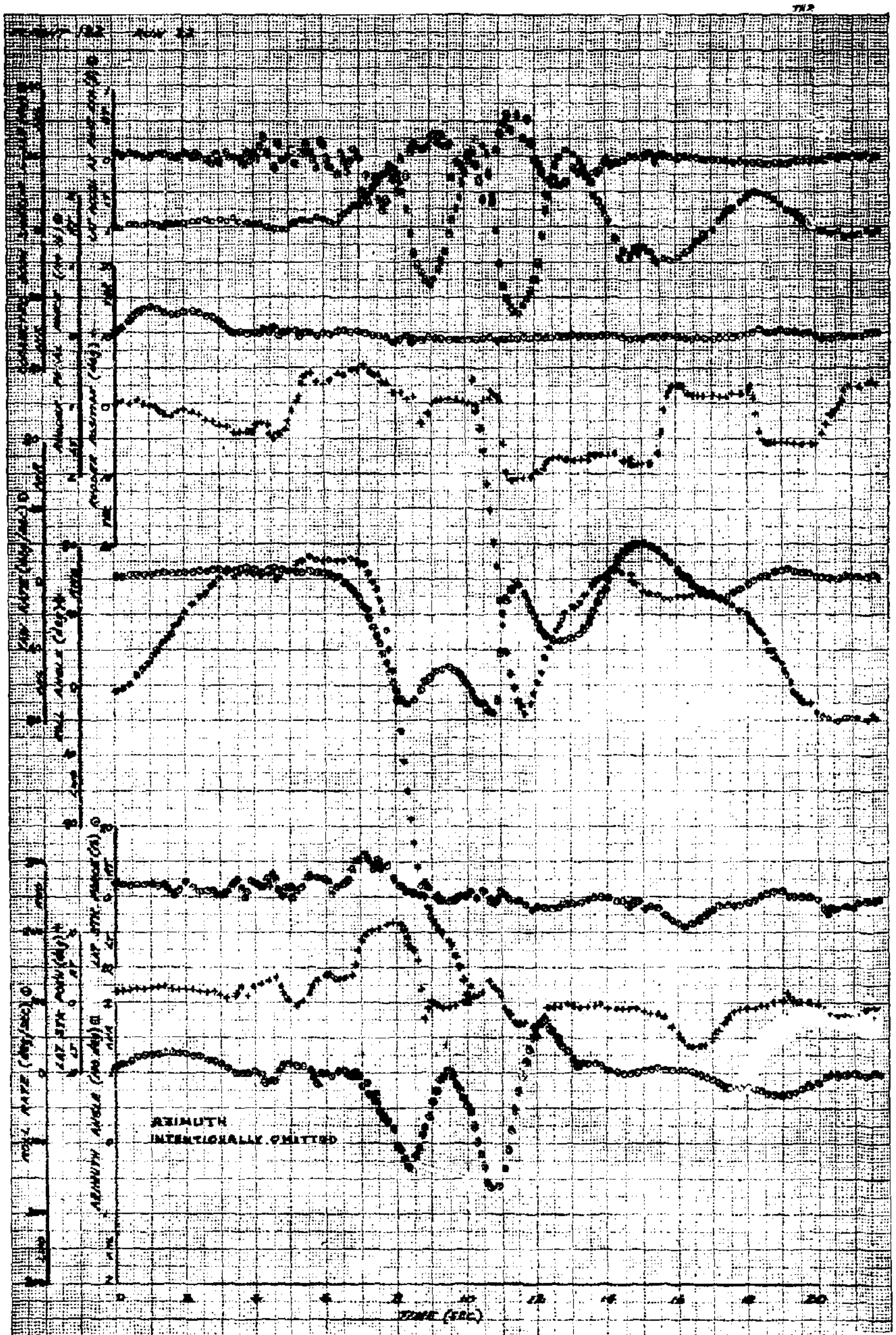

FIGURE [illegible] CONTINUED

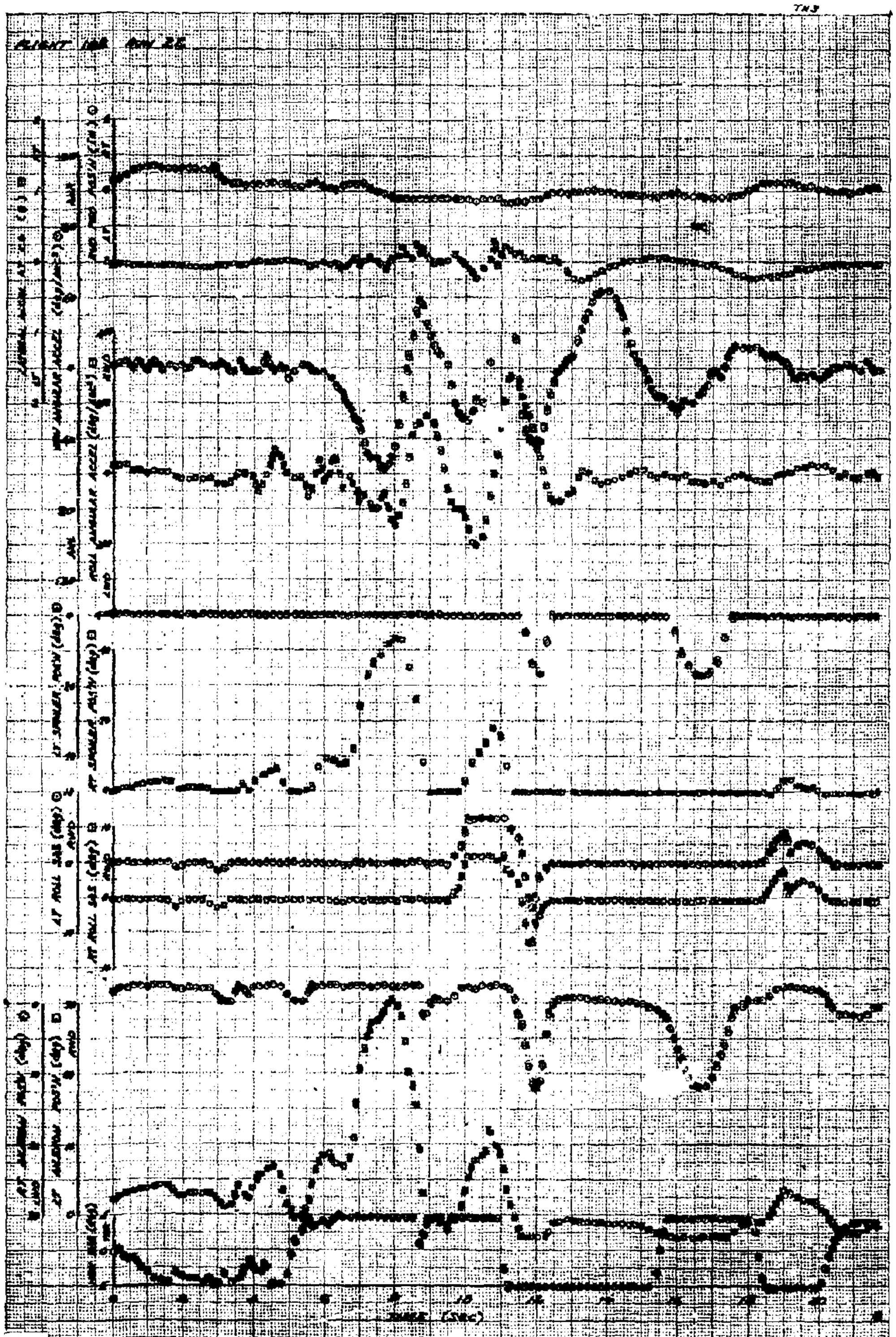

FIGURE 38 CONTINUED

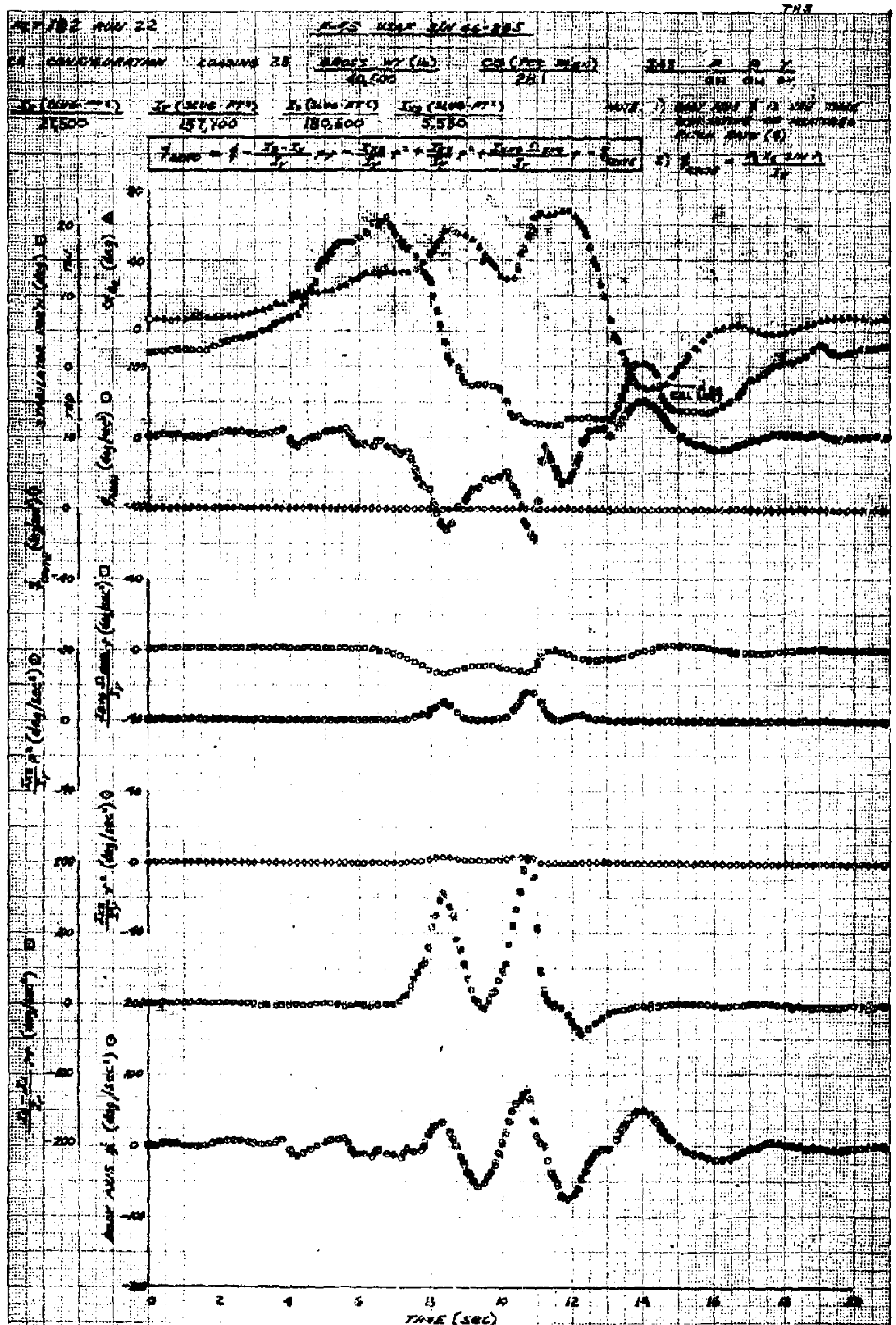

FIGURE 88 CONTINUED

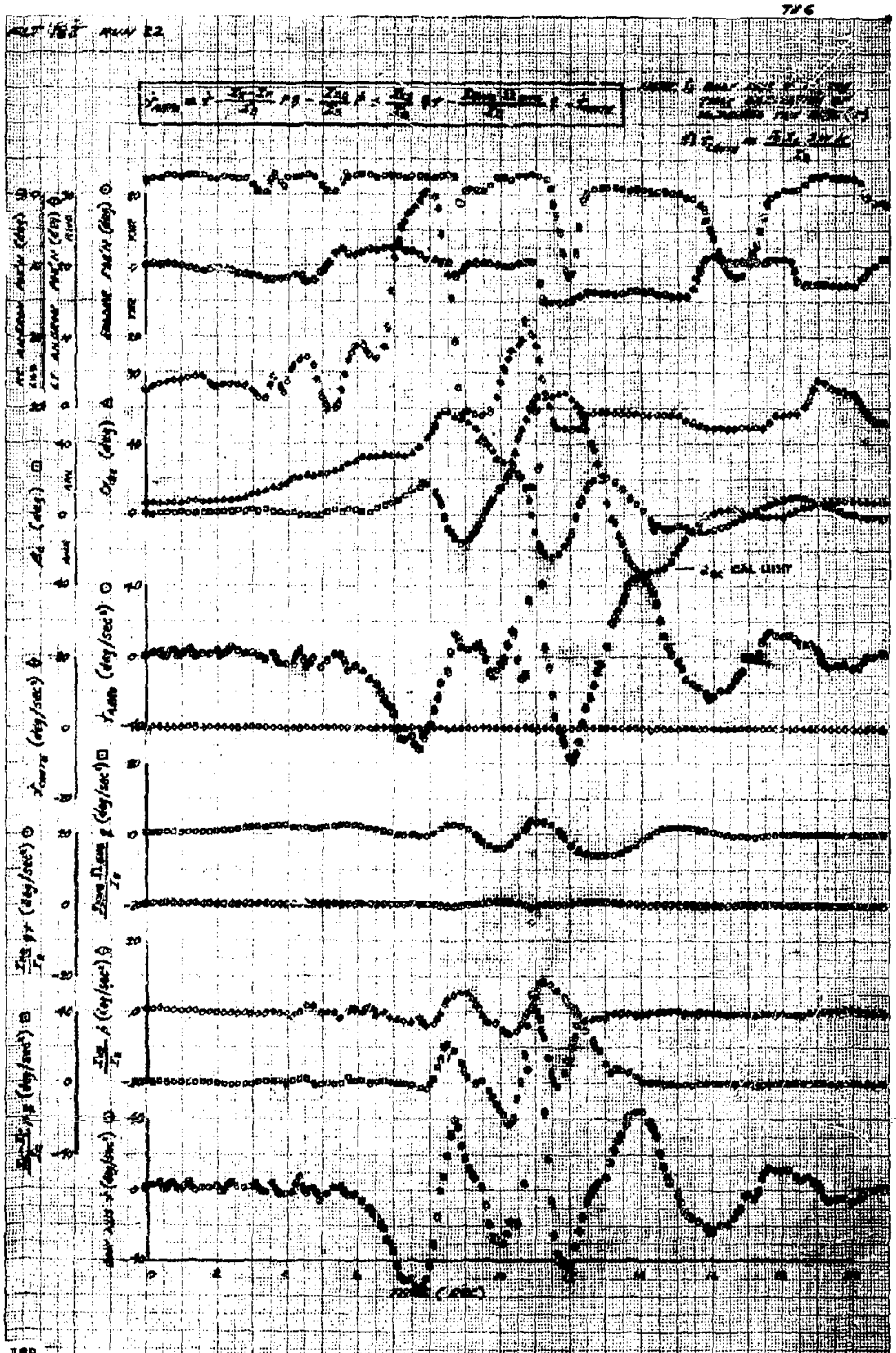

FIGURE 56 CONTINUED

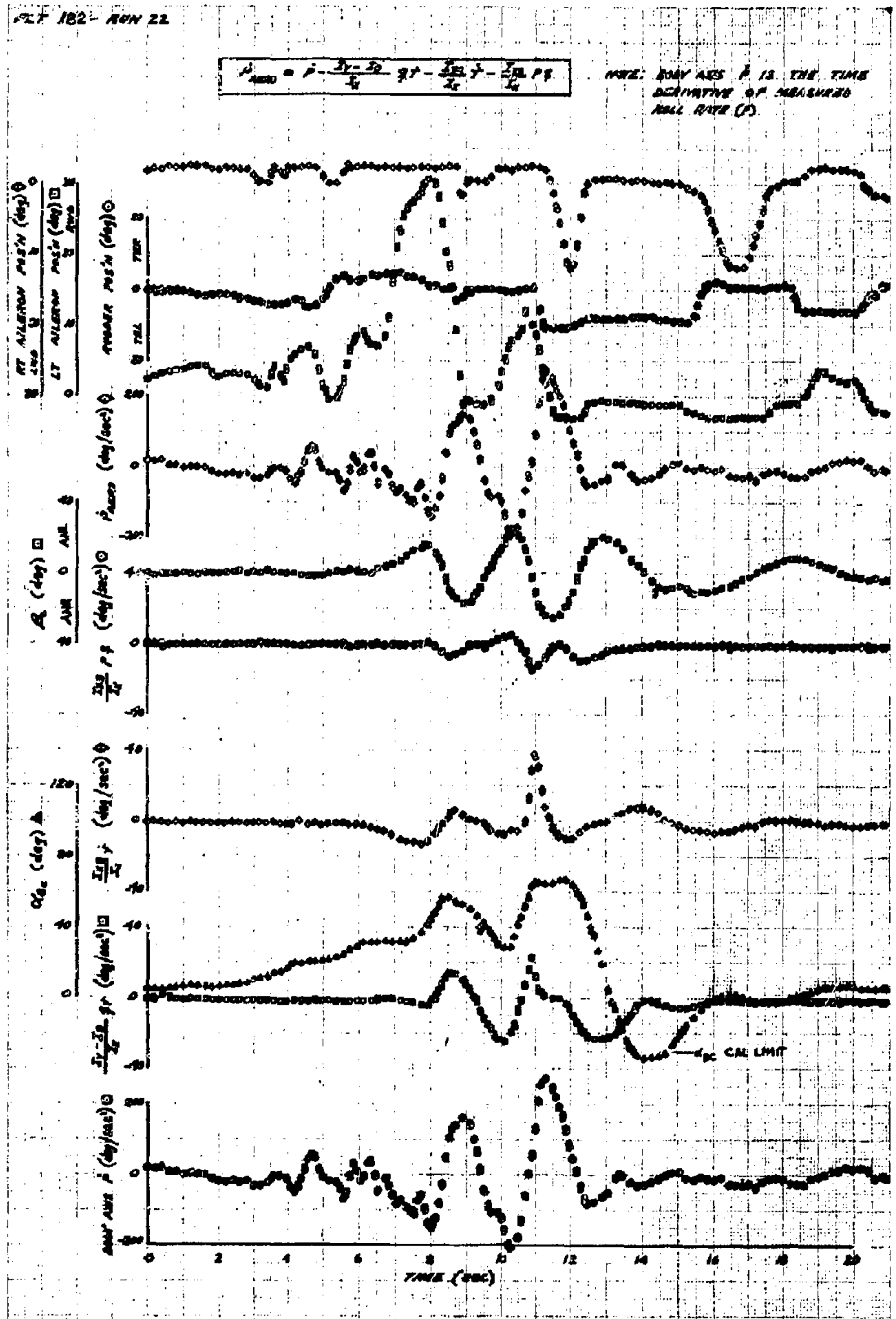

FIGURE 38 CONTINUED

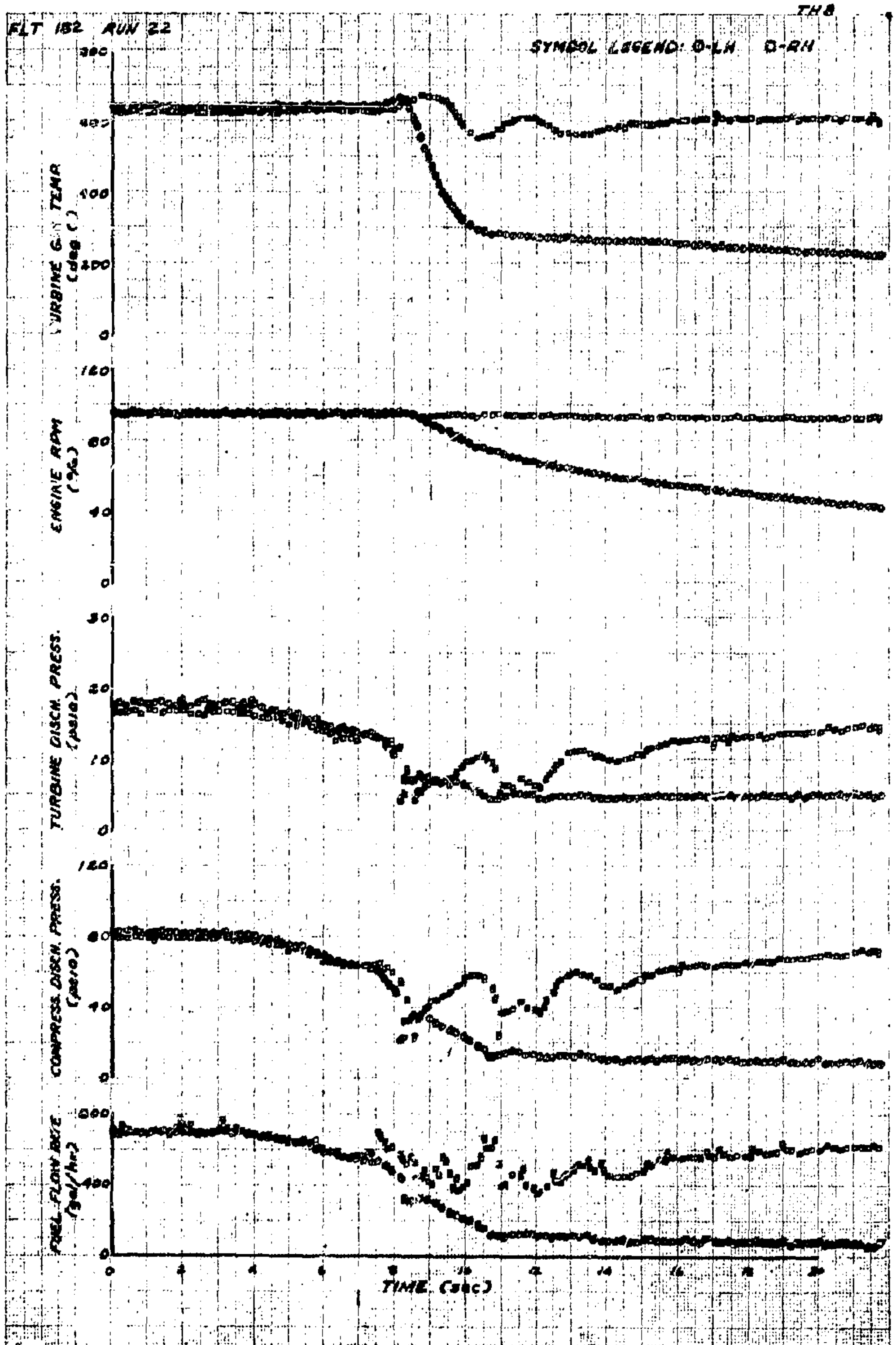

FIGURE 58 CONTINUED

THIS PAGE LEFT BLANK FOR PRESENTATION PURPOSES

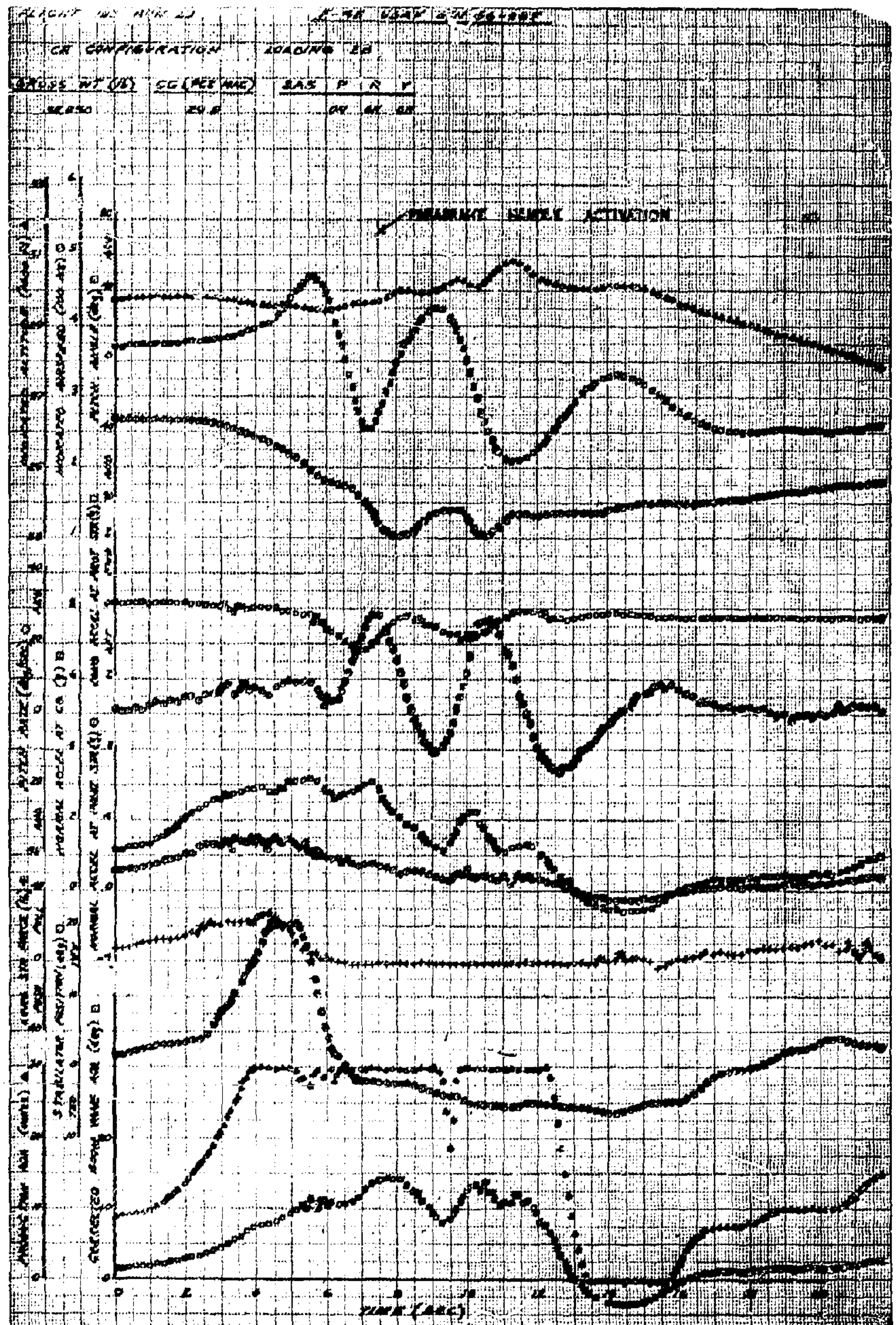

 FIGURE 38 L TURN, STEEP - MILDLY

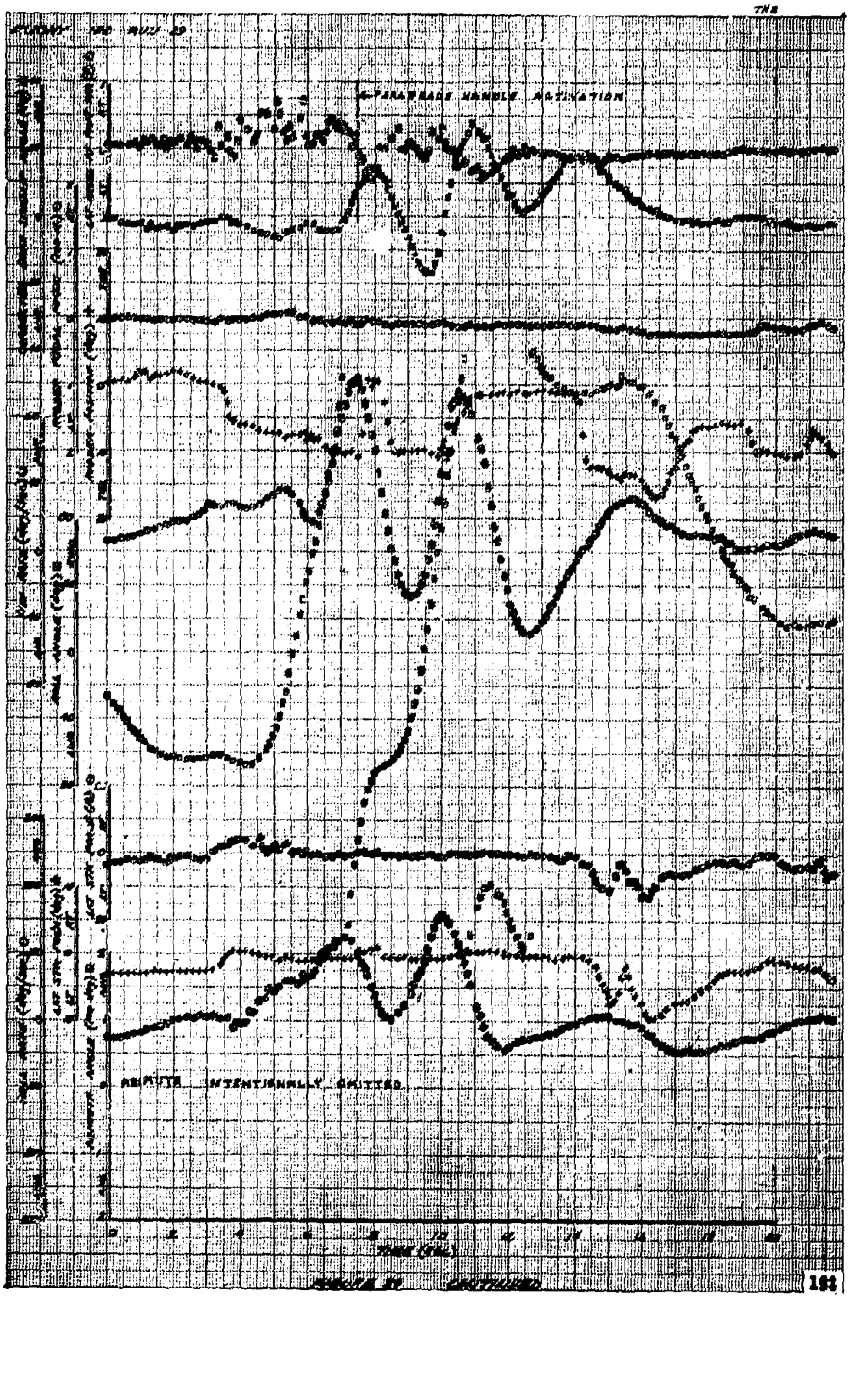
HANDLE ACTIVATION
INTENTIONALLY OMITTED

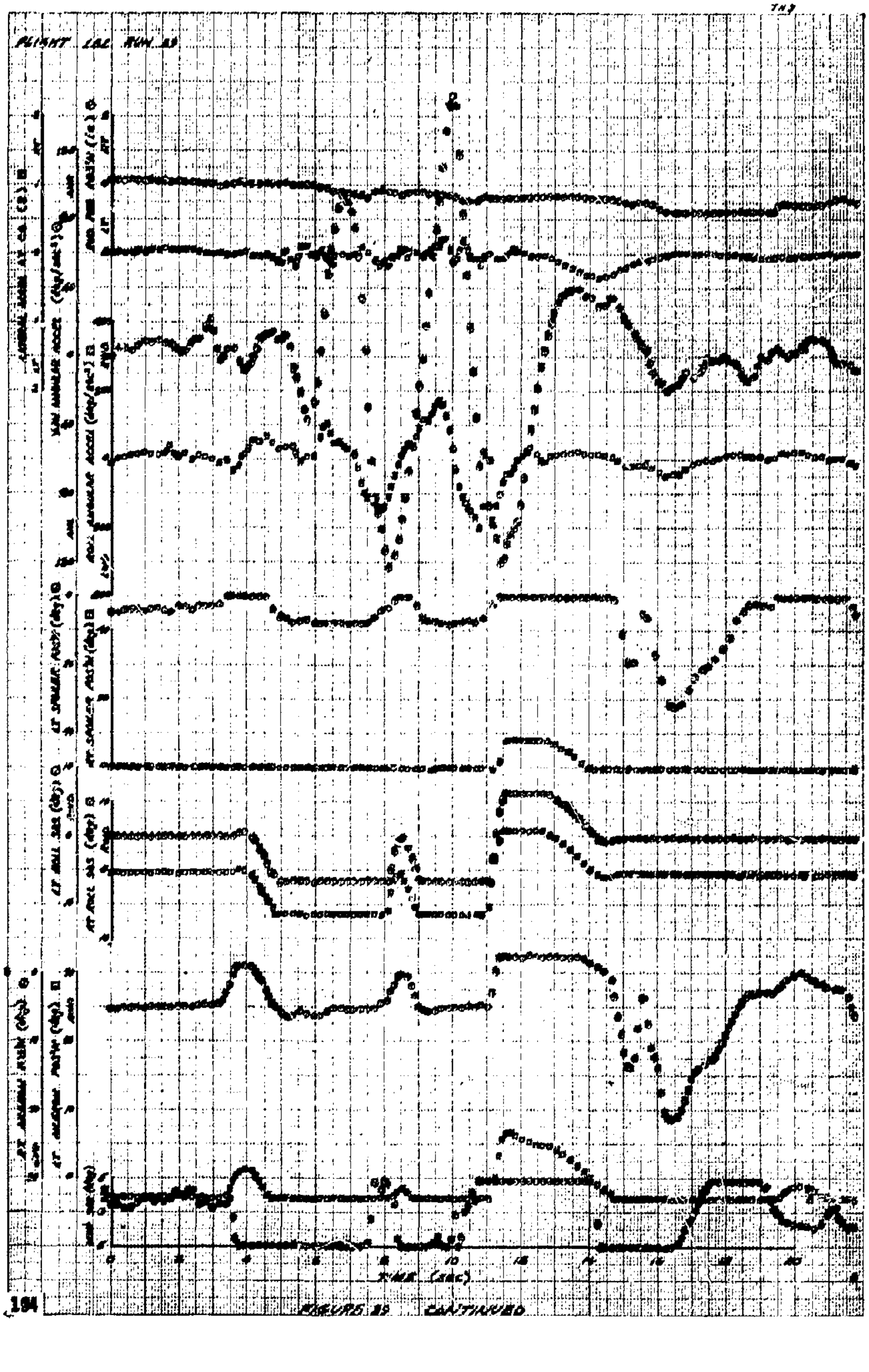

FIGURE 29 CONTINUED

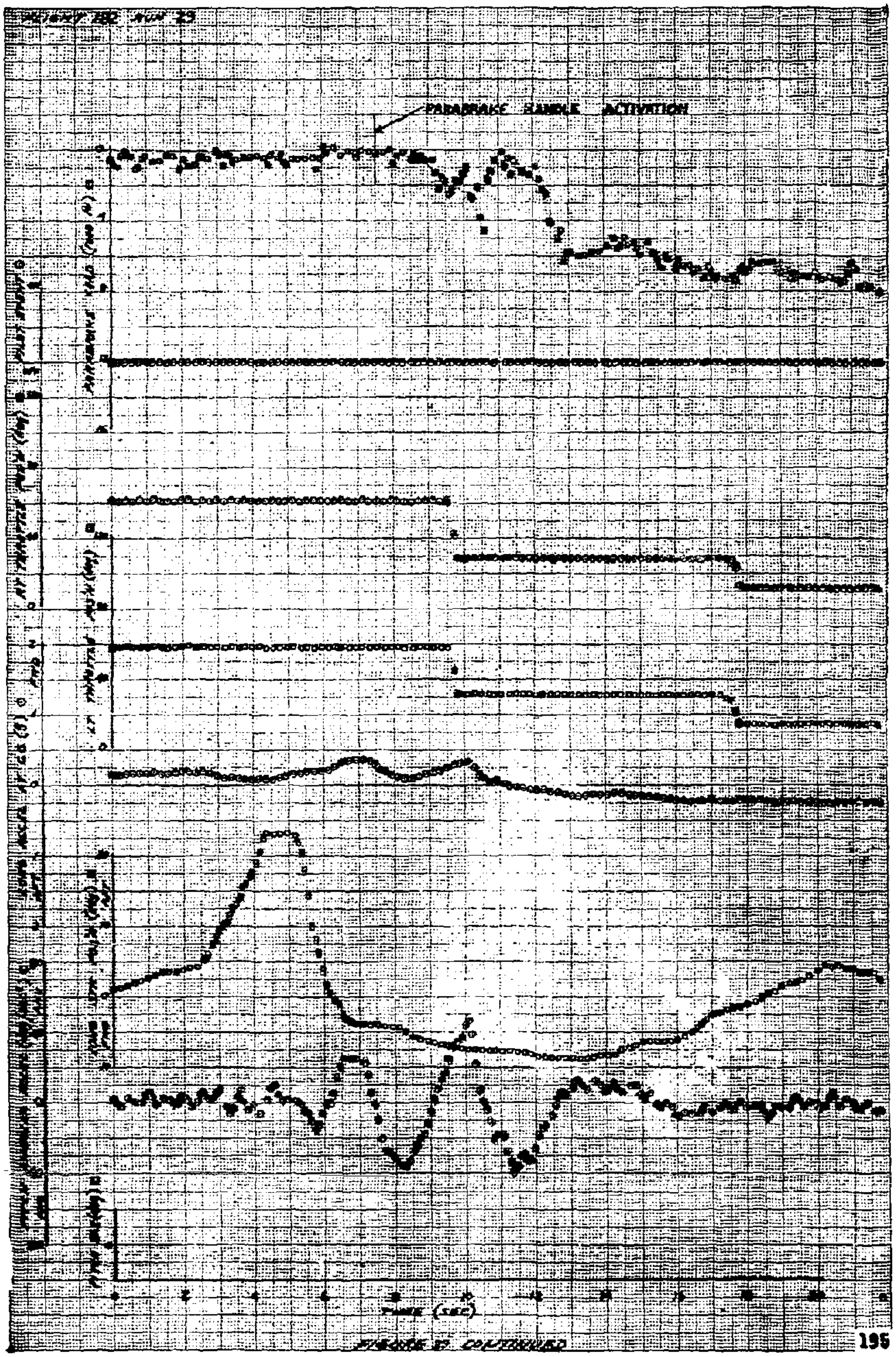

FIGURE 27 CONTINUED

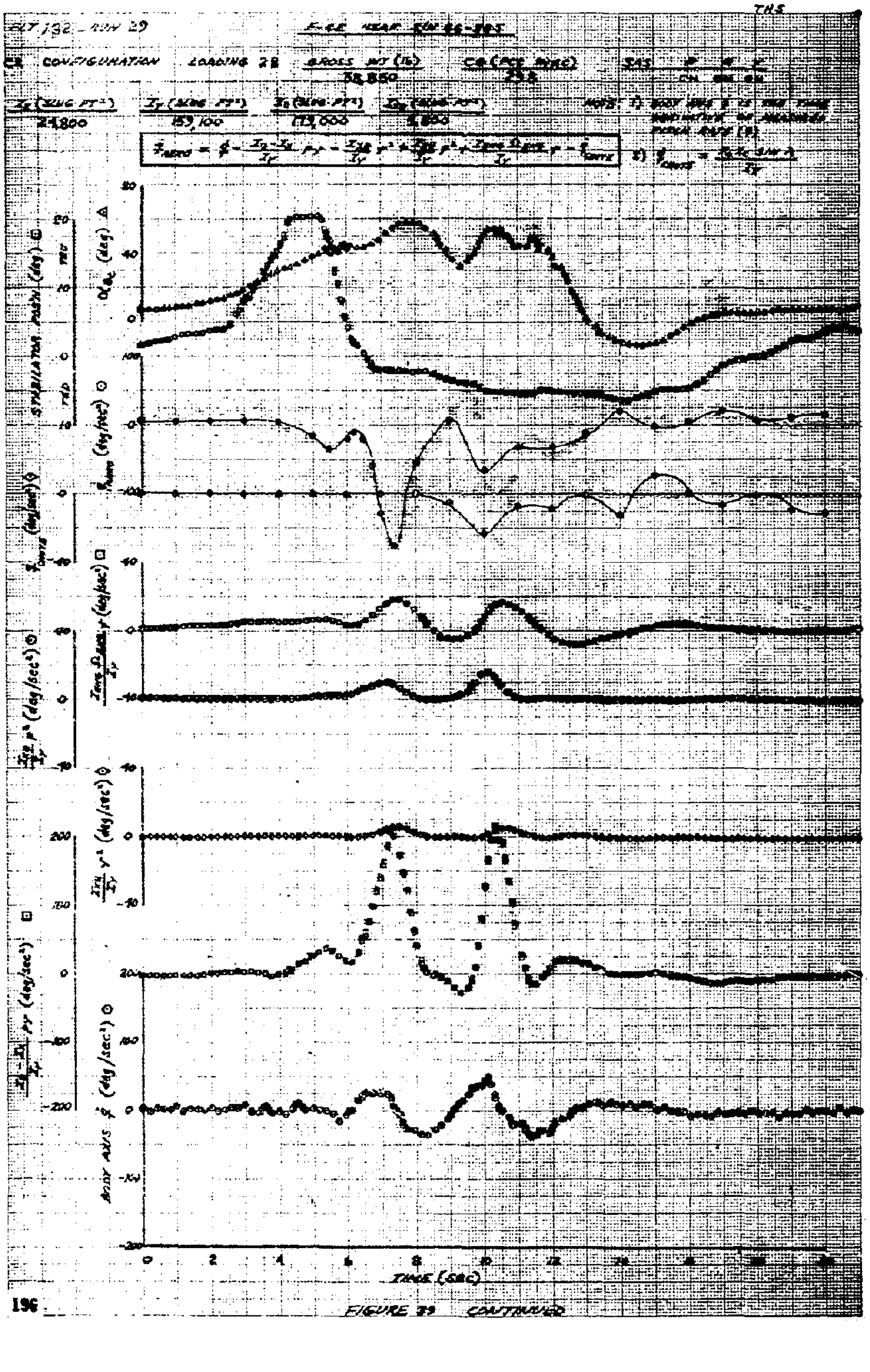

FIGURE 39 CONTINUED

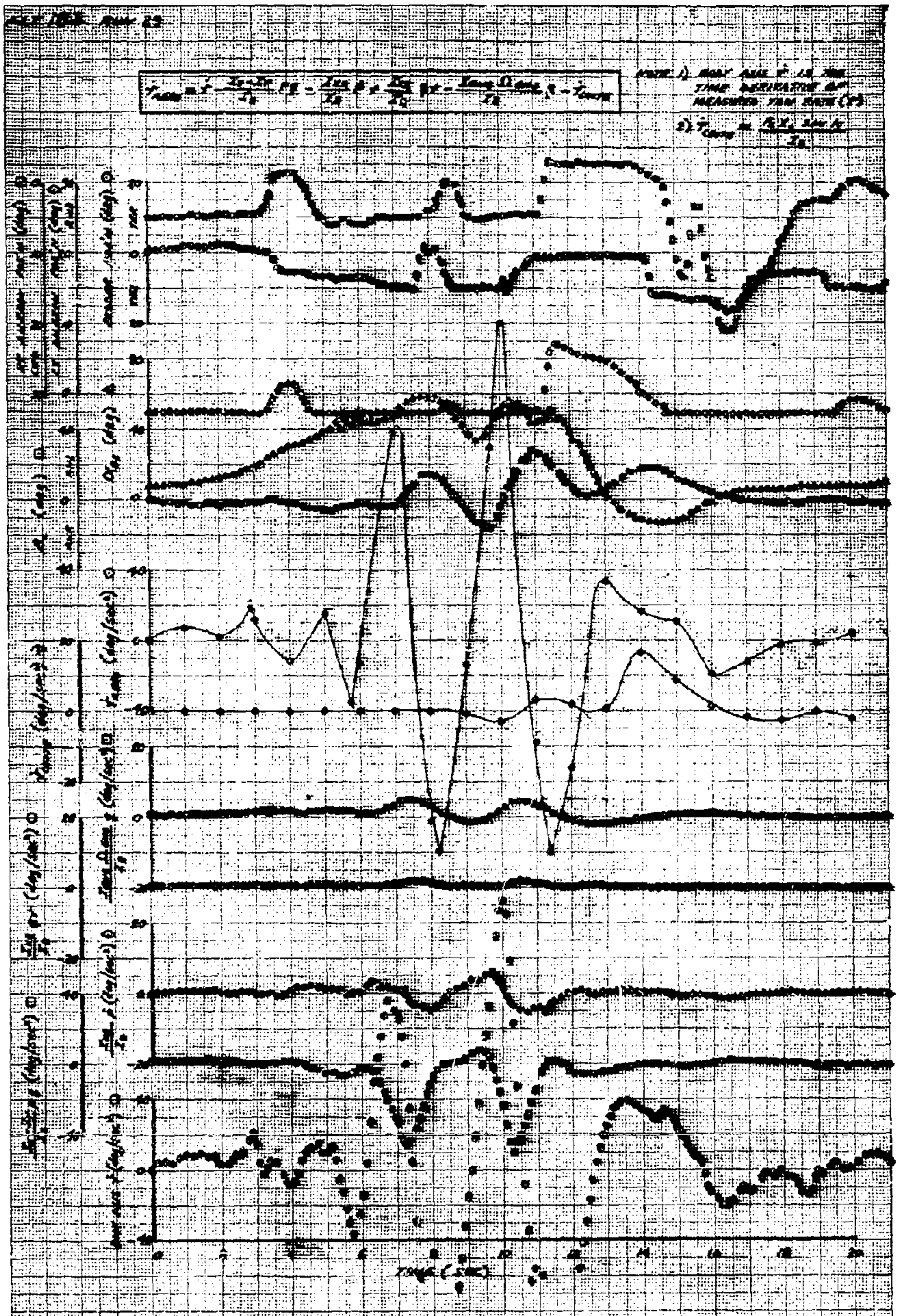

FIGURE 33 CONTINUED

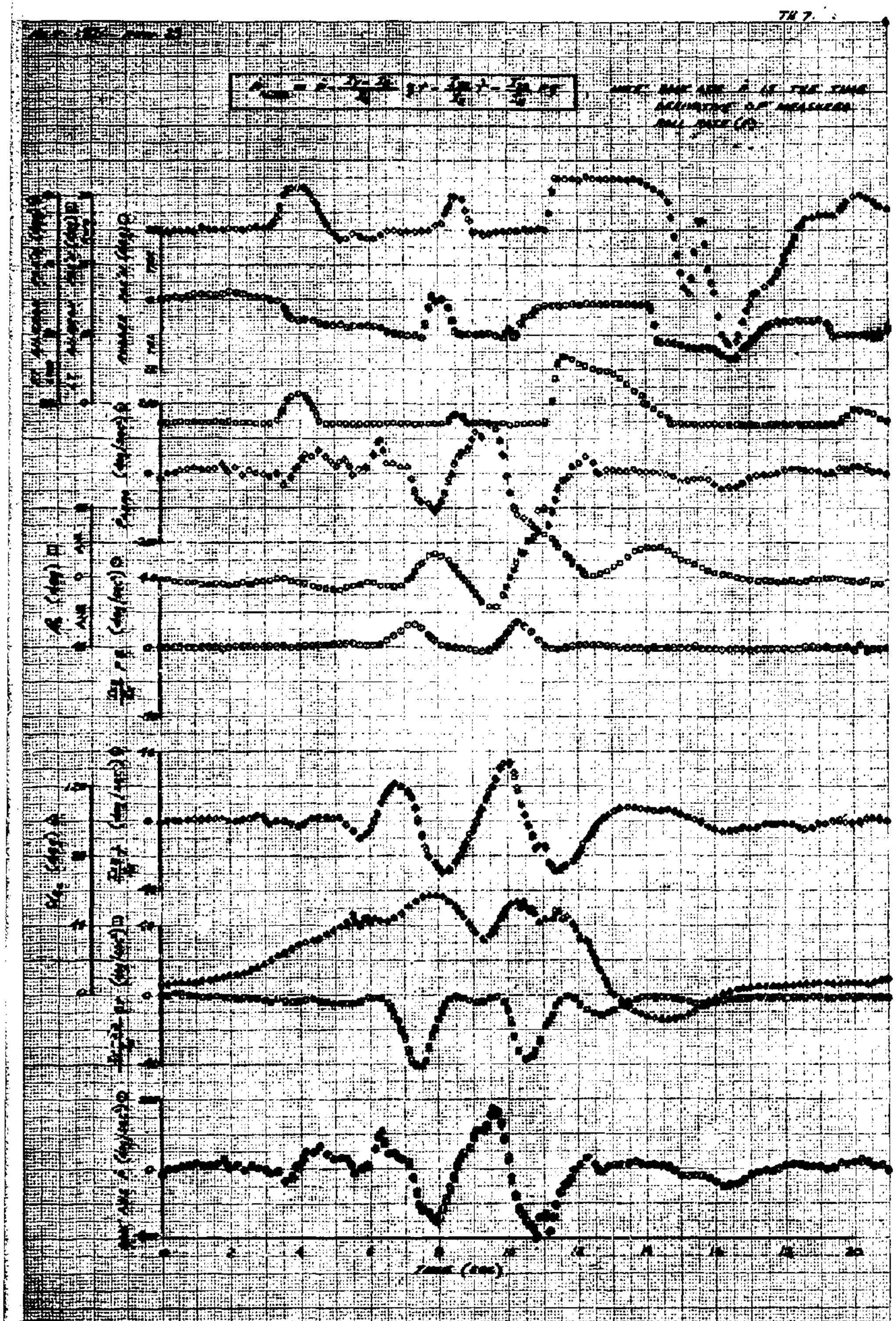

FIGURE 33 CONTINUED

THIS PAGE LEFT BLANK FOR PRESENTATION PURPOSES

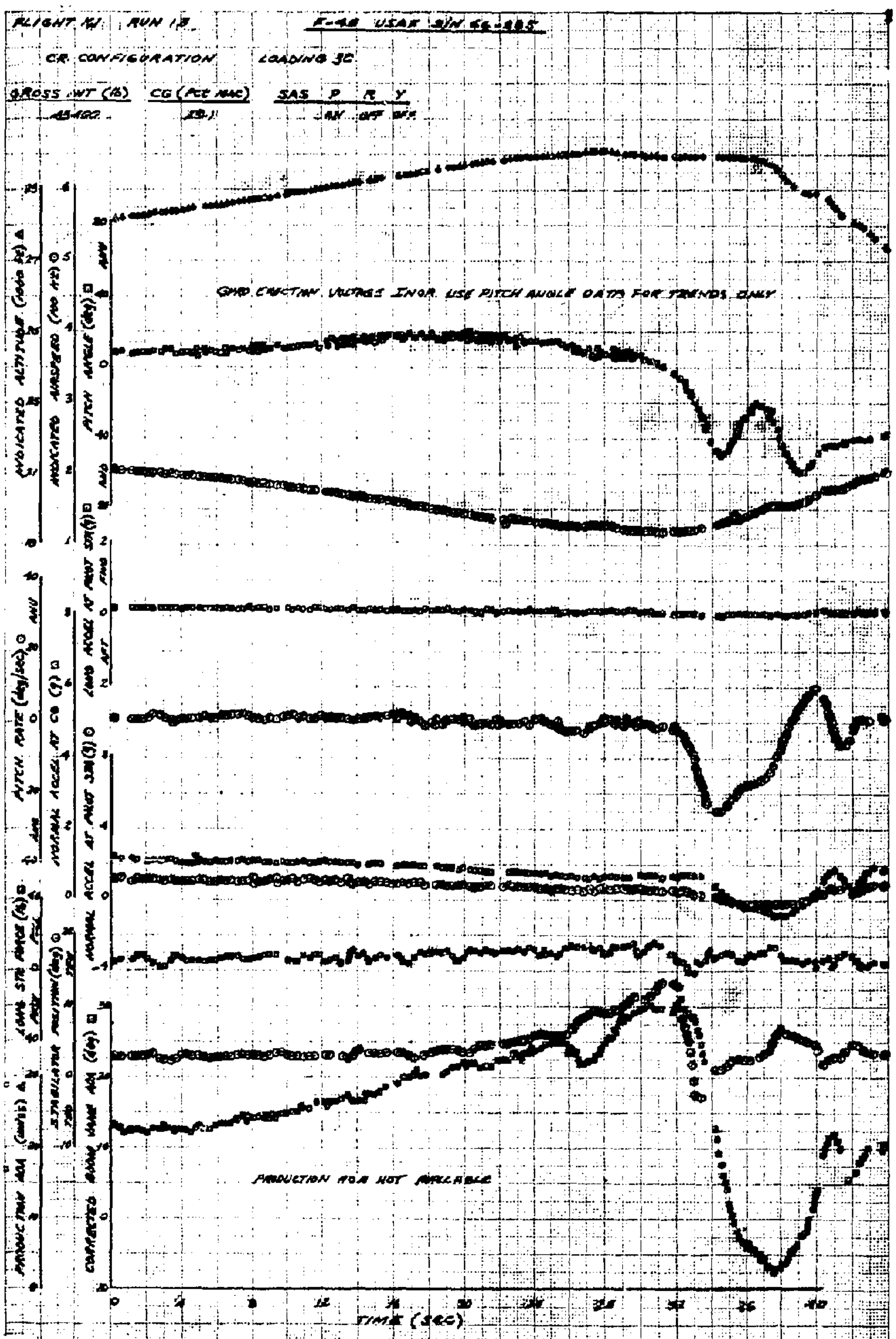

 FIGURE 40 ROLLING DEPARTURE WITH ASYMMETRIC LOADING

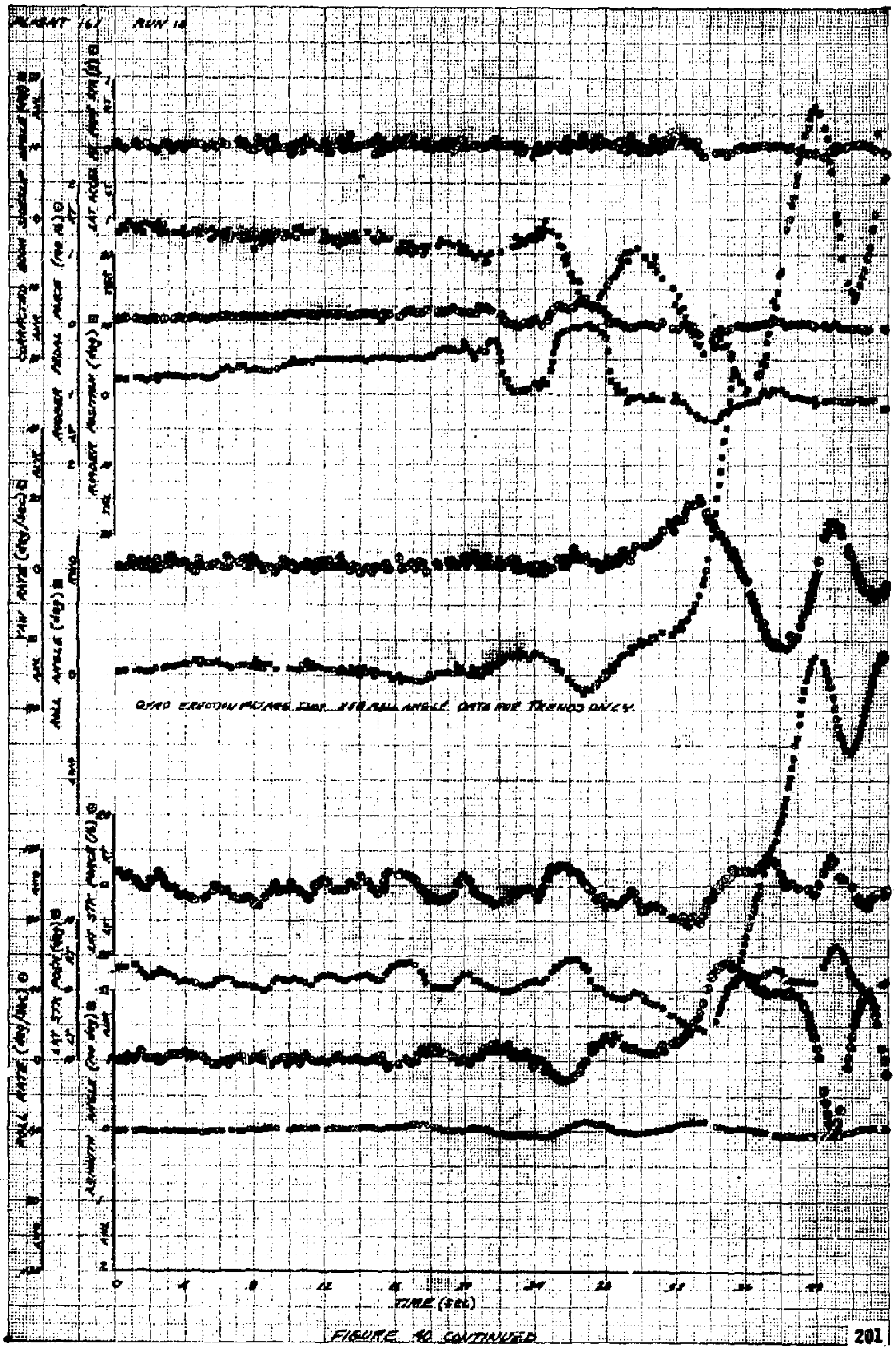

FIGURE 40 CONTINUED

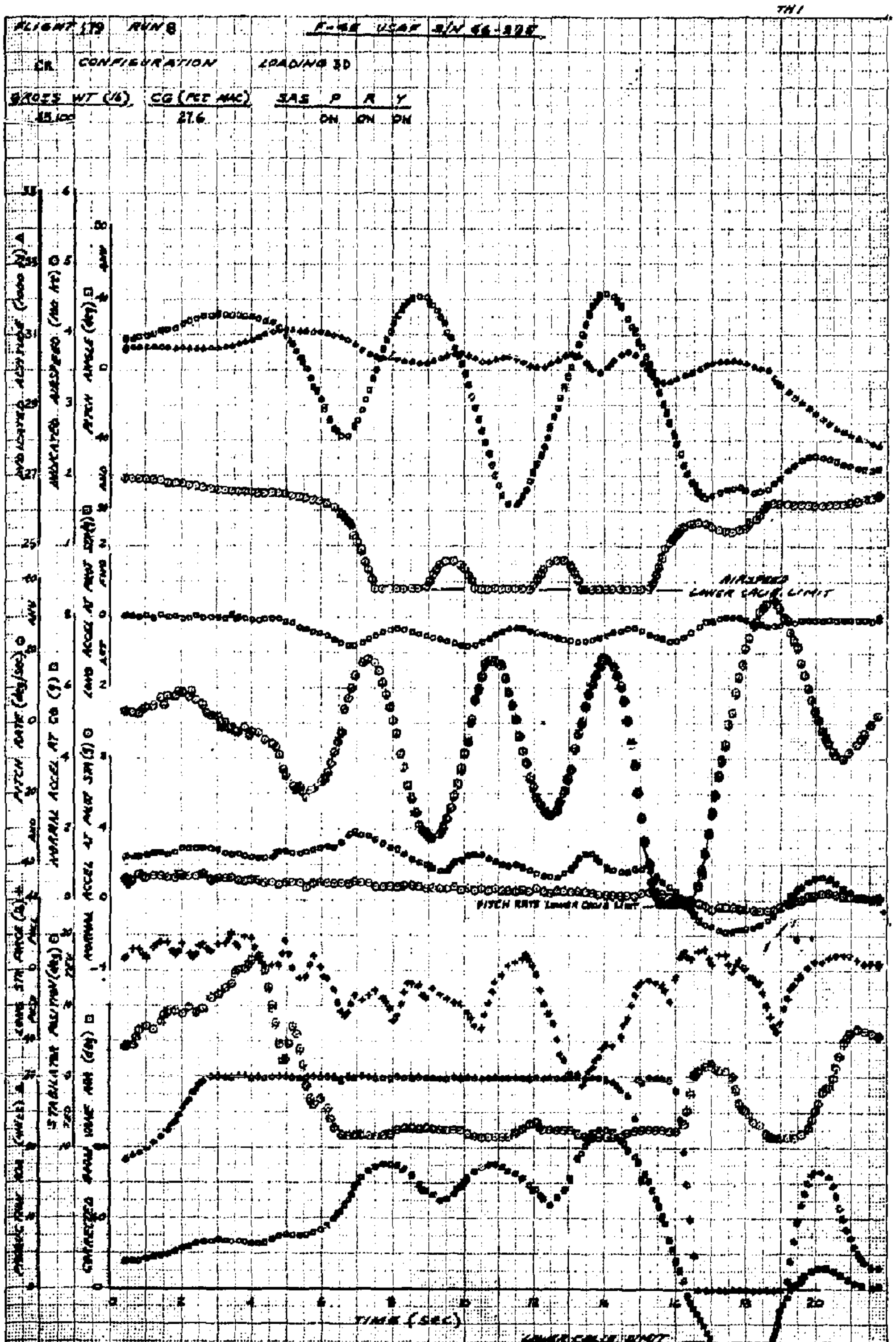

202 FIGURE 41 2 TURN, HIGH AOA - HIGHLY OSCILLATORY SPIN

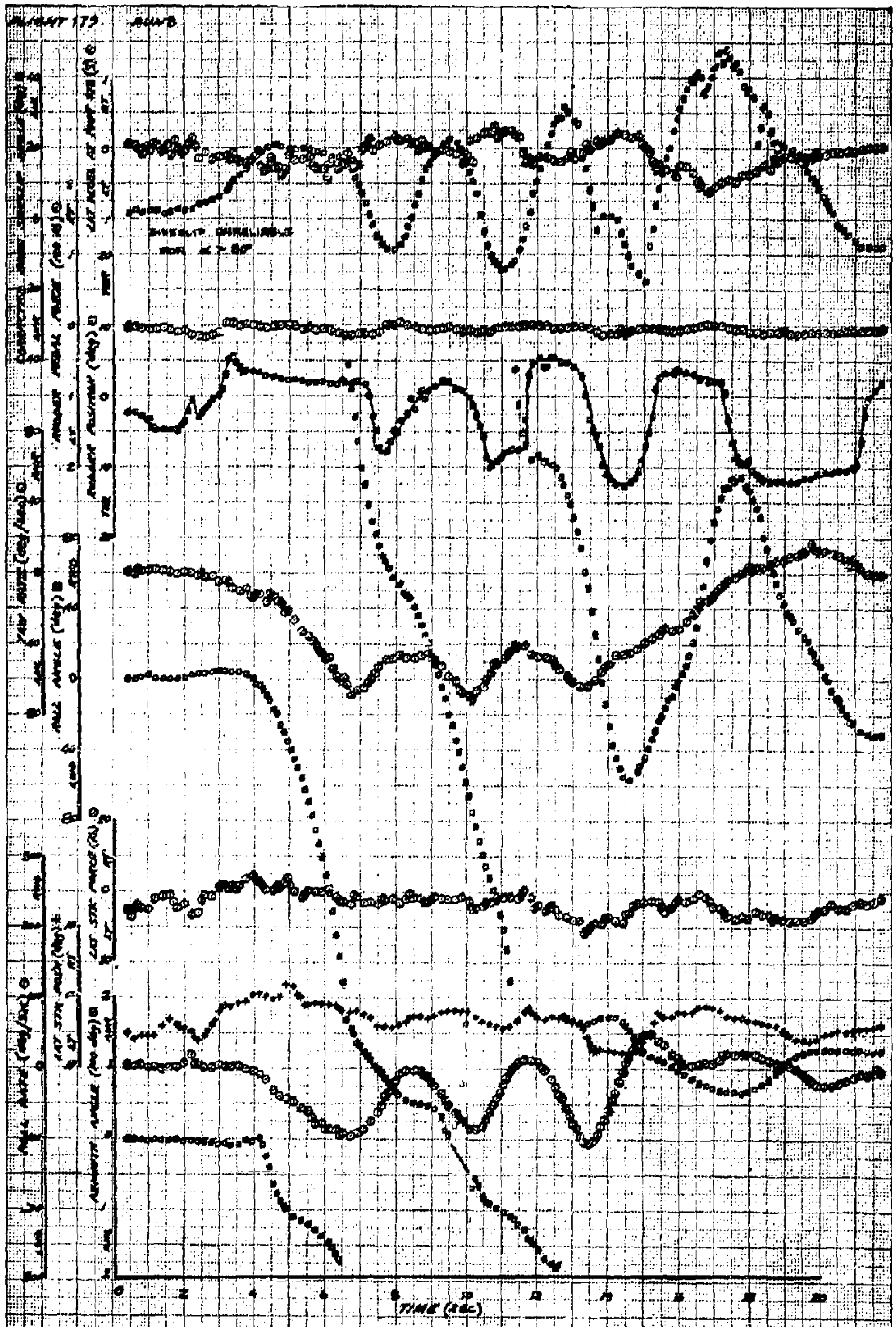

FIGURE 41 CONTINUED

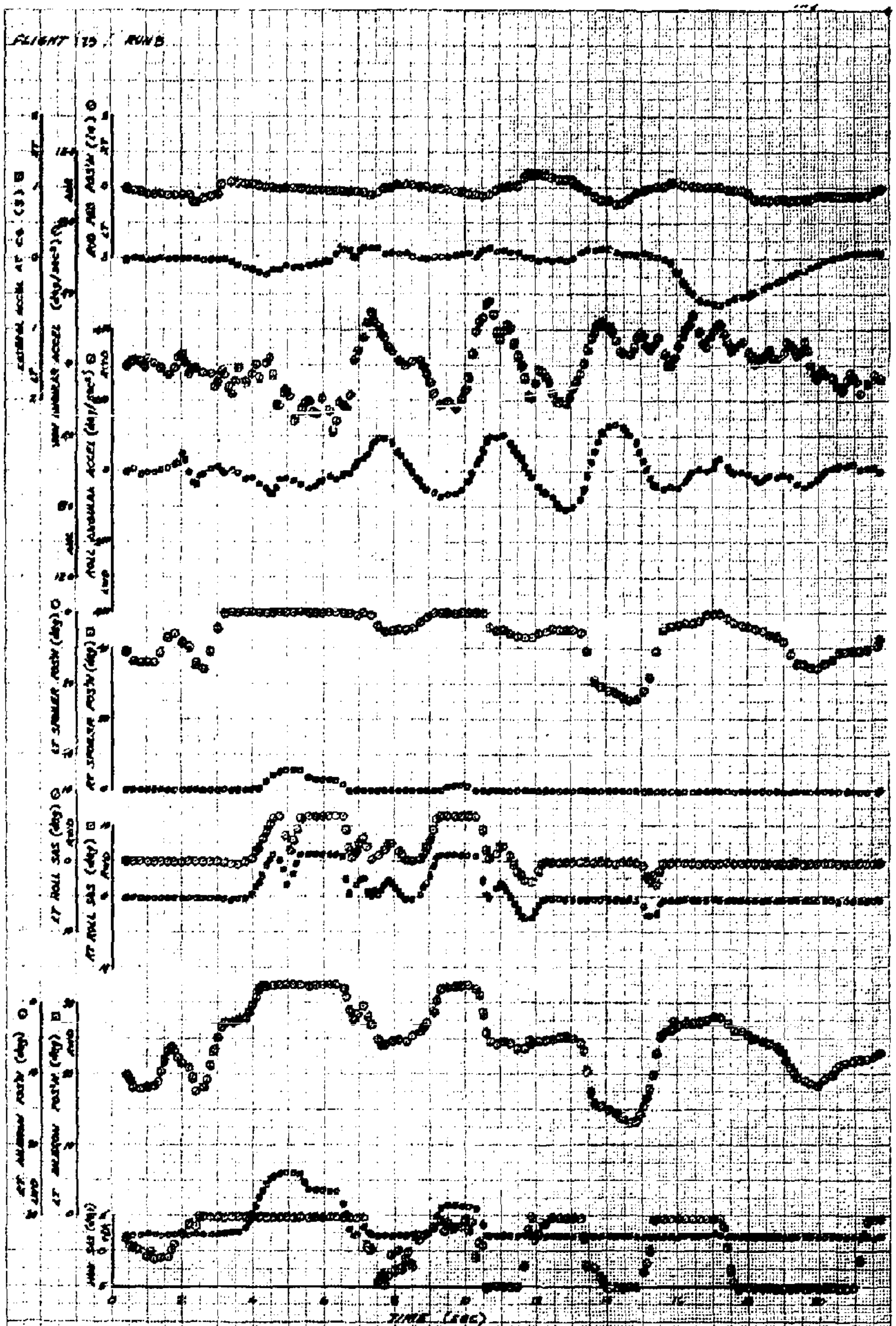

FIGURE 41 CONTINUED

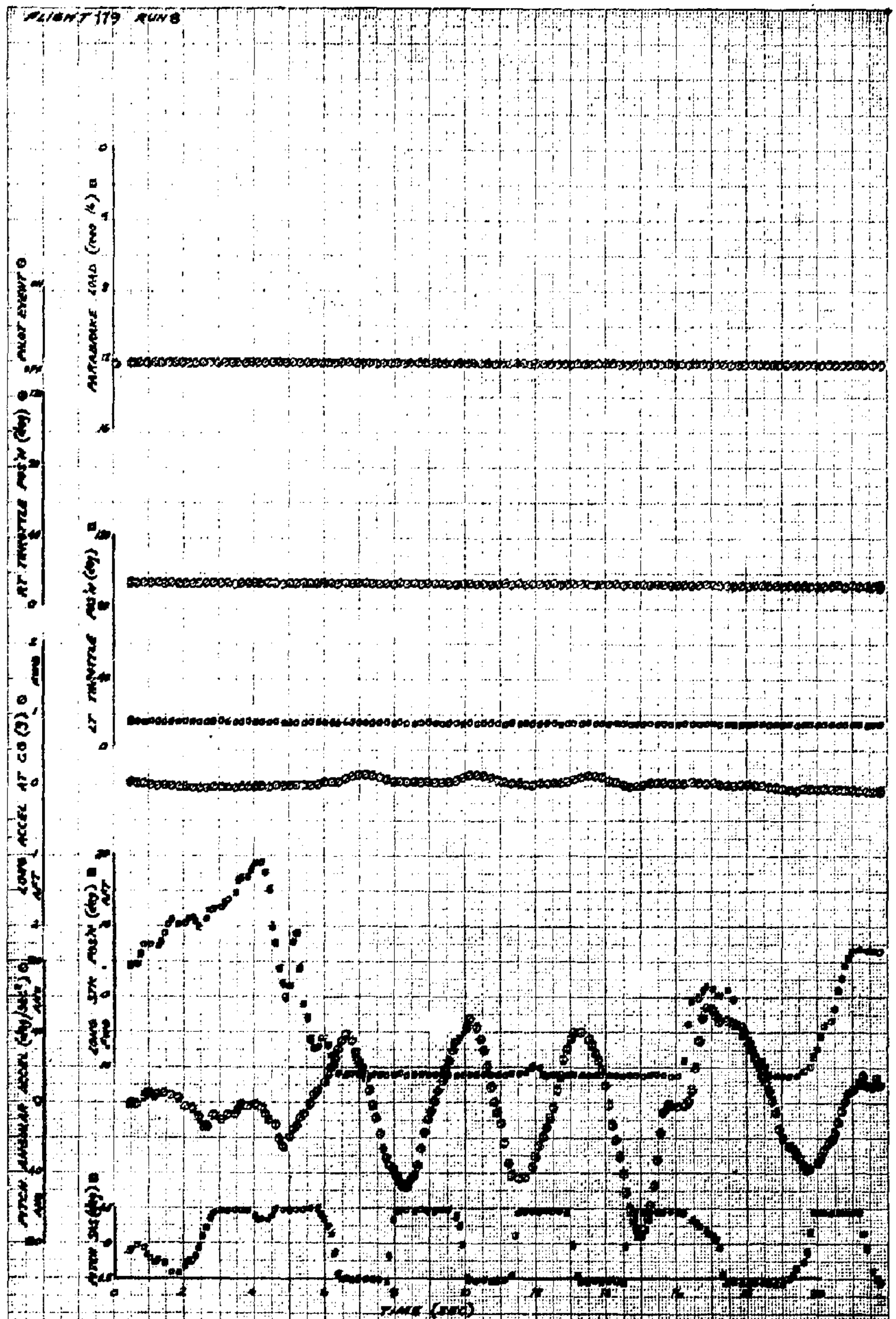

FIGURE 41 CONTINUED

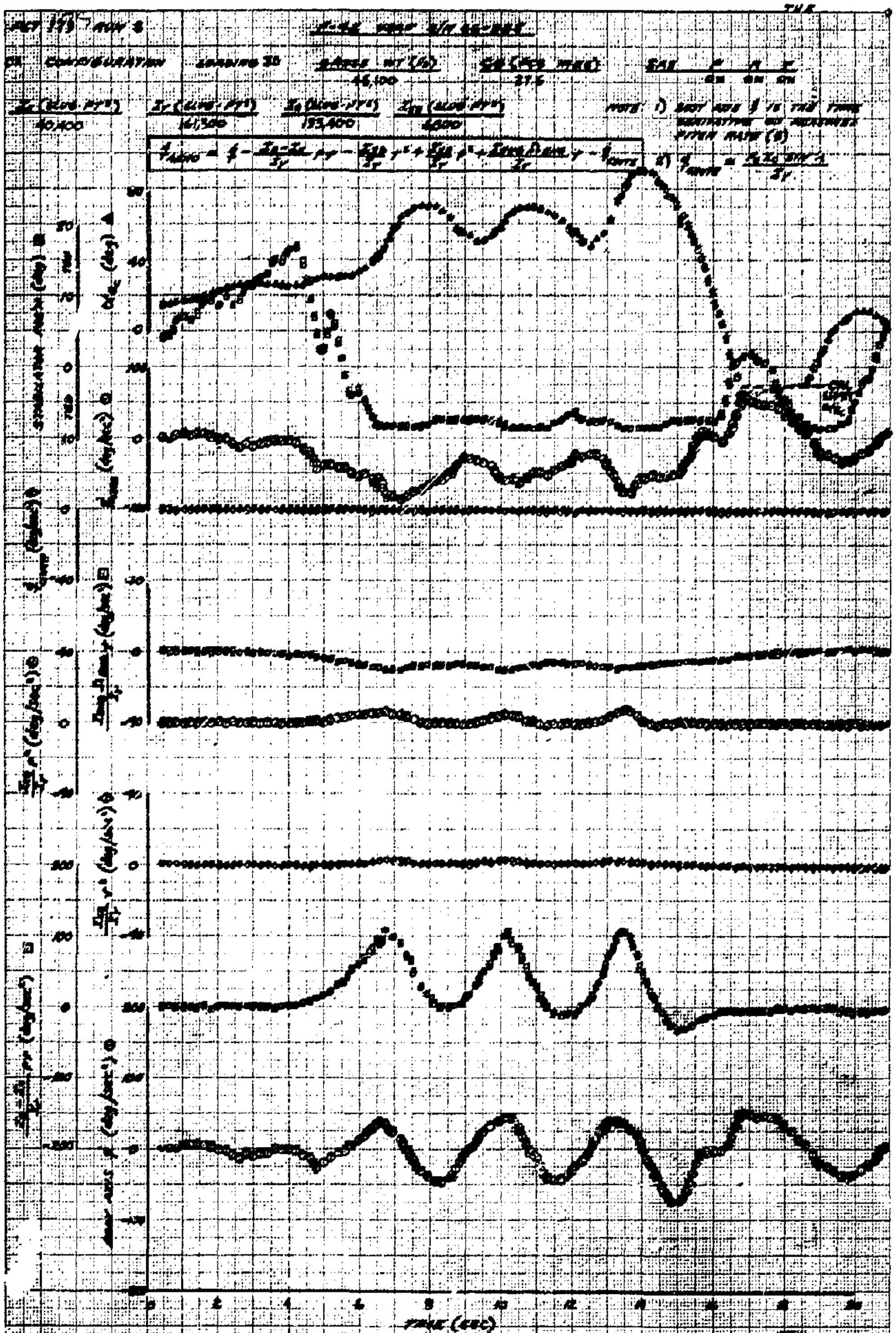

FIGURE 41 CONTINUED

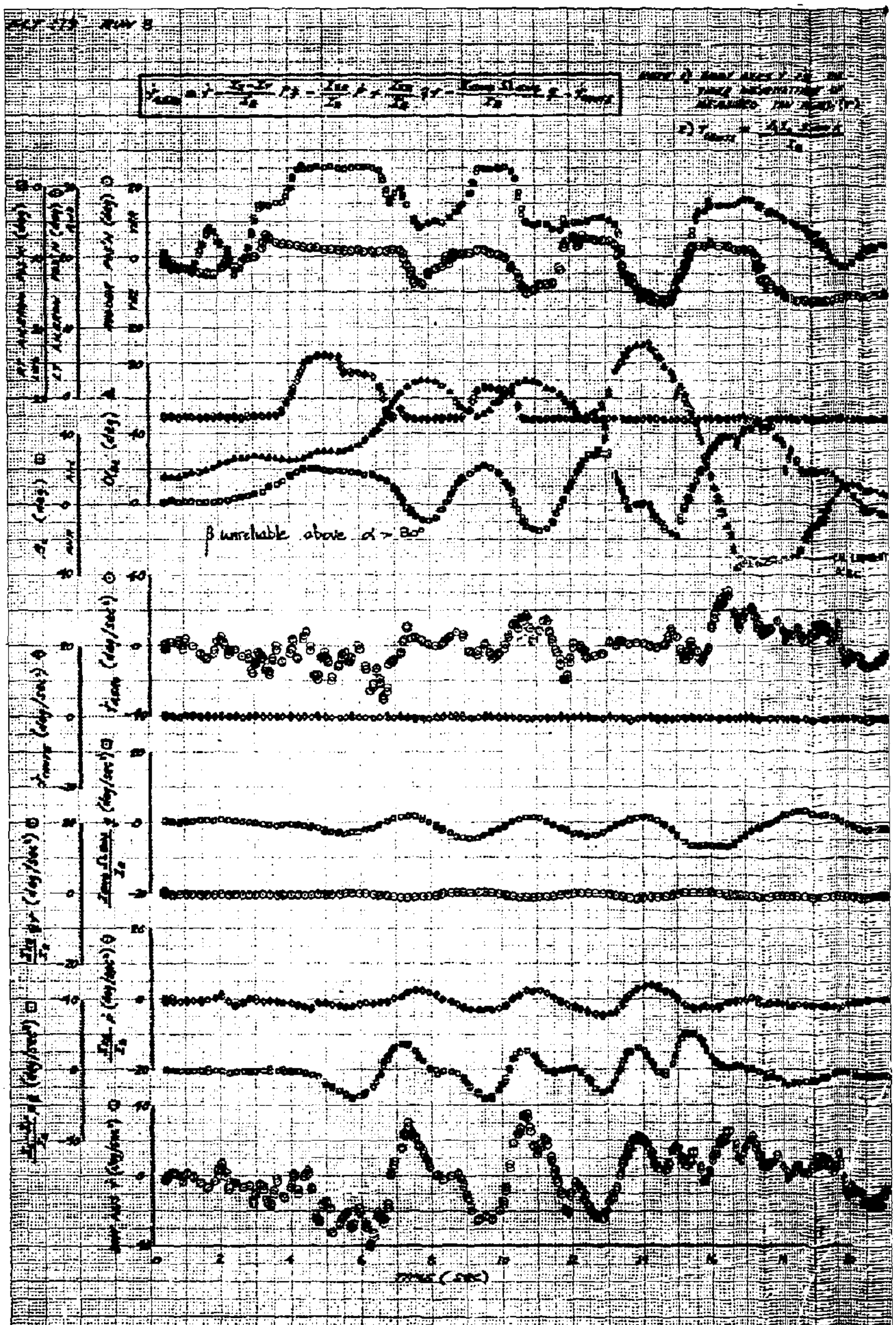

FIGURE 41 CONTINUED

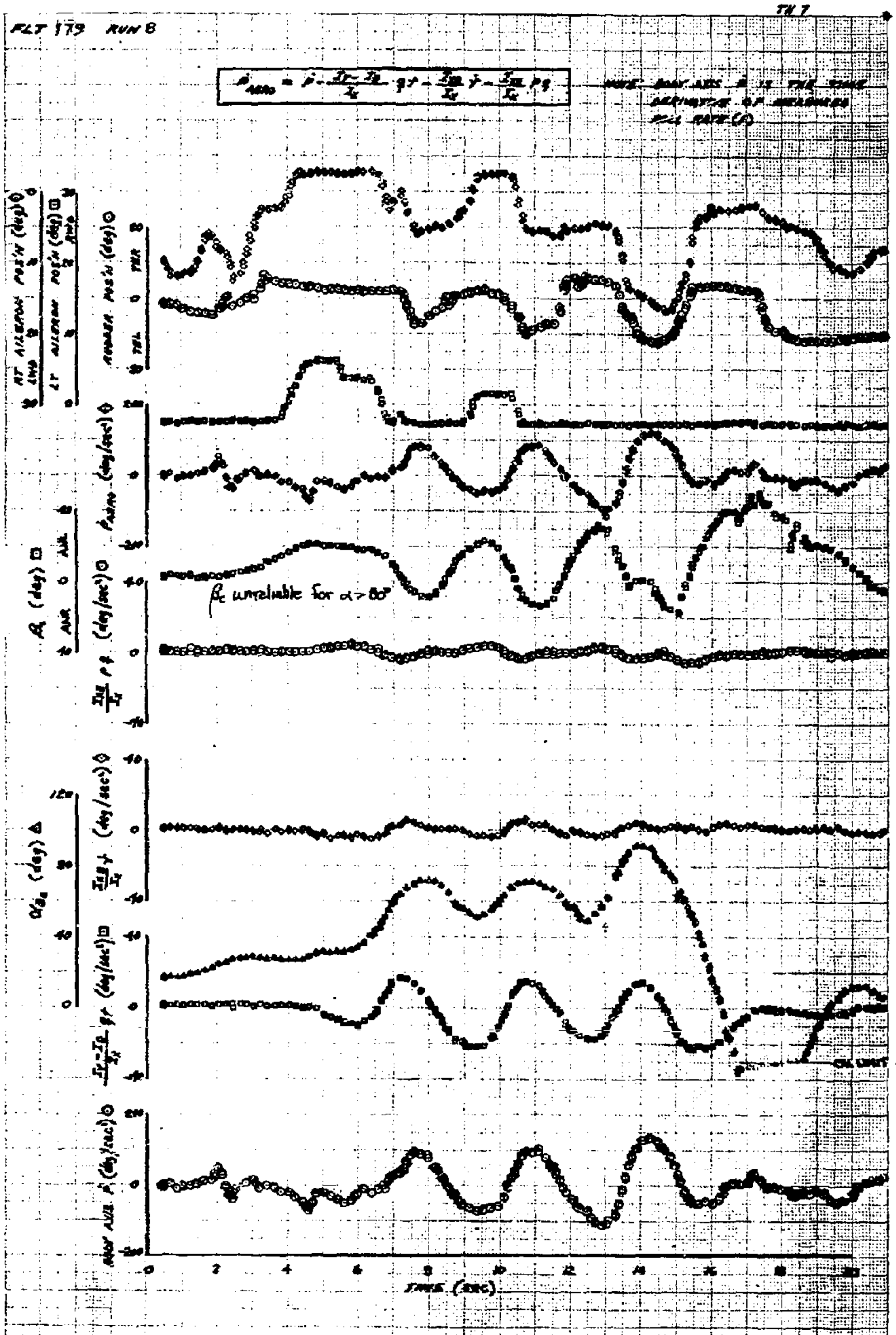

FIGURE 41 CONTINUED

PRECEDING PAGE BLANK-NOT FILMED

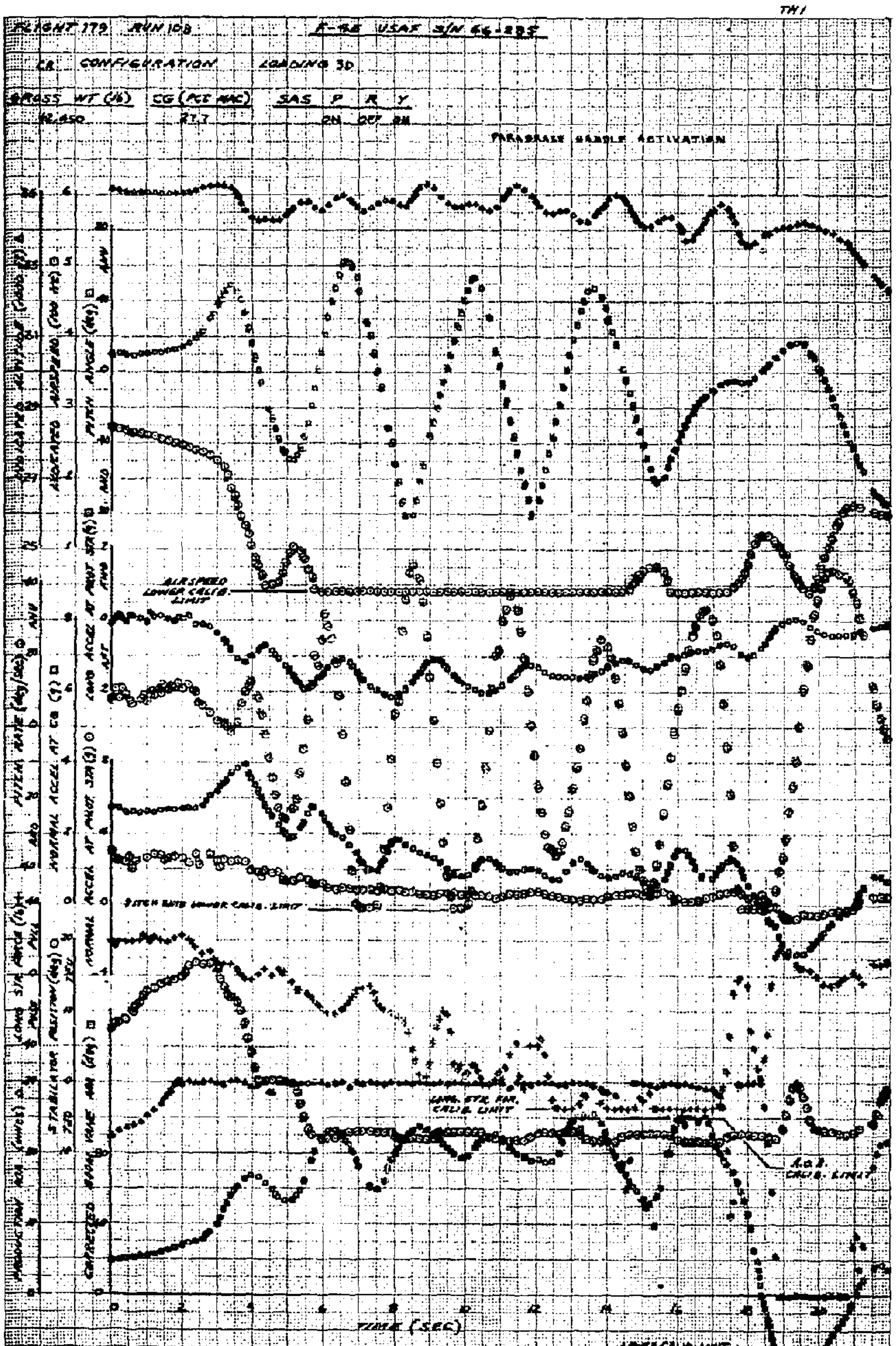

FIGURE 42 4 TURN, HIGH AOA - HIGHLY OSCILLATORY SPIN

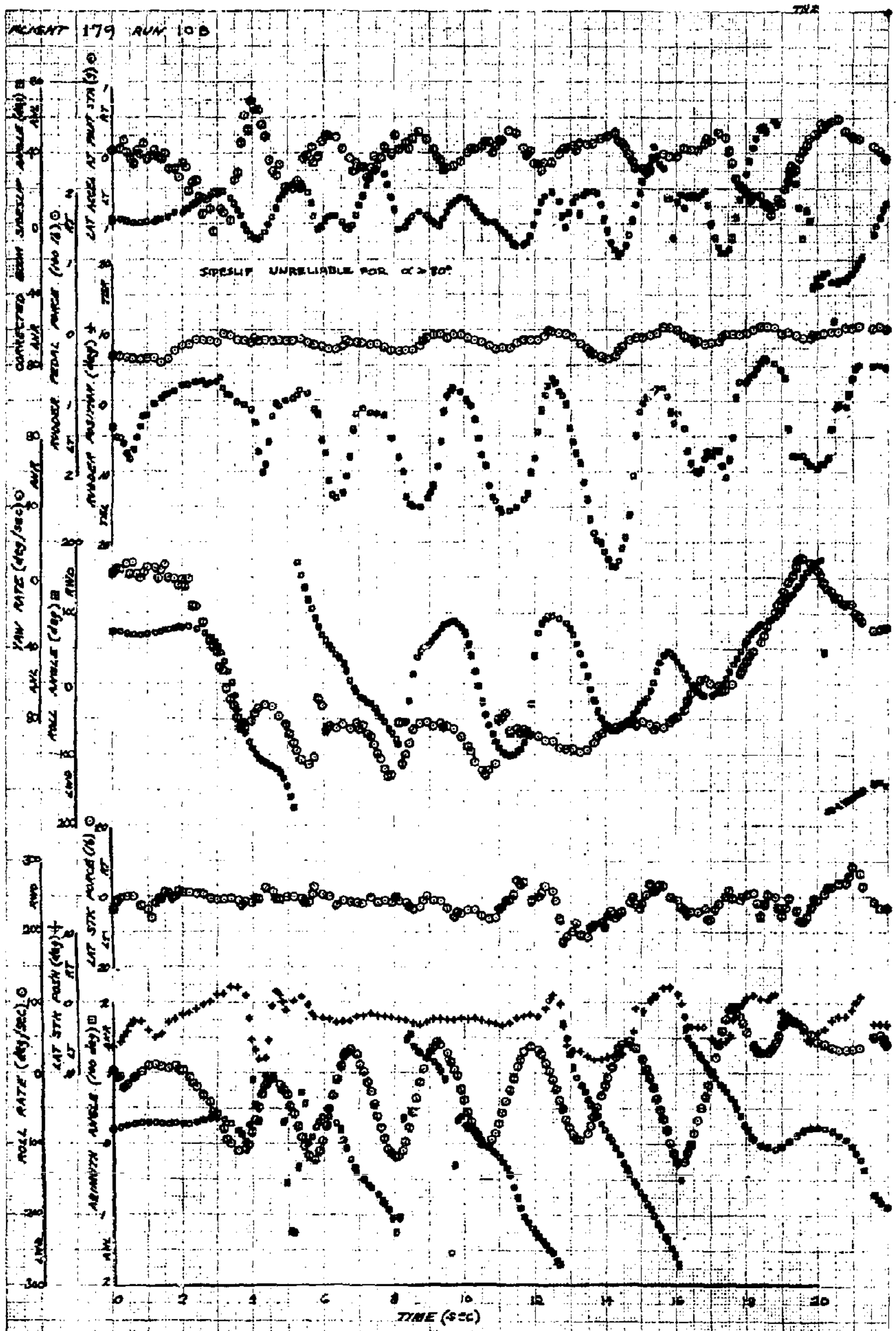

FIGURE 42 CONTINUED

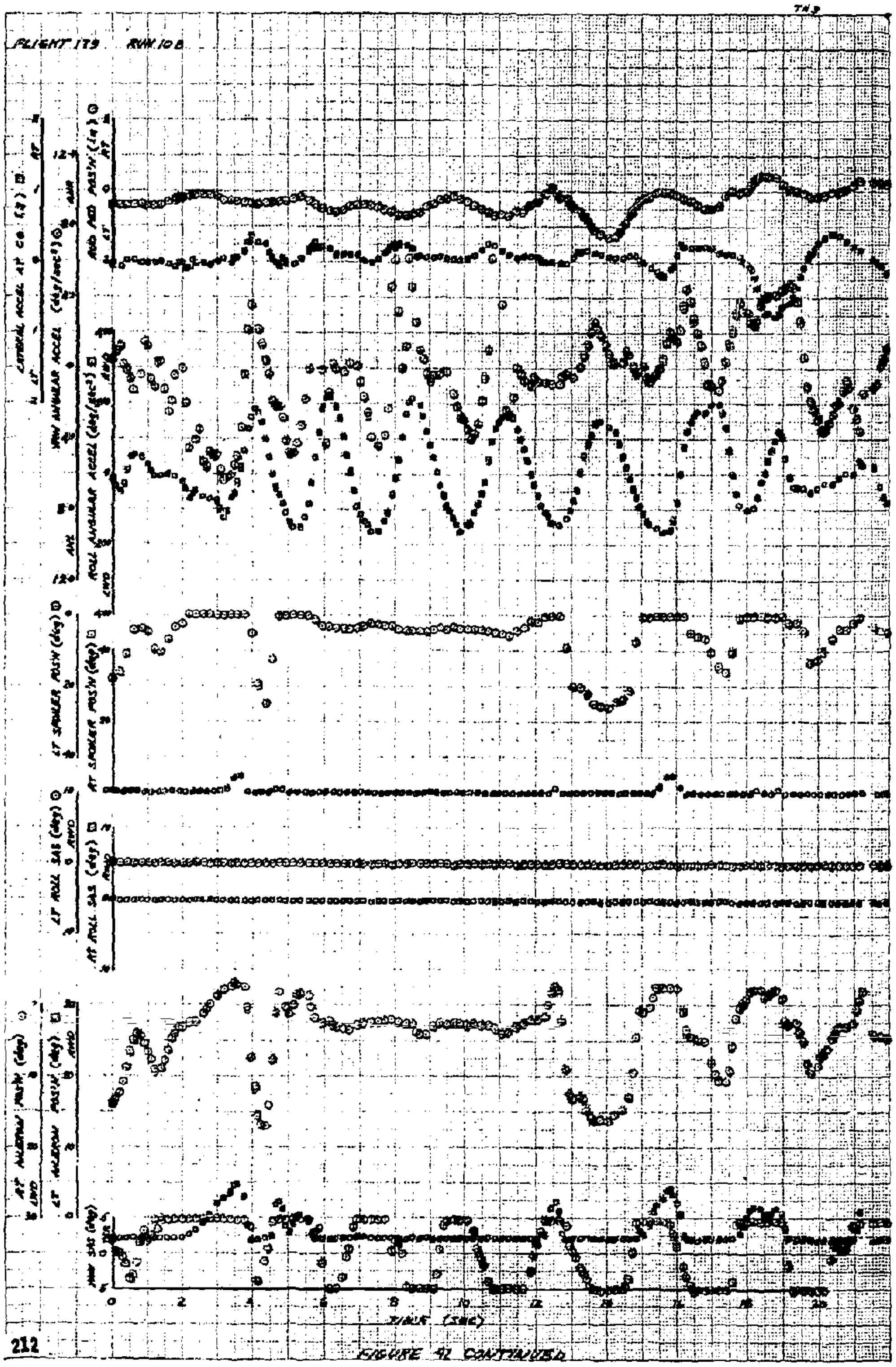

FIGURE 41 CONTINUED

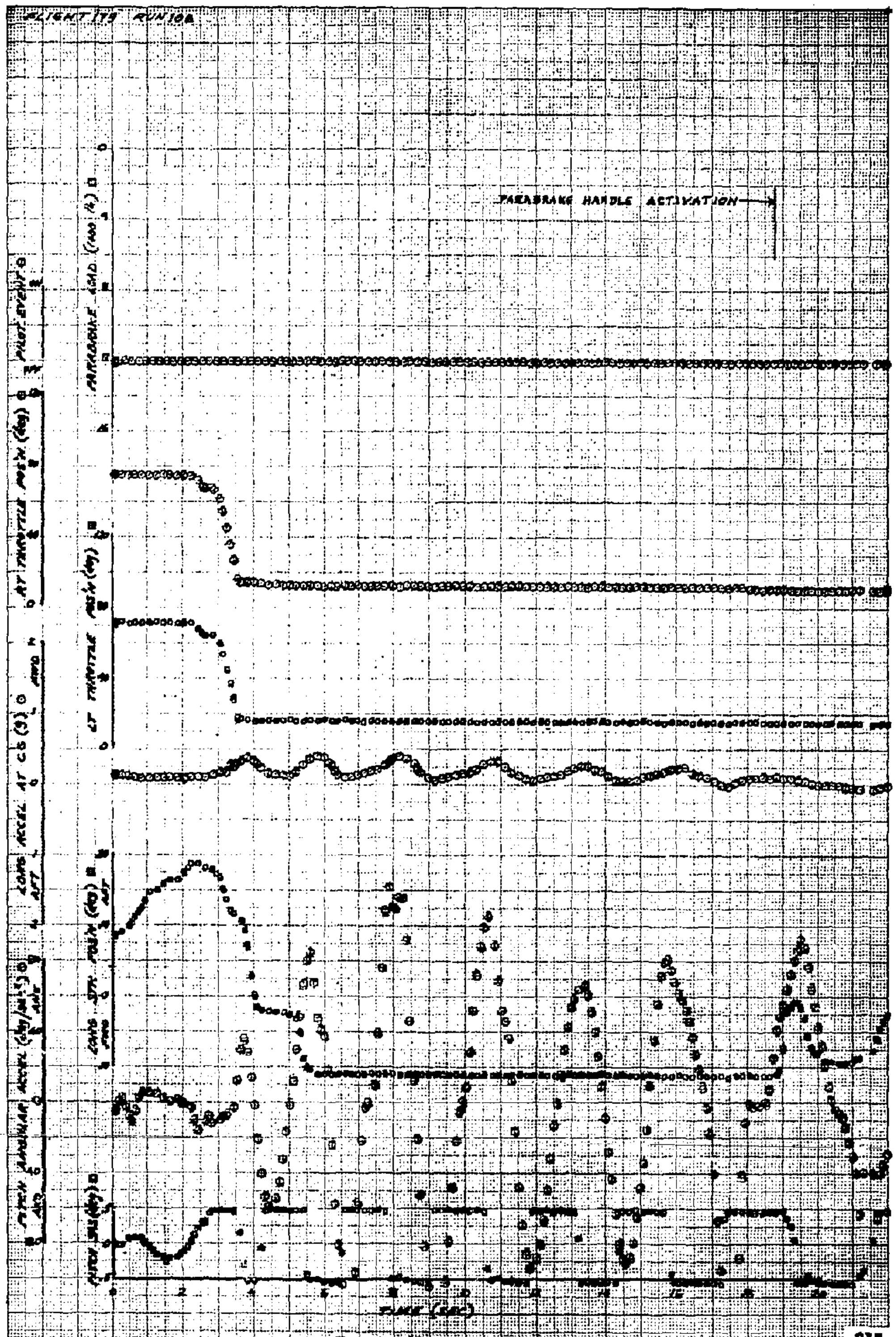

FIGURE 47 CONTINUED

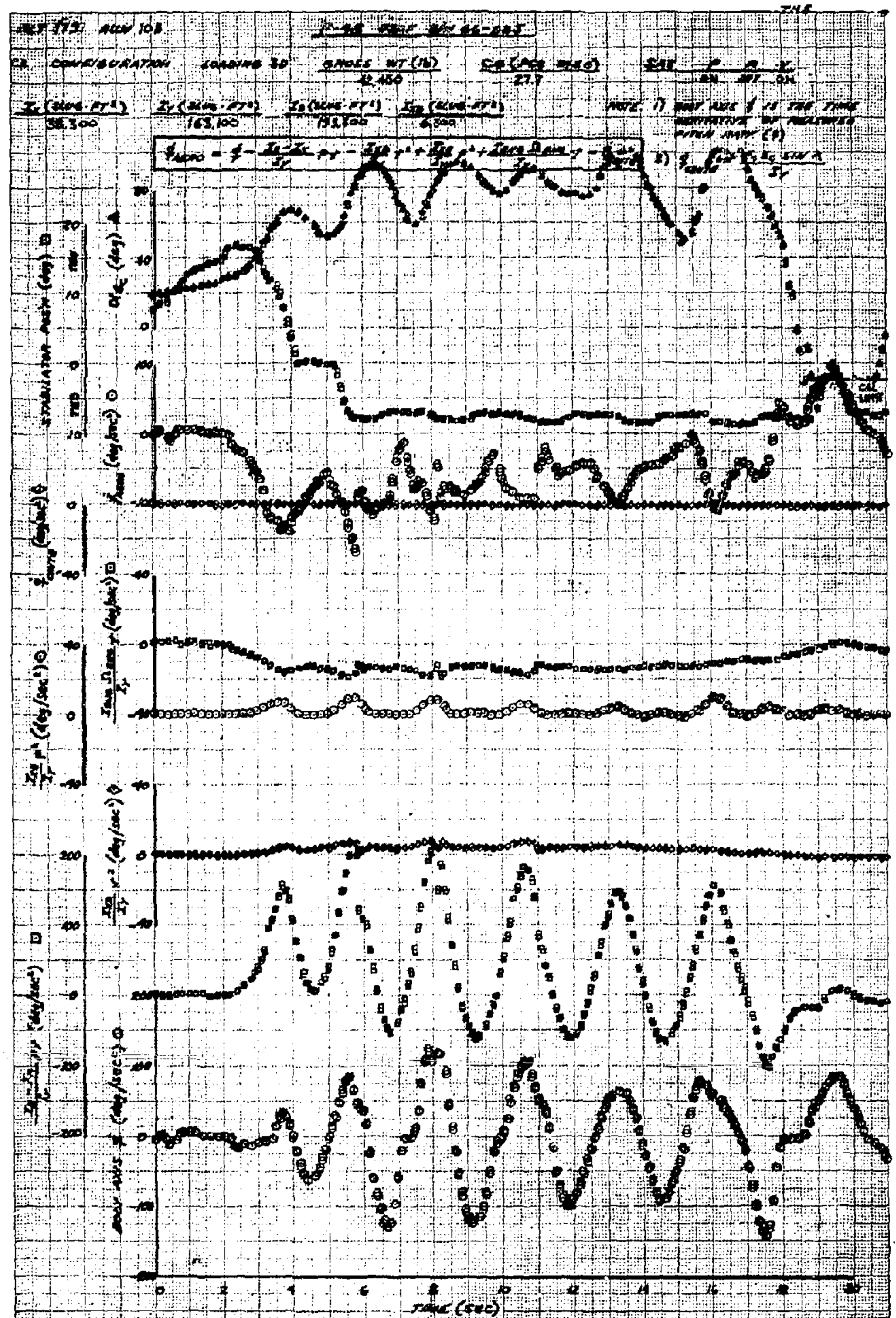

FIGURE 42 CONTINUED

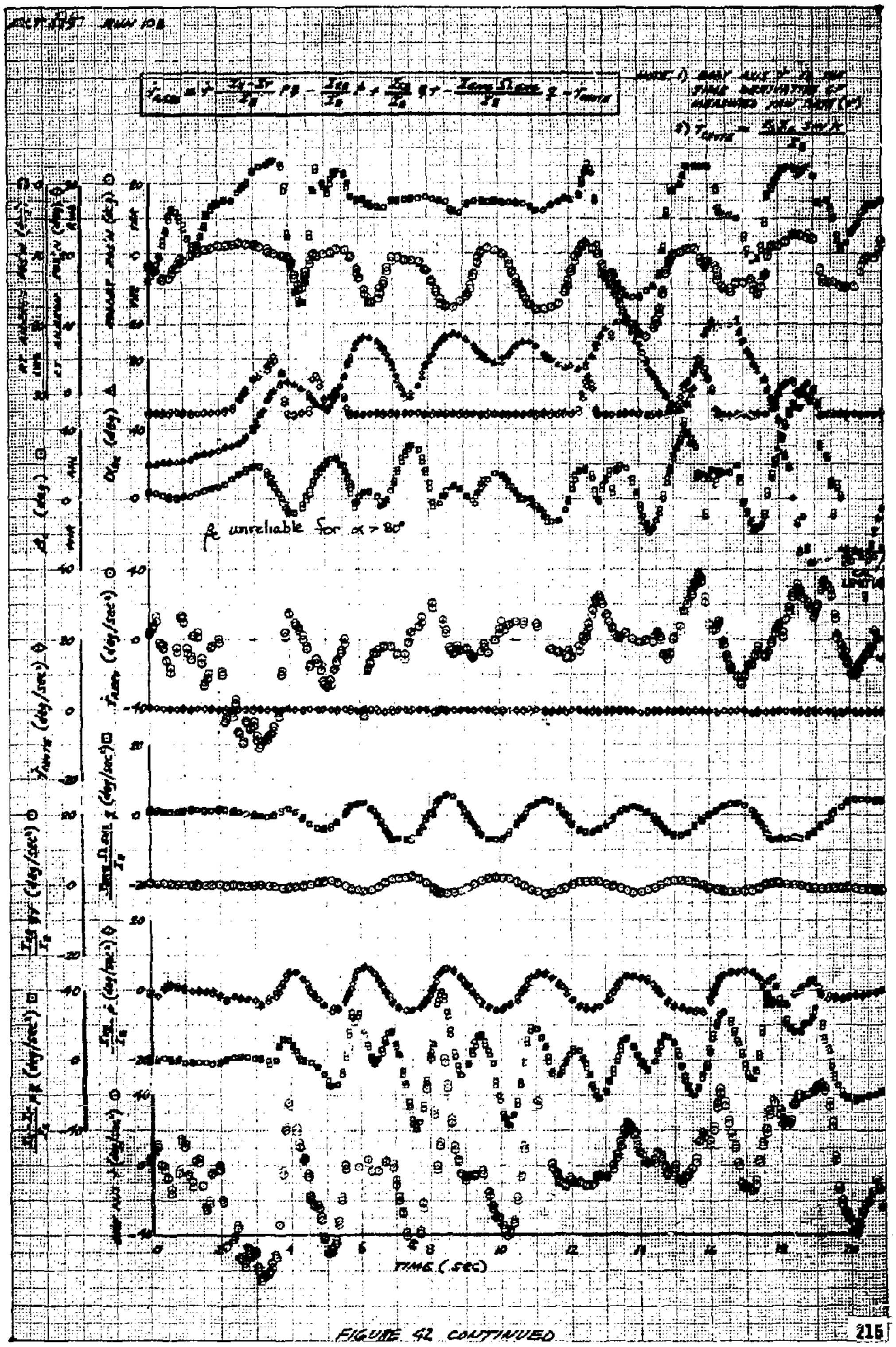

FIGURE 42 CONTINUED

FLT 179 RUN 10B

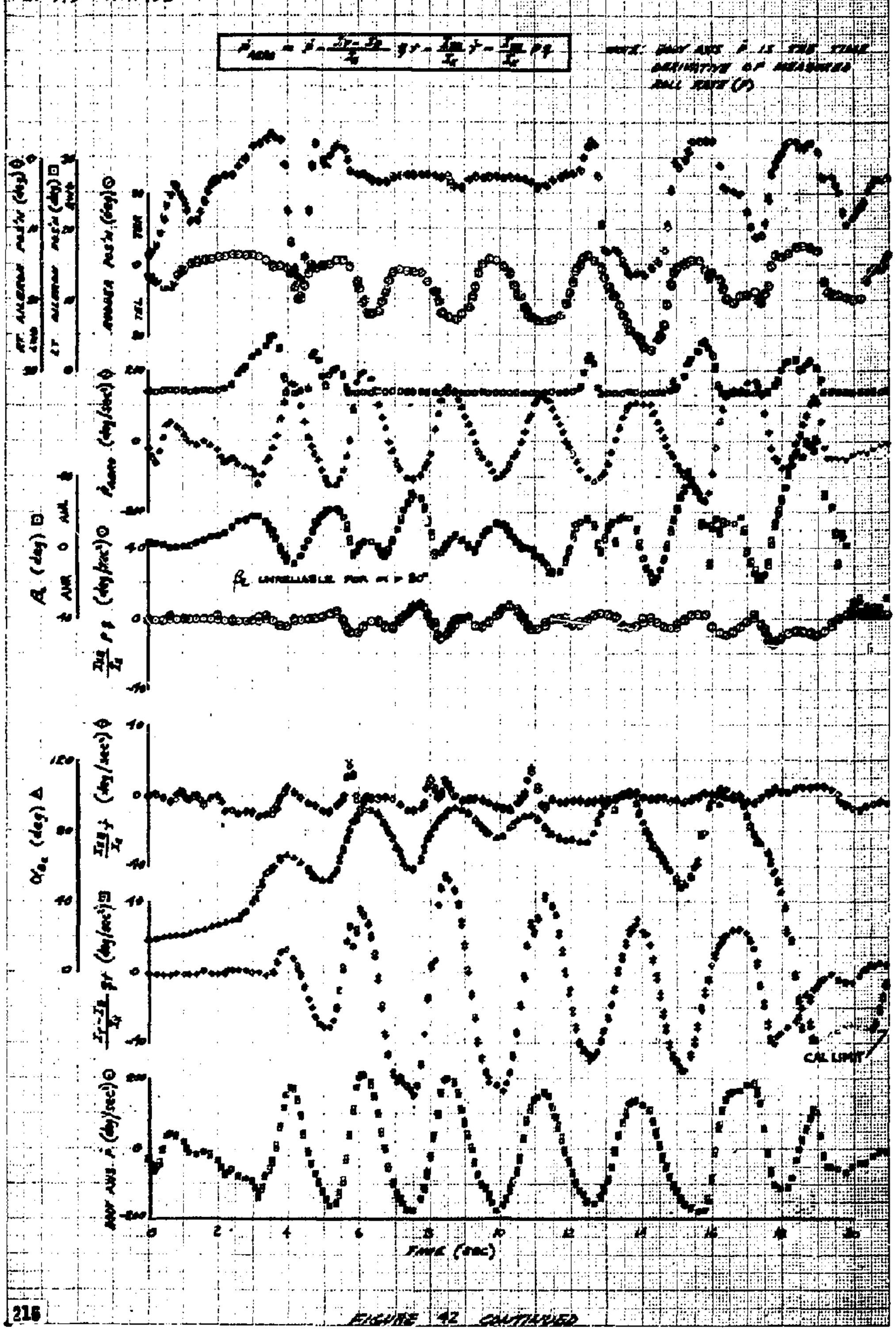

FIGURE 42 CONTINUED

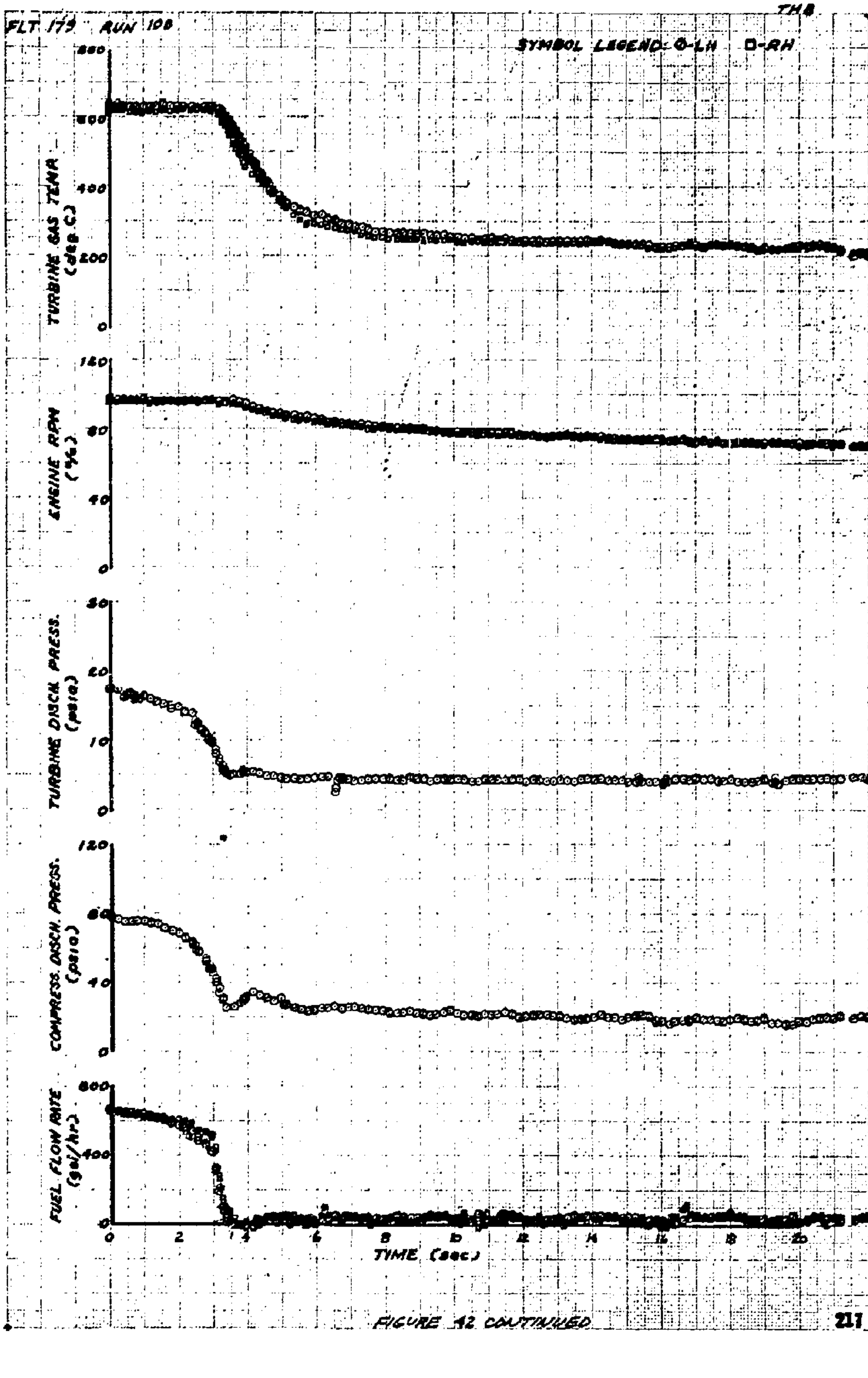

FIGURE 42 CONTINUED

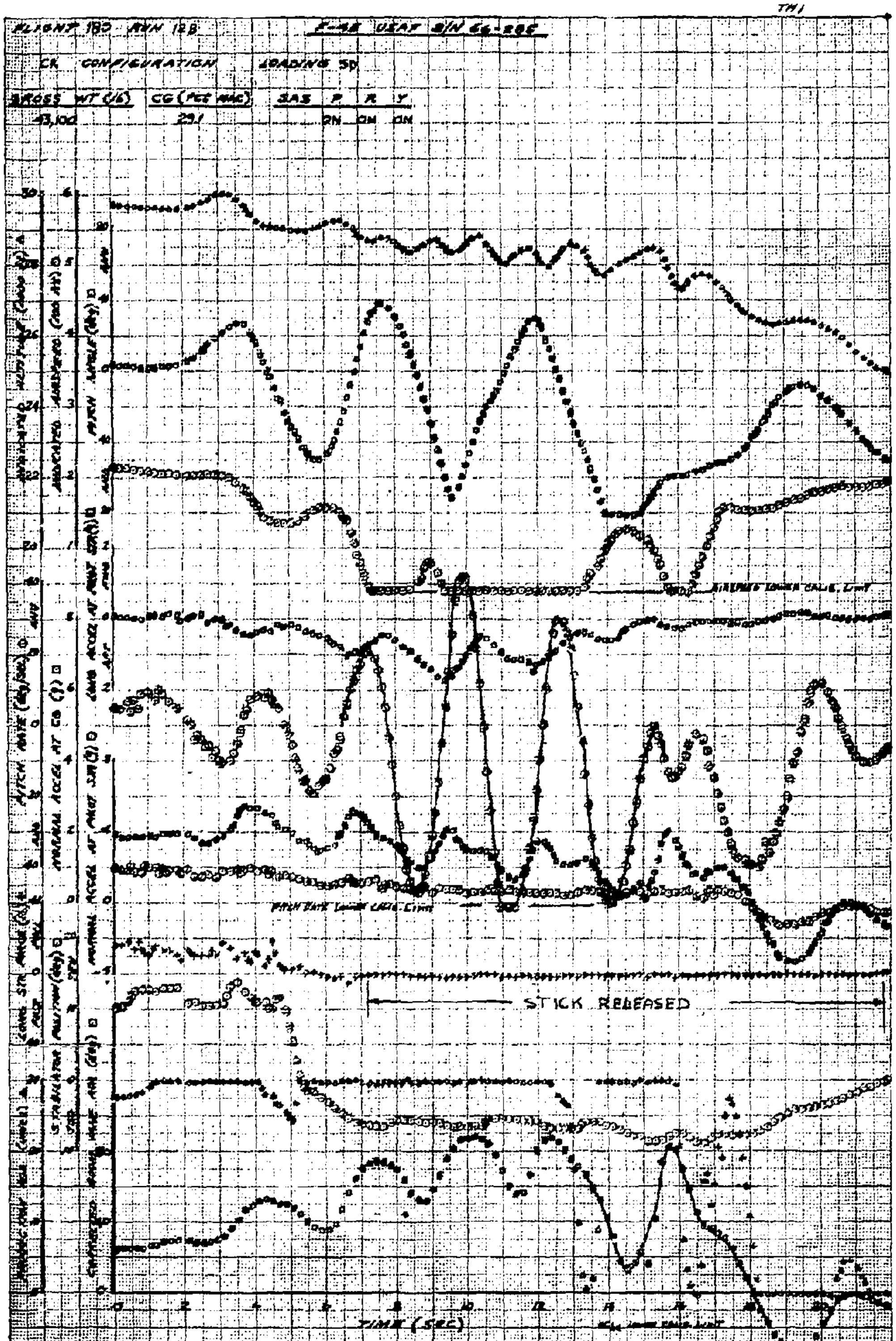

FIGURE 43 3½ TURN, HIGH AOA - HIGHLY OSCILLATORY SPIN; STICK RELEASE

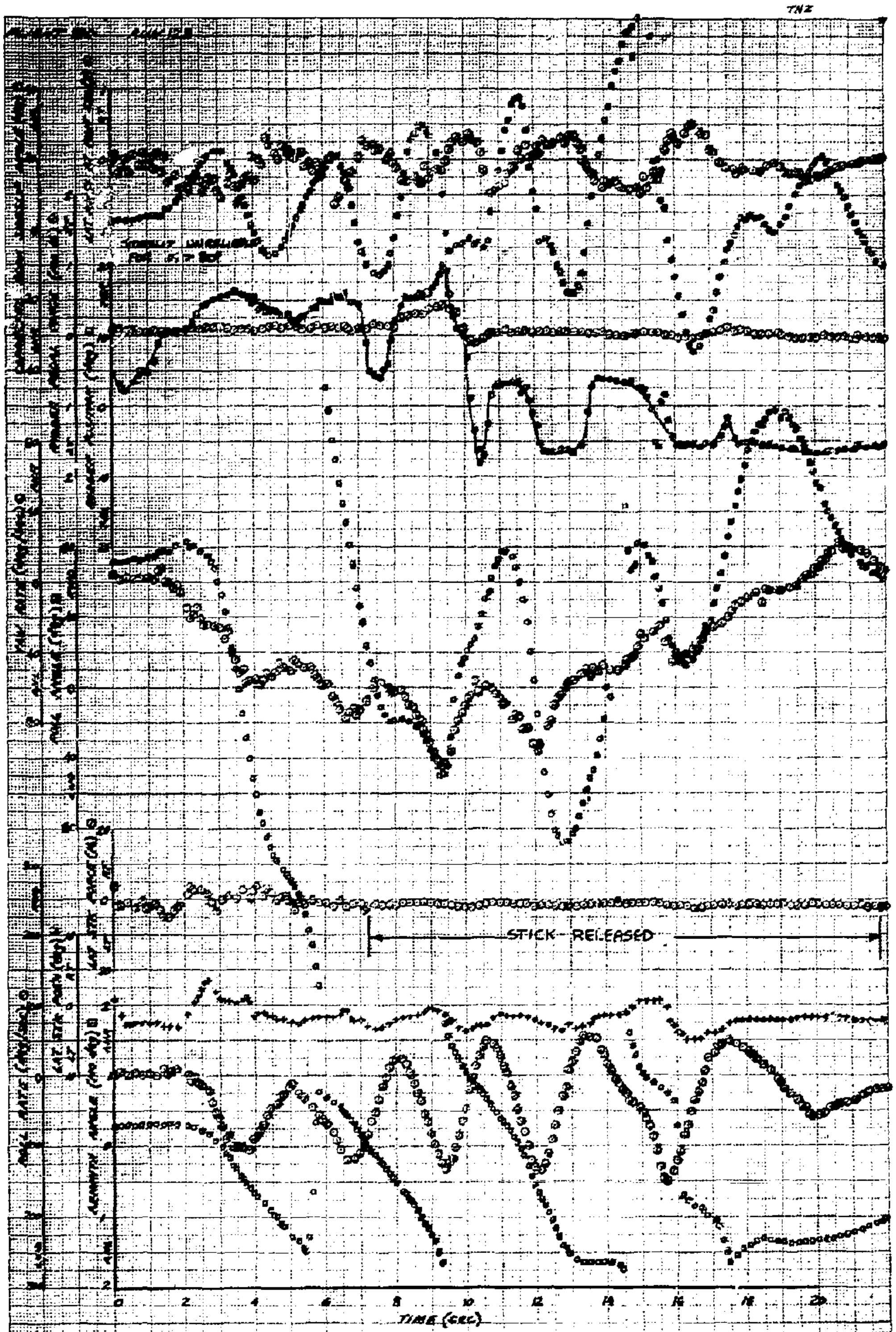

FIGURE 43 CONTINUED

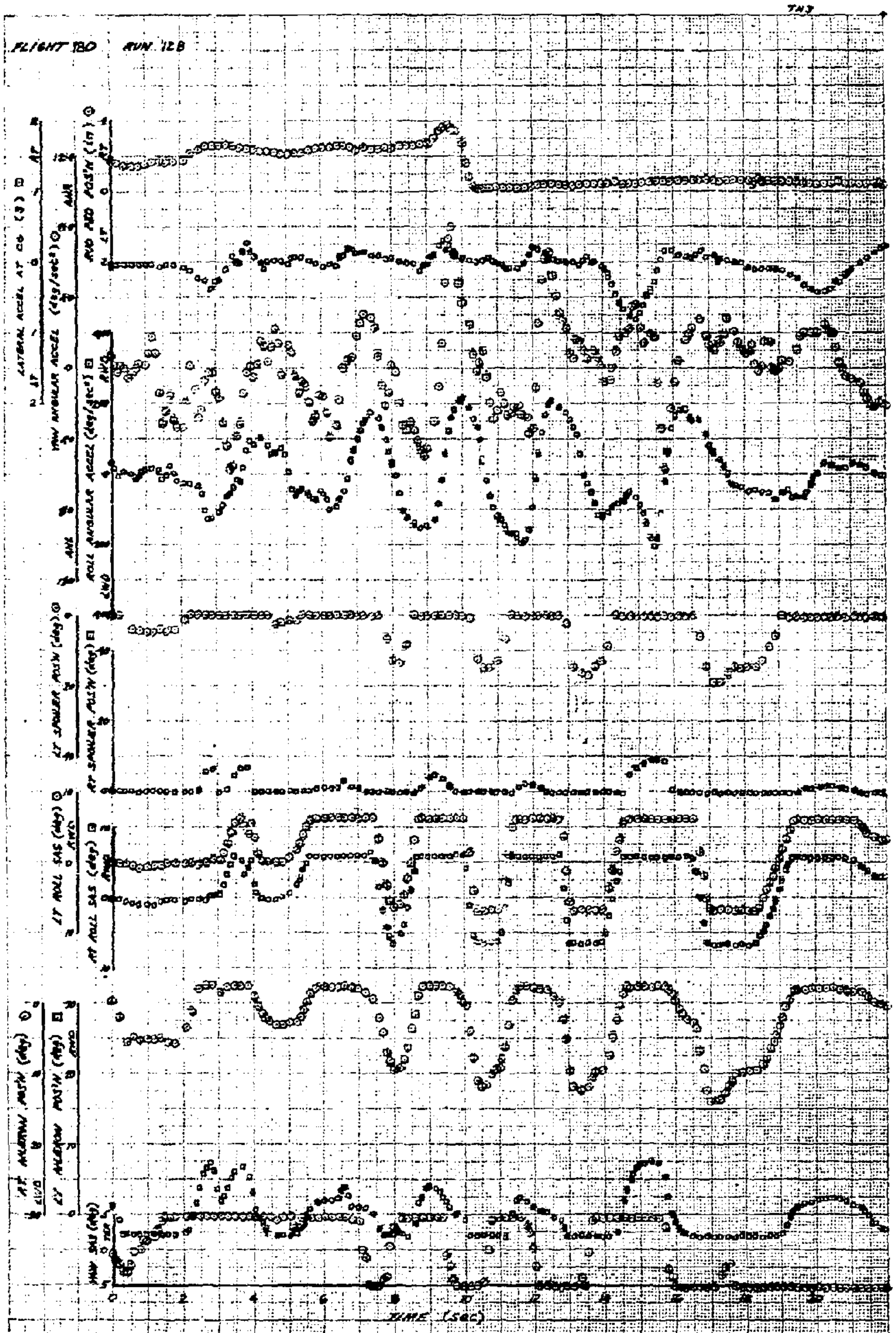

FIGURE 43 CONTINUED

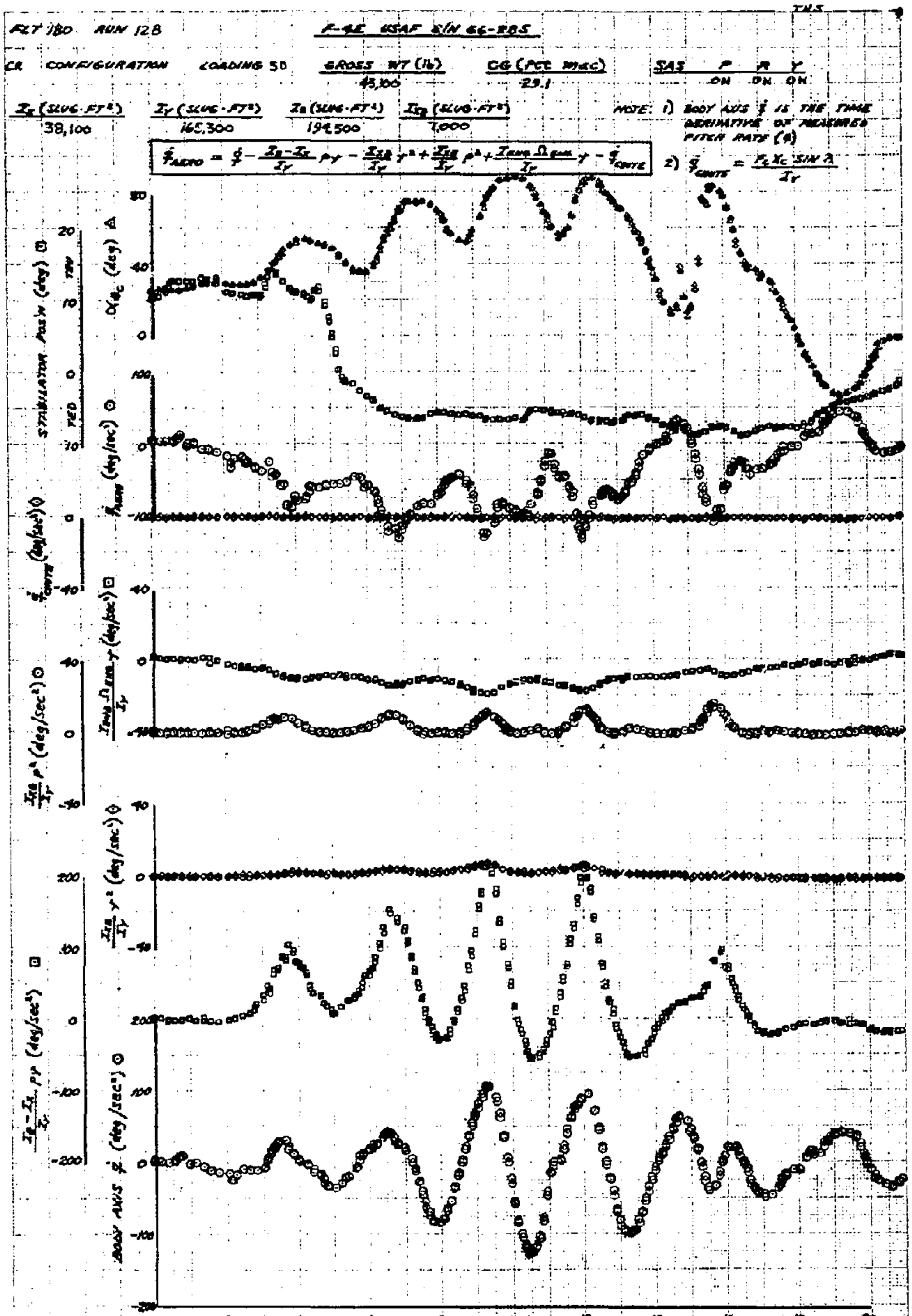

FIGURE 43 CONTINUED

TN6

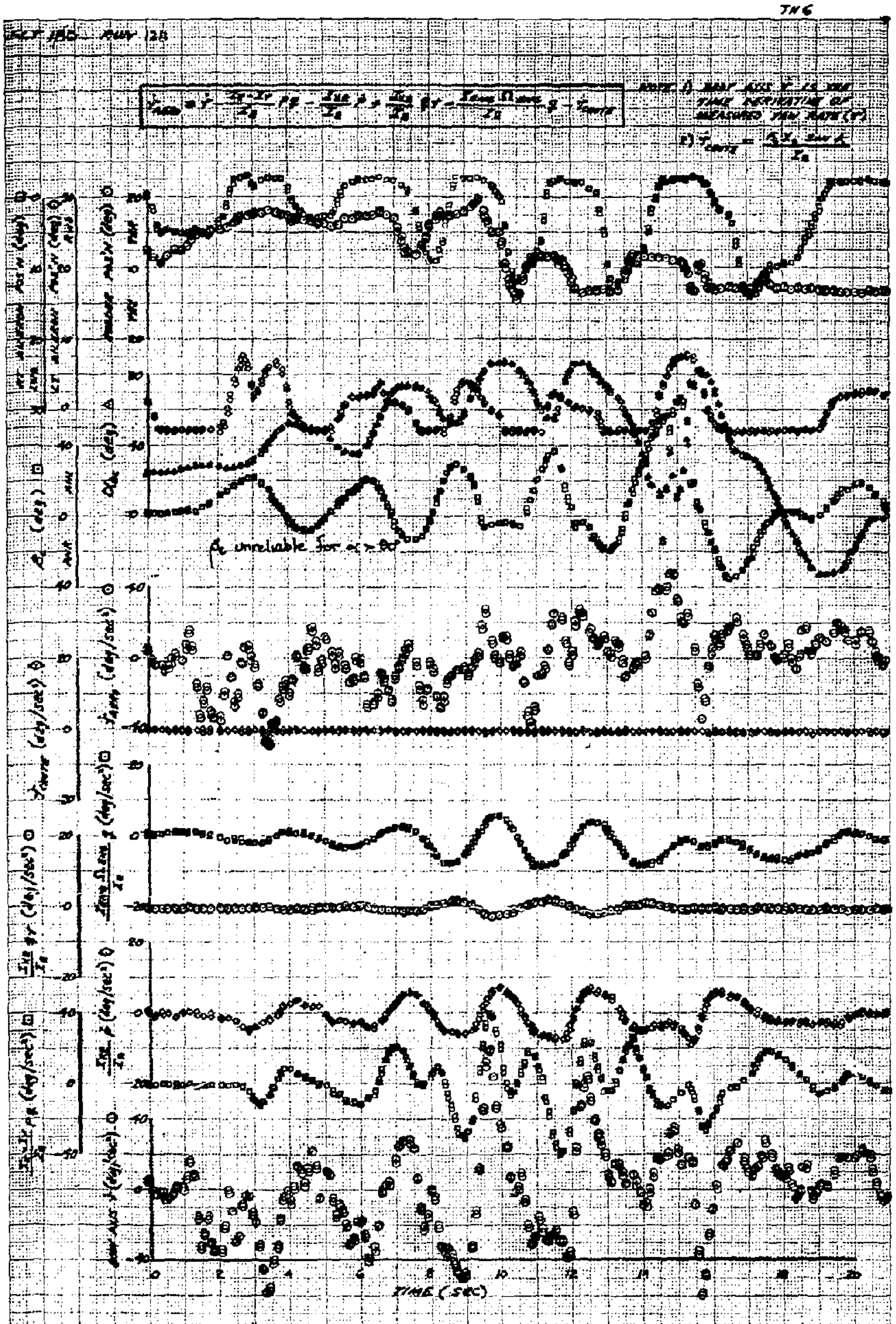

FIGURE 43 CONTINUED

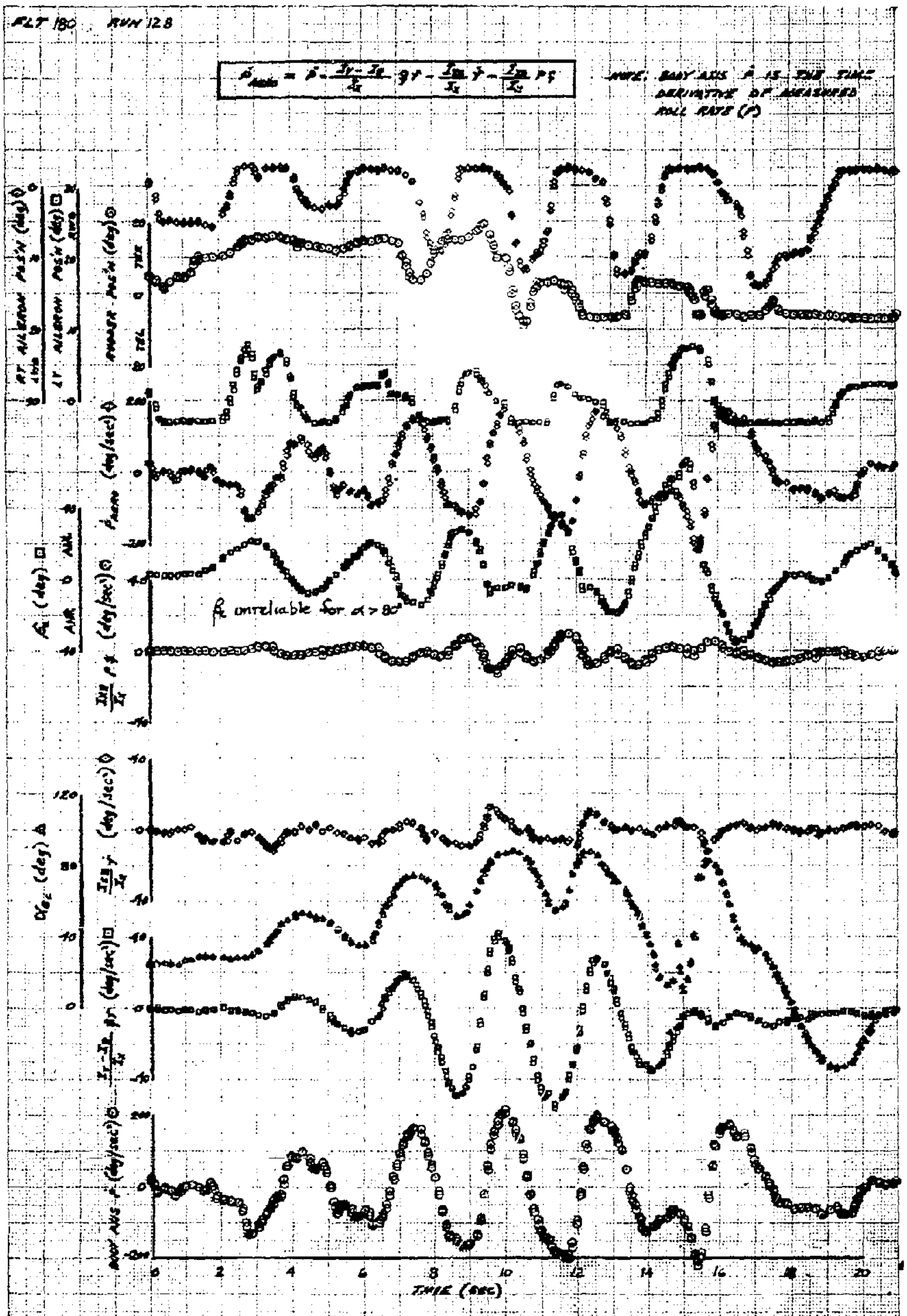

FIGURE 43 CONTINUED

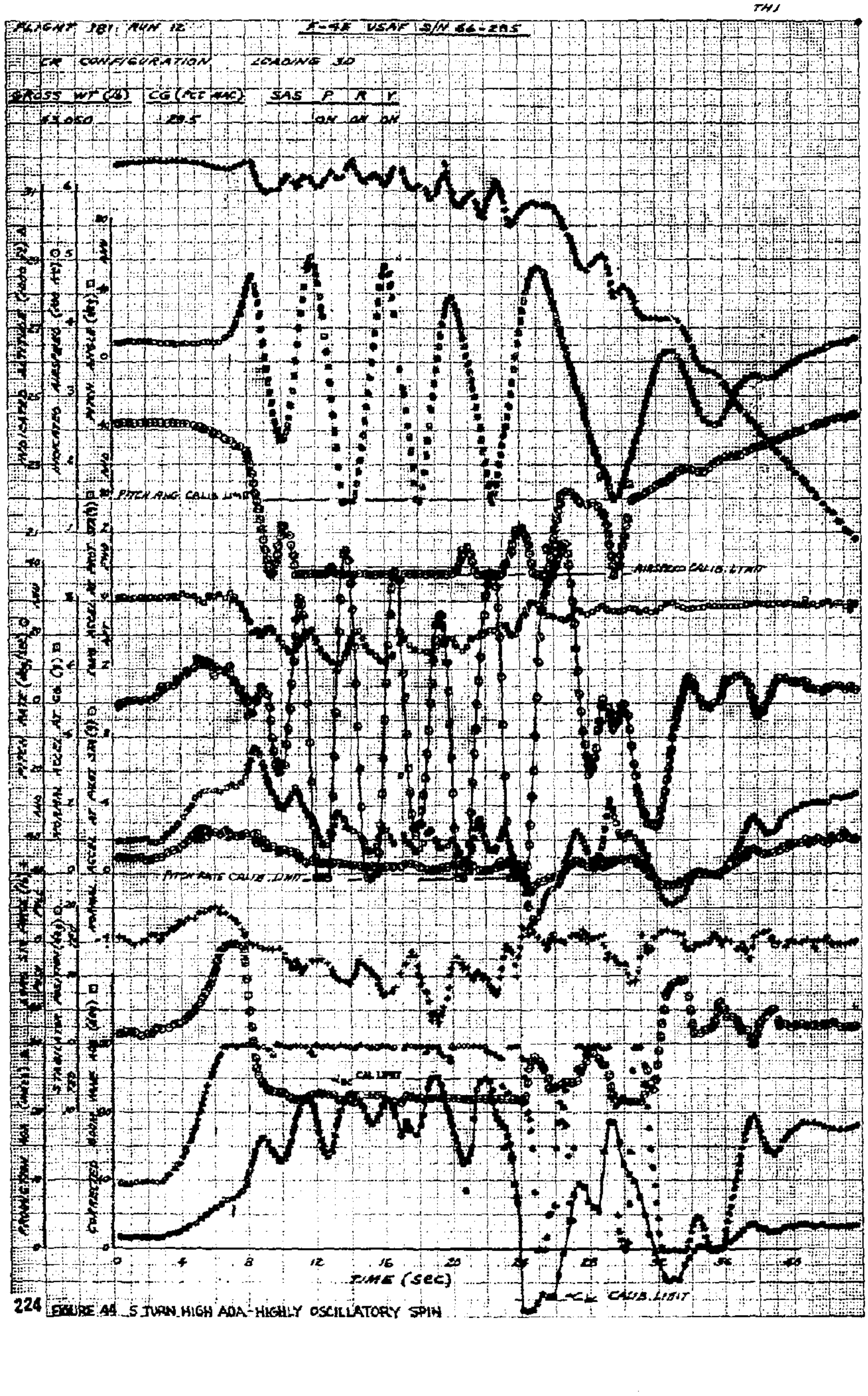

 FIGURE 44 S TURN HIGH AOA - HIGHLY OSCILLATORY SPIN

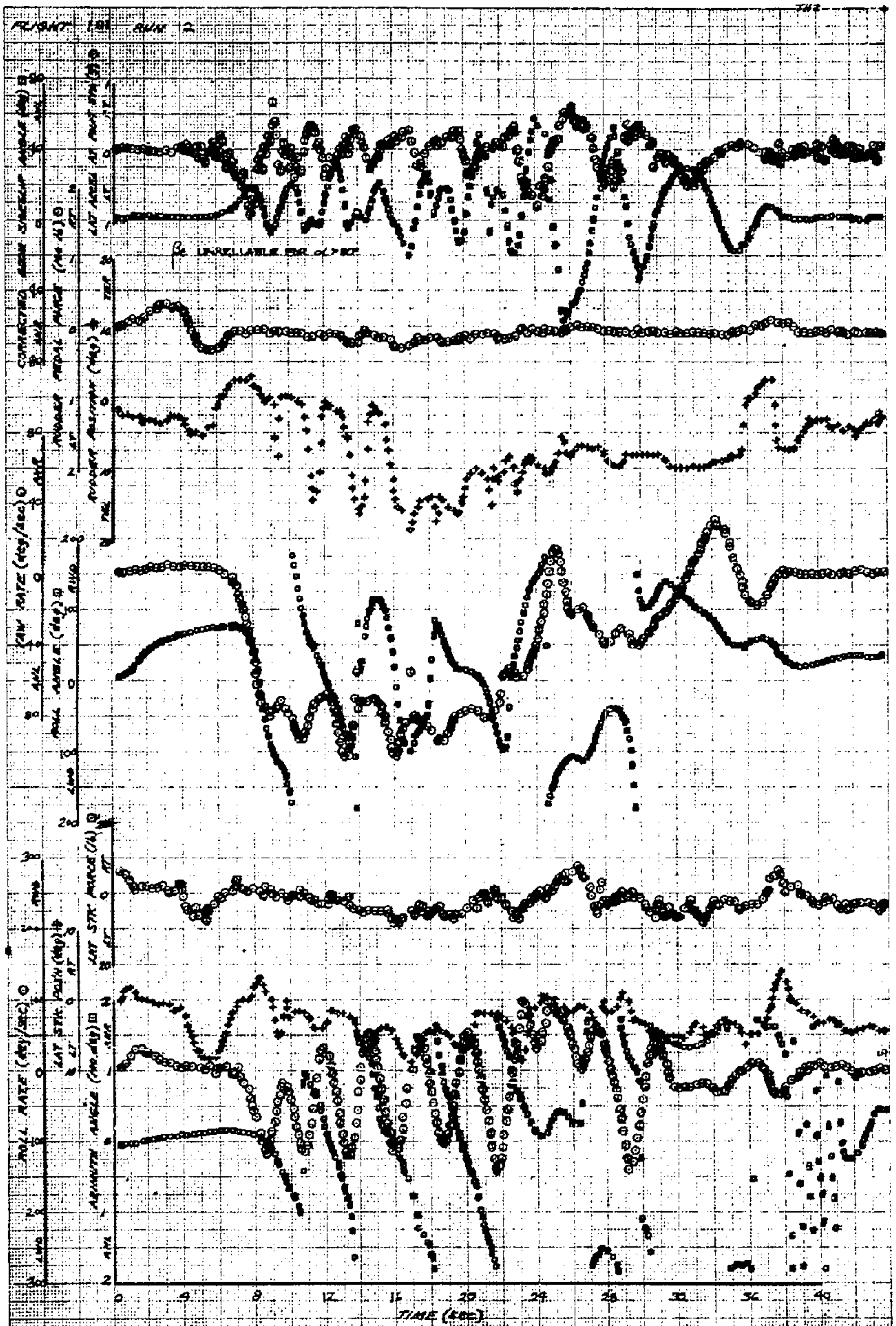

FIGURE 44 CONTINUED

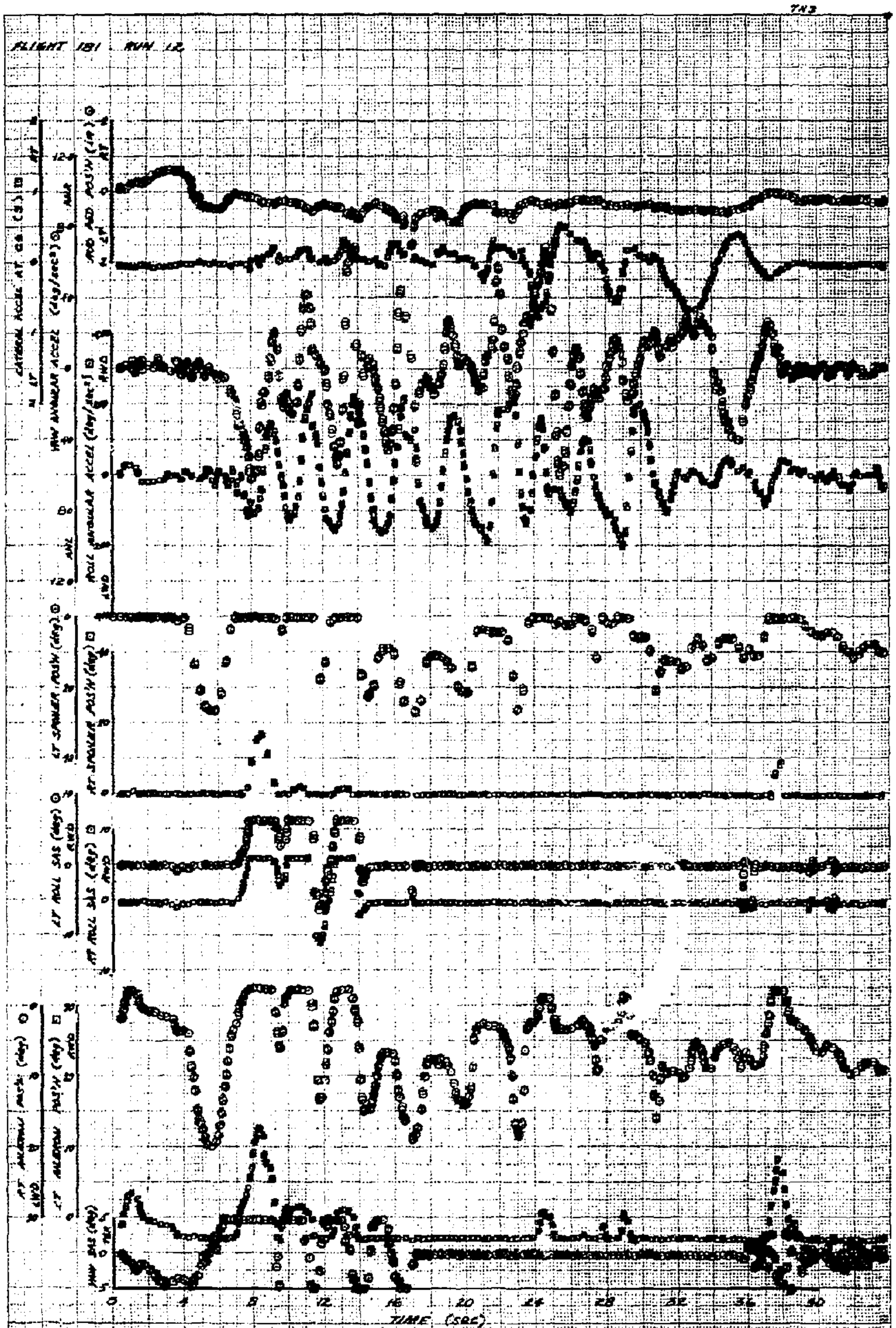

FIGURE 44 CONTINUED

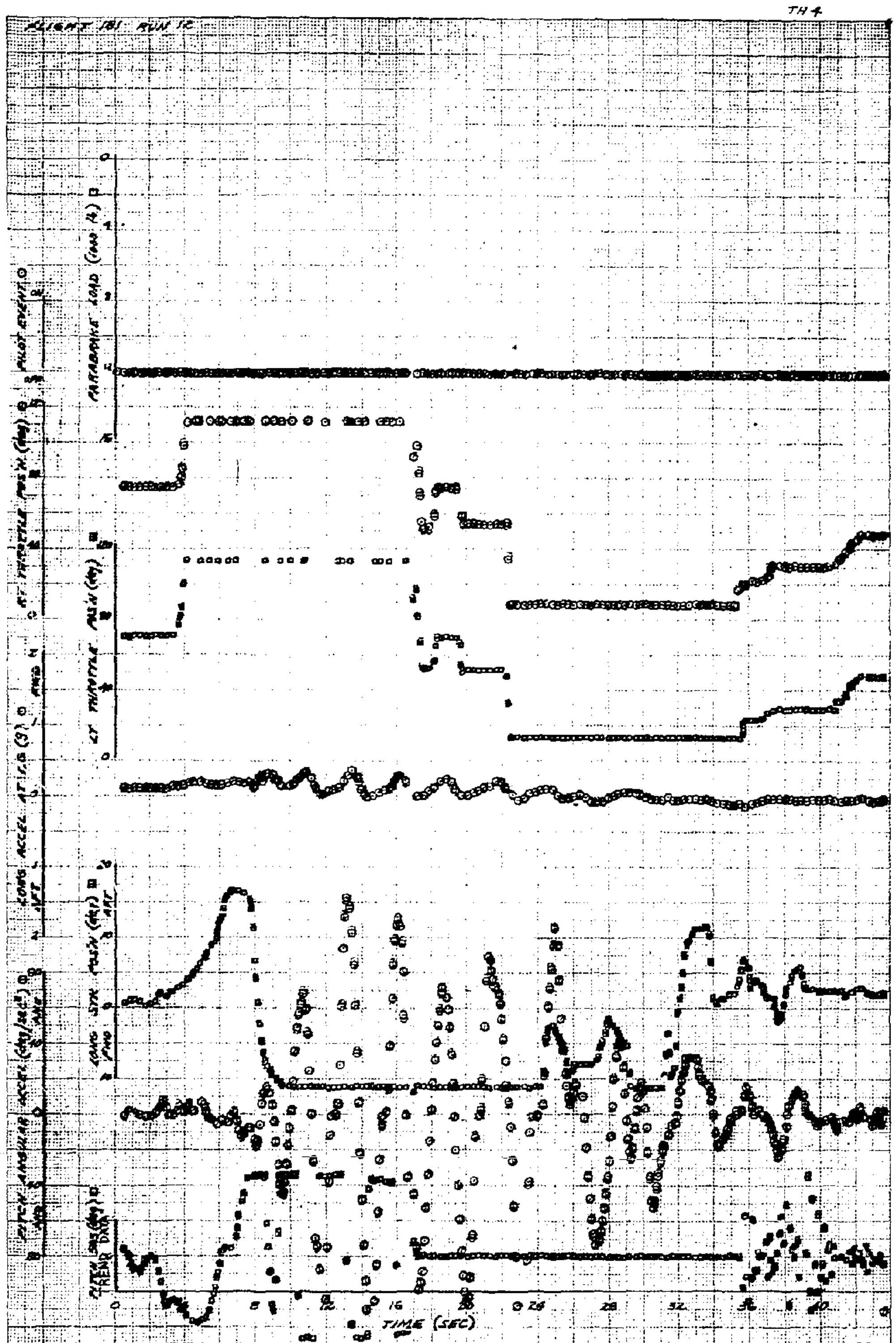

FIGURE 44 CONTINUED

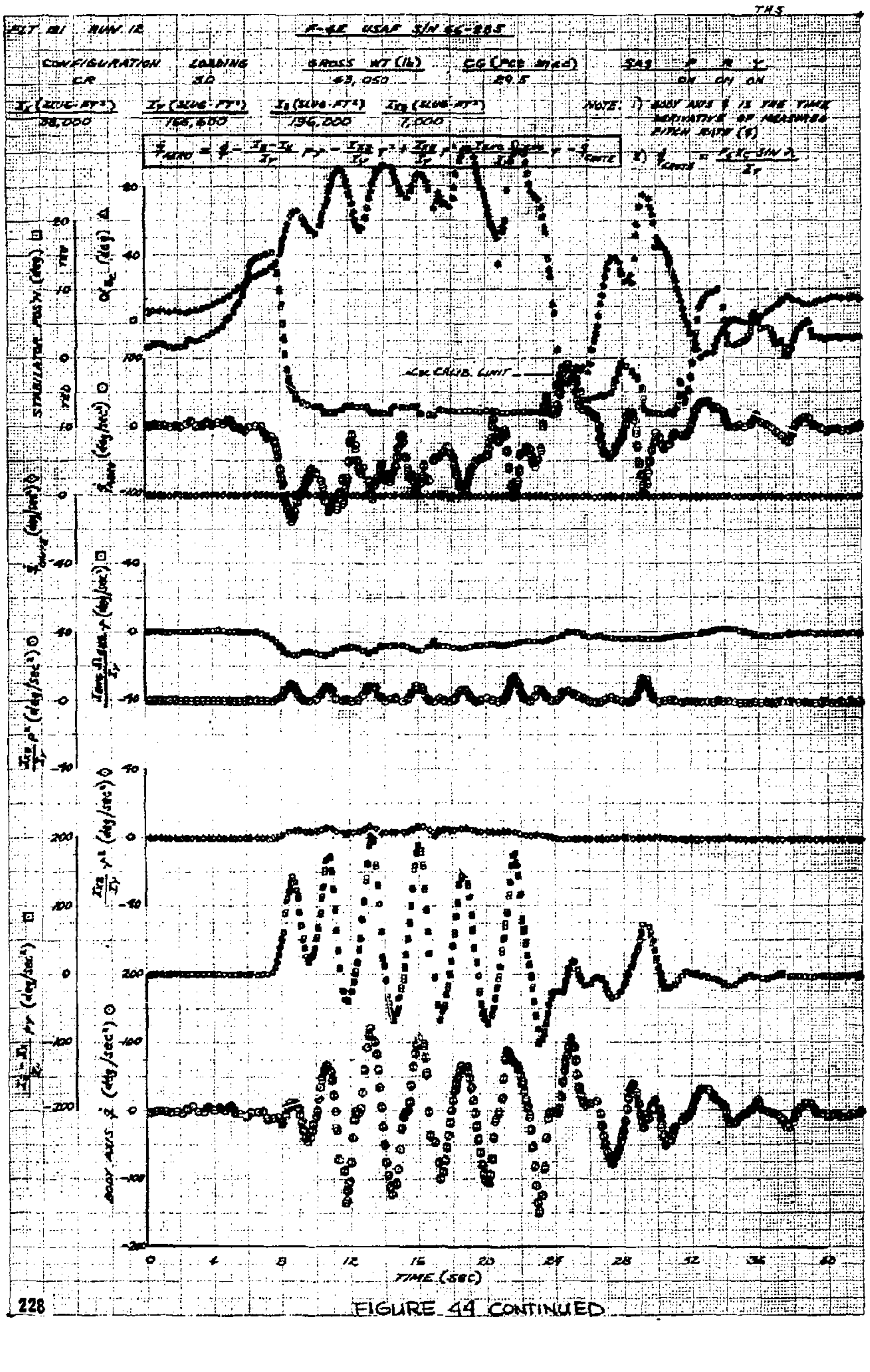

FIGURE 44 CONTINUED

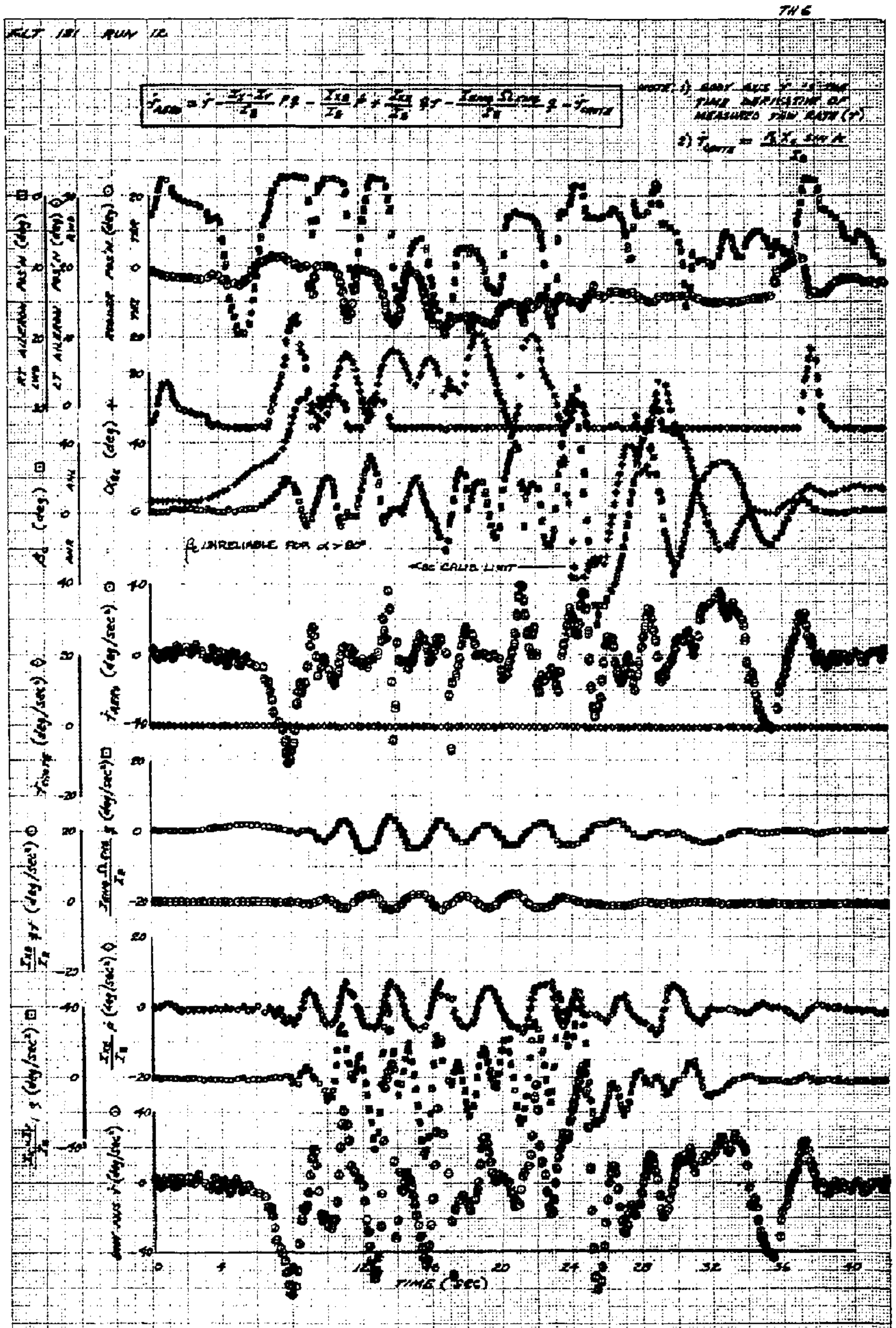

FIGURE 44 CONTINUED

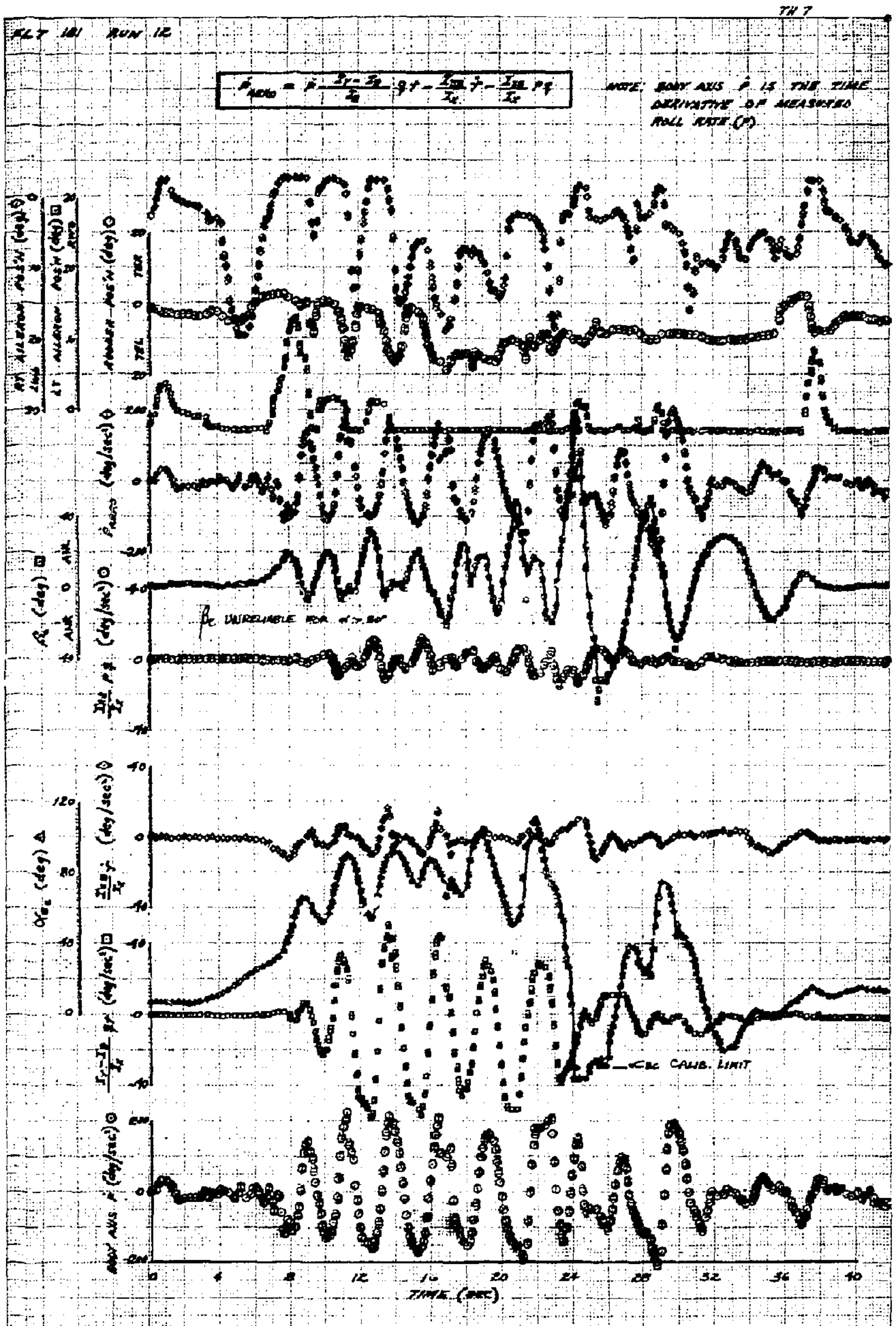

FIGURE 44 CONTINUED

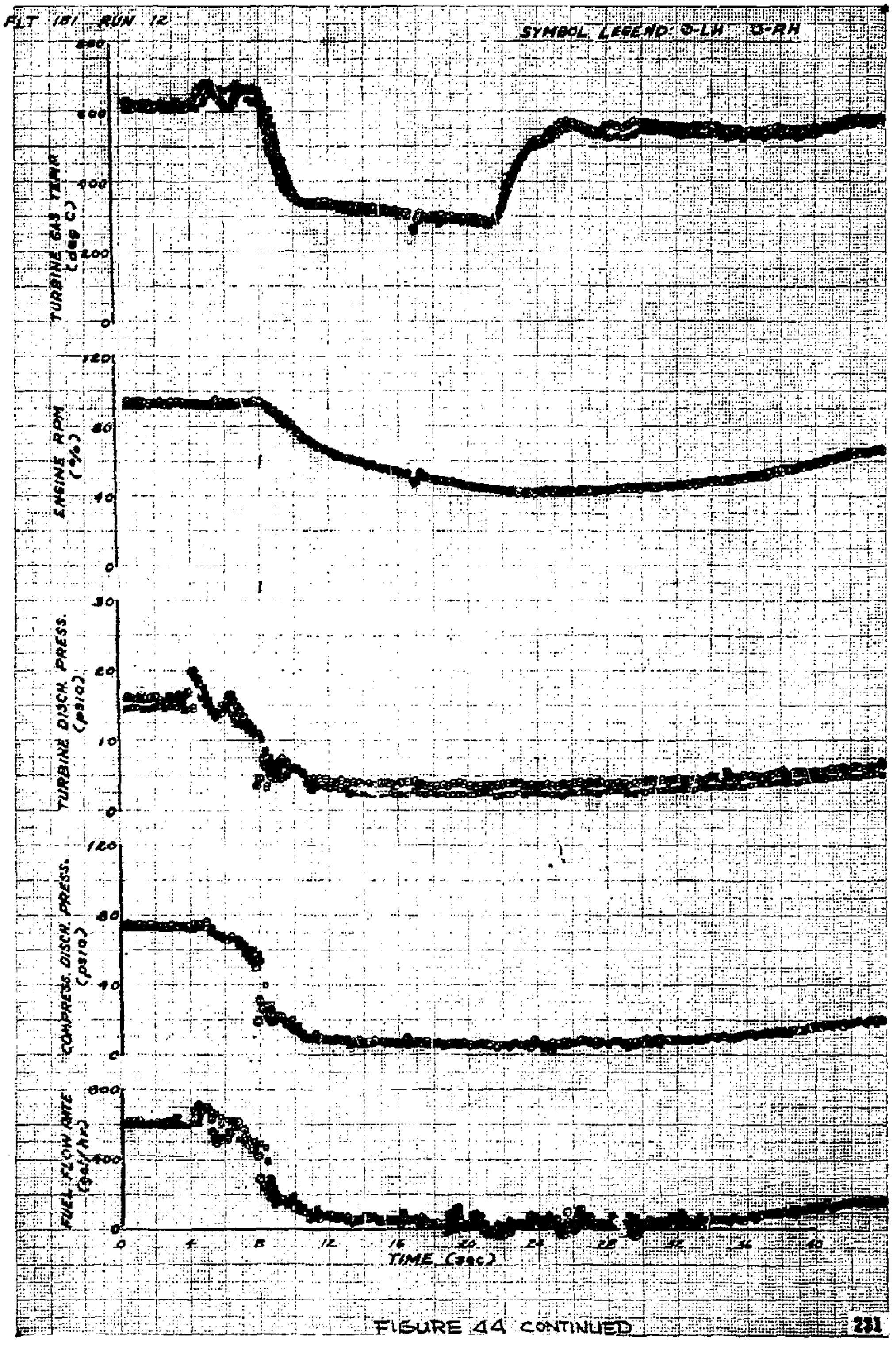

FIGURE 44 CONTINUED

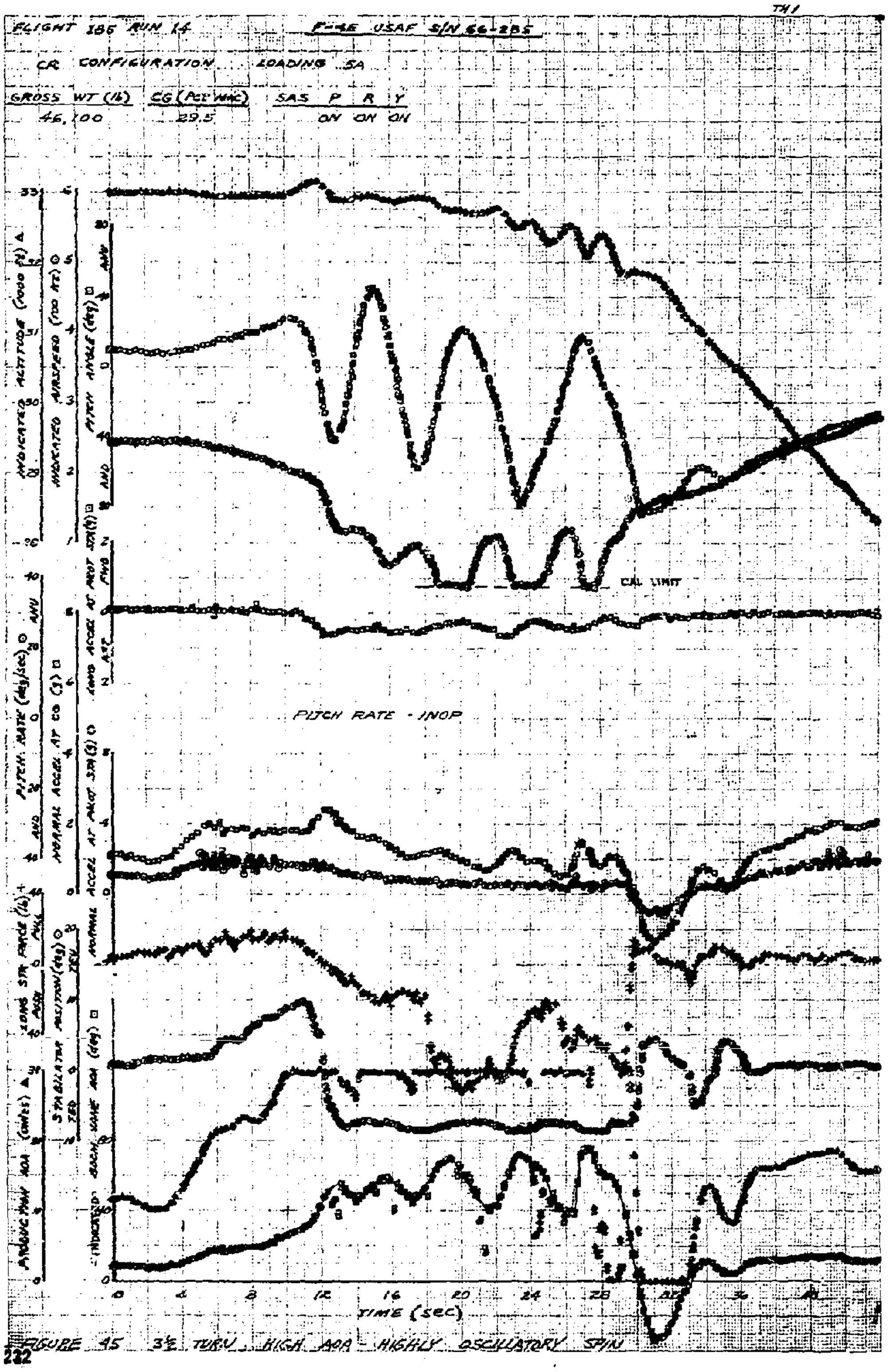

FIGURE 45 3½ TURN, HIGH AOA - HIGHLY OSCILLATORY SPIN

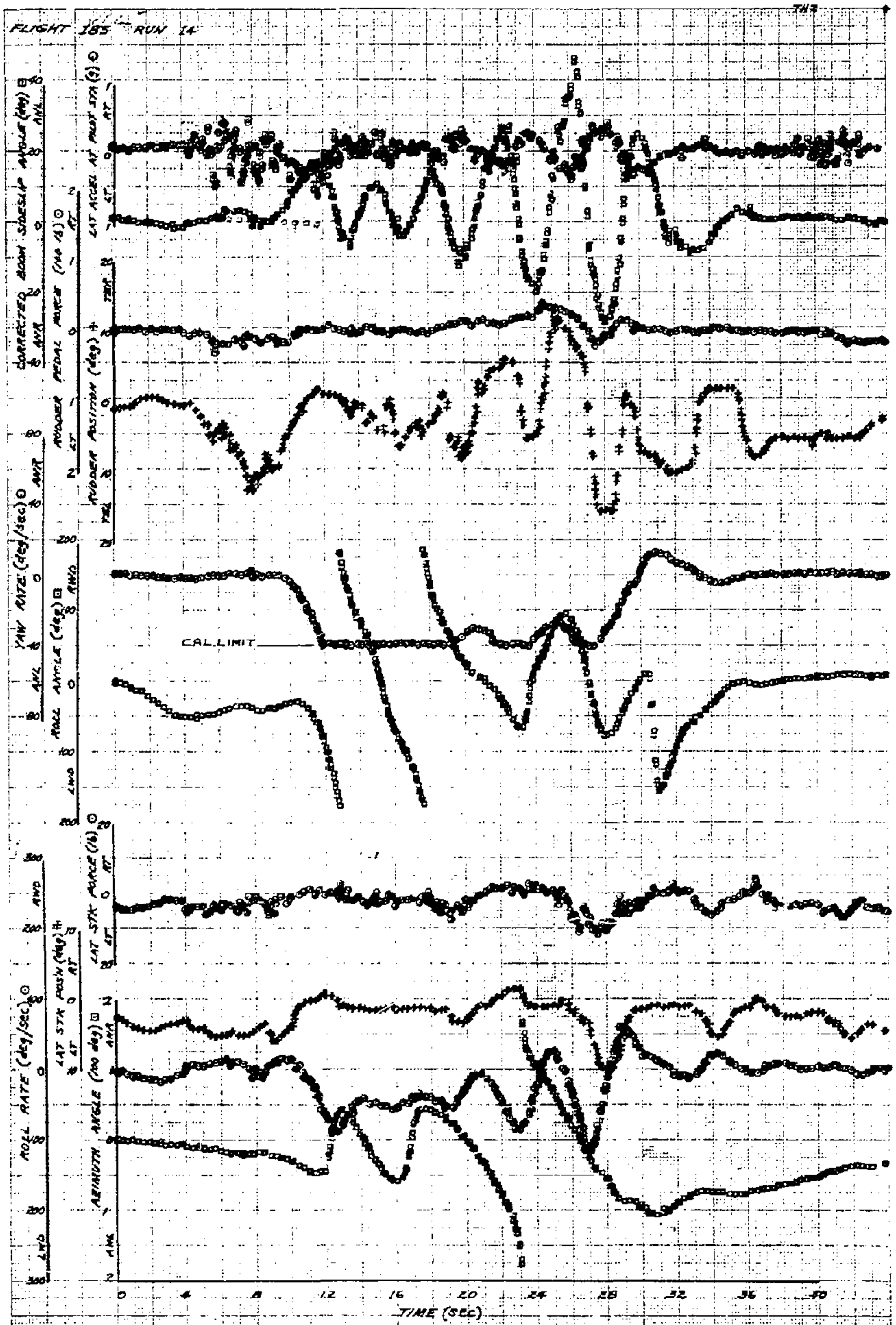

FIGURE 45 CONTINUED

TH4

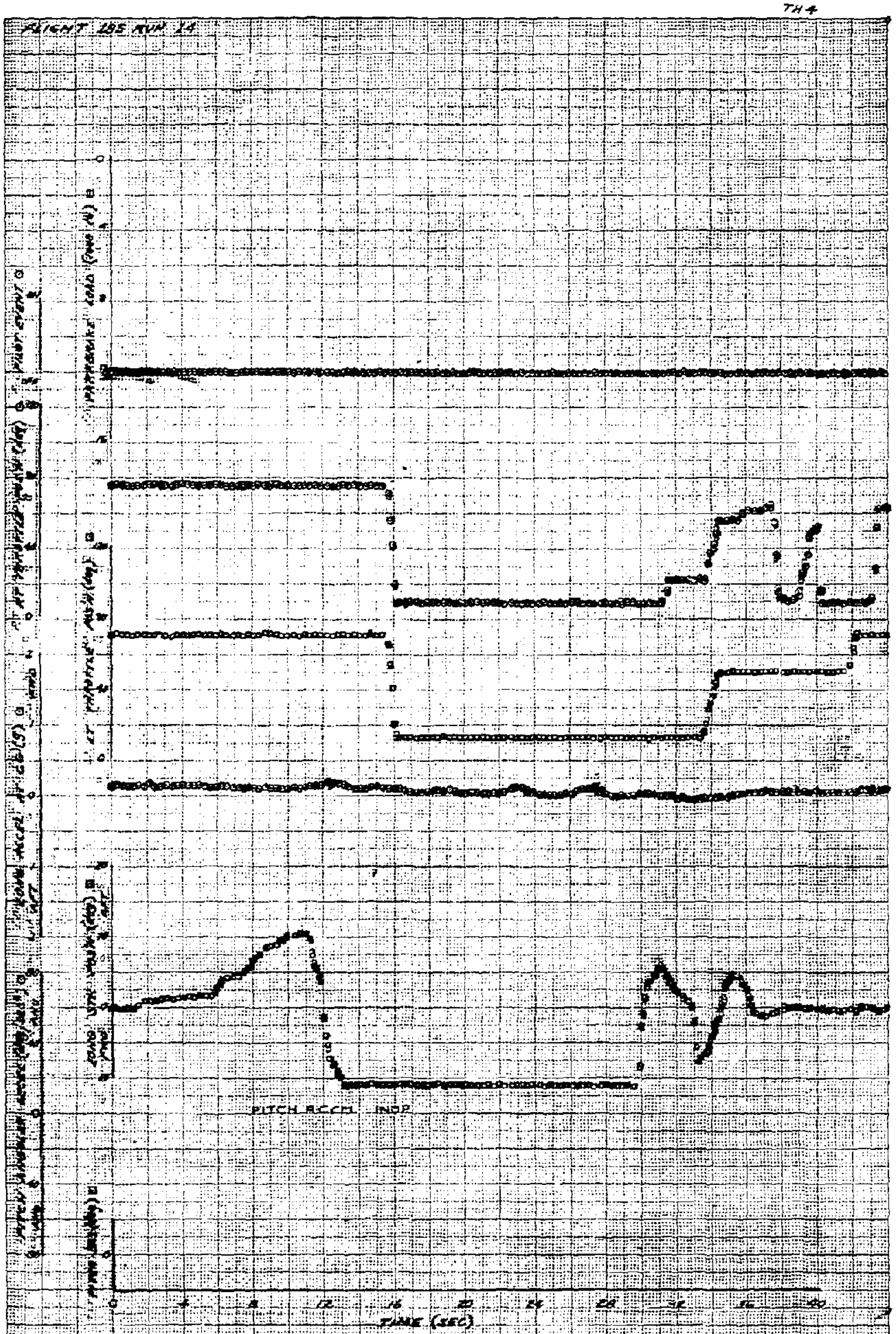

FIGURE 45 CONTINUED

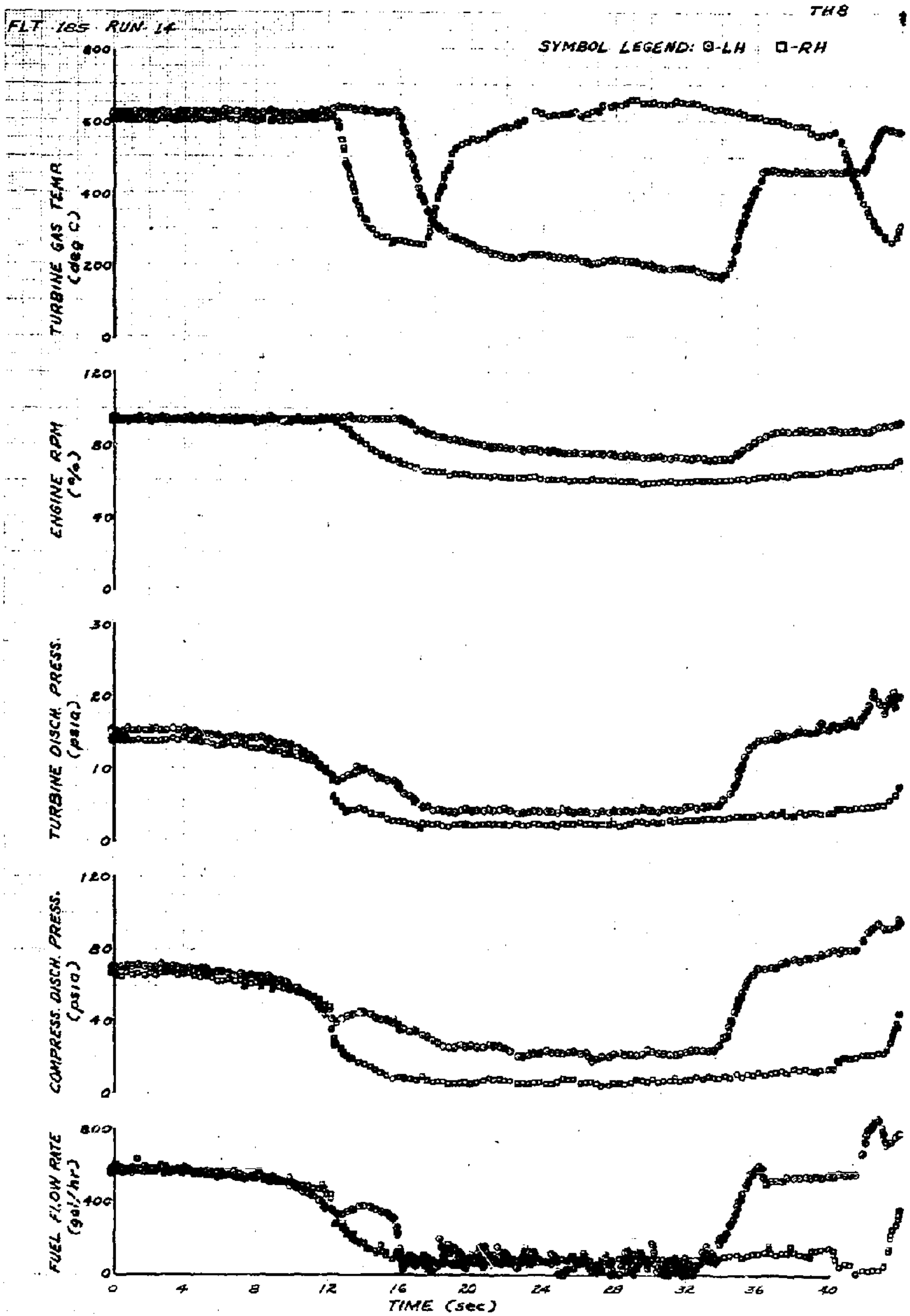

FIGURE 45 CONTINUED

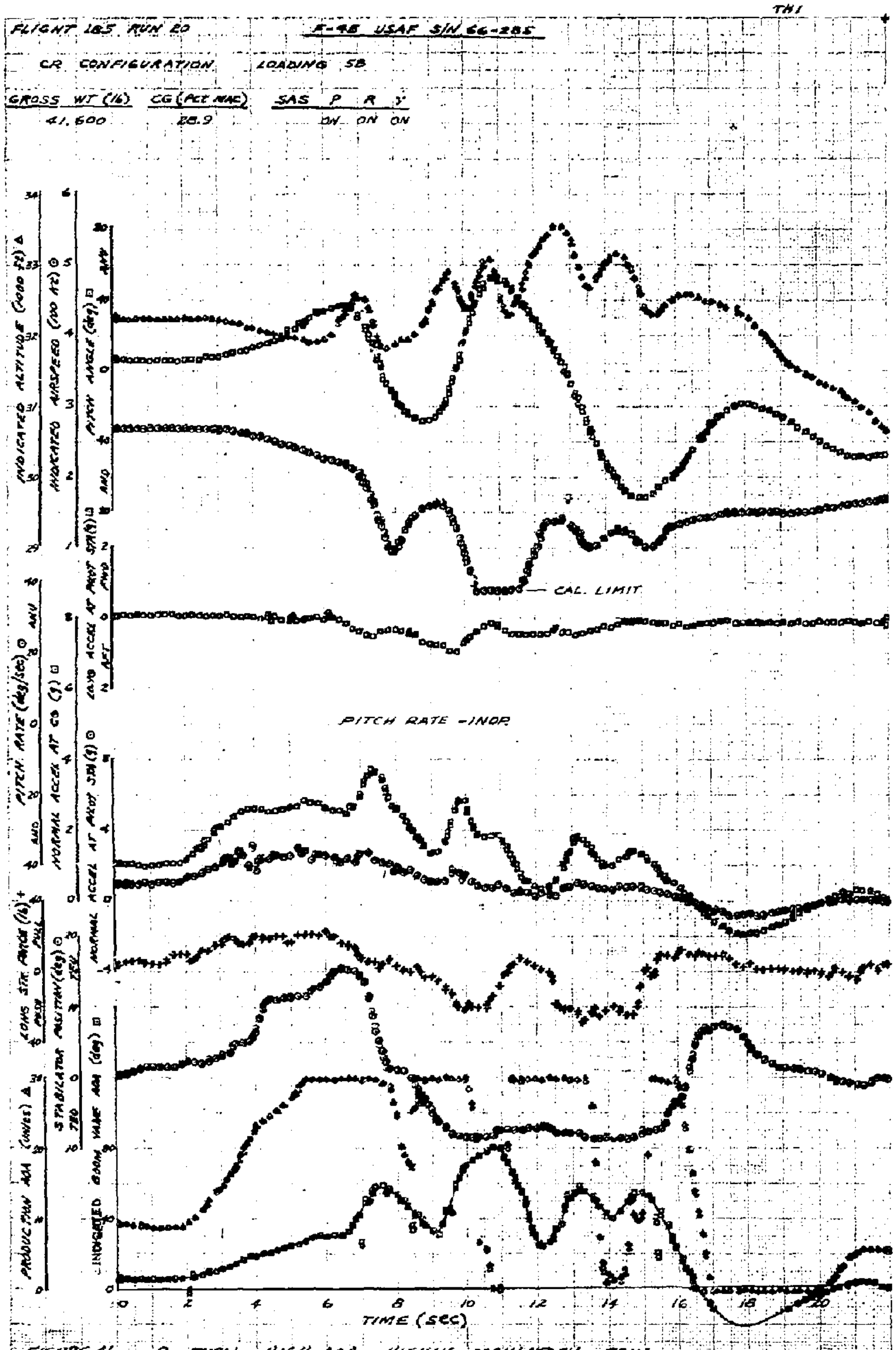

FIGURE 46 2 TURN, HIGH AOA - HIGHLY OSCILLATORY SPIN

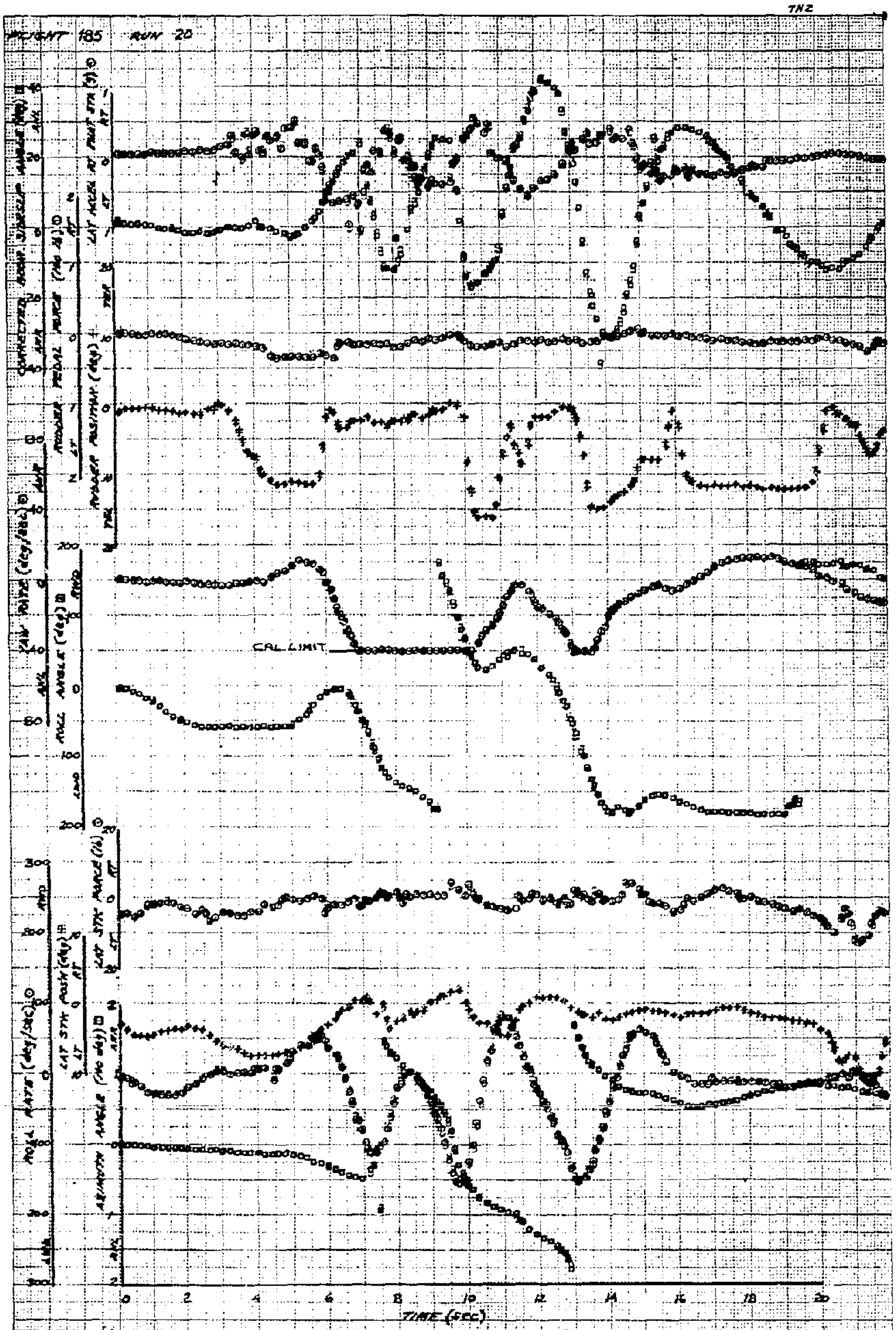

FIGURE 46 CONTINUED

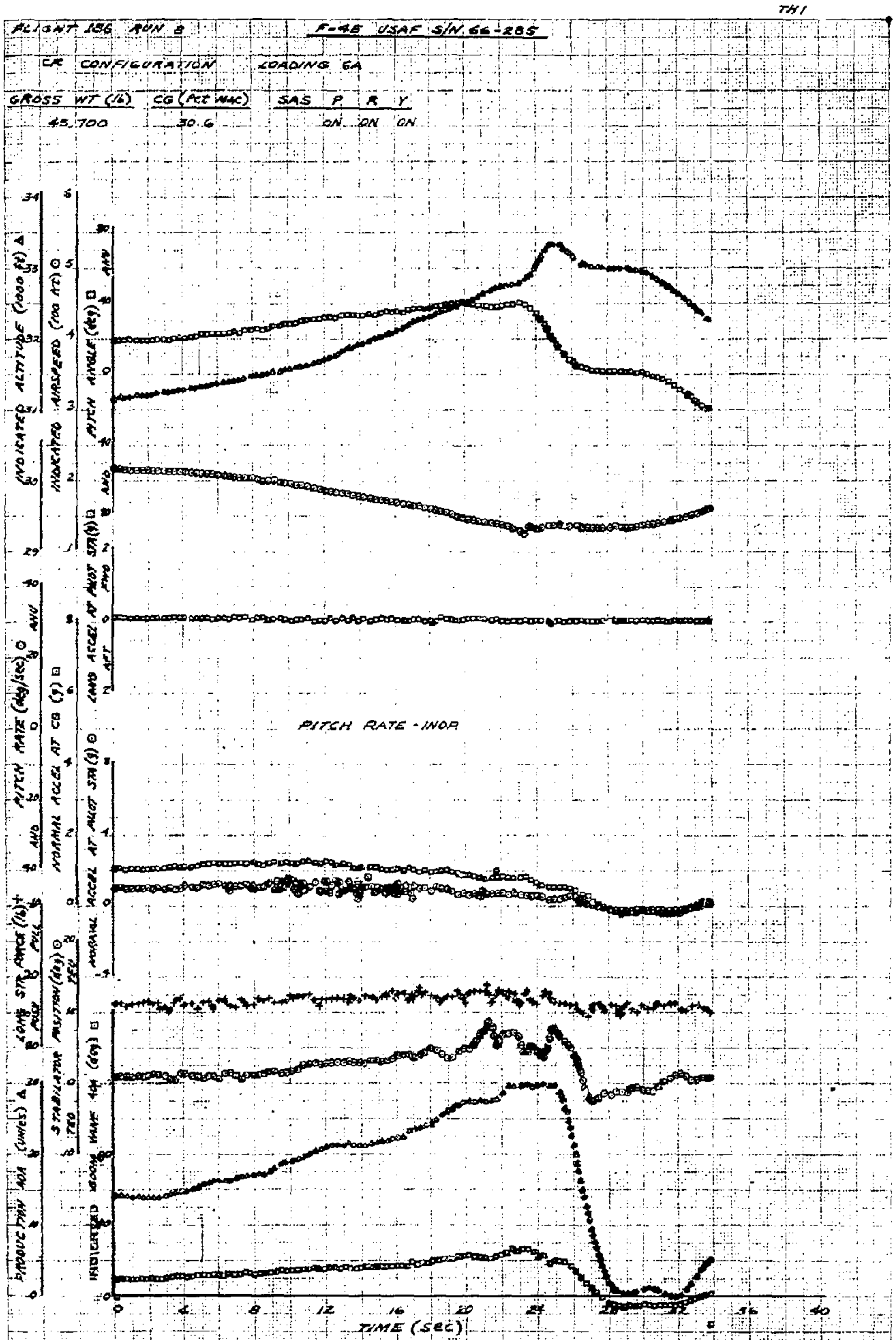

FIGURE 47 ROLLING DEPARTURE WITH MAXIMUM ALLOWABLE ASYMMETRY

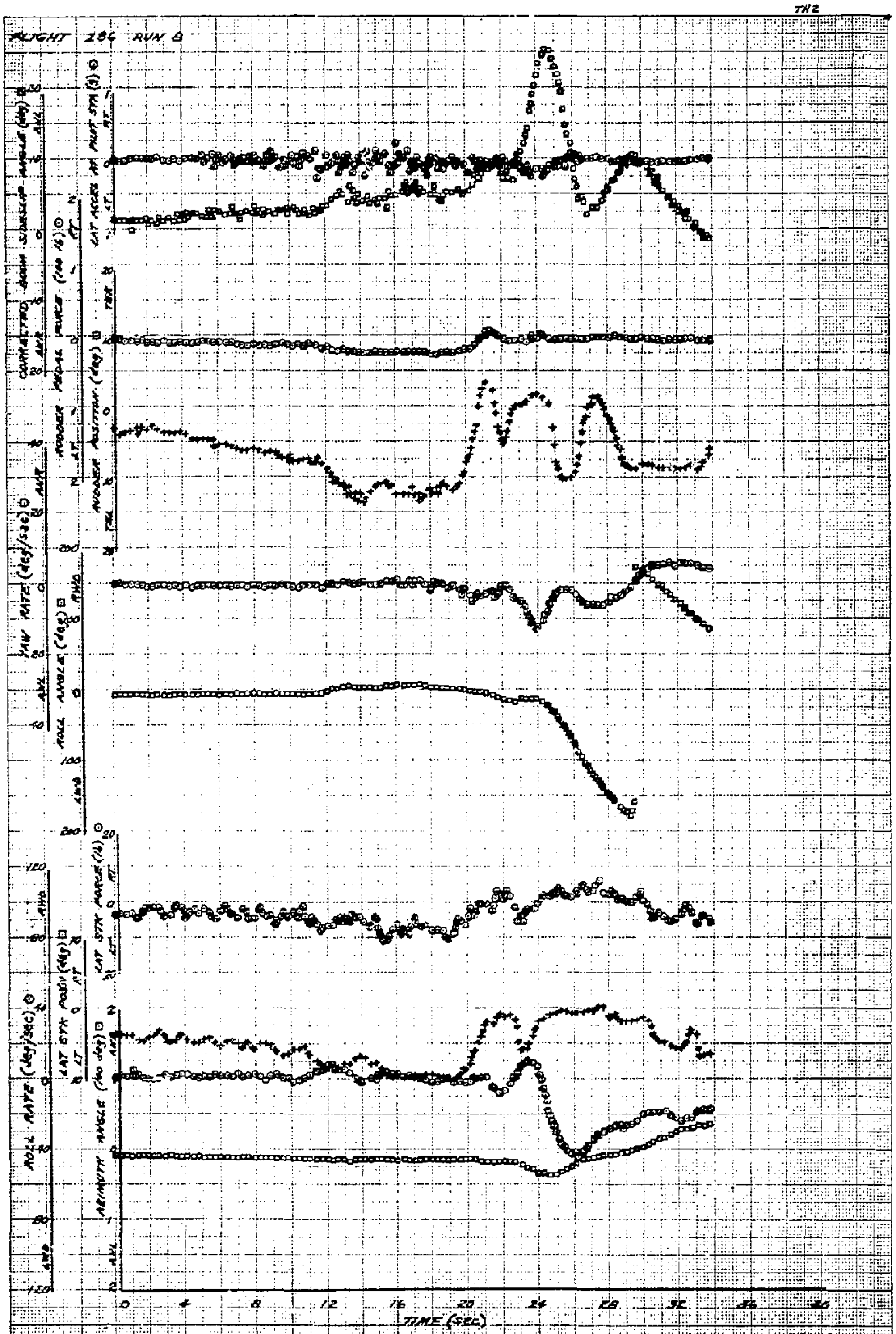

FIGURE 47 CONTINUED

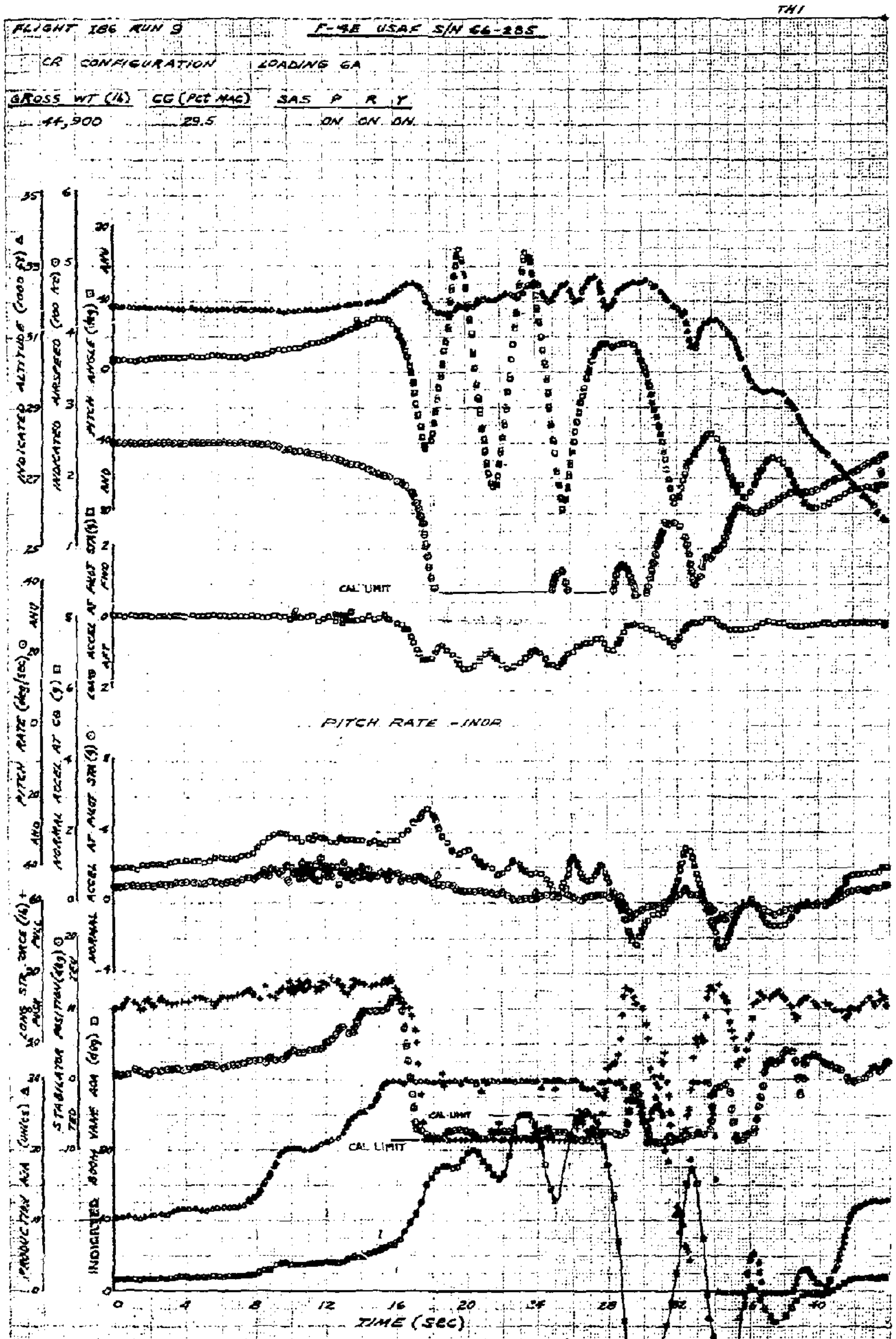

FIGURE 48 2½ TURN, HIGH AOA - HIGHLY OSCILLATORY SPIN (1)

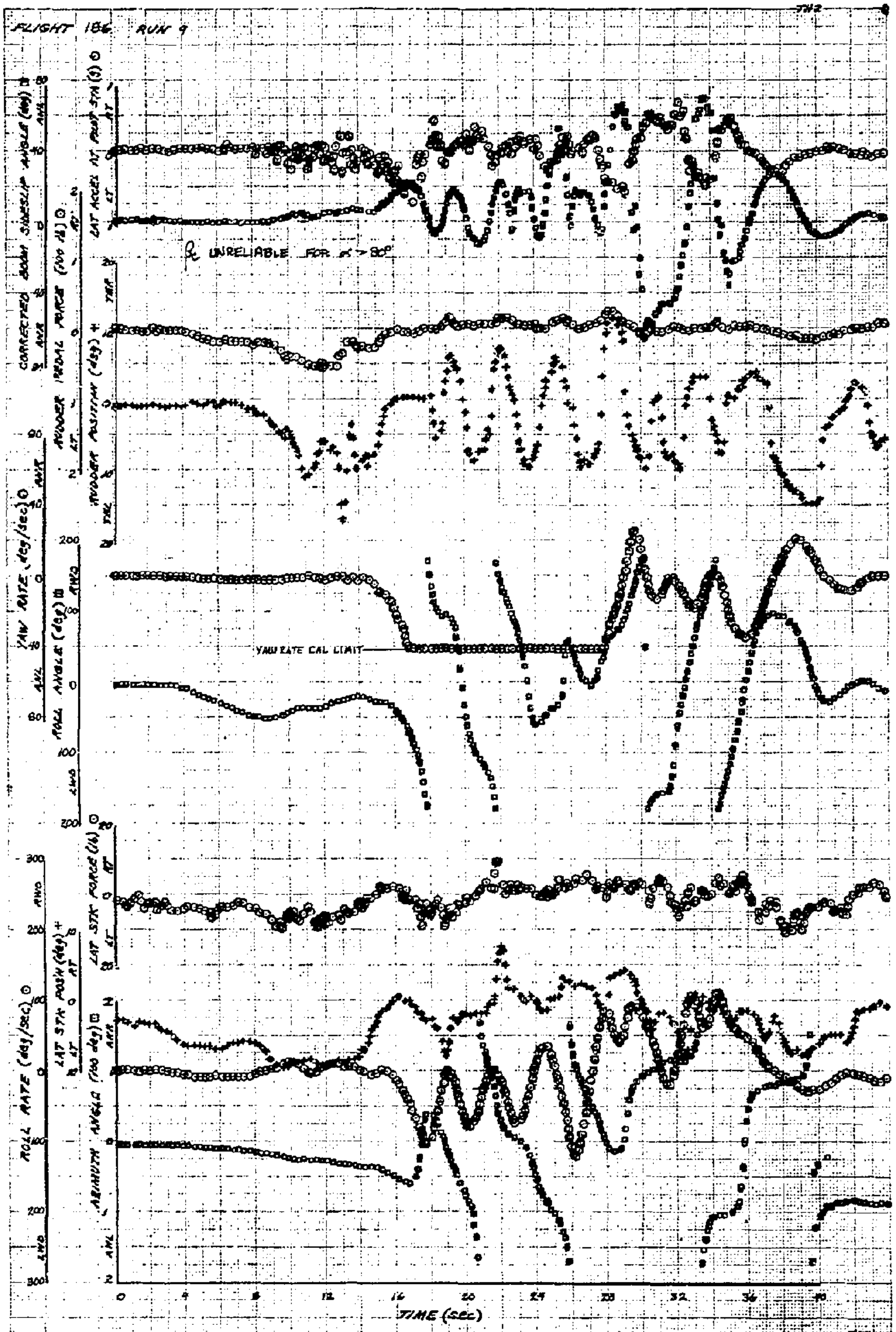

FIGURE 48 CONTINUED

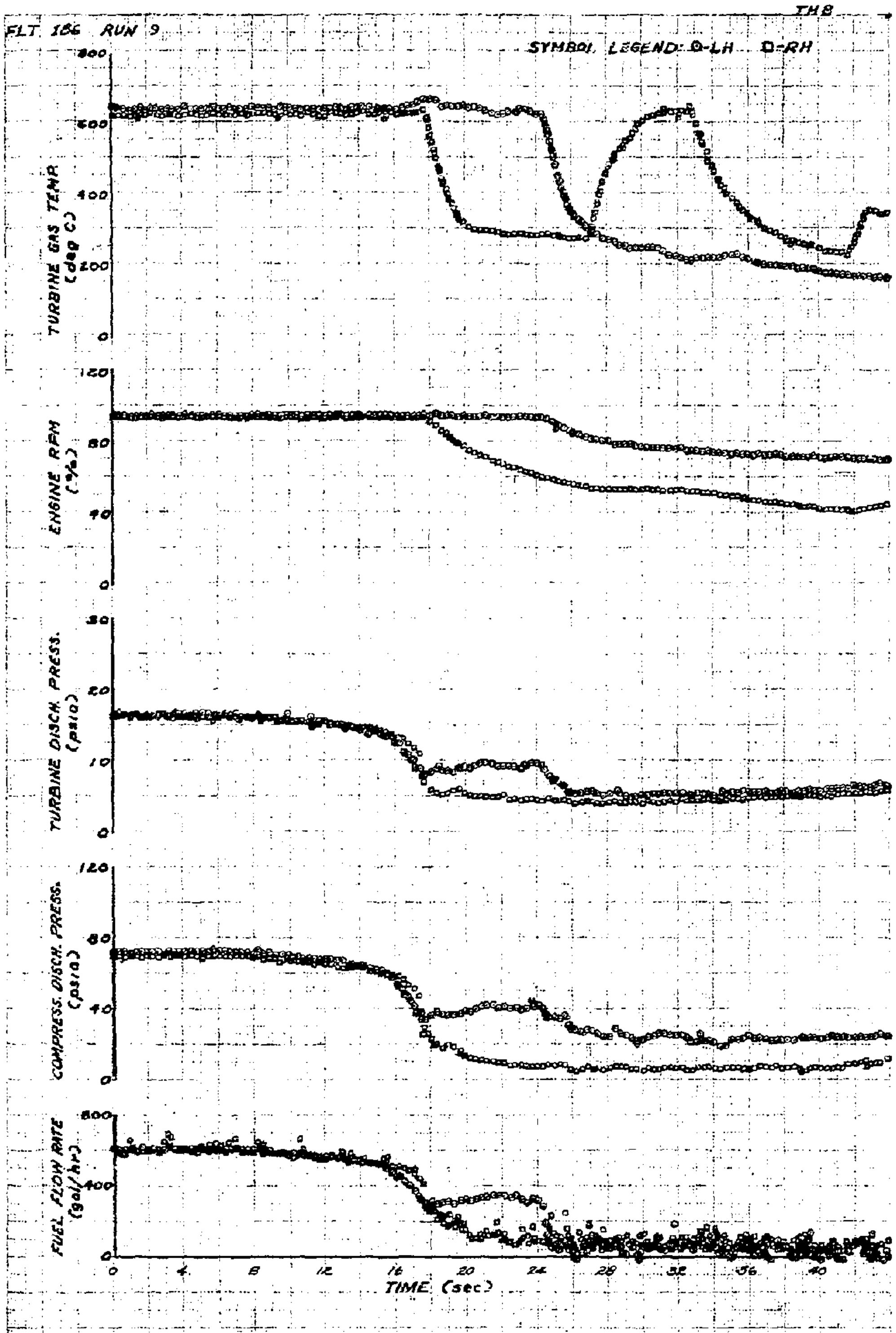

FIGURE 48 CONTINUED

PRECEDING PAGE BLANK-NOT FILMED

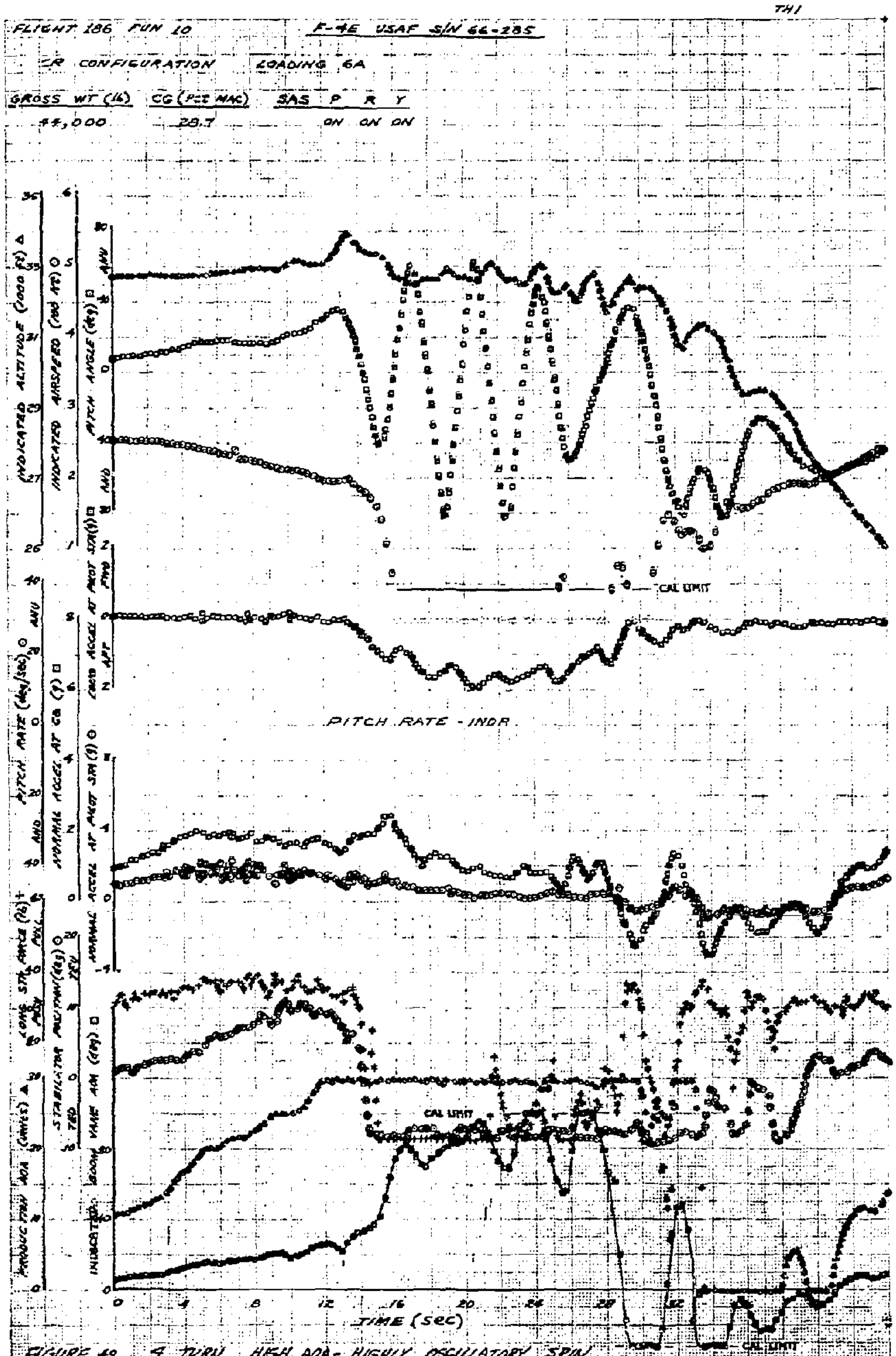

FIGURE 49 4 TURN, HIGH AOA - HIGHLY OSCILLATORY SPIN

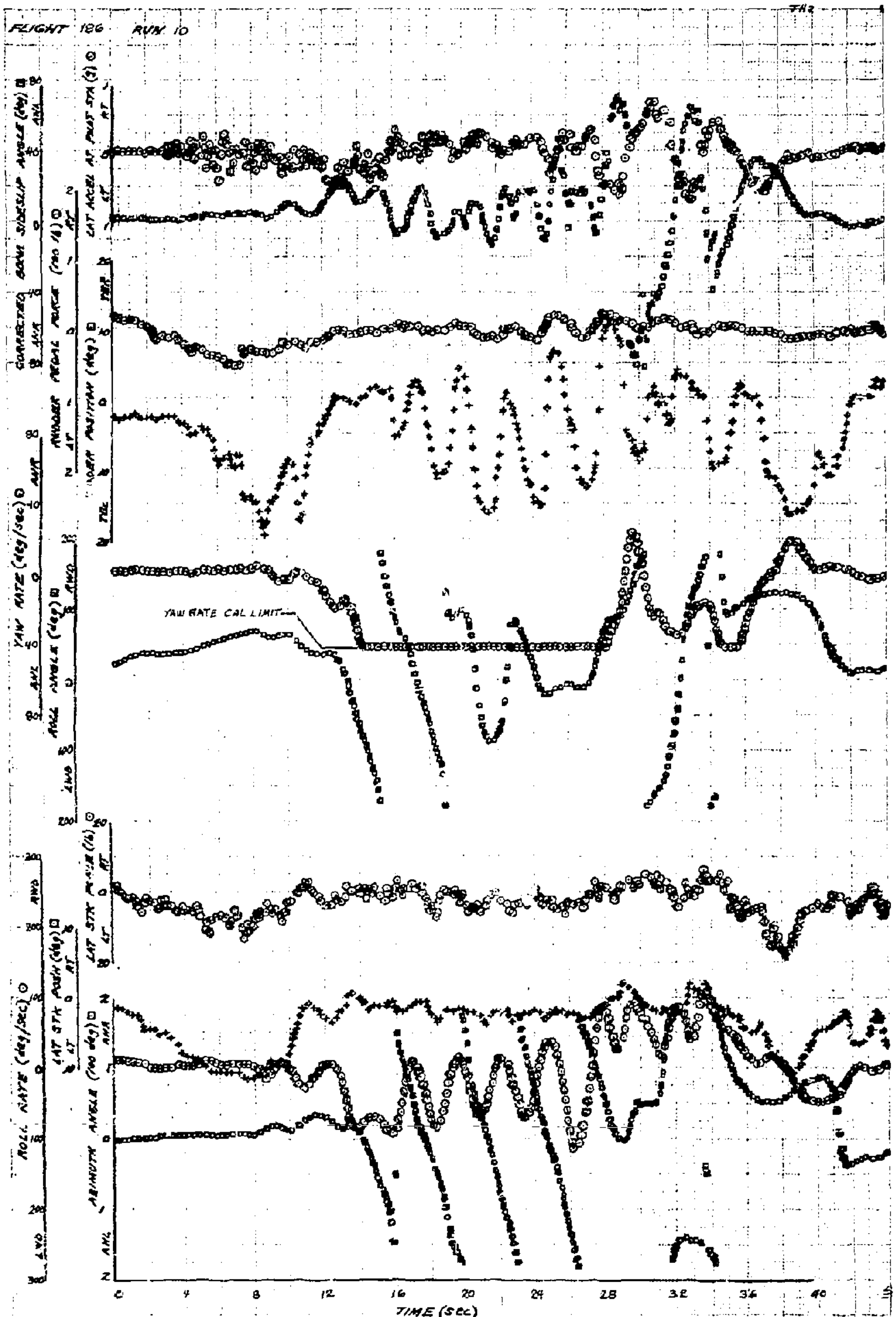

FIGURE 49 CONTINUED

TH8

FLT 186 RUN 10

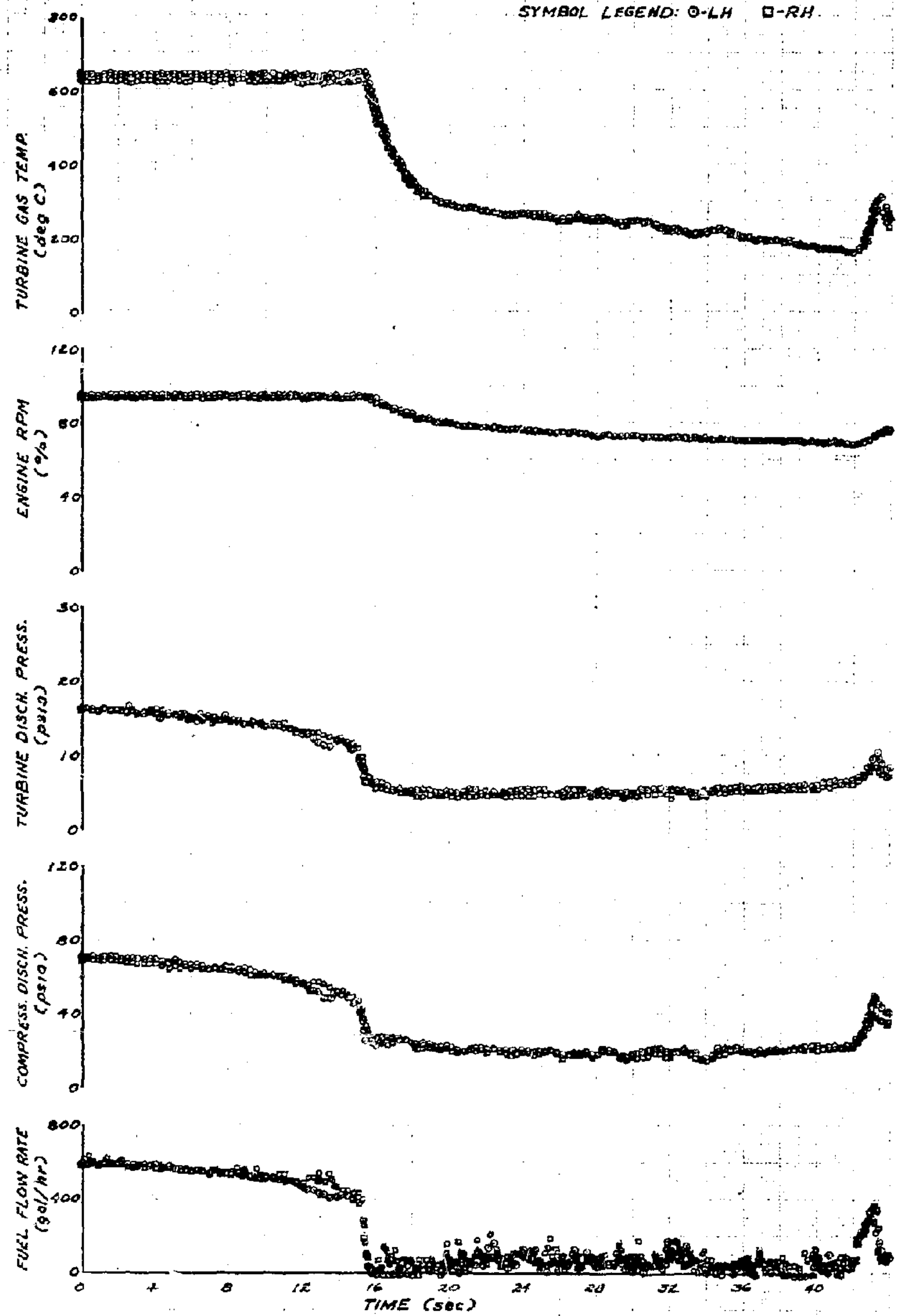

FIGURE 49 CONTINUED

.PRECEDING PAGE BLANK-NOT FILMED

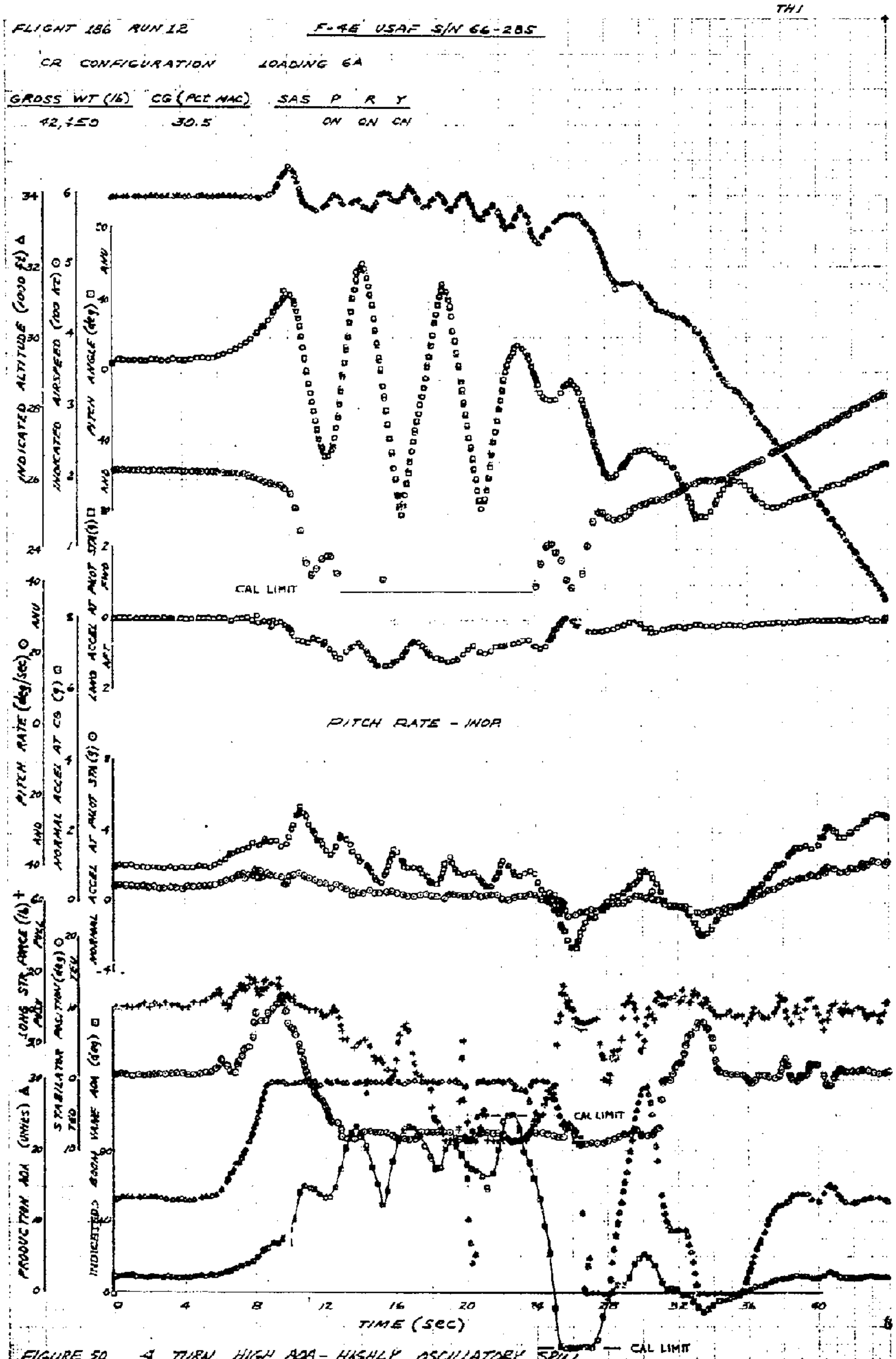

FIGURE 50. 4 TURN, HIGH AOA - HIGHLY OSCILLATORY SPIN

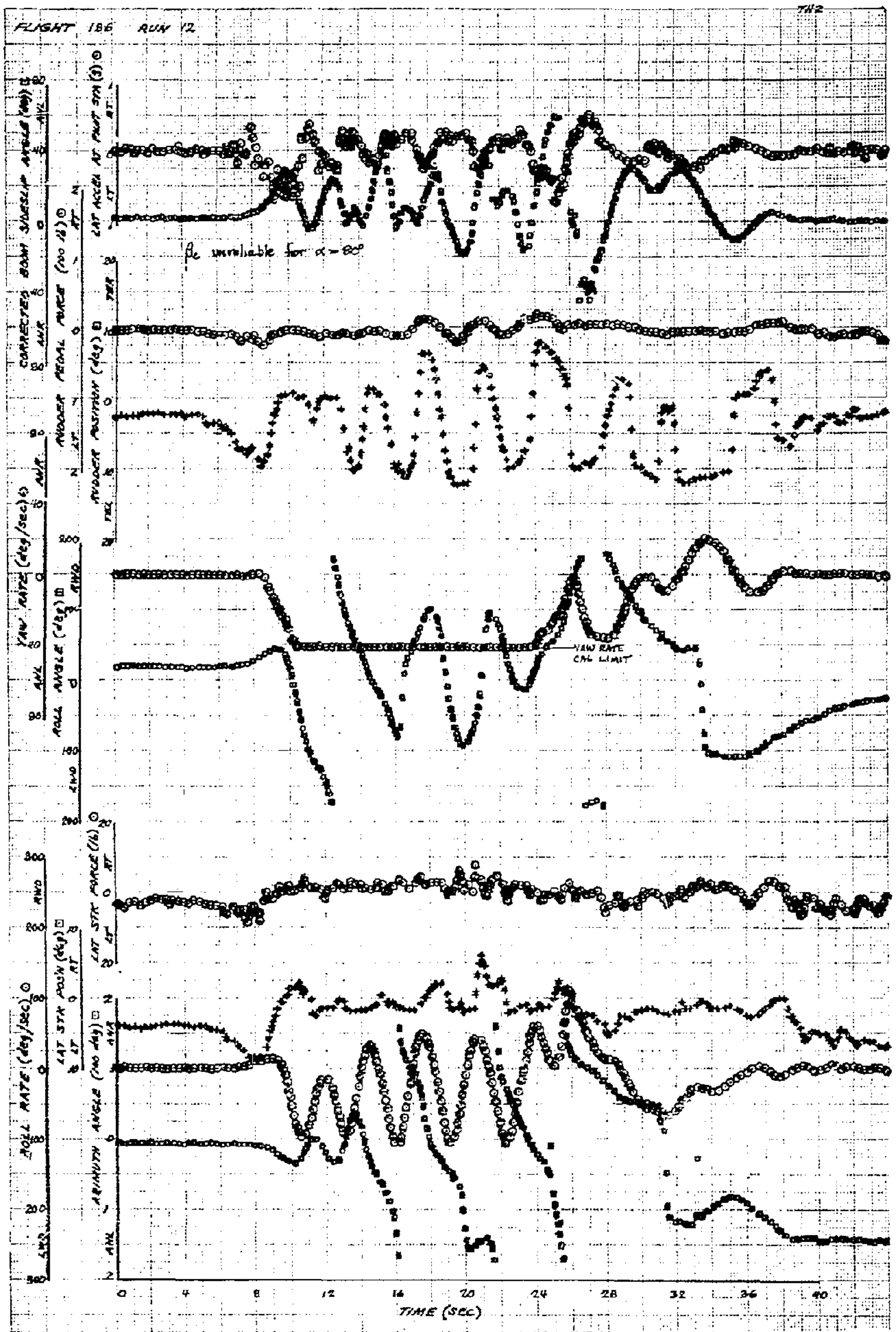

FIGURE 50 CONTINUED

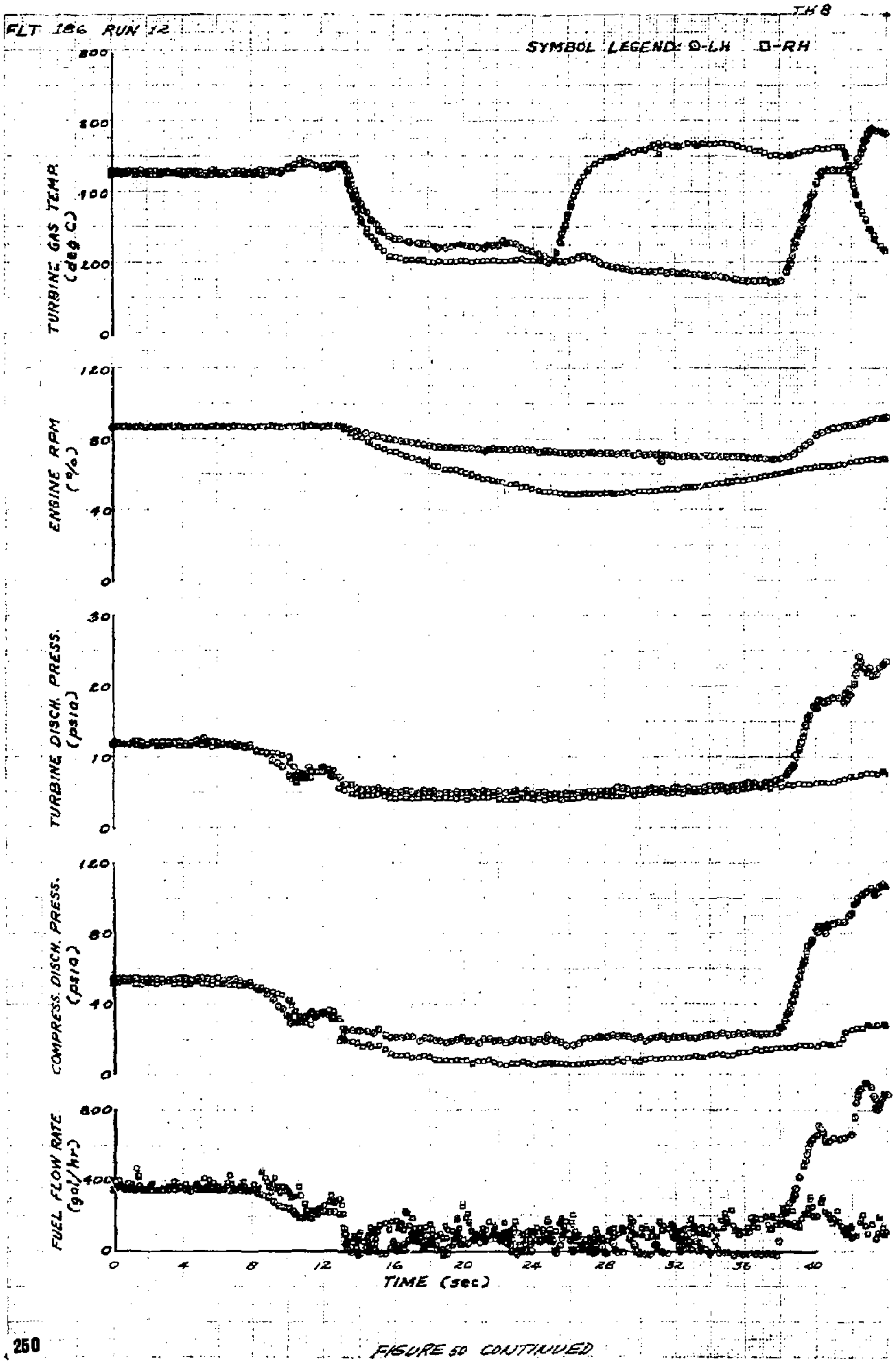

FIGURE 50 CONTINUED

PRECEDING PAGE BLANK-NOT FILMED

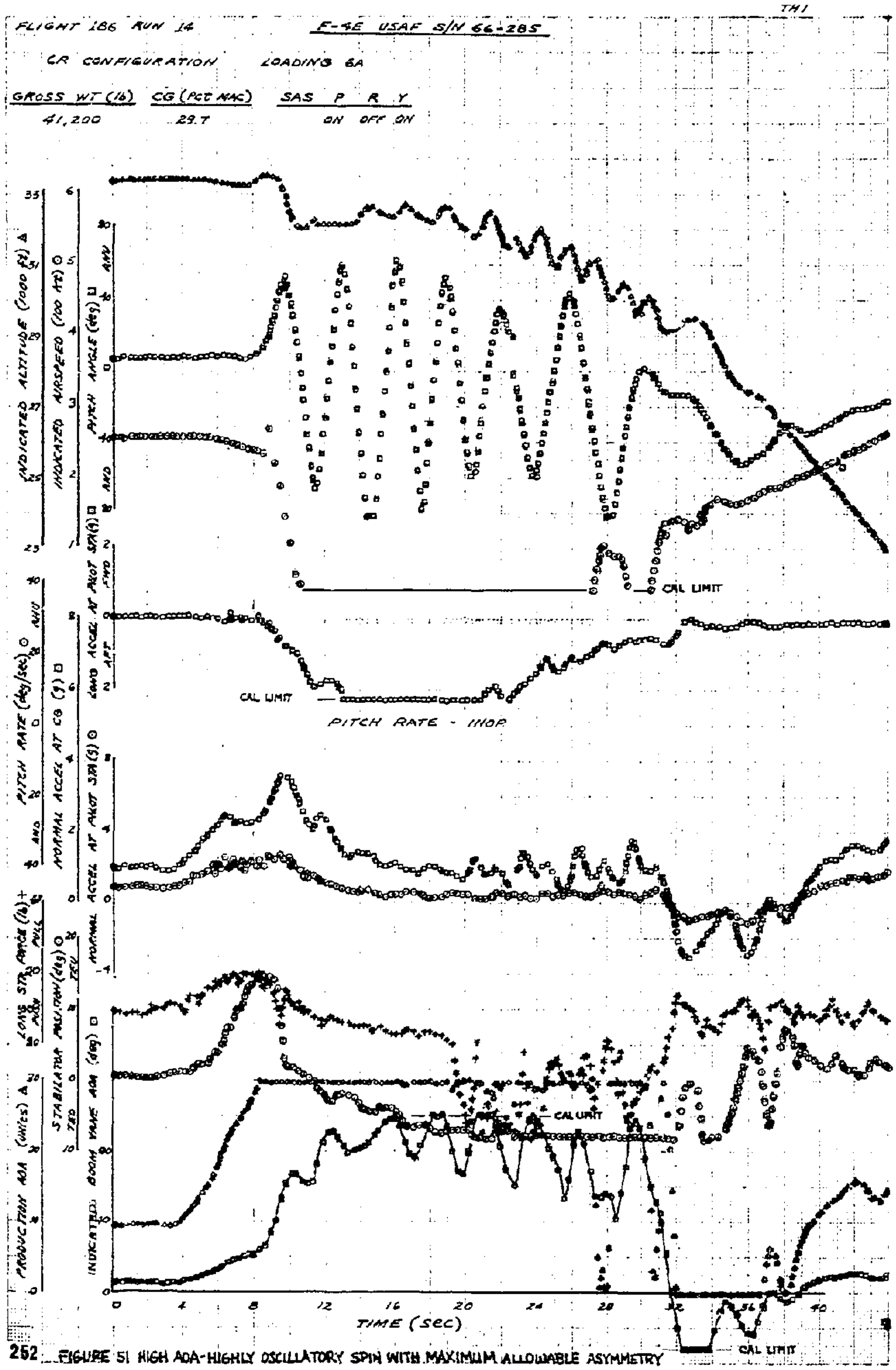

FIGURE 51 HIGH AOA-HIGHLY OSCILLATORY SPIN WITH MAXIMUM ALLOWABLE ASYMMETRY

FLIGHT 186 RUN 14

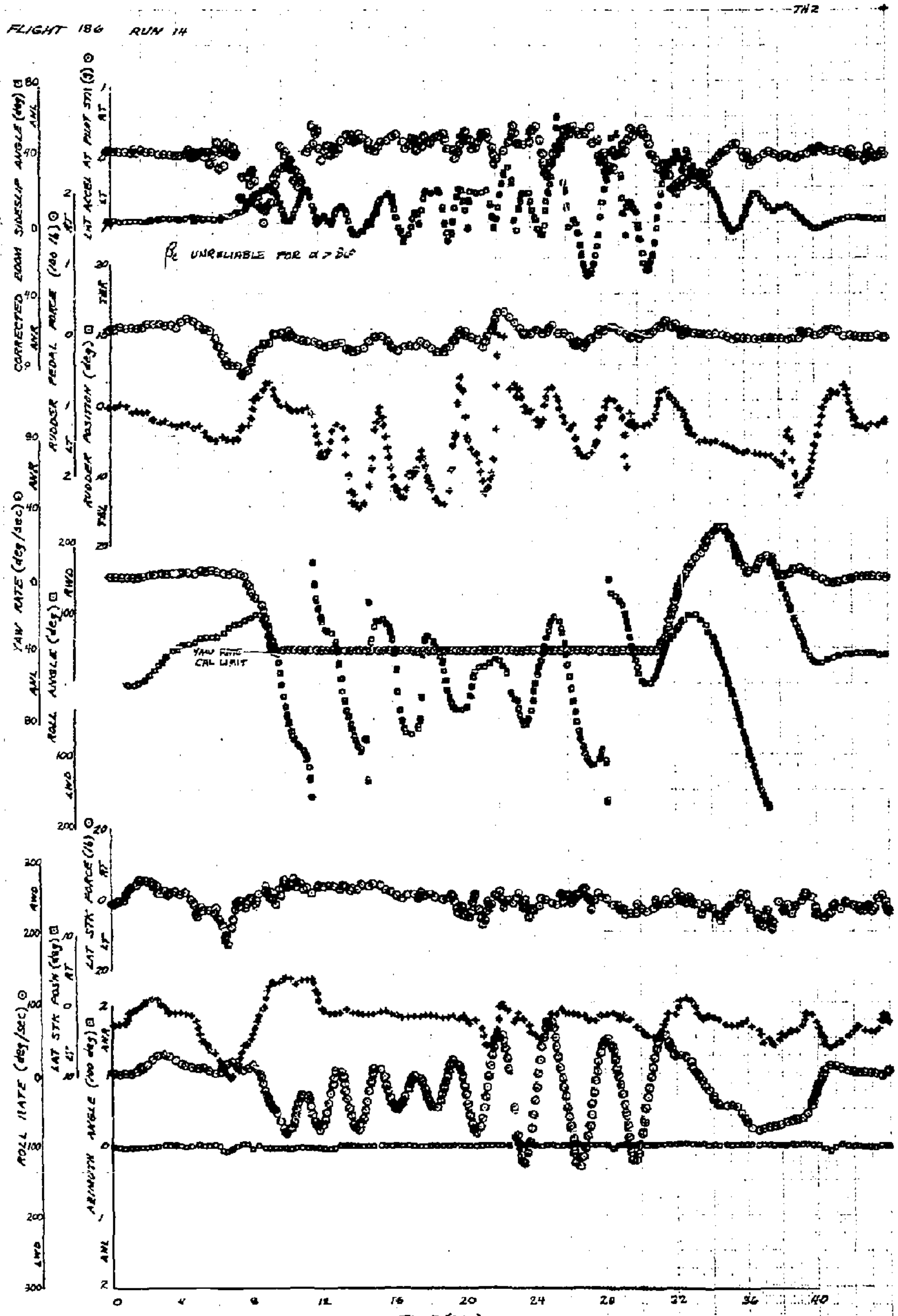

FIGURE 51 CONTINUED

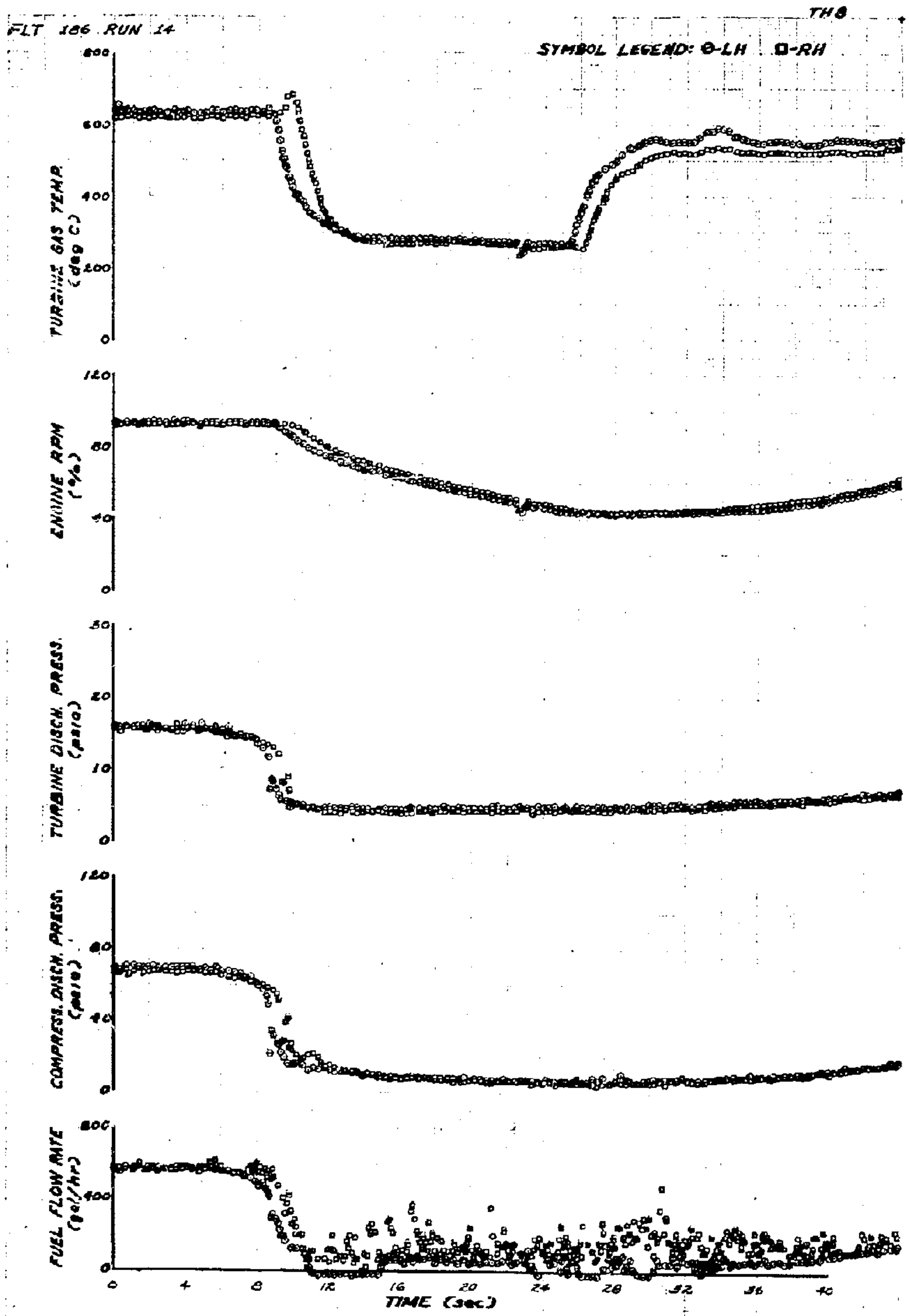

FIGURE 51 CONTINUED

PRECEDING PAGE BLANK-NOT FILMED

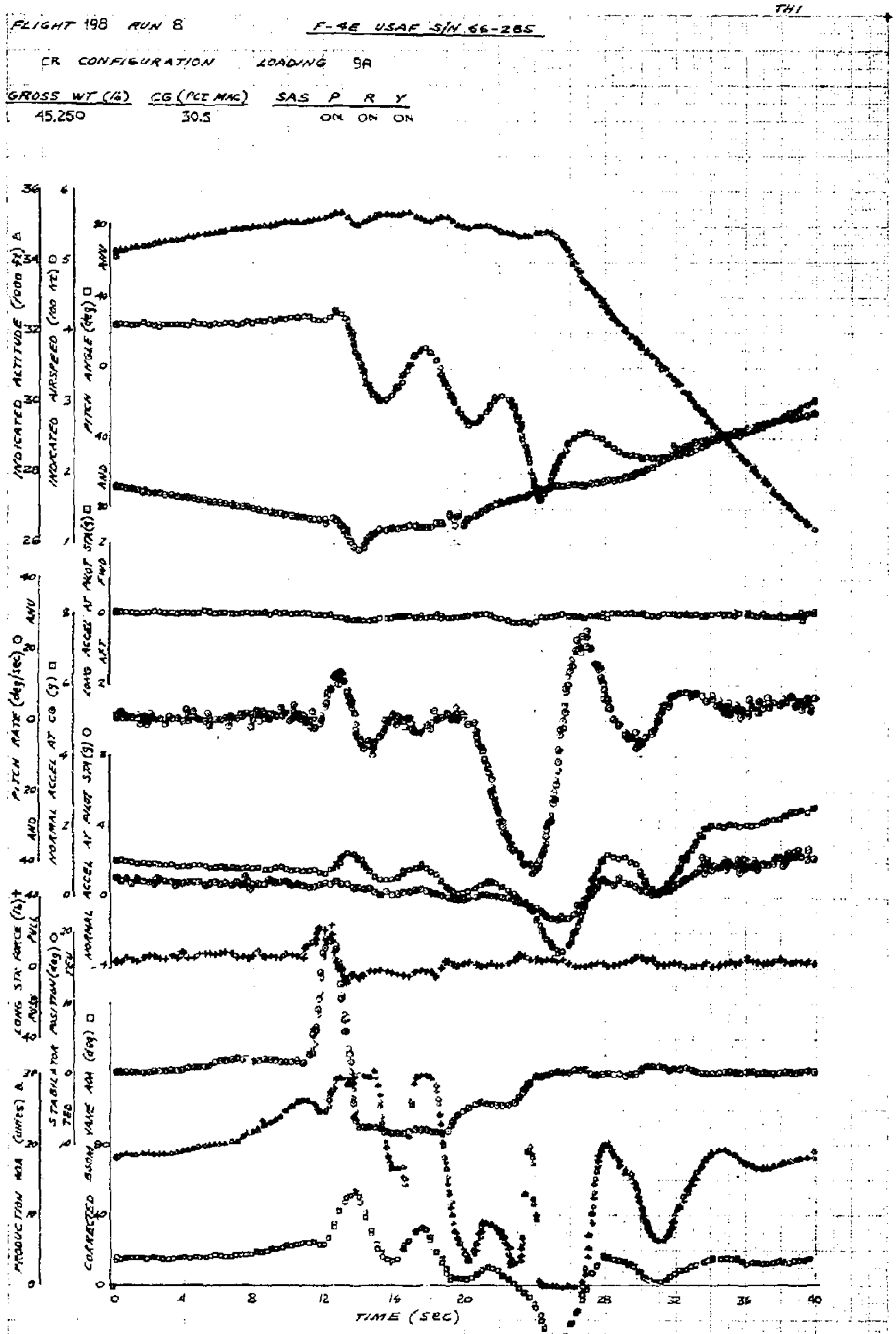

FIGURE 52 ROLLING DEPARTURE WITH RECOVERY ROLLS

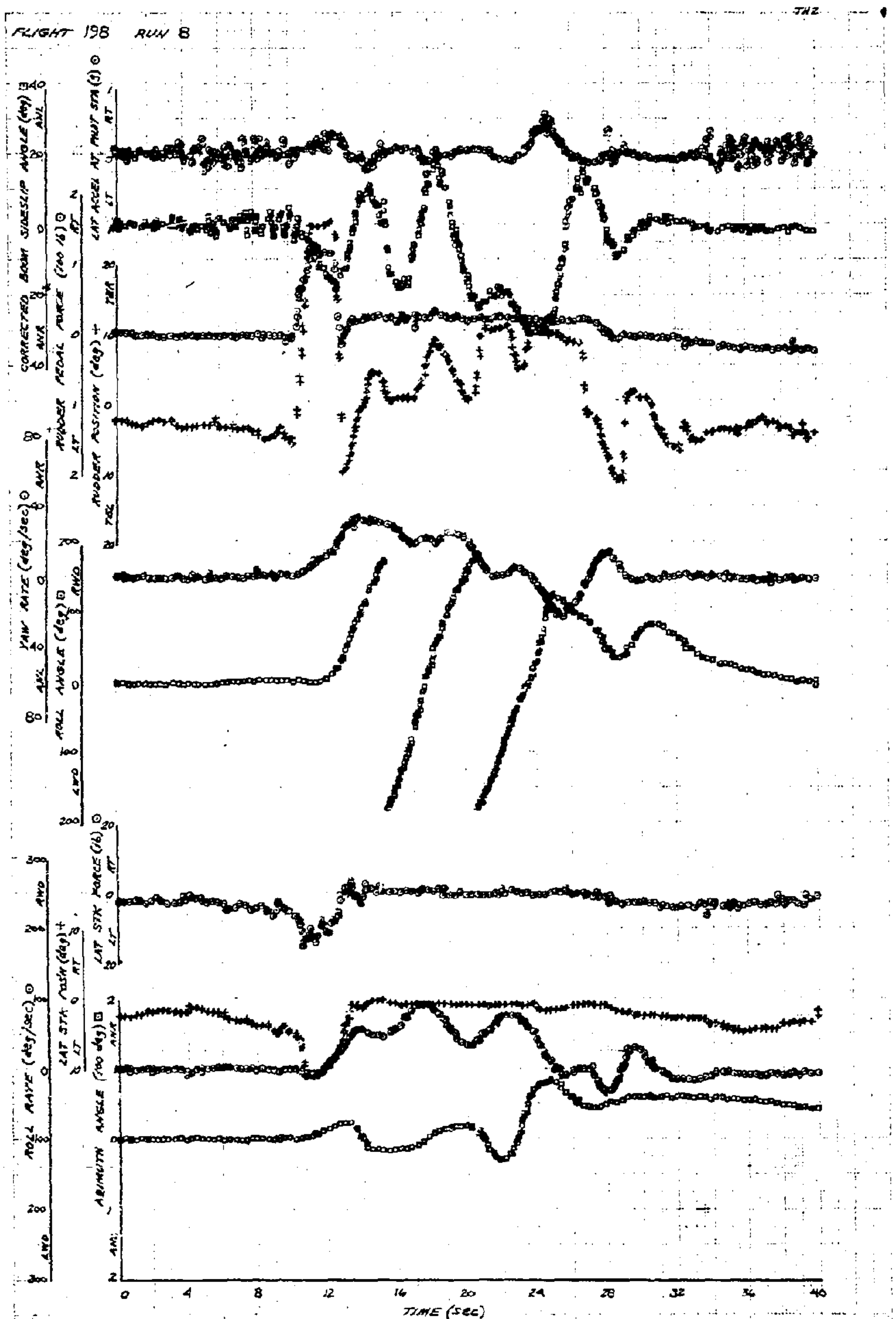

FIGURE 52 CONTINUED

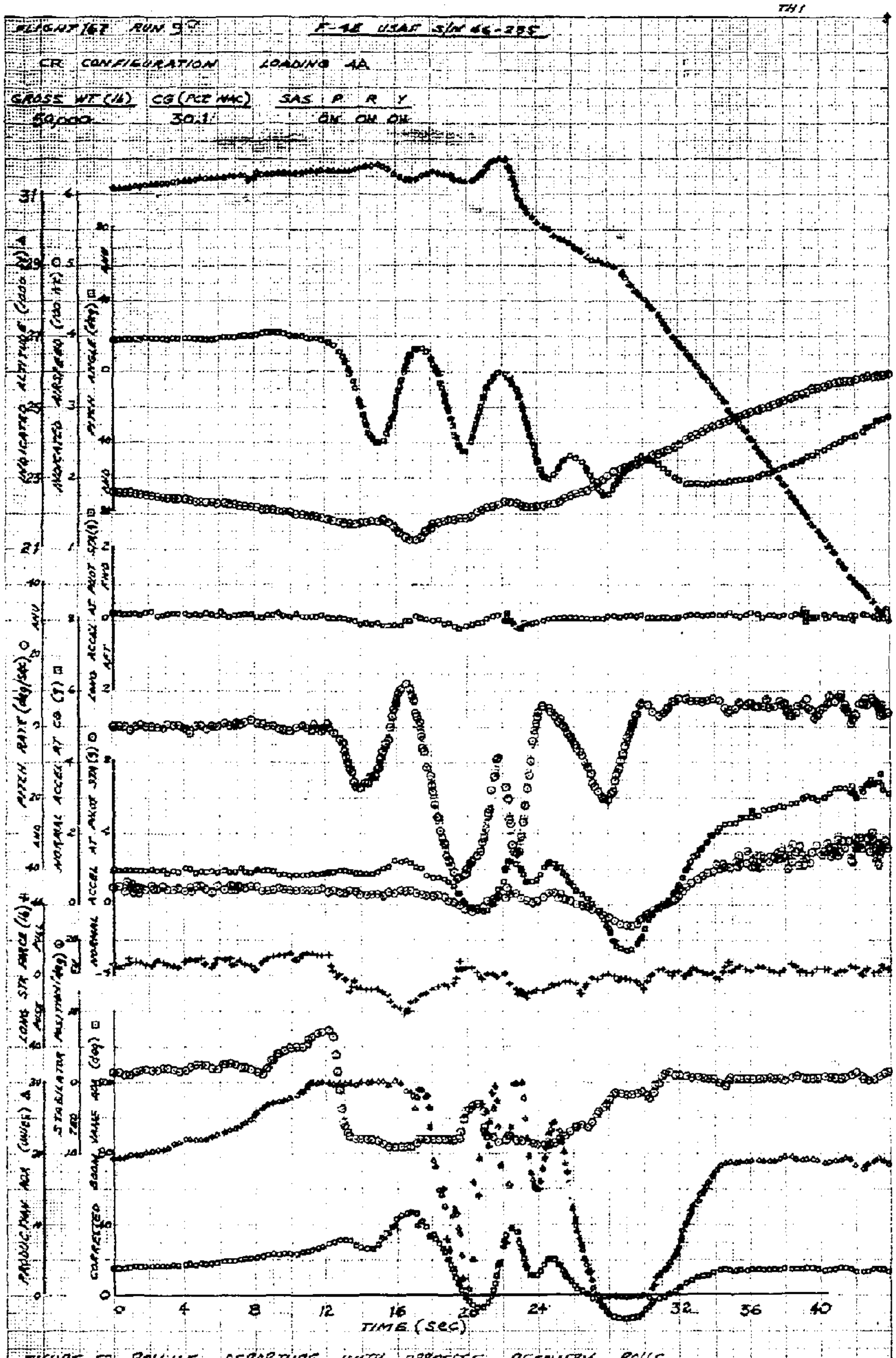

FIGURE 53 ROLLING DEPARTURE WITH OPPOSITE RECOVERY ROLLS

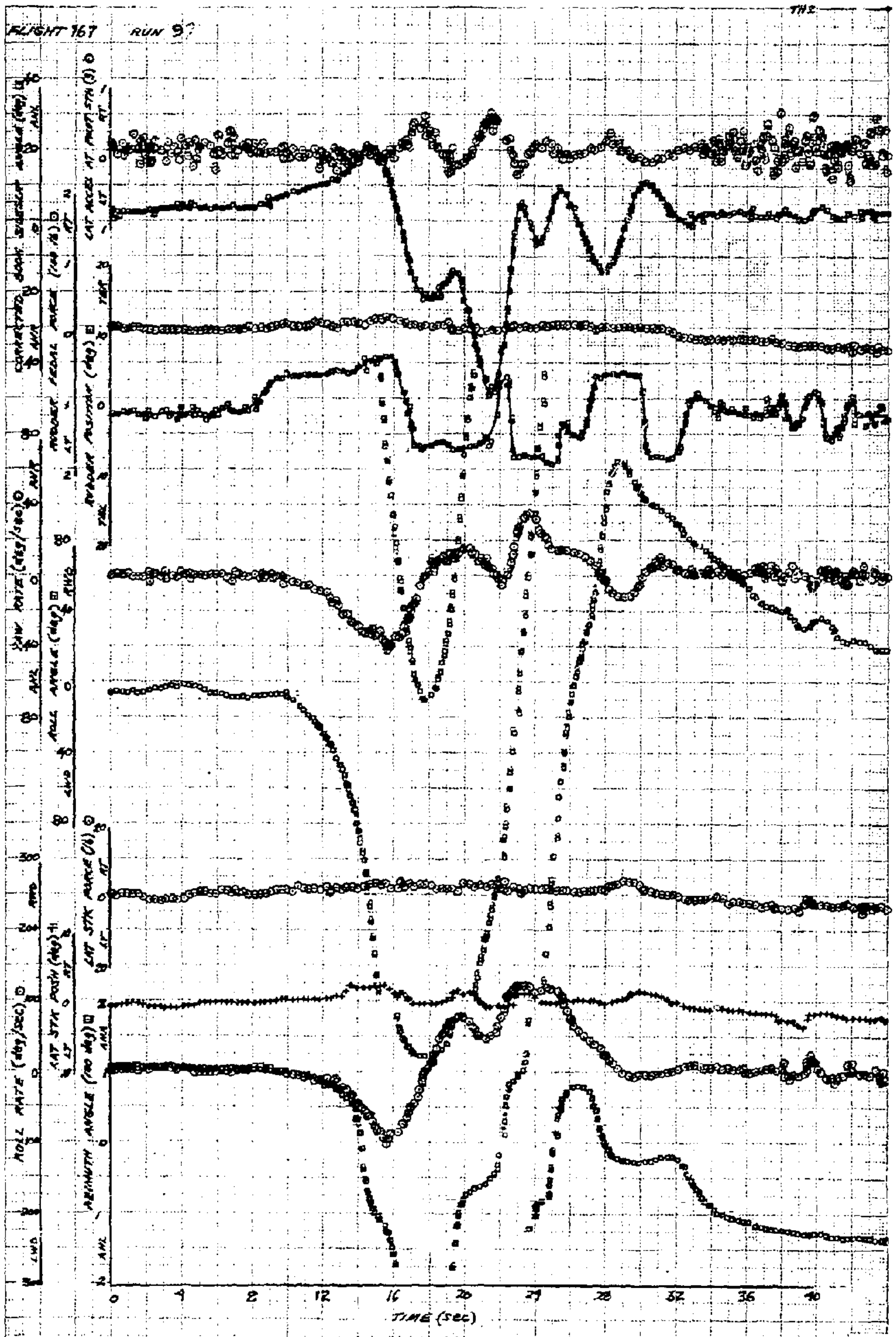

FIGURE 53 CONTINUED

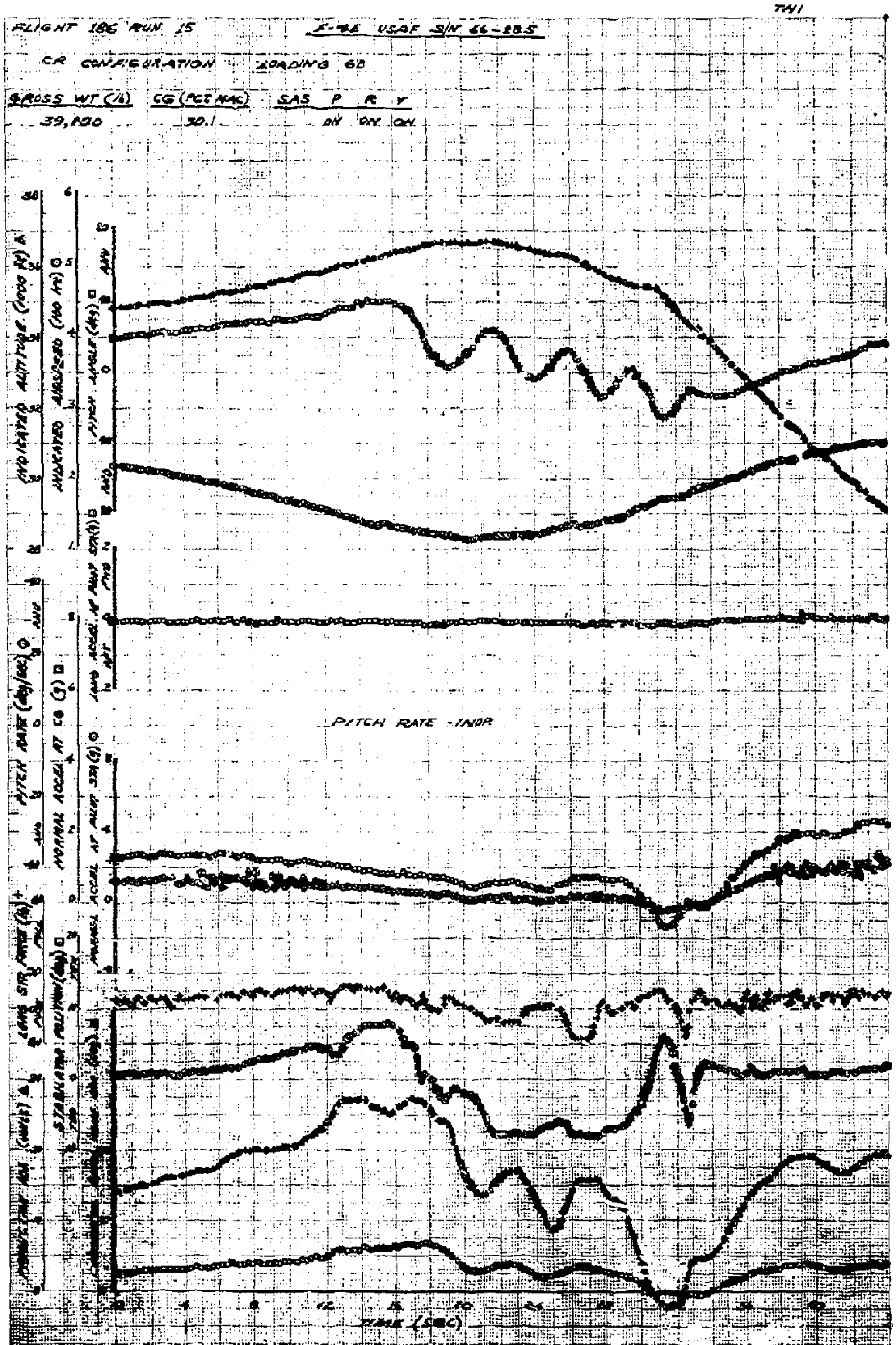

FIGURE 54 RECOVERY ROLLS FROM A ROLLING DEPARTURE

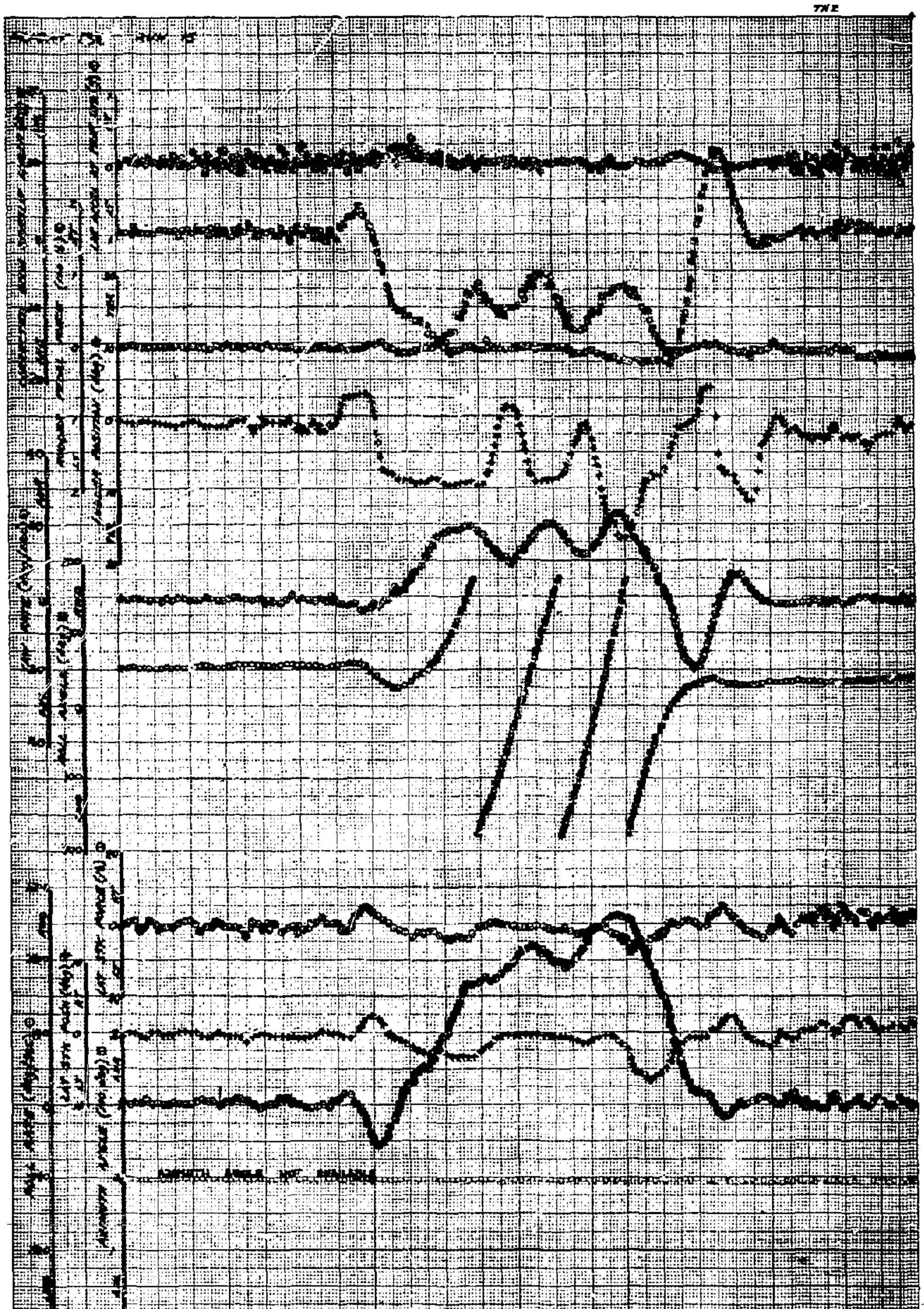

FIGURE 24 CONTINUED

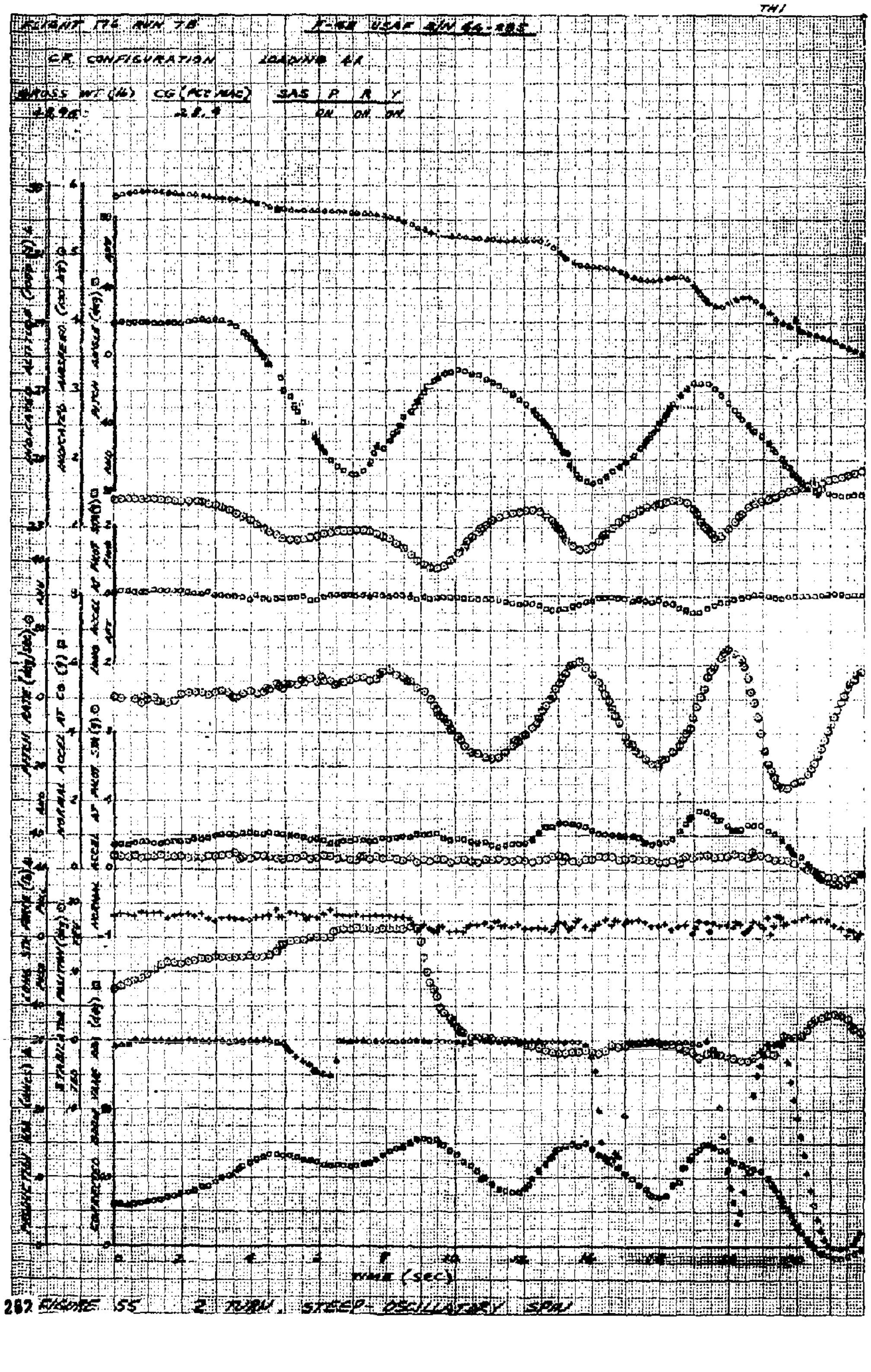

FIGURE 55 2 TURN, STEEP- OSCILLATORY SPIN

FIGURE 55 CONTINUED

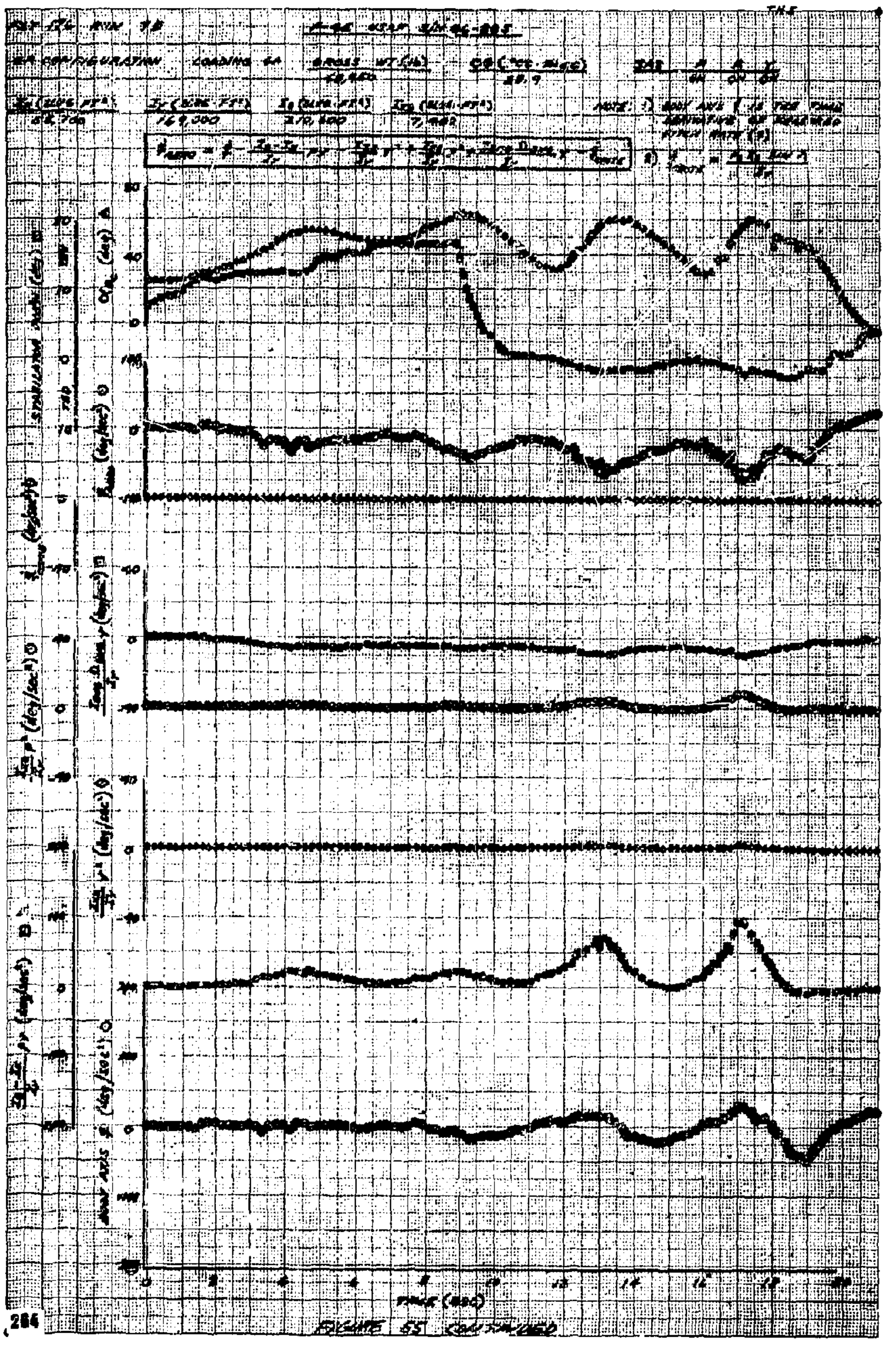

FIGURE 55 CONTINUED

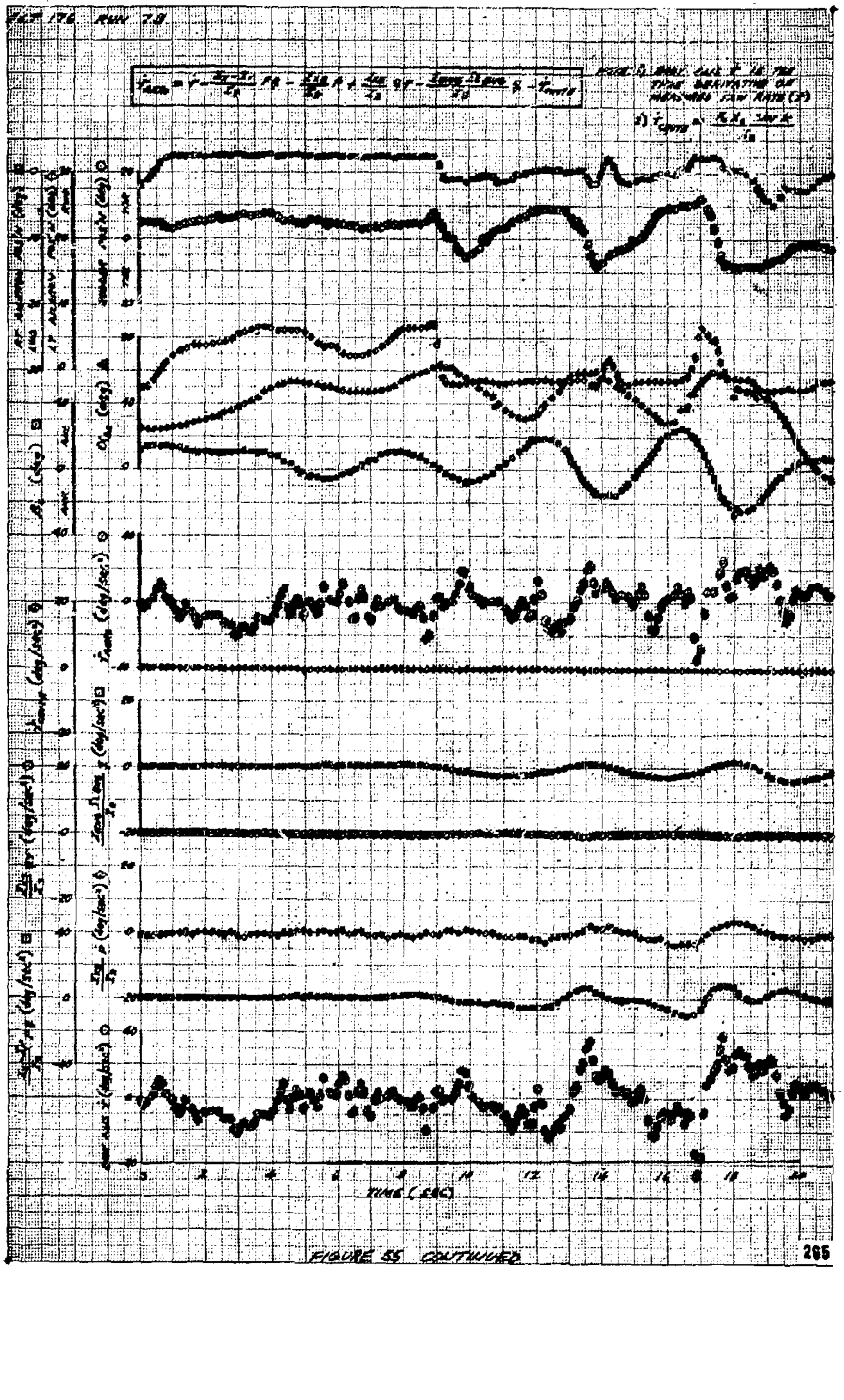

FIGURE 55 CONTINUED

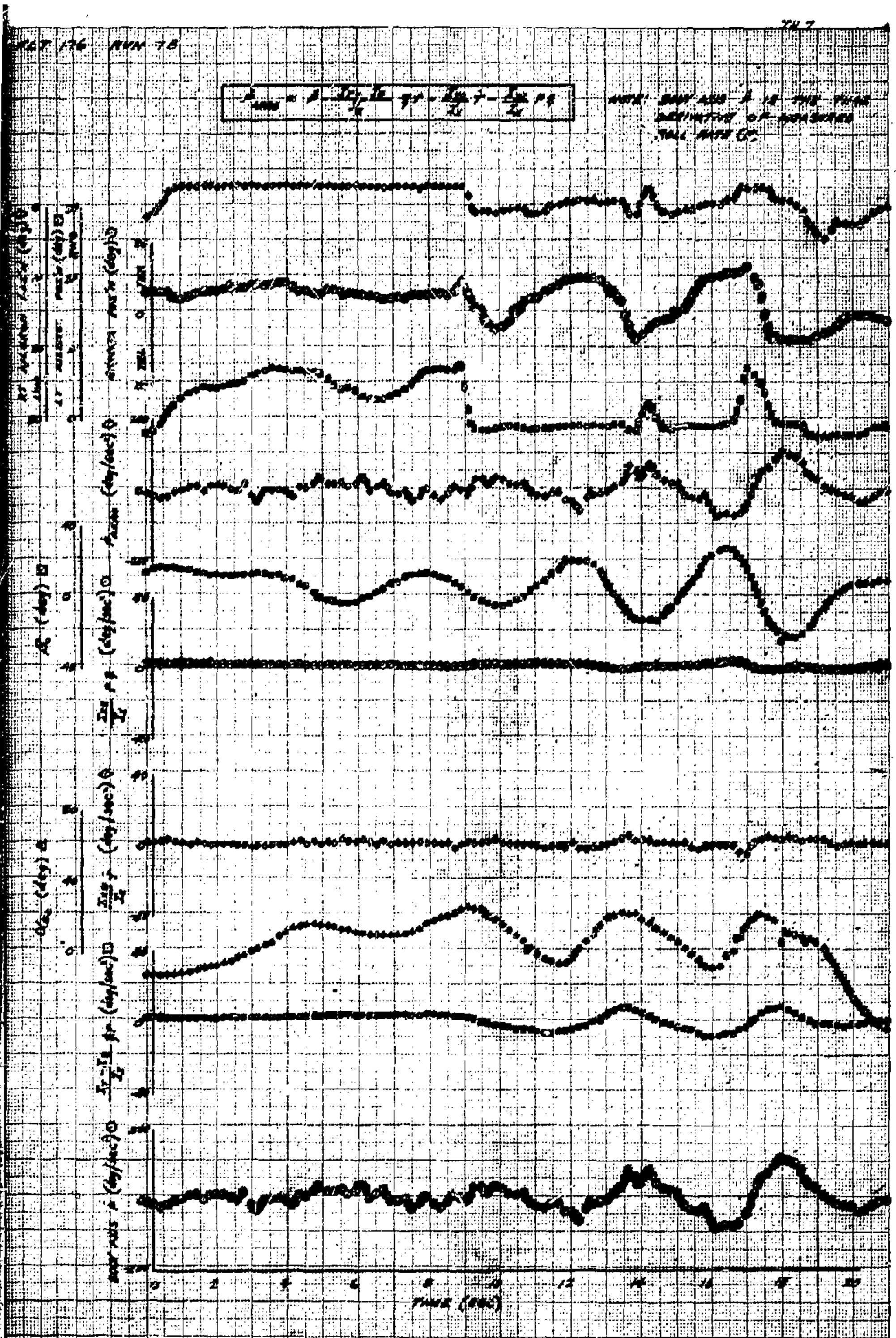

FIGURE 55 CONTINUED

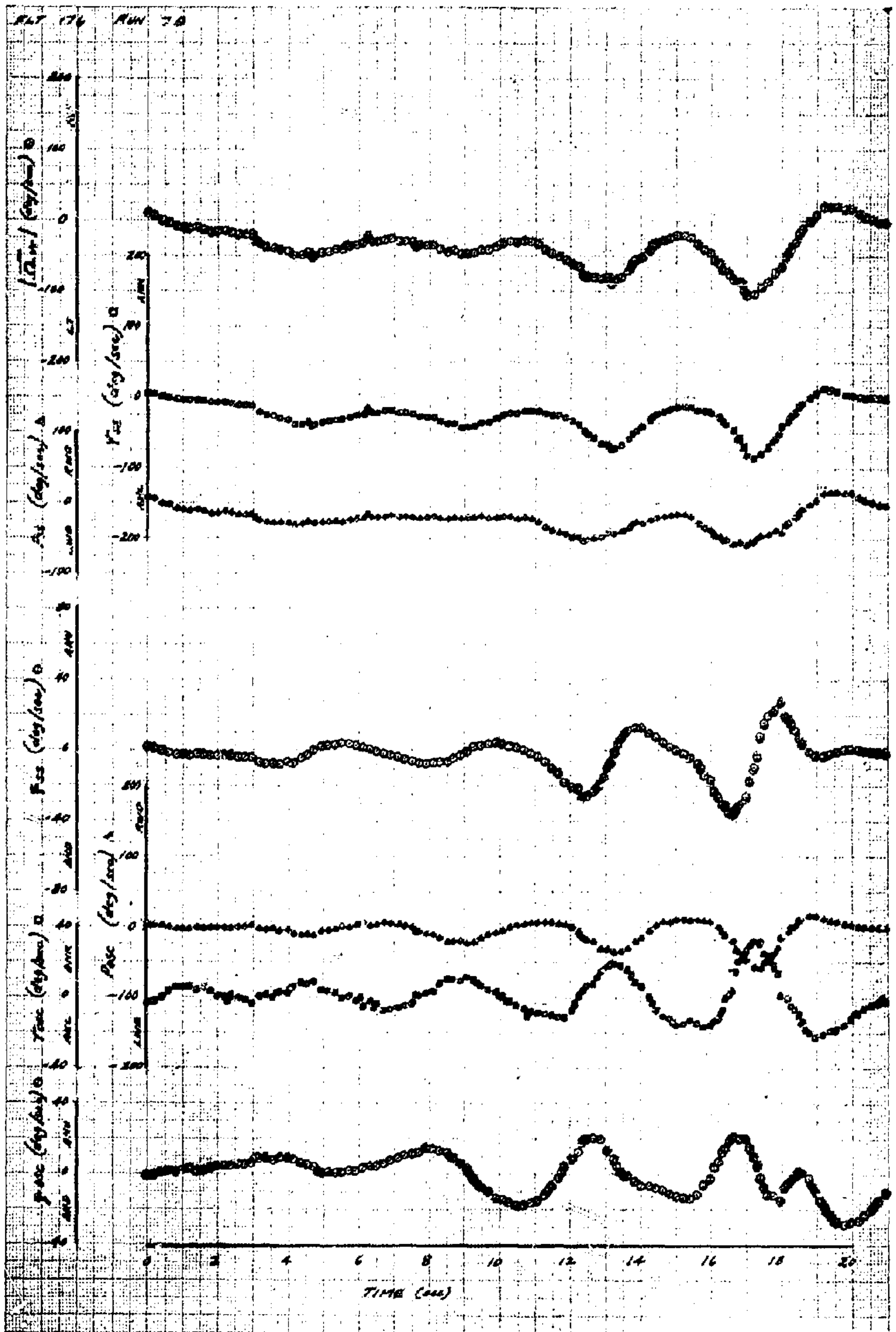

FIGURE 55 CONTINUED

 FIGURE 56 DRAG CHUTE DEPLOYMENT AT ALTITUDE

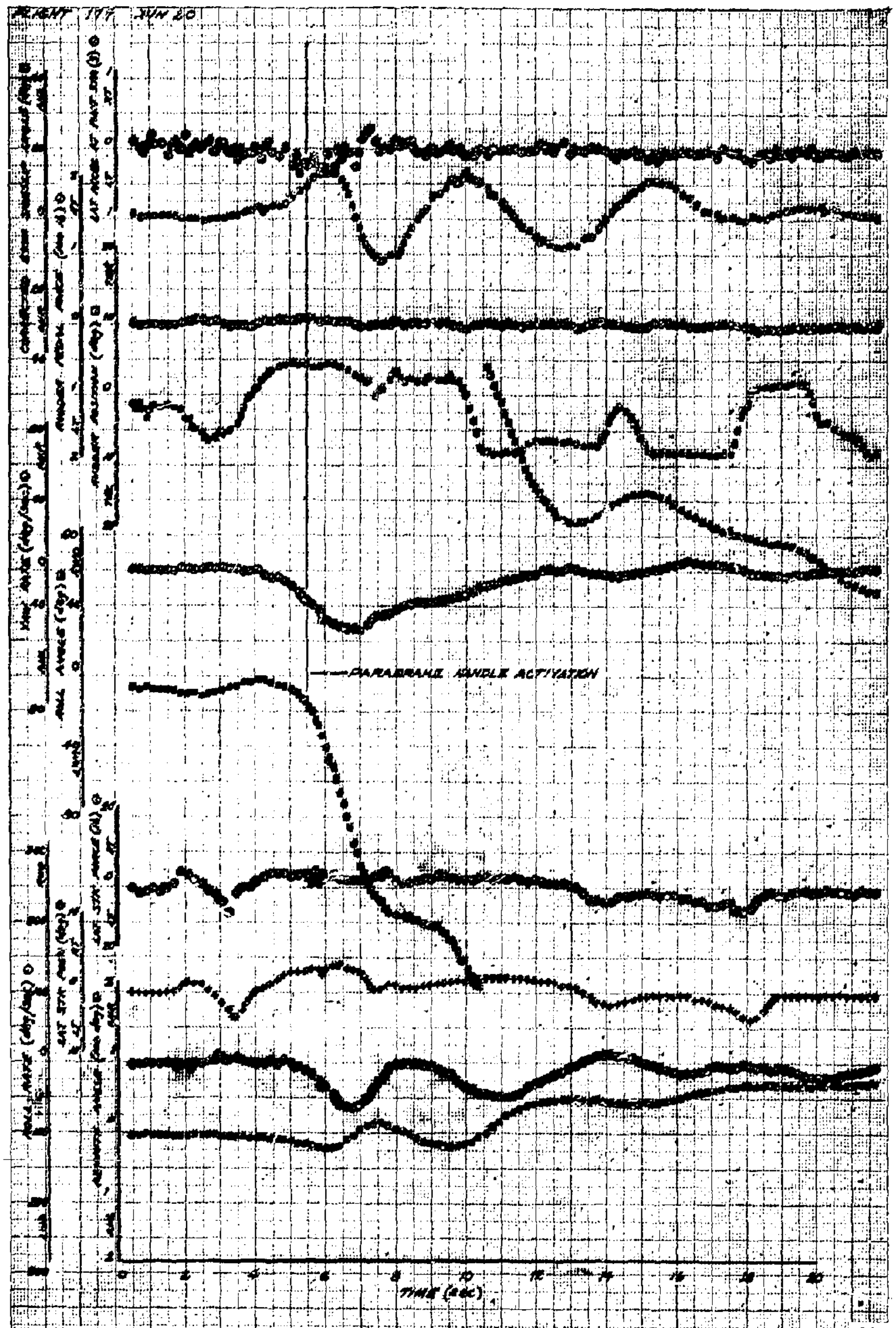

FIGURE 56 CONTINUED

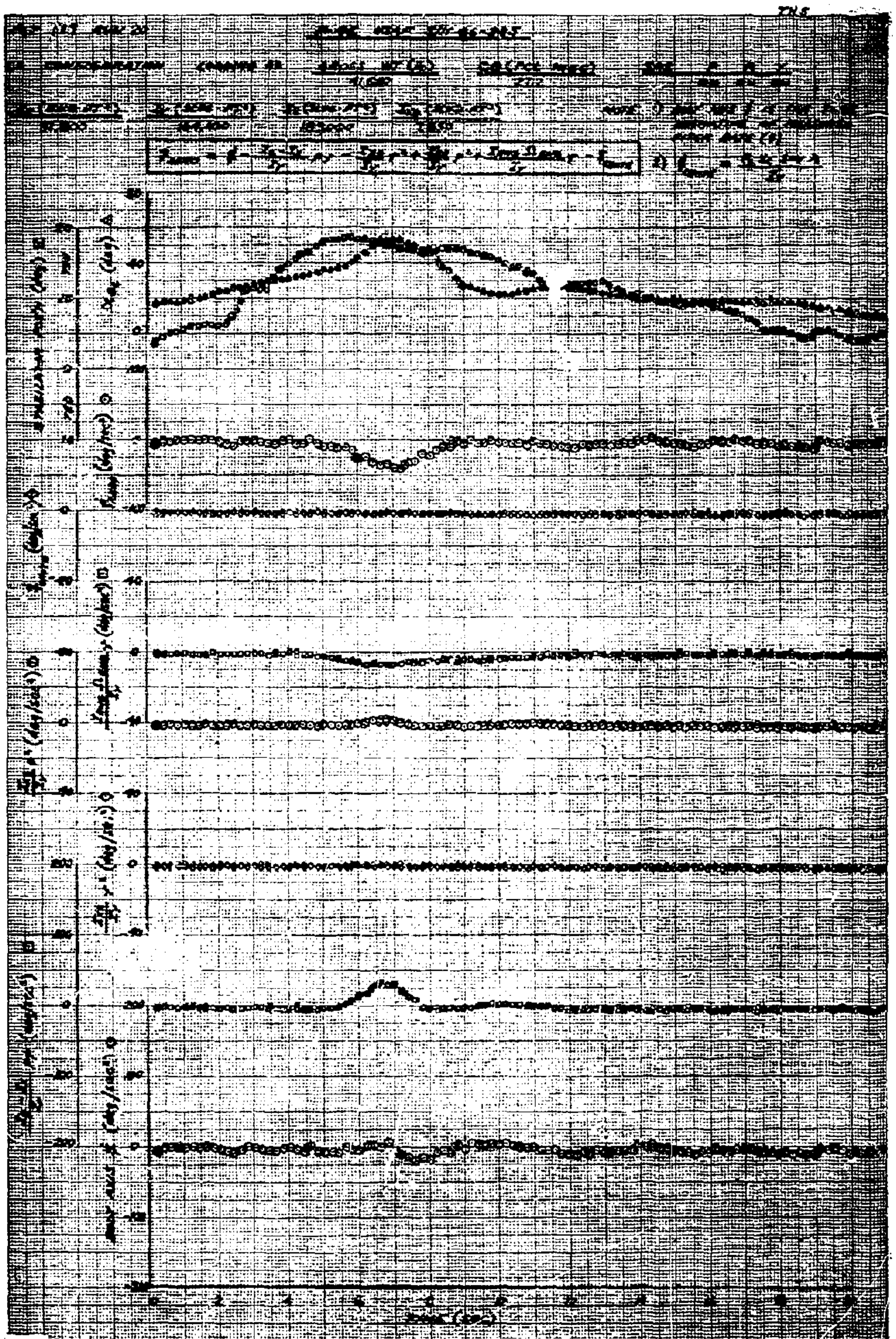

FIGURE 56 CONTINUED

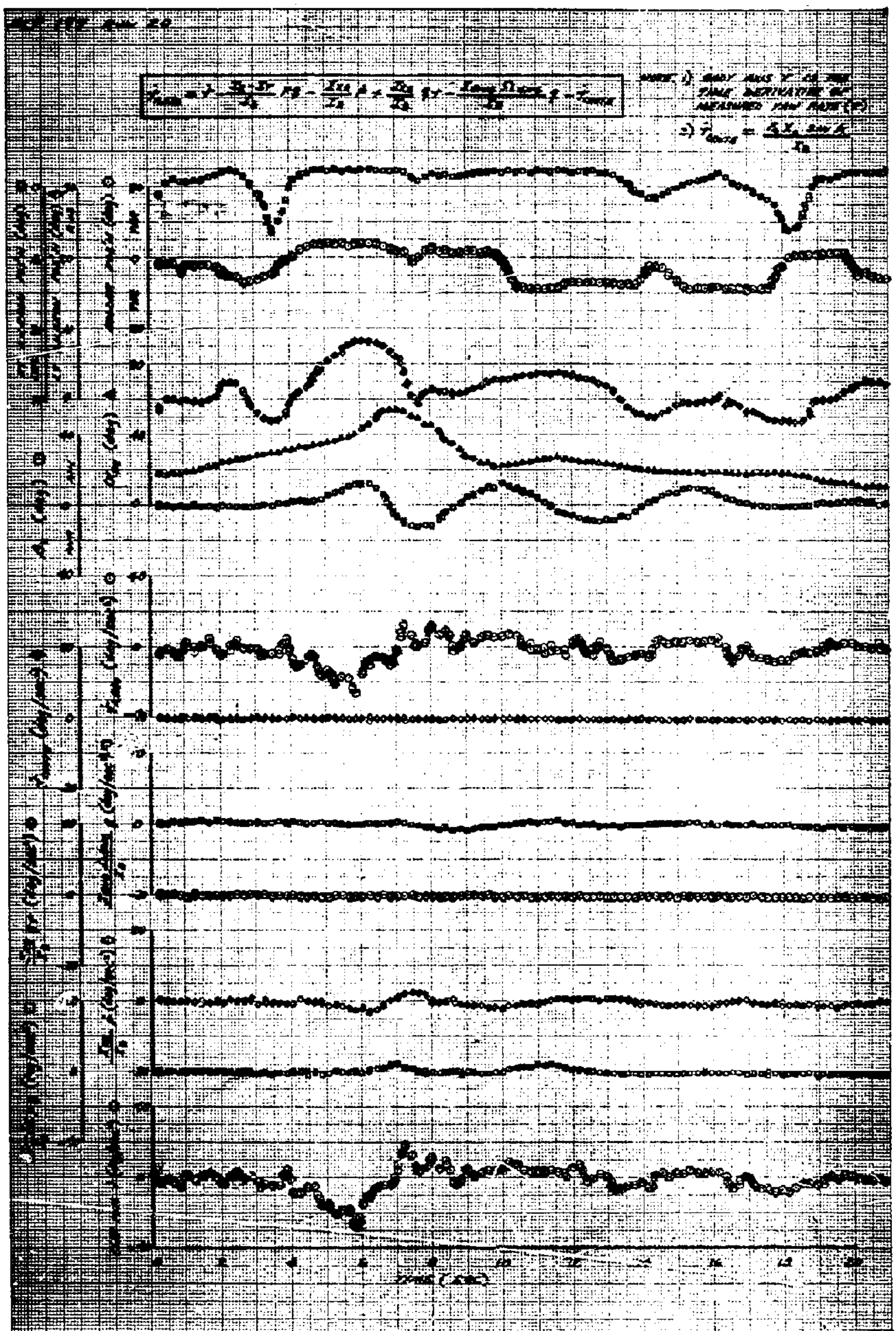

FIGURE 56 CONTINUED

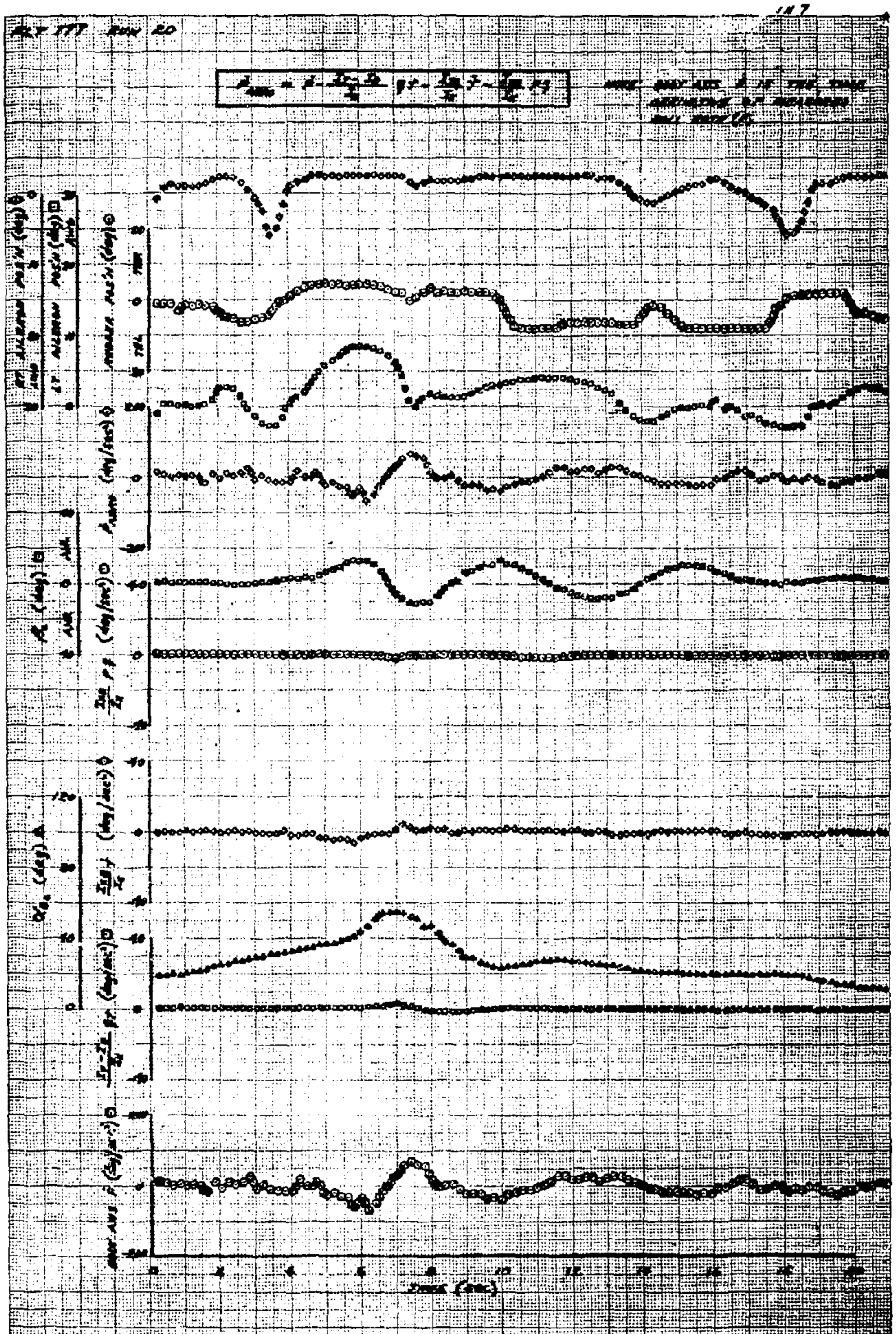

FIGURE 36 CONTINUED

PRECEDING PAGE BLANK-NOT FILMED

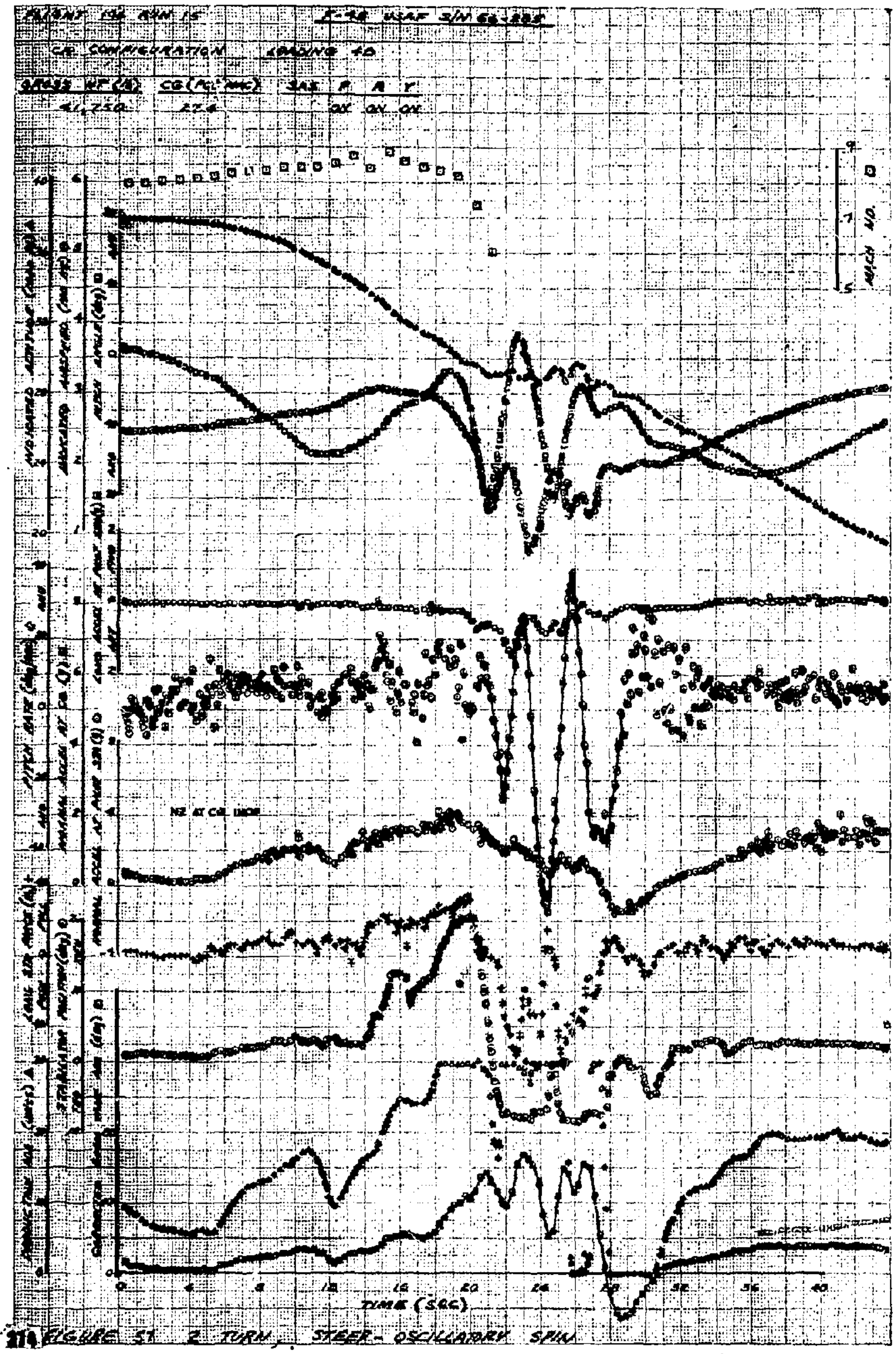

 FIGURE 57 2 TURN, STEER- OSCILLATORY SPIN

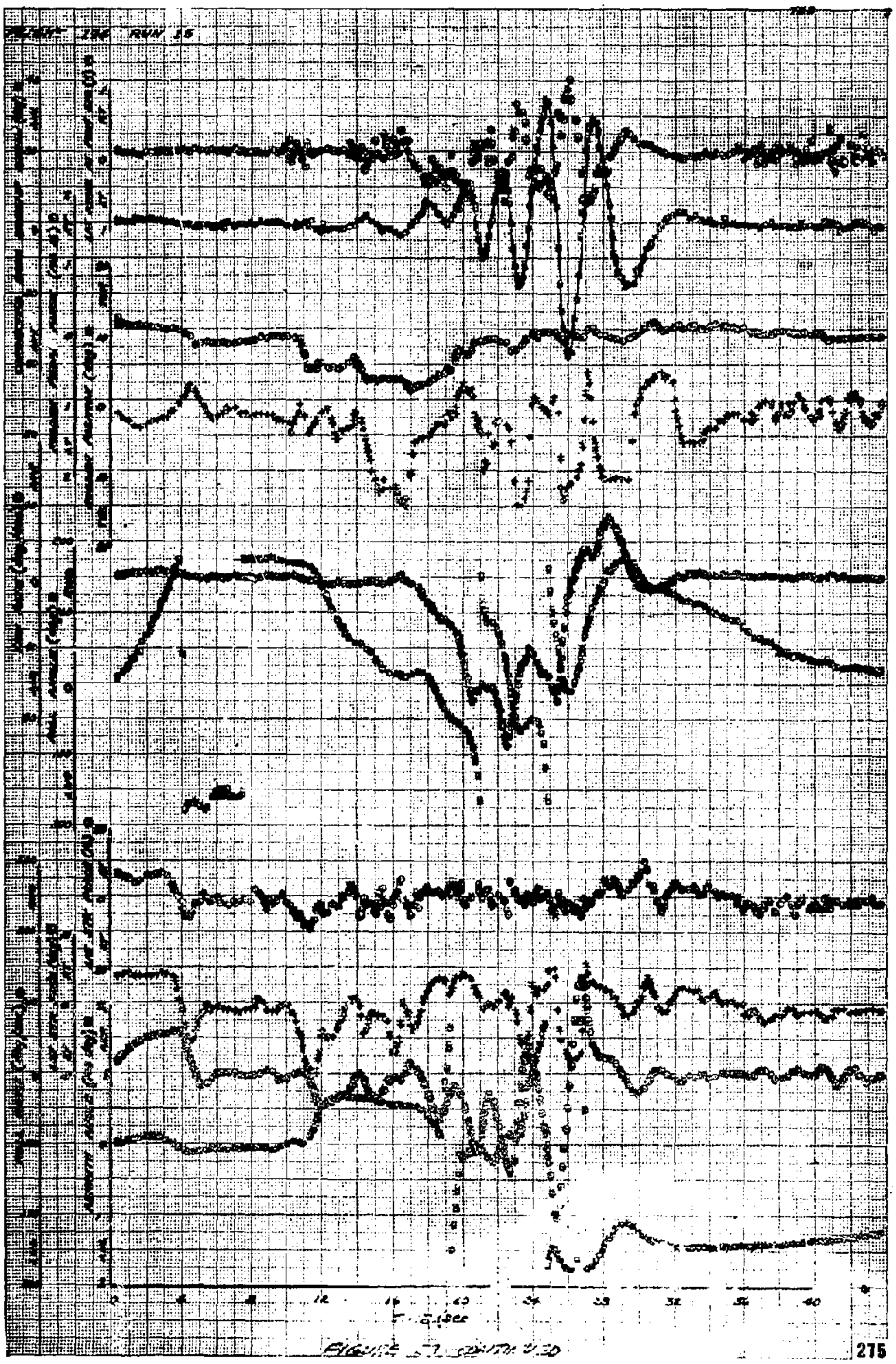

FIGURE 57 CONTINUED

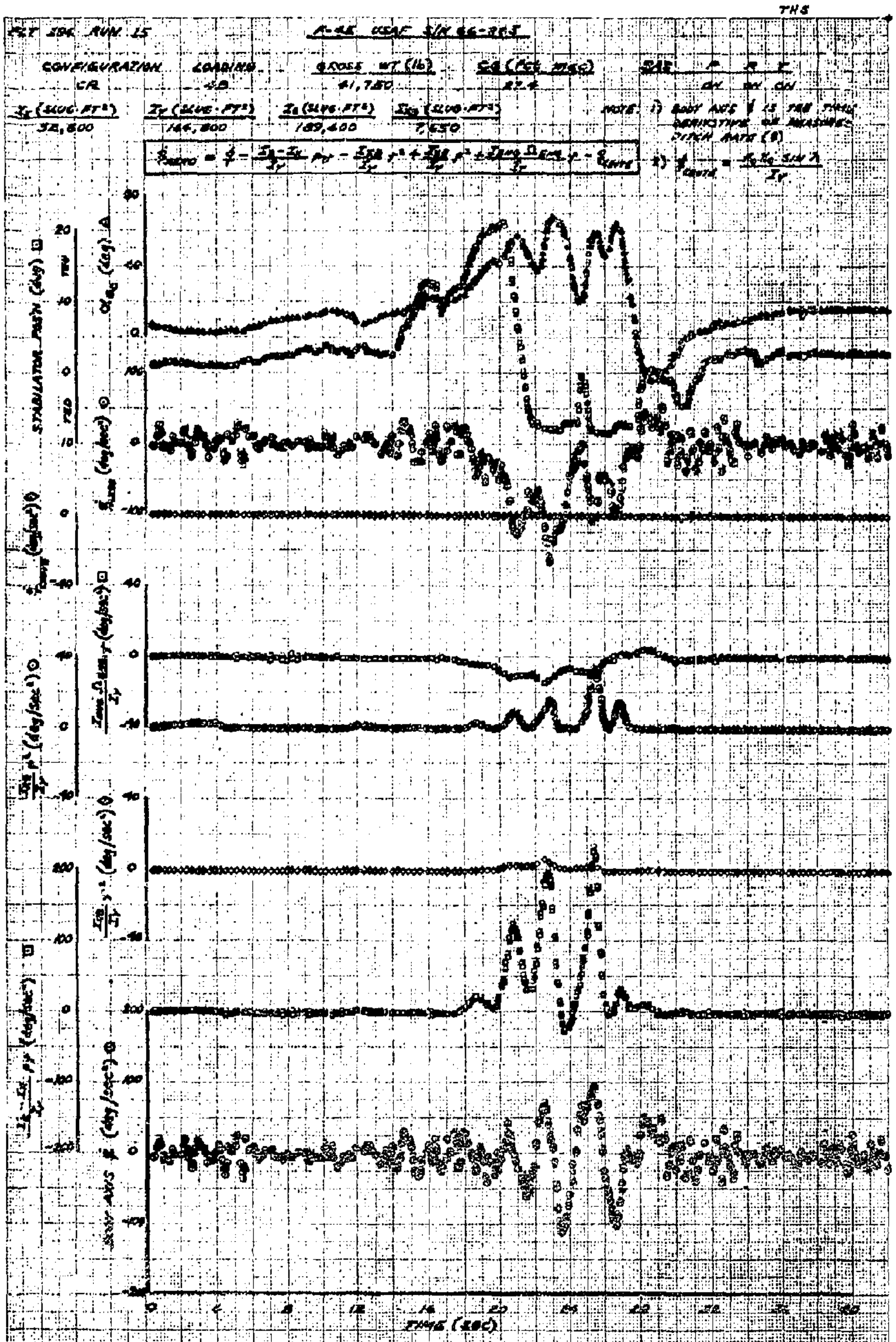

FIGURE 57 CONTINUED

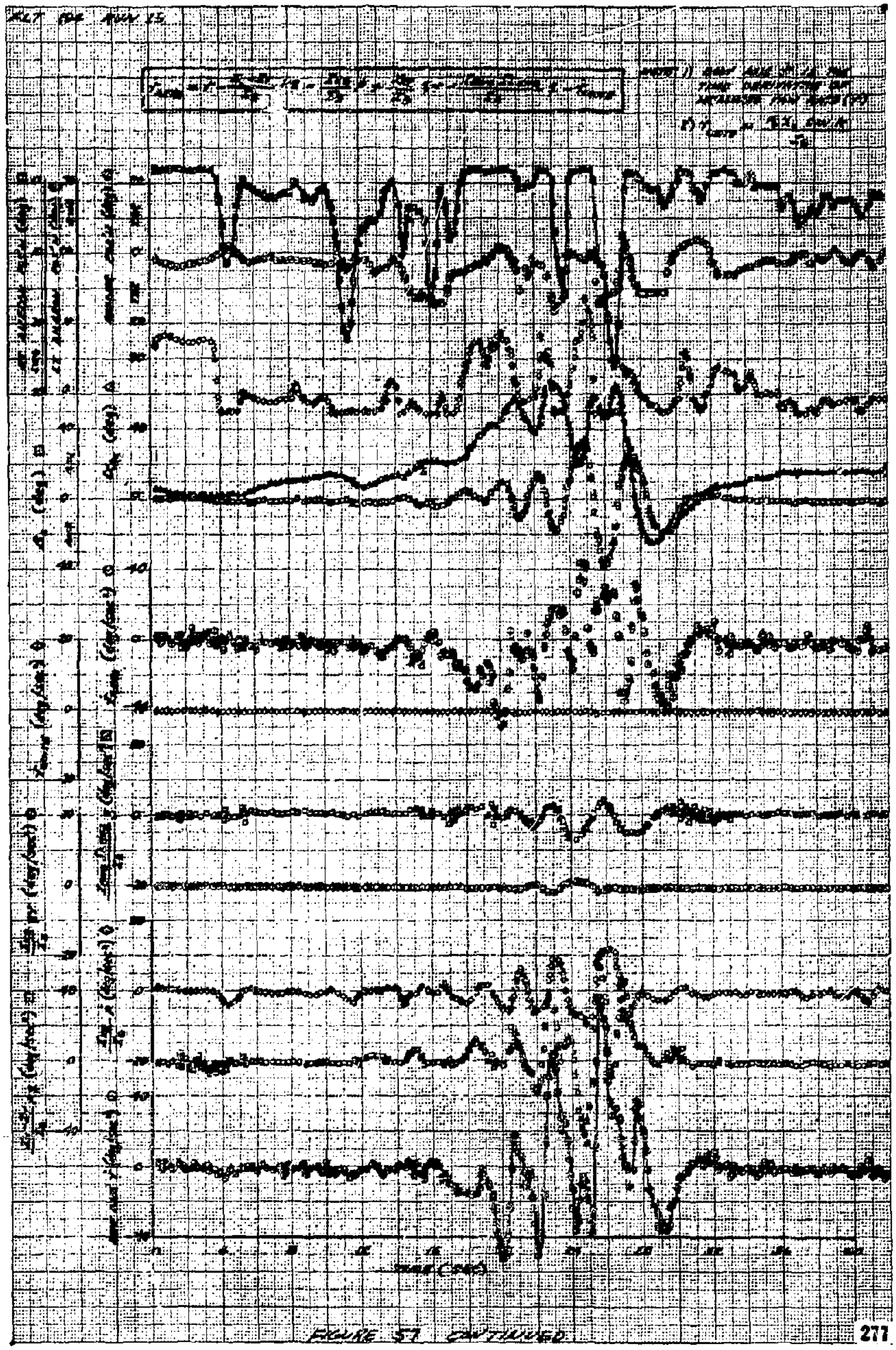

FIGURE 57 CONTINUED

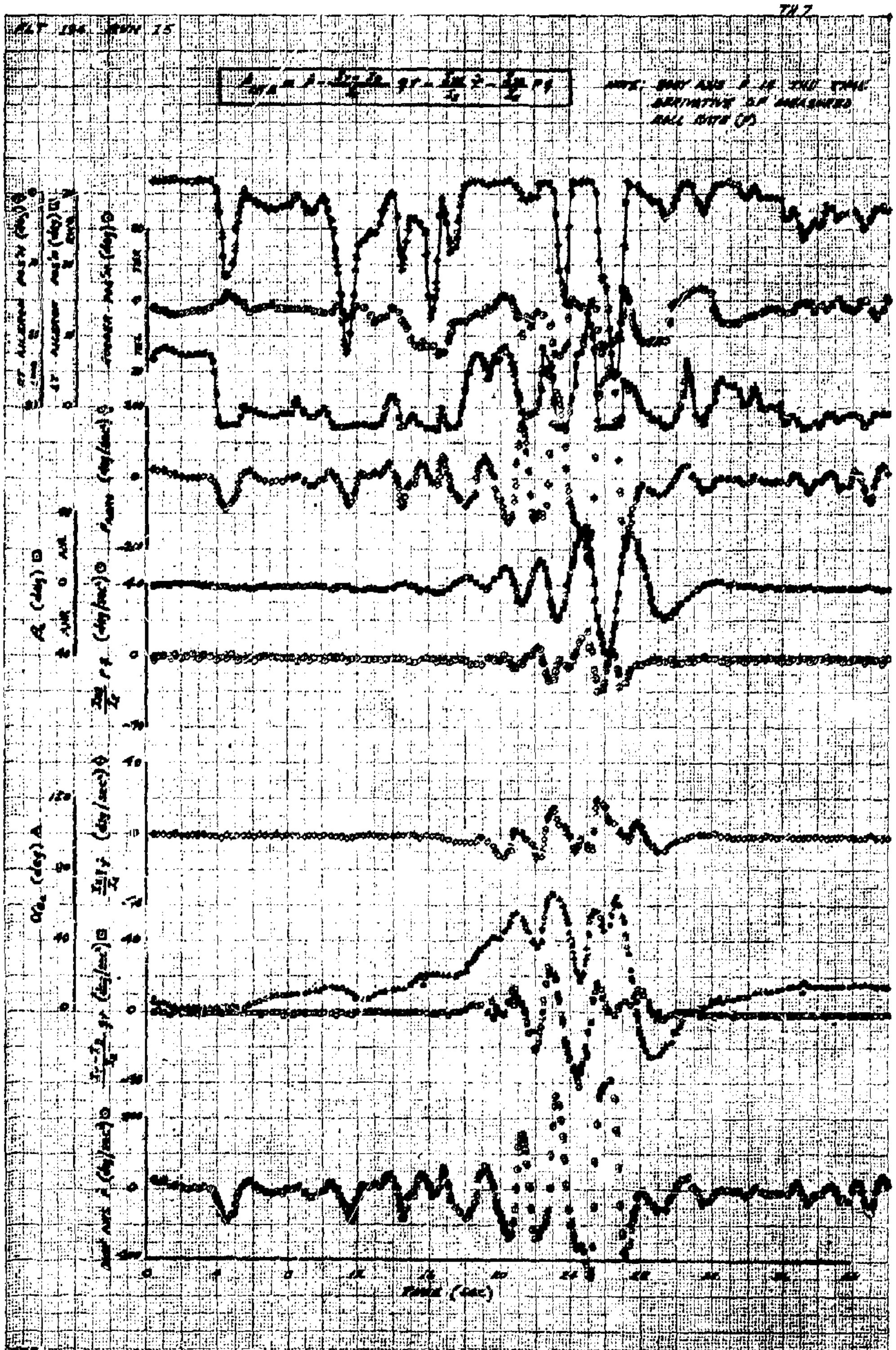

FIGURE 57 CONTINUED

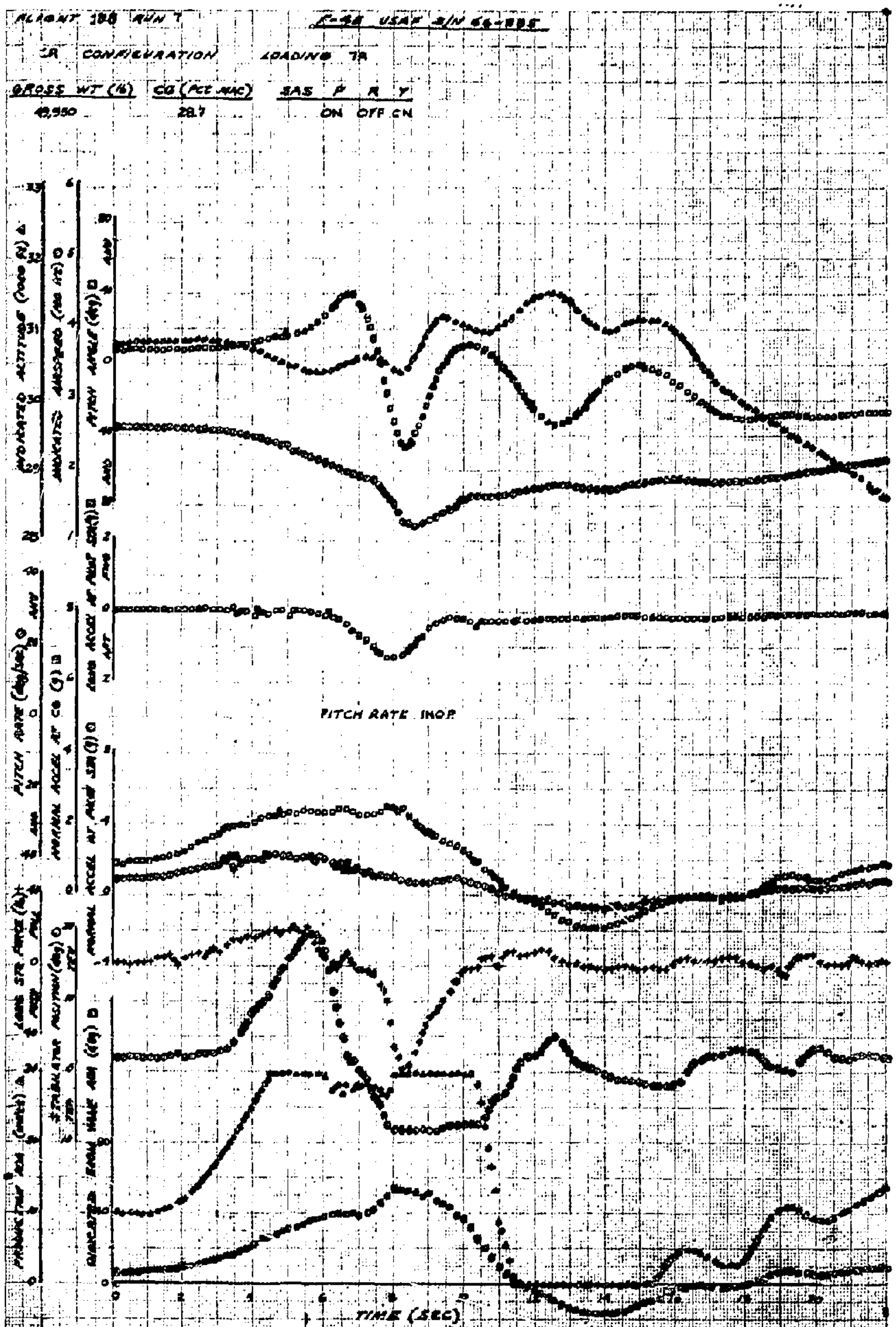

FIGURE 59 ROLLING DEPARTURE

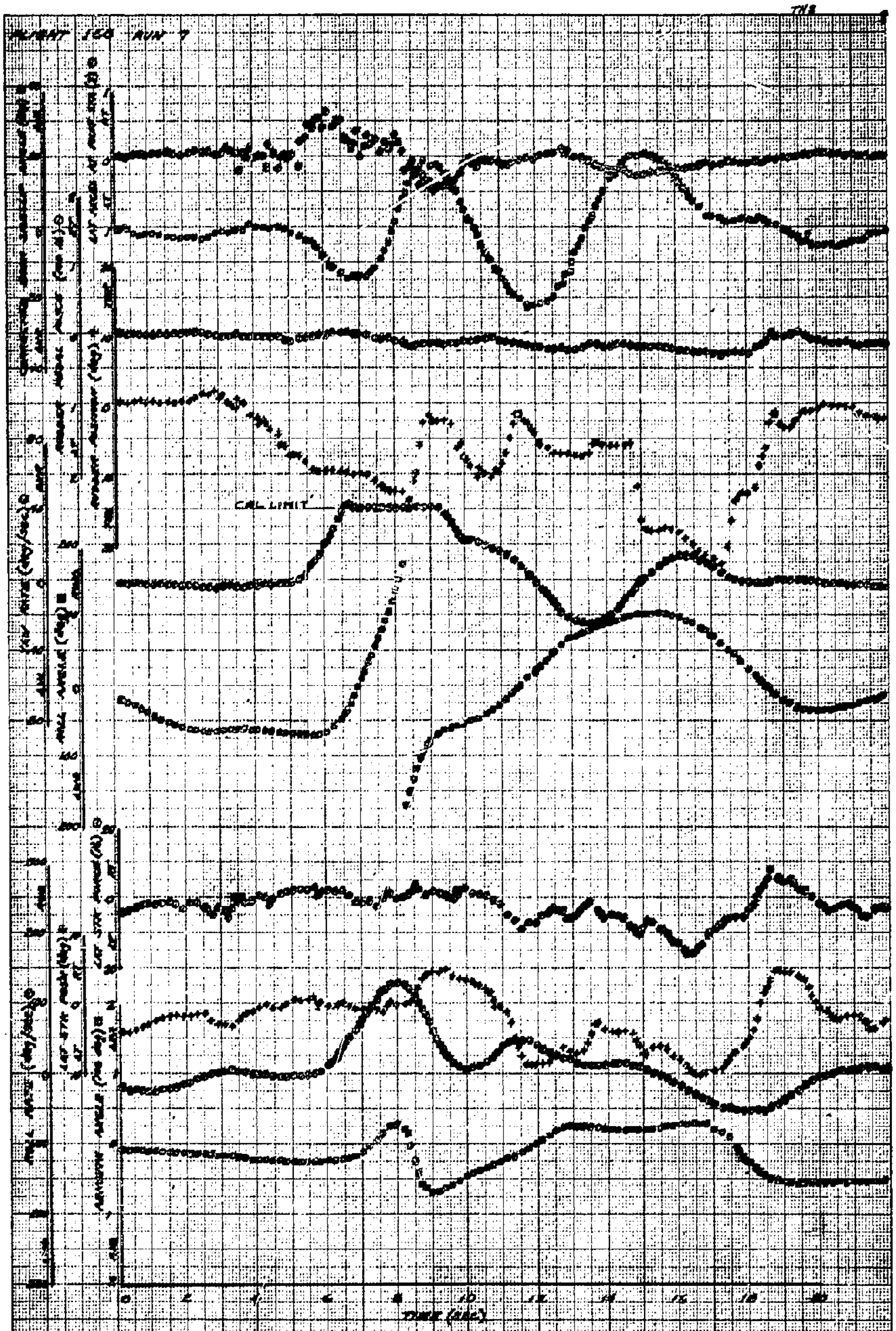

FIGURE 58 CONTINUED

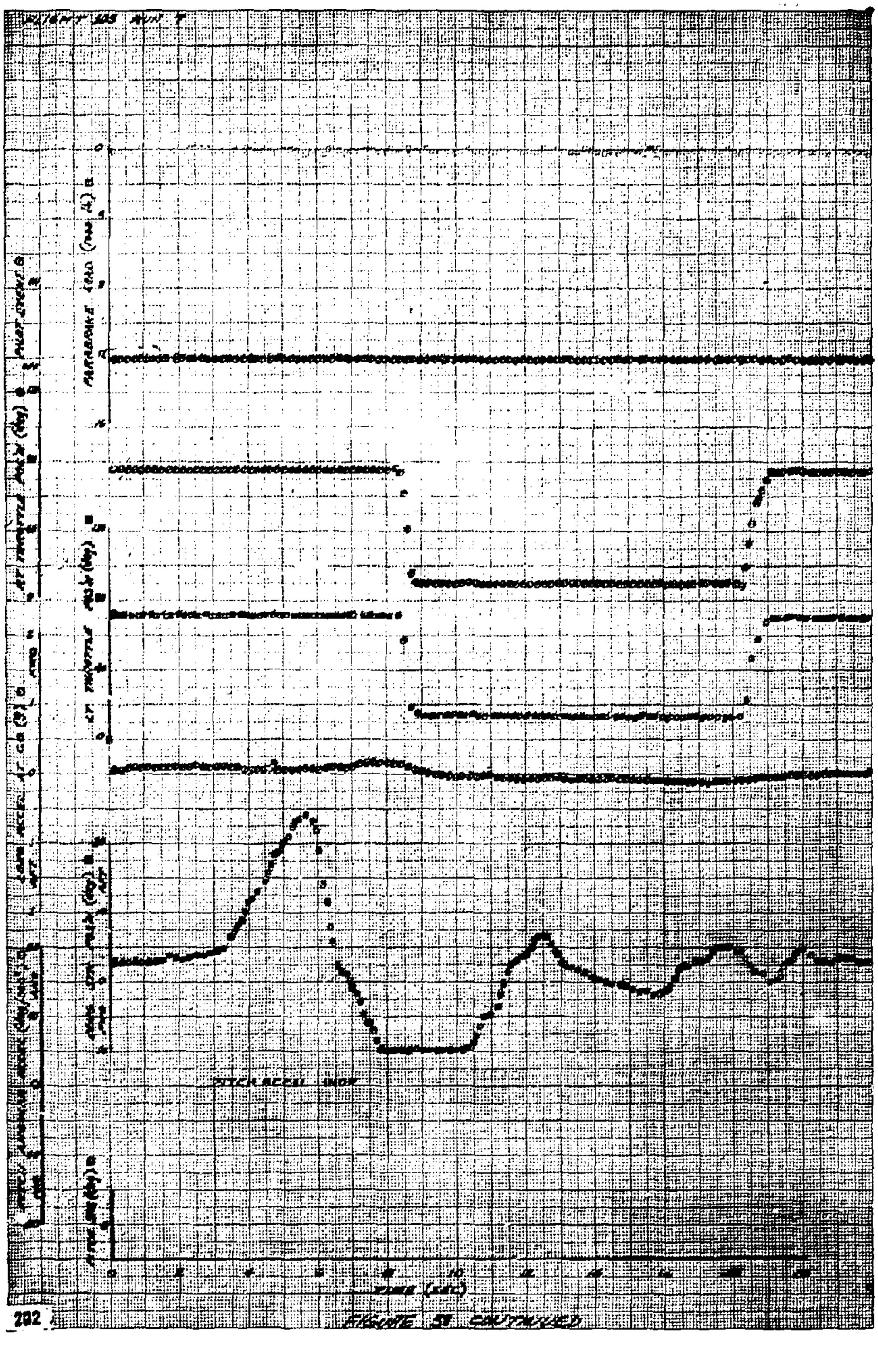

FIGURE 58 CONTINUED

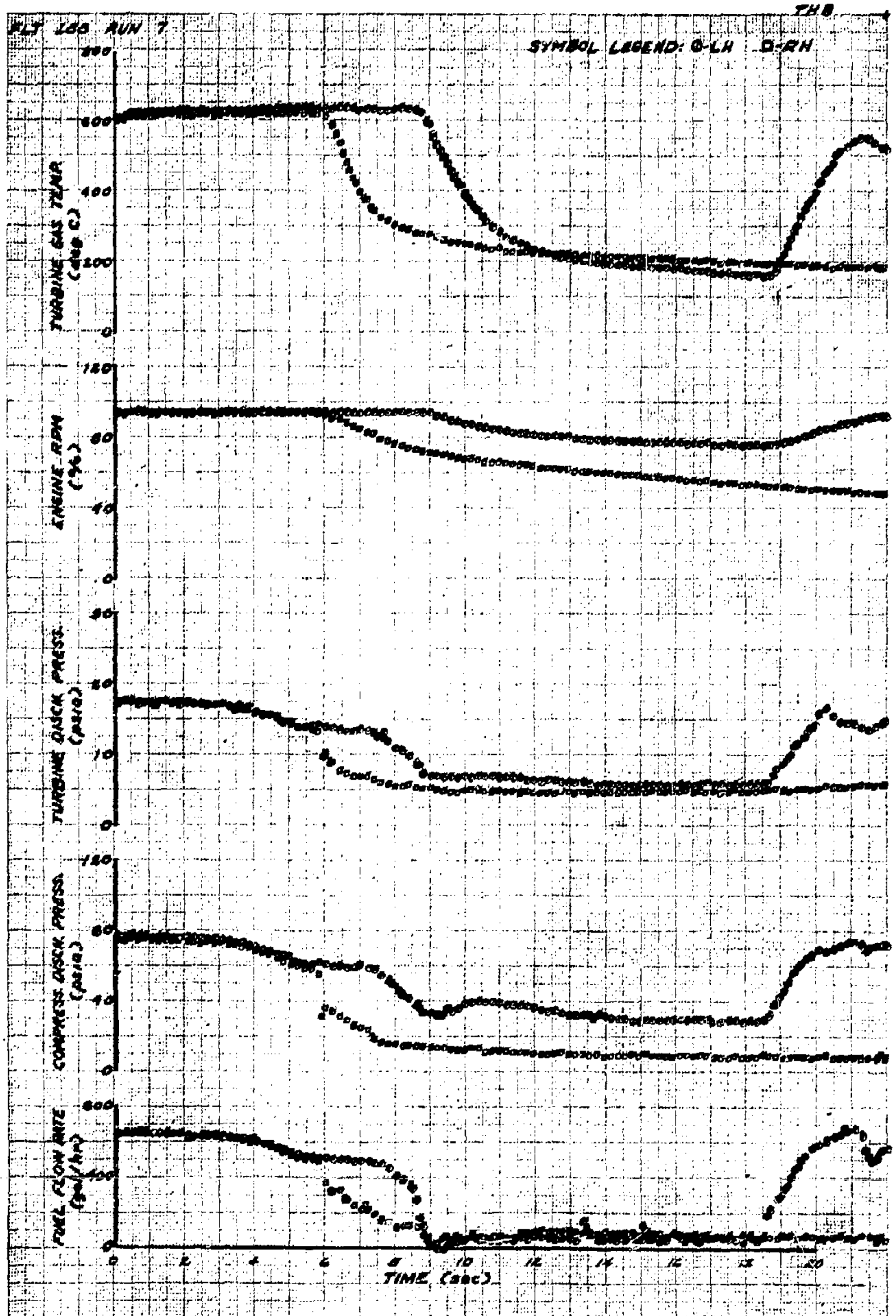

FIGURE 58 CONTINUED

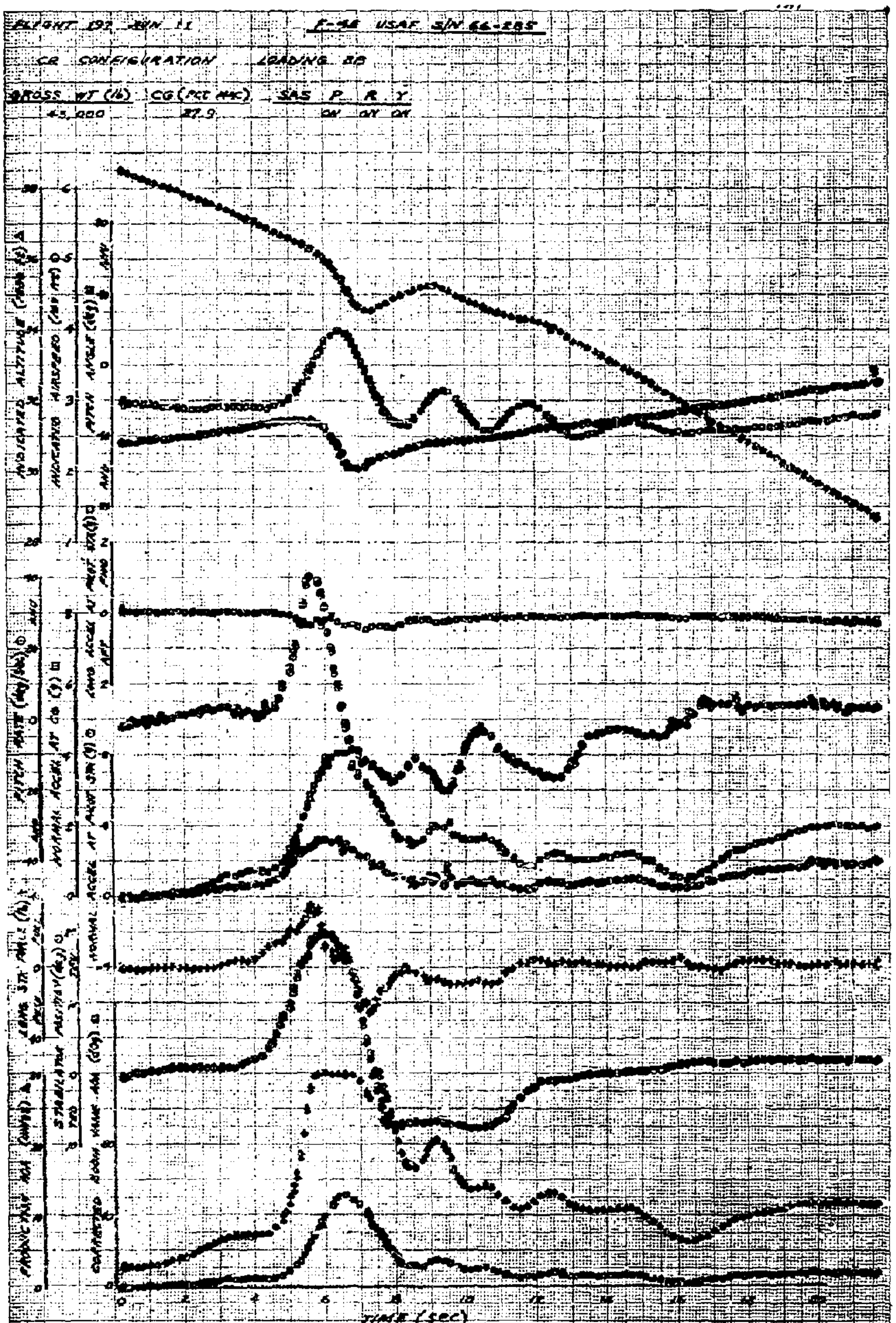

 FIGURE 59 RECOVERY ROLLS FROM A ROLLING DEPARTURE

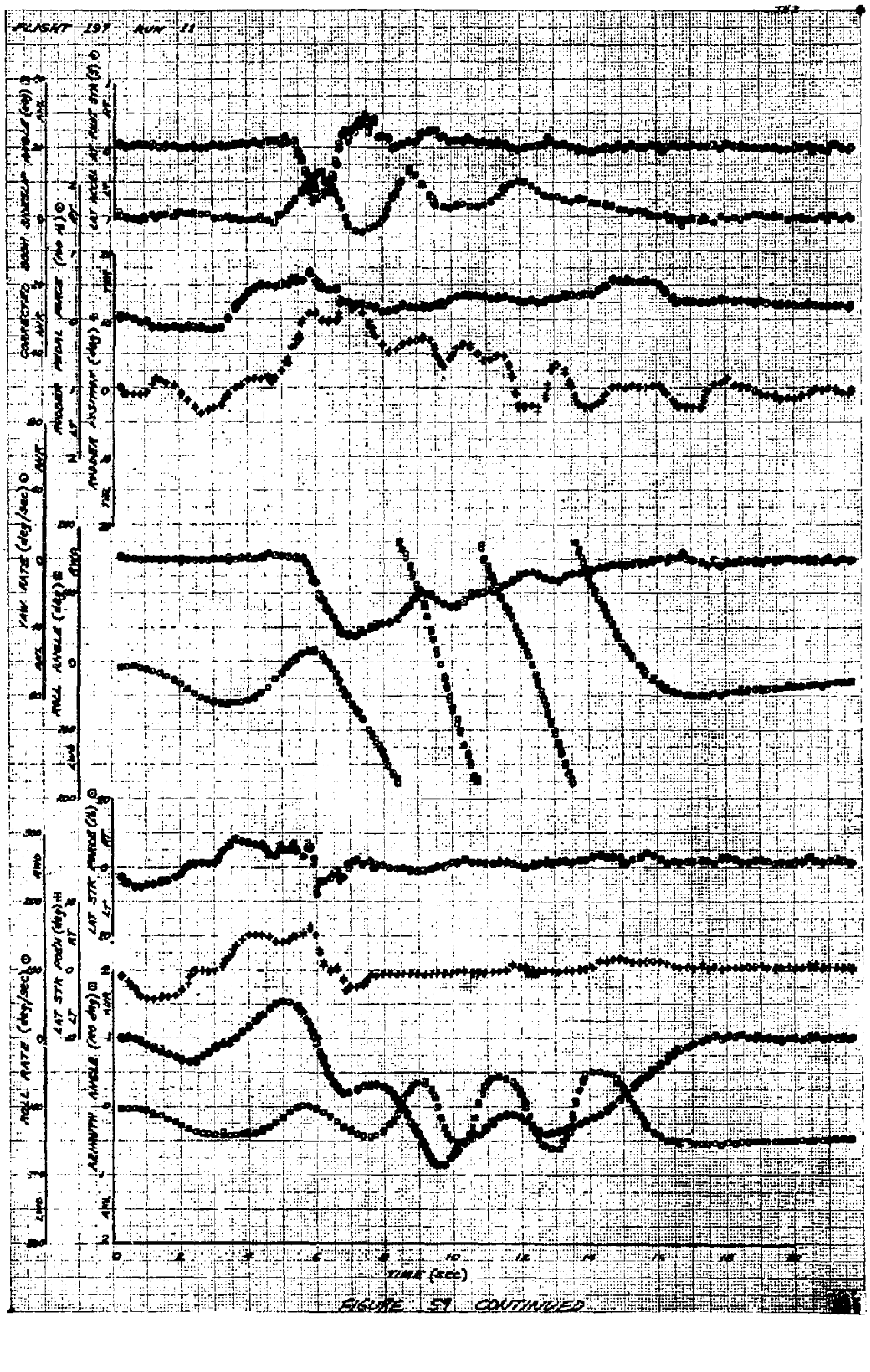

FIGURE 57 CONTINUED

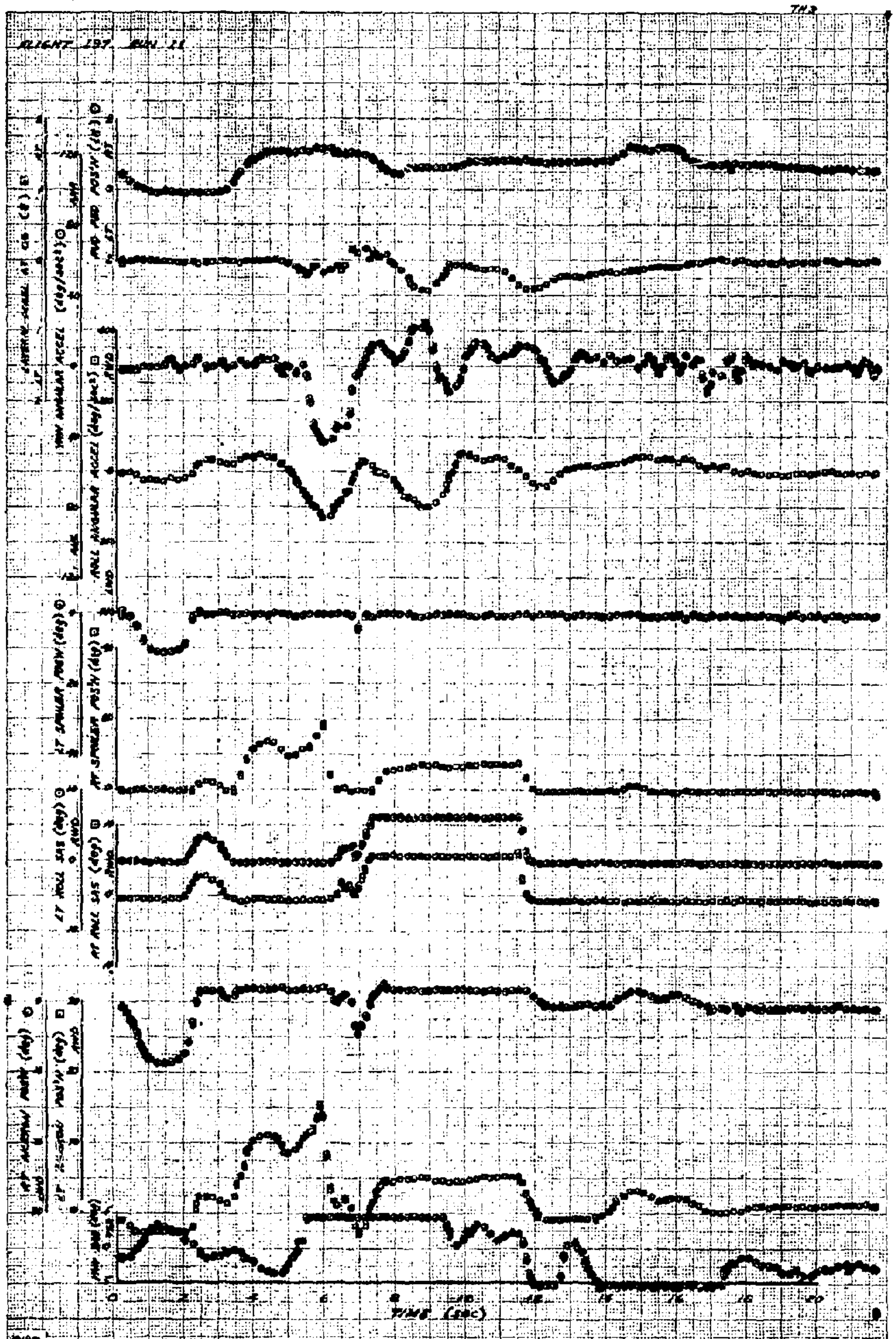

FIGURE 59 CONTINUED

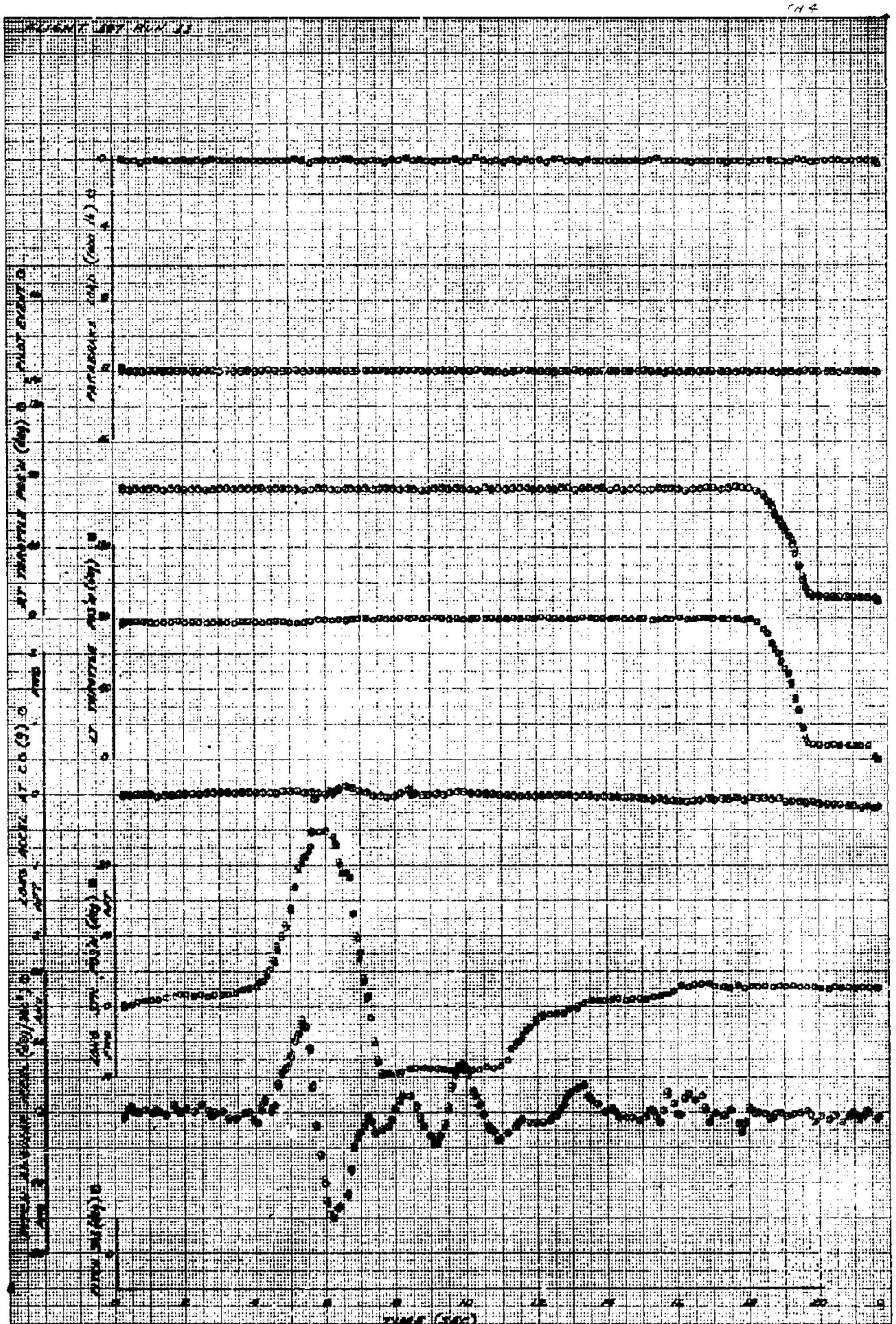

FIGURE 59 CONTINUED

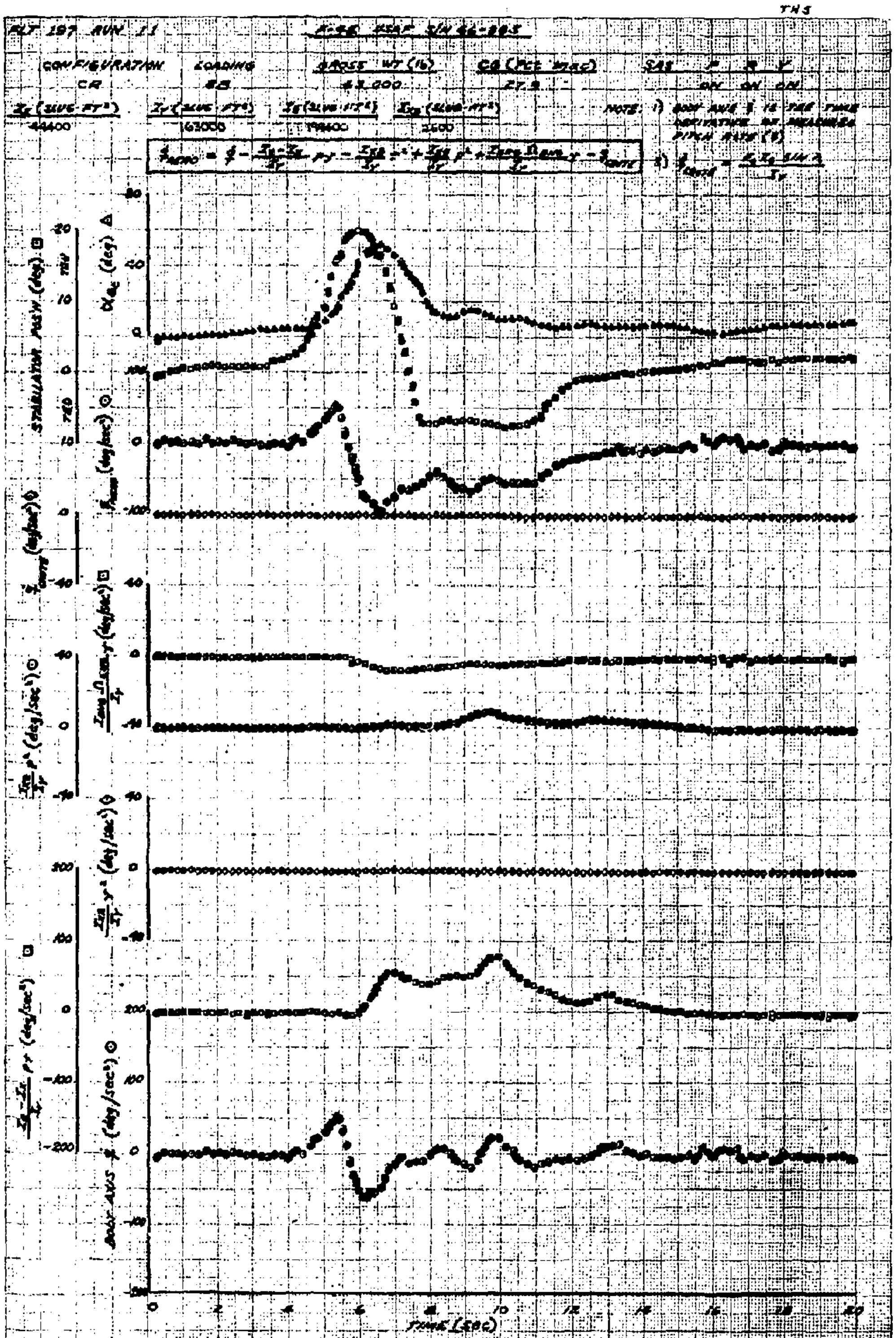

FIGURE 59 CONTINUED

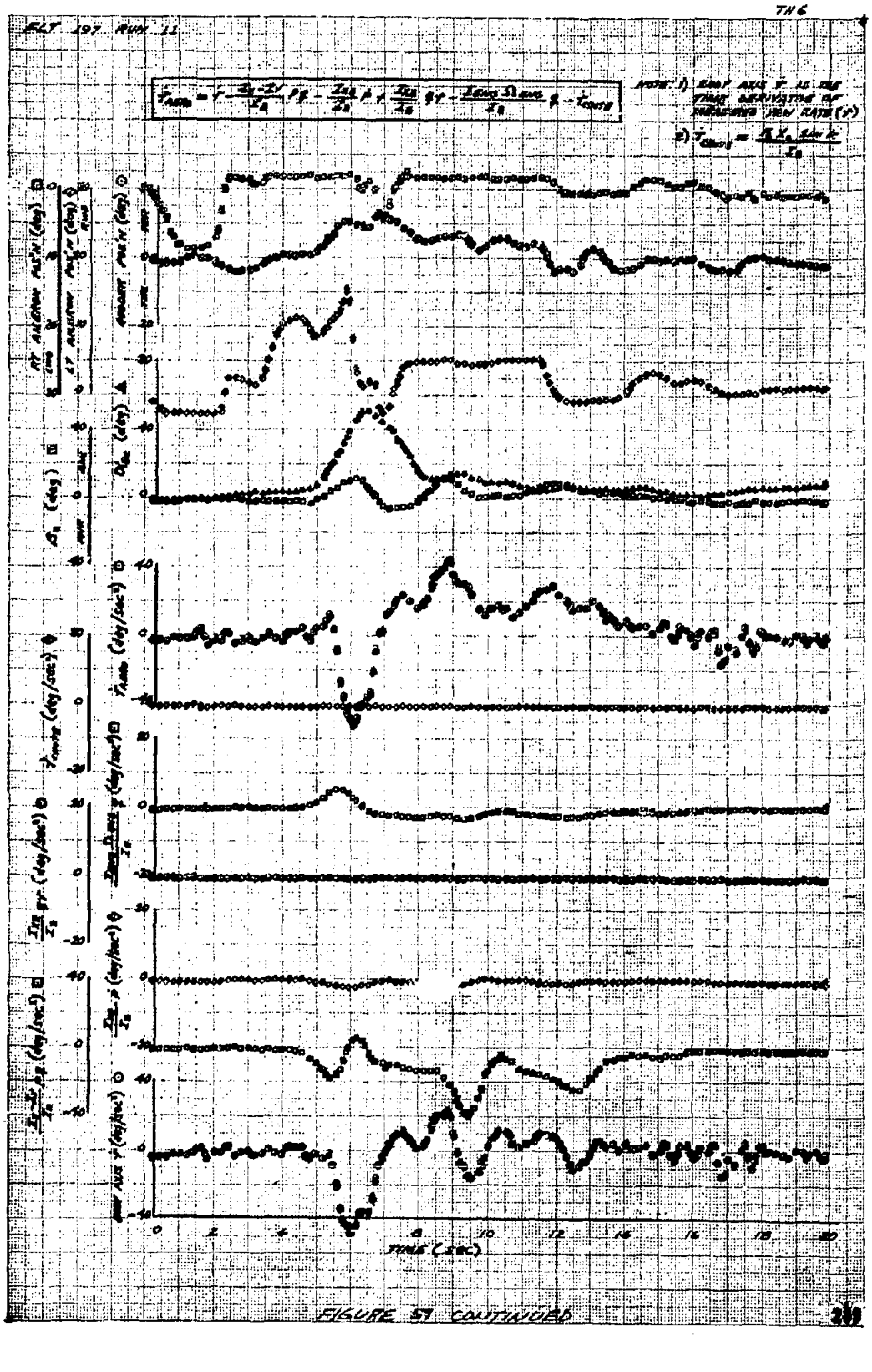

FIGURE 57 CONTINUED

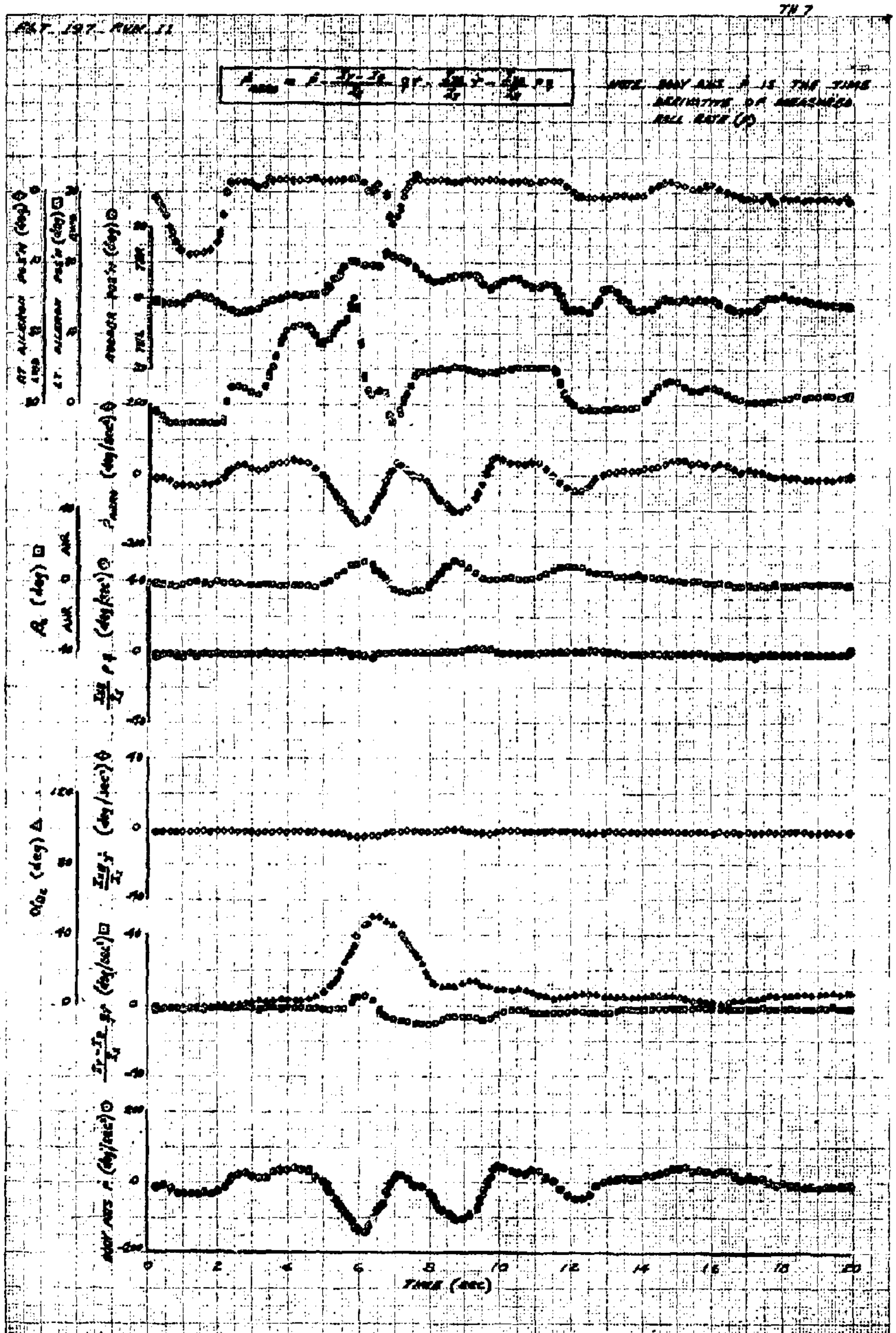

FIGURE 57 CONTINUED

PRECEDING PAGE BLANK-NOT FILMED

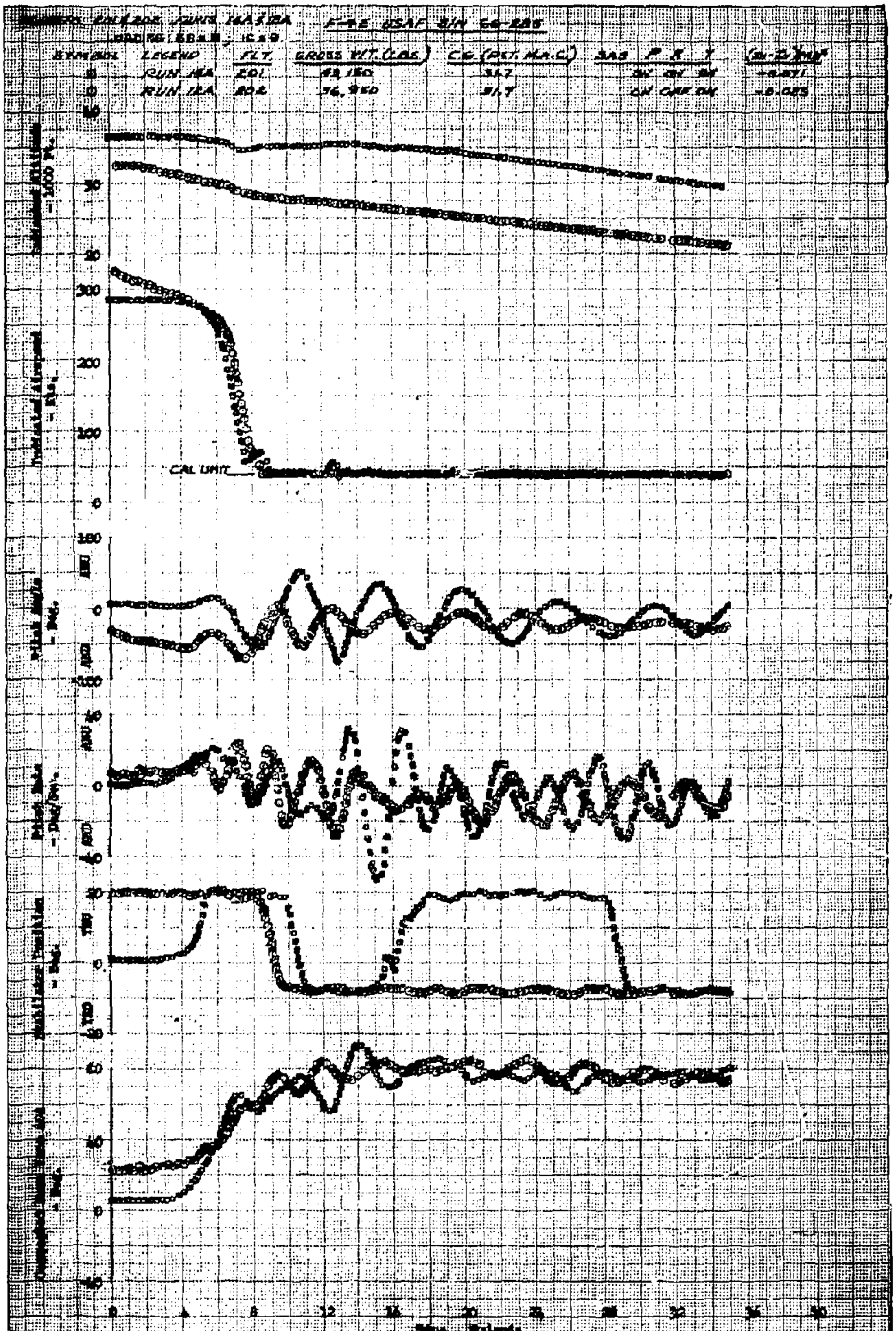

 FIGURE 60 COMPARISON OF FLAT SPIN ENTRIES

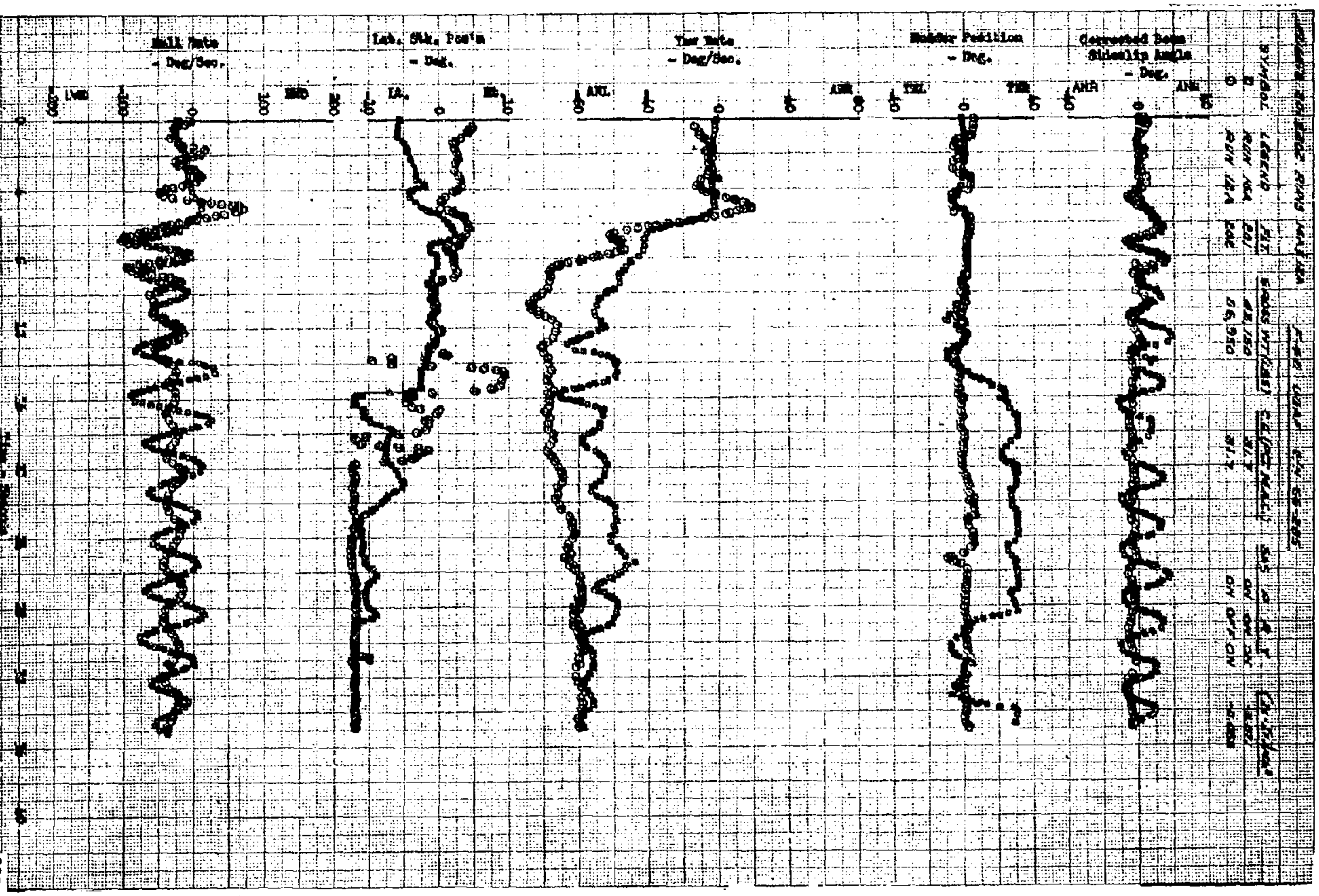

FIGURE 60 CONTINUED

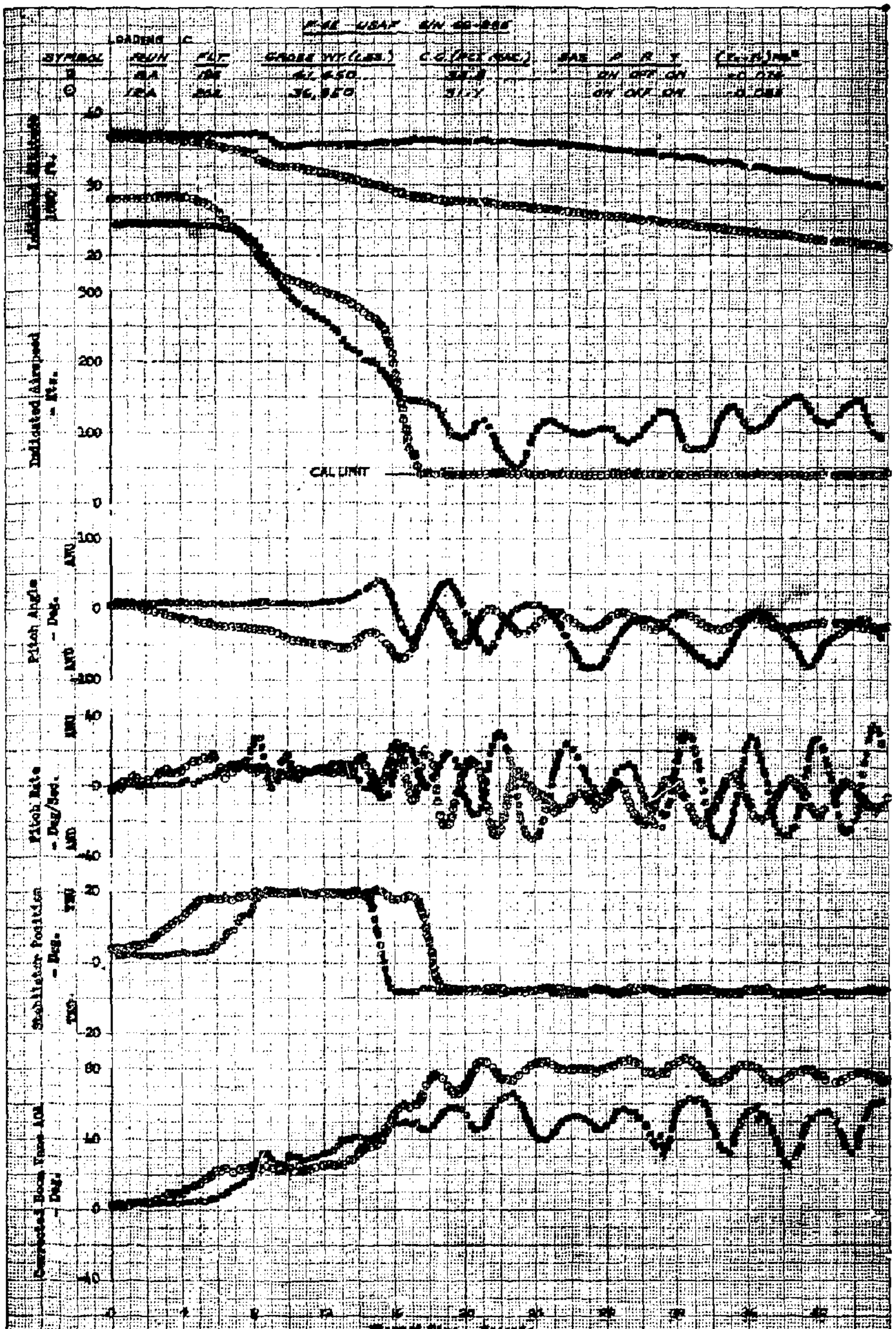

FIGURE 61 COMPARISON OF FLAT AND STEEP MILDLY OSCILLATORY SPIN CURVES

F-4E USAF S/N 66-283

SYMBOL	RUN	TP	GROSS WT (LBS)	C.G. (PCT MAC)	SAS P R Y	C_{l}-TRIM
○	22	188	41,450	32.8	ON OFF ON	-0.002
○	126	206	36,950	31.7	ON OFF ON	-0.003

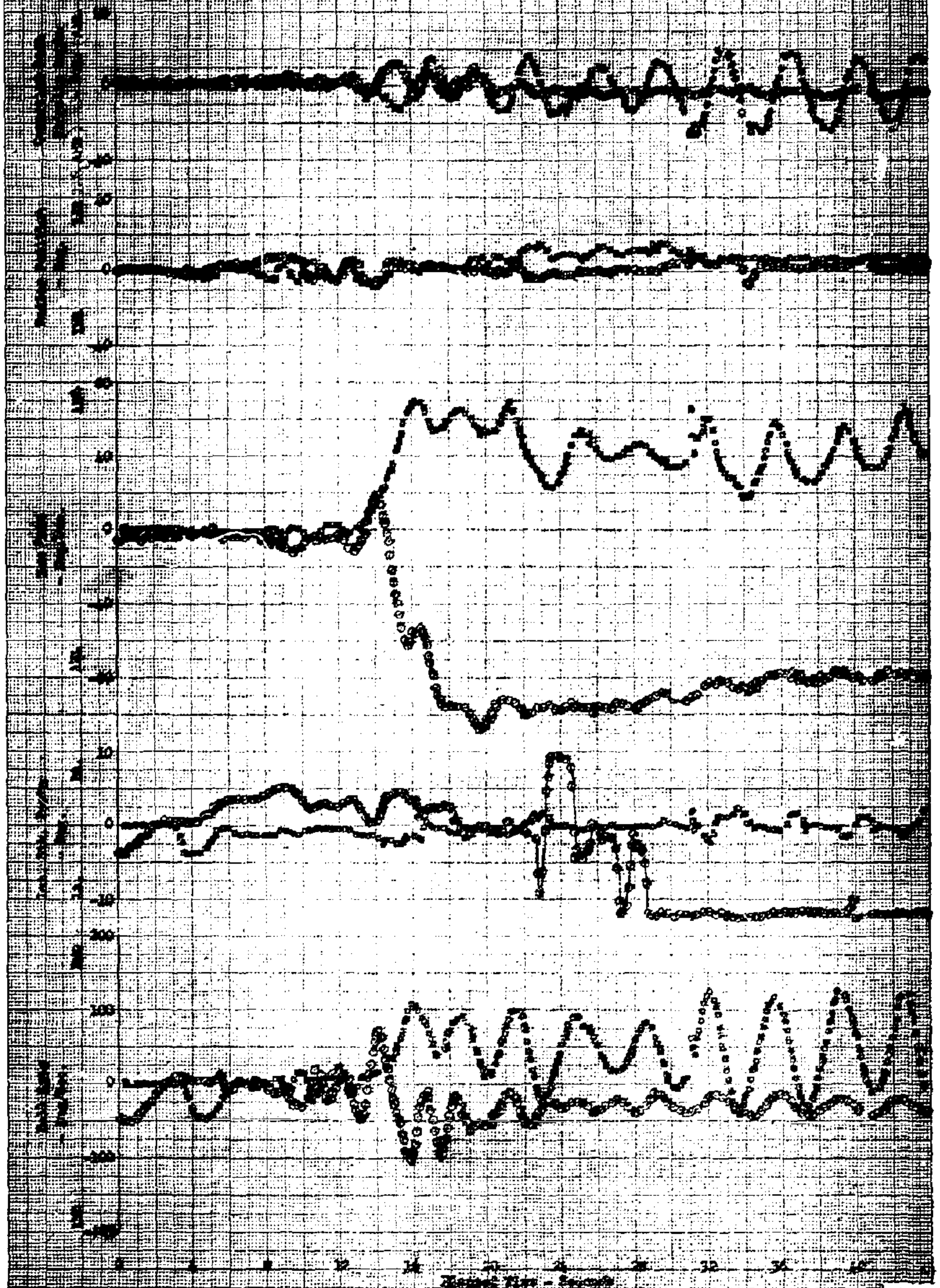

FIGURE 61 CONTINUED

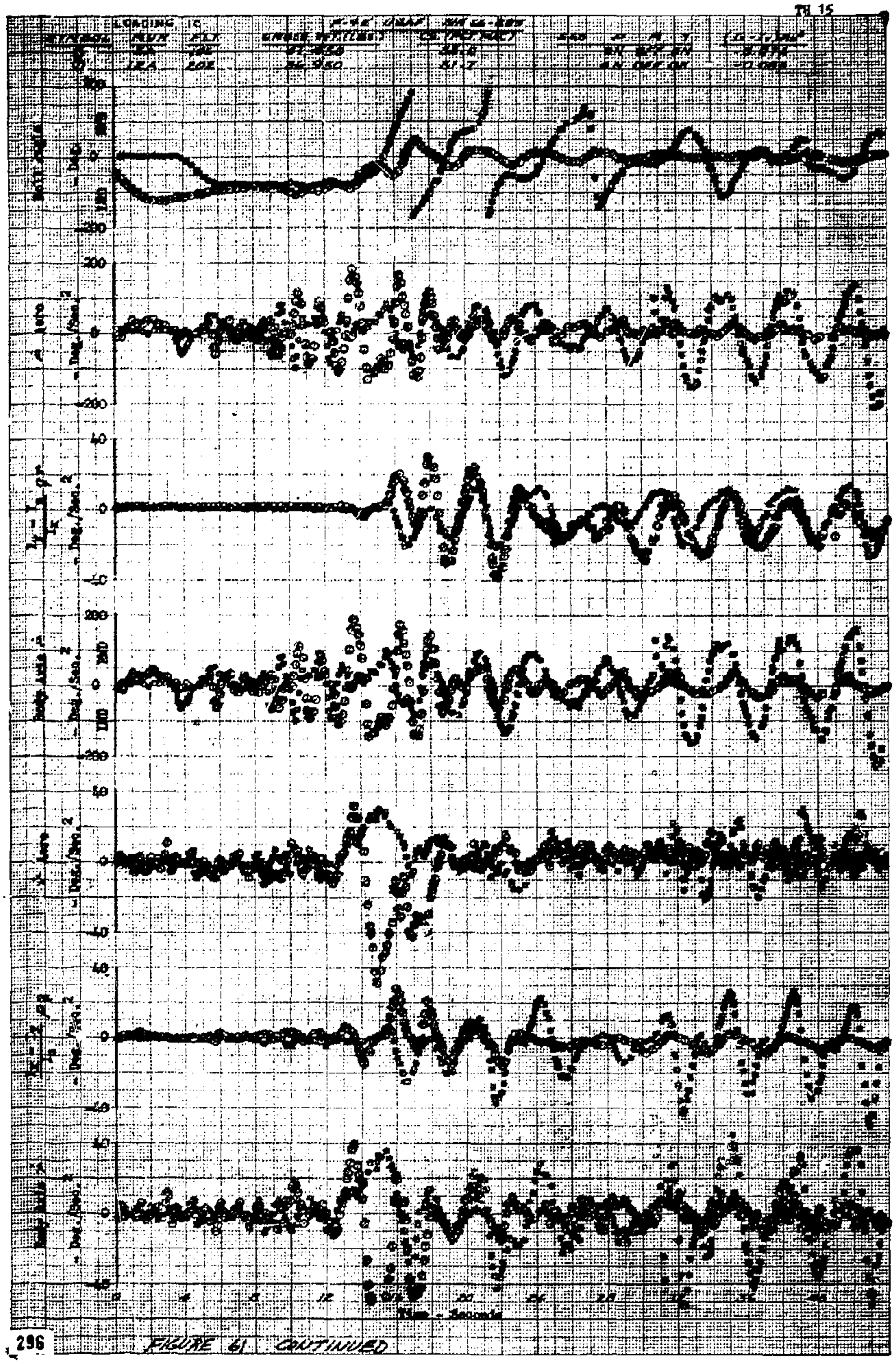

FIGURE 61 CONTINUED

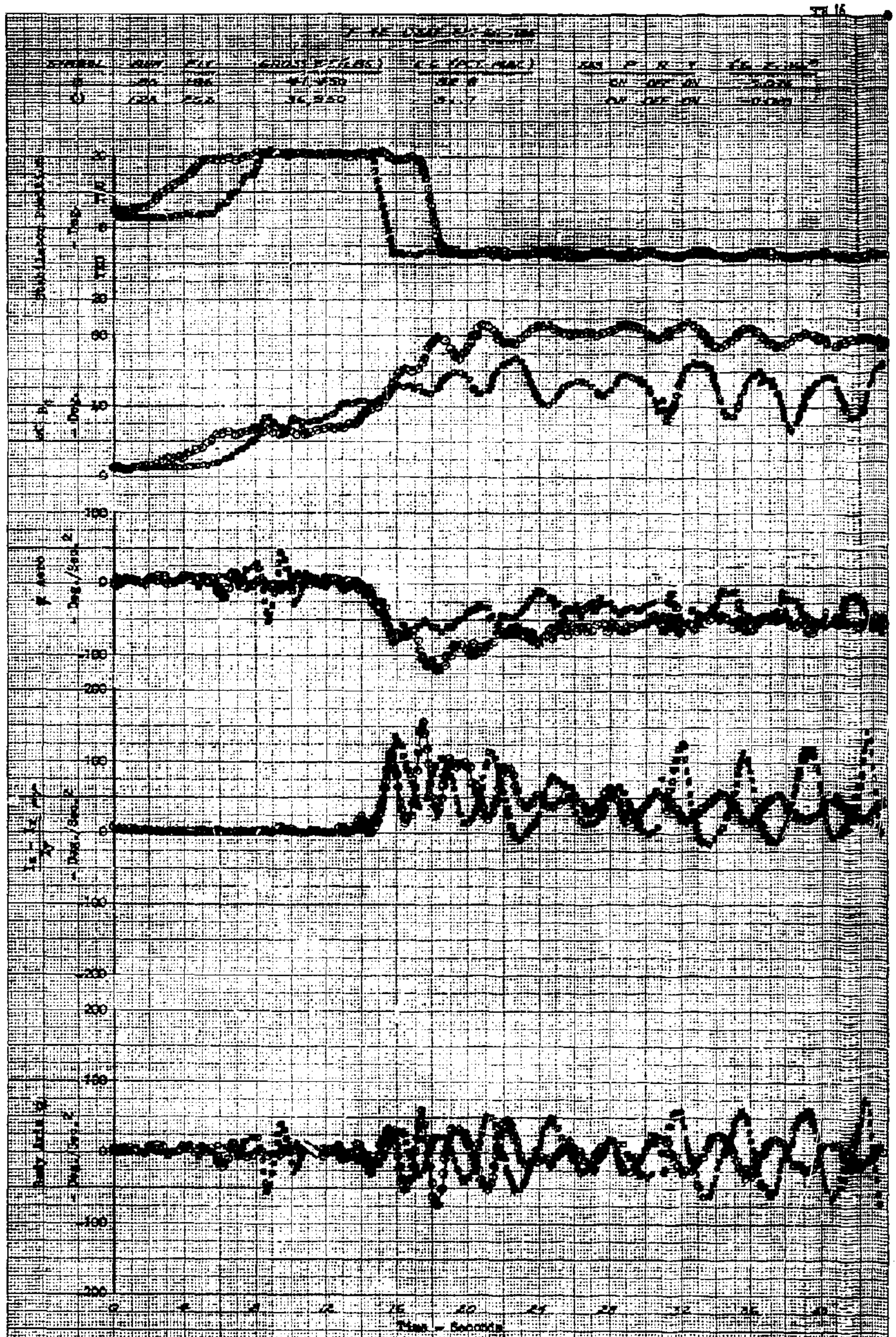

FIGURE 61 CONTINUED

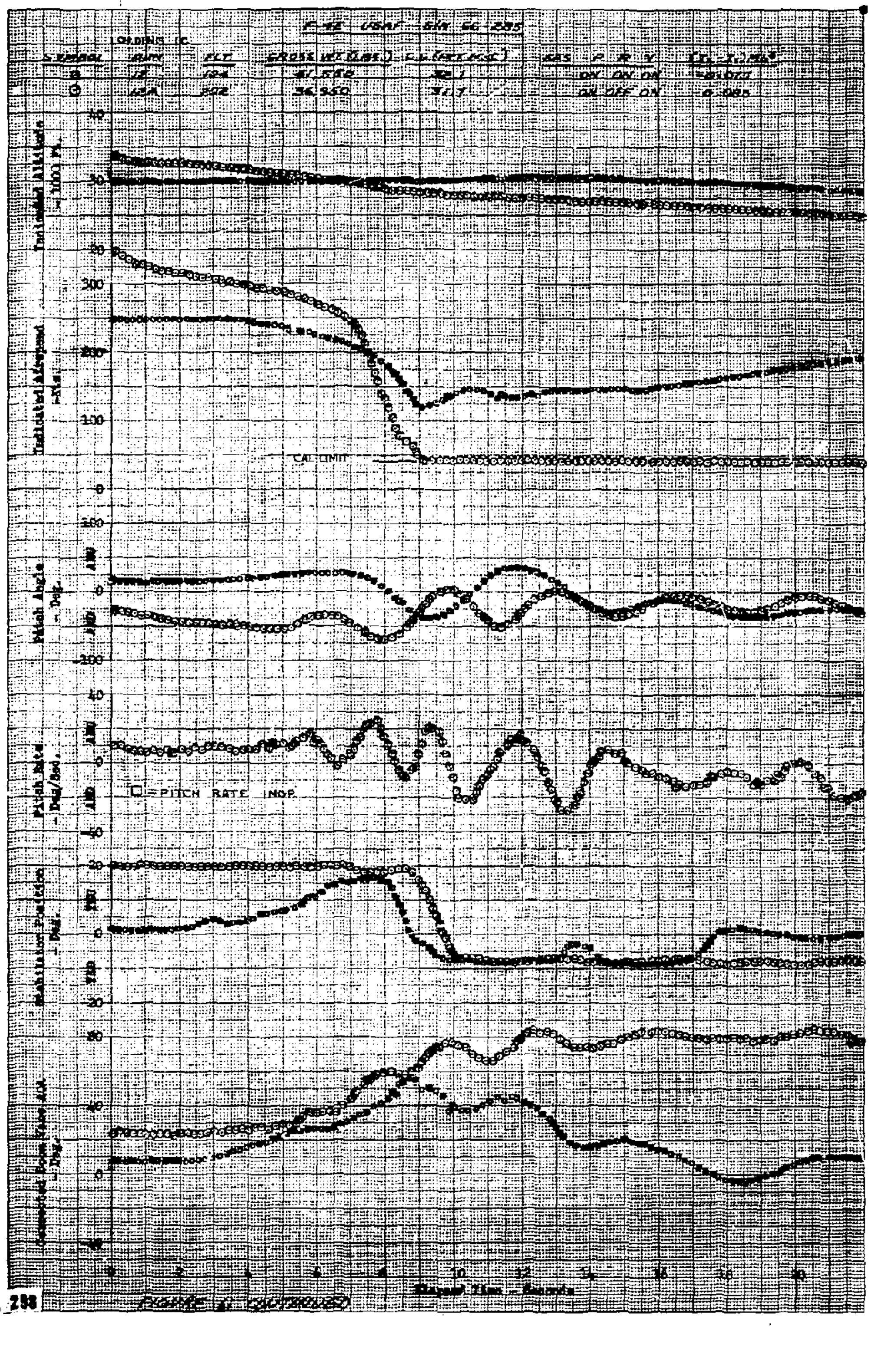

FIGURE 11 (CONTINUED)

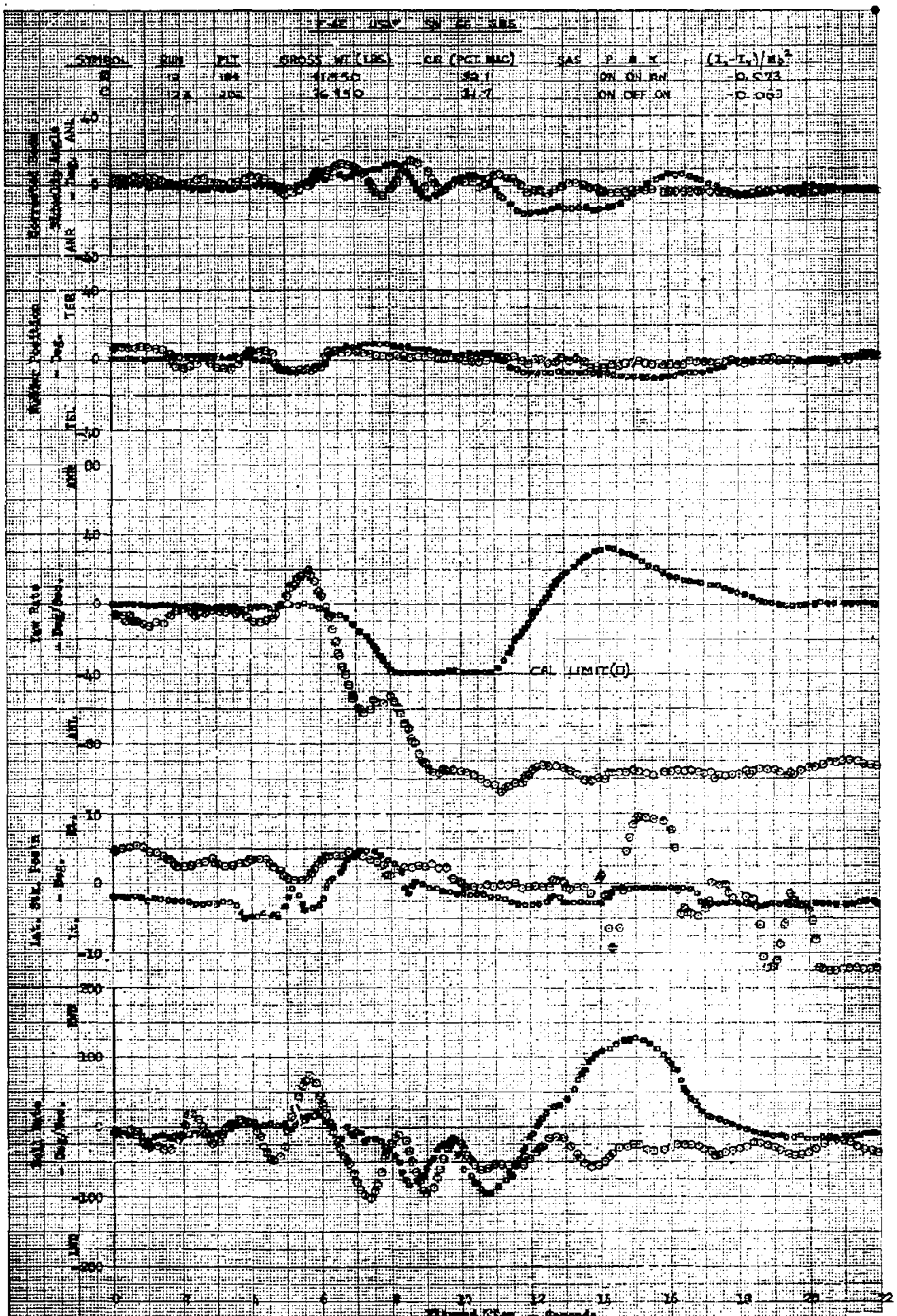

FIGURE 21 CONTINUED

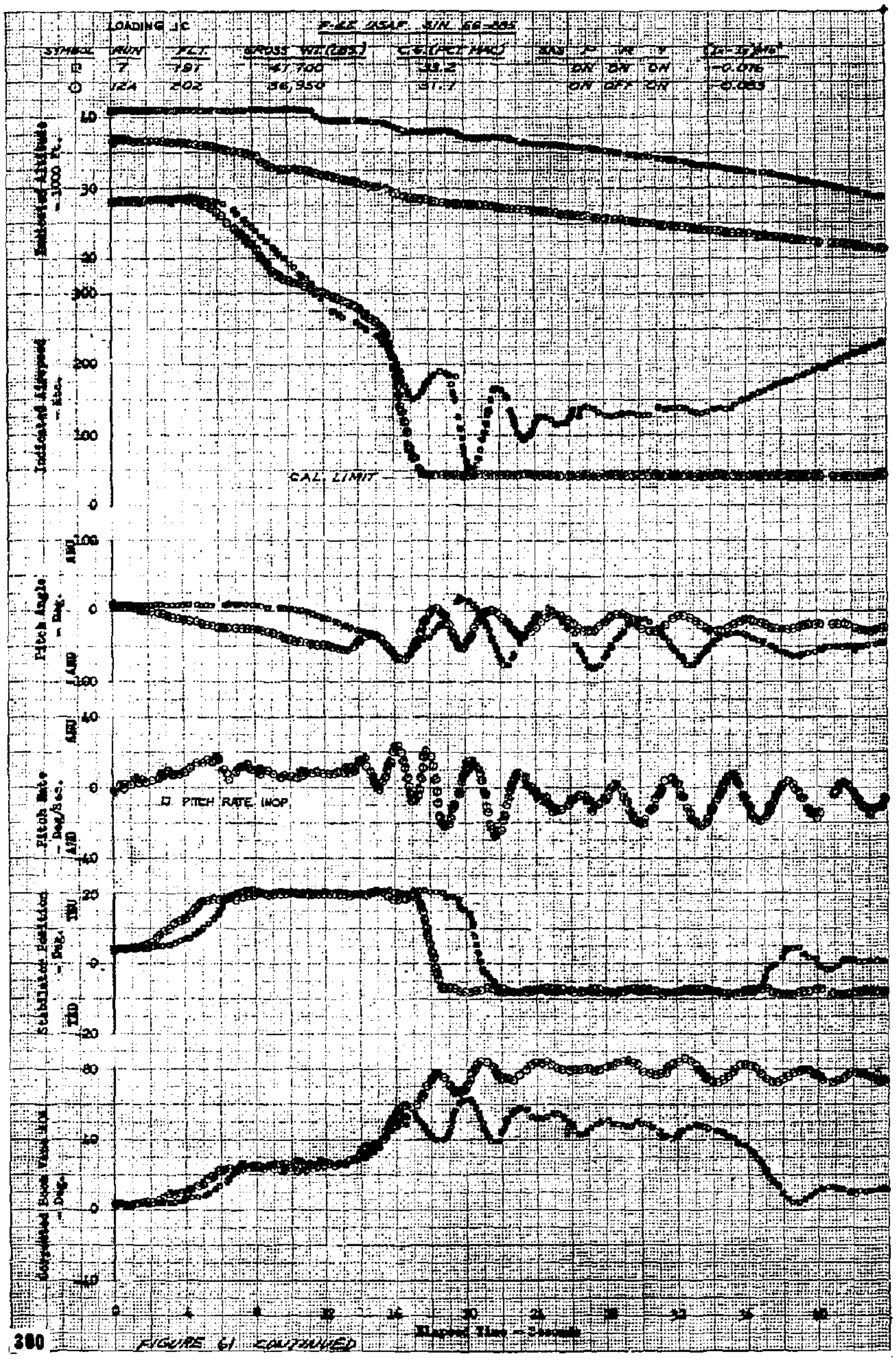

FIGURE 61 CONTINUED

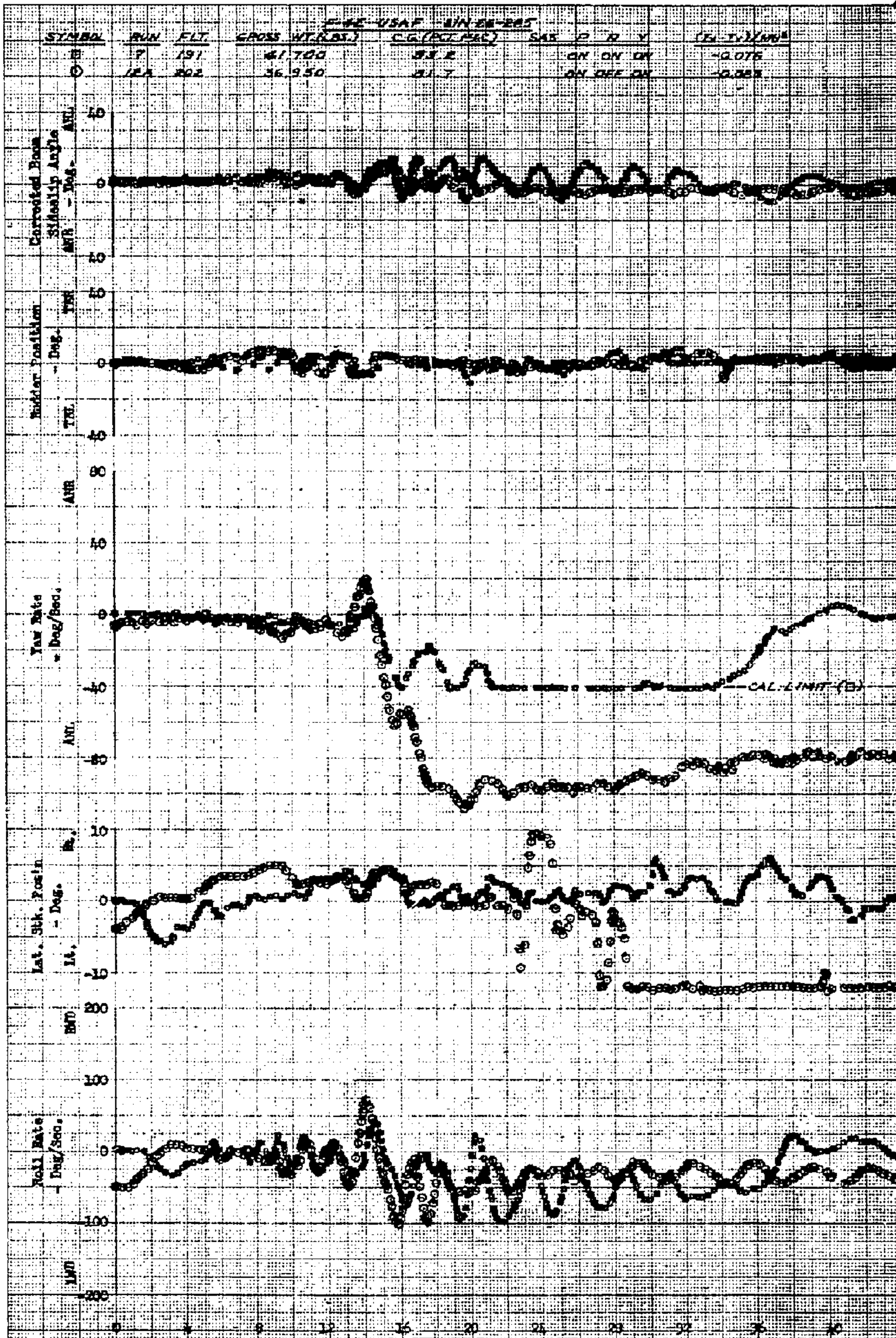

FIGURE 61 CONTINUED

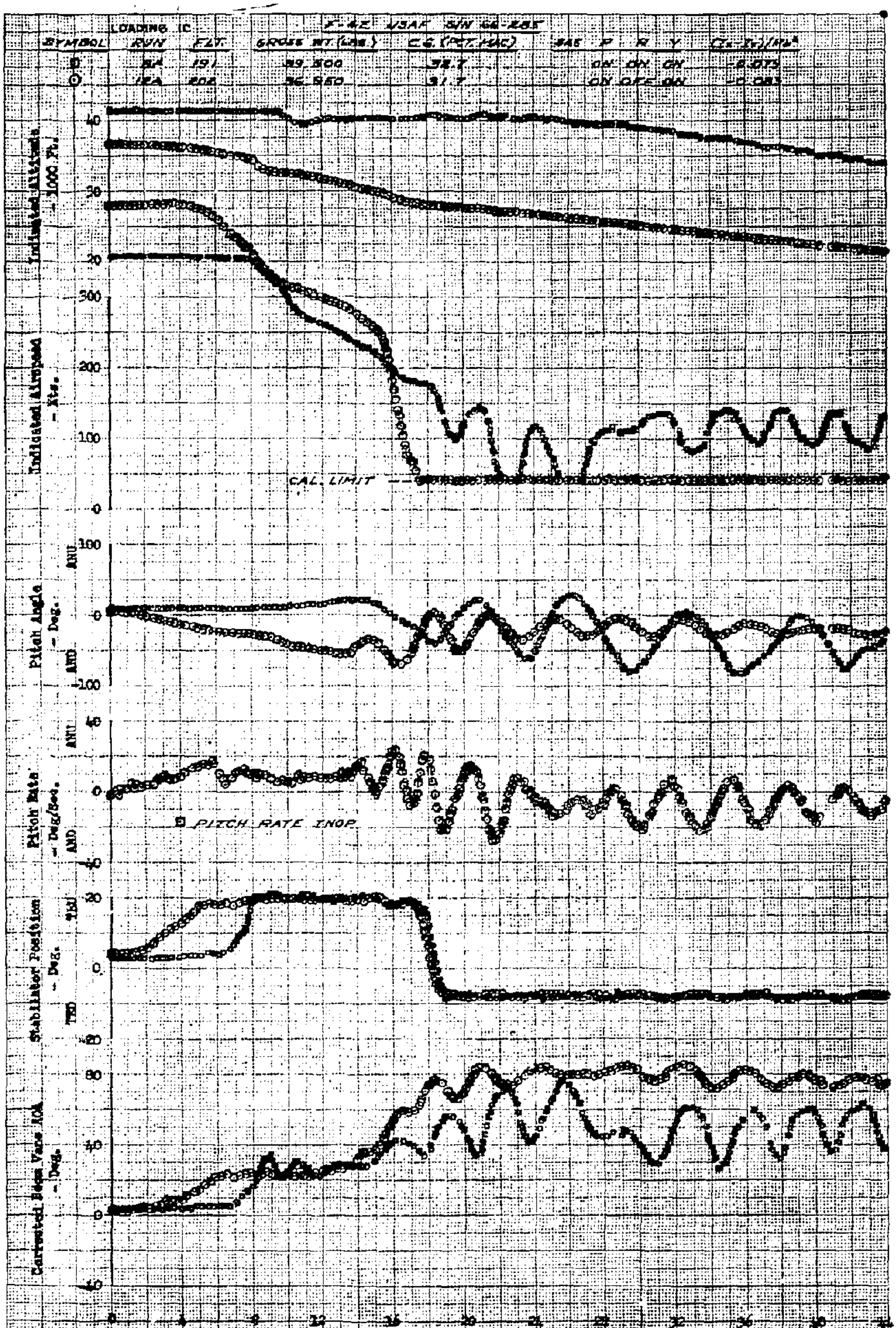

FIGURE 61 CONTINUED

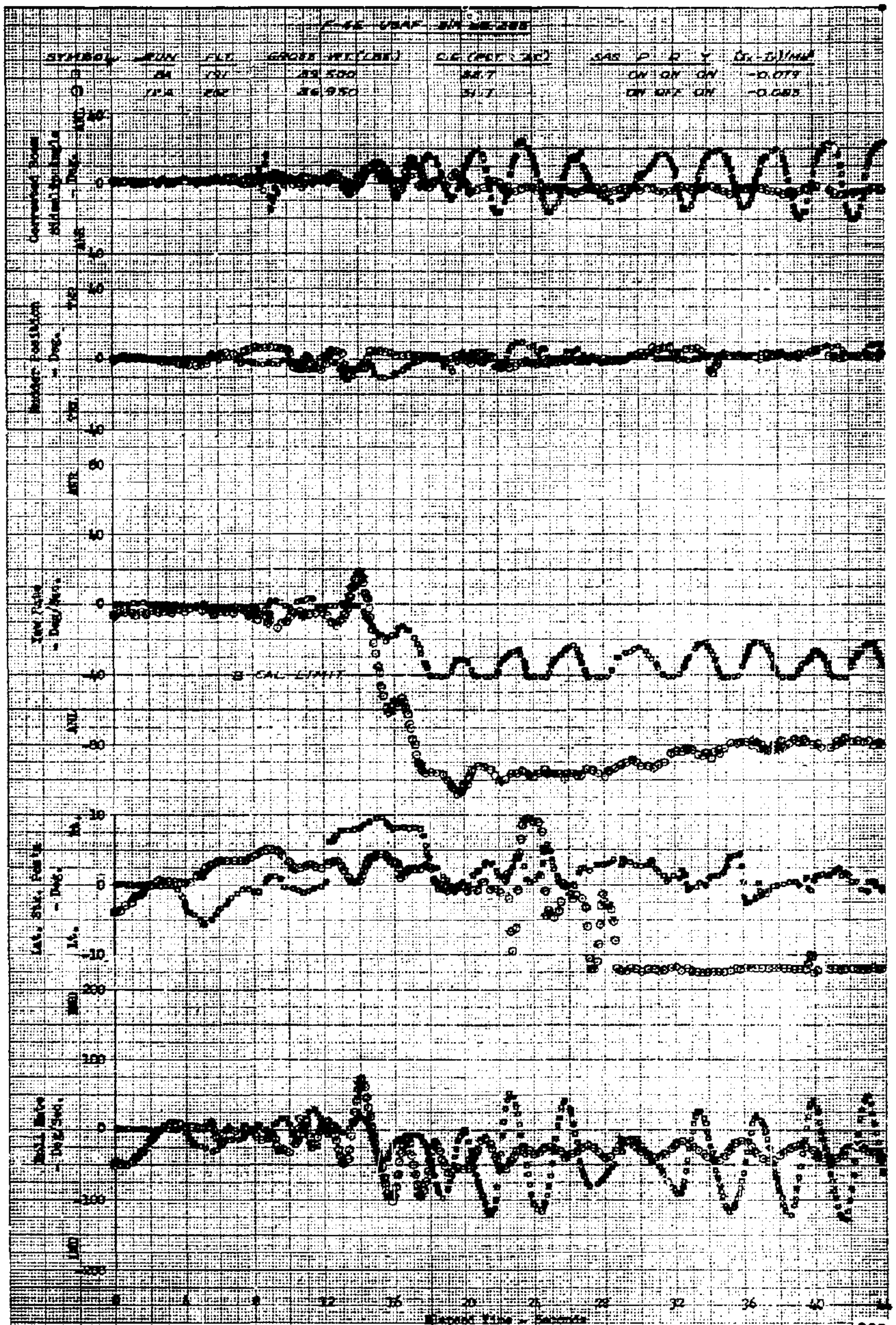

FIGURE 61 CONTINUED

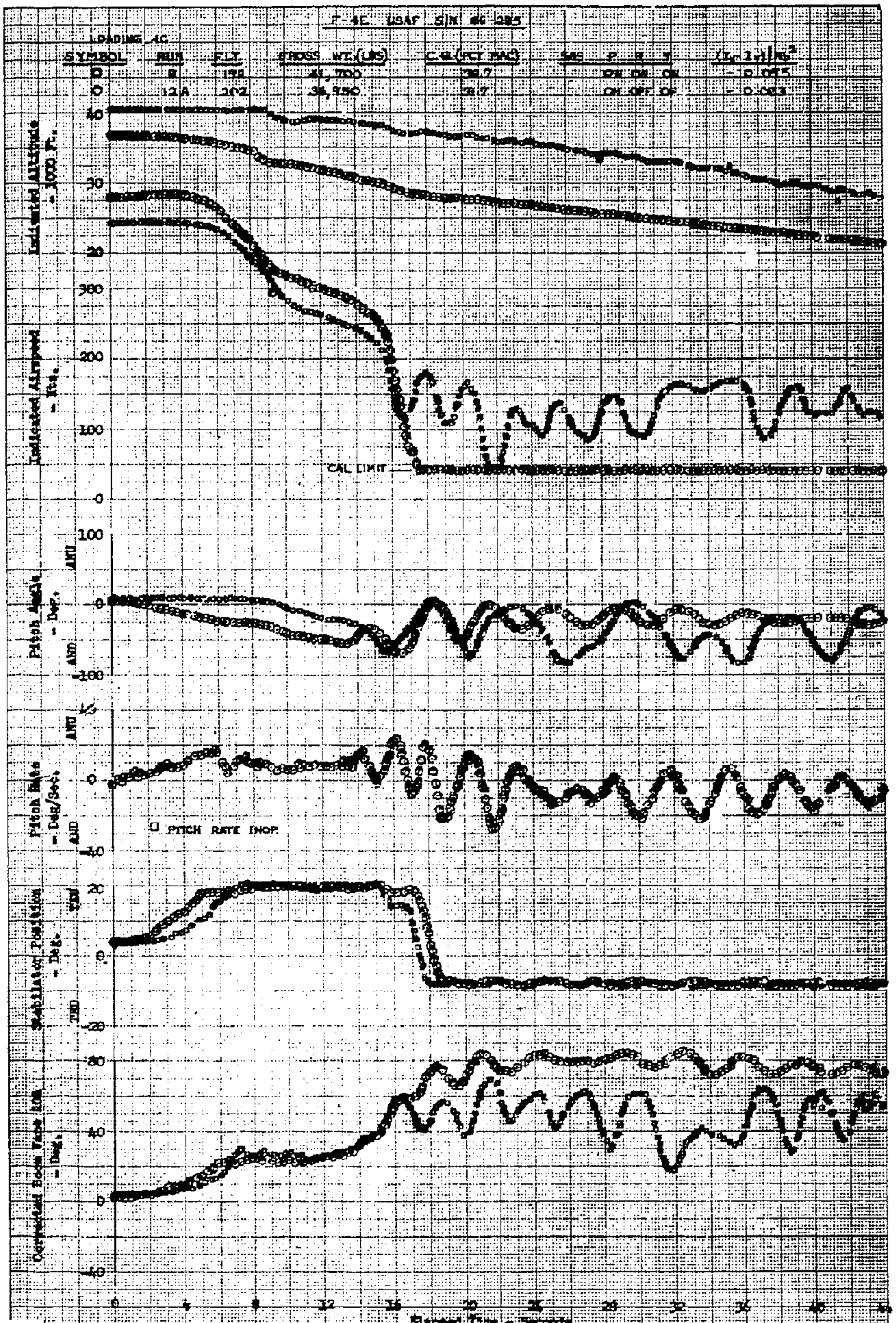

304 FIGURE 61 CONTINUED

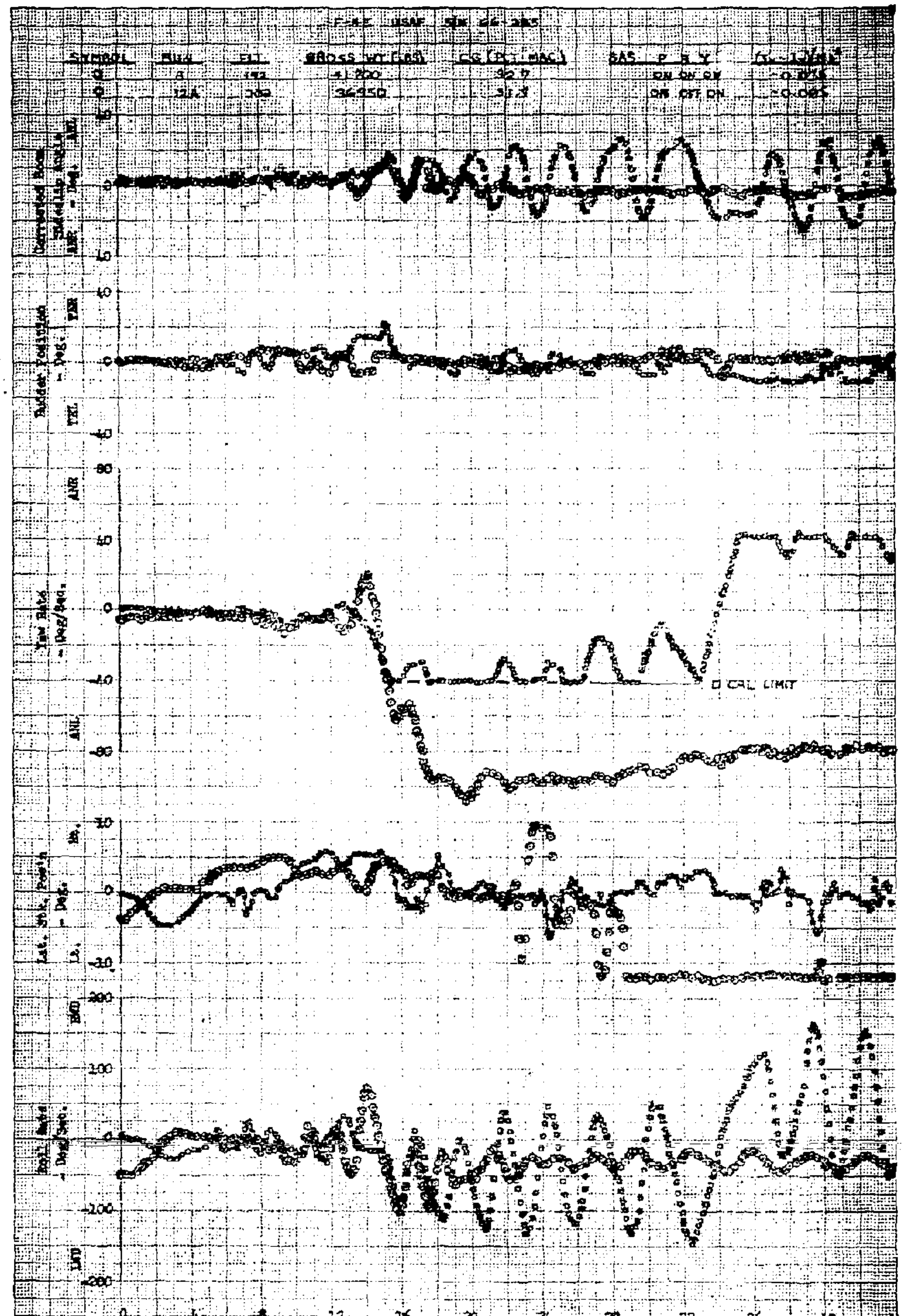

FIGURE 61 CONTINUED

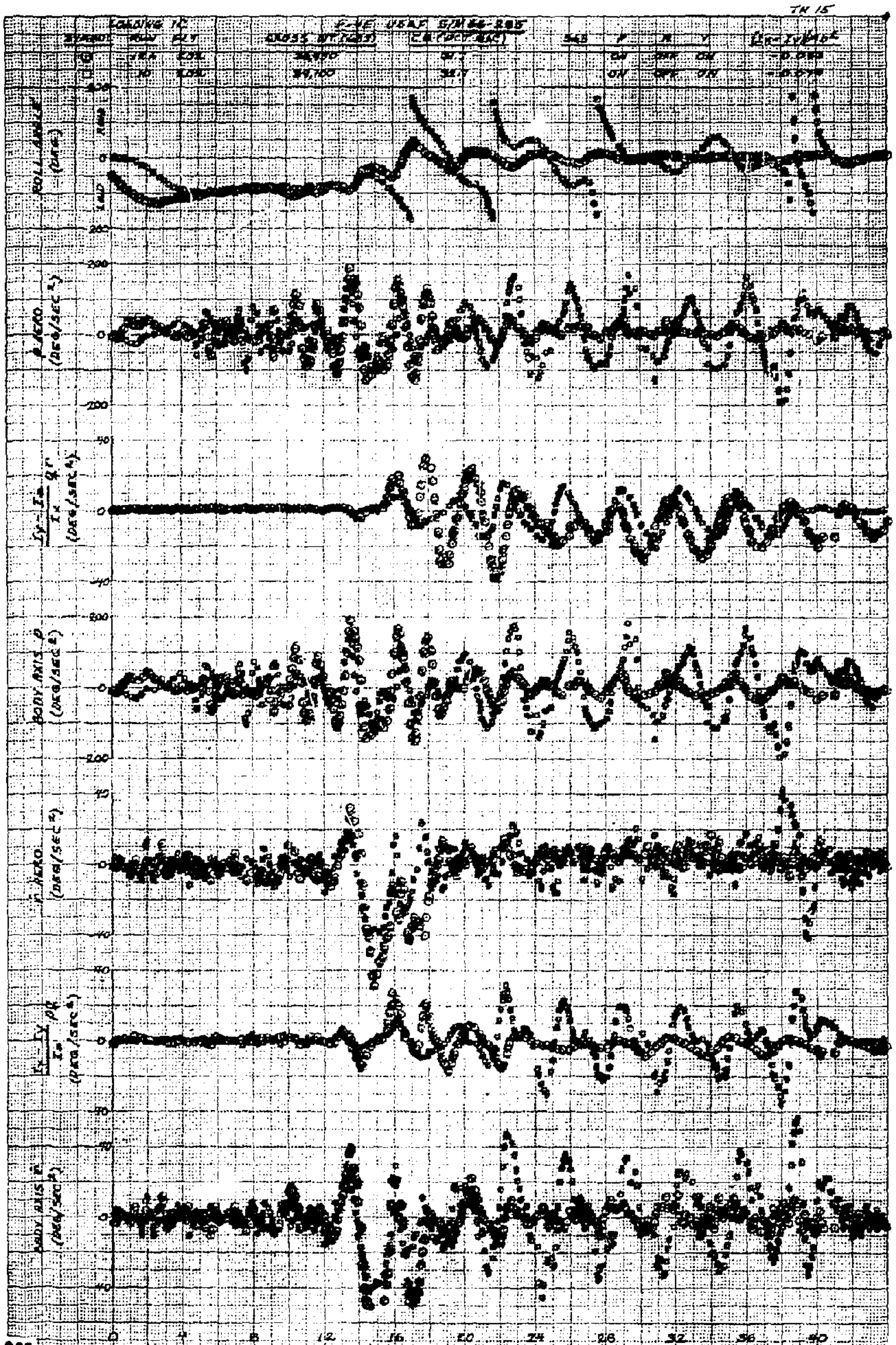

FIGURE 61 CONTINUED

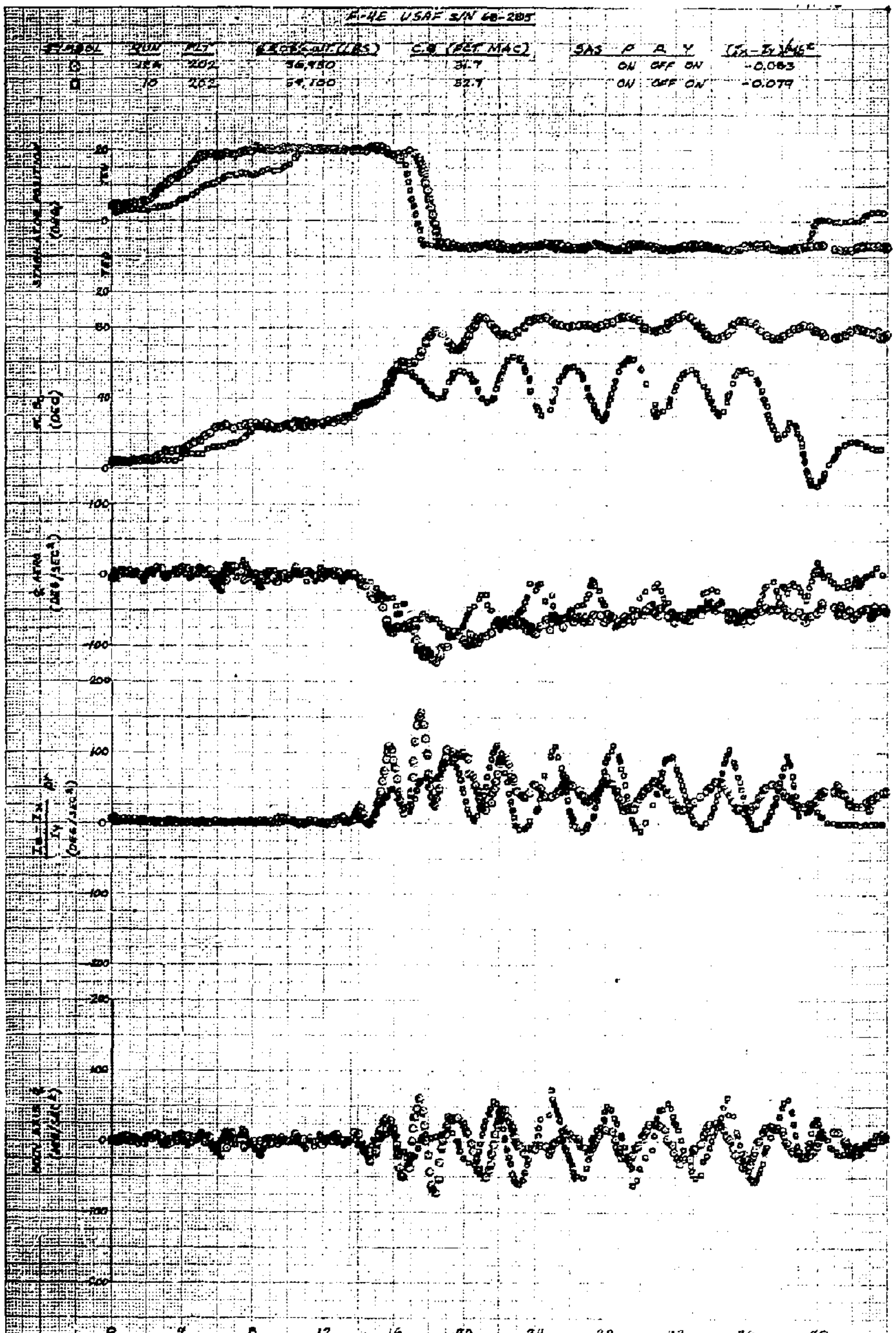

FIGURE 61 CONTINUED

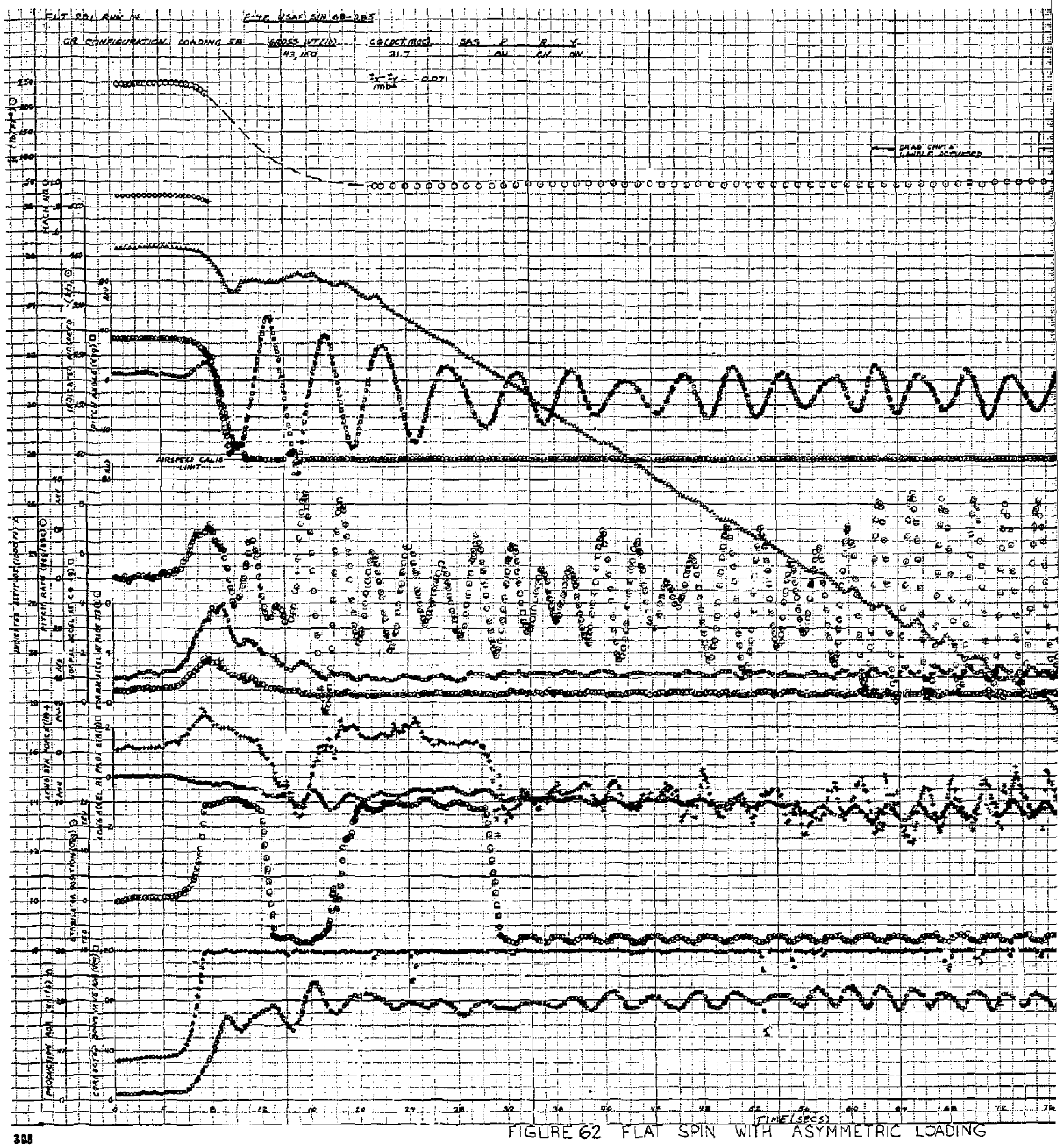

FIGURE 62 FLAT SPIN WITH ASYMMETRIC LOADING

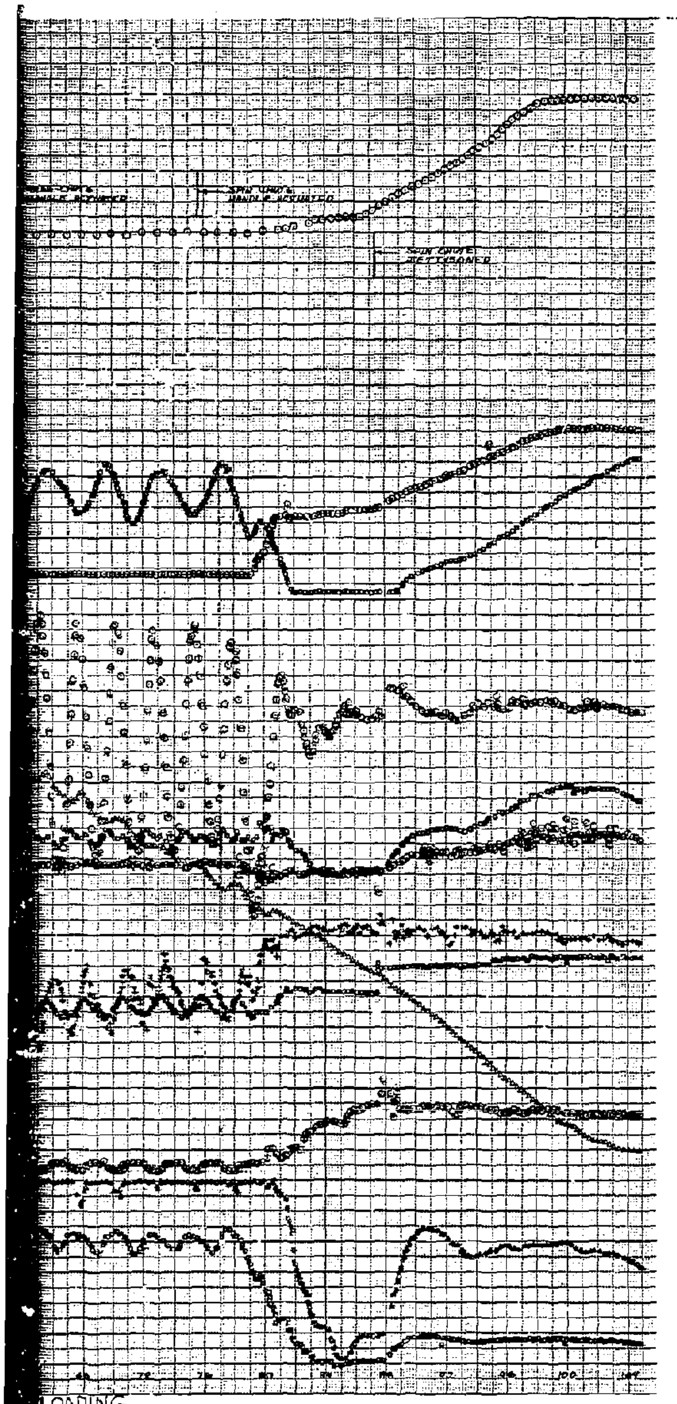

LOADING

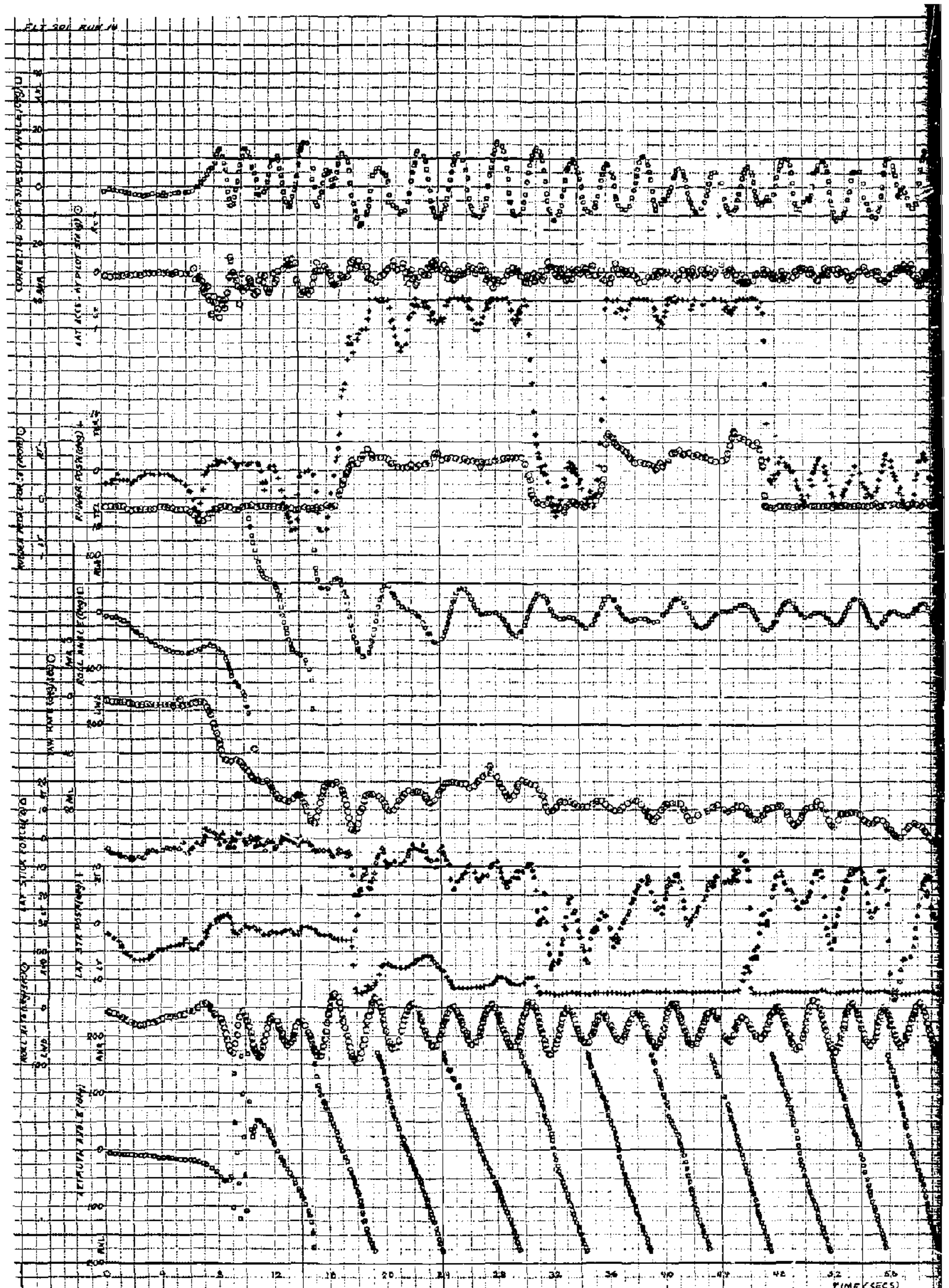

FIGURE 62 CONTINUED

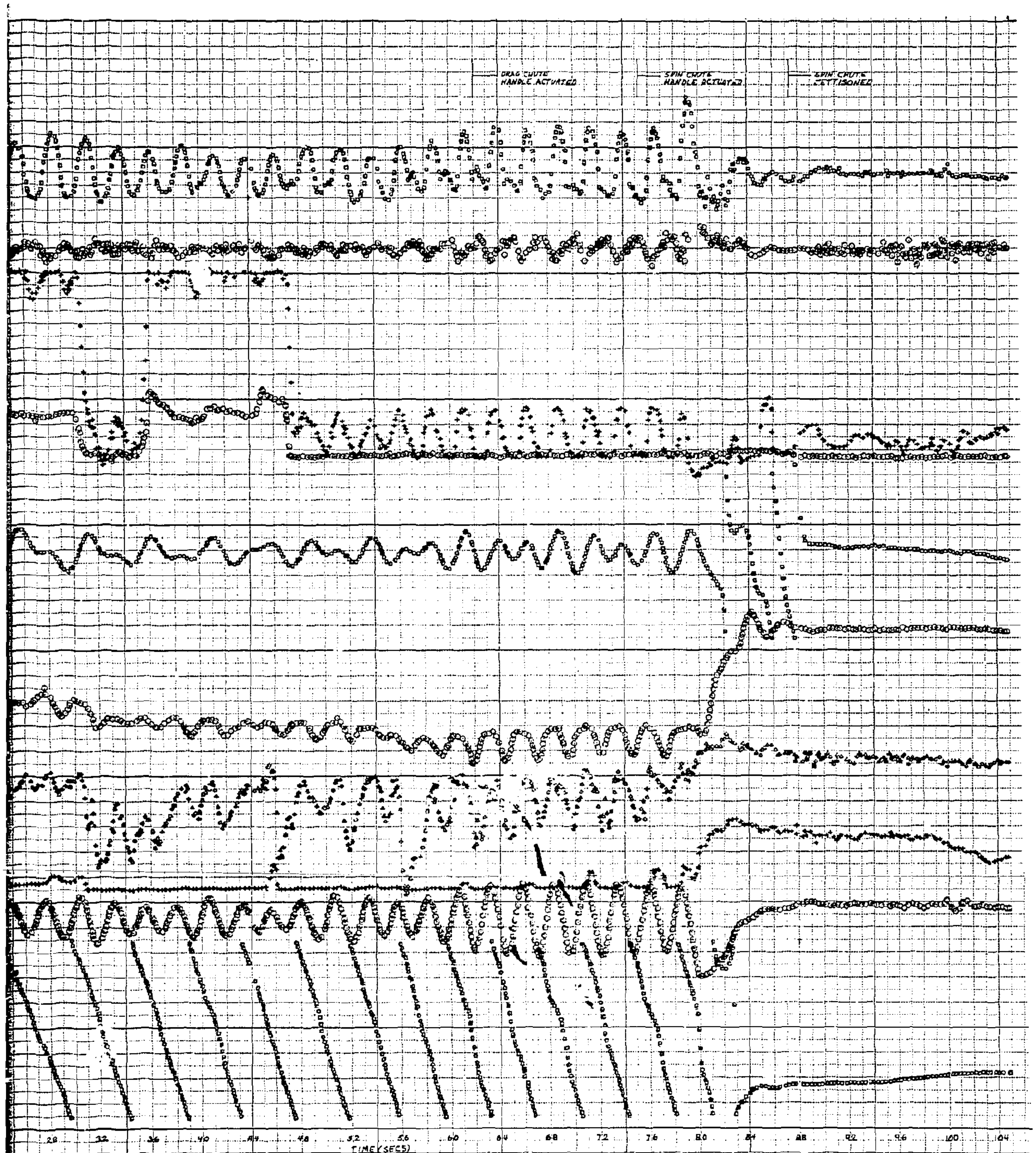

FIGURE 62 CONTINUED

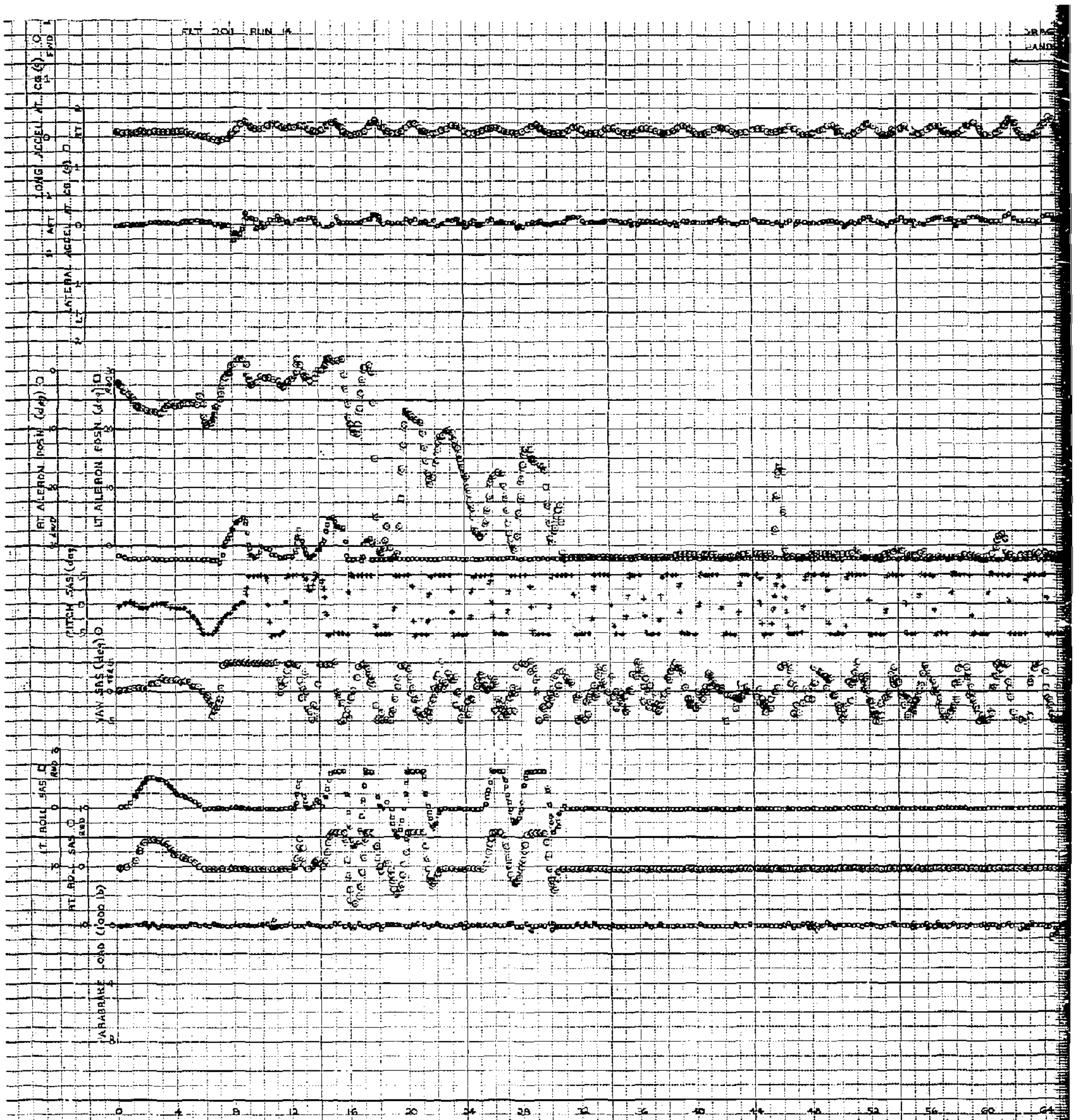

FIGURE 62 CONTINUED

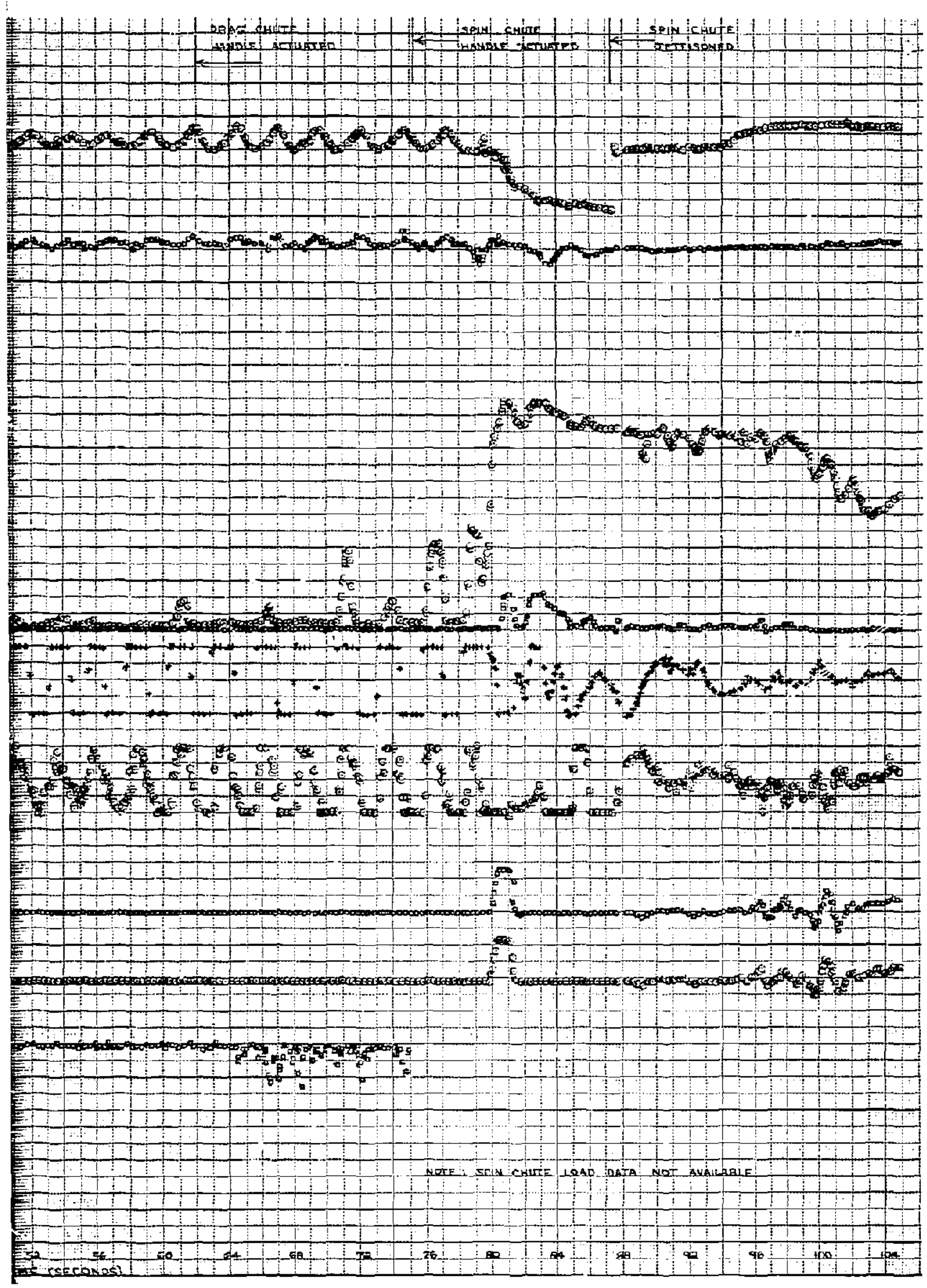

DRAG CHUTE HANDLE ACTUATED
SPIN CHUTE HANDLE ACTUATED
SPIN CHUTE JETTISONED
NOTE: SPIN CHUTE LOAD DATA NOT AVAILABLE
52
56
60
64
68
72
76
80
84
88
92
96
100
104
TIME (SECONDS)

2

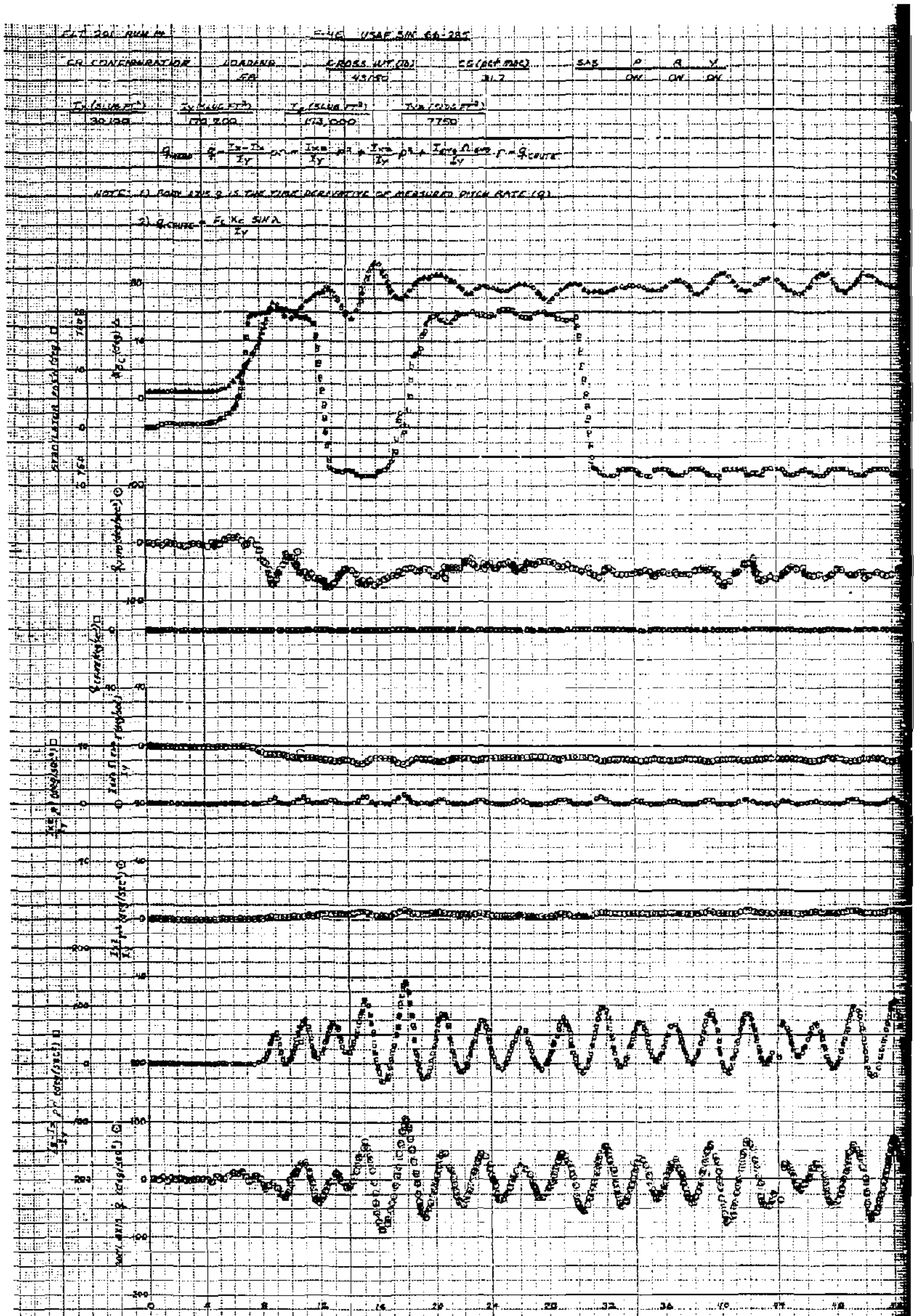

FIGURE 62 CONTINUED

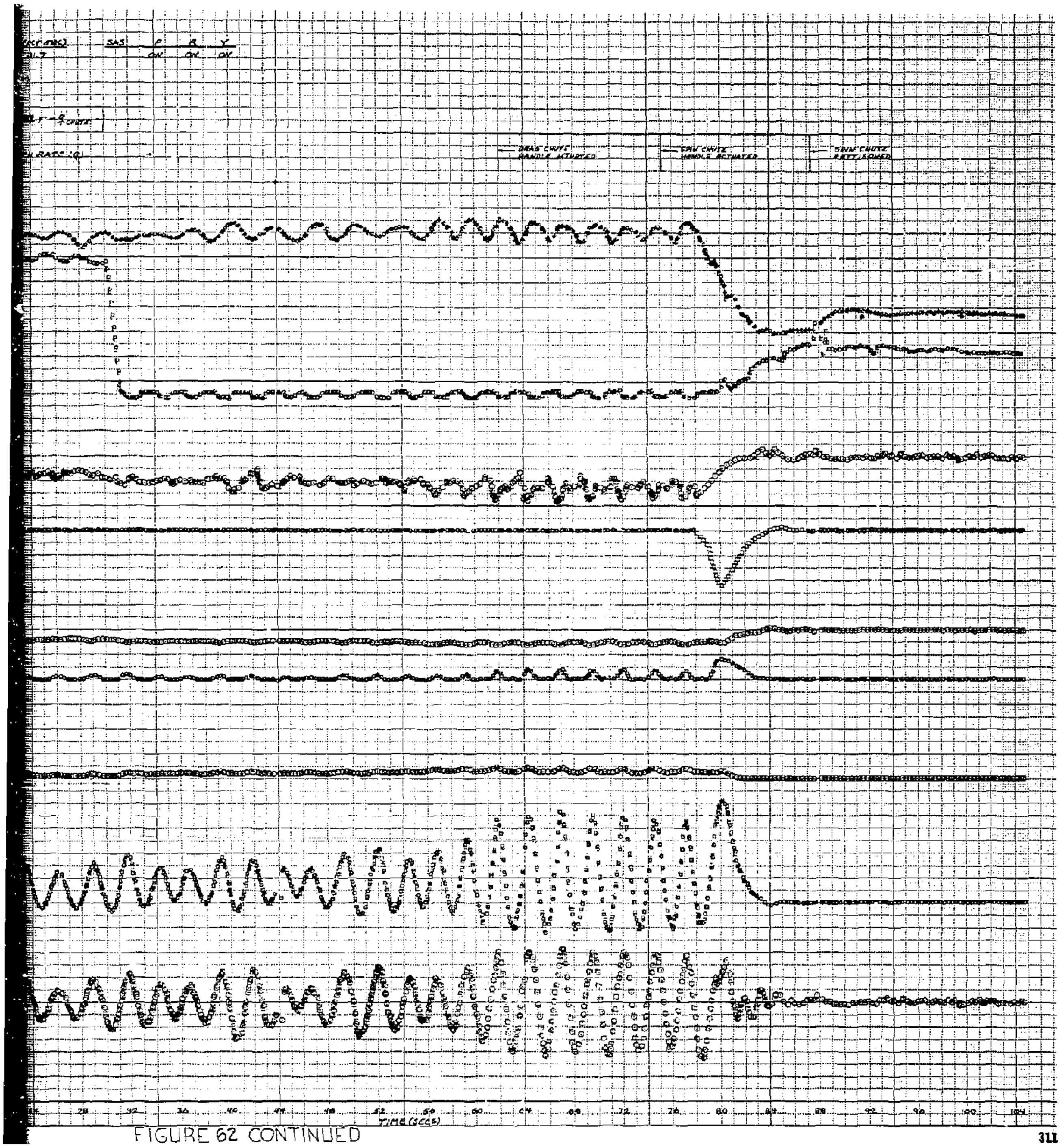

FIGURE 62 CONTINUED

2

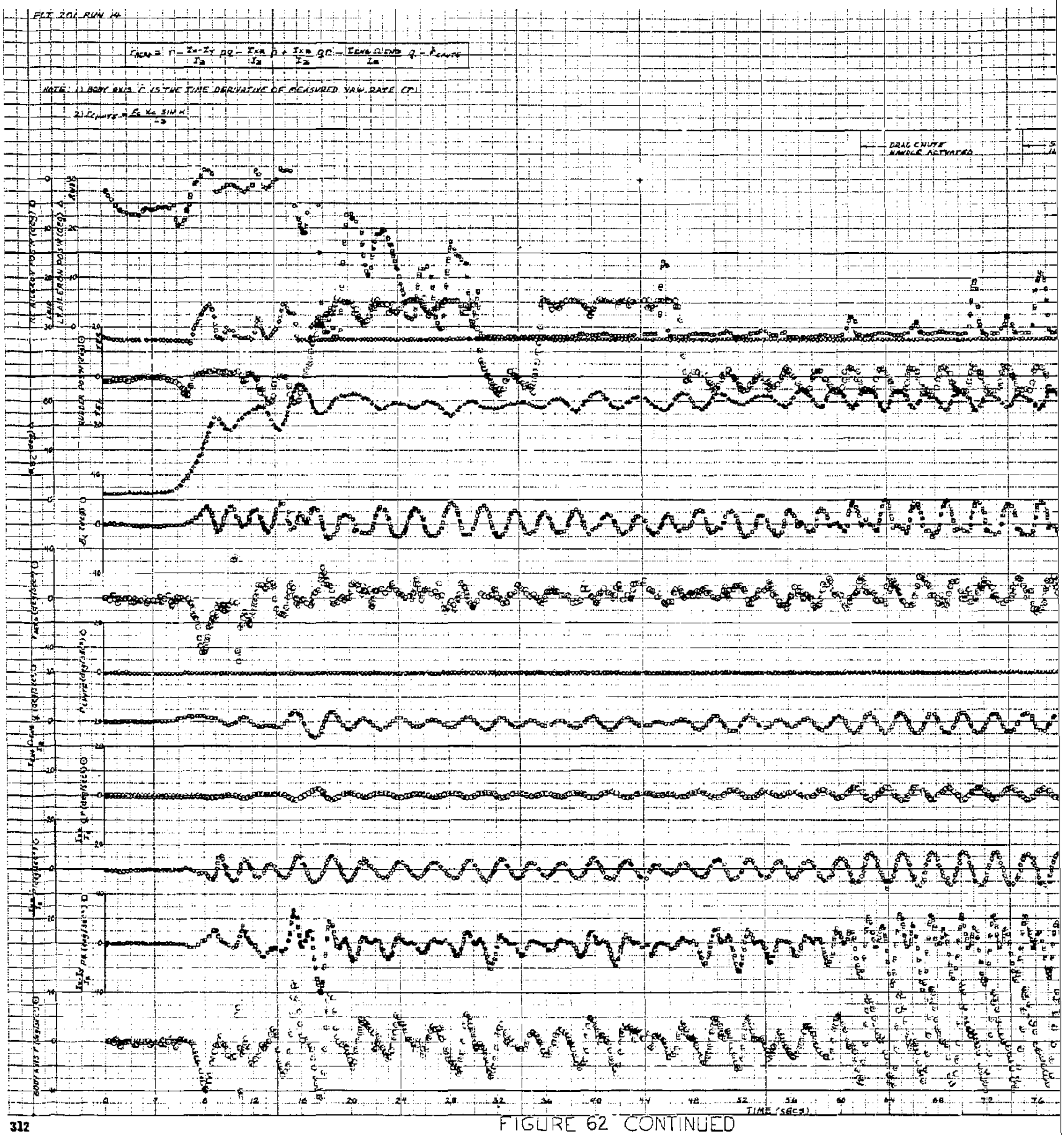

FIGURE 62 CONTINUED

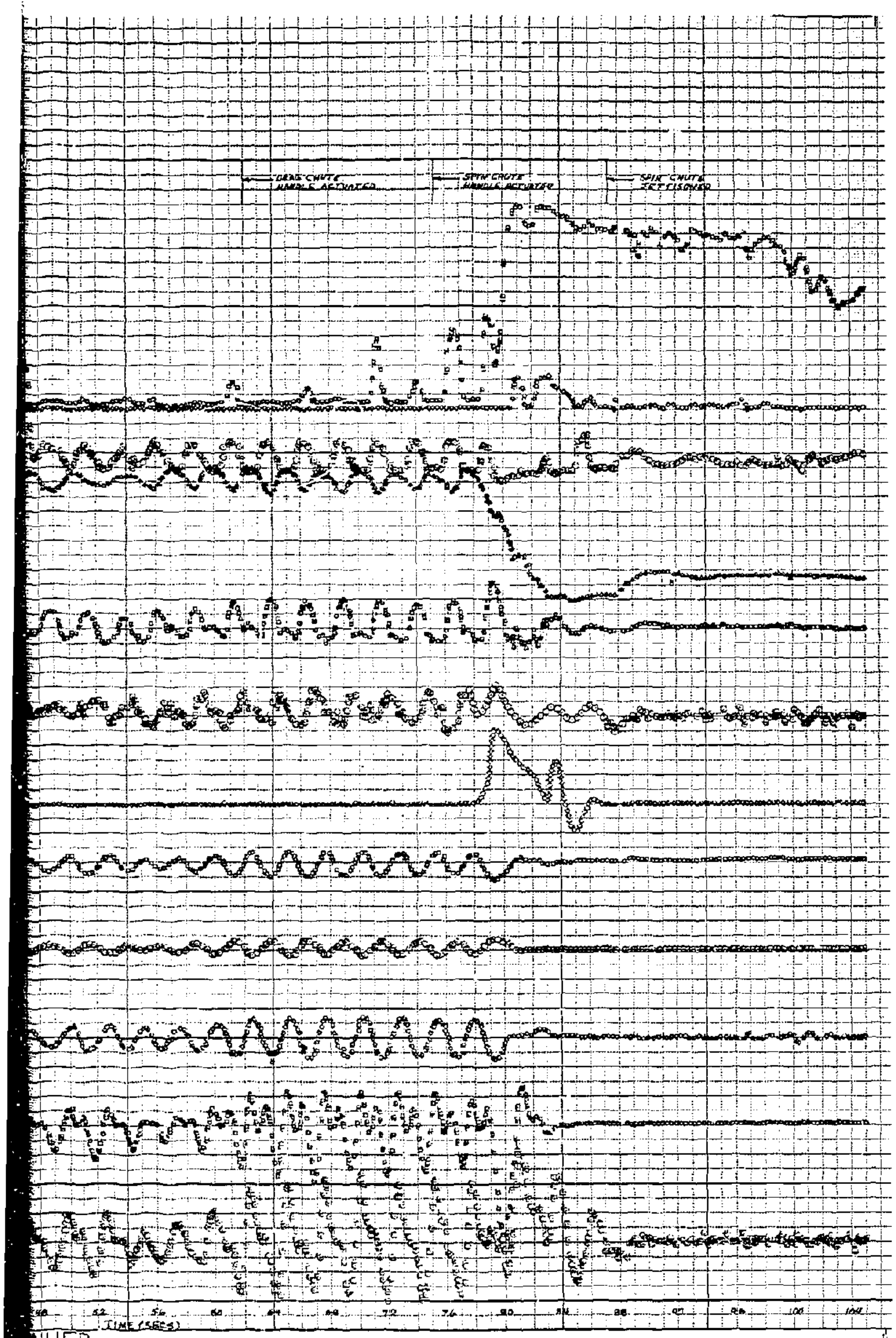

DRAG CHUTE HANDLE ACTUATED
SPIN CHUTE HANDLE ACTUATED
SPIN CHUTE JETTISONED
48
52
56
60
64
68
72
76
80
84
88
92
96
100
104
TIME (SECS)

NUED

2)

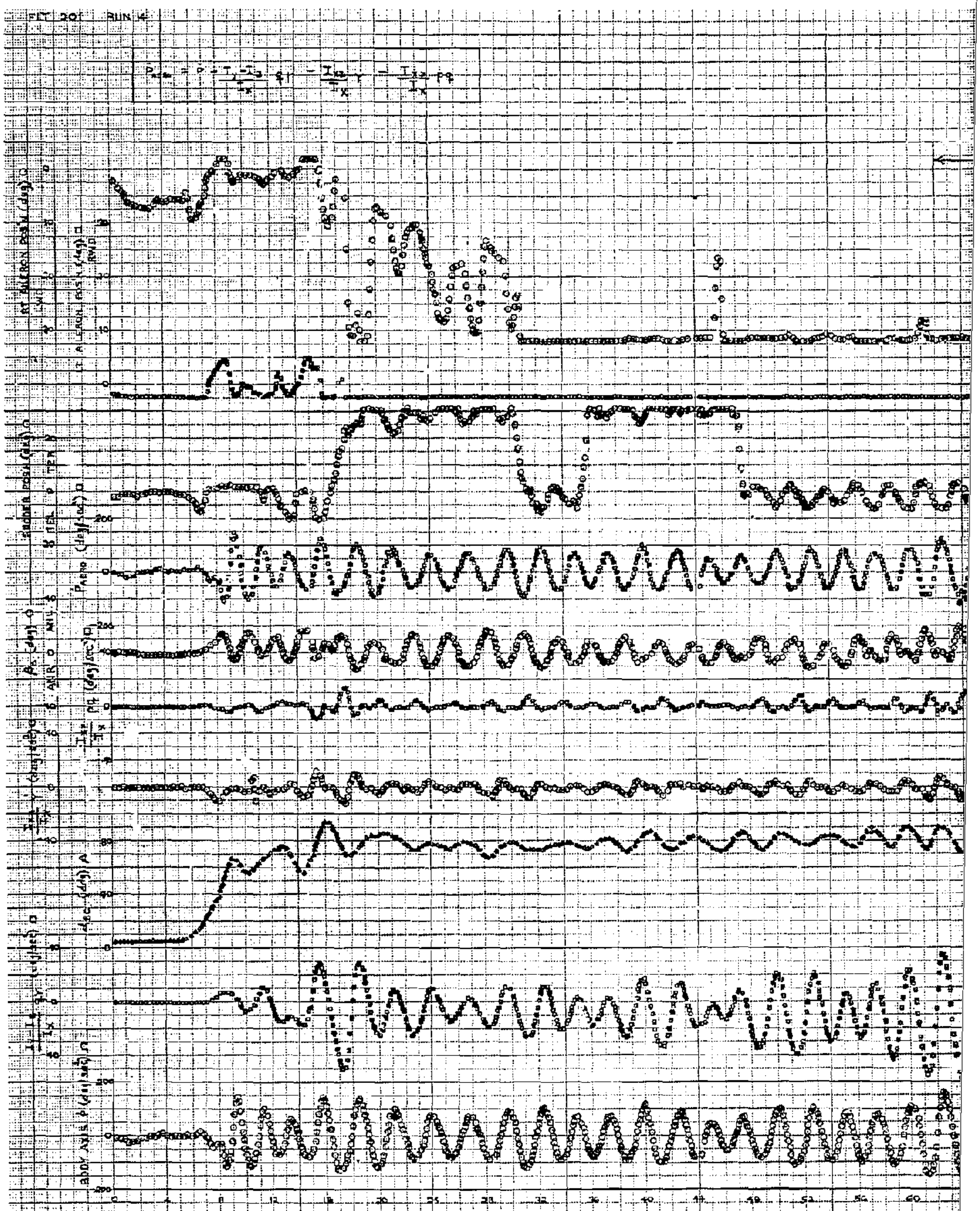

FIGURE 62 CONTINUED

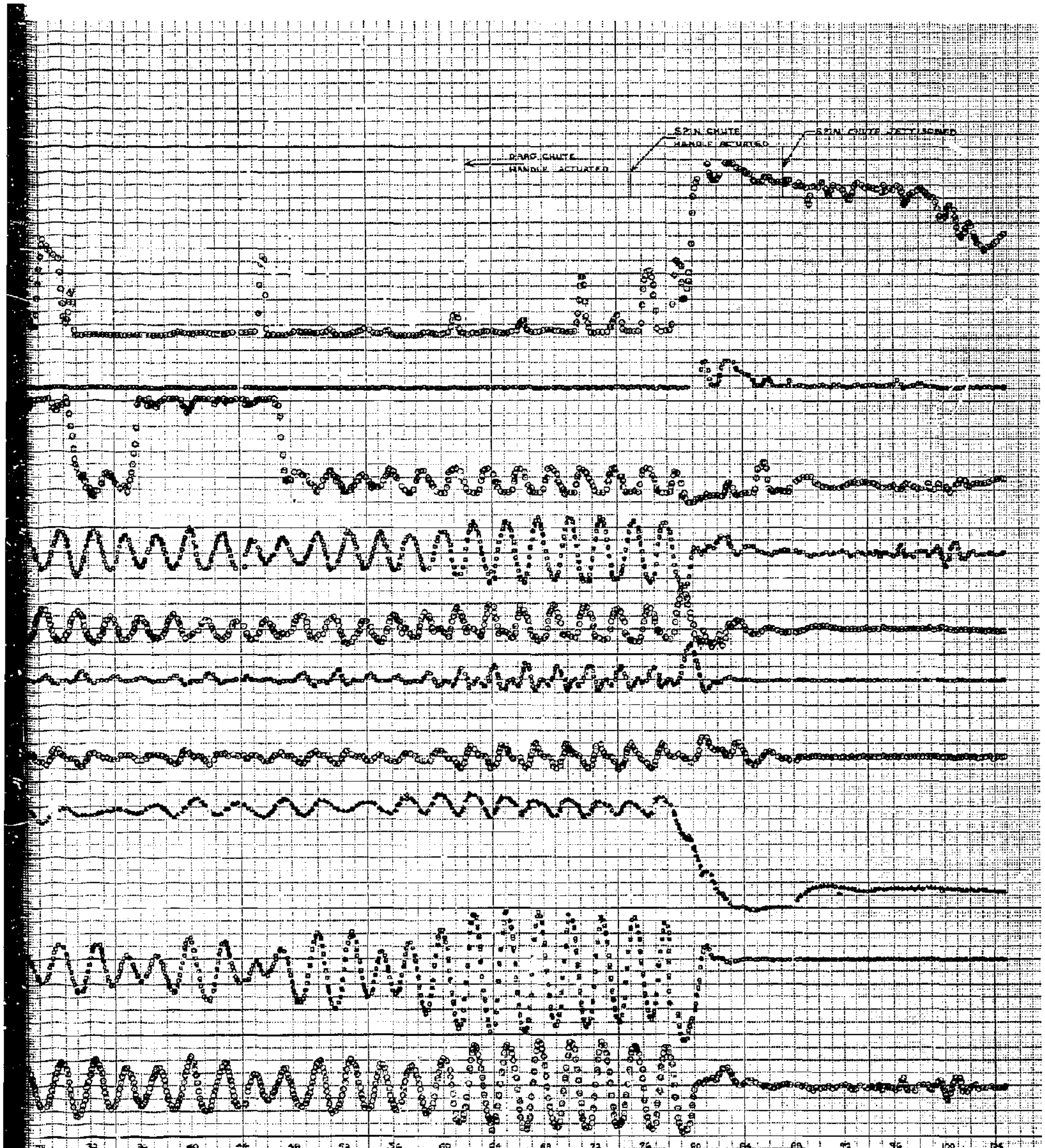

FIGURE 62 CONTINUED

2

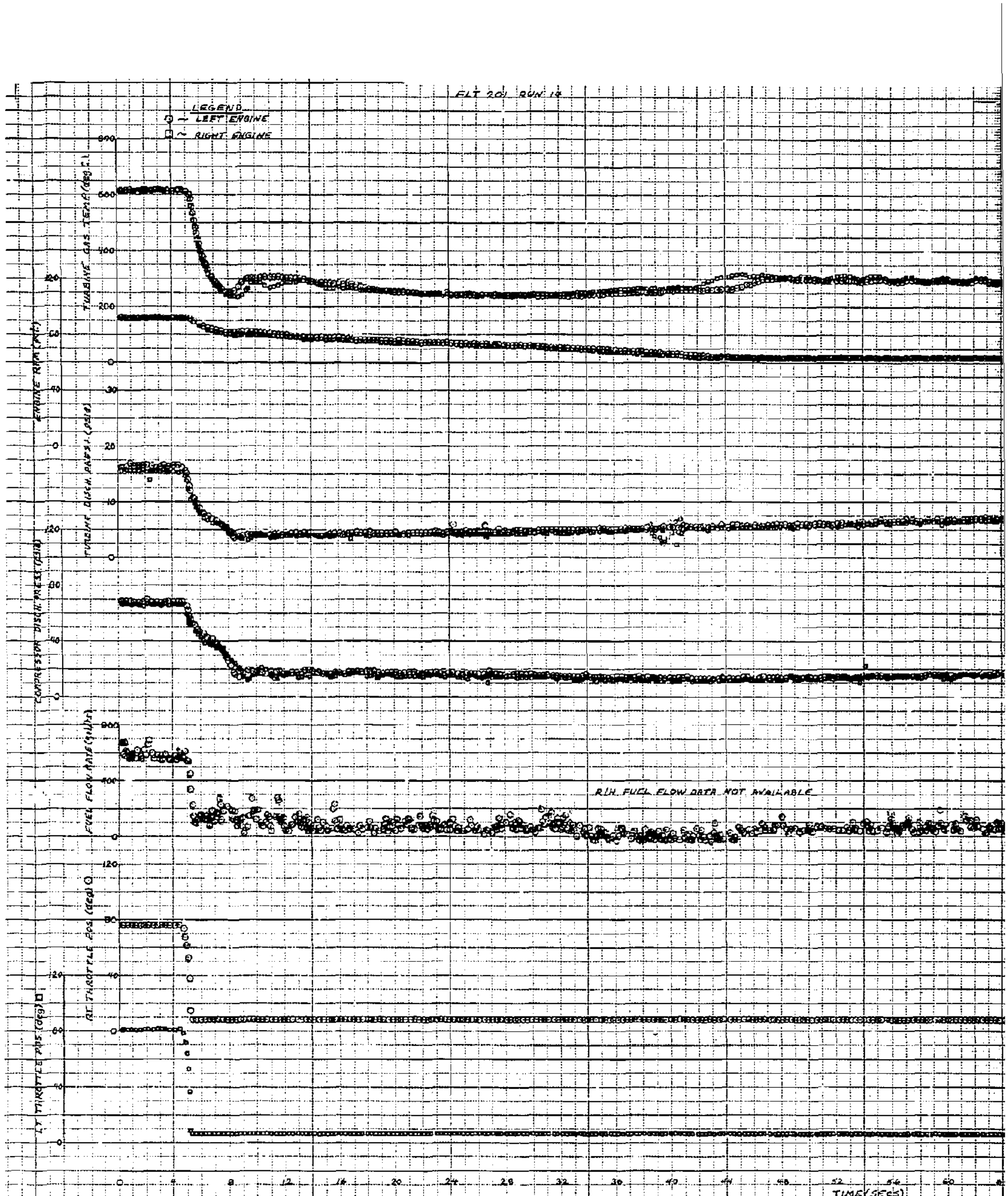

FIGURE 62 CONTINUED

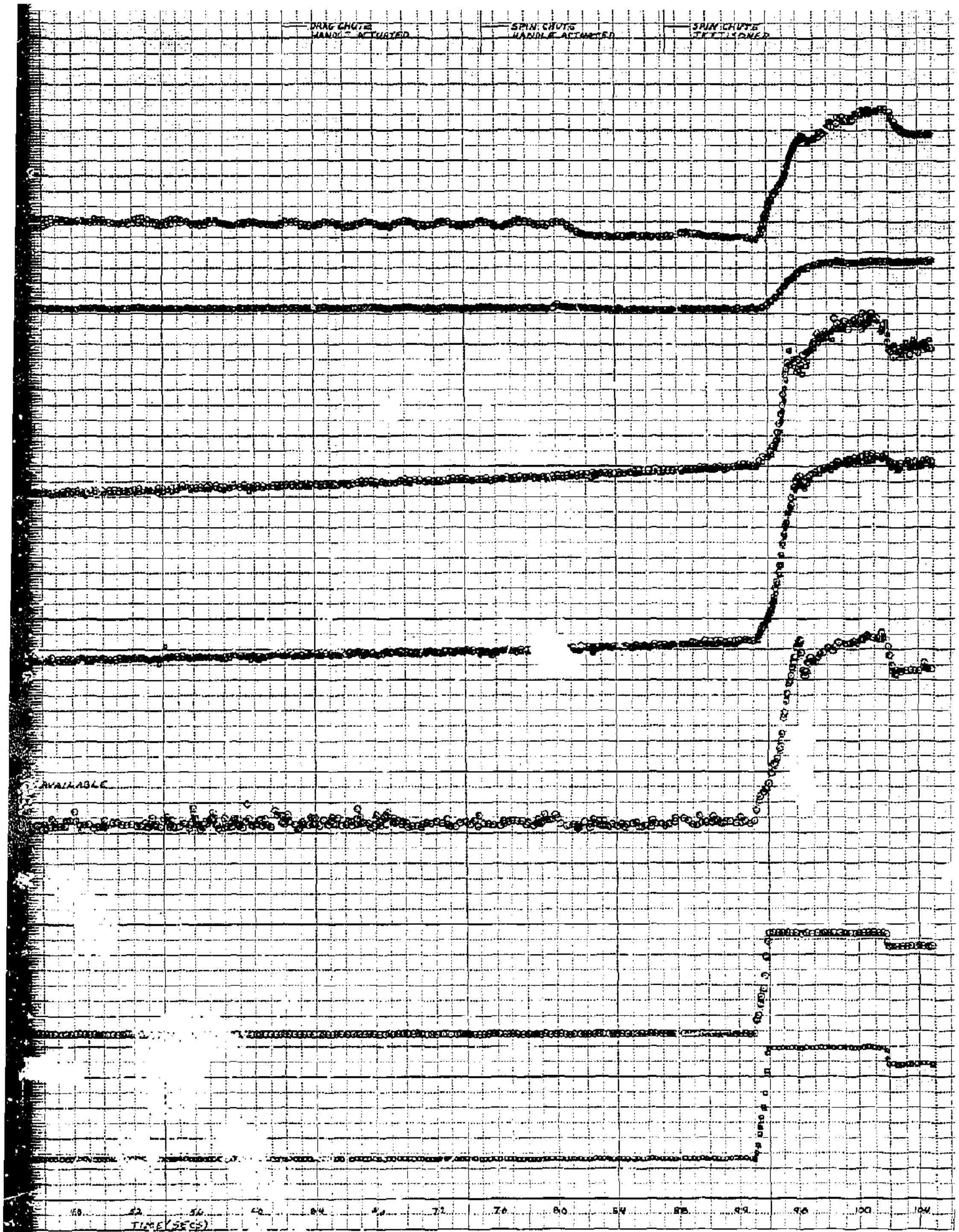
DRAG CHUTE HANDLE ACTUATED
SPIN CHUTE HANDLE ACTUATED
SPIN CHUTE JETTISONED
AVAILABLE
TIME (SECS)

TINUED

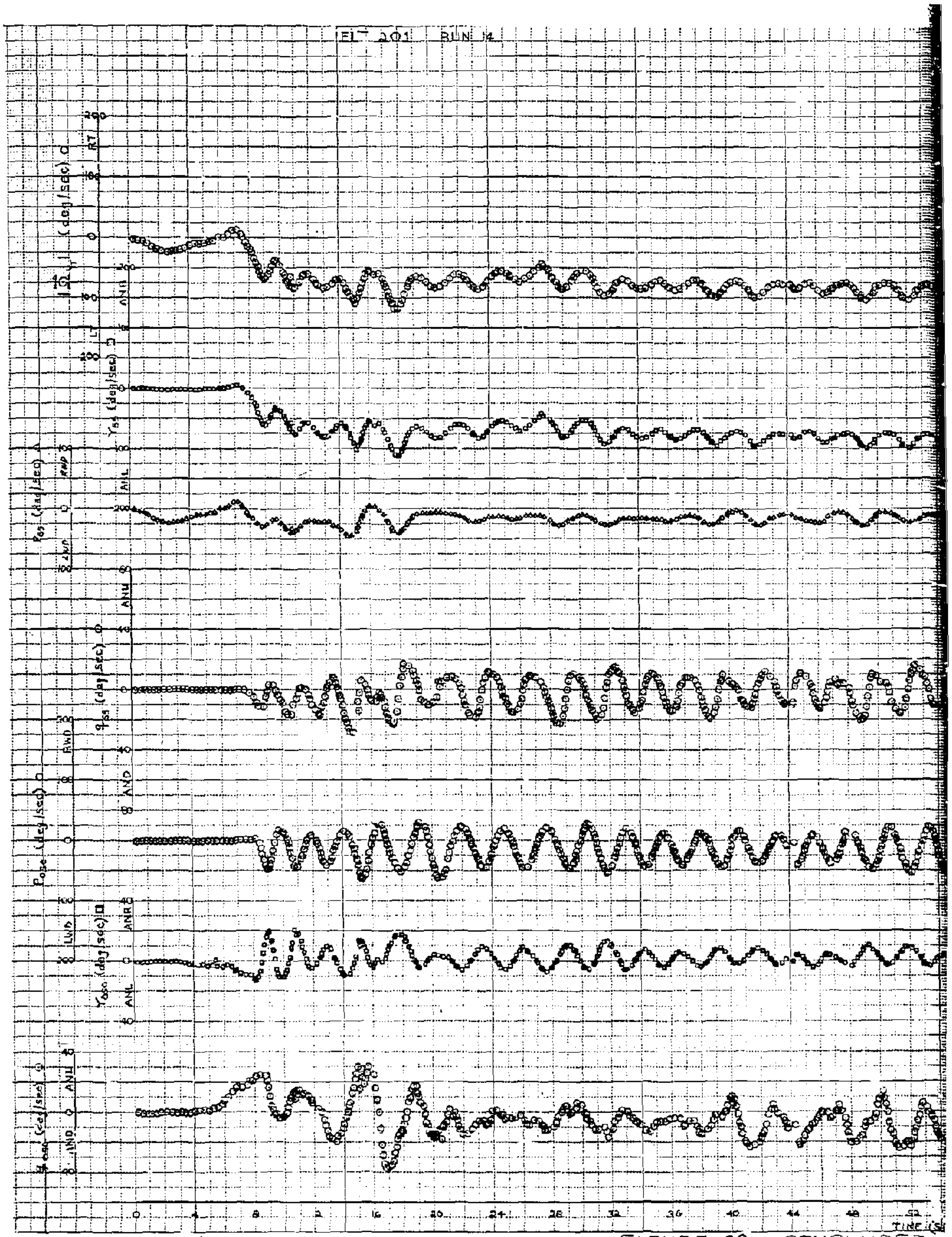

FIGURE 62 CONCLUDED

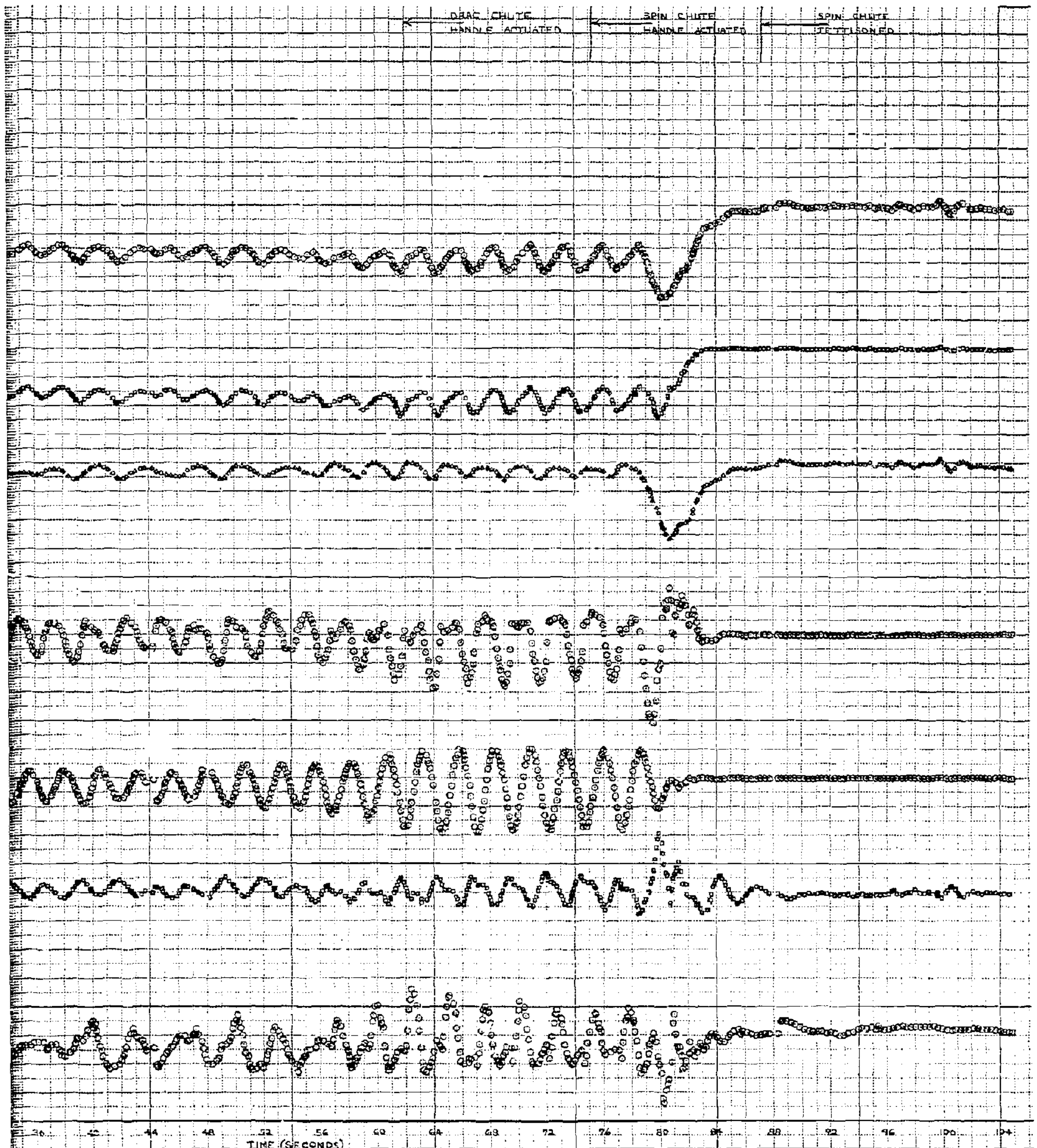

GURE 62 CONCLUDED

2

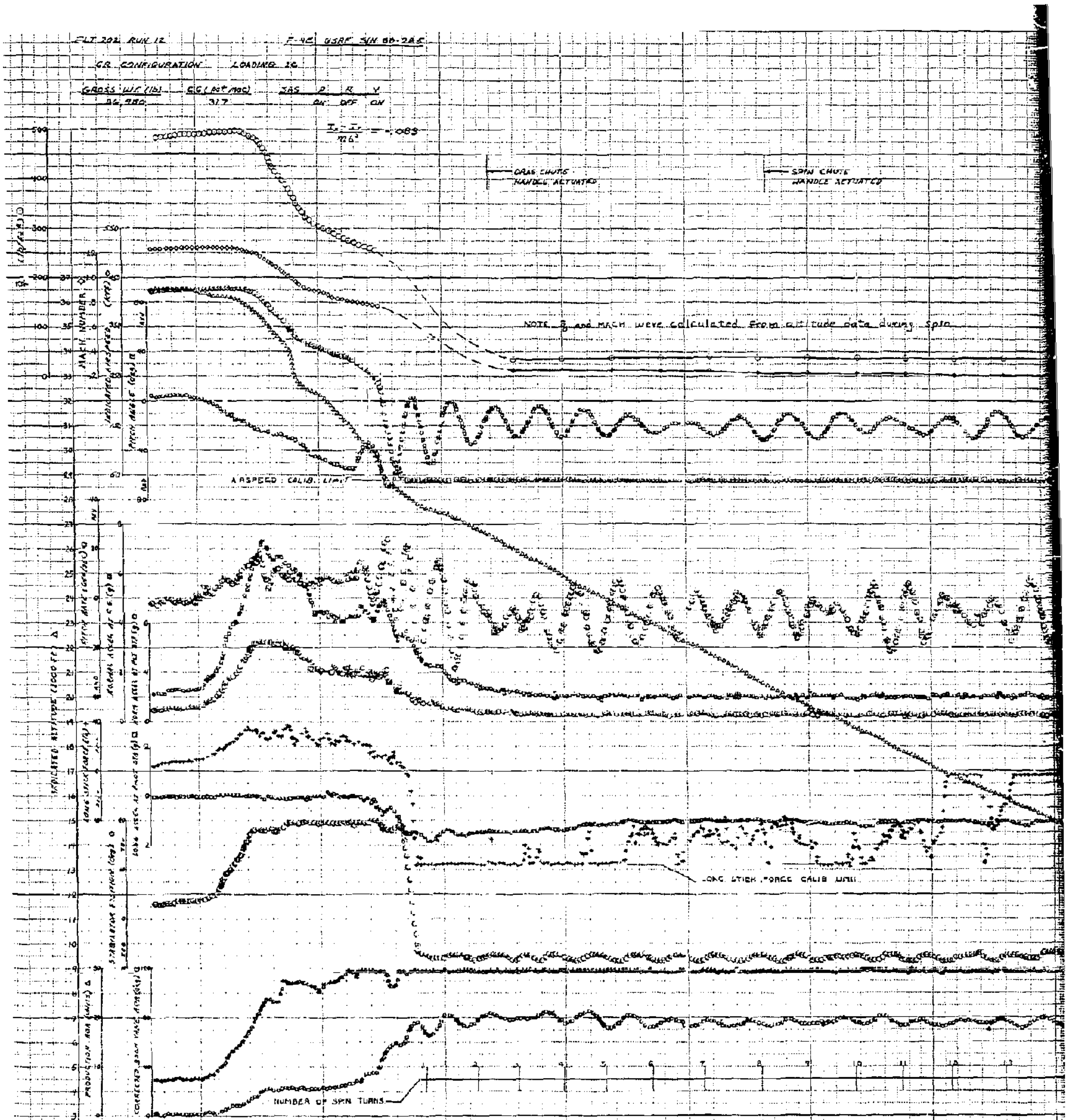

FIGURE 63 FLAT SPIN WITH CLEA

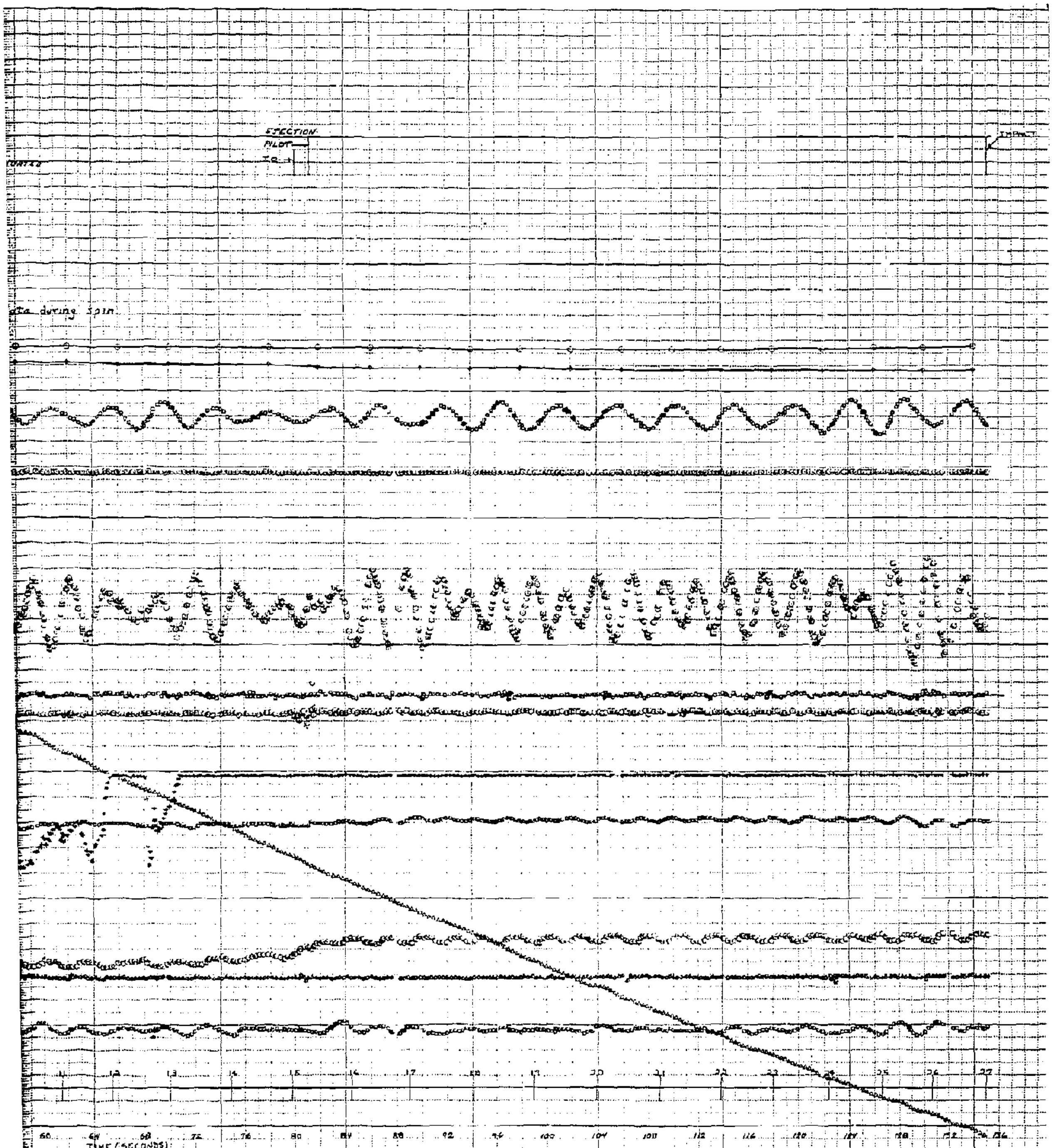

LAT SPIN WITH CLEAN LOADING

2

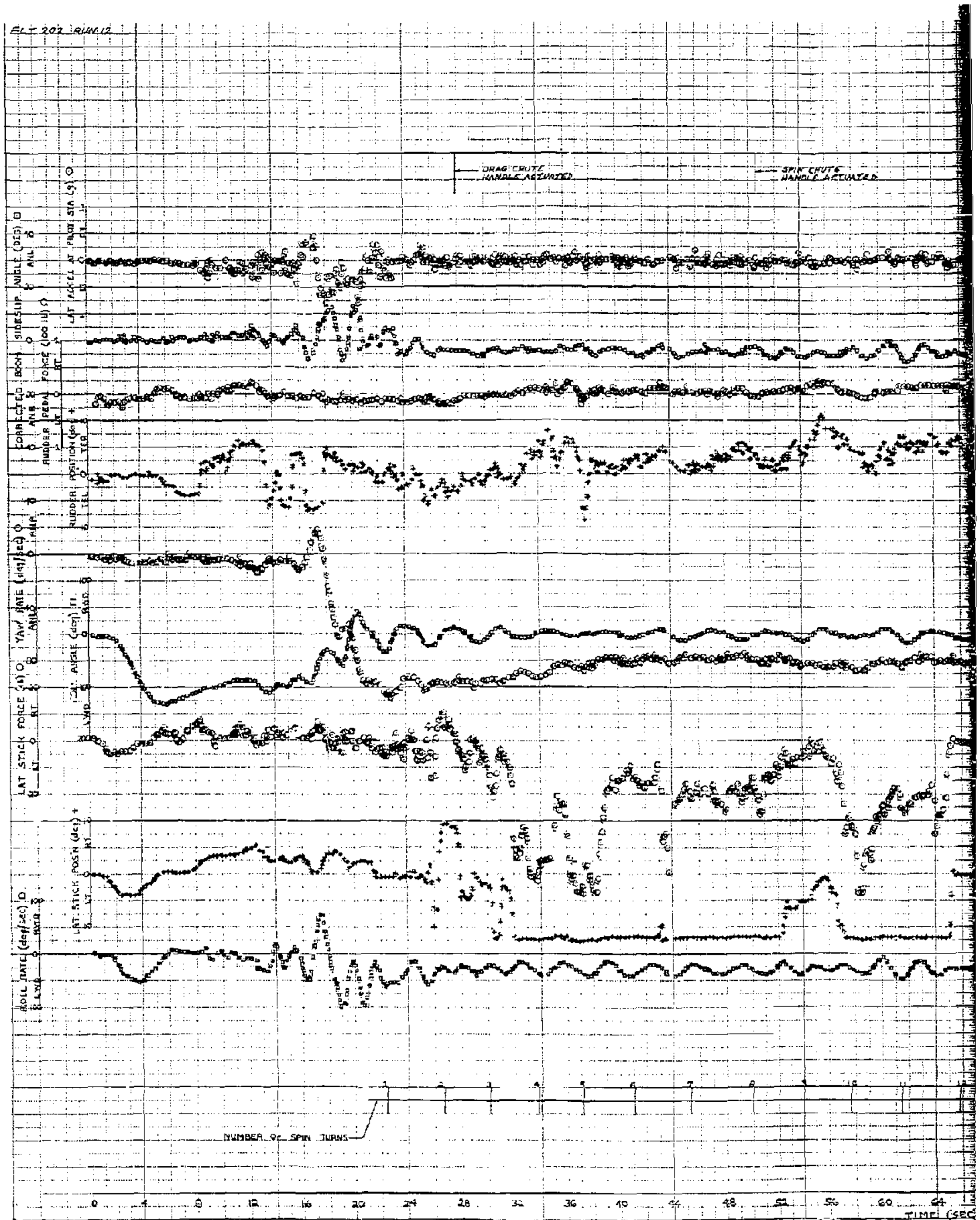

FIGURE 63 CONTINUED

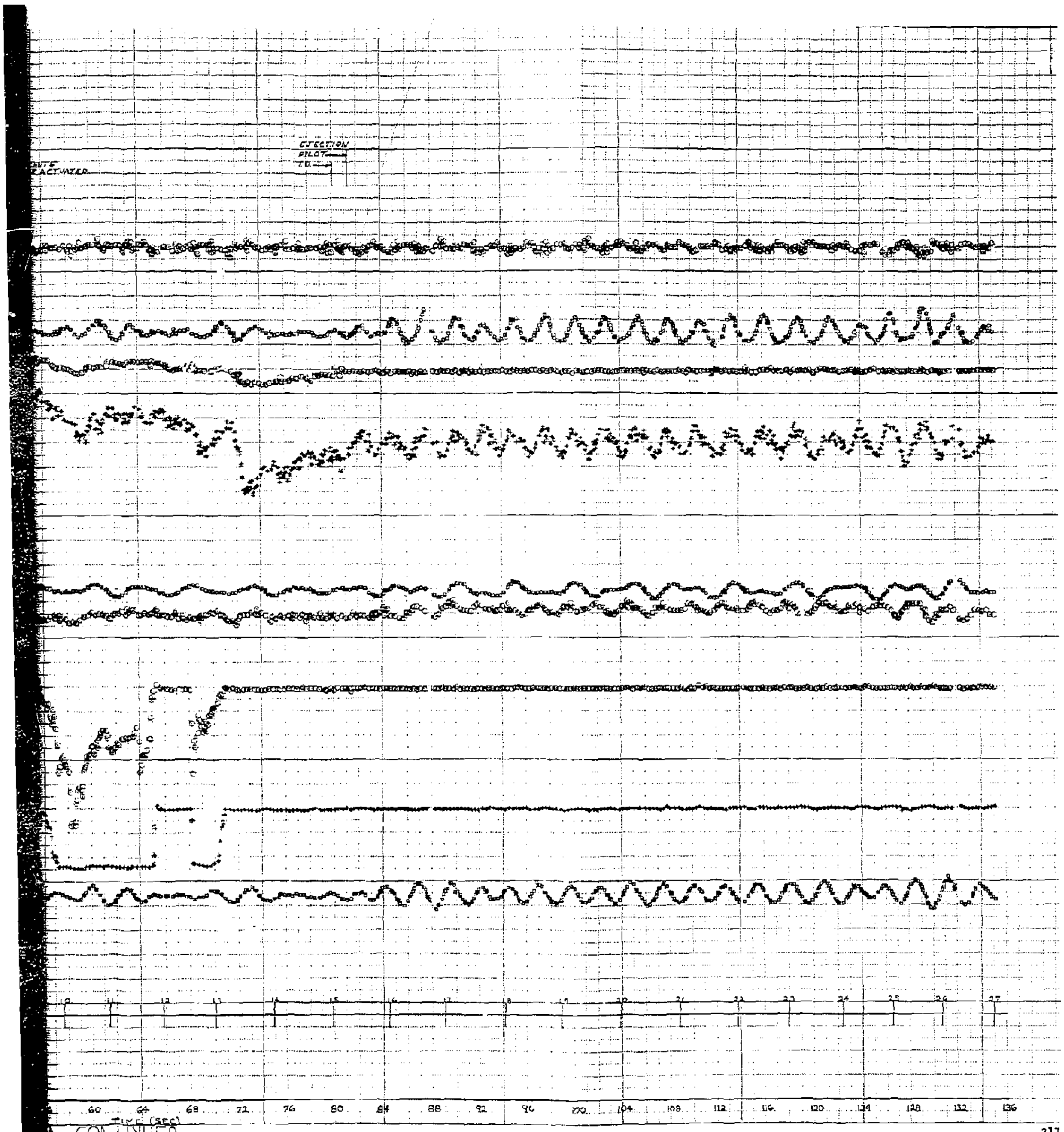

EJECTION
PILOT
T.D.
CHUTE
DEACTIVATED
60
64
68
72
76
80
84
88
92
96
100
104
108
112
116
120
124
128
132
136
TIME (SEC)

CONTINUED

2

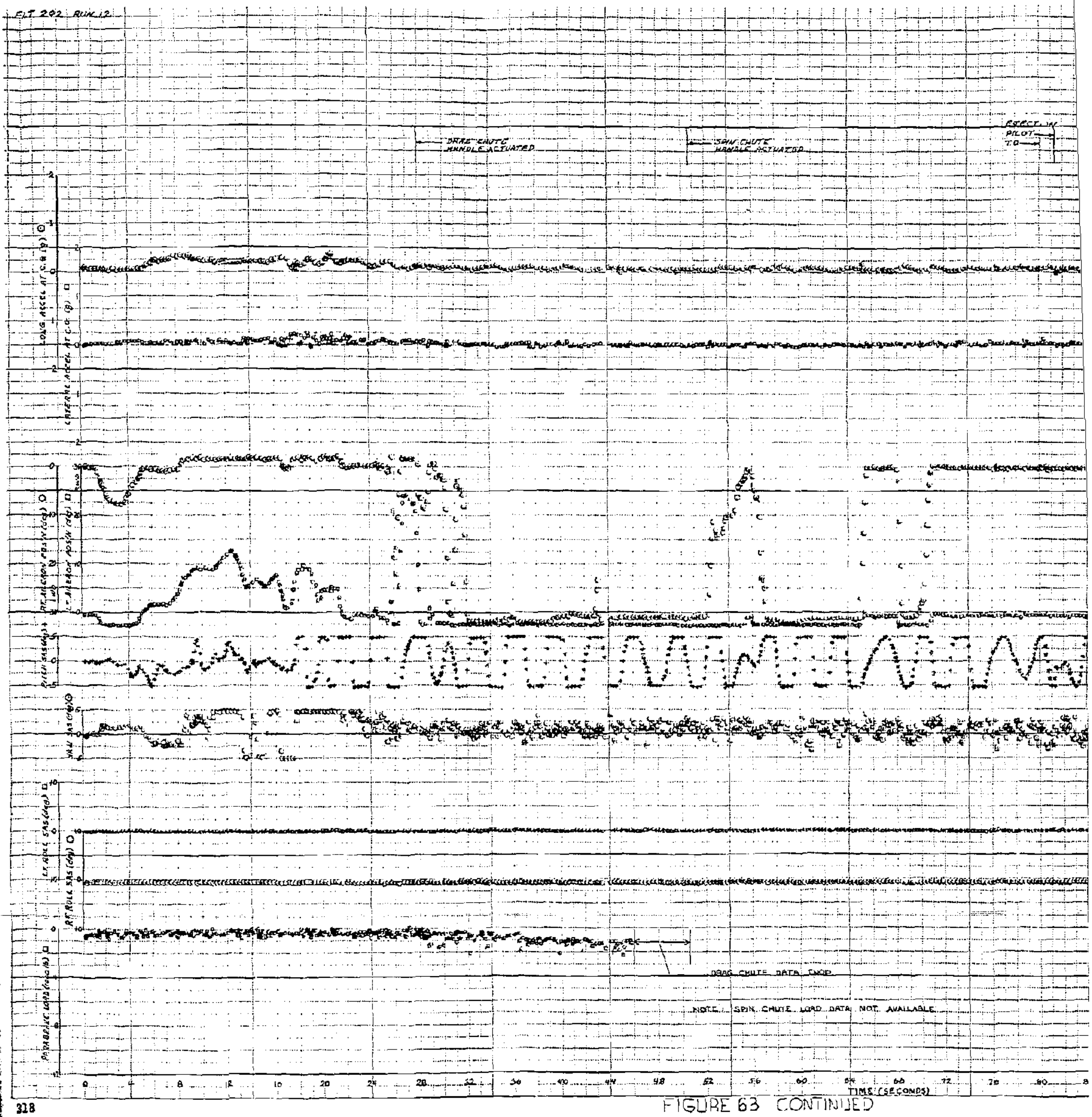

FIGURE 63 CONTINUED

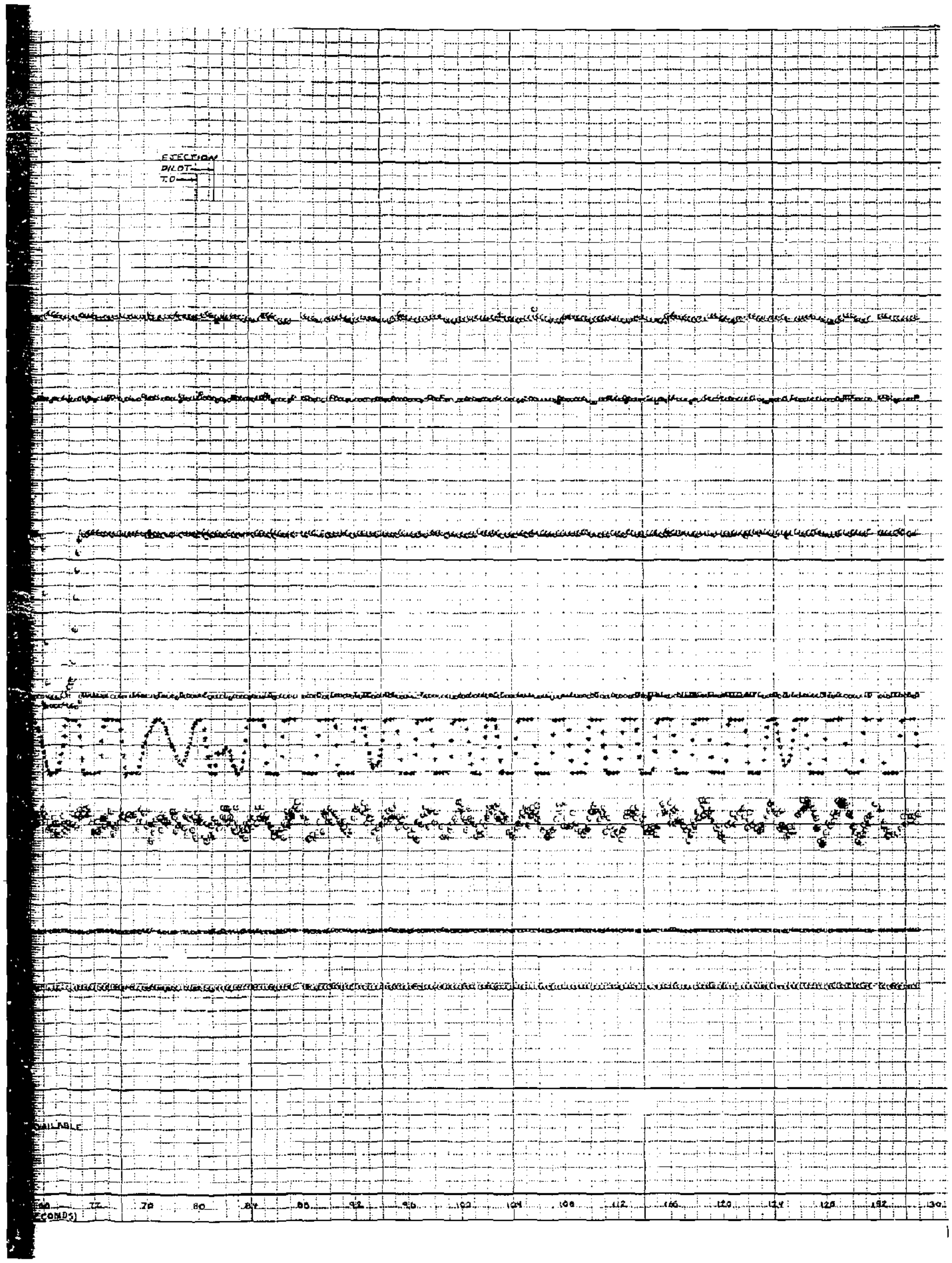

EJECTION
PILOT
T.O.
AILABLE
72
76
80
84
88
92
96
100
104
108
112
116
120
124
128
132
136
ECONDS)

2

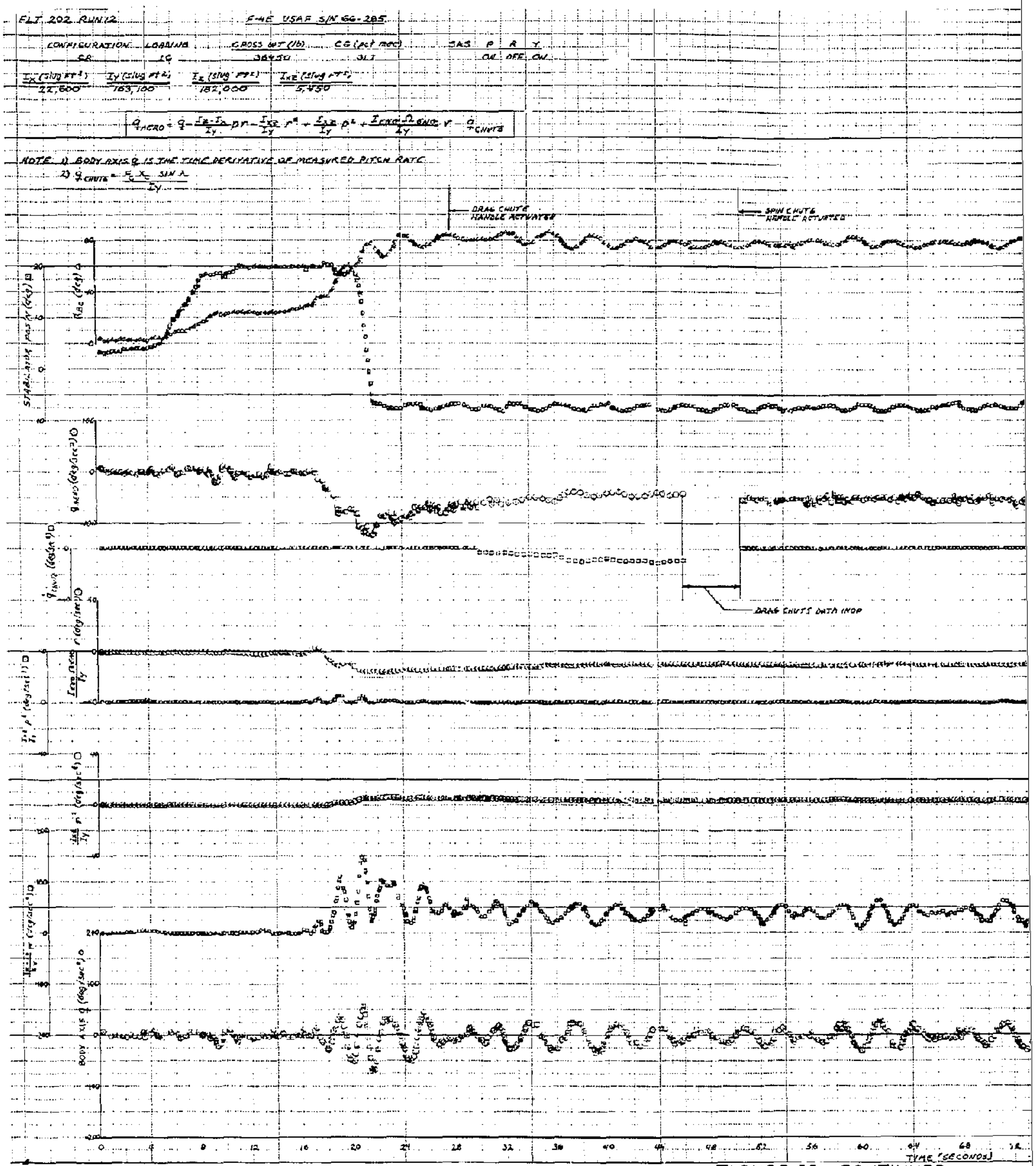

FIGURE 63 CONTINUED

63 CONTINUED

2

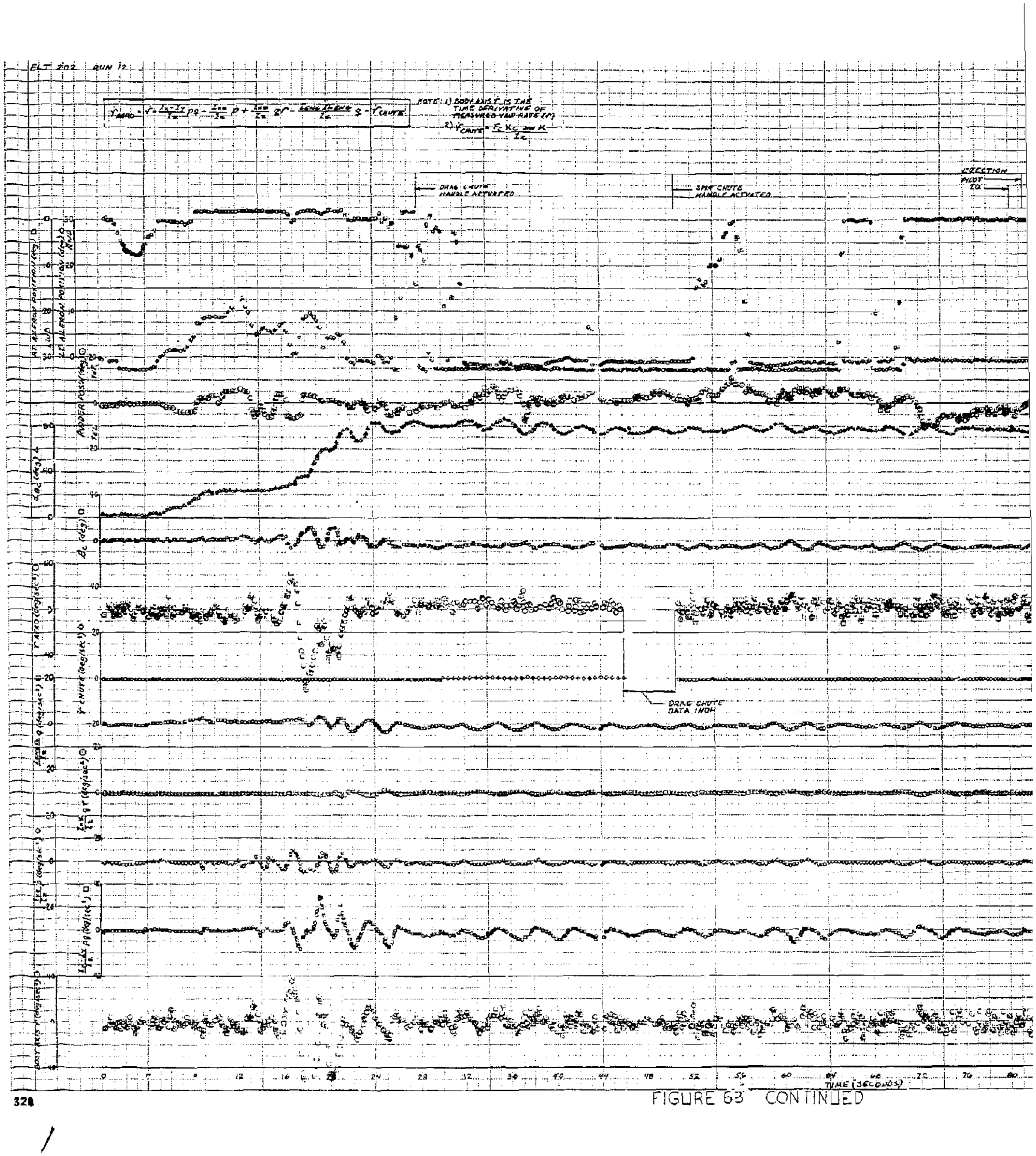

FIGURE 63 CONTINUED

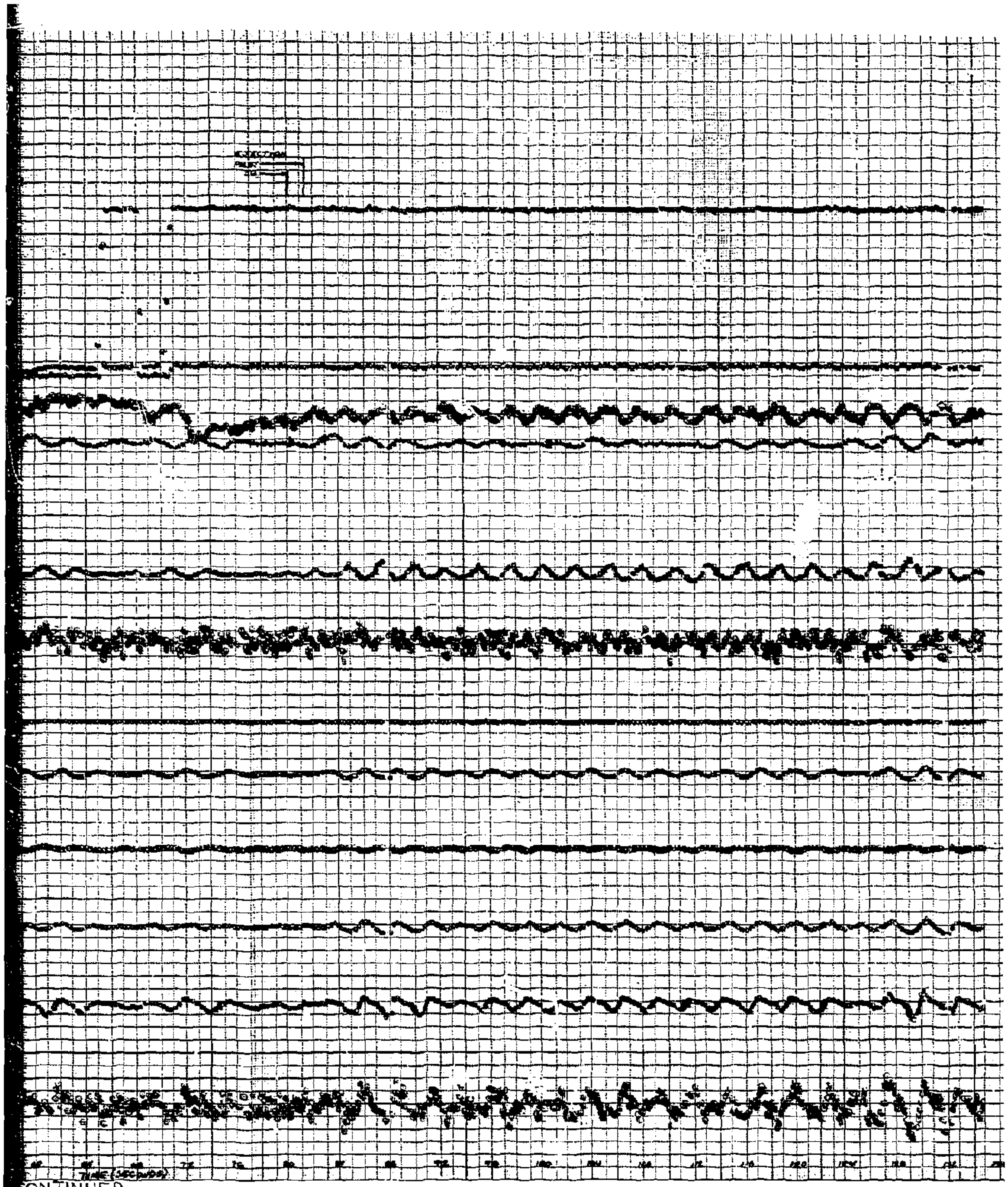

CONTINUED

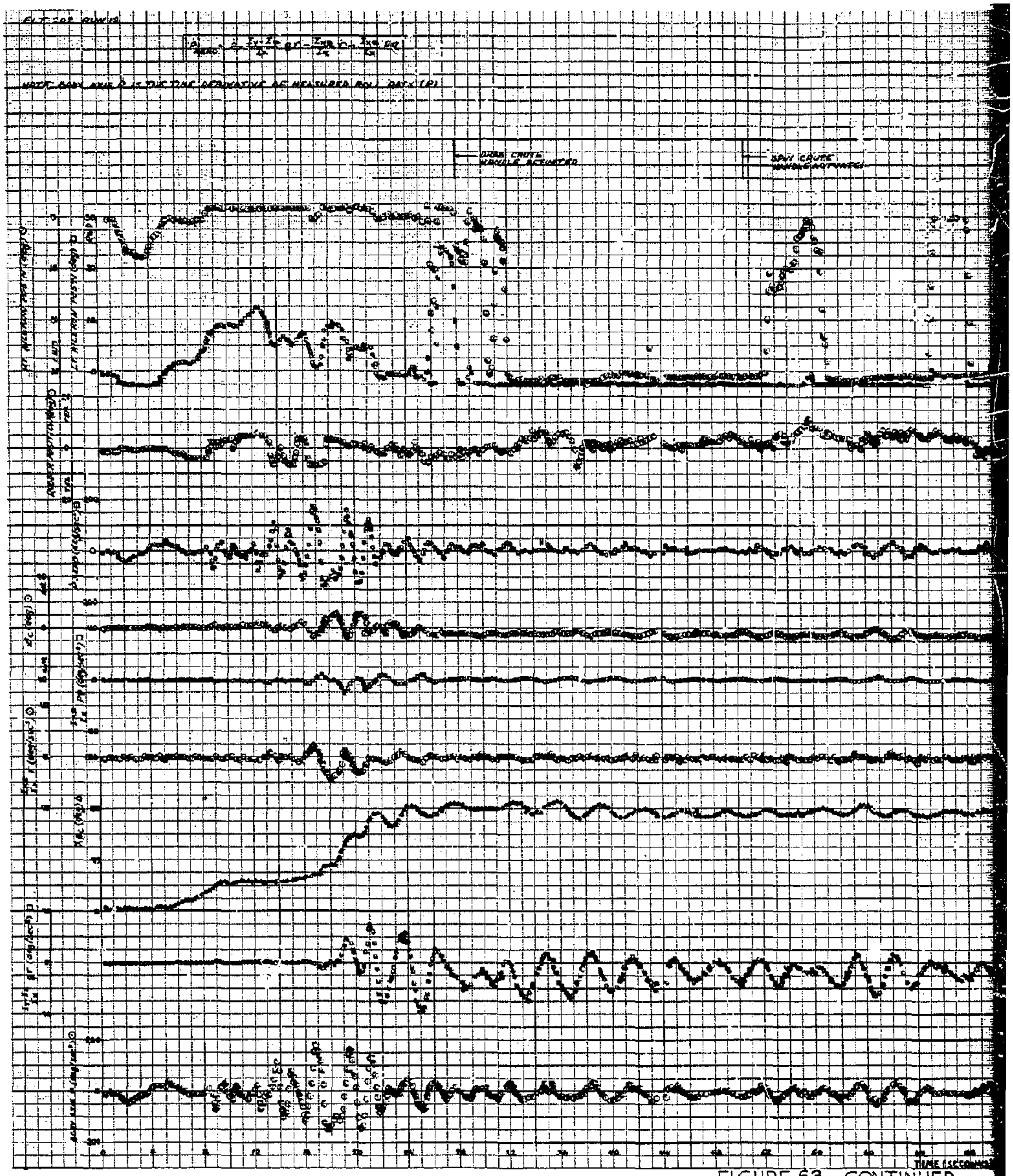

FIGURE 63. CONTINUED

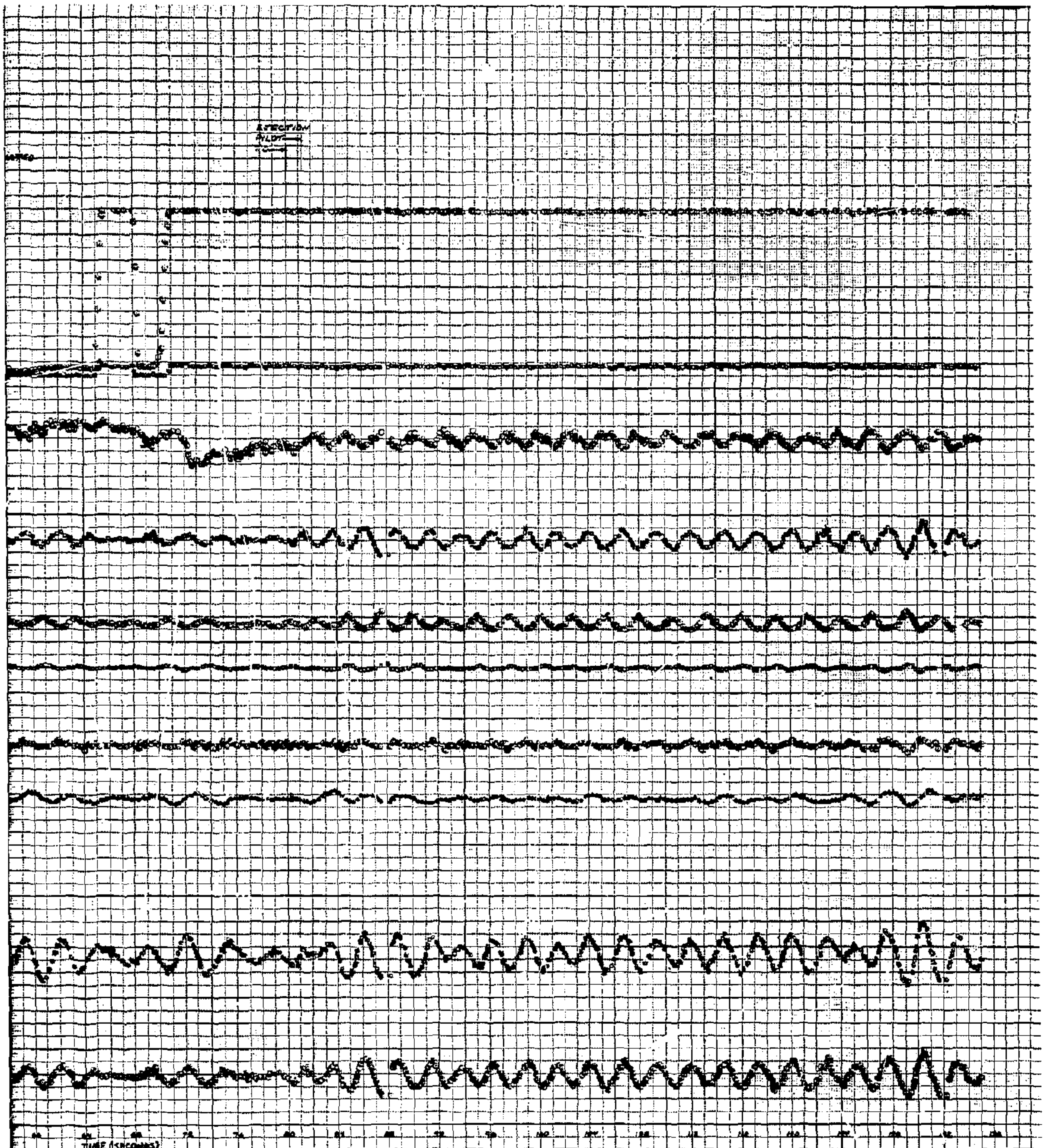

CONTINUED

2

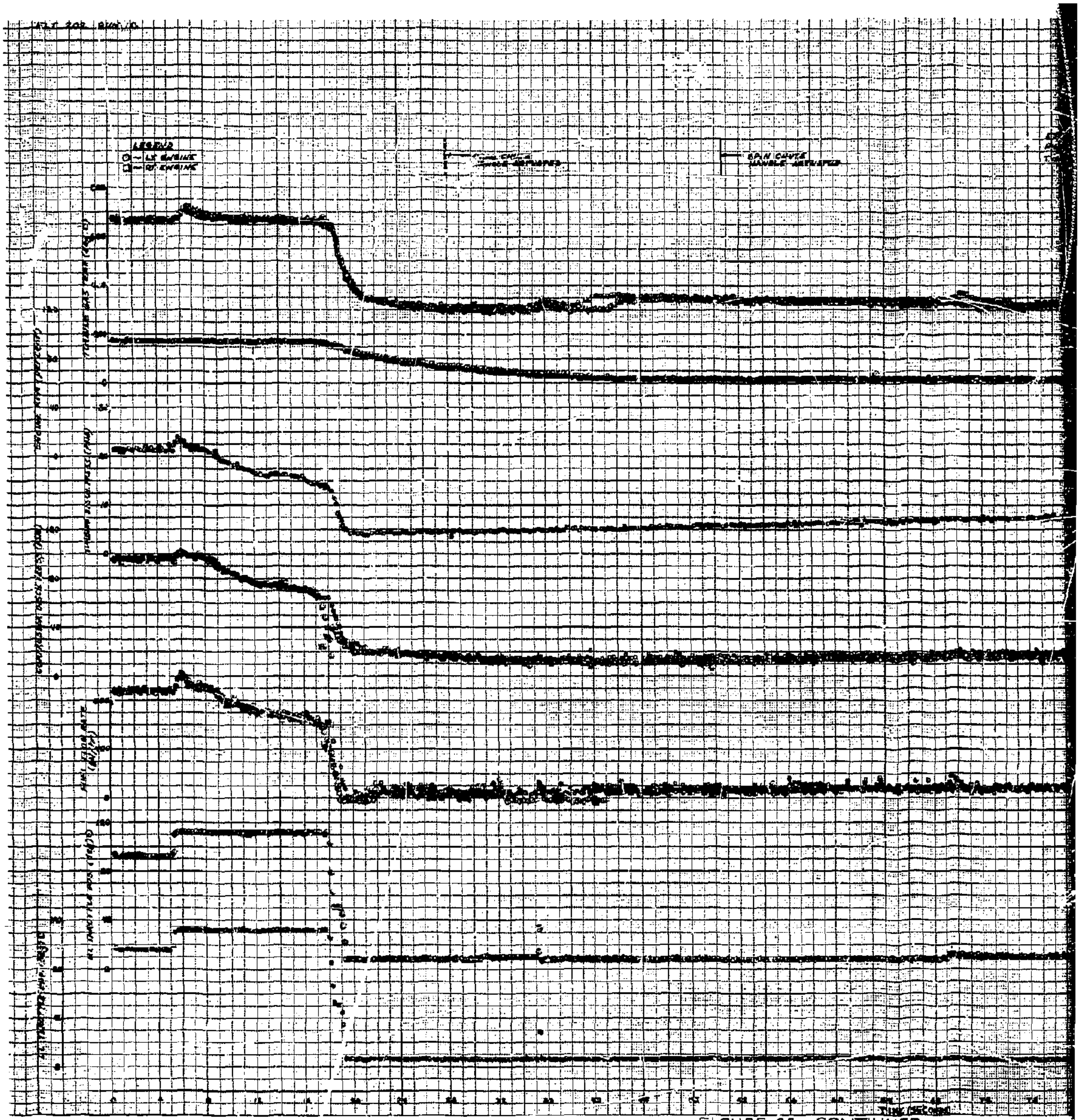

FIGURE 63 CONTINUED

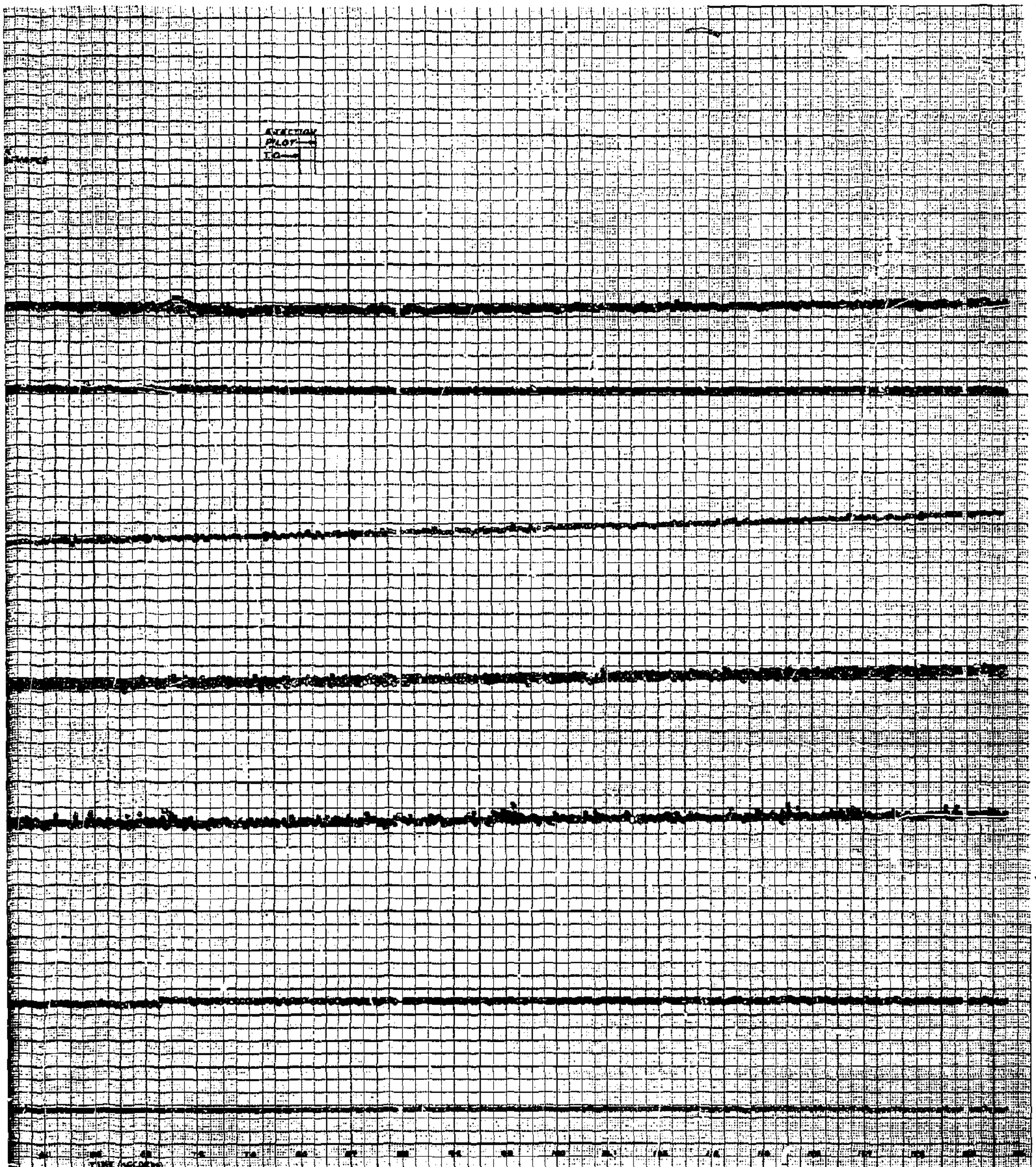

CONTINUED

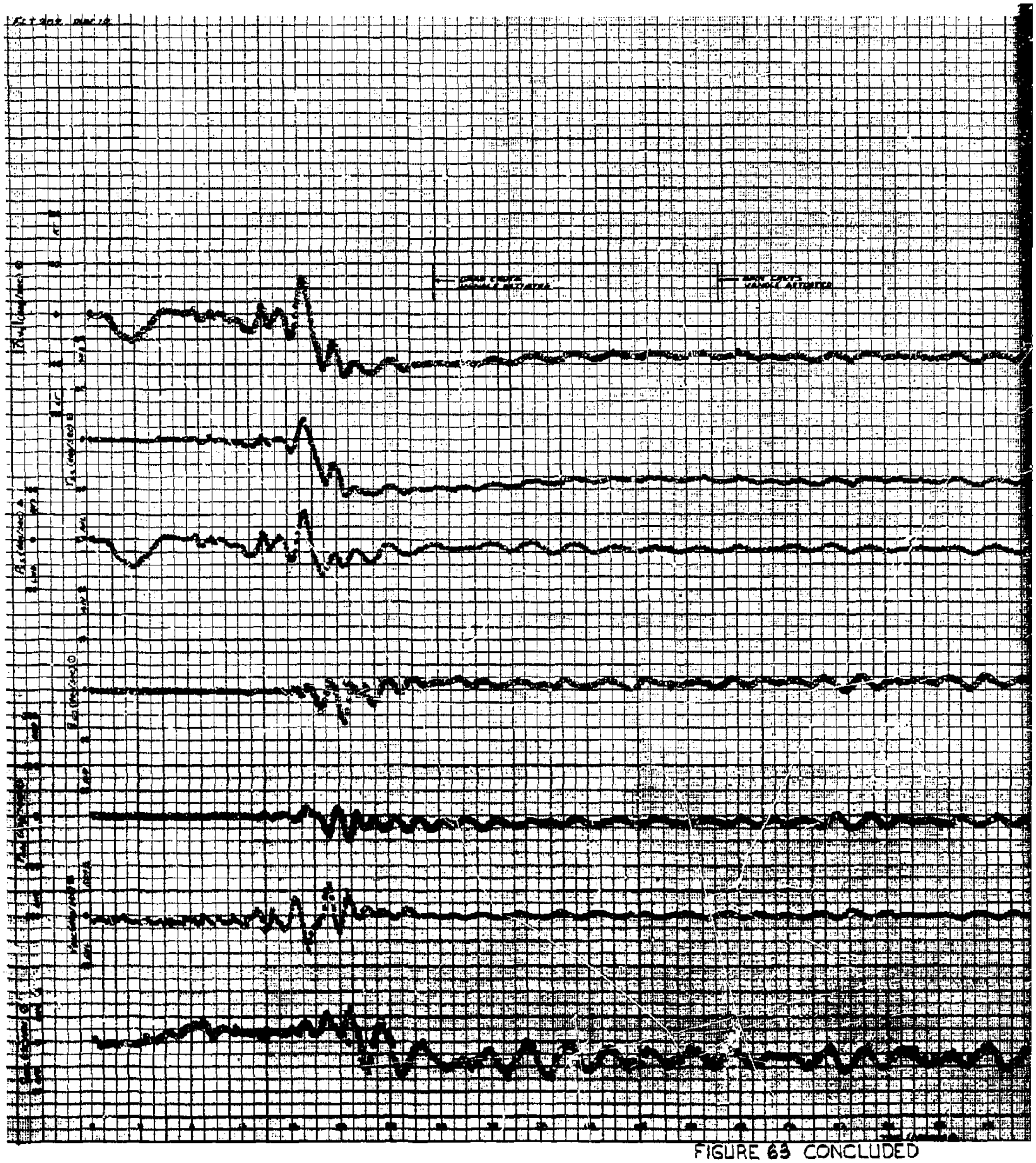

FIGURE 63 CONCLUDED

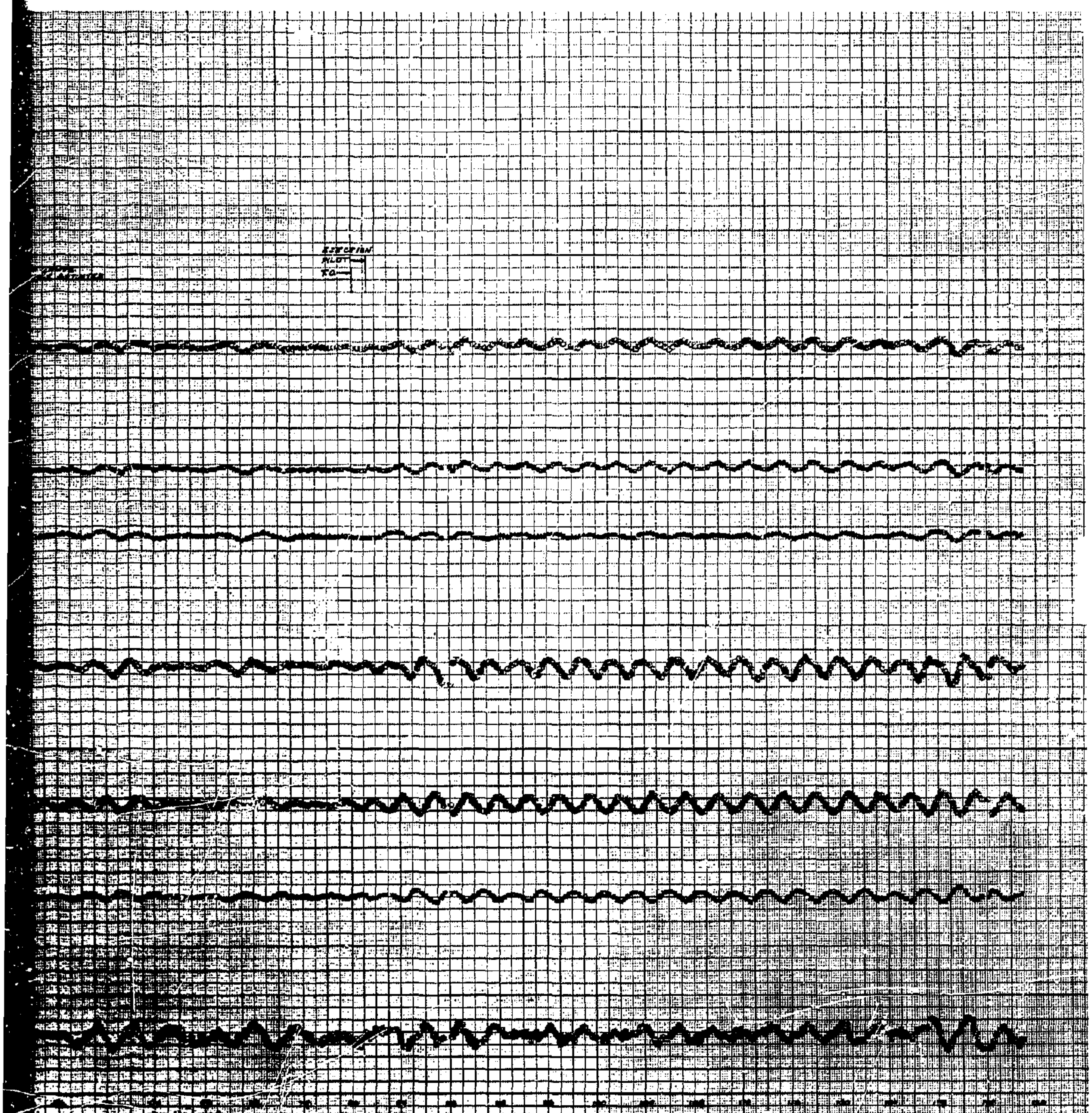

63 CONCLUDED

2

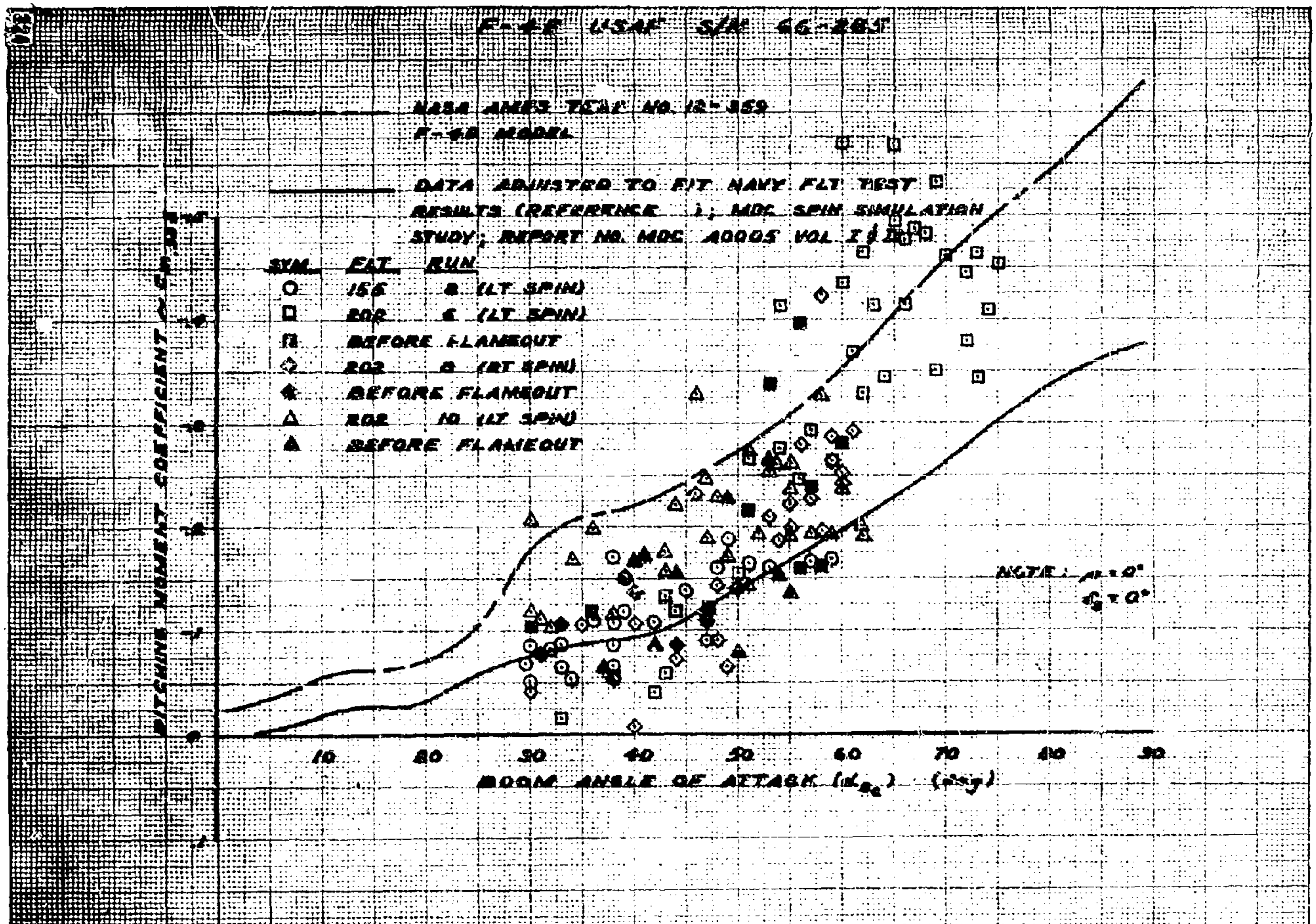

FIGURE 68 PITCHING MOMENT COEFFICIENT VS. ANGLE OF ATTACK

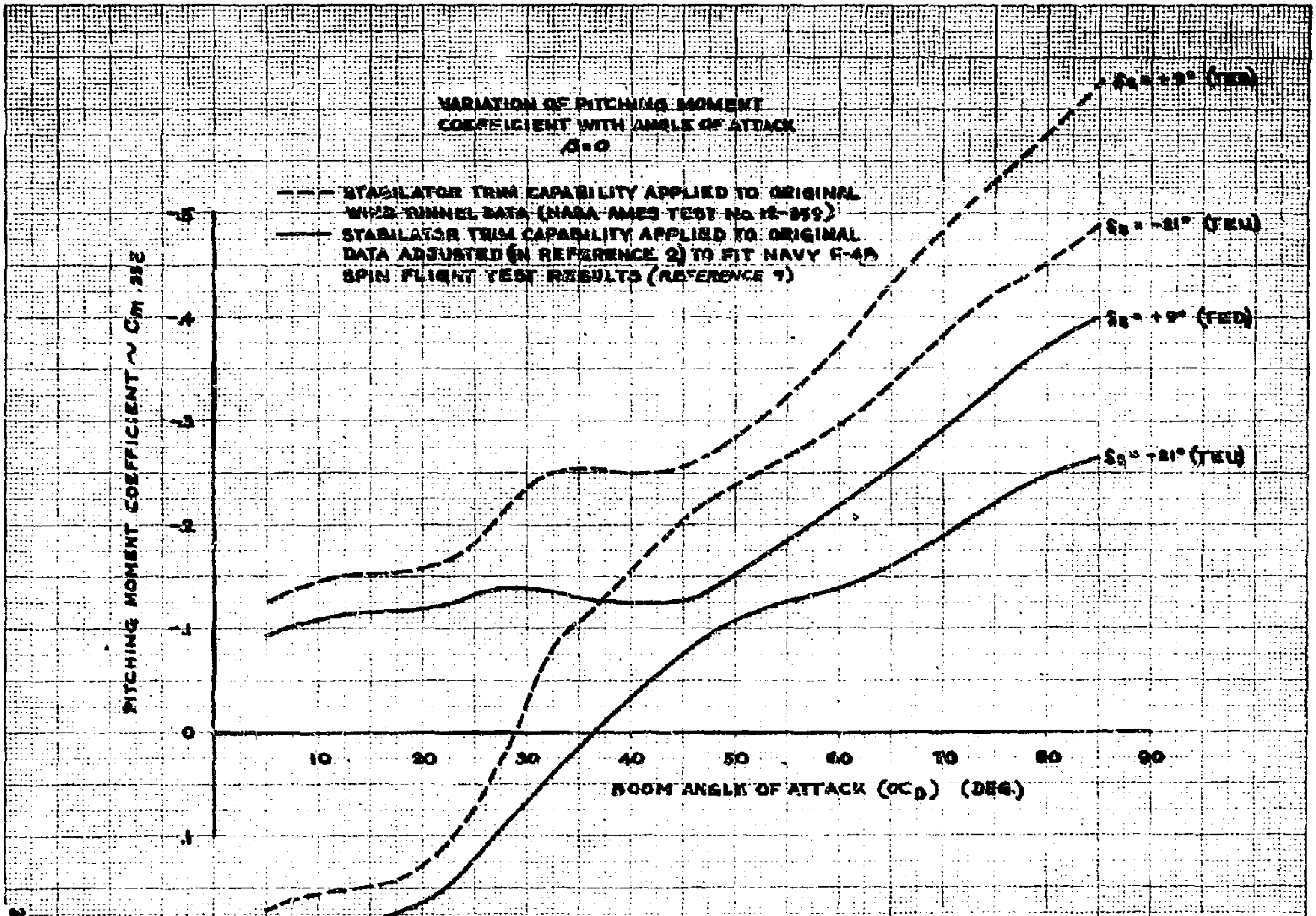

FIGURE 65 PITCHING MOMENT VS ANGLE OF ATTACK

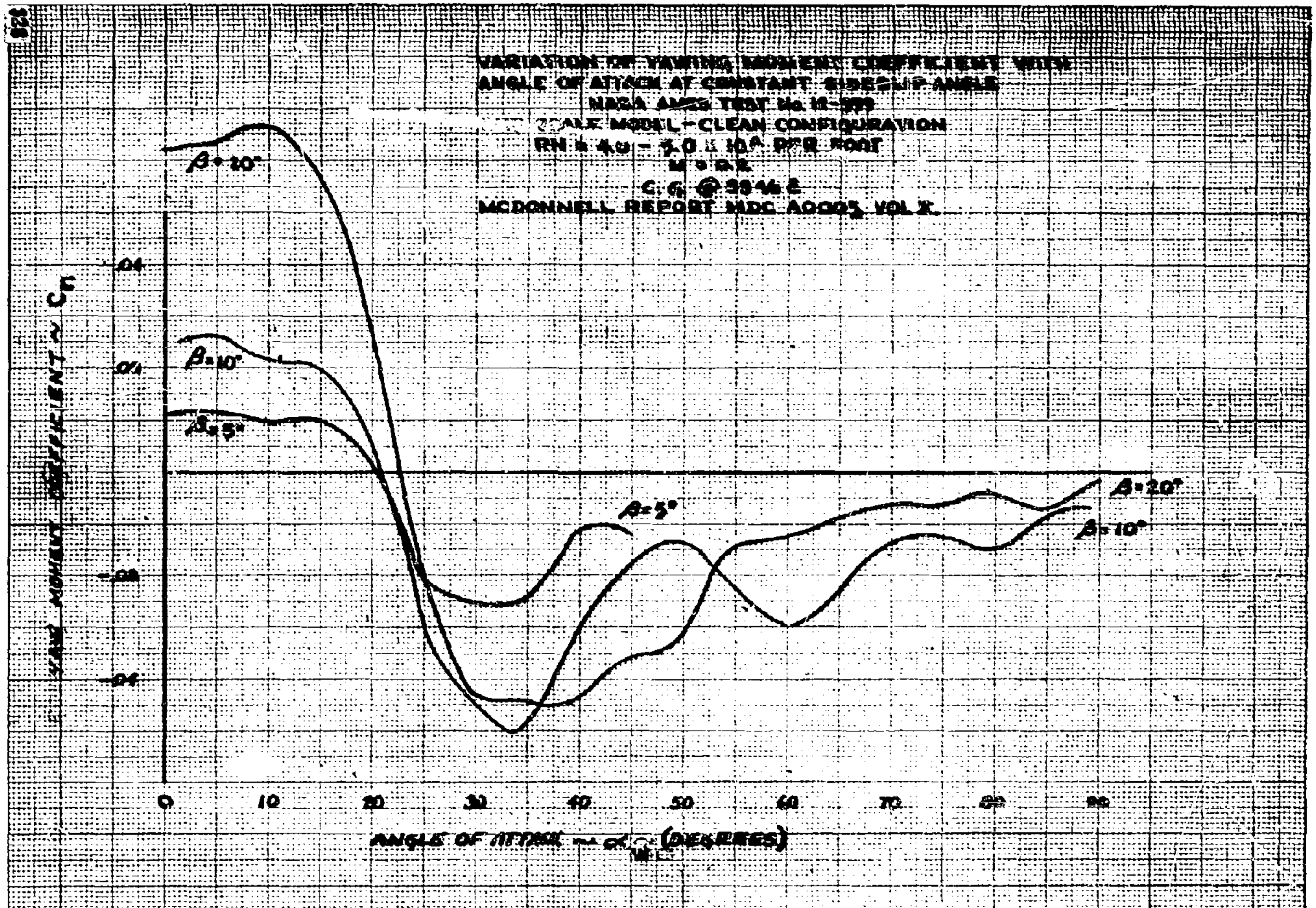

FIGURE 66 YAWING MOMENT COEFFICIENT VS ANGLE OF ATTACK

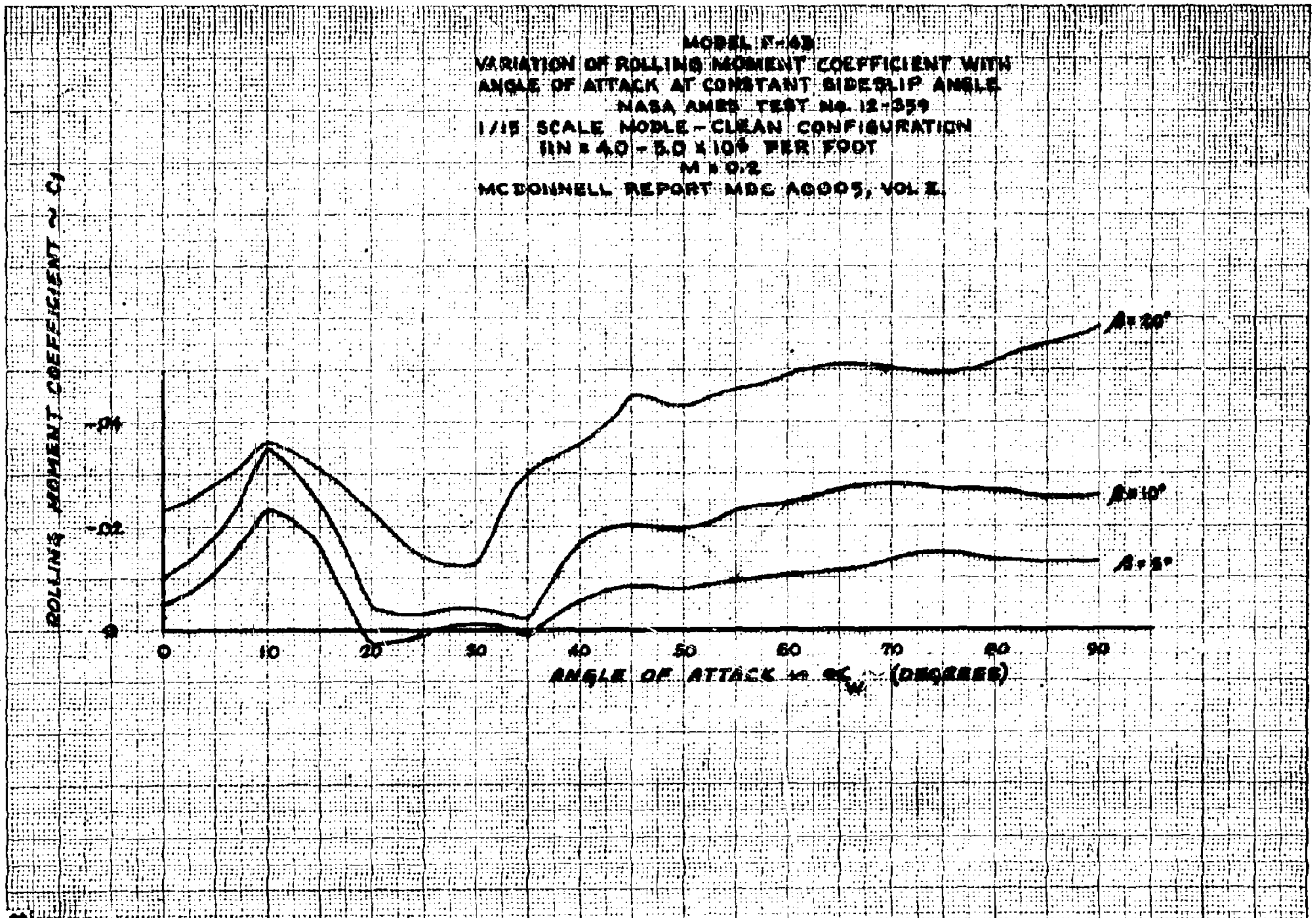

FIGURE 67 ROLLING MOMENT COEFFICIENT VS ANGLE OF ATTACK

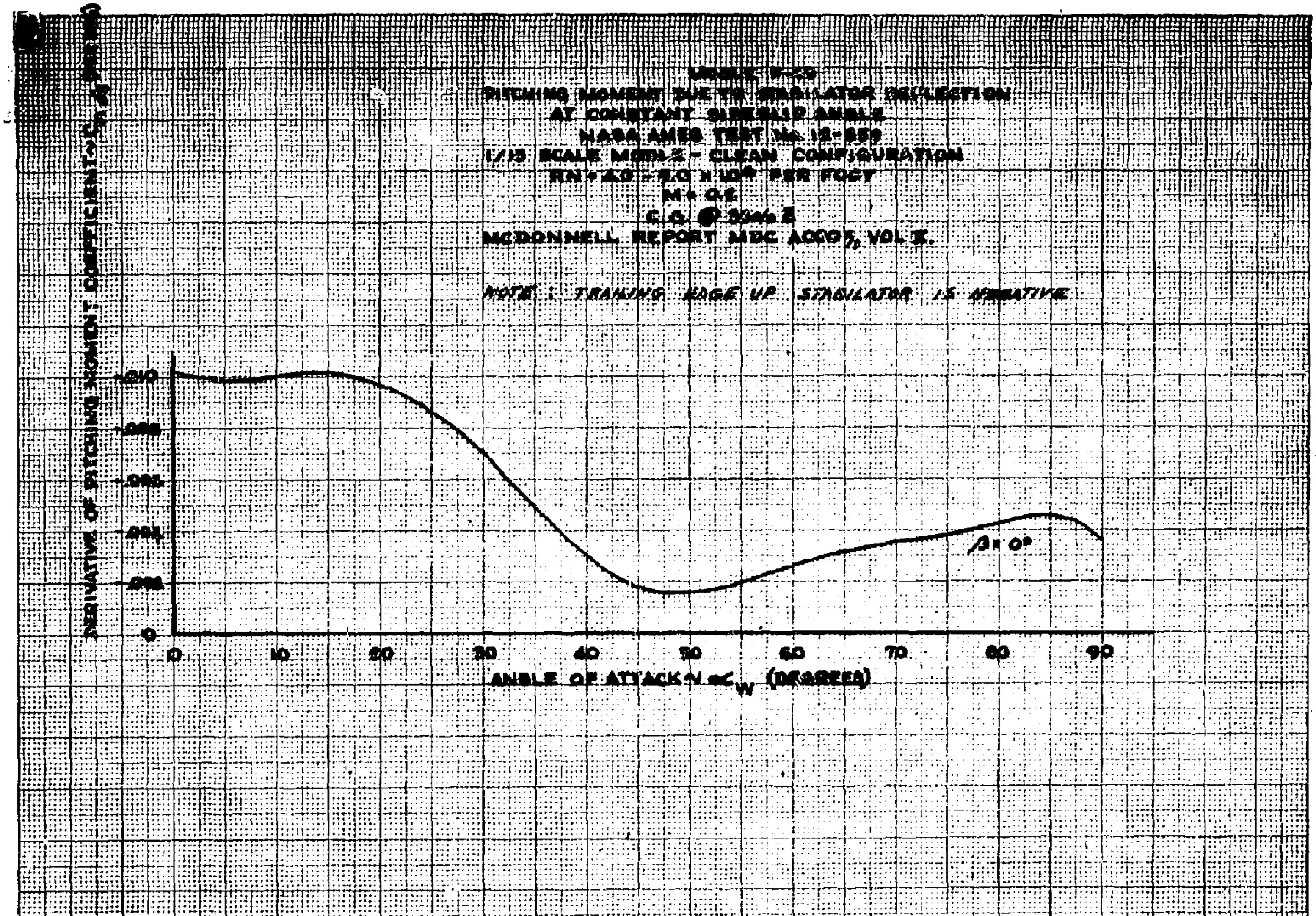

FIGURE 68 STABILATOR EFFECTIVENESS VS ANGLE OF ATTACK

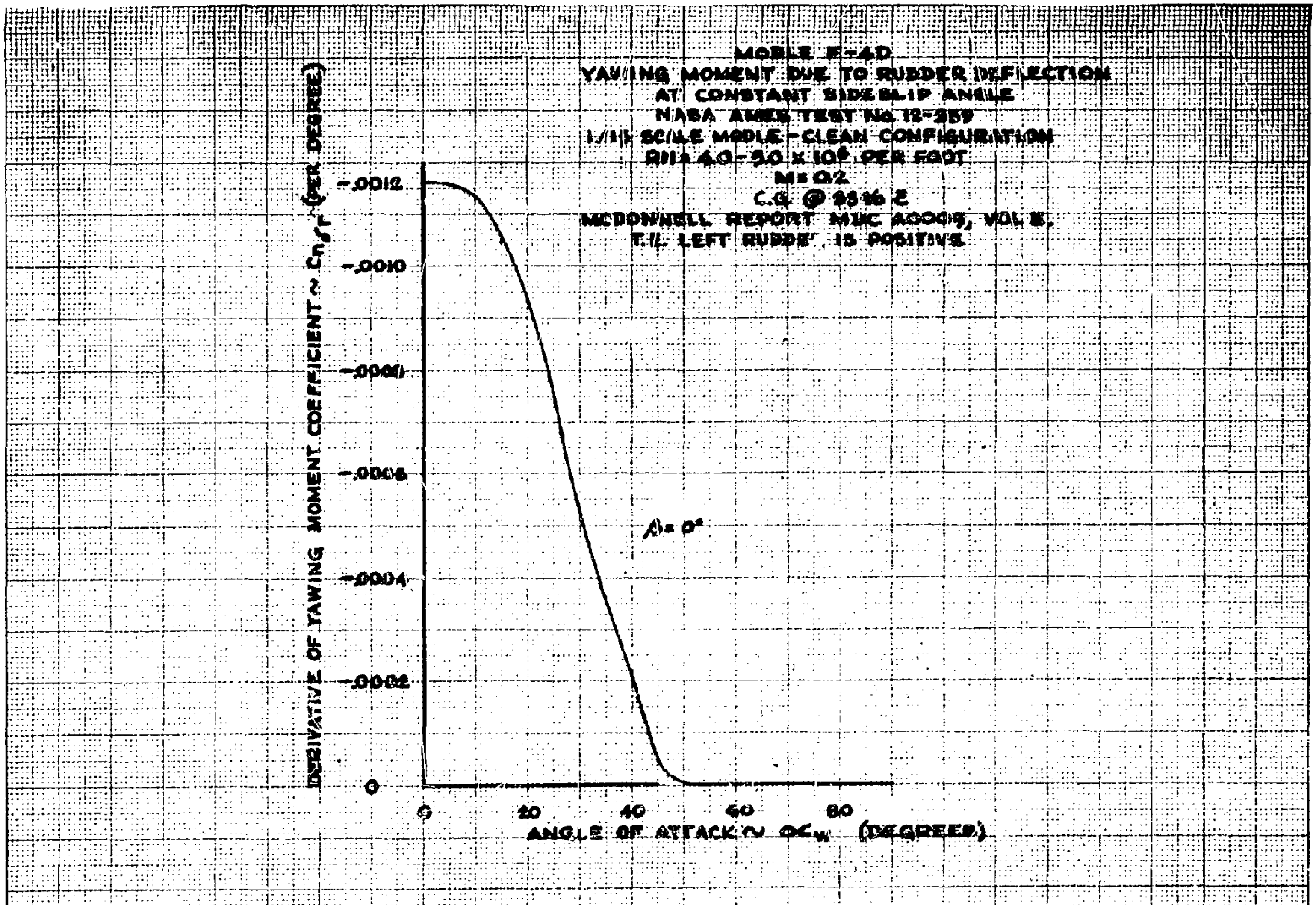

FIGURE 69 RUDDER EFFECTIVENESS VS ANGLE OF ATTACK

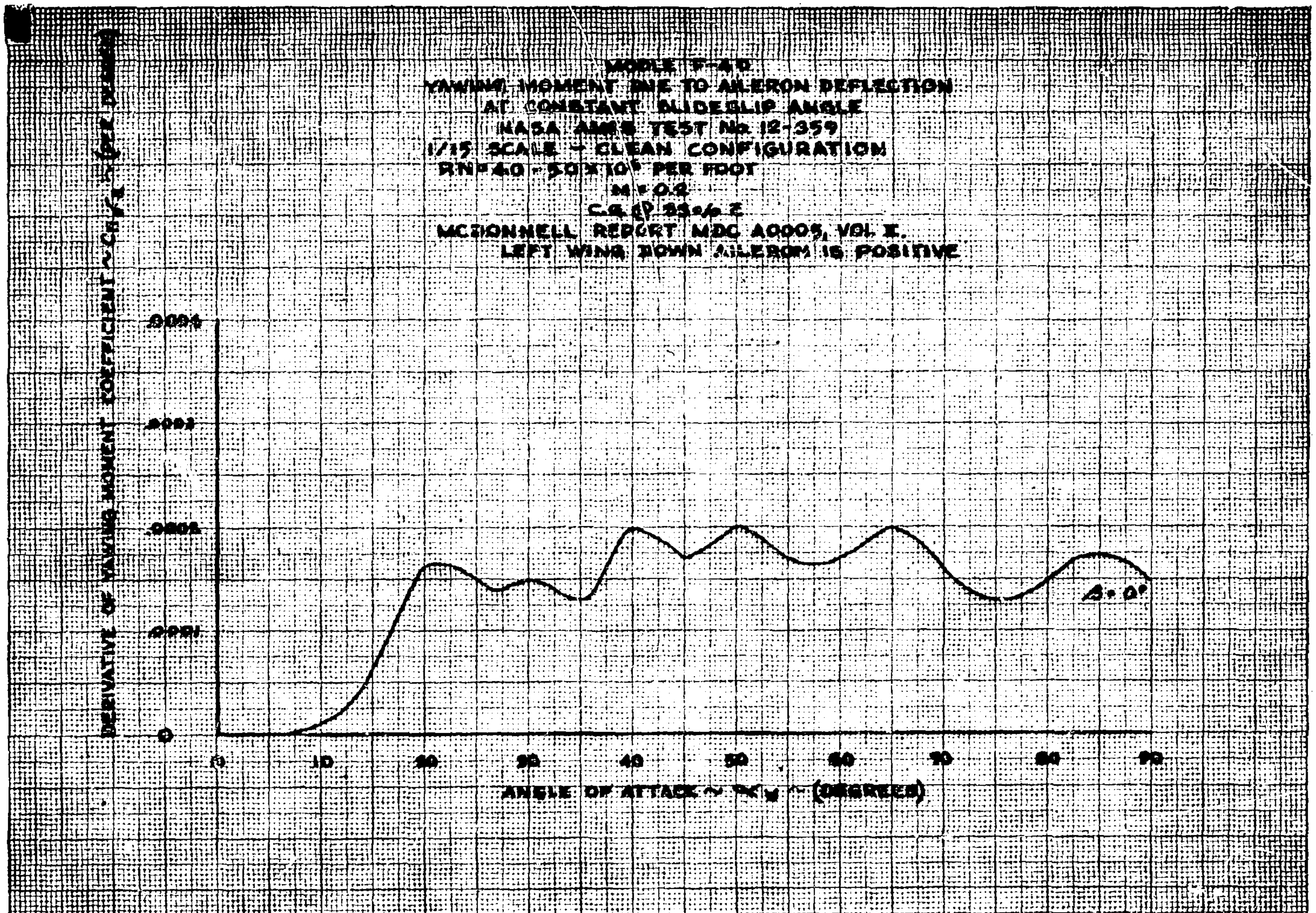

FIGURE 70 YAWING MOMENT DUE TO AILERON DEFLECTION

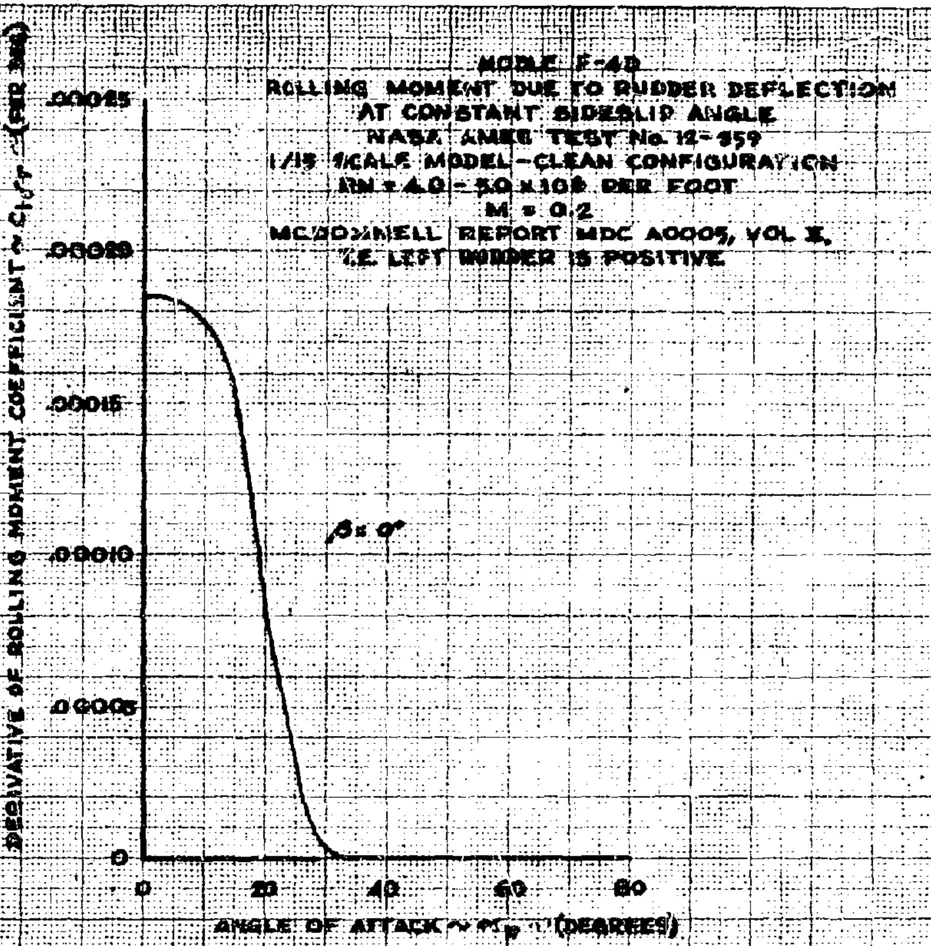

FIGURE 71 ROLLING MOMENT DUE TO RUDDER DEFLECTION

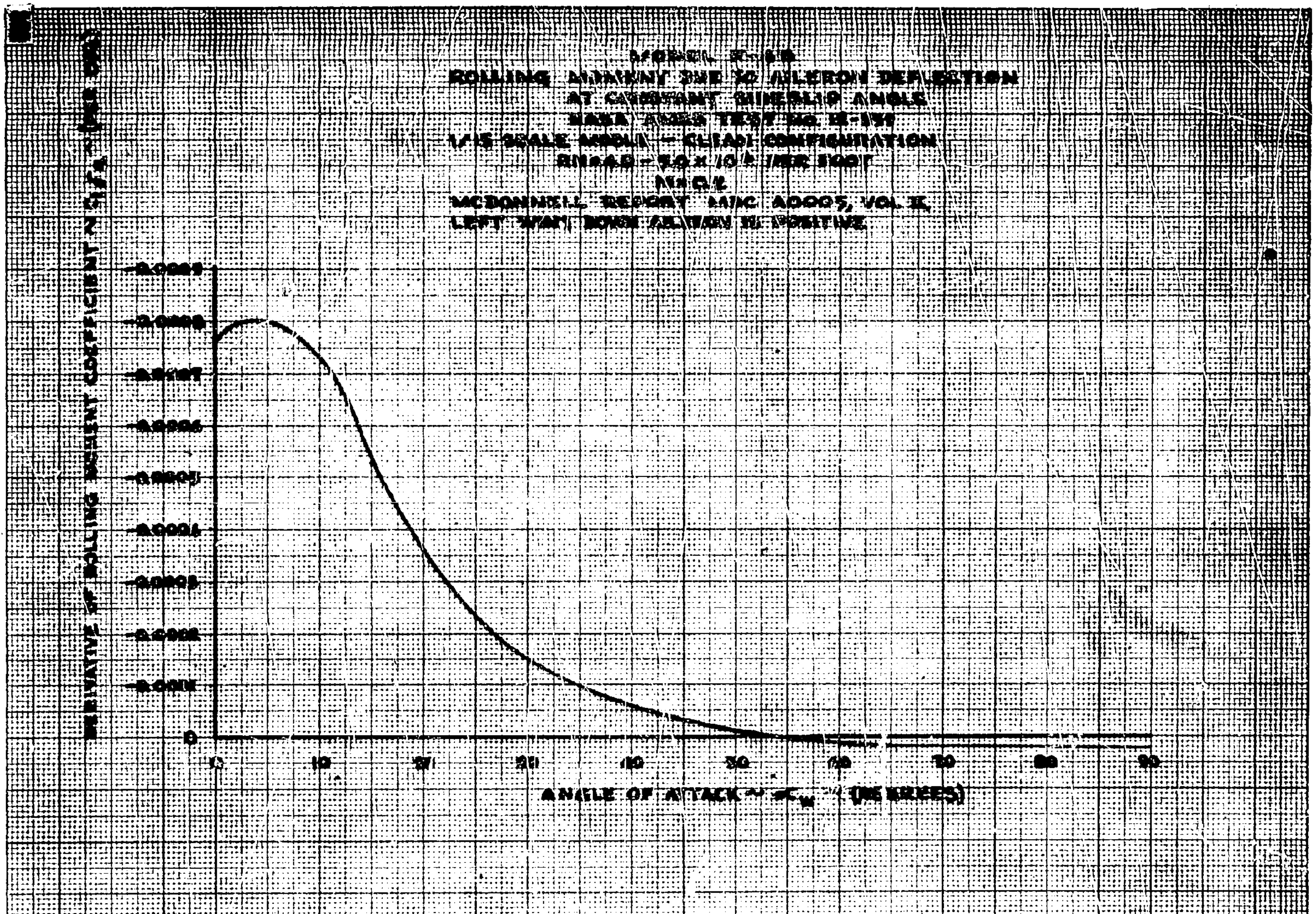

FIGURE 72 AILERON ROLL EFFECTIVENESS VS ANGLE OF ATTACK

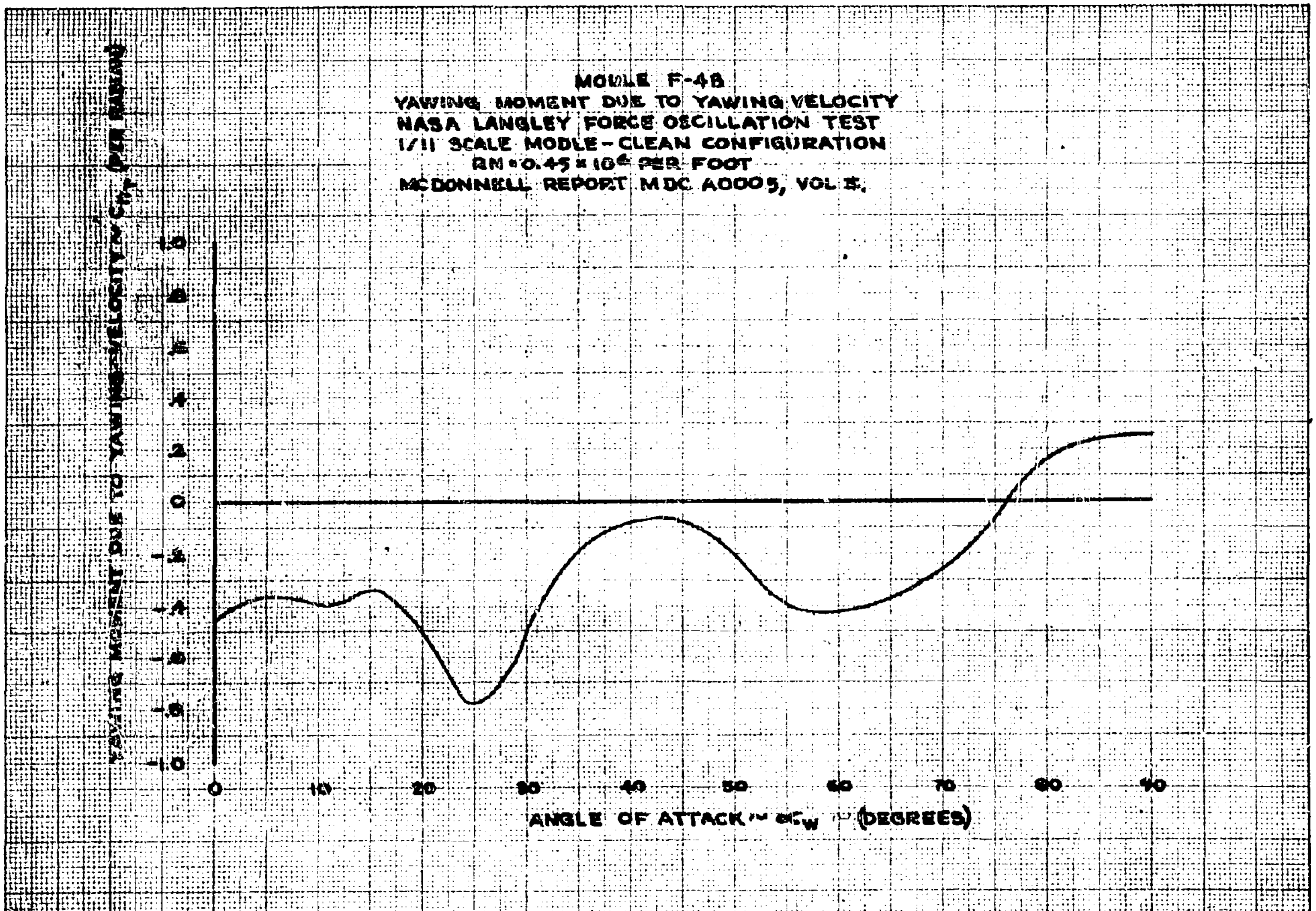

FIGURE 73 YAWING MOMENT DUE TO YAWING VELOCITY

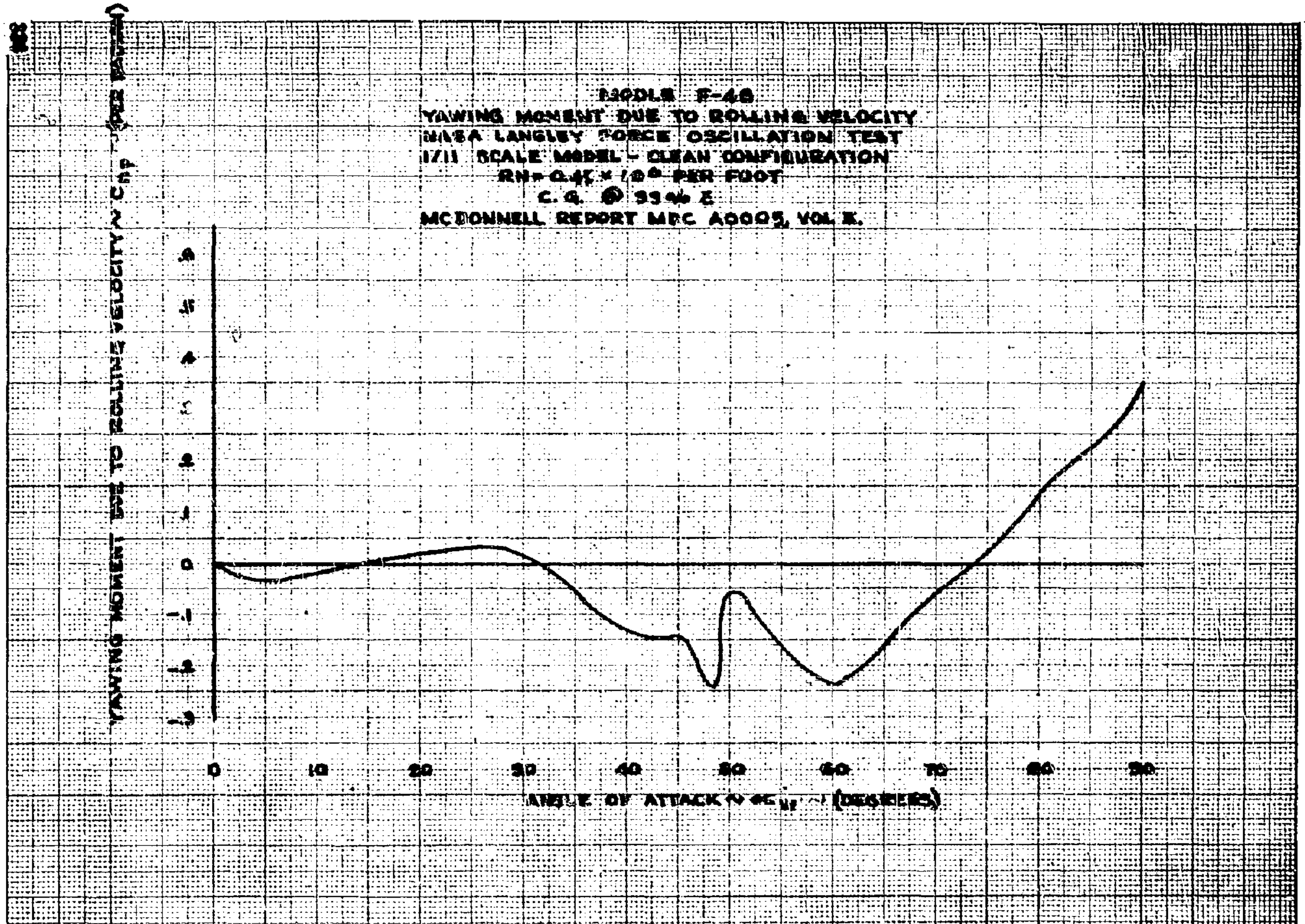

FIGURE 74 YAWING MOMENT DUE TO ROLLING VELOCITY

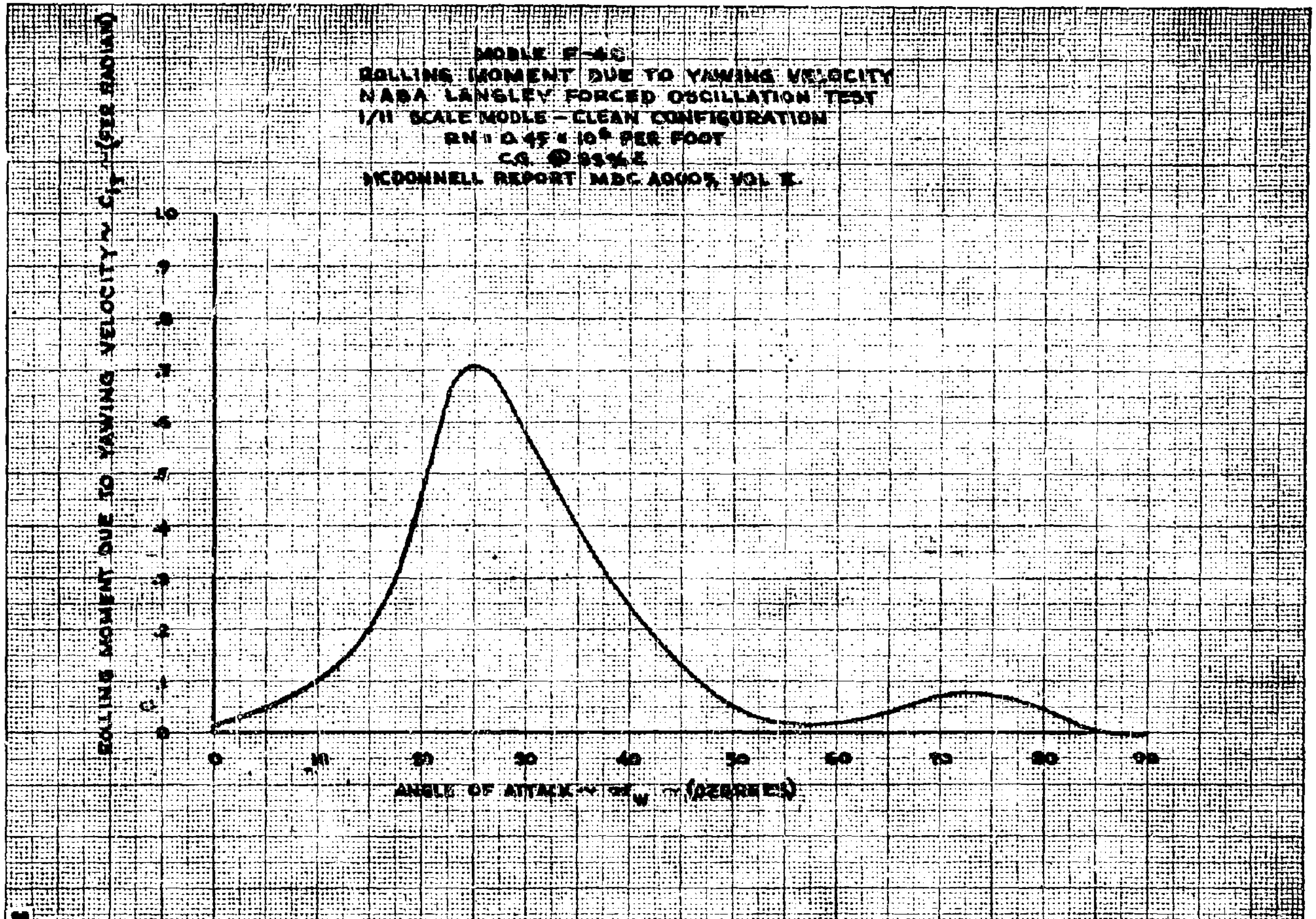

FIGURE 7.5 ROLLING MOMENT DUE TO YAWING VELOCITY

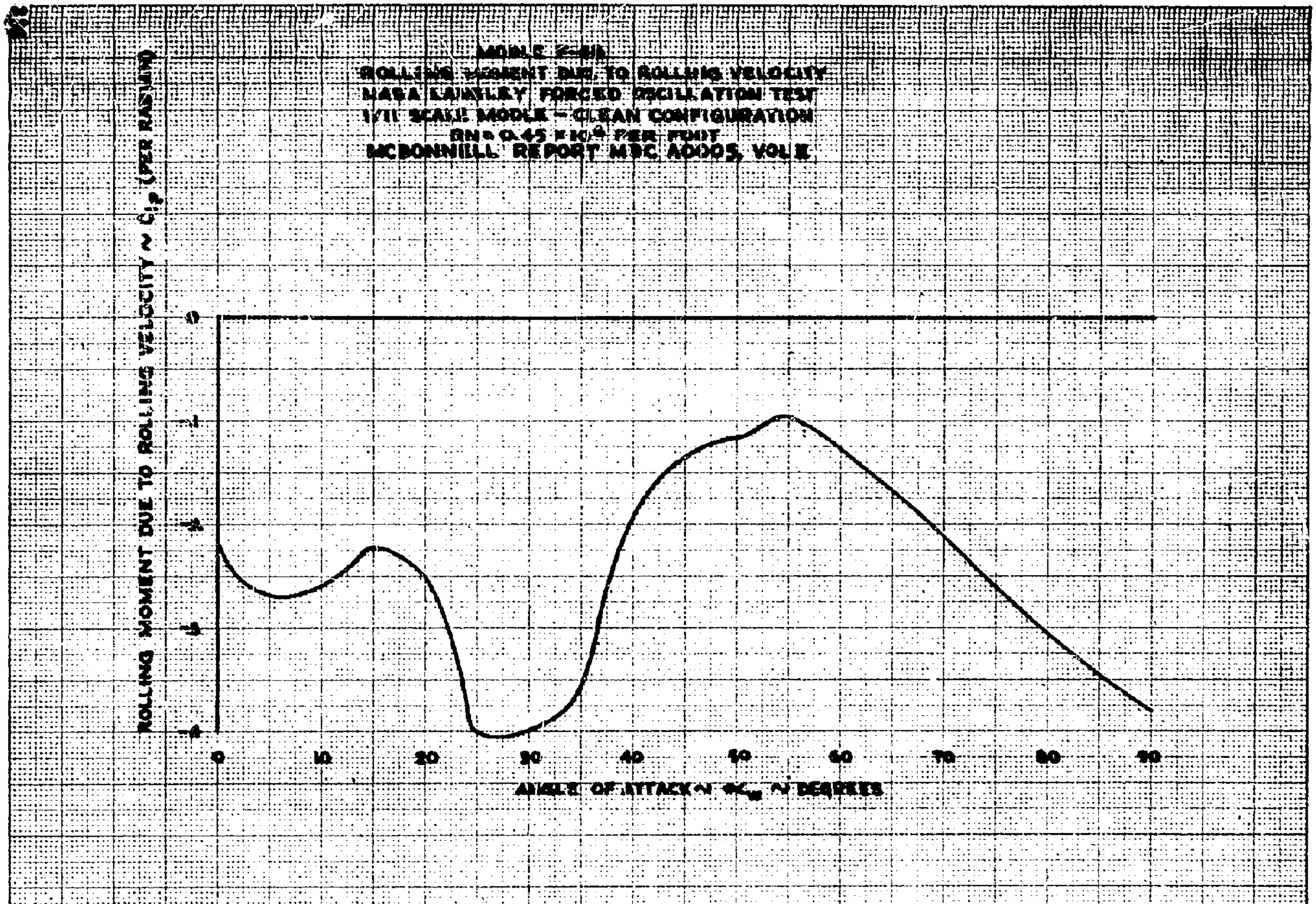

FIGURE 76 ROLLING MOMENT DUE TO ROLLING VELOCITY

APPENDIX II
Flight Log

F-4E USAF S/N 66-285

Flt No.	Duration Hr & Min	Loading	Phase	Test Results
146	1 + 20	1	Airspeed Calibration	Airspeed Calibration - Tower Fly-by
147	1 + 15	1A	Baseline Stability	Baseline stability at forward cg; dynamic and maneuvering longitudinal stability, rudder roll performance at 15 and 19 units; PA static longitudinal stability.
148	1 + 10	1B	Baseline Stability	Baseline Stability Mission at aft cg; dynamic and maneuvering longitudinal stability; rudder roll performance at 15, 17, and 19 units.
149	1 + 05	1	TAC Maneuver	TAC Training Maneuvers: adverse yaw demo-hi and low AOA, CR and PA configuration.
150	1 + 20	1A	TAC Maneuver	TAC Training Maneuvers: steady sideslip, CR 19 units; rudder and aileron demo's for adverse yaw; various combinations of SAS and ARI; CR and PA.
151	1 + 15	1A	I	Forward cg stall investigation; out-of-control recoveries from 1 g and accelerated stalls in CR and PA. Parabrake deploy at 29 units, CR configuration.
152	1 + 10	1B	Airspeed Calibration	Airspeed calibration - low speed pace (T-37)
153	1 + 15	1B	I	Mid-aft cg stall approaches in CR and PA; SAS on and off; drag chute deploy at 29U accelerated stall.
154	1 + 20	1A	I	Forward cg stall penetrations; rolling departure recoveries with forward stick; full aileron inputs near 25 units; drag chute deploy in half-flap configuration at 27 units.
155	0 + 30	1B	I	Mid-aft [illegible] CR static lateral-directional at 19 units; two turn spin left after normal stall approach; drag chute out to aid forward stick recovery.
156	1 + 0	1B	Baseline Stability	Chase abort; mid-aft cg; CR and PA TAC training maneuver; supersonic acceleration; steady sideslip at 19 units.

Flt No.	Duration Hr & Min	Loading	Phase	Test Results
157	1 + 15	1B	I	Mid-aft cg; normal and accelerated CR stalls; rudder and aileron inputs from 19 to 27 units; drag chute deploy near 30 units.
158	1 + 15	4A	Baseline Stability	Weather prohibited stall tests; conducted static longitudinal and lateral-directional stability tests; evaluated longitudinal maneuvering stability at .8 and .9 mach number.
159	1 + 40	4A & 4B	I	Normal and accelerated stalls; full aileron inputs near 25 units; drag chute deploy at 30 units, required forward stick for recovery.
160	1 + 10	4A & 4B	I	Normal stalls; CR configuration; rolling departures; first encounter with recovery rolls.
161	1 + 10	3C	I	Forward cg; normal and accelerated stalls; CR configuration; all departures were to the right; drag chute deployed in rolling departure near 30 units.
162	0 + 35	3C	I	Mid cg; normal stalls; CR configuration; rolling departures only; lost PC1.
163	1 + 10	3C	I	Mid cg; normal and accelerated stalls; CR configuration; 3 spins, 1 rolling departure to the right; drag chute out on 5-turn spin.
164	1 + 15	1A	I	Forward cg; normal and accelerated stalls; CR configuration; only 2 rolling departures; good AOA response to forward stick; drag chute deploy.
165	1 + [illegible]	1B	I	Normal cg; normal and accelerated stalls; CR configuration; 6 rolling departures; control pulses at high AOA; drag chute deployed/stick released.
166	1 + 05	4A & 4B	I	Weather prohibited stall maneuvers; drag chute deploy and stick fixed trim points.
167	1 + 45	4A & 4B	I	Normal cg; normal and accelerated stalls; CR configuration; 6 rolling departures, 3 spins; drag chute deploy.
168	0 + 45	1A	TAC Training Maneuver	Training maneuvers evaluated by representative from Tactical Fighter Weapons Center.

Flt No.	Duration Hr & Min	Loading	Phase	Test Results
169	0 + 55	1A	TAC Training Maneuver	Training maneuvers evaluated by representative from Tactical Fighter Weapons Center.
170	0 + 25	1A	II	T/M failure: air abort.
171	1 + 15	7A	II	Forward cg; normal and accelerated stalls; CR configuration; 6 rolling departures, 1 spin; drag chute deployed during rolling departure.
172	1 + 0	1B	II	Mid-aft cg; normal and accelerated stalls; CR configuration; 9 rolling departures, 1 steep-smooth spin; chute deploy in rolling departure.
173	1 + 10	1C	II	Mid-aft cg; normal and accelerated stalls; CR configuration; 4 spins, 3 rolling departures; drag chute aided departure recovery.
174	1 + 30	1B	II	Normal cg; normal and accelerated stalls; CR configuration; 6 mild rolling departures.
175	1 + 30	4A & 4B	II	Forward cg; normal and accelerated stalls; CR configuration; 4 spins, 4 rolling departures.
176	1 + 30	4A & 4B	II	Forward-mid cg; normal and accelerated stalls; CR configuration; 2 spins, 9 rolling departures
177	1 + 30	4A & 4B	II	Mid-aft cg; normal and accelerated stalls; CR configuration; 12 rolling departures, 1 spin; evaluated different forward stick rates; drag chute deployed at high AOA, aircraft recovered with stick held aft.
178	1 + 30	1B	II	Normal cg; normal and accelerated stalls; CR configuration; 6 rolling departures, 4 spins; drag chute deployed, but forward stick was effecting recovery.
179	1 + 0	3D	II	Forward cg; normal and accelerated stalls; CR configuration; 6 spins, 2-4 turns; varied rate of forward stick; drag chute near vertical tail.
180	1 + 10	3D	II	Forward cg; normal and accelerated stalls; CR configuration; 6 spins, 2-4 turns; drag chute deployed and caught on q-bellows probe on vertical tail.
181	1 + 0	3D	II	Mid-aft cg; normal and accelerated stalls; CR configuration; 6 spins, 2-5 turns; one inverted turn at recovery from a 5-turn erect spin.

Flt No.	Duration Hr & Min	Loading	Phase	Test Results
182	1 + 15	2A,B	I, II	Forward cg; normal and accelerated stalls (smooth and abrupt); CR configuration; 8 spins (1-3 turns) and 3 rolling departures; drag chute aids recovery from spin.
183	1 + 15	1D	II	Tuft photos of empennage and lower wing at stabilized AOA's.
184	1 + 15	1E	II	Forward cg; normal and accelerated stalls; CR and PA configuration; 4 spins (1-7 turns) and 4 rolling departures; drag chute aids recovery from spin.
185	1 + 30	5A, B	II	Forward cg; normal and accelerated stalls; CR configuration; 7 spins (1-3 1/2 turns, all to left); tuft photos of empennage.
186	1 + 20	6A, B	I, II	Forward cg; normal and accelerated stalls (smooth and abrupt); CR configuration; 6 spins (1 1/2-6 1/2 turns); 2 rolling departures; extreme recovery oscillations.
187	0 + 45	7A	I, II	Forward cg; normal and accelerated stalls (smooth and abrupt); CR configuration; 4 mild rolling departures; very positive recoveries with forward stick only.
188	0 + 45	7A	II	Forward cg; normal and accelerated stalls; CR configuration; 4 rolling departures, 1 spin (1 turn).
189	1 + 10	1A	III	Forward cg; accelerated stalls and high pitch attitude zoom stalls; CR configuration; 2 rolling departures; 1 spin; 8 high pitch attitude stalls with and without lateral-directional control inputs.
190	1 + 10	1A	III	Normal cg; normal and accelerated stalls; high pitch attitude zoom stalls; CR configuration; 2 rolling departures; 1 spin; 6 high pitch attitude zoom stall entry maneuvers; including a vertical entry and controls release.
191	0 + 45	1C	III	Aft cg; accelerated stalls and one 60° pitch attitude stall; CR configuration; 2 spins (4 and 8 turns); drag chute aided recovery from the steep-mildly oscillatory spin mode.

Flt No.	Duration Hr & Min	Loading	Phase	Test Results
192	0 + 25	1C	III	Aft cg; CR configuration; one 60° pitch attitude zoom stall; accelerated stall resulting in steep-mildly oscillatory spin with a reversal in turn direction; drag chute aided recovery.
193	0 + 50	1B	III	Aft cg; CR configuration; accelerated stalls and zoom entry stalls; one rolling departure; three spins; drag chute deployed to aid recovery from spin.
194	1 + 15	4A,B	III	Forward cg; normal and accelerated stalls, CR and DIVE configuration; four rolling departures; four spins (1-2 turns); simulated ground attack maneuvers/inadvertant stalls.
195	1 + 10	1B	III	Aft cg; normal and accelerated stalls and oblique loop; CR configuration; two rolling departures; 3 spins (2-5 1/2 turns).
196	1 + 05	1C	III	Aft cg; accelerated stalls; CR and CO configuration; two rolling departures, one spin; inverted stall; aileron with the spin direction aids recovery.
197	1 + 0	8A,B	III	Mid cg; normal and accelerated stalls; CR configuration; three rolling departures, one spin; positive recoveries with forward stick only.
198	1 + 30	9A,B	III	Mid cg; normal and accelerated stalls; CR configuration; four rolling departures; two spins; lateral-directional controls required to obtain a departure into the heavy wing.
199	1 + 05	5A,B	IV	Mid-aft cg; normal and accelerated stalls; CR configuration; one rolling departure, five spins (1-7¼ turns).
200	0 + 45	5A,B	IV	Non-productive. Weather in spin area/chase lost communication.
201	1 + 20	5A,B	IV	Mid-aft cg; accelerated stalls; CR configuration; first attempt to evaluate the aft stick.. spin recovery procedure resulted in a flat spin; 33' chute deployed for recovery.
202	1 + 0 (estimated)	1C	IV	Aft cg; accelerated stalls; CR configuration; one rolling departure; three steep spins; one flat spin; 33' chute attach mechanism failed, chute left airplane, crew ejected.

REFERENCES

1. Rutan, Elbert L., McElroy, Collet E., First Lieutenant, USAF and Gentry, Jerauld R., Major, USAF, Stall/Near Stall Investigation of the F-4E Aircraft, FTC-TR-70-20, Air Force Flight Test Center, Edwards AFB, California, August 1970.

2. Brady, C. C., Moran, W. A., and Rosenstein, M. L., Model F-4 Spin Evaluation Program, MACAIR Report MDC A0005, St. Louis, Missouri, Volumes I and II, 15 August 1969.

3. Chambers, Joseph R. and Anglin, Ernie L., Analysis of Lateral-Directional Characteristics of a Twin-Jet Fighter Airplane at High Angles of Attack, NASA TN D-5361, Washington D.C., August 1969.

4. Rutan, Elbert L. and Gentry, Jerauld R., Major, USAF, Category II Stability and Control Evaluation of the F-4E Aircraft, FTC-TR-69-14, Air Force Flight Test Center, Edwards AFB, California, April 1969.

5. Rutan, Elbert L., and Gentry, Jerauld R., Major, USAF, Category II Stability and Control Evaluation of the F-4E Aircraft, FTC-SD-69-14, Air Force Flight Test Center, Edwards AFB, California, July 1969.

6. Williams, George H., Major, USAF, and Twinting, William T., Captain, USAF, F-4C Category II Stability and Control Test, FTC-TR-65-30, Air Force Flight Test Center, Edwards AFB, California, December 1965.

7. DeAnda, Albert G., AFFTC Standard Airspeed Calibration Procedures, FTC-TIH-68-1001, Air Force Flight Test Center, Edwards AFB, California, April 1968.

8. Luckey, R. A., and Brockhagen, B. J., F-4E Stall and Near Stall Investigation - Test Airplane Modification - Final Engineering Report, MDC A0023, McDonnell-Douglas Corporation, St. Louis, Missouri, 8 December 1969.

9. Clexton, Edward W., Lieutenant USN, Sullivan, Dennis A., Lieutenant USN, and Dunn, Joseph L., Evaluation of the Spin and Recovery Characteristics of the F-4B Airplane, NATC-TR-FT-88R-67, Naval Air Test Center, Patuxent River, Maryland, December 1967.

10. Densford, W. G., F4H-1F Airplane Demonstration Data Report, Volume II, Supplement II - Spins, McDonnell-Douglas Corporation Report 6088, St. Louis, Missouri, 9 October 1961.

11. Bonnie, W. J., Niemann, C. R., Sonntag, A. H., and Weber, W. B., Model F/RF-4B-C Aerodynamic Derivative, McDonnell-Douglas Corporation Report 9842, St. Louis, Missouri, 10 February 1964, revised 16 April 1969.

12. Wykes, J.H., Casteel, G. R. and Collins, R. A., An Analytical Study of the Dynamics of Spinning Aircraft, WADC Technical Report 58-38, Wright-Patterson AFB, Dayton, Ohio, December 1958.

13. Neihouse, Anshal I., Klinar, Walter J., and Scher, Stanley H., Status of Spin Research for Recent Airplane Designs, NASA TR R-57, Washington, D. C., 1960.

14. Polhamus, Edward C. and Spreemann, Kenneth P., Subsonic Wind-Tunnel Investigation of the Effect of Fuselage Afterbody on Directional Stability of Wing-Fuselage Combinations at High Angles of Attack, Washington, D.C., NACA TN 3896, 1956.

15. Moul, Martin T. and Paulson, John W., Dynamic Lateral Behavior of High-Performance Aircraft, NACA RM L58E16, Washington, D.C., 1958.

16. Stone, Ralph W. and Polhamus, Edward C., Some Effects of Shed Vortices on the Flow Fields Around Stabilizing Tail Surfaces, AGARD Report 108, Paris, France, April-May 1957.

17. Chambers, Joseph R., Bowman, J.S. Jr., and Anglin, Ernie L., Analysis of the Flat-Spin Characteristics of a Twin-Jet Swept-Wing Fighter Aircraft, NASA Langley Working Paper, LWP-663. Langley Research Center, Hampton, Virginia, October 1968.

18. Casteel, G. R. and Weyl, Carl J., A Design Approach to Provide Satisfactory Spin Characteristics for a Modern Fighter Aircraft, AIAA 70-928, July 1970.

19. Sullivan, D.A., Lt, USN, Gentry, J.R., Major, USAF, et al, Final Report - Military Evaluation of the F-4 Wing Leading Edge Slats, NATC Rpt FT-119R-69, Patuxent River, Maryland, 15 Oct 1969.

UNCLASSIFIED
Security Classification

DOCUMENT CONTROL DATA - R & D

(Security classification of title, body of abstract and indexing annotation must be entered when the overall report is classified)

1. ORIGINATING ACTIVITY (Corporate author) Air Force Flight Test Center Edwards Air Force Base, California	2a. REPORT SECURITY CLASSIFICATION Unclassified 2b. GROUP N/A

3. REPORT TITLE

Stall/Near Stall Investigation of the F-4E Aircraft

4. DESCRIPTIVE NOTES (Type of report and inclusive dates)

Final

5. AUTHOR(S) (First name, middle initial, last name)

Collet E. McElroy, First Lieutenant, USAF
Patrick S. Sharp, Sergeant, USAF

6. REPORT DATE	7a. TOTAL NO. OF PAGES	7b. NO. OF REFS
October 1970	343	19

8a. CONTRACT OR GRANT NO.	9a. ORIGINATOR'S REPORT NUMBER(S)
b. PROJECT Directive 70-30 and 70-30A	FTC-SD-70-20
c.	9b. OTHER REPORT NO(S) (Any other numbers that may be assigned this report)
d.	N/A

10. DISTRIBUTION STATEMENT

This document may be further distributed by any holder only with specific prior approval of ASD (ASZMT), Wright-Patterson AFB, Ohio 45433.

11. SUPPLEMENTARY NOTES	12. SPONSORING MILITARY ACTIVITY
None	6512th Test Group Edwards AFB, Calif

13. ABSTRACT

This report includes test techniques, data reduction methods, analytical studies and substantiating data for the Stall/Near Stall Investigation of the F-4E aircraft. Discussion of results, conclusions, and recommendations were included in FTC-TR-70-20, Stall/Near Investigation of the F-4E Aircraft, August 1970.

DD FORM 1 NOV 65 1473

UNCLASSIFIED
Security Classification

14. KEY WORDS	LINK A		LINK B		LINK C	
	ROLE	WT	ROLE	WT	ROLE	WT
F-4E aircraft						
stall testing						
spin testing						
stall warning						
asymmetric loading						
spin modes						
aerodynamic data						
inertial coupling						
engine gyroscopic effects						
forward stick						
departure						
recovery						
drag chute						
position error						
angle of attack and sideslip						
moment coefficients						